Investigation of growth limitations in (pseudo-)steady states with *Corynebacterium glutamicum*

DISSERTATION

Von der Fakultät Energie-, Verfahrens- und Biotechnik der Universität Stuttgart zur Erlangung der Würde eines Doktor-Ingenieurs (Dr.-Ing.) genehmigte Abhandlung

Vorgelegt von

Michaela Graf, M.Sc.

aus Ulm

Hauptberichter: Prof. Dr.-Ing. Ralf Takors
Mitberichter: Prof. Dr. rer. nat. Bernhard Eikmanns

Tag der mündlichen Prüfung: 22. Oktober 2019

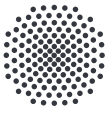

Universität Stuttgart

Institut für Bioverfahrenstechnik

2019

Für Tobias

Wenn die Menschen nur über das sprächen, was sie begreifen, dann würde es sehr still auf der Welt sein.

Albert Einstein

Danksagung

Bevor der interessierter Leser in die Tiefen von *Corynebacterium glutamicum* abtaucht, sei er an dieser Stelle auf einige Personen aufmerksam gemacht, die mich maßgeblich in dieser Doktorarbeit unterstützt haben.

Zunächst sei meinem Doktorvater Prof. Dr.-Ing. Ralf Takors gedankt, dessen Vorlesung „Bioverfahrenstechnik“ mich während meinem Verfahrenstechnikstudium auf die Biotechnologie aufmerksam gemacht und letztendlich dazu geführt hat, in diesem Fachbereich zu promovieren. Während meiner Zeit am Institut für Bioverfahrenstechnik, in dem der experimentelle Teil der Arbeit entstand, sowie in der folgenden Schreibphase fernab vom IBVT, stand er immer für Fragen und zur Diskussion bereit.

Ich möchte Prof. Dr. Bernhard Eikmanns danken, der während der Projketreffen von ’0.6Plus’ bereits wertvolles Feedback für meine Arbeit lieferte und nun als Mitberichter dieser Thesis fungiert. Prof. Dr. Bernhard Hauer sei für die Übernahme des Prüfungsvorsitzt gedankt. Dem Bundesministerium für Bildung und Forschung (BMBF) danke ich für die finanizielle Unterstützung des Projekts ’0.6Plus’ im Rahmen der e:Bio Initiative (Fördermittel 031A302A).

Meinen Projektpartnern Dr. Marcus Persicke und Dr. Tobias Busche am CebiTec Bielefeld sowie Dr. Katharina Nöh und Dr. Martin Cerff am FZ Jülich danke ich für die sehr gute Kooperation und Diskussion in Hinblick auf Genomsequenzierung, Transkriptom- und Fluxomuntersuchungen.

Herzlicher Dank gilt außerdem Prof. Dr. Bastian Blombach, der immer eine offene Tür für Coryne-spezifische Diskussionen, für Nachhilfe im mikrobiellen Metabolismus

und motiverenden Worte für alle anderen Wehwechen eines Doktoranden hatte.

Der guten Seele am IBVT, Frau Reu sage ich Danke für jegliche administrative Hilfestellung vor und nach meiner Doktorandenzeit und ihre schwäbischen Weisheiten.

Meinen damaligen Studentinnen Frederike Froriep, Julia Zieringer und Anna-Lena Mayer danke ich für ihren Fleiß und Einsatz im Rahmen ihrer Abschlussarbeiten und HiWi-Tätigkeiten, womit sie maßgeblich zu den Ergebnissen dieser Arbeit beigetragen haben. An dieser Stelle sei auch Julia Harm-Bekbenbetova für ihre Unterstützung im gesamten '0.6Plus' Projekt gedankt.

Meinen ehemaligen Kollegen Andre Feith und Dr. Attila Teleki möchte ich für die lehrreiche Einführung in die Metabolomuntersuchung mittels LC-MS danken, sowie ihrer wertvollen und tatkräftigen Unterstützung während des ^{13}C-Markierungsversuchs.

Alexander Dietrich, Salaheddin Laghrami, Mira Lenfers-Lücker, dem eisernen Kern des IBVT, danke ich für ihre Hilfe, Bereitschaft und Einsatz in technischen und analytischen Fragestellungen. Ein großes „Danke!“ geht an ein weiteres Urgestein des Instituts, Andreas Freund, der mit mir AuP betreut hat und mit unendlicher Geduld jede neue Idee bezüglich der Optimierung der kontinuierlichen Prozessführung getestet und umgesetzt hat - unter anderem mit Hilfe des großen Sai Baba und Untermalung toller Reiseberichte.

Bei meinen ehemaligen Mitdoktoranden (und teilweise wieder Kollegen) Joana, Michi, Alex, Max, Lisa und Maria möchte ich mich für ihr Wissen, ihre tolle Kameradschaft, ihre Sportivität und ihren Rückhalt bedanken - ihr habt meine Zeit am Institut und in Stuttgart maßgeblich geprägt!

Meinen Bürojungs Julian, Andy und Felix danke ich dafür, dass sie mir jede Bio- und Coryne-Frage beantwortet haben, immer für Motivation und Rat bereitgestanden sind und so für ein produktives und äußerst angenehmes Miteinander sorgten und auch nach der Zeit am IBVT immer noch sorgen - einmal Corynemafia immer La Famiglia!

Meinem Projektmitstreiter Thorsten gilt großer Dank für Theorien, Diskussionen und Ideen rund um Coryne und das Projekt '0.6Plus', nächtliche Einsätze während der ALE Studien, dem Batch-Marathon am Ende unserer Doktorandenzeit und zu guter Letzt für seine und Minas kulinarischen Künste.

Der größte Dank gilt meiner Familie und Freunden und ganz besonders meinen Eltern, Danie und Alexander, Andreas und Tobias. Eure ständige Unterstützung, euer Fachwissen, euer Verständnis, eure Ratschläge und eure motivierenden Worte haben den Rahmen gestellt, der diese Arbeit für mich möglich gemacht hat. Ich danke euch!

Contents

List of Figures

List of Tables

Nomenclature

1,3PG	1,3-Bisphosphoglycerate
2PG	2-phosphoglycerate
3PG	3-phosphoglycerate
a	Average gene expression
Ace	Acetat
AceCoA	Acetyl-Coenzym A
AKG	α-ketoglutarate; 2-oxoglutarate
Ala	L-alanine
ALE	Adaptive laboratory evolution
Arg	L-arginine
Asn	L-asparagine
ATCC	American Type Culture Collection
ATP	Adenosine triphosphate
AU	Arbitrary unit
BHI	Brain-heart-infusion
bn	Billion
C	Carbon
c	Concentration of a component ($\mathrm{g\,L^{-1}}$)
CCM	Central carbon metabolism
CDW	Cell dry weight (g)
CER	Carbon dioxide evolution rate ($\mathrm{mmol\,CO_2\,L^{-1}\,h^{-1}}$)
cf.	*confer*, 'compare'
Cit	Citrate
COG	Clusters of orthologous groups

Cys	L-cysteine
c_{CO_2}	CO_2 concentration in liquid phase ($\mathrm{mol\,L^{-1}}$)
c_s	Substrate concentration ($\mathrm{g\,L^{-1}}$)
c_x	Biomass concentration ($\mathrm{g\,L^{-1}}$)
D	Dilution rate, $D = F/V_R$ ($\mathrm{h^{-1}}$)
cDNA	Complementary DNA
DEG	Differentially expressed gene
DHAP	Dihydroxyacetonphosphate
DNA	Deoxyribonucleic acid
e.g.	*exempli gratia*, 'for example'
E4P	Erythrose 4-phosphate
EDS	Experimental design study
et al.	et alii, 'and other'
F	Feed flow rate
F6P	Fructose 6-phosphate
FACS	Fluorescence-activated cell sorting
FBA	Flux balances analysis
FbP	Fructose 1,6-bisphosphate
FC	Log fold-change, M-value
FCT	Fast-centrifugation-treatment
Fig.	Figure
Fum	Fumarate
FZJ	Forschungszentrum Jülich
G6P	Glucose 6-phosphate
GAM	Growth associated maintenance
GAP	Glycerinaldehyde 3-phosphate
Glc	Glucose
Gln	L-glutamine
Glu	L-glutamate
Glucn	Gluconate
Gly	Glycin
GRAS	Generally recognized as safe
GTP	Guanosine triphosphate
H_0	Null-hypothesis
HILIC	Hydrophilic interaction liquid chromatography
His	L-histidine
HPLC	High-pressure liquid chromatography
HWE	Hot-water-extraction

i.e.	*id est*, 'that is'
IBVT	Institut für Bioverfahrenstechnik
IDMS	Isotopic dilution mass spectrometry
Ile	L-isoleucine
IsoCit	Isocitrate
K_s	Saturation concentration of the substrate ($g\,L^{-1}$)
LC	Liquid chromatography
Leu	L-leucine
Lys	L-lysine
M	Log fold-change, FC-value
m	Mass of a component (g)
m_S	Maintenance parameter
CE	Chloroform-methanol extraction
Mal	Malate
Met	L-methionine
MFA	Metabolic flux analysis
MOPS	3-(N-morpholino)propanesulfonic acid
MQ	Cold-methanol quenching
MS	Mass spectronomy
MTHF	Methylenetetrahydrofolate
$\dot{n}$	Molar flow ($mol\,s^{-1}$)
n.d.	Not detected
NAD	Nicotinamide adenine dinucleotide
NADP	Nicotinamide adenine dinucleotide phosphate
NGAM	Non-growth associated maintenance
NMR	Nuclear magnetic response
OAA	Oxaloacetate
OD	Optical density
OTR	Oxygen transfer rate ($mol\,O_2\,L^{-1}\,h^{-1}$)
OUR	Oxygen uptake rate ($mmol\,O_2\,L^{-1}\,h^{-1}$)
p	Total pressure (bar)
pO_2	Dissolved oxygen saturation (%)
-P	...-phosphate
PCA	Protochatechuate
PCR	Polymerase chain reaction
PEP	Phosphoenolpyruvate
pH	Negative decadic logarithm of the proton concentration
Phe	L-phenylalanine

ppGpp	Guanosine pentaphosphate
PPP	Pentose phosphate pathway
Pro	L-proline
PTS	Phosphotransferase system
Pyr	Pyruvat
q_{CO_2}	Biomass specific carbon dioxide evolution rate ($\mathrm{g\,g^{-1}\,h^{-1}}$)
q_{O_2}	Biomass specific oxygen consumption rate ($\mathrm{g\,g^{-1}\,h^{-1}}$)
q_s	Biomass specific substrate consumption rate ($\mathrm{g\,g^{-1}\,h^{-1}}$)
RQ	Respiratory quotient
r	Pearson's correlation factor
R	Ideal gas constant = $8.314\,\mathrm{J\,mol^{-1}\,K^{-1}}$
mRNA	Messenger RNA
R5P	Ribose 5-phosphate
RNA	Ribonucleic acid
RNA-Seq	RNA-Sequencing
RPK	Reads per kilobase
rRNA	Ribosomal RNA
Ru5P	Ribulose 5-phosphate
S7P	Sedoheptulose 7-phosphate
SAM	S-Adenosyl methionine
SD	Standard deviation
Ser	L-serine
SNM	Stoichiometric network model
Suc	Succinate
SucCoA	Succinyl-CoA
T	Temperature (°C)
t	Time
t_d	Generation doubling time (h)
TC	Total carbon
TCA	Tricarboxylic acid cycle
TES	Trace element solution
Thr	L-threonine
TIC	Total inorganic carbon
TOC	Total organic carbon
TPM	Transcript per kilobase million
Trp	L-tryptophan
TY	Tryptone-yeast
Tyr	L-tyrosine

$\dot{V}_g$ ..... Volumetric gas flow ($L\,h^{-1}$)
V ..... Volume (mL, L)
V_R ..... Reaction volume (L)
Val ..... L-valin
(v/v) ..... Volume to volume proportion
WT ..... Wild type
(w/w) ..... Weight to weight proportion
X5P ..... Xylulose 5-phosphate
y ..... Molar exhaust gas fraction (–)
Y_{xs} ..... Yield coefficient of biomass per unit substrate consumed

Greek letters .....
Δ ..... Difference between two quantities
°C ..... Degree Celsius
μ ..... Specific growth rate (h^{-1})
μ_{max} ..... Maximum specific growth rate (h^{-1})
% ..... Percent

Indices .....
$\tilde{}$ ..... Indicates steady state conditions
0 ..... Point in time at a certain start, e.g. t=0 h
C ..... Carbon
exp ..... Experimental
G ..... Gaseous phase
Glc ..... Glucose
in ..... In-flowing
L ..... Liquid phase
max ..... Maximum
out ..... Out-flowing
R ..... Reaction
ref ..... Reference
$feed$ ..... Feeding conditions
s ..... Substrate
t ..... Certain point in time
theo ..... Theoretical
x ..... Biomass

Units .....

g ..... Gram
h ..... Hour
J ..... Joule
K ..... Kelvin
L ..... Liter
m ..... Meter
min ..... Minute
mol ..... Mol
s ..... Second
V ..... Volt

Zusammenfassung

Corynebacterium glutamicum ist aufgrund seiner vorteilhaften intrinsischen Eigenschaften einer der wichtigsten Produktionsstämme in biotechnologischen industriellen Prozessen. Allerdings kann seine vergleichsweise geringe maximale Wachstumsrate (μ) von $0.6\,\mathrm{h}^{-1}$ einen negativen Einfluss auf die Produktivität zugehöriger Bioprozesse haben. Daher war das Ziel dieser Thesis, potentielle Wachstumslimitationen des Stammes unter (pseudo-)stationären Bedingungen und in adaptiven Laborevolutionsexperimenten (ALE) zu identifizieren. Durch das Öffnen dieser Flaschenhälse könnte μ erhöht werden was schlussendlich die Position von *C. glutamicum* gegenüber konkurrierenden Produktionsstämmen stärkt.

Daher wurde das Wachstum von *C. glutamicum* unter metabolisch-pseudo stationären Bedingungen in substratunlimitierten Satzprozessen in Bioreaktoren analysiert. Das Hinzufügen verschiedener Wachstumssupplemente [Hirn-Herz-Boullion, eng.'brain-heart-infusion' (BHI): (1–37) $\mathrm{g\,L}^{-1}$, 18 essentieller Aminosäuren: jeweils $5\,\mathrm{mmol\,L}^{-1}$, $0.1\,\mathrm{mmol\,L}^{-1}$ Protokatechuat (PCA), $0.2\,\mathrm{mg\,L}^{-1}$ Thiamin] zu glukosehaltigem CGXII Minimalmedium erhöhte μ von $0.32\,\mathrm{h}^{-1}$ im Bereich (0.44–0.67) h^{-1}. Anschließend zeigten engergetische Betrachtungen, dass der ATP-Vorteil durch extrazellulär zugefütterte Aminosäuren gering war (4 ATP pro Gramm Biomasse), aber dass ATP-aufwendige Komponenten wie Fettsäuren und Nukleotide schnelles Wachstum von *C. glutamicum* bis zu einer maximalen Rate von $0.67\,\mathrm{h}^{-1}$ begünstigen. Die maximale Glukoseaufnahmerate ($q_{Glc} = 0.0277$ C-mol $\mathrm{g}^{-1}\,\mathrm{L}^{-1}\,\mathrm{h}^{-1}$) wurde durch die geringe Zugabemenge von $1\,\mathrm{g\,L}^{-1}$ BHI erreicht. Unabhängig vom Wachstumssupplement war die Gesamtkohlenstoffaufnahmerate immer strikt proportional zur Wachstumsrate, was zu einer konstanten Biomasse-Kohlenstoffausbeute von ungefähr 18 g Biomasse pro C-mol führte und die maximale Kohlenstoff- und Stickstoffverarbeitungskapazität des Stammes darstellt. In diesem Zusammenhang wurde die Aminosäureaufnahme mit dem kurierten und erweiterten stöchiometrischen

Netzwerkmodel *iMG481* weiter untersucht. Darauffolgende Flussbilanz- und Sensitivitätsanalysen beleuchteten so die experimentell bestimmten Aufnahmeraten der 18 supplementierten Aminosäuren. Die Zugabe von Aminosäuren mit ATP-intensiver Biosynthese hatte einen positiven Einfluss auf das zelluläre Wachstum, während Glutamin und Asparagin essentielle Rollen als Vorläuferbausteine für Aminosäuren des Transaminasenetzerks spielten. Eine zusätzliche Transkriptomanalyse der PCA-supplementierten Bedingung bestätigte die vorherrschende Meinung, dass PCA die intrazelluläre Eisenaufnahme begünstigt und/oder den Tricarbonsäure Zyklus (TCA) speist. Zusätzlich konnte in Hinblick auf Expression von Aufnahme und Assimilierung elementarer Nährstoffe eine potentielle regulatorische Funktion von PCA aufgedeckt werden. Die Transkriptomanalyse der $37\,\mathrm{g\,L^{-1}}$ BHI-supplementierten Bedingung, die zum ersten Mal für *C. glutamicum* durchgeführt wurde, wurde als Werkzeug eingesetzt um potentiell wachstumsfördernde Supplemente im Komplexmedium zu untersuchen. Die Analyse bestätigte die μ-steigernden Spezies, die in der vorherigen physiologischen Untersuchung charakterisiert wurden und deckte außerdem auf, dass die Anwesenheit von elementaren Stoffen wie Schwefel deren ATP-teure Assimilierung oder Transport überflüssig machte. Schlussendlich wurden differentiell exprimierte Gene (DEGs), die eine mögliche transkriptionelle Kontrolle über μ haben, aus den supplementierten Kultivierungen [(1–37) $\mathrm{g\,L^{-1}}$ BHI, $0.1\,\mathrm{mmol\,L^{-1}}$ PCA] identifiziert. Allerdings hat keines der identifizierten und re-engineerten Zielgene eine Wachstumsratensteigerung bewirkt.

Neben den Supplementierungsstudien wurden potentielle Wachstumslimitationen von *C. glutamicum* untersucht, als der Stamm in in PCA-haltigem CGXII Minimalmedium ($12\,\mathrm{g\,L^{-1}}$ Glukose) unter metabolisch stationären Bedingungen in kontinuierlichen Chemostaten bei verschiedenen μ kultiviert wurde. Kinetische Parameter wurden für $\mu = 0.2$, 0.3 und $0.4\,\mathrm{h^{-1}}$ als Basis für Metabolom- und Transkriptomstudien bestimmt. In diesem Zusammenhang wurden erste Schritte unternommen, um intrazelluläre Metabolitpools des Stamms absolut zu quantifizieren, wobei die Schnelle-Zentrifugations-Methode (engl. fast-centrifugation-treatment) gekoppelt mit der Heißwasserextraktion (engl. hot-water-extraction) die Kombination der Wahl für die meisten analysierten Metaboliten darstellte. Gleichzeitig wurde jedoch gezeigt, dass für die zuverlässige Quantifizierung von intrazellulären Metaboliten mehrere Extraktionsmethoden angewandt werden müssen. Die Kombination von Metabolom- und Transkriptomdaten dieser Arbeit mit korrespondierenden Proteomdaten aus der Literatur ließen erkennen, dass unter den getesteten glukoselimitierten Bedingungen die Glukoseaufnahme über das Phosphotransferasesystem (PTS) unter transkriptioneller Kontrolle, und die Glykolyse und der Pentosephosphatweg (PPW) unter metabolischer Kontrolle waren, während für den TCA Zyklus kein eindeutiges Kontrollschema festgestellt werden konnte. Darüber hinaus enthüllten die Metabolom- und Transkriptomdaten einen möglichen Wachstumsflaschenhals aufgrund eines unvorteilhaften NADH/$\mathrm{NAD^+}$-Verhältnisses, das wahrscheinlich in einer Nicht-Proportionalität zwischen μ und der Versorgung

mit anabolischen Bausteinen resultierte. Ein zweiter möglicher Flaschenhals könnte sich im Methionin S-Adenosylmethionin (SAM)-Zyklus befinden, was zu einer unzureichenden Bereitstellung bei steigendem μ des aktivierten C_1-Körpers 5,10-Methylentetrahydrofolat und/oder SAM führte. Außerdem zeigte der Vergleich der transkriptionellen Antwort mit entsprechenden Literaturdaten aus transienten Satzverfahr-Experimenten, dass die Verfügbarkeit von extrazellulärer Glukose, und damit der Prozessmodus der Kultivierung, der Schalter zwischen metabolischer und transkriptioneller Kontrolle der Glykolyse in diesem Mikroorganismus sein könnte. Schlussendlich wurde ein stationärer ^{13}C-Markierungsversuch in Chemostatfahrweise durchgeführt, um das Fluxom in zentralen Kohlenstoffmetabolismus (ZKM) von *C. glutamicum* bei $\mu = 0.4\,h^{-1}$ zu bestimmen. Der etablierte experimentelle Versuchsaufbau hat zudem gezeigt, dass er für zukünftige nicht-stationäre Experimente geeignet ist, da dynamische ^{13}C-Isotopologprofile nach dem Wechsel zu ^{13}C für jedes der analysierten Metaboliten aufgenommen werden konnten. Abgeleitet von diesen Markierungsmustern wiesen Unterbrechungen in der Markierungsanreicherung nahezu aller ZKM Metaboliten daraufhin, dass unmarkierter Kohlenstoff von Puffer- oder Speicherstoffen in die Glykolyse geschleust wurden. Außerdem waren die langsame Markierung von Metaboliten aus der oberen Glykolyse, die im Gegensatz dazu schnelle Markierung von Metaboliten aus der unteren Glykolyse und des PPWs, sowie die Anwesenheit ^{13}C-markierten Glukonats Indikatoren für einen potentiellen zweiten Glukoseaufnahmeweg neben dem PTS, der vom Stamm unter glukoselimiterten Bedingungen verwendet wird. Abgeleitet von Wachstumskinetiken und stationären Markierungsmustern zeigten die intrazellulären Metaboliteflüsse, dass 54 % der aufgenommenen Glukose in den PPW geschleust wurden, während 45 % und 66 % jeweils Richtung Glykolyse und TCA Zyklus geleitet wurden. Der Vergleich mit Flussverteilungen bei $\mu < 0.4\,h^{-1}$, die von ^{13}C-Markierungsversuchen aus der Literatur abgeleitet wurden, und korrespondierender berechneter theoretischen Mengen an NADPH, zeigte ein Überschuss dieses Reduktionsequivalents bei $\mu \geq 0.15\,h^{-1}$. Diese scheinbar wachstumsabhängige Überproduktion von NADPH wurde zum ersten Mal beschrieben.

ALE Experimente wurden in einem kontinuierlichen Bioreaktor durchge-führt, um *C. glutamicum* durch natürliche Selektionsprozesse zu höheren μ hin zu evolvieren. Der Stamm wurde dabei drei Selektionsdrücken ausgesetzt, indem die Verdünnungsrate nahe μ_{max} eingestellt wurde, der Hefeexktraktanteil im CGXII-basierten Wachstumsmedium graduell erniedrigt wurde und die Standardkomponente PCA weggelassen wurde. Innerhalb von 2.5 Monaten wurden fünf Prozesse in Folge durchgeführt, wobei 1700 Generationen von *C. glutamicum* erzeugt wurden. Der schlussendlich abgeleitete und evolvierte Stamm EVO5 zeigte ein μ von $0.54\,h^{-1}$ in PCA-freiem CGXII Minimalmedium, was eine Erhöhung von 58 % gegenüber dem Wildtyp darstellte. Die Sequenzierung des Genoms von EVO5 identifizierte zehn Mutationen, unteranderem in *ramA*, das für den globalen Kohlenstoffregulator des Stammes kodiert, in *dtxR*, das für dessen

Haupteisenregulator kodiert, und in *rpoA*, das für die alpha-Untereinheit seiner DNA-gerichteten Polymerase kodiert. Das Re-Engineering der *ramA*-Mutation und die folgende Charakterisierung des resultierenden Stamms Cg ReRamA in Bioreaktor Satzkultivierungen offenbarte eine Wachstumssteigerung von 8 % gegenüber dem WT, aber eine nicht-proportionale Zunahme der Glukoseaufnahmerate um 25 %. Diese konnte auf die Bildung von Pyruvat als metabolisches Überflussprodukt zurückgeführt werden, was die Folge eines hohen glykolytischen aber nicht-angepasstem niedrigeren TCA-Flusses war. Dies bestätigte wiederum den identifizierten Wachstumsflaschenhals der metabolisch-stationären Untersuchung.

Summary

Corynebacterium glutamicum is one of the most important producer strains in industrial biotechnological processes, based on its advantageous intrinsic attributes. However, its comparably low maximum growth rate (μ) of $0.6\,h^{-1}$ may negatively influence the productivity of related bioprocesses. Hence, this thesis focused on identifying potential growth limitations of the strain under (pseudo)-stationary conditions and in adaptive laboratory evolution (ALE) experiments. Upon opening these bottlenecks μ might be boosted, ultimately strengthening the position of *C. glutamicum* over competing production hosts.

Therefore, growth of *C. glutamicum* was analyzed under metabolic pseudo-stationary conditions installed in substrate-unlimited bioreactor batch cultivations. Addition of varying growth supplements [brain-heart-infusion (BHI): $(1–37)\,g\,L^{-1}$, 18 essential amino acids: $5\,mmol\,L^{-1}$, respectively, $0.1\,mmol\,L^{-1}$ protocatechuate (PCA), $0.2\,mg\,L^{-1}$ thiamin] to glucose-containing CGXII minimal medium individually enhanced μ from $0.32\,h^{-1}$ to $\mu = (0.44–0.67)\,h^{-1}$. Subsequent energetic analysis revealed that the ATP-benefit from extracellularly fed amino acids was only minor (4 ATP g_{CDW}^{-1}) but indicated that ATP-costly compounds like fatty acids and nucleotides in BHI facilitate fast growth of *C. glutamicum* up to its apparent maximum of $0.67\,h^{-1}$. The maximum glucose consumption rate ($q_{Glc} = 0.0277$ C-mol $L^{-1}\,g^{-1}\,h^{-1}$) was obtained by adding mere amounts of $1\,g\,L^{-1}$ BHI. Irrespective of the growth supplement, total carbon consumption rates were always strictly proportional with μ resulting in a constant biomass carbon yield of about $18\,g_{CDW}$ C-mol^{-1} which represents the strain's maximum capacity of processing carbon and nitrogen. In this context, amino acid consumption was further investigated with the curated and expanded stoichiometric network model *iMG481*. Subsequent flux balance and sensitivity analyses elucidated the experimentally determined uptake rates of the 18 supplemented amino acids. Adding amino acids with ATP-intensive

biosynthesis had a positive effect on cellular growth, whilst Gln and Asn played crucial roles as precursors for amino acids of the transaminase network. Additional transcriptome analysis for the PCA-supplemented condition confirmed the dominating opinion that PCA enhances the intracellular iron availability and/or is used to fuel the tricarboxylic acid (TCA) cycle. Moreover, a potential regulatory function of PCA was revealed based on the corresponding expression regarding uptake and assimilation of elemental nutrients. Transcriptome analysis of the $37\,g\,L^{-1}$ BHI-supplemented condition, performed for the first time with *C. glutamicum*, was employed as tool to investigate potential μ-increasing supplements in this complex medium. The analysis confirmed the characterized growth enhancing species from the previous physiological investigation and further revealed the presence of elemental compounds like sulfur making ATP-costly assimilation or transport unnecessary. Finally, μ-dependent differentially expressed genes (DEGs) detected in supplemented cultivations [(1–37) $g\,L^{-1}$ BHI, $0.1\,mmol\,L^{-1}$ PCA] with potential transcriptional control over μ were singled out. However, none of the identified and re-engineered target genes induced a growth rate increase.

Besides the supplement studies, potential growth limitations of *C. glutamicum* cultivated under metabolic stationary conditions in PCA-containing CGXII minimal medium ($12\,g\,L^{-1}$ glucose) were investigated in continuous chemostat cultivations at different μ. Kinetic parameters were determined for $\mu = 0.2\,h^{-1}$, $0.3\,h^{-1}$ and $0.4\,h^{-1}$ as basis for metabolome and transcriptome studies. In this context, first steps towards absolute quantification of the strain's intracellular metabolite pools were made revealing the fast-centrifugation-treatment coupled with hot-water-extraction as combination of choice for the majority of analyzed metabolites. However, it was simultaneously shown that several extraction techniques have to be employed for reliable absolute quantification of intracellular metabolites. Combining metabolome and transcriptome data from this work with corresponding proteome values from literature revealed that under the tested glucose-limited conditions, glucose uptake via phosphotransferase system (PTS) was under transcriptional control, glycolysis and pentose phosphate pathway (PPP) were under metabolic control, and no distinct control scheme could be assessed for the TCA cycle. Moreover, metabolome and transcriptome data revealed a potential growth bottleneck in glycolysis due to an unfortunate $NADH/NAD^+$-ratio possibly resulting in a non-proportionality between μ and anabolic precursor supply for biomass formation. A second potential bottleneck was located in the methionine S-Adenosyl methionine (SAM)-cycle leading to insufficient supplies of the activated C_1-compound 5,10-methylenetetrahydrofolate and/or SAM with rising μ. Besides, comparison of the transcriptional response with corresponding data of transient batch experiments from literature revealed that the availability of extracellular glucose, and thereby the process mode of the cultivation, might be the switch between metabolic and transcriptional control of glycolysis in this microogranism. Finally, a stationary ^{13}C-labeling experiment in chemostat mode was performed to determine the central carbon metabolism (CCM)-fluxome of

C. glutamicum at $\mu = 0.4\,h^{-1}$. The established experimental setup also proved to be applicable for future non-stationary experiments since dynamic ^{13}C-isotopologue profiles were recorded for each of the analyzed metabolites after switching to ^{13}C feed. Derived from these labeling patterns, disruptions in the labeling enrichment of nearly all CCM metabolites hinted at channeling of unlabeled carbon from buffer or storage compounds into glycolysis. Also, slow labeling in metabolites of upper glycolysis but fast labeling of lower glycolysis and PPP metabolites as well as the presence of ^{13}C-labeled gluconate were an indicator for a potential second route of glucose uptake, employed by the strain under glucose-limited conditions in addition to PTS. Intracellular metabolite fluxes derived from growth kinetics and stationary labeling patterns revealed that 54 % of consumed glucose was channeled towards PPP, whilst 45 % and 66 % were channeled towards glycolysis and TCA cycle, respectively. Comparison to ^{13}C-derived flux distributions from literature for $\mu < 0.4\,h^{-1}$ and correspondingly calculated amounts of theoretically produced NADPH revealed a surplus of this reduction equivalent for $\mu \geq 0.15\,h^{-1}$. This apparent growth-related overproduction of NADPH was described for the first time.

ALE experiments were performed in a continuous bioreactor to evolve *C. glutamicum* towards higher μ by means of natural selection. Thus, the strain was exposed to three selection pressures by installing dilution rates near μ_{max}, by gradually decreasing the yeast-extract portion in the CGXII-based growth medium over the processes, and by omitting the standard CGXII component PCA. Five consecutive processes were conducted within 2.5 months generating 1,700 generations of *C. glutamicum*. Finally derived and evolved strain EVO5 exhibited $\mu = 0.54\,h^{-1}$ in PCA-free CGXII minimal medium which was an increase of 58 % over the parental wild type (WT). Whole genome sequencing revealed ten mutations in the genome of EVO5, amongst them *ramA*, encoding the strain's global carbon regulator, *dtxR* encoding its major iron regulator, and *rpoA* coding for the alpha subunit of its DNA-directed polyermase. Re-engineering of the *ramA* mutation and subsequent characterization of resulting strain Cg ReRamA in bioreactor batch cultivations revealed a growth increase of 8 % over the WT, but a non-proportional increase by 25 % of the glucose consumption rate. This could be traced back to formation of pyruvate as metabolic overflow product due to high glycolysis, but unbalanced lower TCA cycle fluxes, ultimately confirming the μ-bottleneck identified in the investigation under metabolic stationary conditions.

CHAPTER 1

Motivation and objectives

1.1. *Corynebacterium glutamicum* - an industrial workhorse with one fundamental drawback

The white biotechnology industry sector covers the production of bulk and fine chemicals, foodstuffs, and biofuels. The market volume of corresponding goods steadily increases since 2010 (91.9 bn €) and is expected to reach six-fold higher sales by 2020 (Festel et al., 2012). In biotechnological processes, a broad spectrum of microorganisms, e.g. bacteria, fungi, yeasts, enzymes, and derived cell parts are available as production platform. Amongst the microbial producers, *Corynebacterium glutamicum* is one of the most important industrial workhorses. It is a Gram-positive, non-sporulating, facultative anaerobic prokaryote (Liebl, 2006; Nishimura et al., 2007) that is able to grow anaerobically in the presence of nitrate (Nishimura et al., 2007), but only grows insignificantly without this terminal electron acceptor under the same conditions (Michel et al., 2015). *C. glutamicum* is generally recognized as safe organism (GRAS) making it most suitable for applications in health, cosmetic, food, and feed industries (Takors et al., 2007; Vertès et al., 2013). It was discovered that the *C. glutamicum* wild type (WT) strain naturally secrets the amino acid glutamate under biotin-insufficient conditions (Kinoshita et al., 1957), whereby the organism became the main source for producing the flavor enhancer. Subsequently, the WT was subjected to random mutagenesis and

selection processes that resulted in mutant strains with enhanced secretion of other amino acids such as L-lysine, L-arginine, ornithine, and L-threonine (Becker et al., 2010; Udaka, 2008). The ability of *C. glutamicum* to produce a variety of amino acids ultimately led to the establishment of industrial amino acid fermentation in Japan replacing the traditional approach of chemically decomposing proteins to obtain amino acids (Kinoshita, 2005). Until now, the production of L-glutamate, L-lysine, and L-valine remains the major application of *C. glutamicum* (Hermann, 2003).

The simultaneous unraveling of the genome of *C. glutamicum* WT ATCC 13032 by Ikeda & Nakagawa (2003) and Kalinowski et al. (2003) and the following construction of genome scale metabolic network models (Kjeldsen & Nielsen, 2009; Shinfuku et al., 2009) enabled the application of metabolic engineering techniques. Thus, the strain's genome was targetedly modified instead of randomly whereby the production of organic acids like lactate, succinate, and pyruvate (Dominguez et al., 1993; Okino et al., 2005; Wendisch et al., 2006b; Wieschalka et al., 2012) could be further enhanced (Nishimura et al., 2007). In addition, heterologous *C. glutamicum* producers were constructed by integrating artificial reactions and pathways into the parental genome to produce new or non-natural compounds like diamins (Kind et al., 2010; Wendisch et al., 2018) and heterologous proteins (Freudl, 2017; Scheele et al., 2013), or to enable mutant growth on renewable feedstocks relevant for industrial production (Becker & Wittmann, 2012). Furthermore, the organism advances in the popular field of bio-based production of chemicals, materials, and fuels such as isobutanol (Blombach et al., 2011) and ethanol (Inui et al., 2004), and is able to grown on side streams from bio-refineries (Lange et al., 2017). *C. glutamicum* naturally grows on a variety of sugars with glucose, fructose, and sucrose the most important for amino acid production (Lindner et al., 2011), but also readily consumes organic acids such as acetate, pyruvate and lactate (Ikeda, 2012). In addition to its immense product and substrate scope, the organism is a popular choice for industrial processes based on its advantageous intrinsic attributes. For instance, *C. glutamicum* cannot be infected or lyzed by bacteriophages in contrast to *Escherichia coli* and is regarded as a moderately alkali-tolerant strain [pH 7-8.5, *E. coli*: pH 6-7; Follmann et al. (2009)]. Additionally, several scale-down studies showed that the organism can endure harsh production conditions typically encountered in large-scale bioreactors (Buchholz et al., 2014a; Käß et al., 2014a,b). A multitude of further attributes distinguishing *C. glutamicum* as an ideal industrial producer can be found in Vertès et al. (2013).

Despite *C. glutamicum*'s advantageous characteristics, the organism has one general drawback compared to competing production hosts: its biomass specific maximum

growth rate is significantly smaller than that of, e.g., *E. coli* or *Bacillus* species. Under standard batch process conditions using minimal medium with glucose as carbon source, exponential growth rates (μ, in h^{-1}) of $0.4\,h^{-1}$ were observed. Only under highly diluted conditions, that are non-typical for production processes, maximum growth rates of $0.6\,h^{-1}$ were determined (Bäumchen et al., 2007; Grünberger et al., 2013; Unthan et al., 2013). In general, the production of a target compound is either growth-coupled or growth-decoupled. An example for the former are primary metabolites or recombinant proteins (Feist et al., 2010; San et al., 1994) where a high growth rate consequentially leads to a high cell specific productivity. As a result, low growth rates decrease the overall process performance which makes *C. glutamicum* a less attractive production host, e.g. for production of recombinant proteins, than *E. coli* (Gopal & Kumar, 2013). Processes decoupled from growth, such as production of whole cells or cell parts (e.g. enzymes), naturally benefit from a high μ as well. In this case, the space time yield of the process is positively influenced due to a shorter initial batch phase facilitated by a high intrinsic exponential growth rate. Hence, the target biomass concentration required to start the subsequent production phase (e.g. in fed-batch mode) is reached faster. In either scenario, the economic performance of a bioprocess benefits if the employed producer strain features a high intrinsic growth rate. Thus, it is not surprising that other microorganisms like the fast growing *E. coli* with μ_{max} of up to $1.73\,h^{-1}$ (Cox, 2004) are preferred over *C. glutamicum* when choosing a suitable industrial production host for a (new) bioprocess. In this context, the recently characterized strain *Vibrio natriegens* revealing μ_{max} of $4.43\,h^{-1}$ in complex medium and high substrate consumption rates under (an)aerobic conditions (Hoffart et al., 2017) can be considered as serious future competitor for *C. glutamicum*.

1.2. *C. glutamicum* growth related studies

Prior to the start of project '0.6plus' that focused on identifying *C. glutamicum*'s growth limitations (cf. section 1.4), already several *C. glutamicum* studies addressed growth-related topics. For instance, batch cultivations were conducted to assess the growth phenotype of *C. glutamicum* WT in mineral media, e.g. CGXII (Keilhauer et al., 1993; Kind et al., 2010) or MM (Liebl et al., 1989) featuring different iron siderophores. Moreover, WT growth under standard conditions (mineral medium and glucose as sole carbon source) served as reference to study different growth environments typically

encountered during production, e.g. varying carbon sources (Cocaign et al., 1993; Frunzke et al., 2008; Krause et al., 2010; Netzer et al., 2004; Wendisch et al., 2000), changing dissolved O_2- (Käß et al., 2014a,b) and CO_2-levels in the fermentation broth (Blombach et al., 2013; Buchholz et al., 2014a), or to generally compare the WT phenotype with that of genome-altered mutant strains. Deduced from these investigations, average growth rates of the WT ATCC 13032 observed in minimal media range around $0.4\,h^{-1}$, whilst another WT (ATCC 17965) revealed a growth rate of up to $0.58\,h^{-1}$ in the exponential growth phase (Cocaign-Bousquet et al., 1996; Gourdon et al., 2003).

The growth phenotype of *C. glutamicum* was also studied in continuous bioreactors. In chemostat mode, for instance, a broad range of growth rates can be stablely installed with the same growth medium to study the physiology of cells. Cocaign-Bousquet et al. (1996) used this process type to install growth rates between $(0.1–0.55)\,h^{-1}$ to examine the orgranism's growth kinetics and determine corresponding glucose consumption phenotypes. Findings on the latter confirmed that a secondary transport system for glucose next to the phosphotranferase system (PTS) is active accounting for up to 15 % of the global glucose transport in *C. glutamicum* ATCC 17965 at high growth rates and glucose excess. This implied (i) an evolutionary advantage over strains only possessing one uptake system and (ii) that an additional carbon flux is channeled into the pentose pathway which enables a more efficient carbon substrate transformation into biomass (Cocaign-Bousquet et al., 1996). They further concluded that at high μ, glucose transport becomes the limiting factor for growth. A continuous bioreactor was also used in the studies of Zhao & Lin (2002) to examine growth dependent flux distribution and partitioning in the central metabolism of *C. glutamicum* lysine-producer ATCC 21253. At high growth rates, additional carbon was channeled through the tricarboxylic acid cycle to enhance amino acid production for anabolic reactions. Silberbach et al. (2005) employed chemostats to investigate the response of *C. glutamicum* ATCC 13032 to ammonium limitation at two different growth rates. Transcriptome and proteome analysis were performed and in addition to gaining insights into nitrogen metabolism, growth rate dependent expression of ribosomal proteins and F_0F_1 subunits of ATP-synthase was determined (Silberbach et al., 2005). Similar to the batch studies introduced above, continuous cultivations were also performed to study specific phenotypes of *C. glutamicum* under large-scale production conditions. For instance, Bäumchen et al. (2007) applied elevated levels of dissolved carbon dioxide in highly diluted turbidostat processes and measured the corresponding maximum applicable growth rate of WT ATCC 13032. Under reference conditions (no additional CO_2 was channeled into the bioreactor) and

slightly enhanced partial CO_2 pressures of up to 0.14 bar, a maximum growth rate of $0.58\,h^{-1}$ was observed. Until this time, that was the highest growth rate of WT ATCC 13032 measured in minimal medium.

Apart from these classical bioreactor investigations, another type of continuous cultivation system was employed in the investigation of Grünberger et al. (2013). The authors studied the growth behavior of *C. glutamicum* ATCC 13032 on single cell level in microfluidic devices allowing organisms to grow on a single focal plane in continuous mode (Grünberger et al., 2014). With this device, the maximum achievable specific growth rate in minimal growth medium CGXII was determined applying different biomass detection techniques, i.e. optical density (OD), cell volume via coulter counter, and cell number via fluorescence-activated cell sorting (FACS). They found 1.5 times higher μ_{max} in the microfluidic device ($\mu \approx 0.6\,h^{-1}$) compared to growth rates determined in batch cultivations ($\mu \approx 0.4\,h^{-1}$) conducted in microtiter plates, shaking flasks, or lab-scale batch bioreactors using the same growth medium. Ultimately, they identified that the highly diluted environment in the microfluidic device [comparable to those installed by Bäumchen et al. (2007)] was the cause for the μ-increase and concluded that the constant dilution by fresh medium removes by-products such as acetate that impairs growth (Grünberger et al., 2013). Based on these results, Unthan et al. (2013) performed batch cultivations in a bioreactor with low starting biomass concentrations of OD $\approx$ 0.005 (approx. $1.5 \cdot 10^{-3}$ $g_{CDW}L^{-1}$) to simulate the highly diluted conditions in the microscale bioreactor. This experimental setup lead to a bi-phasic growth phenotype and the strain revealed $\mu = 0.61\,h^{-1}$ in the first and $\mu = 0.46\,h^{-1}$ in the second growth phase. The maximum growth rate observed in phase one confirmed Grünberger et al. (2013)'s assumption that highly diluted conditions are advantageous for the strain. Besides, Unthan et al. (2013) used quantitative transcriptomics, metabolomics, and integrative *in silico* analysis to further analyze this first growth phase, revealing that protocatechuate (PCA) is a hidden co-substrate for accelerated growth within the minimal medium CGXII. The reason for PCA's growth boosting abilities could not be answered yet. It is suggested that the compound facilitates iron acquisition (Liebl et al., 1989) and/or fuels *C. glutamicum*'s tricarboxylic acid (TCA) cycle (Shen et al., 2012; Unthan et al., 2013).

Towards the end of this project in July 2018, two studies were published investigating possible growth deficits of *C. glutamicum* by employing yet another approach. Pfeifer et al. (2017) and Wang et al. (2018b) respectively performed adaptive laboratory evolution (ALE, cf. section 2.4) experiments to mimick natural selection processes and thereby increase *C. glutamicum*'s fitness, i.e. growth rate, in minimal growth medium. Indeed,

both working groups were able to enhance *C. glutamicum*'s intrinsic μ in minimal growth medium by 26 % and 42 %, respectively, compared to WT growth. Since named investigations are similar to one working package of this thesis (cf. section 1.5), detailed information and results of both studies are accordingly provided in section 4.8.

1.3. Growth studies of other production hosts

Apart from the presented *C. glutamicum* growth studies, potential growth limitations of other industrial producer strains were examined more thoroughly by employing different techniques with the ultimate aim to increase the growth performance. As starting point, Cox (2004) conducted chemostat experiments with *E. coli*, *Mycobacterium tuberculosis*, and *Streptomyces coelicolor* species and derived the following common attributes of an ultra-fast grower from the individual results: (a) highly efficient mechanisms for the uptake and metabolism of nutrient sources for carbon and energy; (b) ability to become polyploid and thereby increase the average number of rRNA operons per cell; (c) capacities for rapid rRNA synthesis; (d) capacities for rapid protein synthesis. These attributes could be confirmed in subsequent investigations, e.g. by studies of Potrykus et al. (2011) with *E. coli*. Besides, they revealed that the alarmone ppGpp, functioning as global regulator in response to nutritional stress and limited fatty acid synthesis, is the major determinant of growth rate control in *Enterobacteriaceae*. In more detail, RNA/DNA- and RNA/protein-ratios declined with increased ppGpp basal levels that manifested due to low growth rates. Attributes (c) and (d) were also identified as relevant for the eukaryotic producer *Saccharomyces cerevisiae*. Pir et al. (2012) identified translation and transcription as bottlenecks for fast growth when cultivating the strain in chemostat processes with exceeding nutrient supply. Furthermore, they observed a positive influence on growth of *S. cerevisiae* by reducing the levels of either proteins negatively regulating growth processes or that of toxic cytosolic monomers.

A more descriptive investigation was conducted by Ishii et al. (2007) examining the response of *E. coli* to genetic and environmental perturbations in continuous cultivations by means of OMIC tools (cf. section 2.3), i.e. metabolomics, transcriptomics, and proteomics. The authors found that the *E. coli* WT actively regulates the expression of global genes and enzyme levels to meet rising metabolic demands at enhanced growth rates. Simultaneously, they observed stable metabolite pool levels as consequence of said growth-dependent protein expression. Other research made use of another systems

biology tool (cf. section 2.3) flux balance analysis (FBA) to predict the theoretical maximum growth rate of *E. coli* (Ibarra et al., 2002). Since predictions of said *in silico* models are often not consistent with experimental data, Ibarra et al. (2002) suggested that this might be due to laboratory strains not having completed adaptive evolution under the examined conditions yet. Indeed, the strain could optimize its biological functions in subsequent ALE studies and met the growth performance previously predicted by FBA simulations. Later, Teusink et al. (2009) confirmed this approach and the results for the strain *Lactobacillus plantarum*.

Apart from studying growth phenotypes *in vivo* or *in silico*, ALE experiments were also conducted to select for mutant strains with increased growth rates. One of the best known examples is the long-term study of the Lenski group (Lenski et al., 1991) that cultivated *E. coli* WT in glucose-supplemented minimal medium to identify evolutionary processes altering the organism's genome. After about 20,000 generations, the evolved strain revealed a 1.85-fold increased fitness over the parental strain due to manifestation of beneficial mutations. From there on, however, the occurrence of advantageous genome alterations declined (Barrick et al., 2009). Apart from this study, only a few other investigations aimed at evolving *E. coli* (LaCroix et al., 2015), *Salmonella enterica* (Knöppel et al., 2018), or *Pichia pastoris* (Moser et al., 2017) in ALE cultivations featuring industrial-relevant minimal medium and a standard carbon source like glucose.

1.4. Framework of project '0.6Plus'

Motivated by existing fundamental *C. glutamicum* growth studies and investigations having successfully increased growth rates of other industrial producer strains, project '*0.6Plus: Improving Fundamental Properties of* C. glutamicum *to Expand its Scope for Industrial Application*' was established in scope of the e:Bio-initiative of the German Federal Ministry for Education and Research (Bundesministerium für Bildung und Forschung, BMBF). The overarching aim of '0.6Plus' was to investigate which attributes of *C. glutamicum* WT ATCC 13032 limit its intrinsic growth rate and how these bottlenecks could be resolved. Since an increase of μ can only be achieved if a nutrient source, e.g. the carbon donor glucose, is consumed proportionally fast to provide precursors for catabolism and anabolism, the biomass specific glucose consumption rate was of equal interest for this project. In this sense, nine German *C. glutamicum*-expert groups contributed to the project by focusing on different aspects of *C. glutamicum*, e.g. carbon uptake, cell division,

ribosome numbers, intracellular carbon fluxes. Thereby, two common goals should be reached: (i) decipher which (intracellular) mechanisms control and/or limit growth to the supposed maximum of $\mu = 0.6\,h^{-1}$, and based on this knowledge, (ii) attempt to enhance μ to make *C. glutamicum* even more attractive for industrial applications.

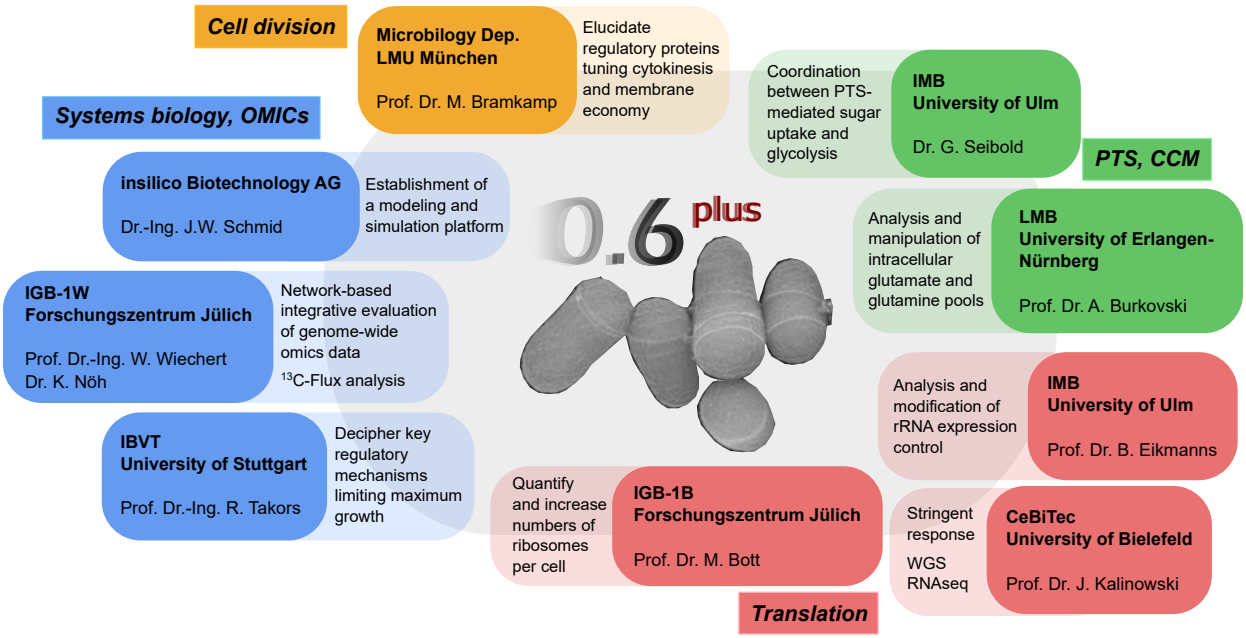

Figure 1.1.: Project partners contributing to project '0.6Plus' and their distinctive topics. Snapshot of *C. glutamicum* was adapted from REM figure of Wittmann & Becker (2007).

A short overview of each of the nine specific working areas and corresponding working packages is illustrated in figure 1.1. Besides the single topics, several collaborations between project partners were established whenever topics overlapped or specific expertise was needed. The Institute of Biochemical Engineering (Institut für Bioverfahrenstechnik, IBVT, University of Stuttgart) contributed with three topics to '0.6Plus'. Thorsten Haas and I worked on sub-projects one and two, respectively, focusing on deciphering growth limitations from a systems biology point of view. Systems biology approaches target the metabolome, transcriptome, proteome, and fluxome level of a cell which are in short referred to as OMIC-layers (cf. section 2.3). In this context, Thorsten Haas conducted transcriptome analysis under transient growth environments (batch cultivations) in sub-project one, whilst my work focused on metabolic (pseudo-)steady state investigations installed in batch and continuous bioprocesses. Within this sub-project, I collaborated with my colleague Thorsten Haas, the CeBiTec (working group

of Prof. Dr. Jörn Kalinowski, University of Bielefeld), and the modeling group of Dr. Katharina Nöh [working group of Prof. Dr.-Ing. Wolfgang Wiechert, IBG-1 Forschungszentrum Jülich (FZJ)]. In the third sub-project, Thorsten Haas and I together conducted ALE experiments to select for evolved *C. glutamicum* mutants with superior growth performance over the parental WT. Consequently, this thesis covers three topics that are individually defined by specific objectives presented in the next subsection.

1.5. Objectives of this thesis

The first part of this thesis focused on investigating growth phenotypes at pseudo metabolic steady states, namely substrate unlimited growth conditions. Therefore, bioreactor batch cultivations were conducted with different growth media (minimal, complex, 'synthetic complex' media) to install varying environments in terms of the nutrient spectrum. Apart from examining corresponding growth kinetics, a metabolic network model was employed and transcriptome analysis were performed. In detail, the single working packages comprised:

- Determine the strain's physiological response to varying media supplementation
- Curate an existing stoichiometric network model of *C. glutamicum* with regard to amino acid uptake and biosynthesis
- Determine amino acid consumption of the *in vivo* and *in silico* cell
- Determine the (growth rate dependent) transcriptional response to different media supplementation
- Characterize growth phenotypes of correspondingly modified *C. glutamicum* mutant strains

With regard to the transcriptome analysis, I collaborated with Dr. Tobias Busche from the CeBiTec who performed the transcriptome measurements. *C. glutamicum* mutant strains were kindly constructed by my colleague Felix Müller. Parts of this first topic were published in the contribution *'Physiological Response of* Corynebacterium glutamicum *to Increasingly Nutrient-Rich Growth Conditions'* (Graf et al., 2018) in the journal 'Frontiers in Microbiology' section 'Systems Microbiology' and is attached in

the appendix. Accordingly, the main results were summarized in this thesis and were expanded by the results and discussion of the transcriptome studies.

In the second part of this dissertation, 'real' stationary growth conditions were installed in a continuous bioreactor. The installed dilution rate in a chemostat process dictates the strain's growth rate by limiting the substrate supply accordingly. Thus, the cellular phenoytpe of *C. glutamicum* was preliminary assessed at different growth rates. Additionally, the metabolic and transcriptional response was analyzed as well as the carbon flux through the cell's central metabolism. Therefore, the following working packages were addressed to identify potential growth limitations of *C. glutamicum* under metabolic stationary conditions:

- Analyze the physiology of *C. glutamicum* in metabolic steady states
- Establish *C. glutamicum*-specific metabolome sampling and extraction techniques
- Evaluate and analyze intracellular metabolic pool sizes of central carbon metabolism metabolites and amino acids at different growth rates
- Analyze the transcriptional response of *C. glutamicum* to metabolic steady state growth and identify growth rate-related gene expressions
- Establish an experimental setup for non-stationary ^{13}C-labeling experiments
- Conduct a (non-)stationary ^{13}C-labeling experiment at $\mu = 0.4\,\mathrm{h}^{-1}$
- Compare the carbon flux distribution at $\mu = 0.4\,\mathrm{h}^{-1}$ to flux patterns determined at other growth rates

LC-MS analytics for metabolome analysis was performed in collaboration with my colleagues Dr. Attila Teleki and André Feith. In this context, data of this thesis was published in the contribution *'HILIC-Enabled ^{13}C Metabolomics Strategies: Comparing Quantitative Precision and Spectral Accuracy of QTOF High- and QQQ Low-Resolution Mass Spectrometry'* (Feith et al., 2019) in the journal 'Metabolites'. Moreover, the isotopic ^{13}C-flux experiments were designed together with Dr. Martin Cerff and Dr. Katharina Nöh (FZJ), who also modeled and simulated the corresponding carbon flux distribution. Transcriptome measurements were again performed at the CeBiTec, whilst growth related expression patterns of differentially expressed genes were identified in collaboration with Thorsten Haas.

The third part of this thesis outlines the setup and results of continuous ALE experiments performed equally by Thorsten Haas and me. The following objectives were addressed:

- Establishment of an experimental setup for long-term continuous ALE processes
- Evolving the *C. glutamicum* WT strain in continuous ALE bioreactor processes
- Characterization of evolved mutants to identify growth-enhancing mutations

Deduced from several ALE experiments, genomes of potentially evolved *C. glutamicum* strains were sequenced by Dr. Marcus Persicke from CeBiTec and Felix Müller again constructed a mutant strain. The results of the ALE processes were presented in the paper *'Continuous Adaptive Evolution of a Fast-Growing Corynebacterium glutamicum Strain Independent of Protocatechuate'* (Graf et al., 2019) that was published in the journal 'Frontiers in Microbiology' in the section 'Systems Microbiology' and is attached in the appendix. The main results of this contribution are summarized in this thesis.

CHAPTER 2

Theoretical background

2.1. *Corynebacterium glutamicum*

2.1.1. Brief history and taxonomy

With the isolation of the diphteroid bacillus *Corynebacterium diphteriae*, the genus *Corynebacterium* was defined (Lehmann & Neumann, 1896) and classified within the *Actinobacteria*. Bacteria of this genus have a straight or rod-shaped form and therefore the greek word 'coryne' translating to 'tapered' or 'clubbed ends' gave this genus its name. *Corynebacteriae* are non-motile and non-sporulating, have a high G+C content, and their snapping cell division takes place in the corynebacterial V-form (Udaka, 2008). The protagonist of this work *C. glutamicum* belongs to this genus and was discovered in 1956 by Kyowa Hakko Kogyo Co. Ltd. Kinoshita and co-workers searched for microorganisms showing the ability to extracellularly accumulate glutamate and were thus scanning different natural environments such as soils, sewage waters, and zoological gardens (Kinoshita et al., 1957). Ultimately, strain 'No. 534' was isolated from soil of the Ueno Zoo in Tokyo. Due to the organisms ability to produce 10 g glutamate from 50 g glucose in a biotin-limited growth medium, they called the non-pathogenic strain *Micrococcus glutamicus* that was later renamed to *Corynebacterium glutamicum*. Besides glutamate, it was early discovered that *C. glutamicum* is also able to excrete other amino acids like lysine, arginine, ornithine, and threonine. Until today, *C. glutamicum* is one of the

most employed production hosts for amino acid production (Leuchtenberger et al., 2005). Apart from this, the strain serves as model organism for pathogenic bacteria of the *Mycobacterium tuberculosis* complex (Kalinowski et al., 2008; Mentz et al., 2013) and for *Corynebacterium diphteriae* (Mentz et al., 2013).

2.1.2. Central carbon metabolism

Most of the *C. glutamicum* cultivations performed in this work comprised glucose as limiting carbon source in growth media. Hence, an overview of the organism's central carbon metabolism (CCM) is provided summarizing information about (i) glycolysis from Arndt & Eikmanns (2008), Ikeda (2012), and Yokota & Lindley (2005); (ii) TCA cycle from Arndt & Eikmanns (2008) and Eikmanns (2005); and (iii) pentose phosphate pathway (PPP) from Yokota & Lindley (2005). The CCM is illustrated in figure 2.1 and additionally shows annotated genes of *C. glutamicum* encoding enzymes required for glucose metabolism, serving as quick reference for the reader with regard to transcriptome studies discussed in section 4.3 and section 4.6. Normally, glucose is taken up by a glucose-specific PTS (Malin & Bourd, 1991; Sugimoto & Shiio, 1987) that is located in the cell membrane and phosphorylates glucose during its transport into the cytoplasm. However, it was noted that other transport capacities for glucose have to exist in *C. glutamicum* (Cocaign-Bousquet et al., 1996; Dominguez et al., 1997; Gourdon et al., 2003) which was later confirmed by Ikeda et al. (2011) and Lindner et al. (2011) identifying PTS-independent glucose uptake by inositol permeases (IolT1 and IolT2) and subsequent phosphorylation by glucokinases. In either scenario, the resulting glucose 6-phosphate (G6P) is channeled into glycolysis for catabolic or into PPP for anabolic purposes (cf. figure 2.1). Following the eight steps of glycolysis, G6P is metabolized to the C_3-keto acid pyruvate (Pyr) whereby two molecules of adenosine triphosphate (ATP) and one molecule of oxidized nicotinamide adenine dinucleotide (NAD, oxidized form: NADH) are obtained along the way. *Vice versa*, all involved reactions from fructose 6-phosphate (F6P) to Pyr are reversible (partially due to a second set of respective enzymes, cf. figure 2.1) and are thus referred to as glucoeneogenetic reactions. Following the catabolic route, Pyr is catalyzed via pyruvate dehydrogenase complex to acetyl-coenzyme A (AceCoA) that marks the entryway into the TCA cycle. This eight-step reaction cycle provides the cell with catabolic precursors such as ATP and guanosine triphosphate (GTP), reducing equivalents like NADH and nicotinamide adenine dinucleotide phosphate (NADPH), and with anabolic precursors like α-ketoglutarate (AKG; also referred to as

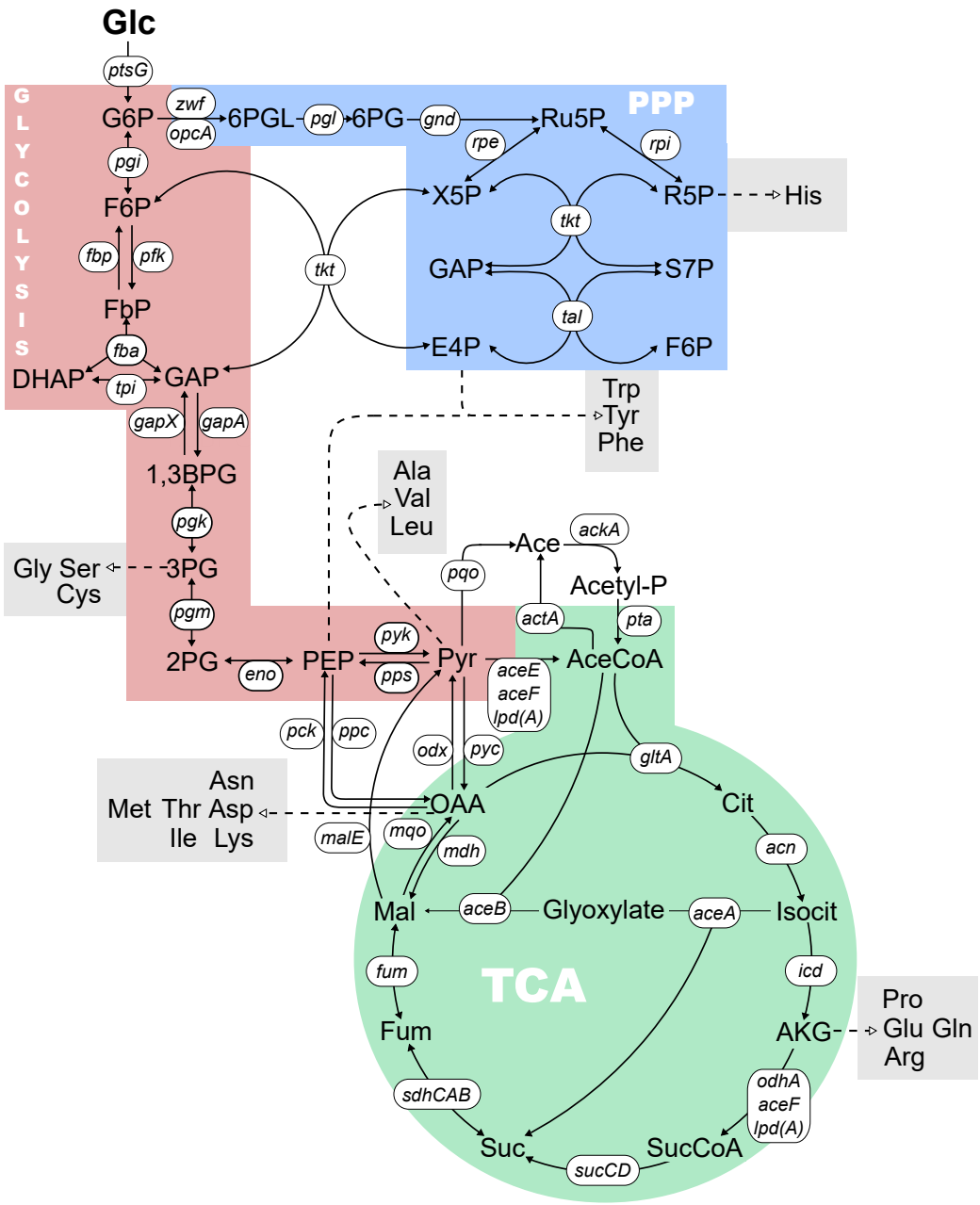

Figure 2.1.: Illustration of the CCM of *C. glutamicum* including branches towards amino acid biosynthesis (dottet lines). The pictured genes (italic) encode the following enzymes: *aceA*: IsoCit lyase; *aceB*: Mal synthase; *aceE*, *aceF* (*sucB*), *lpd*: Pyr dehydrogenase complex; *ackA*: Ace acetohydroxyacid isomeroreductase; *acn*: aconitase; *actA*: Ace CoA-transferase; *eno*: enolase; *fba*: FbP aldolase; *fbp*: fructose-bisphosphatase; *fum*: fumarase; *gapA*: GAP dehydrogenase; *gapX*: GAP dehydrogenase; *gltA*: Cit synthase; *gnd*: 6P-gluconate dehydrogenase; *icd*: IsoCit dehydrogenase; *malE*: malic enzyme; *mdh*: Mal dehydrogenase; *mqo*: malate:quinone oxidoreductase; *odhA*, *aceF* (*sucB*), *lpdA*: AKG dehydrogenase; *odx*: OAA decarboxylase; *pck*: PEP carboxykinase; *pfk*: 6P-fructokinase; *pgi*: G6P isomerase; *pgk*: 3PG kinase; *pgl*: 6P-gluconolactonase; *pgm*: phosphoglycerate mutase; *ppc*: PEP carboxylase; *pps*: PEP synthase; *pqo*: pyruvate:quinone oxidoreductase; *pta*: phosphotransacetylase; *ptsG*: Glc-specific phosphotransferase system; *pyc*: Pyr carboxylase; *pyk*: Pyr kinase; *rpe*: Ru5P-epimerase; *rpi*: R5P-isomerase; *sucC*, *sucD*: SucCoA synthetase; *sdhC*, *sdhA*, *sdhB*: Suc dehydrogenase; *tal*: transaldolase; *tkt*: transketolase; *tpi*: triosephosphate isomerase; *opcA*, *zwf*: G6P dehydrogenase. For abbreviations, the reader is kindly referred to the nomenclature.

2-oxoglutarate) or oxaloacetate (OAA) which is also the 'end product' after one cycle. Besides, the glyoxylate shunt is active in the *C. glutamicum* WT whenever substrates like acetate, fatty acids, or ethanol are present in the growth medium. These metabolites enter the TCA cycle at the level of AceCoA and are channeled from iso-citrate (IsoCit) via the glyoxylate shunt towards succinate (Suc) or malate (Mal) by-passing oxidative decarboxylation reactions. To replenish the TCA cycle or channel carbon once again towards glycolysis, *C. glutamicum* possesses a complex anaplerotic network featuring (de)carboxylating reactions around the metabolites phosphoenol-pyruvate (PEP), Pyr, malate, and OAA. The physiological function of this anaplerotic structure is not fully understood yet (Kappelmann et al., 2015). The major pathway for generating anabolic precursors is the PPP. Under physiological conditions, G6P is irreversibly transformed to ribulose 5-phosphate (Ru5P) in the oxidative branch of the PPP whereby two molecules of the anabolic reducing equivalent NADPH are formed. In the adjacent non-oxidative part of the PPP, the reversible formation of anabolic precursors ribose 5-phosphate (R5P) and erythrose 4-phosphate (E4P) is catalyzed. Simultaneously, glycolysis is replenished by simultaneous formation of F6P and/or glyceraldehyde 3-phosphate (GAP).

2.1.3. Amino acid biosynthesis and transporters

One working package of this dissertation dealt with *C. glutamicum*'s *in vivo* and *in silico* amino acid consumption (cf. section 4.2.2), wherefore corresponding information on amino acid biosynthesis, uptake, and metabolism is summarized here. The 20 proteinogenic amino acids can be distinguished into six families as illustrated in figure 2.1: (i) L-serine (Ser) family comprising glycine (Gly), Ser, and L-cysteine (Cys); (ii) Pyr family with L-valine (Val), L-alanine (Ala), and L-leucine (Leu); (iii) L-glutamate (Glu) family containing Glu, L-glutamine (Gln), L-proline (Pro), and L-arginine (Arg); (iv) L-aspartate (Asp) family including Asp, L-asparagine (Asn), L-lysine (Lys), L-threonine (Thr), L-isoleucine (Ile), and L-methionine (Met); (v) aromatic amino acid family comprising L-tyrosine (Tyr), L-phenylalanine (Phe), and L-tryptophan (Trp); (vi) L-histidine (His). In table 2.1, references for amino acid biosynthesis pathways of *C. glutamicum* are listed, whilst a short overlook with regard to their CCM metabolite precursors is provided in the following. The Ser family branches of from glycolysis at the height of 3-phosphoglycerate (3GP), whilst the Pyr family has its origin in Pyr as the name already suggests. The Glu family makes use of AKG as precursor, whilst the Asp family requires OAA. His derives from PPP precursor R5P via phosphoribosyl pyrophosphate (PRPP), the aromatic amino

acid family requires equimolar amounts of PPP metabolite E4P and glycolysis metabolite PEP to feed the shikimate pathway leading to the respective amino acid synthesis reactions. Based on their aliphatic side-chain, Val, Leu, and Ile are also described as branched-chain amino acids and share several enzymes for their biosynthesis [summarized in Pátek (2007)].

For most of the proteinogenic amino acids, uptake systems in *C. glutamicum* were either experimentally identified or are assumed to be present based on bioinformatic investigations [cf. table 2.1; and supplementary table 1 of Graf et al. (2018), section A]. Accordingly, Ala, Gln, His, Ile, Leu, Thr , Trp, Tyr and Val are taken up by secondary systems. For Asp, only primary transport was observed, whilst for Glu and Met secondary and primary transporters were identified. Lys is taken up via an antiporter in exchange with Lys, Ala, Ile, or Val. Phe is taken up via a secondary and another unspecified transporter. Since Pro serves as compatible solute for *C. glutamicum* for osmo-protection, basal uptake systems as well as an unspecified transporter are available. A transport system for Arg was not described yet but consumption of the amino acid was experimentally observed (Graf et al., 2018).

2.1.4. Genome and transcriptional regulation

In 2003, Kalinowski et al. (2003) and Ikeda & Nakagawa (2003) simultaneously unraveled the genome of *C. glutamicum* ATCC 13032. The ordered-clone approach applied by Kalinowski et al. (2003) resulted in a genome sequence with 3,282,708 base pairs (bp), a G+C content of 53.8 %, and 3002 coding genes. Ikeda & Nakagawa (2003) employed a whole-genome shotgun strategy and revealed a total genome sequence of 3,309,401 bp, a G+C content of 53.8 %, and predicted the existence of 3099 coding genes. The discrepancy between both genomes is due to a higher number of insertion sequences and the presence of an additional putative prophage region in the latter genome. Therefore, ATCC 13032 is distinguished into the 'Bielefeld' or 'Kyowa Hakko' type.

On the one hand, annotated genes give insights into the metabolic reaction network of an organism by representing encoded enzymes that ultimately catalyze metabolic reactions. On the other hand, genes encode proteins that are involved in transcriptional regulation processes representing the link between extracellular stimuli and cellular responses. According to current knowledge, the minimal regulatory repertoire of *C. glutamicum* ATCC 13032 consists of DNA-binding transcription regulators, sigma factors, and other proteins that are encode by 159 genes (Schröder & Tauch, 2013). In response

Table 2.1.: Overview of literature references for amino acid (AA) biosynthesis and transporters of *C. glutamicum*. n.d.a.: no data available

AA	References for biosynthesis pathways	References for transporters
Ala	Marienhagen & Eggeling (2008)	Trötschel et al. (2008)
Arg	Sakanyan et al. (1996)	n.d.a. but Arg consumption was observed by Graf et al. (2018)
Asn	Summarized in Oikawa (2007)	n.d.a.
Asp	Summarized in Oikawa (2007)	Krämer & Lambert (1990)
Cys	Wada & Takagi (2006)	n.d.a.
Gln	Summarized in Rehm et al. (2010)	Siewe et al. (1995)
Glu	Summarized in Rehm et al. (2010)	Burkovski et al. (1996), Krämer et al. (1990)
Gly	Peters-Wendisch et al. (2005)	n.d.a.
His	Kulis-Horn et al. (2014)	Shang et al. (2013)
Ile	Summarized in Pátek (2007)	Tauch et al. (1998), Ebbighausen et al. (1989)
Leu	Summarized in Pátek (2007)	Ebbighausen et al. (1989)
Lys	Sonntag et al. (1993)	Bröer & Krämer (1990), Seep-Feldhaus et al. (1991)
Met	Summarized in Trötschel (2005)	Trötschel et al. (2008)
Phe	Summarized in Sprenger (2007)	Wehrmann et al. (1995), Shang et al. (2013), (Zhao et al., 2011)
Pro	Summarized in Shimizu & Hirasawa (2007)	Weinand et al. (2007), Peter et al. (1997)
Ser	Peters-Wendisch et al. (2002), Peters-Wendisch et al. (2005)	Palmieri et al. (1996)
Thr	Summarized in Eikmanns et al. (1991)	Palmieri et al. (1996)
Trp	Summarized in Sprenger (2007)	Wehrmann et al. (1995), Shang et al. (2013)
Tyr	Summarized in Sprenger (2007)	Wehrmann et al. (1995), Shang et al. (2013)
Val	Summarized in Pátek (2007)	Ebbighausen et al. (1989)

to external stimuli, transcription regulators recognize and bind to operator sites of target genes (the regulon) and thereby influence their expression in a positive or negative way. The collectivity of transcriptional regulator and regulon is called network motif and stands for a specific physiological function of the cell. The regulatory network of *C. glutamicum* harbors local, master, and global regulators (Brinkrolf et al., 2010). Local regulators control the expression of smaller regulons that consist of a low number of genes and are usually clustered within the group of target genes, e.g. forming an operon (Rodionov et al., 2008). Master regulators control several units of functionally related regulons forming functional modules within the transcriptional network (Kohl & Tauch, 2009). Until know, eleven master regulators were identified controlling genes of six modules: (i) RamA, RamB, SugR, and SigB controlling carbon metabolism; (ii) AmtR, McbR, PhoR controlling macroelement homeostasis; (iii) DtxR controlling metal homeostasis; (iv) SigH controlling the heat and oxidative stress response; (v) LexA controlling the cellular SOS response; (vi) ArnR controlling anaerobic respiration (Toyoda & Inui, 2015). Global regulators have the highest position in the regulation hierarchy and control more than 20 target genes that belong to a minimum of four different functional moduls (Toyoda & Inui, 2015). Another form of regulatory mechanism concerns the replacement of (alternative) sigma factors from the RNA polymerase holoenzyme. Usually, the housekeeping sigma factor is carried by an RNA polymerase to initiate transcription and an alternative sigma factor redirects the RNA polymerase towards a subset of promoters. Thus, sigma factors have positive control over gene expression when bound to the RNA polymerase, and negatively affect the RNA polymerase in their absence. In turn, DNA-binding transcription regulators influence gene expression by blocking or allowing the RNA polymerase access to the promoter region (Schröder & Tauch, 2010). *C. glutamicum* harbors seven sigma factors: the primary housekeeping sigma factor SigA, the nonessential primary-like sigma factor SigB, and the five alternative sigma factors SigC, SigD, SigE, SigH, and SigM (Brinkrolf et al., 2007). For detailed literature on *C. glutamicum*'s transcriptional network, transcriptional units and sigma factors, the reader is kindly referred to Brinkrolf et al. (2010), Schröder & Tauch (2013, 2010), and Toyoda & Inui (2015). Besides, regulatory functions of the introduced transcription factors are summarized in the ontology-based database CoryneRegNet (Pauling et al., 2012) which served as main reference for transcript discussions in this thesis.

2.2. Microbial growth and the metabolic steady state

2.2.1. Pseudo metabolic stationarity in batch processes

Batch processes in shaking flask or bioreactor experiments are performed by seeding the organism into a growth environment with an initial unlimited substrate supply and a fixed reaction volume. Usually, one of the growth nutrients, e.g. the carbon source, is supplied in a limited amount whilst nitrogen-, phosphorous-, sulfurous-sources, and trace elements are supplied in manifold. After inoculation of the growth medium, a potential 'lag' phase with no apparent cell growth might occur (cf. figure 2.2), where the strain adapts to the potentially new growth environment (different growth nutrients, pH, temperature, etc.). Subsequently, the growth rate accelerates, finally leading to exponential growth. In this correspondingly called exponential (or logarithmic) growth phase, the cell exhibits a constant growth rate and substrate consumption rate as long as all growth nutrients are available in excess. Therefore, this cellular state is referred to as pseudo metabolic steady state even though the growth environment is highly dynamic (increase of biomass concentration, decrease of nutrients, potential decrease of oxygen availability, increase of dissolved carbon dioxide, etc.). Within this phase, all relevant kinetic parameters of conducted batch processes were calculated in this thesis as stated in section 3.10.1. As soon as one of the growth nutrients ultimately becomes limiting, the organism first enters the decelerating transition phase and then the stationary phase if the growth medium is depleted of elemental substrate(s). Without any further supply of nutrients, cell death is eminent.

2.2.2. Metabolic stationarity in continuous processes

In a continuous process setup, feed medium containing essential growth substrates is constantly added to the bioreactor, and cultivation broth comprising residual substrates, metabolic products, and biomass is simultaneously and constantly removed from the vessel. If the reaction volume is moreover kept constant, a stationary growth environment is established wherein all process parameters are stable and the feed supply, represented by the dilution rate, determines a fixed growth rate and ultimately constant biomass and substrate concentrations (cf. figure 2.3). Based on this stationary growth environment, derived kinetic parameters originate from a 'real' metabolic steady state of the cell, contrary to the dynamic and therefore pseudo-stationary growth environment of a batch process in the exponential phase. This makes the continuous bioreactor an ideal

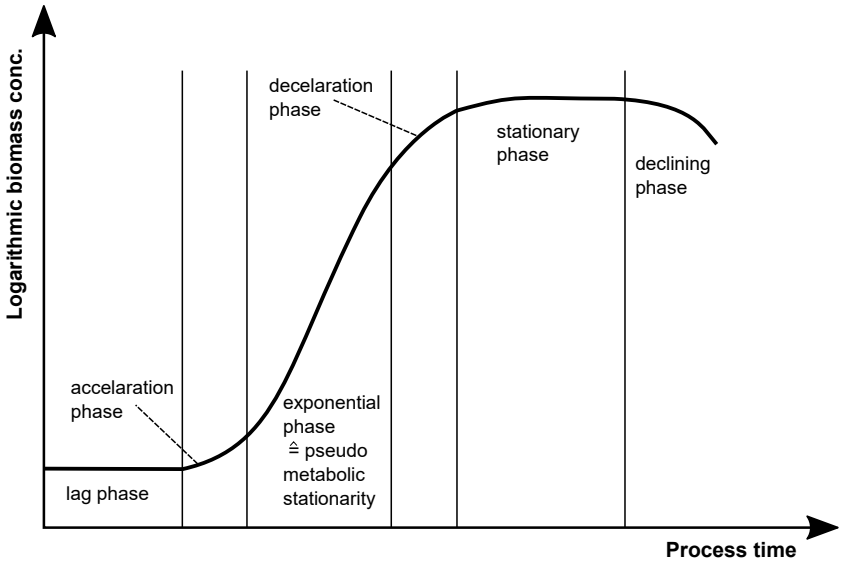

Figure 2.2.: Illustration of substrate-unlimited batch growth of microorganisms that can be distinguished into six growth phases. In the exponential growth phase, cells are in pseudo metabolic stationarity and exhibit constant growth kinetics. Biomass formation is pictured as logarithmic curve over the process time.

device for systems biology investigations since highly reproducible experiments can be conducted. Besides, this is an essential prerequisite for OMIC disciplines such as transcriptomics, metabolomics, and proteomics, or metabolic flux analysis [MFA; Bull (2010) and Hoskisson & Hobbs (2005)].

In most continuous bioreactor studies, chemostat processes (Larsson et al., 1990; Martin & Hempfling, 1976; Monod, 1950; Novick & Szilard, 1950) are employed where the dilution rate through the system is set below the maximum growth rate keeping cell growth substrate-limited. This is advantageous with regard to the robustness of the system making it auto-stable: whenever the dilution rate increases or decreases, resulting in a momentary excess or reduction of substrate, the system shortly responds with an increase or decrease in biomass. However, when the fluctuation in the dilution rate returns to its normal setpoint, biomass accordingly declines or increases and ultimately returns to its stable working point (Agrawal & Lim, 1984; Zhao & Skogestad, 1997). If experiments shall be performed near the maximum growth rate of a cell, continuous process types such as the nutristat or turbidostat are usually employed (Davey et al., 1996; Gostomski et al., 1994; Martin & Hempfling, 1976). In contrast to the chemostat, these setups ensure a stable process performance when approximating the critical dilution rate (=maximum growth rate) in the wash out regime, cf. figure 2.3 and the mathematical description of the continuous process in section 3.10.2.

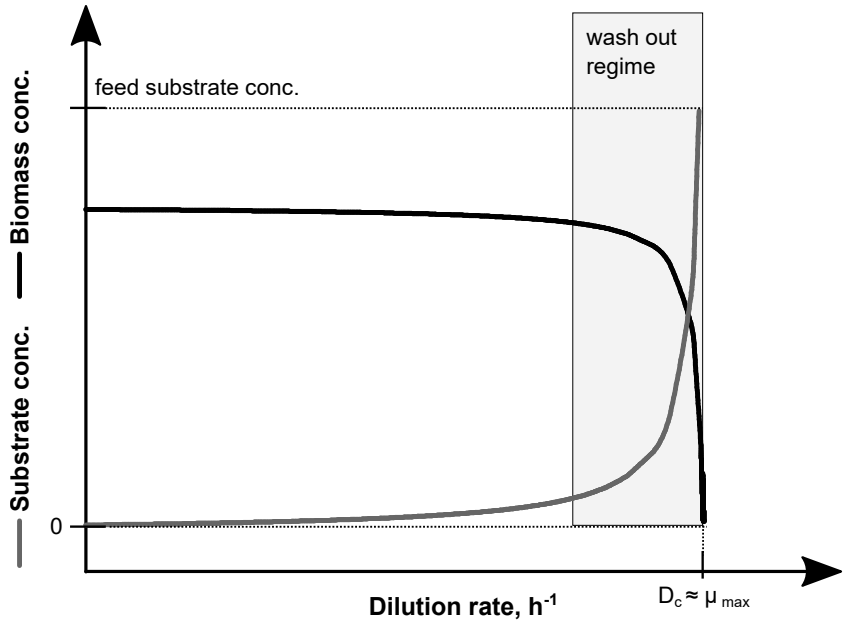

Figure 2.3.: Illustration of steady state biomass and substrate concentrations in dependency of different dilution rates D in a continuous bioreactor. Dilution rates approximating the critical dilution rate (D_c) represent the wash out regime which is highly sensitive to changes in D, biomass, or substrate concentration. The wash out region can be controlled by employing turbidostat or nutristat control, whilst D below D_c can be stably set with chemostat control.

2.3. Systems biology and OMICs

2.3.1. Systems biology

The aim of systems biology is the holistic and quantitative description of biological systems and the interaction of different modules within these systems (Fiehn, 2001; Kitano, 2002). Regarding the discipline of biochemical engineering, this might cover the description of heterogeneous cell populations as found in large scale production cultivations or the description and optimization of producers strains. In the latter case, a systems biology approach might comprise the description of the different control levels within the cell (Takors et al., 2007). This is exemplarily illustrated in figure 2.4 where these levels are distinguished into genome, transcriptome, proteome, metabolome, and fluxome. To analyze these layers, the so called 'OMICs' techniques are employed to (i) sequence the cell's genome; (ii) determine the sum of RNA and especially mRNA representing the gene expression status of the cell (transcriptomics); (iii) assess all identifiable/analyzable proteins (proteomics); (iv) identify and quantify all intra- and extracellular metabolites (metabolomics); and (v) determine intracellular fluxes between

metabolite pools (fluxomics). Moreover, the interaction within or between these modules is of interest. Thus, systems biology tries to identify gene interactions, biochemical pathways, and corresponding regulatory structures; investigate system dynamics (e.g. via metabolic or sensitivity analysis) and system control (e.g. via metabolic control analysis); and model complete *in silico* cells or parts of it (e.g. via topological network models). Hence, upon exposing the investigated strain to extracellular stimuli, combining OMIC techniques and systems biology approaches facilitates a deep insight into the cellular phenotype by simulating and predicting *in vivo* cell physiology (Kitano, 2002). Based on the retrieved information, metabolic engineering or synthetic biology tools can be applied to modify and construct an optimal production cell.

The following sections provide a short introduction of OMIC tools employed in this work.

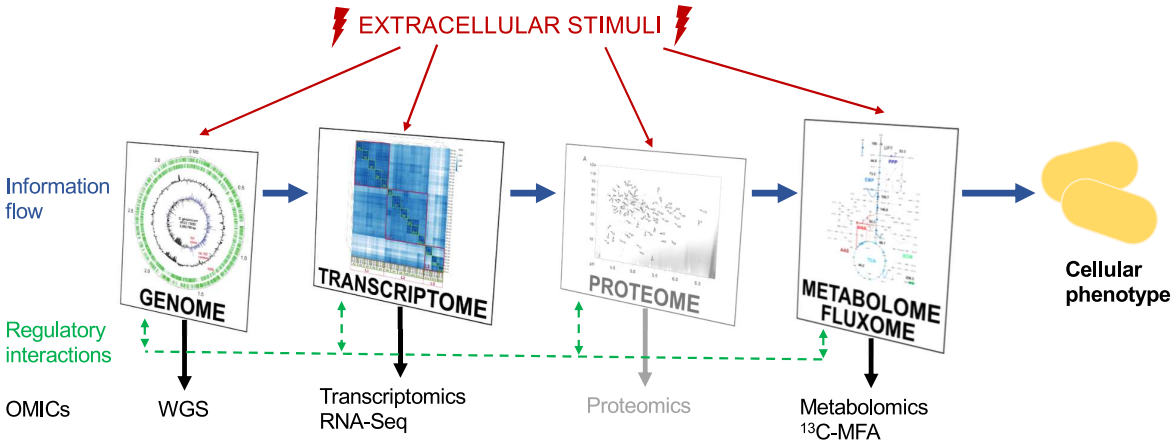

Figure 2.4.: Illustration of cellular regulation on the level of the genome, transcriptome, proteome, metabolome, and fluxome from a systems biology viewpoint. Extracellular stimuli can impact each (or several) level(s) resulting in the information flow as pictured, ultimately leading to a phenotypic response of the investigated strain. Simultaneously, regulatory interactions between all layers are possible. The respective OMIC technique employed in this work to capture information flows or regulatory interactions are additionally depicted. WGS: whole genome sequencing, RNA-Seq: RNA sequencing, MFA: metabolic flux analysis. Since the proteome level was not investigated in this thesis it is illustrated in gray.

2.3.2. Transcriptomics

In the discipline of transcriptomics, the complete transcriptional repertoire of a cell in a specific physiological state is quantified and analyzed (Wang et al., 2009). Amongst the different RNA species, the mRNA is of great interest because it is the blueprint for protein synthesis. Therefore, quantifying the amount of mRNA gives a first insight into

which proteins are potentially expressed under certain physiological conditions without the need to measure the entire proteome of the cell. Besides, mRNA expression analysis can also provide insight into underlaying gene clusters, gene networks, and regulatory structures (cf. section 2.1.4). Therefore, a transcriptomics work flow roughly comprises: (i) the isolation of RNA from biomass samples; (ii) mRNA isolation; (iii) conversion of mRNA strands into a library of cDNA fragments; (iv) addition of sequencing adapters to the fragments; (v) obtaining short sequences (=sequencing reads) from the cDNA fragments via a high-throughput sequencing technology such as RNA-Sequencing (RNA-Seq); (vi) alignment of the reads with a reference genome (Wang et al., 2009). Finally, the reads represent a base-resolution expression profile of each gene. This 'raw' data is then further processed with bioinformatic tools such as DESeq2 (Love et al., 2014) and maSigPro (Nueda et al., 2014) to identify differentially expressed genes (DEGs). Genes classified as DEGs exhibit a statistically significant decreased or increased gene expression in comparison to a reference state. This allows the assessment of the transcriptional response of the cell to specific external stimuli or to genetic changes. In this dissertation, mRNA isolation from biomass samples, sequencing, and subsequent mapping of reads was kindly performed by our project partners at the CeBiTec. Identification of DEGs from corresponding raw count data was performed by two methods based on the absence (cf. section 3.12.2) or availability of biological replicates (cf. section 3.12.3). The latter was kindly performed by my colleague Thorsten Haas (Haas et al., 2019).

2.3.3. Metabolomics

In the discipline of metabolomics, a cell's endometabolome (intracellular metabolites) and exometabolome (extracellular metabolites) is analyzed. The entity of the endo- and exometabolome represents the current status of genetic regulations in the cell and therefore mirrors the phenotype of the microogranism (Dunn et al., 2005). Hence, by quantifying intracellular metabolite pools and identifying the underlying metabolic pathways/network, the cell's response to specific growth environments or stimuli can be measured. Depending on the aim of the metabolome analysis, different experimental variants exist which can be subdivided into (i) target analysis: analysis of one or several metabolites of a specific metabolic reaction; (ii) metabolic profiling: measuring predefined metabolites generally related to a specific pathway; (iii) metabolic footprinting: measuring all extracellular metabolite concentrations in the cultivation broth; and (iv) metabolic fingerprinting: a rapid, high-throughput analysis aiming at a global analysis

of the whole metabolome (Ellis et al., 2007; Takors et al., 2007; Wendisch et al., 2006a). Within the scope of this work, metabolic profiling was employed to quantify the majority of metabolites from the CCM (glycolysis, TCA, PPP) and intracellular amino acids to identify growth-related effects. In principle, quantification of the endometabolome comprises the rapid quenching of the cell's metabolism, the extraction of intracellular metabolites from biomass, and the subsequent quantification of pool sizes. The very first step of this procedure already proofs to be challenging since the stopping of all intracellular activities has to be performed such as not to distort the recorded 'snapshot' of the cell's metabolic state (Fiehn, 2001). Simultaneously, the employed quenching technique must not damage the cell to prevent leakage of intracellular metabolites. Moreover, specific extraction techniques shall be employed that enable a holistic capture of the targeted intracellular metabolite pools (Winder et al., 2008). Besides nuclear magnetic resonance (NMR), the analysis of extracted metabolites is nowadays usually performed with mass spectrometry (MS) coupled to gas or liquid chromatography [LC; Ellis et al. (2007) and Patti et al. (2012)]. With this method, metabolites are selected for by their specific mass-charge-ratio (m/z) within the complex metabolite sample matrix. In this work, a LC-MS QQQ device was employed to quantify intracellular metabolite pools (cf. section 3.11.3) whilst a LC-MS QTOF device was used to analyze ^{13}C-isotopoluge distributions of intracellular metabolites (cf. section 3.11.4).

2.3.4. Fluxomics

The main target of fluxomics is the determination and quantification of intracellular metabolite fluxes that comprise all conversion and transport rates of metabolites (Klein & Heinzle, 2012). These fluxes embody the connection between intracellular pools of metabolites and therefore grand insights into the principles of cell growth, maintenance, and the response of microorganisms to external stimuli (Sauer, 2006). To determine intracellular fluxes, isotopic ^{13}C-tracer experiments are performed and the resulting labeling information in intracellular metabolites is used as basis for metabolic network-based flux simulation. Ideal ^{13}C-labeling patterns in analyzed metabolites are obtained by firstly performing an experimental design study (EDS). Thus, a specific mixture of isotopically labeled substrates is identified that produces advantages labeling patterns for the following flux simulation (Nöh & Wiechert, 2006).

Regarding the experimental execution of a ^{13}C-tracer process, the establishment of time-invariant and constant endometabolome pool sizes in the investigated cell is a

prerequisite to determine intracellular fluxes. This is achieved by establishing a metabolic steady state in the cell, i.e. by cultivating the strain in substrate-unlimited batch conditions (pseudo metabolic steady state) or in substrate-limited continuous conditions (real metabolic steady state; cf. section 2.2). Subsequently, the ^{13}C-tracer experiment is conducted by employing one of the following approaches (Niedenführ et al., 2015; Wiechert & Nöh, 2005): (i) stationary ^{13}C-analysis: stationary ^{13}C-labeling patterns in the intracellular metabolites of interest are obtained in batch cultivations by using isotopically labeled substrate as growth substrate from the very start, and in continuous bioprocesses by feeding the isotopic substrates for at least 4–5 residence times (Zamboni et al., 2009) whereupon sampling is performed; (ii) non-stationary ^{13}C-analysis: fast metabolome sampling is employed right after a ^{13}C-pulse is set (batch cultivation) or the ^{13}C-feed is started (continuous process) and feeding is stopped before stationary labeling patterns in metabolites are reached [for detailed information on ^{13}C-analysis, the reader is kindly referred to Antoniewicz (2015), Sauer (2006), and Wiechert & Nöh (2005)]. Therefore, non-stationary ^{13}C-labeling is profoundly less time- and cost-intensive compared to the stationary labeling approach. However, since dynamic changes of labeling patterns are the prerequisite for this type of analysis, a high number of samples has to be taken with a sampling rate that ideally is in the range or even below the metabolite pool-turn over rates of the targeted metabolites. Only if this is given, dynamics in labeling patterns can be captured properly before stationary isotopolouge distributions are reached. This is especially challenging for metabolites of the upper glycolysis with observed turn over rates of around (1–5) s in microorganisms (Heijnen, 2010). Moreover, non-stationary ^{13}C-analysis requires quantitative information of metabolite pool sizes to predict the fluxes (Wiechert & Nöh, 2013). In the case of stationary ^{13}C-analysis, rapid sampling and pool size information is not required.

Apart of building the basis for flux simulations, ^{13}C-labeling experiments are employed to identify new metabolic pathways/reactions in the metabolism of the investigated strain and to gather knowledge about reversible reactions or futile cycles, ultimately improving stoichiometric network models [SNMs; Vertès et al. (2012)].

2.3.5. Metabolic network models

In principle, a metabolic network model is the mathematical reconstruction of a cell's metabolism and comprises a huge amount of metabolites and connecting chemical reactions. Based on information gathered by the OMICs techniques, e.g. genome sequence,

annotated genes, enzymatic repertoire, endometabolome, reversibility of reactions, etc., the complexity of network models reaches genome-scale. These models are employed to investigate the cell's phenotypes or the outcome of external stimuli *in silico*, i.e. simulate and predict metabolic fluxes within the cell (Winter & Krömer, 2013). One type of metabolic network models are SNMs. They are based on stoichiometric properties of enzymes (Vertès et al., 2012) whereby stoichiometric mass balances at (pseudo) stationary conditions are derived and formulated. This resulting linear equation system is then solved with MFA. Therefore, MFA requires information on experimentally determined extracellular fluxes, e.g. substrate consumption and biomass formation rates. Due to the complexity of the SNMs, the corresponding system is most often under-determined (i.e. the degree of freedom is > 0), wherefore linear optimization algorithms such as FBA are employed (Terzer et al., 2009). Since classical MFA only predicts net fluxes in a metabolic system and are limited with regard to bidirectional, parallel, branched, or cyclic reactions (Wiechert & Nöh, 2005), additional information is required to simulate intracellular metabolic fluxes. Thus, information gathered within isotopic ^{13}C-labeling experiments enhance the validity of a SNM by providing information on the fate of ^{13}C-atoms within the metabolic model. In this dissertation, SNMs were either employed to predict growth phenotypes with a modified metabolic network model of *C. glutamicum* (cf. section 4.2.1), or to simulate intracellular metabolite fluxes of the strain (cf. section 4.7.3). The latter was kindly performed by our project partners at the FZJ.

2.4. Adaptive laboratory evolution

In an ALE experiment, microogranisms are cultivated for a prolonged time in clearly defined growth environments. The extracellular conditions are chosen by the experimenter such as to expose the strain to specific selection pressures that ultimately trigger intracellular adaption processes. Hence, mutations in the genome of the cell are observed after 100 to 1,000 generations (Winkler et al., 2013), that are extrinsically observed as increase of the organism's fitness (Dettman et al., 2012; Ryall et al., 2012). In the last years, genome sequencing techniques developed rapidly and made the identification of gene mutations easier. Concomitantly, this increased the popularity of ALE applications for industrial biotechnology topics as well (Wang et al., 2018b). With regard to strain optimization, this technique is an alternative to molecular metabolic engineering procedures targeting the improvement of the same cellular attributes, e.g.

growth rate, substrate spectrum, substrate uptake rate, production rate (Dragosits & Mattanovich, 2013; LaCroix et al., 2015; Rugbjerg et al., 2018; Sandberg et al., 2016), or robustness to (toxic) by-products (McCloskey et al., 2018; Mohamed et al., 2017; Tremblay et al., 2015). In contrast to metabolic engineering approaches, where targeted alterations are introduced into the host genome, long-term ALE approaches allow the cell to develop 'natural' mutations whereby balanced protein expression levels might be more easily obtained than with 'artificial' molecular biotechnology techniques (Dragosits & Mattanovich, 2013).

The experimental execution of the ALE experiment can be performed in batch or continuous process mode. Whilst repetitive batch experiments are comparably easy to perform, the extracellular growth conditions are highly dynamic. This could lead to unwanted side-selection pressures potentially altering the outcome of the experiment. On the contrary, continuous processes provide constant growth environments and the selection pressure can be set more precisely. However, experimental costs and efforts are higher than in the repetitive batch process (Dragosits & Mattanovich, 2013). With regard to ALE experiments involving *C. glutamicum*, several publications appeared within the last years following the general trend of increased interest in ALE. For instance, enhancing the growth performance of the WT strain cultivated in mineral medium was the subject of two publications [Pfeifer et al. (2017) and Wang et al. (2018b), cf. section 4.8]. Other studies aimed at adapting the strain to different carbon sources, e.g. methanol (Sinumvayo et al., 2018), to improve its productivity [e.g. putrescine, Li et al. (2018) or recombinant proteins, Choi et al. (2018)], or to enhance *C. glutamicum*'s stress tolerance (Oide et al., 2015; Wang et al., 2018a; Xu et al., 2019). Besides, the ALE setup itself was also the focus of different investigations (Mahr et al., 2015; Radek et al., 2017). For further background knowledge on ALE, the reader is kindly referred to the reviews of Dragosits & Mattanovich (2013) and Stella et al. (2019), and to the contribution of Winkler et al. (2013).

CHAPTER 3

Material and Methods

In this chapter, material and methods are summarized that were employed in this thesis. Contents of this section have been (partially) published and corresponding references are provided.

3.1. Bacterial strains

Several *C. glutamicum* strains were cultivated in this dissertation. For pseudo-steady state growth investigations (supplementation experiments), investigation of metabolic steady states in continuous processes, and in the initial ALE process, WT *C. glutamicum* ATCC 13032 obtained from the American Type Culture Collection (ATCC, Manassas, VA, USA) was used. Derived from transcript results of supplementation experiments (cf. section 4.3), deletion mutants *C. glutamicum* Δcg1296, *C. glutamicum* Δcg3329, and *C. glutamicum* Δcg3374 were constructed and cultivated. Likewise, over-expression mutants *C. glutamicum* pVWEx1-cg1296 [*C. glutamicum* (pFEM19)] and *C. glutamicum* pVWEx1-cg0936 [*C. glutamicum* (pFEM18)] were created and studied. Strains EVO1, EVO2, EVO3, EVO4, and EVO5 were obtained from growth evolution studies after each ALE process, respectively. *C. glutamicum* reRamA (Cg reRamA; cf. section 4.8.3 and section B) was constructed bearing the point mutation S101C in gene cg2831 (*ramA*). All re-engineered or evolved strains were derived from *C. glutamicum* ATCC 13032.

3.2. Media

3.2.1. Complex media 2 × TY

For cryogenic and precultures of *C. glutamicum* (cf. section 3.6), tryptone-yeast extract complex medium (2 × TY) was used (Sambrook & Russell, 2001) as given in table 3.1.

Table 3.1.: Composition of 2 × TY complex medium for pre-cultures on agar plates and in glass reaction tubes.

Component	Concentration, $g\,L^{-1}$
Tryptone	16
Yeast Extract	10
NaCl	5

All components of the 2 × TY medium were dissolved in deionized water. For preculture stage 1 (cf. section 3.6.2), 5 mL of the solution were filled in glass reaction tubes, sterilized for 20 min at 121 °C, and afterwards stored at room temperature. For a solid culture medium (agar plates), $18\,g\,L^{-1}$ agar was added to the listed components prior to sterilization. 20 mL of the sterile solution was poured into Petri dishes which were left to dry in the clean bench. Agar plates were stored at 4 °C.

3.2.2. Minimal media

Cultivations in shaking flasks and bioreactors (cf. section 3.7) were performed in modified CGXII minimal medium (Buchholz et al., 2014b) with optional supplementation of different carbon and nitrogen sources. The components are listed in the following tables.

Shaking flask medium

The components listed in table 3.2 were dissolved in deionized water and $MgSO_4 \cdot 7\,H_2O$ and $CaCl_2 \cdot H_2O$ were added from separately sterilized stock solutions (cf. table 3.4). The pH was adjusted to 7 (carbon source: glucose) or 6.5 (carbon source: acetate) with $5\,mol\,L^{-1}$ KOH. The salt solution was sterilized for 20 min at 121 °C and residual supplements were added afterwards according to table 3.6. 500 mL sterile baffled shaking flasks were filled with 50 mL of the complemented CGXII medium prior to inoculation.

Table 3.2.: Composition of modified CGXII minimal medium for shaking flask cultures.

Component	Concentration, $g\,L^{-1}$
$(NH_4)_2SO_4$	10
K_2HPO_4	1
KH_2PO_4	1
Urea	5
3-(N-morpholino)propanesulfonic acid (MOPS)	21

Bioreactor and feed medium

The components listed in table 3.3 were dissolved in deionized water and $MgSO_4 \cdot 7\,H_2O$ and $CaCl_2 \cdot H_2O$ were added from separately sterilized stock solutions (table 3.4). The resulting salt solution was sterilized for 20 min at 121 °C and residual supplements were added according to table 3.6. pH was set to 7.4 in the bioreactor using 25 % NH_4OH prior to inoculation (section 3.7.3).

For feed media in continuous cultivations, all salts of the CGXII minimal medium were dissolved in 47 kg deionized water in a feed reservoir which was sterilized for 20 min at 121 °C. The supplements and the required amount of sterilized deionized water for a total of 50 kg growth medium were added through a feeding bottle after the feed reservoir had cooled down.

Table 3.3.: Composition of modified CGXII minimal medium for main cultures in bioreactors (cf. section 3.7.3).

Component	Concentration, $g\,L^{-1}$
$(NH_4)_2SO_4$	10
K_2HPO_4	1
KH_2PO_4	1

Salt stock solutions

$MgSO_4$- and $CaCl_2$-solutions were prepared as individual 1000 × stock solutions. The respective amounts (cf. table 3.4) were dissolved in deionized water, sterilized for 20 min at 121 °C, and stored at 4 °C.

Table 3.4.: Composition of $MgSO_4$- and $CaCl_2$-stock solutions as supplements for modified CGXII media given in table 3.2 (shaking flask cultures) and table 3.3 (bioreactor cultivation).

Component	Concentration, $g\,L^{-1}$
$MgSO_4 \cdot 7\,H_2O$	250
$CaCl_2 \cdot H_2O$	10

Trace element solution

All components of the trace element solution (TES; cf. table 3.5) were dissolved in deionized water and 32 % HCl was added to reach pH 1 to give a 1000 × concentrated stock solution. The solution was filtered aseptically through 0.2 µm cellulose-acetate filters and stored at room temperature.

Table 3.5.: Composition of trace element solution (TES) as supplement for modified CGXII media given in table 3.2 (shaking flask cultures) and table 3.3 (bioreactor cultivation).

Component	Concentration, $g\,L^{-1}$
$Fe(II)SO_4 \cdot 7\,H_2O$	16.40
$MnSO_4 \cdot H_2O$	10.00
$CuSO_4 \cdot 5\,H_2O$	0.20
$ZnSO_4 \cdot 7\,H_2O$	1.00
$NiCl_2 \cdot 6\,H_2O$	0.02

^{12}C-glucose stock solution

To prepare 1 L 500 $g\,L^{-1}$ ^{12}C-glucose stock solution, 652.12 mL deionized water was added to 550 g glucose $\cdot H_2O$, sterilized for 20 min at 121 °C, and stored at room temperature. The stock-solution was used in varying amounts for shaking flask and bioreactor cultures as given in the respective sections.

^{13}C-labeled glucose stock solutions

For generation of isotopically ^{13}C-labeled biomass from shaking flask cultures, a 400 $g\,L^{-1}$ solution of uniformly labeled U^{13}C-glucose was prepared. For (non-)stationary labeling in the continuous bioreactor cultivation, 113 $g\,L^{-1}$ U^{13}C- and 129 $g\,L^{-1}$ C_1-^{13}C-glucose stock solutions were prepared, respectively. Either type of labeled glucose was dissolved in deionized water, solutions were filtered aseptically through 0.2 µm cellulose-acetate filters, and stored at room temperature.

Biotin stock solution

The biotin solution was prepared as a 1000 × stock solution. 0.2 g biotin was dissolved in 1 L deionized water, aseptically filtered through a 0.2 µm cellulose-acetate filter, aliquoted, and stored at −20 °C.

Thiamin stock solution

The thiamin solution was prepared as a 500 × stock solution. 0.1 g thiamin·HCl was dissolved in 1 L deionized water, aseptically filtered through a 0.2 µm cellulose-acetate filter, aliquoted, and stored at −20 °C.

Protocatechuate stock solution

The PCA solution was prepared as a 1000 × stock solution. 30 g PCA was dissolved in 1 L 0.4 mol L^{-1} NaOH, aseptically filtered through a 0.2 µm cellulose-acetate filter, aliquoted, and stored at −20 °C.

Supplements

The stock solutions listed in table 3.6 were individually and aseptically added as supplements to modified CGXII minimal media. Whilst glucose, $MgSO_4$, $CaCl_2$, TES, and biotin were always added, thiamin and PCA were only added when indicated in the corresponding sections. Besides, different amounts of brain-heart-infusion (BHI) or 5 mmol L^{-1} of 18 essential amino acids, respectively, were supplemented as additional carbon and nitrogen sources in supplementation experiments (cf. section 4.1). The preparation is given in detail in the attached publication Graf et al. (2018) (cf. section A). Moreover, varying amounts of YE were used for the ALE studies as stated in section 4.8.1. The detailed preparation is described in the attached manuscript Graf et al. (2019) (cf. section B).

Table 3.6.: Supplements for modified CGXII pre-culture (cf. table 3.2) or main culture (cf. table 3.3) media.

Component	Stock concentration, $g\,L^{-1}$	Added stock solution, $mL\,L^{-1}$
^{12}C-glucose	500.0	varies
$MgSO_4 \cdot 7\,H_2O$	250.0	1
$CaCl_2 \cdot H_2O$	10.0	1
TES	-	1
Biotin	0.2	1
Thiamin	0.1	2
PCA	30.0	1

3.3. Devices, software, and databases

All devices, software, and databases employed in this thesis are summarized in table 3.7 and table 3.8.

3.4. Whole genome sequencing

Whole genome sequencing of *C. glutamicum* WT ATCC 13032 and evolved strain *C. glutamicum* EVO5 was performed by our project partners at the CeBiTec as described in Graf et al. (2019) (cf. section B).

3.5. Construction of strains

Construction of mutants derived from *C. glutamicum* ATCC 13032 was kindly performed by my colleague Felix Müller as stated in the following. Deletion mutants of ATCC 13032 lacking either of the genes cg1296, cg3329, or cg3374 were generated by applying the integration/deletion system based on plasmid pK19mobsacB (Schäfer et al., 1994). In order to delete the entire gene sequence [as identified by Pfeifer-Sancar et al. (2013)], 500 bp genomic sequences up- and downstream of the target gene were amplified with the appropriate primer pair as indicated in table 3.9. PCR amplification products of both flanking regions (flank1 and flank2) were cloned simultaneously into *Bam*HI, *Nhe*I linearized pK19mobsacB by isothermal assembling (Gibson, 2011). Competent cells of *E. coli* DH5α (Hanahan, 1983) were transformed by electroporation (Eppendorf Eporator,

Table 3.7.: Devices employed in this thesis.

Device	Name	Manufacturer
Bioreactor	Triple glass reactor system	HWS Labortechnik, Mainz, Germany
	KLF 2000	Bioengineering, Wald, Switzerland
Temperature sensor	Pt100	Bioengineering, Wald, Switzerland
Pressure probe	PR-35 X HT	KELLER Druckmesstechnik, Jestetten, Germany
pH probe	405-DPAS-SC-K8S	Mettler-Toledo, Gießen, Germany
Dissolved oxygen probe	InPro 6800	Mettler-Toledo, Gießen, Germany
Oxygen sensor	BCPO2	BlueSens, Herten, Germany
Carbon dioxide sensor	BCPCO2	BlueSens, Herten, Germany
Mass flow controller	MFC GFC171S	Analyt-MTC GmbH, Müllheim, Germany
Peristaltic pumps	120 U/DV (200RPM)	Watson Marlow, Falmouth, UK
Syringe pump	LA-30	Landgraf HLL, Langenhagen, Germany
Laboratory scale	AE200	Mettler Toledo, Gießen, Germany
	Combics 3	Sartorius, Göttingen, Germany
Analytical scale	XS204	Mettler Toledo, Gießen, Germany
Spectrophotometer	DR 3900	Dr. Lange, Berlin, Germany
	Ultrospec 2100 pro	Biochrom, Cambridge, UK
Centrifuge	5403 R	Eppendorf, Hamburg, Germany
TC/TN analyzer	Multi N/C 2100s	Analytik Jena, Jena, Germany
HPLC	Agilent 1200	Agilent Technologies, Santa Clara, USA
LC-MS QQQ	LC: 1200 Series, MS: TripleQuad LC/MS 6410	Agilent Technologies, Santa Clara, USA
LC-MS QTOF	LC: 1260 Infinity, MS: Agilent 6540 Quadrupole	Agilent Technologies, Santa Clara, USA
HILIC columns for LC-MS	SeQuant ZIC-pHILIC column PEEK 150 × 2.1 mm, 5 µm	Merck Millipore, Burlington, USA
	SeQuant ZIC-pHILIC guard column PEEK 20 × 2.1 mm, 5 µm	Merck Millipore, Burlington, USA
LC columns for HPLC	ZORBAX Eclipse Plus C18 column 250 × 4.6 mm, 5 µm	Agilent Technologies, Santa Clara, USA
	ZORBAX Eclipse Plus C18 guard column 12.5 × 4.6 mm, 5 µm	Agilent Technologies, Santa Clara, USA
	Rezex ROA organic acid column H^+ 8 % column 300 × 7.8 mm, 8 µm	Phenomenex, Torrance, USA
	Rezex ROA organic acid column H^+ 8 % guard column 50 × 7.8 mm, 8 µm	Phenomenex, Torrance, USA
Bench-top rotary shaker	HAT CH-4203	Infors HT, Bottmingen, Switzerland

Table 3.8.: Software and databases employed in this thesis.

Software	Manufacturer
Windows XP (SP5)	Microsoft, Redmond, USA
Windows 8.1	Microsoft, Redmond, USA
Office 2010	Microsoft, Redmond, USA
Office 2013	Microsoft, Redmond, USA
LABVIEW 2009 SP1	National Instruments, Austin, USA
MatLab R2014b	The MathWorks, Natick, USA
Mass Hunter Workstation (Ver. B.05.519.0)	Agilent Technologies, Santa Clara, USA

Databases	Link
KEGG	`http://www.genome.jp/kegg/`
Biocyc	`http://biocyc.org/`
CoryneRegNet	`http://coryneregnet.compbio.sdu.dk/v6/index.html`

2500 V, 2 mm gap width cuvettes) according to a slightly modified protocol after Dower et al. (1988). Plasmids were amplified in *E. coli* DH5α cells and eventually isolated using a commercial plasmid preparation kit (E.Z.N.A. Plasmid Mini kit I, Omega Bio-Tek Inc., Norcross, Georgia, USA).

Correct plasmids were verified by sequencing (GATC Light run service, Konstanz, Germany) using the generic primer pair pK19fw_seq and pK19rev_seq. Competent cells of ATCC 13032 [preparation according to Kirchner & Tauch (2003)] with slight modifications: cells were harvested at OD = 1.75 and washed three times with 10 % (v/v) glycerol] were transformed with (300–800) ng of the appropriate plasmid preparation by electroporation [Eppendorf Eporator, 2500 V, 2 mm gap width, achieving time constants of (4.3–4.7) ms] in accordance with an optimized protocol (van der Rest et al., 1999). Excision of the vector backbone was promoted in the presence of sucrose by the *sacB* gene on the plasmid as described by Schäfer et al. (1994). The gene deletion was finally confirmed by colony polymerase chain reaction (PCR) using the appropriate amplification primer pair flank1_fw and flank2_rev for either of the genes resulting in a 1000 bp amplification product.

Re-engineering of the $C \rightarrow G$ point mutation inside cg2831 (*ramA*) was carried out with the pK19mobsacB integration/deletion system as before. Primers overlapping at the point mutation were designed and the point mutation itself was encoded on both primers. Regions of 500 bp flanking the point mutation (cf. table 3.10: ramA-flank1_fw + ramA-flank1_rev and ramA-flank2_fw + ramA-flank2_rev) were amplified by PCR

and inserted simultaneously in *Hind*III, *Bam*HI linearized pK19mobsacB by isothermal assembling (Gibson, 2011).

Vector integration and excision of the backbone was performed as described above. The point mutation was finally confirmed by sequencing of the PCR product using the primer pair ramAfw_seq and ramArev_seq (cf. table 3.11). Overexpression of cg0936 (*rpf1*) and cg1296 in *C. glutamicum* was based on the replicative pVWEx1 vector construct, allowing strong IPTG inducible expression of the target gene under control of the hybrid promoter P_{tac}. The respective gene was amplified from the genomic DNA of *C. glutamicum* ATCC 13032 with the primer pair indicated in table 3.9. The purified PCR product was inserted in *Pst*I and *Bam*HI linearized pVWEx1 by isothermal assembling as before.

Table 3.9.: Overview of all bacterial strains generated within this thesis.

Strain	Specification
C. glutamicum Δcg1296	deletion of gene Δcg1296 in ATCC 13032 background
C. glutamicum Δcg3329	deletion of gene Δcg3329 in ATCC 13032 background
C. glutamicum Δcg3374	deletion of gene Δcg3374 in ATCC 13032 background
C. glutamicum (pFEM18)	for strong inducible expression of cg0936 (*rpf1*)
C. glutamicum (pFEM19)	for strong inducible expression of cg1296
C. glutamicum ramA(C302G)	point mutation yielding phenotype: RamA(S101C) (*ramA* = cg2831)

3.6. Seedtrain

Preculture cultivation was carried out in several stages forming a seedtrain as described in the following section to generate biomass for the main cultivation.

3.6.1. Cryogenic cultures

For the preparation of cryogenic cultures, cells grown in 2 × TY medium in glass reaction tubes were harvested at an OD of 5. 700 µL of the cell suspension was thoroughly mixed with 300 µL sterile glycerin and stored at −70 °C as working cell bank.

Table 3.10.: Overview of amplification primers. Regions binding to the respective genomic sequence are depicted in uppercase. Sequences designed for overlaps during Gibson assembly are depicted in lowercase. Nucleotides encoding the point mutation in *ramA* for the Ser → Cys substitution on the protein level are printed in bold.

Name	Sequence (5'→3')	PCR amplification product
cg1296-flank1_fw	cctgcaggtcgactctagaggatccCGGGATAGGTATTCGGAGGC	flank1 (cg1296)
cg1296-flank1_rev	aataaaccaaGGCACTATAATAGACCTAGTATCTATAGATTGATAG	
cg1296-flank2_fw	ttatagtgccTTGGTTTATTGGCGCCTCGT	flank2 (cg1296)
cg1296-flank2_rev	gtgcttgcggcagcgtgaagctagcCAATTCTGCTTTTGGATGAACC	
cg3329-flank1_fw	cctgcaggtcgactctagaggatccGACATCACCACGGCACAGTT	flank1 (cg3329)
cg3329-flank1_rev	ttaatgcgctAGCGATTCCTTAAATTCGGG	
cg3329-flank2_fw	aggaatcgctAGCGCATTAACGGTAAAGTG	flank2 (cg3329)
cg3329-flank2_rev	gtgcttgcggcagcgtgaagctagcAGCACTGGTCAAACATGGTG	
cg3374-flank1_fw	cctgcaggtcgactctagaggatccGGATAATACTTGCTAACCGTCCTAAAC	flank1 (cg3374)
cg3374-flank1_rev	caactctcctCAAAGGCTCCATTCGATCGA	
cg3374-flank2_fw	ggagcctttgAGGAGAGTTGACATGAAGGTTTTC	flank2 (cg3374)
cg3374-flank2_rev	gtgcttgcggcagcgtgaagctagcAAACCATCCCCTGCCTCATC	
rpf1_fw	attacgccaagcttgcatgcctgcagAAATGAGAGGAAAACTTTTCATG	rpf1
rpf1_rev	aattcgagctcggtacccggggatccTTAGCCGACGAAAGCG	
cg1296_fw	attacgccaagcttgcatgcctgcagACTAGGTCTATTATAGTGCCATGAG	cg1296
cg1296_rev	aattcgagctcggtacccggggatccCTATCCCACCACCTCCTC	
ramA-flank1_fw	aacagctatgaccatgattacgccaagcttGGGGGTTAACTACCTCTTCGG	flank1 ramA(c302g)
ramA-flank1_rev	cgacaatG**C**AATGAAGGCCC	
ramA-flank2_fw	GGGCCTTCATT**G**Cattgtcg	flank2 ramA(c302g)
ramA-flank2_rev	agtgaattcgagctcggtacccggggatccTTAAGGCAGTGCGCCGATC	

Table 3.11.: Overview of sequencing primers.

Name	Sequence (5'→3')
pK19fw_seq	CAGGCTTTACACTTTATGC
pK19rev_seq	ACCTGCTTTCTCTTTGCG
pVWEx1fw_seq	GGTTCTGGCAAATATTCTG
pVWEx1rev_seq	TGCCGCCAGGCAAATTC
cg1296fw_seq	GTTGAATCGGCAGTGTTC
cg1296rev_seq	CAAAGAGTCAGGATAACG
ramAfw_seq	GTTGCAGGACAATCGCC
ramArev_seq	CCCATCTCTTCAGCAGC

3.6.2. Precultures

Cryogenic cultures were spread on 2 × TY agar plates. After incubation for (48–60) h at 30 °C, colonies were used to inoculate 5 mL of 2 × TY complex medium filled in glass reaction tubes, forming the preculture stage 1. 8 h later, the content of one reaction tube was used to inoculated 50 mL of CGXII medium containing 40 g L^{-1} glucose filled in 500 mL sterile baffled shaking flasks. This second preculture stage (stage 2) was incubated overnight for (10–13) h. All pre-culture stages were incubated at 30 °C on a bench-top rotary shaker at 120 min^{-1}. On the day of the main cultivation, the second preculture was used to inoculate CGXII medium in another shaking flask or in a bioreactor.

3.7. Cultivation systems for main cultures

Main cultivations were performed in different scales: (i) 500 mL shaking flasks with a reaction volume of 50 mL; (ii) triple glass reactor system with three identical and in parallel-operated bioreactors with a reaction volume of 200 mL (working volume: 250 mL); (iii) lab-scale bioreactor (KLF) with a reaction volume of either 1.2 or 1.5 L (working volume: 3 L).

3.7.1. Cultivation in shaking flasks

Main cultivations in shaking flasks were initiated with 45 mL complemented CGXII minimal medium. Inoculum from the preculture stage 2 was harvested and centrifuged for 10 min at 7173×g and 4 °C. The supernatant was discarded and the biomass pellet was resuspended in 5 mL sterile 0.9 % (w/v) NaCl-solution to reach an OD of 1 (carbon source: glucose) or 2 (carbon source: acetate).

3.7.2. Batch cultivation in triple glass reactor system

For supplementation experiments described in section 4.1 and Graf et al. (2018) (cf. section A), a reactor system with three identical glass vessels was employed which were operated in parallel. Each vessel was equipped with a dissolved oxygen (pO_2) probe and a pH probe. The pO_2-probes were calibrated at 30 °C in the bioreactors (0 %-setpoint was set by aeration with N_2; 100 %-setpoint was set with aeration of process air), whilst pH probes were calibrated externally using pH 4 and pH 7 buffers. Heating jackets on each reactor ensured constant temperatures. For aeration, compressed air was channeled

through individual mass flows and filtered aseptically before entering each bioreactor. Mixing of the liquid volume was realized via magnetic stirrers, whilst vortexes were prevented with baffles mounted on the stirrer shafts. Reactors were filled with specific growth media and after calibration of pO_2- and pH-probes, the full-equipped vessels were autoclaved for 20 min at 121 °C. After cooling down, the sterile supplements were added aseptically via syringes. Process conditions of the supplementation experiments are given in in section 4.1 and Graf et al. (2018) (cf. section A).

3.7.3. Batch cultivation in lab-scale bioreactor (KLF)

Batch cultivations for amino acid supplementation experiments (section 4.1 and Graf et al. (2018); cf. section A) and growth evolution studies (section 4.8.1 and Graf et al. (2019); cf. section B) were performed in a 3 L laboratory-scale steel bioreactor (KLF) equipped with cooling and heating elements, a temperature sensor, a pO_2-probe, and a pH probe. A pressure sensor was installed at the head of the reactor, an automatic exhaust valve was used to regulate pressure in the reactor, and molar fractions of O_2 and CO_2 were monitored in the exhaust gas. For aeration, compressed air was channeled through a mass flow controller and filtered aseptically before entering the bioreactor. Mixing of the liquid phase was realized with a Rushton turbine, whilst vortexes were prevented by baffles. Prior to fermentation, the reactor was sterilized with 1 mol L^{-1} K_2HPO_4/1 mol L^{-1} KH_2HPO_4 buffer (pH 7) for 20 min at 121 °C. The drain of the reactor was sterilized *in situ* with pure steam for 10 min and the buffer was removed. The KLF was then filled with separately sterilized and complemented CGXII medium. Process and operation conditions are given in section 4.1 and Graf et al. (2018) (cf. section A) for amino acid supplementation experiments and in section 4.8.1 and Graf et al. (2019) (cf. section B) for ALE experiments.

3.7.4. Continuous cultivation in KLF

Continuous cultivations were performed in the same KLF bioreactor described in section 3.7.3. To enable a continuous process in chemostat mode at a fixed dilution rate (D), an advanced controller scheme as described in Graf et al. (2019) (cf. description and figure 1 in section B) was implemented to maintain a defined reaction volume in the bioreactor and constant feed and harvest rates. The initiation of a chemostat process from a previous batch cultivation is given in Graf et al. (2019) (cf. section B). Shortly

summarized for the ALE studies, CGXII minimal medium (Buchholz et al., 2014b) supplemented with $10\,g\,L^{-1}$ glucose and varying amounts of YE was employed as growth medium, whilst dilution rates were altered whenever constant process parameters, i.e. constant respiratory signals, could be observed. For more details and process parameters, the reader is kindly referred to Graf et al. (2019) (cf. section B).

In contrast to this, investigations of *C. glutamicum*'s growth under metabolic stationary conditions (cf. section 4.4) at $D = 0.2$, 0.3, and $0.4\,h^{-1}$ differed: (i) CGXII minimal medium ($12\,g\,L^{-1}$ glucose) was supplemented with $30\,mg\,L^{-1}$ PCA; (ii) a working volume of 1.5 L was used, and fixed impeller speeds of 700 rpm and aeration rates of $1\,L\,min^{-1}$ were installed independently from the dilution rate; (iii) antifoam agent was added with varying feed rates of (80–160) $\mu L\,h^{-1}$ to maintain a constant antifoam concentration of $267\,\mu L\,L^{-1}$; (iv) dilution rates were only increased if the set dilution rate had been hold for at least five residence times (RTs) which is considered as threshold for metabolic stationarity (Zamboni et al., 2009). Thus, at $D = 0.2\,h^{-1}$ the chemostat was not perturbed for 25 h, at $D = 0.3\,h^{-1}$ for 16.67 h, and at $D = 0.4\,h^{-1}$ for 12.5 h. After these periods, biosuspension samples were withdrawn for biomass determination (OD and CDW measurements), to produced cell-free filtrates, and to determine total inorganic carbon (TIC) and organic carbon (TOC). Moreover, metabolome and transcriptome samples were taken as described in section 3.11.1 and section 3.12, respectively. Sampling was repeated for three times in 1.5 h intervals for all growth rates and in all processes. Each chemostat process was completed with a dynamic wash out (cf. section 3.10.2) by setting $D \approx 0.6\,h^{-1}$ and following the decline of biomass over time. All chemostat processes were performed in biological triplicates.

3.8. Stationary ^{13}C-labeling in chemostat mode

3.8.1. Process setup and characterization of feed switch

An isotopic ^{13}C-labeling experiment was performed in chemostat mode to record the progress of ^{13}C-labeling patterns in intracellular metabolites to ultimately simulate carbon flux distributions in *C. glutamicum*'s CCM via MFA. Therefore, the first phase of ^{13}C-labeling was performed as non-stationary labeling experiment that requires rapid metabolome sampling to capture non-stationary ^{13}C-patterns in intracellular metabolites. The second phase of ^{13}C-labeling was executed as a stationary labeling experiment by maintaining the ^{13}C-feed until stationary labeling patterns in metabolites were achieved.

For this expanded stationary labeling experiment, the 'standard' continuous bioreactor setup introduced in section 3.7.4 was technically expanded. Firstly, a semi-automatic sampling device was installed in the harvest tubing of the bioreactor for rapid sampling during the non-stationary phase. The device was able to automatically provide 1 mL of biosuspension and samples were withdrawn in 4 s-intervals. Secondly, the feed section was altered to enable a switch from a ^{12}C- to a ^{13}C-labeled feed reservoir without sabotaging the cell's metabolic steady state. The setup is depicted in figure 3.1 and the feed switch was performed as following. Situated behind the ^{12}C-feed reservoir, a T-piece was integrated in the tubing indicated by ① in the figure. A second T-piece ② connected the ^{13}C-reservoir and a sterile syringe ③. In non-labeling mode, T-piece ① was disconnected from the ^{13}C-feed reservoir by a hose clamp. Prior to switching the feeds, the syringe was used to draw the labeled medium from the reservoir into the connecting tubing. Since the tubing between T-piece ① and ② was disconnected by the hose clamp, the ^{12}C- and ^{13}C-feeds were separated by an air bubble, whose size depended on the length of tubing between T-pieces ① and ②. To initiate the ^{13}C-feed, the clamp was removed and simultaneously, another one was placed between the ^{12}C-feed and T-piece ①. Thereby, withdrawal of medium from the unlabeled feed reservoir was stopped and instead drawn from the labeled reservoir. The exact moment of the labeling start could be determined by following the the air bubble's progress into the bioreactor.

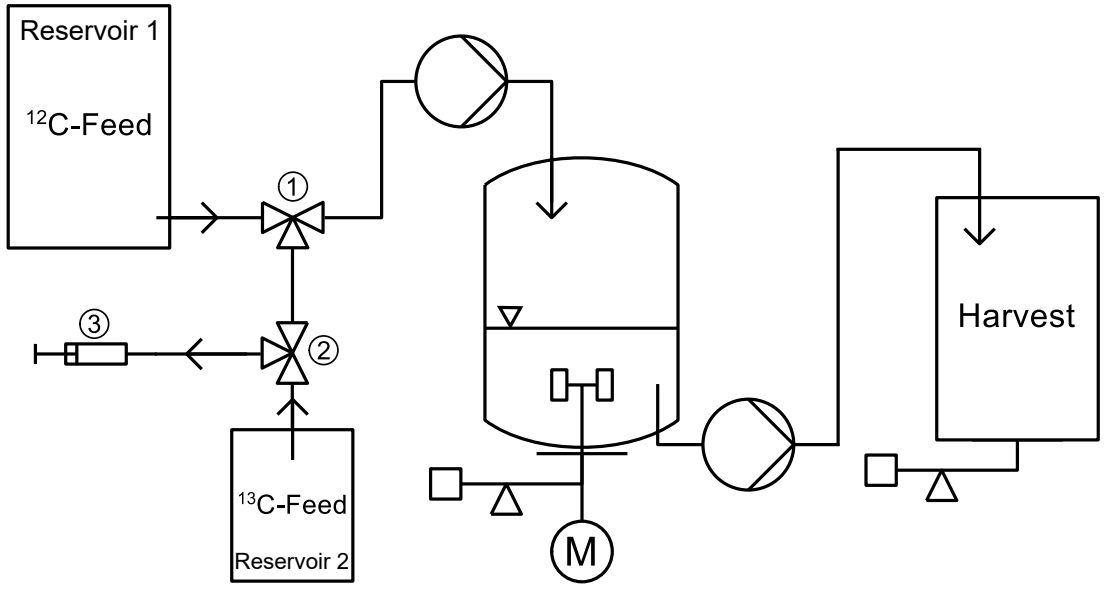

Figure 3.1.: Illustration of the experimental setup employed to switch between ^{12}C- and ^{13}C-feed in a continuous bioreactor.

To test the functionality of the setup, a salt-tracer experiment was performed under process conditions (dilution rate $D = 0.4\,h^{-1}$, $p = 1.5\,bar$) to imitate the ^{12}C-^{13}C-switch. Therefore, reservoir 1 was filled with demineralized water and reservoir 2 with a K_2HPO_4-KH_2PO_4 buffer solution. A probe was installed in the vessel to measure the conductivity of the working volume in time intervals of seconds (illustrated by the gray line in figure 3.2). In the exact moment the air bubble entered the bioreactor and therefore vanished from view, a timer in the process control system of the reactor was started (cf. dotted line at 200 s in figure 3.2). As soon as the conductivity signal surpassed the mean value (dashed line) of deionized water ± the standard deviation (black lines), visible by a sharp increase of conductivity, the tracer solution had reached the liquid phase. According to three individually performed experiments, the time lag between the vanishing of the air bubble and increase of conductivity was 5 s which was then considered in the following design of the sampling plan for the ^{13}C-labeling experiment (cf. table D.8).

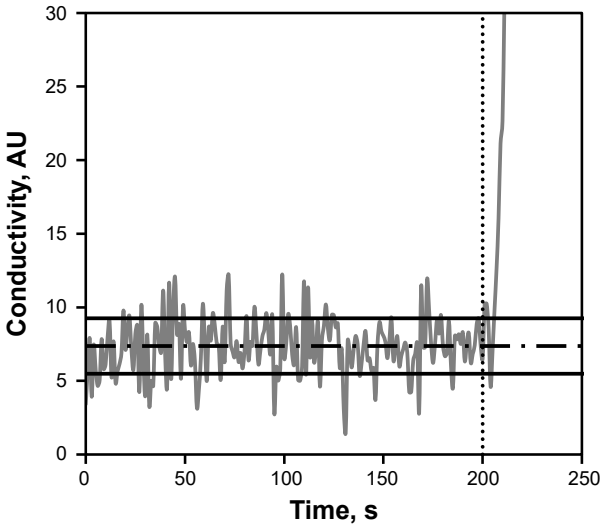

Figure 3.2.: Illustration of the conductivity signal (gray line) over time after deionized water feed was replaced by a tracer solution feed to simulate the ^{12}C-^{13}C-feed switch of the ^{13}C-labeling experiment. 5 s after the salt solution entered the bioreactor (indicated by the dotted line at t = 200 s), the conductivity signal abruptly rose above the mean value (dashed line) ± standard deviation (black line) from deionized water.

3.8.2. Experimental design study

An EDS was performed by our project partners at FZJ to determine the ideal ^{13}C-labeled glucose mixture producing unique and 'informative' patterns in CCM metabolites of

C. glutamicum. Thus, mixing 67 % uniformly labeled ^{13}C- (U-^{13}C) and 33 % C_1-^{13}C-glucose was identified as the mixture of choice (Mix I) and simultaneously proved to be the most cost-effective option in comparison to other mixtures (c.f. figure 3.3). Moreover, the EDS predicted that stationary labeling patterns at a growth rate of 0.4 h^{-1} in CCM metabolites are reached after 3 RT (7.5 h), whilst amino acid pools should display constant labeling patterns after 4 RT (10 h). Thus, the ^{13}C-labeling phase should be held up for at least 4 residence times at $D = 0.4\,h^{-1}$ equaling 10 h to produce stationary ^{13}C-patterns for the stationary-labeling part of the experiment. Besides, the EDS confirmed that the 4 s intervals between metabolome samples in the preliminary non-stationary labeling phase of the experiment should be fast enough to capture non-stationary labeling patterns of CCM metabolites. With this information, a sampling scheme for both labeling phases was designed as given in table D.8.

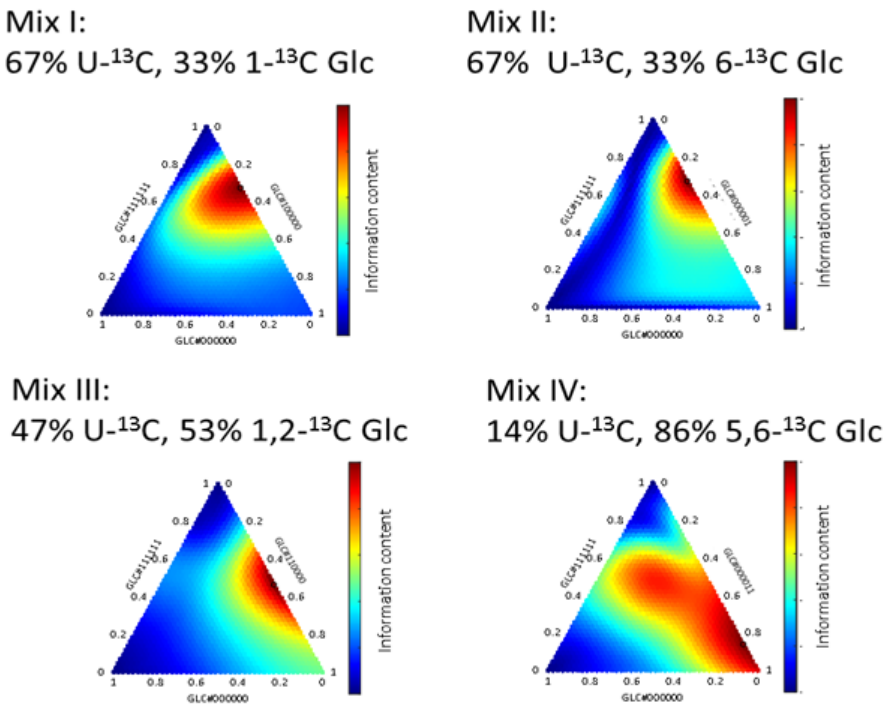

Figure 3.3.: Illustrations of potential ^{13}C-glucose mixtures for employment in the isotopic ^{13}C-experiment. Mix I was revealed as most informative and cost-effective. The experimental design study was kindly performed by our project partners Dr. Katharina Nöh and Dr. Martin Cerff of the FZJ.

3.8.3. Cultivation and process parameters

The continuous ^{13}C-labeling experiment was prepared and initiated as described in section 3.7.4 with a working volume of 1.2 L, a fixed dilution rate of $D = 0.4\,h^{-1}$, and application of CGXII minimal medium supplemented with $30\,mg\,L^{-1}$ PCA and $12\,g\,L^{-1}$ glucose as growth medium. Two media reservoirs containing ^{12}C- and ^{13}C-glucose, respectively, were prepared at the same time. Thereby, the chance of disrupting the metabolic steady state after the feed switch due to media aging was diminished. After the initiating batch phase, a constant stirrer speed of 600 rpm and an aeration rate of $0.8\,L\,min^{-1}$ were installed in the bioreactor and maintained during the experiment. The overall process was divided into the ^{12}C-phase and the ^{13}C-labeling-phase. In the unlabeled phase, samples for biomass determination and cell-free filtrates, and TIC and TOC measurements were taken after more than five RTs to ensure a metabolic steady state. The ^{13}C-labeling-phase was started by switching to the labeled feed and immediate sampling in 4 s-intervals within the first minute. Sampling intervals were exponentially increased afterwards according to the sampling plan (cf. table D.8). Cold methanol quenching was performed to quench all metabolic activities of the cell, intracellular metabolites were extracted and measured as described in section 3.11.1.

3.9. Analytical methods

Bioprocesses were followed and evaluated by determination of biomass formation, analyzing substrates and products in cell-free filtrates via enzymatic assays and high pressure liquid chromatography, and by determination of total amounts of (in)organic (TIC, TOC) carbon and nitrogen (TN).

3.9.1. Detection of biomass formation

Biomass growth in main cultivations was followed by the OD of the cell suspension and determined gravimetrically after the processes to obtain the cell dry weight (CDW). OD was measured as described in Graf et al. (2018). CDW was determined in 1 mL scale in supplementation experiments [Graf et al. (2018); cf. section A] and in ALE studies [Graf et al. (2019); cf. section B].

In the chemostat experiments (stationary growth investigation and in the labeling experiment; cf. section 4.4 and section 4.7), CDW analysis was performed as following.

Glass reaction tubes were dried at 120 °C for 48 h in a drying oven, subsequently left to cool in an exsiccator for at least 30 min, and weighted with a microbalance. During cultivations, technical triplicates of 1.5 (labeling experiment) or 3 mL (stationary growth investigation) cell suspension were filled into the reaction tubes that were subsequently centrifuged at 3000 × g and 4 °C for 10 min. The supernatant was discarded, the residual cell pellet was washed with 5 mL deionized water and again centrifuged. This washing step was repeated for two times and the resulting biomass samples were dried at 120 °C for 48 h to remove residual liquid in the pellets. Subsequently, the biomass-containing tubes were left to cool down in an exsiccator for at least 30 min and weighed again. The difference in weight between the empty and filled tubes gives the CDW.

3.9.2. Determination of extracellular metabolite concentrations

To determine extracellular glucose, pyruvate, and amino acid concentrations, biosuspension was directly filtrated after sampling through 0.20 µm syringe filters and stored at −20 °C until further analysis. Glucose and amino acid concentrations were determined as given in Graf et al. (2018) (cf. section A). Pyruvate was quantified as described in Graf et al. (2019) (cf. section B).

3.9.3. Determination of total carbon and nitrogen amounts

Determination of TIC and TOC of biosuspension, biomass, and cell-free samples was performed as described in Graf et al. (2018) (cf. section A).

3.10. Quantification of bioprocesses and data analysis

In this thesis, batch cultivations and continuous bioprocesses were conducted. Determination of process-dependent kinetic parameters is presented in the following for each process type. Since nearly all cultivations were performed with one limiting substrate (typically the carbon source), Monod-kinetics (Monod, 1949) were moreover applied when appropriate.

3.10.1. Kinetic parameters of batch processes

A bioreactor operated in batch mode presents a closed system where all essential nutrients are provided at the beginning of the process. During the cultivation, no further substrates

except for oxygen via aeration, base for titration, and carbon dioxide via the exhaust are added or removed. To calculate corresponding physiological parameters of the exponential growth phase (cf. figure 2.2), where the strain is in a metabolic pseudo steady-state (cf. section 2.2.1), mass balances of a closed system are employed.

Exponential growth rate

The exponential growth rate μ (in h^{-1}) of a cell cultivated in a batch process is derived from the biomass balance of a closed system:

$$\frac{dm_x}{dt} = \mu\, c_x\, V_R \qquad [1]$$

where m_x (in g) is the mass of the biomass, c_x (in $g\,L^{-1}$) the concentration, and V_R (in L) the reaction volume. Substitution of m_x with $m_x = c_x\, V_R$ gives the left hand side of Eq. 1:

$$\frac{dm_x}{dt} = \frac{d(c_x\, V_R)}{dt} = \frac{dc_x}{dt}\, V_R + \frac{dV_R}{dt}\, c_x \qquad [2]$$

Since the working volume in batch processes is constant ($dV_R/dt = 0$), Eq. 2 is reduced to:

$$\frac{dm_x}{dt} = \frac{dc_x}{dt}\, V_R \qquad [3]$$

A simplified biomass balance for a batch fermentation is gained by introducing Eq. 3 into Eq. 1:

$$\frac{dc_x}{dt} = \mu\, c_x \qquad [4]$$

Finally, the exponential growth rate μ is calculated as:

$$\mu = \frac{1}{c_x}\frac{dc_x}{dt} \qquad [5]$$

During the exponential growth phase, μ is approximately constant over the period of time $t_0 ... t_1$, whereby integration of the differential leads to:

$$\mu = ln\left(\frac{c_{x,1}}{c_{x,0}}\right)\frac{1}{t_1 - t_0} \qquad [6]$$

Considering only one limiting substrate in the growth medium, the Monod-equation (Monod, 1949) can be applied:

$$\mu = \mu_{max}\frac{c_s}{K_s + c_s} \qquad [7]$$

where μ_{max} (in h^{-1}) is the maximum growth rate of the strain in the employed growth medium. K_s (in $g\,L^{-1}$) is the half-saturation constant that equals the concentration leading to the half maximum growth rate. Assuming that $c_s >> K_s$ in the exponential growth phase, which is conform for, e.g. glucose concentrations significantly larger than $14\,\mu mol\,L^{-1}$ (Lindner et al., 2011) for *C. glutamicum* WT, $c_s/(c_s + K_s) \approx 1$ and Eq. 7 simplifies to:

$$\mu = \mu_{max} \quad [8]$$

Consequently, when a single substrate is supplemented unlimited to the organism, the exponential growth rate equals the maximum growth rate in the installed growth environment. Inserting Eq. 6 into Eq. 8 leads to the integral:

$$\mu_{max} = ln\left(\frac{c_{x,1}}{c_{x,0}}\right)\frac{1}{t_1 - t_0} \quad [9]$$

Equation Eq. 9 was used to calculate (maximum) specific growth rates of *C. glutamicum* cultivated in batch processes using linear regression of logarithmic biomass formation over the process time.

Specific substrate consumption rate

The specific substrate consumption rate q_s (in $g\,g^{-1}\,h^{-1}$) of a strain in a batch cultivation is derived from the substrate balance of a closed system:

$$\frac{dm_s}{dt} = -q_s\,c_x\,V_R \quad [10]$$

where m_s (in g) is the substrate mass and q_s is defined as a positive parameter. Assuming that V_R and q_s are constant over a considered period of time $t_o...t_1$ leads to:

$$\int_0^1 dm_s = -q_s\,V_R\int_{t_0}^{t_1} c_x\,dt \quad [11]$$

Substituting $c_x\,dt$ with Eq. 4 and presuming that μ is constant over $t_0...t_1$ gives:

$$\int_0^1 dm_s = \frac{-q_s}{\mu}\,V_R\int_0^1 dc_x \quad [12]$$

With a constant V_R, $m_s = c_s V_R$ and Eq. 12 simplifies to:

$$\int_0^1 dc_s = \frac{-q_s}{\mu} \int_0^1 dc_x \quad [13]$$

After integration, q_s is received:

$$q_s = \mu \frac{c_{s,0} - c_{s,1}}{c_{x,1} - c_{x,0}} \quad [14]$$

All specific substrate consumption rates of batch cultivations were calculated as stated in Eq. 14 using the biomass substrate yield as presented in the following Eq. 15.

Biomass substrate yield

The biomass substrate yield Y_{xs} (in $\mathrm{g\,g^{-1}}$) is defined as ratio between biomass growth and substrate consumption:

$$Y_{xs} = \frac{\mu}{q_s} \quad [15]$$

Inserting Eq. 14 into Eq. 15 gives:

$$Y_{xs} = \frac{c_{x,1} - c_{x,0}}{c_{s,0} - c_{s,1}} \quad [16]$$

Thereby, biomass substrate yields were preliminary determined by linear regression of biomass-substrate curves and further used to calculate the specific substrate consumption rate.

Oxygen consumption rate

Calculation of the specific oxygen uptake rate OUR (in $\mathrm{mol\,L^{-1}\,h^{-1}}$) is based on the assumption that oxygen in the gas phase and dissolved oxygen in the liquid phase are in equilibrium. It is furthermore presumed that the oxygen demand of the cells Q_{O_2} (in $\mathrm{mol\,L^{-1}\,h^{-1}}$) equals their oxygen uptake:

$$Q_{O_2} = OUR = \frac{\Delta \dot{n}_{O_2}}{V_R} \quad [17]$$

where $\Delta \dot{n}_{O_2}$ (in $\mathrm{mol\,h^{-1}}$) is the absorbed oxygen mass flow calculated by the difference of molar oxygen influx and efflux:

$$\Delta \dot{n}_{O_2} = \dot{n}_{O_2,in} - \dot{n}_{O_2,out} \quad [18]$$

$\dot{n}_{O_2,in}$ is the incoming oxygen mass flow in the inlet gas and $\dot{n}_{O_2,out}$ the residual amount of oxygen in the exhaust gas. Inserting the ideal gas law:

$$p\,\dot{V}_g = \dot{n}\,R\,T \qquad [19]$$

where $\dot{V}_g$ (in $\mathrm{L\,h^{-1}}$) is the volumetric gas flow rate, $R = 8.314\,\mathrm{J\,mol^{-1}\,K^{-1}}$ the universal gas constant, and T (in K) and p (in Pa) the calibration temperature and pressure of the mass flow controller used for ventialtion of the bioreactor. Further assuming isobaric and isothermal conditions in the inlet and outlet gas flow, Eq. 18 is transformed:

$$\Delta\dot{n}_{O_2} = (\dot{V}_{g,in}\,y_{O_2,in} - \dot{V}_{g,out}\,y_{O_2,out})\frac{p}{RT} \qquad [20]$$

$y_{O_2,in}$ and $y_{O_2,out}$ are volumetric oxygen fractions and $\dot{V}_{g,in}$ and $\dot{V}_{g,out}$ are the volumetric gas flow rates of the inlet and exhaust gas. $\dot{V}_{g,in}$ and $\dot{V}_{g,out}$ are determined with an inert gas balance leading to the ratio:

$$\frac{\dot{V}_{g,in}}{\dot{V}_{g,out}} = \frac{1 - y_{O_2,out} - y_{CO_2,out}}{1 - y_{O_2,in} - y_{CO_2,in}} \qquad [21]$$

where $y_{CO_2,in}$ and $y_{CO_2,out}$ are carbon dioxide fractions of the inlet and outlet. Inserting this equation into Eq. 20 gives:

$$\Delta\dot{n}_{O_2} = \frac{p}{RT}\dot{V}_{g,in}\left(y_{O_2,in} - y_{O_2,out}\left[\frac{1 - y_{O_2,in} - y_{CO_2,in}}{1 - y_{O_2,out} - y_{CO_2,out}}\right]\right) \qquad [22]$$

Consequently, OUR can be calculated as:

$$OUR = \frac{p}{RT}\frac{\dot{V}_{g,in}}{V_R}\left(y_{O_2,in} - y_{O_2,out}\left[\frac{1 - y_{O_2,in} - y_{CO_2,in}}{1 - y_{O_2,out} - y_{CO_2,out}}\right]\right) \qquad [23]$$

Thus, measurement of molar oxygen and carbon dioxide fractions of the inlet and exhaust gas enables determination of OUR. The specific oxygen uptake rate q_{O_2} (in $\mathrm{mol\,g^{-1}\,h^{-1}}$) is deduced from OUR:

$$q_{O_2} = \frac{OUR}{c_x} \qquad [24]$$

q_{O_2} in batch cultivations is calculated using linear regression of OUR and biomass formation curves.

Carbon Dioxide Evolution Rate

In analogy with OUR, the carbon dioxide evolution rate CER (in $\mathrm{mol\,L^{-1}\,h^{-1}}$) is determined:

$$CER = \frac{p}{RT}\frac{\dot{V}_{g,in}}{V_R}\left(y_{CO_2,out}\left[\frac{1 - y_{O_2,in} - y_{CO_2,in}}{1 - y_{O_2,out} - y_{CO_2,out}}\right] - y_{CO_2,in}\right) \quad [25]$$

Division of CER by the biomass concentration yields the specific carbon dioxide evolution rate q_{CO_2} (in $\mathrm{mol\,g^{-1}\,h^{-1}}$):

$$q_{CO_2} = \frac{CER}{c_x} \quad [26]$$

q_{CO_2} in batch cultivations is calculated using linear regression of CER and biomass formation curves. Since carbon dioxide is highly soluble in water, the measured amount of CO_2 in the exhaust gas only mirrors the produced amount of CO_2 by the cells if the liquid phase (biosuspension) is in equilibrium with the gas phase. Thereby, using CGXII minimal medium at pH 7.4 leads to an underestimation of produced carbon dioxide especially at the beginning of batch cultivations. This missing amount can be accounted for if total carbon (TC) analysis is performed as explained in section 3.10.3.

Respiratory Quotient

The respiratory quotient RQ (in $\mathrm{mol\,mol^{-1}}$) is an indicator for metabolic activity and is derived from CER and OUR:

$$RQ = \frac{CER}{OUR} \quad [27]$$

3.10.2. Kinetic parameters of continuous processes

The operation of a bioreactor in continuous mode is characterized by feed medium containing substrates essential for growth that is constantly added to the bioreactor, whilst cultivation broth comprising substrates, metabolic products, and biomass is simultaneously and constantly removed from the reactor (cf. section 2.2.2). Calculation of corresponding kinetic parameters are based on mass balances of open systems.

Growth rate

The growth rate in a continuous bioreactor is set by the dilution rate D (in $\mathrm{h^{-1}}$). This relation is derived in the following starting with the biomass mass balance of an open system:

$$\frac{dm_x}{dt} = \mu\, c_x\, V_R + c_{x,in}\, F_{in} - c_{x,out}\, F_{out} \quad [28]$$

where m_x (in g) is the current mass of the biomass in the reactor, c_x (in $\mathrm{g\,L^{-1}}$) is the biomass concentration, V_R (in L) is the working volume of the bioreactor, F (in $\mathrm{L\,h^{-1}}$) is the mass flow of feed entering (*in*) or cultivation broth leaving (*out*) the reactor. Assuming that (i) only sterile feed enters the reactor ($c_{x,in} = 0$), (ii) only ideally mixed components leave the reactor ($c_{x,out} = c_x$), and that (iii) V_R is constant ($F_{in} = F_{out} = F$, $dV_R/dt = 0$), Eq. 28 leads to:

$$\frac{dc_x}{dt} = c_x \left(\mu - \frac{F}{V_R} \right) \qquad [29]$$

The term F/V_R is generally referred to as the dilution rate D which is equal to the inverse mean residence time (in h) of liquid in a continuous reactor. According to Eq. 29, which is illustrated in figure 2.3, whenever $D < \mu_{max}$ biomass will accumulate ($dc_x/dt > 0$) in the reactor and when $D > \mu_{max}$ biomass will be washed out of the reactor ($dc_x/dt < 0$). Under process conditions where D and the substrate concentration of the feed ($c_{s,in}$) are kept constant, a steady state equilibrium will be finally reached ($dc_x/dt = 0$) and Eq. 29 becomes:

$$\mu\, \tilde{c_x} = D\, \tilde{c_x} \qquad [30]$$

Hence, if the trivial solution $c_x = 0$ is neglected, the dilution rate fixes the substrate concentration in the bioreactor at the exact value which makes μ equal to D (Herbert et al., 1956) and growth of new cells is balanced by washed out cells (Hoskisson & Hobbs, 2005).

Moreover, μ or D can be expressed in dependence of the generation time t_d (in $\mathrm{h^{-1}}$) of the cell population:

$$\mu = D = \frac{log(2)}{t_d} \qquad [31]$$

Metabolic steady state

Based on the derivation of Eq. 30, biomass and substrate concentrations at metabolic steady state of the cell (cf. section 2.2.2) can be calculated. Thus, the substrate mass balance is formulated as:

$$\frac{dm_s}{dt} = -q_s\, c_x\, V_R + c_{s,in}\, F_{in} - c_{s,out}\, F_{out} \qquad [32]$$

where q_s is the biomass specific substrate uptake rate (in $\mathrm{g\,g^{-1}\,h^{-1}}$). Using the same constraints (i)-(iii) as for the biomass balance, the definition for D, and the definition $q_s = \mu/Y_{xs}$ (see also paragraph below), Eq. 32 simplifies to:

$$\frac{dc_s}{dt} = -\frac{\mu}{Y_{xs}} c_x + D(c_{s,in} - c_s) \quad [33]$$

During metabolic steady state equilibrium, $dc_s/dt = 0$ and Eq. 30 apply whereby Eq. 33 becomes:

$$0 = -\frac{D}{Y_{xs}} c_x + D(c_{s,in} - c_s) \quad [34]$$

Assuming the strain follows Monod-type growth and μ_{max}, K_s, and Y_{xs} are dictated by the strain and the growth medium only (Herbert et al., 1956), inserting Eq. 7 into Eq. 30, and the resulting equation into Eq. 34 leads to the following expressions for the metabolic steady state concentrations of the substrate $\tilde{c_s}$ and of the biomass $\tilde{c_x}$:

$$\tilde{c_s} = K_s \frac{D}{\mu_{max} - D}, \qquad \tilde{c_x} = Y_{xs}(c_{s,in} - \tilde{c_s}) \quad [35]$$

Vice versa, a definition for the maximum specific growth rate is obtained:

$$\mu_{max} = D\left(\frac{K_s}{\tilde{c_s}} + 1\right) \quad [36]$$

Eq. 36 shows that μ_{max} can be obtained in continuous steady states whenever $\tilde{c_s} >> K_s$. This behavior is identical to the circumstances in exponential phase of a batch cultivation. Assuming that Monod-type growth applies and μ_{max}, K_s and Y_{xs} are known for the strain, the biomass and substrate steady state concentrations can be calculated in dependency of D using Eq. 35. Consequentially, figure 2.3 illustrates all non-trivial solutions for the steady state concentrations. In addition, the so-called critical dilution rate D_c which is equal to μ_{max} is shown. Approximating this region, c_x starts to decline while c_s increases and becomes unlimited ($c_s >> K_s$). If D_c is surpassed, however, the culture is washed out ($c_x = 0$) and c_s enhances to $c_{s,in}$.

Dynamic wash out

The region approximating D_c is highly sensitive for small changes in D, c_x or c_s making it difficult to estimate μ_{max}. Thus, Pirt & Callow (1960) proposed a theoretical approach to determine D_c which was experimentally evaluated by Esener et al. (1981):

I Estimate μ_{max} and establish a steady state at $D < \mu_{max}$.

II Increase D to $D + \Delta D > \mu_{max}$ at $t = 0$ where the strain grows at its maximum rate

III Measure the response of the culture via the CDW*

To obtain μ_{max} from the experimental data (III), $\mu \approx \mu_{max}$ (wash out) is inserted into Eq. 29, integrated and solved for c_x at time in point t:

$$c_{x,t} = c_{x,0}\, e^{(\mu_{max}-D)t} \quad [37]$$

where $c_{x,0}$ (in $\mathrm{g\,L^{-1}}$) is the biomass concentration at $t = 0$. Assuming that the strain instantaneously adapted to the increased dilution rate, linear regression of the logarithmic biomass depletion over the wash out time is used to determine μ_{max}. This procedure was performed at the end of stationary growth investigations to estimate μ_{max} of *C. glutamicum* WT grown in PCA-supplemented minimal medium (cf. section 4.4).

Glucose consumption rate

The glucose consumption rate of a cell cultivated in continuous mode can be calculated as given in Eq. 15 making use of the biomass substrate yield calculated with steady state concentrations:

$$Y_{xs} = \frac{\tilde{c_x}}{c_{s,in} - \tilde{c_s}} \quad [38]$$

and substituting μ with D (cf. Eq. 30):

$$q_s = \frac{D}{Y_{xs}} \quad [39]$$

Respiratory rates

Oyxgen consumption, carbon dixoide emission, and RQ are calculated as presented in Eq. 23, Eq. 25, and Eq. 27. Corresponding biomass specific rates are derived by division with the steady state biomass concentration:

$$q_{O_2} = \frac{OUR}{\tilde{c_x}} \quad [40]$$

$$q_{CO_2} = \frac{CER}{\tilde{c_x}} \quad [41]$$

*The oxygen uptake rate and the carbon dioxide evolution rate can also be used.

3.10.3. Carbon Balance

In order to verify the consistency of the obtained experimental data and the physiological understanding of the fermentation processes, an elemental carbon balance (C-balance) is performed. Therefore, a simple black box model is set up as shown in figure 3.4, where the carbon flowing into the system as substrate has to be recovered in carbon flowing out of the system in form of biomass, metabolic (by-)products and CO_2 (Stephanopoulos et al., 1998).

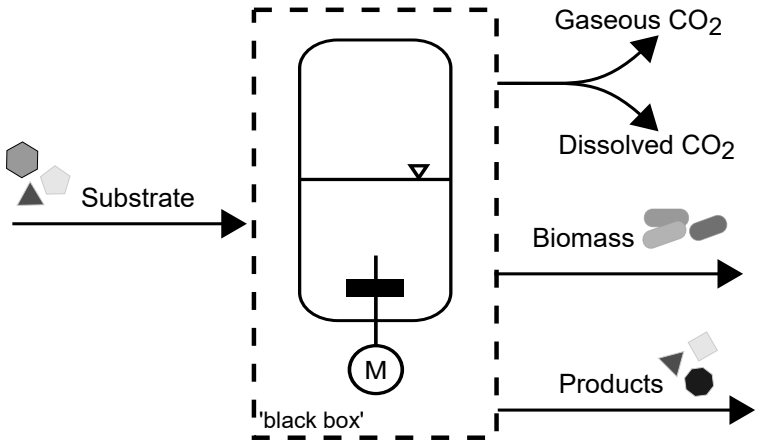

Figure 3.4.: Illustration of elemental carbon balancing as performed in this work. Inflowing carbon in the form of substrate is balanced by outflowing carbon in the form of gaseous CO_2 and dissolved CO_2 species in the liquid phase, biomass, and products. The system boundary of the balance is considered as 'black box' since the actual biochemical transformation processes are not considered. The figure was adapted from an illustration in Buchholz et al. (2014a)

The carbon source in the conducted cultivations varied but could be quantified by TOC analysis, whilst glucose was determined as given in section 3.9.2. (By-)products such as amino acids were determined via amino acid HPLC (cf. section 3.9.2). TOC analysis was employed to determine the carbon content of *C. glutamicum* biomass (cf. section 3.9.2). The percentage of carbon dioxide in the gas phase was calculated for batch cultivations by integrating the CER over the exponential growth phase to obtain the total amount of produced $CO_{2,G}$ $[\Delta n(C_{CO_{2,G}})]$. For continuous cultivations, CER could be used without integration (cf. Eq. 45 below). Through bacification of dissolved carbon dioxide ($CO_{2,L}$) in the biosuspension sample (Buchholz et al., 2014b), the carbonic acid (H_2CO_3) equilibrium (Eq. 42) was shifted towards bicarbonate (HCO_3^-) and carbonate (CO_3^{2-}). These inorganic carbon species, summarized as TIC-value, were quantified with

TC-analysis (cf. section 3.9.3).

$$CO_{2,L} + H_2O \rightleftharpoons H_2CO_3 \rightleftharpoons HCO_3^- + H^+ \rightleftharpoons CO_3^{2-} + H^+ \quad [42]$$

After quantification of all relevant compounds, values were converted to $C-mol$ and inserted in the elemental substrate based carbon balance:

$$C_{substrates} = C_{biomass} + C_{products} + C_{CO_{2,G}} + C_{TIC} \quad [43]$$

Carbon balancing was applied for batch and continuous cultivations. Molar amounts of carbon were determined in batch cultivations by integration of consumed or produced compounds over the time of the exponential growth phase:

$$\Delta n(C_{substrates}) = \Delta n(C_{biomass}) + \Delta n(C_{products}) + \Delta n(C_{CO_{2,G}}) + \Delta n(C_{TIC}) \quad [44]$$

In continuous processes, molar mass flows were used considering the reaction volume V_R and growth rate D:

$$\Delta \dot{n}(C_{substrates}) = \Delta \dot{n}(C_{biomass}) + \Delta \dot{n}(C_{products}) + CER + \Delta \dot{n}(C_{TIC}) \quad [45]$$

where the molar mass flows equal:

$$\Delta \dot{n}(C) = \frac{\Delta n(C) \cdot D}{V_R} \quad [46]$$

and the molar differences are:

$$\Delta n(C) = n(C_{in}) - n(C_{out}) \quad [47]$$

3.10.4. Fitting of Monod parameters

Deduced from the BHI supplementation experiments (cf. section 4.1), corresponding exponential growth rates of *C. glutamicum* revealed a Monod-type behavior with increasing concentration of BHI. Thus, parameters defining the Monod equation (Eq. 7), i.e. maximum growth rate μ_{max} and saturation constant of BHI K_{BHI}, were estimated with non-linear least squares fitting using the Curve Fitting Toolbox of Matlab. The detailed description is given in Graf et al. (2018) (cf. section A).

3.10.5. Determination of cellular maintenance parameters

In principle, the consumed substrate is used by microorganisms for proliferation, cellular maintenance purposes, and product formation. Cellular maintenance comprises functions such as proofreading, synthesis and hydrolysis of enzymes and RNA, cell motility, osmo-regulation, maintaining concentration gradients through transmembrane transport, protection against oxygen stress, and futile cycling (Bodegom, 2007). All these energy consuming reactions are described by the maintenance equation after Pirt (1982):

$$q_s = NGAM + GAM \quad [48]$$

where NGAM (in $\mathrm{g\,g^{-1}\,h^{-1}}$) is the non-growth associated maintenance parameter which comprises all non-growth related maintenance reactions, and GAM (in $\mathrm{g\,g^{-1}\,h^{-1}}$) is the growth associated maintenance parameter which comprises maintenance reactions that are dependent of the cell's growth rate. Equation Eq. 48 can be further resolved to:

$$q_s = m_s + \frac{\mu}{Y_{xs}^{real}} \quad [49]$$

where m_s (in $\mathrm{g\,g^{-1}\,h^{-1}}$) is the maintenance coefficient, and Y_{xs}^{real} (in $\mathrm{g\,g^{-1}}$) is the real biomass substrate yield that describes how much substrate is consumed by the cell to exclusively form biomass.

Both maintenance parameters m_s and Y_{xs}^{real} can be determined from linear regression of q_s-values versus the corresponding growth rate previously observed in continuous metabolic steady state cultivations. The intersection of the linear approximation curves with the ordinate delivers m_s, whilst its slope is equal to the reciprocal Y_{xs}^{real}.

3.10.6. Estimation of ATP biomass yield

The produced amount of adenosine triphosphate (ATP) in different supplementation scenarios was estimated (cf. section 4.1.1). Therefore, respiratory rates were preliminary deduced from carbon balancing (cf. section 3.10.3) under the assumption of a certain P/O-ratio. The P/O-ratio indicates the produced amount of ATP molecules from consumed amounts of oxygen. Thereby, qualitative information of the ATP-requirement of *C. glutamicum* under varying nutrient environments were gained. Gaussian error propagation (Eq. 50) was used to calculate standard deviations (SDs) of kinetic parameters, represented by function $f(x, y)$ in dependency of two variables x and y with known uncertainty (σ),

if no experimental SD was available. The calculation scheme is summarized in Graf et al. (2018) (cf. section A).

$$\sigma_f = \sqrt{\left(\frac{\partial f}{\partial x}\right)^2 \cdot \sigma_x^2 + \left(\frac{\partial f}{\partial y}\right)^2 \cdot \sigma_y^2} \qquad [50]$$

3.10.7. Estimation of ATP demand for amino acid biosynthesis

A modified approach based on the calculation scheme of Kaleta et al. (2013) was employed to estimate *C. glutamicum*'s ATP-demand to synthesize amino acids for 1 g biomass. Kaleta et al. (2013) calculated the value for *E. coli* based on the net ATP-amount of consumed and produced building blocks (precursors) from central metabolism for amino acid biosynthesis. Therefore, produced and consumed ATP, NADH, and NADPH amounts were balanced and ultimately transformed to ATP amounts employing a certain P/O-ratio. NADH and NADPH were considered for the production of ATP via the respiratory chain because *E. coli* equilibrates NADH- and NADPH-pools with membrane-bound nicotinamide nucleotide transhydrogenases. In contrast to Kaleta et al. (2013), produced amounts of ATP for precursor synthesis was not considered in this work since carbon fluxes towards main routes in CCM (glycolysis, pentose phosphate pathway) were unknown in this case. Besides, *C. glutamicum* does not posses transhydrogenases (Kabus et al., 2007) whereby NADPH was not considered as ATP-precursor in the calculations. With these adjustments, amounts of ATP-costs for amino acid synthesis in *C. glutamicum* were calculated and multiplied with the mean-amino acid composition of the strain as given in Graf et al. (2018) (cf. section A). This gives the total ATP-cost for synthesis of all amino acids in *C. glutamicum*.

3.11. Metabolome analysis

3.11.1. Biomass quenching and extraction of metabolites

Metabolome samples for quantification of intracellular metabolite pools or determination of ^{13}C-labeling patterns were withdrawn during the stationary growth investigations and continuous isotopic labeling experiment. Therefore, 2 mL biosuspension was withdrawn from the bioreactor for the fast centrifugation treatment, whilst (1–2) mL were taken for cold-methanol quenching. Different combinations of biomass quenching and intracellular metabolite extraction techniques were performed for samples from stationary growth

investigations, whilst cold-methanol quenching in combination with chloroform-methanol extraction was employed for the ^{13}C-experiment.

Cold-methanol quenching (MQ)

For immediate quenching of the metabolism, an adapted version of the original procedure from Koning & van Dam (1992) was used. 2 mL biosuspension was rapidly mixed after withdrawal from the bioreactor with 3 mL of 60 % (v/v) cold (−70 °C) methanol-solution. The mixture was centrifuged at 4000 ×g and −2 °C for 10 min, the supernatant transferred into a fresh tube, and the residual biomass pellet and the supernatant frozen in liquid nitrogen. Until further treatment, all samples were stored at −70 °C. After each step of the procedure, empty and filled reaction tubes were weighed for quantitative determination of the substances.

Fast-centrifugation-treatment (FCT)

Fast centrifugation was applied as proposed by Teleki et al. (2015). 2 mL biosuspension was centrifuged at 20817 ×g and −2 °C for 30 s, the supernatant discarded or collected, and the remaining cell pellet immediately frozen in liquid nitrogen.

Chloroform-methanol extraction (CE)

Following the treatment proposed by Koning & van Dam (1992), frozen cell pellets (from cold-methanol quenching or FCT) were resuspended in 1 mL cold (−20 °C) 50 % (v/v) methanol solution supplemented with 30 µmol L^{-1} L-norvaline as internal standard for LC-MS quantification. To permanently inactive enzymes and permeabilize cell membranes, 1 mL cold (−20 °C) chloroform was added. The suspension was mixed and incubated for 2 h at −20 °C in an overhead-shaker. Centrifugation of samples at 3824 ×g and −2 °C for 10 min divided the suspension into 3 phases: an aqueous, polar methanol phase containing the metabolites, an interphase containing proteins and cell debris, and a non-polar chloroform phase. The methanol phase containing intracellular metabolites was carefully removed and stored at −70 °C until measurement.

Hot-water-extraction (HWE)

For hot-water-extraction (HWE), the technique proposed by Teleki et al. (2015) was slightly modified. 30 µmol L^{-1} L-norvaline was added to the frozen cell pellets such that a biomass concentration between (15–50) g L^{-1} was obtained. Subsequently, the suspension was incubated in a water bath at 100 °C for 1 min, thoroughly mixed, and again

incubated for 5 min. Whilst the high temperature permanently inactivated enzymes, the temperature difference disrupted the cell membranes allowing the intracellular metabolites to diffuse into the extraction solution. Afterwards, samples were cooled and centrifuged at 20817 $\times g$ and 4 °C for 10 min. The metabolite-containing supernatant was carefully removed and stored at −70 °C until measurement.

3.11.2. Preparation of ^{13}C-extracts for IDMS

Fully labeled ^{13}C-metabolite extracts were prepared from shaking flask cultivations of *C. glutamicum* as described in Feith et al. (2019). Thereby obtained labeled intracellular metabolites were employed for isotopic dilution mass spectrometry (IDMS) which employes isotopic substances as internal standard for external calibration of analyzed metabolites.

3.11.3. Quantification of intracellular metabolites with LC-MS QQQ

Quantification of amino acids and intracellular metabolites (cf. table 3.12) from *C. glutamicum*'s CCM was performed with an LC-Electrospray-ionisation(ESI)-TripleQuad-MS/MS device (LC-MS QQQ). Prior to the mass spectrometry (MS) unit of the device, the investigated sample is separated with liquid chromatography (LC), or more precisely, hydrophilic interaction liquid chromatography (HILIC). A detailed description of chromatographic conditions, data acquisition, employment of isotope IDMS, and subsequent metabolite quantification is given in Feith et al. (2019). Compared to the LC-MS QTOF device, that was also employed in this work, analysis via QQQ did not distinguish between citrate and isocitrate and did not detect pyruvate or acetyl-CoA due to the lower mass resolution of the device (Feith et al., 2019).

3.11.4. Isotopologue analysis with LC-MS QTOF

Relative quantification of isotopic labeling patterns of amino acids and intracellular CCM metabolites (cf. table 3.12) from the ^{13}C-labeling experiment was exclusively performed with an LC-MS Q-Time-of-Flight platform (LC-MS QTOF). Likewise to analysis with LC-MS QQQ, HILIC was employed as preliminary separation stage. A detailed description of the following chromatographic conditions, data acquisition, and subsequent quantification of relative isotopologue distributions was performed as described in Feith et al. (2019). Compared to the LC-MS QQQ device, that was also employed in this work, analysis

Table 3.12.: Intracellular metabolites analyzed LC-MS. Abbreviations for these metabolites used throughout this work are indicated.

Metabolite	Abbreviation
Central metabolism	
glucose 6-phosphate	G6P
fructose 6-phosphate	F6P
fructose 1,6-bisphosphate	FbP
dihydroxyacetonphosphate	DHAP
glyceraldehyde 3-phosphate	GAP
2-phosphoglycerate	2PG
2-phosphoglycerate	3PG
phosphoenolpyruvate	PEP
pyruvate	Pyr[†]
acetyl CoA	AceCoA[†]
citrate	Cit[†]
isocitrate	IsoCit[†]
α-ketoglutarate	AKG
succinate	Suc
fumarate	Fum
malate	Mal
pentose 5-phosphate sugars[‡]	Pen5P
sedoheptulose 7-phosphate	S7P
Amino acids	
L-alanine	Ala
L-asparagine	Asn
L-aspartate	Asp
L-arginine	Arg
L-glutamine	Gln
L-glutamate	Glu
glycine	Gly
L-histidine	His
L-isoleucine	Ile
L-leucine	Leu
L-lysine	Lys
L-methionine	Met
L-phenylalanine	Phe
L-proline	Pro
L-serine	Ser
L-threonine	Thr
L-tryptophan	Trp[*]
L-tyrosine	Tyr
L-valine	Val

[†] Add. detected/distinguished via QTOF

[‡] Pool of rib(ul)ose 5-phosphate

[*] Not measured with QTOF analysis

via QTOF could not properly analyze L-tryptophan signals and the measurements were therefore omitted.

3.12. Transcriptome analysis

3.12.1. Transcriptome sampling and RNA processing

Transcriptome samples were withdrawn in the supplementation experiments and in the stationary growth investigations. In both cases, approximately 1 mL biosuspension was withdrawn from the bioreactor, centrifuged at 20817 $\times g$ and 4 °C for 30 s, and quenched in liquid nitrogen after discarding the supernatant. Extraction and isolation of RNA from the samples, whole transcriptome sequencing, read mapping, and raw read count calculation was performed by our project partners at the CeBiTec as described in Haas et al. (2019).

3.12.2. Transcriptome analysis of supplementation experiments

Transcriptome samples of batch cultivations with optional supplementation of 0.1 mmol L^{-1} PCA and (1–37) g L^{-1} BHI were withdrawn in the mid-exponential growth phase. In contrast to the stationary growth investigations, RNA of biological triplicates of each process was pooled after RNA-extraction and further processed as described in section 3.12.1. Identification of differentially expressed genes (DEGs) was performed as stated in the following paragraph, mirroring an approach of the CeBiTec for samples without biological replicates. Additionally, a filtering method was developed in this dissertation to identify all genes with growth rate-dependent expression levels. Thus, the combination of both methods enabled identification of DEGs with growth-related expression patterns.

Identification of differentially expressed genes of supplementation experiments

Raw reads obtained from sequencing of supplementation experiment samples were analyzed and interpreted based on the typical workflow used at the CeBiTec, expanded by some additional operations (marked with *). The procedure is listed in the following:

- Calculation of 'reads per kilobase' (RPK-values) for the raw read count of each gene to normalize reads to the gene length: $RPK = \frac{\text{raw reads+1}}{\text{gene length}} \cdot 1000$. '1' was added to the raw reads prior to the operation making it possible to logarithmize the values.

- Based on the RPK-values, 'transcripts per kilobase million' (TPM-values) were calculated to adjust the reads to the library size: $TPM = \frac{\mathrm{RPK}}{\sum \mathrm{RPK}/10^6}$.
- *To compare the different TPM data sets of the experiments, Pearson correlations were calculated to check for similarity. If the data sets are alike, correlation coefficients of 1 or -1 are reached, and if the data sets are not similar, the coefficient tends to 0.
- Calculation of log fold changes (FC- or M-value) using TPMs to illustrate gene expression differences between the reference cultivation (CGXII standard minimal medium; index ref) and the supplemented conditions [$0.1\,\mathrm{mmol\,L^{-1}}$ PCA, (1–37) $\mathrm{g\,L^{-1}}$ BHI; index exp]: $M = \log_2 \frac{TPM_{exp}}{TPM_{ref}}$.
- Calculation of the average gene expression level (a-value) using TPMs of the reference and the compared process: $a = (TPM_{exp} + TPM_{ref})/2$
- To identify DEGs in the supplementation data sets, cut-off values for the M- and a-values were set:
  - **M-value:** A null hypothesis was formulated with the assumption that the majority of genes was not differentially transcribed. Therefore, a 95 %* significance level was set and thereby M-values within $1.96 \cdot \sigma$ (σ is the standard deviation of all M-values in the respective data set) are true in terms of the hypothesis.
  - **a-value:** A fixed cut-off of ≥ 1 was set, since a small a-value represents a small read number and in conjunction with the M-value would lead to falsified conclusions with regard to the expression level in comparison to genes with a greater read number.

  Taken together, genes with M-values outside the $1.96 \cdot \sigma$ intervals and a-values ≥ 1 were differentially expressed.
- In a last step, COG-categories and known regulons, operons or target genes of regulators were assigned to the identified DEGs using the CoryneRegNet database (Pauling et al., 2012) and the publication by Schröder & Tauch (2010).

Identification of growth rate dependent gene expression

The following filtering method was used to identify μ-dependent expression levels:

- Assuming that obtained M-values are normally distributed, Pearson's correlation factors (r) of the M-value and the corresponding exponential growth rate of the tested supplementation were calculated.
- To test if these correlation factors were statistically significant, a Null-hypothesis H_0 was formulated presuming that there is no statistical relevant correlation (Pearson's r) between μ and the gene expression level. H_0 was subjected to a two tailed t-test employing the t-distribution: $\widehat{t} = r \cdot \sqrt{n-2/1-r^2}$, where $n = 5$ was the sample size equaling the 5 different supplements.
- The obtained $\widehat{t}$ were then compared to the t-values of the t-distribution with a degree of freedom of 3 ($n - 2 = 3$) and the corresponding probability (p) was retrieved.
- If the found p-value of a correlation factor was $p \geq 0.1$, the Null-hypothesis was rejected (probability that H_0 was true was only 10 %), in turn hinting at a correlation between μ and the gene expression level.

3.12.3. Transcriptome analysis of continuous experiments

In contrast to the supplementation experiments, samples from continuous bioreactor cultivations at different growth rates ($\mu = 0.2\,\mathrm{h}^{-1}$, $0.3\,\mathrm{h}^{-1}$ and $0.4\,\mathrm{h}^{-1}$) featured three biological replicates for each growth rate. Thereby, the data analysis workflow developed by my colleague Thorsten Haas was employed as described in Haas et al. (2019).

3.13. ^{13}C-metabolic flux analysis

The MFA was performed by our project partners at the FZJ and is based on kinetic rates and ^{13}C-isotopic labeling data from the isotopic ^{13}C-labeling experiment conducted in chemostat mode ($D = 0.4\,\mathrm{h}^{-1}$). Roughly summarized, the metabolic network model, that was used as groundwork for the simulation, comprised 44 metabolites and 79 reactions (cf. table D.10) of which 41 were unidirectional and 38 were bidirectional. The biomass building reaction summarizes information on *C. glutamicum*'s composition as given by Marx et al. (1996). Therein described proportionalities were assumed to be growth rate independent and accordingly scale with μ. Fitting of 20 simulated fluxes was facilitated by two experimental fluxes (growth rate, carbon dioxide evolution rate) and 171 ^{13}C-labeling

measurements according to the profile likelihoods computational method [summarized in Theorell et al. (2017)].

3.14. Stoichiometric network model of *C. glutamicum*

3.14.1. Curation of *iEZ475* and expansion to *iMG481*

In this thesis, the SNM *iEZ475* of *C. glutamicum* was curated and expanded with regard to amino acid biosynthesis and uptake systems. Evaluation of *iEZ475* with regard to amino acid handling revealed missing synthesis routes, incorrect reaction directions, or false reactions originating from its origin *iKK446* (Kjeldsen & Nielsen, 2009). Incorporating recent knowledge on amino acid biosynthesis pathways or transporters, several reactions were curated and six reactions added resulting in the new model *iMG481* [cf. supplementary material of Graf et al. (2018)]. These modifications are described in Graf et al. (2018) (cf. section A) and were performed with the CobraToolBox using MATLAB software.

3.14.2. Flux balance analysis

FBA is a linear algorithm that calculates the ideal flux distribution in a stoichiometric network by maximization (or minimization) of an objective function. FBA was used in this thesis to (i) validate model *iMG481* with experimental data; (ii) test the influence of different amino acid transporter systems on growth and amino acid consumption; and (iii) estimate the influence of amino acid supplementation on the growth of *C. glutamicum* (sensitivity analysis). Therefore, experimentally determined kinetic parameters, e.g. glucose or amino acid consumption rates and respiratory rates were used as input and the biomass building reaction of *iMG481* was the objective function to be maximized. Further information is provided in Graf et al. (2018) (cf. section A).

3.14.3. Sensitivity analysis

The impact of amino acid supplementation on the growth rate was studied with sensitivity analysis. Hence, marginal amounts of one single amino acid were provided for the *in silico C. glutamicum* cell in addition to a fixed glucose uptake and a FBA was performed with biomass formation as objective function. The excursion of the resulting growth rate from the reference growth rate (sole glucose supplementation) was calculated and related

to the consumed amount of amino acids showing the cell's sensitivity for a certain amino acid. Details on this procedure are given in Graf et al. (2018) (cf. section A).

CHAPTER 4

Results and Discussion

PART I

Growth under metabolic pseudo-stationary conditions

One focus of this thesis was to identify growth limitations of *C. glutamicum* under metabolic pseudo-stationary conditions. Hence, batch cultivations were performed using CGXII minimal medium as basis and different compounds, i.e. different carbon and nitrogen sources [brain-heart-infusion (BHI), amino acids] or trace elements (thiamin, PCA) were added to vary the nutrient environment and thereby the growth rate. Corresponding physiological parameters and kinetics were derived and interpreted revealing potential intrinsic drawbacks of *C. glutamicum* that might be responsible for the strain's inferior growth performance (Graf et al., 2018). Furthermore, amino acid supplementation investigations were conducted to study the physiological responses of the *in vivo* and *in silico* cell as described in detail in Graf et al. (2018). For the latter, the new SNM *iMG481* was utilized. The different aspects of these pseudo-steady state investigations are summarized in the following sections. For detailed information on supplementation kinetics and *in vivo* and *in silico* amino acids investigations, the reader is kindly referred to the attached publication Graf et al. (2018) (cf. section A). Lastly, transcript analyses were performed in supplementation experiments comprising BHI and PCA to investigate growth rate dependent gene expression in comparison to reference cultivations. This information

was used to construct mutant strains of *C. glutamicum* with potential superior growth rates over the WT. Besides, the transcript patterns gave suggestions for minimal media additives (= 'growth boosters') to increase growth.

4.1. Physiological response to enriched minimal medium

4.1.1. Improving growth by supplementation

Bioprocesses were performed in two different reactor setups to unravel possible growth limitations of *C. glutamicum* in substrate unlimited exponential growth phases. A steel tank bioreactor was employed for the amino acid supplementation experiments to guarantee oxygen unlimited conditions ($1\,\mathrm{g\,L^{-1}}$ biomass inoculation density, $40\,\mathrm{g\,L^{-1}}$ glucose), whilst a triple reactor system was used for all other supplement investigations due to the smaller initial biomass ($0.3\,\mathrm{g\,L^{-1}}$) and total glucose supply ($20\,\mathrm{g\,L^{-1}}$). Reference cultivations with glucose as only carbon source yielded comparable exponential growth rates in both reactor systems [triple reactor system: $(0.32 \pm 0.02)\,\mathrm{h^{-1}}$, steel tank bioreactor: $(0.337 \pm 0.033)\,\mathrm{h^{-1}}$; cf. section A, table 1 and 2]. Thus, the following results can be discussed independently from the employed reactor system.

In all experiments, standard minimal medium CGXII (Buchholz et al., 2014b) was supplemented with varying compounds: (i) $(1\text{–}37)\,\mathrm{g\,L^{-1}}$ BHI; (ii) $5\,\mathrm{mmol\,L^{-1}}$ of all essential amino acids except for L-cysteine and L-tyrosine; (iii) $0.2\,\mathrm{mg\,L^{-1}}$ thiamin; (iv) $0.1\,\mathrm{mmol\,L^{-1}}$ PCA. The latter supplement was investigated by Grünberger et al. (2013) and Unthan et al. (2013) and identified as growth-accelerating compound. However, its positive impact on *C. glutamicum*'s metabolism is not fully understood. One theory designates PCA as additional carbon source (Unthan et al., 2013). Therefore, PCA was omitted as standard compound from CGXII (Keilhauer et al., 1993) in these experiments to prevent misinterpretation of the strain's physiological responses. Nevertheless, adding the compound in control experiments revealed an increased μ of $(0.45 \pm 0.01)\,\mathrm{h^{-1}}$ which confirmed the results of Grünberger et al. (2013). *C. glutamicum*'s transcriptional response to the additive is discussed below (cf. section 4.3.1). Besides, the compound was used in the continuous cultivation experiments to broaden the range of adjustable dilution rates (cf. section 4.4.1).

Supplementation of CGXII with increasing amounts of BHI $[(1\text{–}37)\,\mathrm{g\,L^{-1}}]$ induced significantly enhanced growth rates of $(0.44 \pm 0.01\text{–}0.67 \pm 0.03)\,\mathrm{h^{-1}}$ (cf. section A, table 1) compared to reference conditions. Moreover, a Monod-like saturation curve between

growth rate differences of reference and BHI-experiments against corresponding BHI concentrations was observed (cf. section A, figure 2). Thereby, the maximum growth difference between reference and $37\,\mathrm{g\,L^{-1}}$ BHI was determined with $\Delta\mu$ =0.359 $\mathrm{h^{-1}}$ and the saturation constant K_{BHI} causing half-maximum growth was $2.73\,\mathrm{g\,L^{-1}}$. This value indicated a growth boosting component in BHI that already reached saturating levels at a concentration above $5\,\mathrm{g\,L^{-1}}$ BHI.

Since free amino acids or amino acids bound in peptide species are compounds of BHI, following experiments comprised supplementation of free amino acids to investigate whether the observed growth simulation of BHI could be traced back to them. Thus, abundant amounts of amino acids were added to CGII medium such as to enable kinetically unlimited cellular uptake according to published K_M values of amino acid transporters (K_M values are summarized in supplementary table 1 of Graf et al. (2018), section A). Assuming that the largest part of BHI consists of amino acid-related species, an equally high μ of $(0.67 \pm 0.03)\,\mathrm{h^{-1}}$ as observed with $37\,\mathrm{g\,L^{-1}}$ BHI was expected in the case that amino acids were the only growth enhancing factors in BHI. However, a significantly smaller rate of $(0.468 \pm 0.003)\,\mathrm{h^{-1}}$ (cf. Graf et al. (2018) table 2, section A) was determined indicating that amino acids were not the only growth-enhancing factors in the complex medium.

4.1.2. Characterization of growth stimulating compounds

To unravel additional growth stimulating compounds in BHI apart from amino acids, energetic studies were conducted to estimate the ATP-demand of *C. glutamicum* cultivated in the different nutrient environments. It was assumed that the cell's ATP supply equaled its cellular ATP demand. The estimation of the produced amount of ATP was based on a P/O-ratio of 1.2 which was determined as reasonable operational ratio for industrial producers (van Gulik & Heijnen, 1995). Employing this P/O ratio to estimate cellular ATP production consequently required the knowledge of the cell's consumed amount of oxygen. The information was experimentally available only for the amino acid supplementation studies and reference experiments in the steel tank bioreactor whereby q_{O_2} values of $(9.49 \pm 0.85)\,\mathrm{mmol\,g^{-1}\,h^{-1}}$ and $(6.06 \pm 0.48)\,\mathrm{mmol\,g^{-1}\,h^{-1}}$, respectively (cf. Graf et al. (2018) table 2, section A), were determined. For the BHI-supplementation experiments, respiratory rates were derived from carbon balancing assuming that consumed amounts of carbon (provided by glucose and BHI) were transformed to either biomass or carbon dioxide, but not to by-products. Based on thereby obtained theoretical

carbon dioxide emission rates, a RQ of 1 was further presumed (that was experimentally validated by said steel-tank cultivations, cf. Graf et al. (2018) table 2, section A) and in turn lead to the estimated oxygen consumption rates listed in Graf et al. (2018), table 1 (cf. section A). Next, the ATP-biomass yields of the different supplement scenarios were calculated with the help of experimental (for amino acid supplementation experiments) or theoretical (BHI supplementation experiments) oxygen consumption rates, the assumed P/O of 1.2, and final normalization with the respective growth rates observed under the respective supplementation scenario. Finally, the estimation of respiratory rates calculated for the BHI-experiments was evaluated. Therefore, the described q_{O_2}-estimation procedure was employed for the amino acid supplementation and reference experiments where experimental data was available. Experimentally determined and estimated q_{O_2}-values were comparable which qualified the described approximation of the cell's energetic ATP-status for the BHI experiments as valid. Hence, an ATP-biomass yield of $(26.02 \pm 2.08)\,\mathrm{mmol\,g^{-1}}$ was observed for the reference, whilst $1\,\mathrm{g\,L^{-1}}$ BHI and amino acid supplementation revealed yields about $22\,\mathrm{mmol\,g^{-1}}$, further dropping to ca. $14\,\mathrm{mmol\,g^{-1}}$ for $(5\text{–}37)\,\mathrm{g\,L^{-1}}$ BHI (cf. Graf et al. (2018) figure 3, section A). The ATP-yield of the reference was in the experimentally determined range of Cocaign-Bousquet et al. (1996), but only half the value recently observed by Pfelzer (2016). This discrepancy indicated that the assumed P/O-ratio highly influences the quantitative amount of produced ATP. Consequently, the following discussion only qualifies as qualitative interpretation of the ATP-differences amongst different media.

On the one hand, the energetic similarity between $1\,\mathrm{g\,L^{-1}}$ BHI and amino acids mirrored the growth boost of small BHI concentrations as previously described by the Monod-type relation between BHI and μ. On the other hand, it showed that the energetic advantage of amino acid supplementation was only minor and could be achieved to the same extend with small amounts of BHI. The equal ATP-yields calculated for $(5\text{–}37)\,\mathrm{g\,L^{-1}}$ BHI likewise depicted the Monod-like saturating conditions observed before. Nevertheless, the massive ATP-drop of around 46 % from reference conditions compared to $(5\text{–}37)\,\mathrm{g\,L^{-1}}$ BHI growth environments was striking. Ruling out that this drop was due to futile cycling within cellular metabolism or supplement-dependent P/O-ratios, it was most likely that higher concentrations of BHI comprise extremely energy-rich components making cellular biosynthesis of these compounds unnecessary. The only slightly smaller ATP requirement under amino acid addition in comparison to the reference hinted at a moderate energy-advantage for the cell when amino acids were added to minimal media.

To evaluate if these hypotheses were reasonable, the ATP-requirement for *C. glutami-*

cum's amino acid demand was calculated. Therefore, the approach introduced by Kaleta et al. (2013) for *E. coli* was modified [cf. section 3.10.7 and supplementary tables 2 and 3 of Graf et al. (2018)]. Shortly summarized, calculation was started from precursors of central metabolism and NADPH was not considered as ATP-yielding compound due to *C. glutamicum*'s lack of nicotinamide nucleotide transhydrogenases equilibrating NADH and NADPH-pools as in *E. coli* (Sauer et al., 2004). After calculating the amounts of ATP necessary to built one mol of a specific amino acid, the mean amino acid-composition of the *C. glutamicum* cell (cf. Graf et al. (2018) table 4, section A) was consulted to correctly weight the ATP amounts according to the amino acid-ratio in the biomass. As a result, the cell apparently only required approx. 4 mmol ATP per gram biomass for amino acid biosynthesis. This result fitted the observed minor energy-advantage of the cell due to amino acid supplementation (reference: $Y_{ATP,x} = (26.02 \pm 2.08)\,\mathrm{mmol\,g^{-1}}$ vs. amino acid supplementation: $22\,\mathrm{mmol\,g^{-1}}$). Comparing these results to previous studies of Ingraham et al. (1983) confirmed our hypothesis that ATP costs for protein formation rather than amino acid synthesis were more ATP-intensive for *C. glutamicum*. Moreover, the latter authors observed an equal ATP-drop to ours when cultivating *E. coli* in complex instead of minimal medium. Deduced from these observations, it seemed that BHI contains energy-rich building blocks such as fatty acids or nucleotides apart from amino acids. Supplementing BHI with concentrations above $5\,\mathrm{g\,L^{-1}}$ thereby most likely provided *C. glutamicum* with efficient amounts of these building blocks and released the strain of their ATP-intensive production.

Consequently, the μ-boosting effect of BHI concentrations below $5\,\mathrm{g\,L^{-1}}$ could not be attributed to energy-rich building blocks since the ATP-yield of $1\,\mathrm{g\,L^{-1}}$ BHI was reference-like. Thus, it was suspected that trace elements such as PCA or vitamins might improve growth as well. Since the growth-boosting effect of iron chelators was already known for *C. glutamicum* (Grünberger et al., 2013; Liebl et al., 1989; Unthan et al., 2013), results of the transcript analysis conducted for the BHI-supplemented conditions (cf. section 4.3.2) were revised with regard to potential growth stimulating compounds (cf. section 4.1.2). Thus, thiamin was identified as promising candidate which is also regularly used in other minimal media for cultivations of *C. glutamicum* (Kind et al., 2010), and is a standard compound in industrial *C. glutamicum* processes (personal communication Ralf Takors). Indeed, subsequently performed duplicate batch processes showed that addition of $0.2\,\mathrm{mg\,L^{-1}}$ thiamin-HCl to glucose supplemented CGXII medium increased the growth rate of the strain to around $0.44\,\mathrm{h^{-1}}$ which was equivalent to the impact of PCA or $1\,\mathrm{g\,L^{-1}}$ BHI.

In summary, the growth boosting effect of small BHI dosages was most likely due to the presence of iron chelators and vitamins. Higher concentrations of BHI stimulated growth to a large extent due to the availability of external energy-rich building blocks such as fatty acids and nucleotides, whilst amino acids only contributed to a smaller extend to the growth increase. This later observation might represent a potential growth limiting factor in *C. glutamicum* regarding amino acid biosynthesis. Thus, externally supplied amino acids could have eliminated kinetic limitations of the cell by fueling intracellular transaminases to prevent 'slow' biosynthesis routes (cf. section 4.2). Amino acid addition might have also been advantageous for cellular short term needs to charge tRNAs as a prerequisite of fast translation for protein formation Nieß et al. (2017). To further investigate these hypotheses, the *in vivo* amino acid studies with *C. glutamicum* were analyzed in more detail and expanded by *in silico* simulations. The results are presented in section 4.2

4.1.3. Carbon to biomass conversion

With regard to glucose consumption (q_{Glc}) determined from the supplementation experiments, addition of $1\,\mathrm{g\,L^{-1}}$ BHI enhanced q_{Glc} from the reference level 0.0214 ± 0.0015 C-mol $\mathrm{g^{-1}\,h^{-1}}$ to 0.0277 ± 0.0016 C-mol $\mathrm{g^{-1}\,h^{-1}}$, which was an increase of 29 %. As illustrated in figure 1 in Graf et al. (2018) (cf. section A), BHI concentrations above $1\,\mathrm{g\,L^{-1}}$ did not further elevate q_{Glc}. In contrast, a declining tendency from this plateau was observed reaching values below the reference with $37\,\mathrm{g\,L^{-1}}$ BHI: 0.0191 ± 0.0019 C-mol $\mathrm{g^{-1}\,h^{-1}}$. Amino acid supplementation likewise led to reference-like levels (0.0205 ± 0.0006 C-mol $\mathrm{g^{-1}\,h^{-1}}$). However, total carbon consumption rates (q_C), accounting for consumption of glucose plus other available C-sources, were proportional to μ in all tested nutrient scenarios (section A, figure 1). Thereby, a constant biomass carbon yield (Y_{xc}) was obtained with a mean value of approx. 18 g C-mol^{-1}.

Similar observations regarding this yield were made in other studies employing varying carbon sources such as sugar- (Dominguez et al., 1997) or sugar-organic acid-mixtures (Wendisch et al., 2000), Frunzke et al. (2008). The first study, also conducted in bioreactors, yielded 17.6 g C-mol^{-1} that was comparable to our results. The two other studies revealed yields of 12 g C-mol^{-1} and 13 g C-mol^{-1} in shaking flask cultivations. The different biomass carbon yields from bioreactor and shaking flask studies might have been the result of the different cultivation systems. Possibly, the more stable growth environments installed in a bioreactor (constant pH and sufficient oxygen supply) in

contrast to shaking flasks could have promoted the higher yield in the former experimental setups. Nevertheless in either case, the respective yields deduced from the mixed carbon source investigations might reflect *C. glutamicum*'s total cellular capacity limits of processing carbon through metabolism. Due to supplementing amino acids, our study additionally showed the cell's limits of processing carbon and nitrogen and therefore indicated the limits of translation as well. The similarity between Y_{xc} derived from this work and from Dominguez et al. (1997)'s results might indicate equally adjusted capacities for carbon and amino acid processing, i.e. protein formation, which might limit growth in its present state.

4.2. Amino acid consumption of *C. glutamicum*

The physiological response of a cell to extracellular stimuli, e.g. varying nutrient supplies, can be predicted *in silico* by SNMs. Based on corresponding results, the number of wet lab experiments can be reduced to the most promising settings which minimizes experimental efforts and costs. In this dissertation, such an SNM of *C. glutamicum* was curated and then employed to study external nutrient stimuli in the form of amino acids. Hence, the employed model *iMG481* is introduced at the beginning of this section, whereupon *in vivo* wet lab- and *in silico* simulation-amino acid studies are discussed. The following section summarizes the main results presented in Graf et al. (2018) and for further details, the reader is kindly referred to this contribution (cf. section A).

4.2.1. Stoichiometric network model *iMG481*

The SNM *iMG481* established and employed in this thesis is based on the reconstruction *iEZ475* of Zelle et al. (2015). This predecessor model originated from one of the first *C. glutamicum* metabolic networks designed by Kjeldsen & Nielsen (2009) (*iKK446*) to investigate lysine production. In contrast, *iEZ475* focused on the energy metabolism of *C. glutamicum* by incorporation of protons and was finally validated with experimental data from Koch-Koerfges et al. (2012). Recently, a second *C. glutamicum* model was published by Zhang et al. (2017) originating from *iYS502* of Shinfuku et al. (2009). This new model is not considered here due to its curation with *E. coli*-specific pathways that are not present in *C. glutamicum*. Since the investigation of amino acid consumption of *C. glutamicum* was one topic of this thesis, *iMG481* comprises 6 new reactions in amino acid biosynthesis or transport reactions and 4 alterations in existing transport

reactions. For an overview, the following table 4.1 summarizes the pathways and number of reactions from *iEZ475* and expansions in *iMG481* with respective literature references.

The suitability of the curated model was checked by FBA simulations comparing growth of *C. glutamicum* under reference and amino acid supplemented conditions (μ_{ref} = $(0.337 \pm 0.033)\,\mathrm{h}^{-1}$, μ_{AA} = $(0.468 \pm 0.003)\,\mathrm{h}^{-1}$; cf. section A, table 2). Glucose and individual consumption rates of the 18 supplemented amino acids (cf. section A, table 2 and 3) were used as constraints, whilst constraining respiratory rates was omitted. Reference conditions could be met ($\mu_{sim,ref} = 0.337\,\mathrm{h}^{-1}$) and simulated amino acid-based growth was slightly higher ($\mu_{sim,ref} = 0.481\,\mathrm{h}^{-1}$). Besides, *iMG481* proofed to employ both added amino acid synthesis pathways (table 4.1) under reference conditions, whilst the least-ATP costly transporter [cf. supplementary table 1 of Graf et al. (2018)] was employed if individual amino acids were presented to the *in silico* cell in abundance. Both observations agree with the *in vivo* physiological understanding of the strain.

4.2.2. *In vivo* and *in silico* amino acid consumption phenotypes

Apart from investigating the cumulative effect of amino acid supplementation on physiological parameters of *C. glutamicum*, i.e. growth-enhancement, reference-like glucose consumption, proportional increase of total carbon consumption (cf. section 4.1), the cell's consumption of individual amino acids was studied *in vivo* as well. Uptake of amino acids was kinetically unlimited by adding abundant concentrations of $5\,\mathrm{mmol\,L}^{-1}$ of each essential amino acid except for L-cysteine und L-tyrosine in standard CGXII minimal medium ($40\,\mathrm{g\,L}^{-1}$ glucose). Obtained consumption profiles for each amino acids are pictured in supplementary table 1 of Graf et al. (2018) (cf. section A), whilst respective consumption rates are listed in table 3 of Graf et al. (2018).

Apart from Asp, all amino acids were consumed by *C. glutamicum* and Asn consumption started around the time Gln was depleted from the medium. Siewe et al. (1995) suggested that Asn might be transported into the cell by the same transporter(s) as Gln which perfectly explains the sequential uptake of Gln and Asn in our experiments. Besides, q_{Gln} = $(0.694 \pm 0.005)\,\mathrm{mmol\,g}^{-1}\,\mathrm{h}^{-1}$ was in the range of the maximum uptake rate observed for its transporter [v_{max} = $0.75\,\mathrm{mmol\,g}^{-1}\,\mathrm{h}^{-1}$, Siewe et al. (1995)] confirming the experiment's approach to enable kinetically unlimited transport.

Besides these general observations, three different amino acid consumption phenotypes were differentiated by comparison of derived amino acid biomass yields ($Y_{X,AA}$) with mean values calculated from published amino acid compositions of three *C. glutamicum*

Table 4.1.: Strucutre of the stoichiometric network model (SNM) *iMG481*. The SNM is based on the model *iEZ475* which was curated and expanded in this work with regard to amino acid biosynthesis and uptake. Corresponding adjustments in existing reactions or addition of new reactions are based on the listed references. Reactions are shown in bold font.

Pathway	Expansion/Curation	Reference	# Reactions
Central carbon metabolism			43
Amino acid synthesis			112
	Addition of glutaminase reaction **'glsK'**	Buerger et al. (2016)	
	Addition of Ala synthesis **'alaT'**	Marienhagen & Eggeling (2008)	
Oxidative phosphorylation			13
Membrane lipid metabolism			20
Nucleotide salvage pathway			48
Cofactor & prosthetic group biosynthesis			61
Biomass formation			52
Alternate carbon metabolism			35
Transport reactions			97
	Addition of ATP-dependent Arg-importer **'ARG_t_ATP'**	Gong et al. (2003)	
	Addition of Na^+-dependent Asn-importer **'ASN_t_NA'**	Siewe et al. (1995)	
	Addition of ATP-dependent Asp-importer **'ASP_t_ATP'**	Krämer et al. (1990), Marin & Krämer (2007)	
	Addition of Na^+-dependent Met-importer **'MET_t_NA'**	Trötschel et al. (2008)	
	Curation of Gln-Na^+ antiport to symport **'GLN_t_NA'**	Siewe et al. (1995)	
	Alteration from Leu-dependent to Ile-dependent Lys-antiport **'LYS_t_ILE'**	Bröer & Krämer (1990)	
	Curation of Na^+-dependent Ser-export to import **'SER_t_NA'**	Palmieri et al. (1996)	
	Curation of Na^+-dependent Thr-export to import **'THR_t_NA'**	Palmieri et al. (1996)	
Total number of reactions			481

strains (Cocaign-Bousquet et al., 1996; Kimura, 1963; Marx et al., 1996) as listed in table 4 of Graf et al. (2018) (cf. section A). Amino acids of the first group (Arg, His, Ile, Leu, Met, Phe, Ser, Thr, Trp) were consumed according to the mean amino acid biomass composition. The second group consisted of Asn, Gln and Pro and their individual consumed amounts were more than threefold higher than expected from respective $Y_{X,AA}$ values. In contrast, the third group made up of Ala, Asp, Glu, Gly, Lys, and Val was consumed remarkably below the expected threshold. In order to explain the formation of the three groups, SNM *iMG481* was employed. Since *iMG481* reproduced experimental results correctly, *in silico* consumption of single amino acids provided in either abundant amounts or in limited infinitesimal amounts (sensitivity study) was investigated. Corresponding experimental and simulated results are illustrated in figure 4 of Graf et al. (2018) (cf. section A). Together with the experimental data, the *in silico* uptake investigation yielded the following explanations for the observed phenotypes.

Most of the amino acids belonging to the first group share two common traits: (i) the biosynthesis of 1 mol amino acid is very energy intensive, e.g. net-ATP for Arg: $3.8\,\mathrm{mol\,mol^{-1}}$, His: $3.6\,\mathrm{mol\,mol^{-1}}$, Met: $8.8\,\mathrm{mol\,mol^{-1}}$ [cf. supplementary table 2 of Graf et al. (2018)]; (ii) in general, these amino acids do not serve as precursor for other biosynthesis processes. As consequence of the first trait, the cell saves energy if named amino acids are consumed instead of synthesized *de novo*. The *in silico* model confirmed this by attributing the highest impact on growth to amino acids of this group (except for Ser and Thr) in the sensitivity studies [cf. figure 4B in Graf et al. (2018), section A]. Thus, the saved energy in form of ATP or other valuable building blocks such as NADPH could be used by the cell to fuel other pathways. Thereby, biomass formation could be accelerated which is detected as increased growth rate. The second trait explains why the identified amino acids are not overly-consumed: the cell cannot use them (in contrast to the other amino acids, see below) for other cellular processes than protein formation. The only exception to this is Ser, where over-consumption would be reasonable to either fuel glycolysis, MTHF-synthesis (Netzer et al., 2004), or serve as a precursor for L-cysteine (Wada & Takagi, 2006) which was not supplemented in the experiments.

Consumption characteristics of the second and third group are discussed together by taking a look at the transaminase network of *C. glutamicum* as pictured in figure 4.1. The protagonists of this network are Glu and Asp and serve as amino donors for several biosynthesis routes in *C. glutamicum* (Marienhagen & Eggeling, 2008). In turn, Gln and Asn can serve as precursors for Glu and Asp, making use of the hydrolayses glutaminase GlsK (Buerger et al., 2016) or asparaginase AsnA (Mesas et al., 1990), respectively. As

a result of the hydrolysis reaction, the strain is simultaneously provided with ammonia. Considering that Gln was overly consumed (three fold higher than expected from the biomass composition), and Glu, Ala, and Val were consumed below the expected threshold, it was suspected that the over-consumption of Gln ultimately served to fill the 'gaps' of Glu, Ala, and Val. The reasons why these three amino acids could not be sufficiently consumed by *C. glutamicum* in the first place, could be as follows. Glu uptake might have been hampered by the presence of glucose in the minimal growth medium, causing catabolite repression (Krämer et al. (1990), Kronemeyer et al. (1995)). Ala uptake might have stood in competition with Met uptake because both amino acids are imported by the secondary transporter MetP showing a higher affinity for Met [Ala: 69 ± 11 μM, Met: 53 ± 16 μM; Trötschel et al. (2008)]. Lastly, studies of Lange et al. (2003) disqualified Val as carbon or nitrogen source. Hence, the transaminase network around the Glu knot could have served as compensating cascade for missing amounts of Glu, Ala, and Val. Firstly, Gln was over-consumed by the cell and hydrolyzed via GlsK to Glu. Next, Glu served as building block for Ala synthesis via AlaT which simultaneously required Pyr as organic acid for the transferase reaction (Marienhagen & Eggeling, 2008). Thereby, intracellular Ala amounts above the actual Ala-threshold could have been generated, too. Finally, a surplus of Ala could be employed to fill the Val gap via the AvtA-reaction (Marienhagen & Eggeling, 2008). Indeed, comparing the over-consumed molar amount of Gln with the actual consumed molar amounts of Glu, Ala, and Val, revealed that the Gln surplus was sufficient to serve as molar building block.

A similar compensation scheme can be attributed to Asn, Asp, and Lys. Likewise to Gln, Asn was overly consumed, whilst Asp consumption was not observed in the experiments. This fits previous results of Ziert (2014) categorizing Asp as (poor) nitrogen source and excluding it as carbon source. Concerning Lys consumption, the experimentally determined consumption rate in this work was in the range of values determined by Seep-Feldhaus et al. (1991). However, neither of the rates were high enough to satisfy the cellular Lys demand at $\mu = 0.468\,\mathrm{h}^{-1}$. Thus, the over-consumed amount of Asn could have served as precursor for Asp formation via the AnsA reaction (Mesas et al., 1990). In turn, Asp could have been used as precursor for Lys-formation. In sum, the over-consumed amount of Ans was sufficient to fill the respective gaps of Asp and Lys. Apart from potentially compensating Asp and Lys gaps, the Asn surplus might have been employed to directly fuel the TCA cycle by hydrolysis via AspA yielding Fum and ammonia, or via AspB yielding OAA and Glu. *Vice versa*, the reverse reaction might have been used by the strain to degrade a Glu surplus into Asp, ultimately fueling the

AspA reaction and the thereby the TCA cycle.

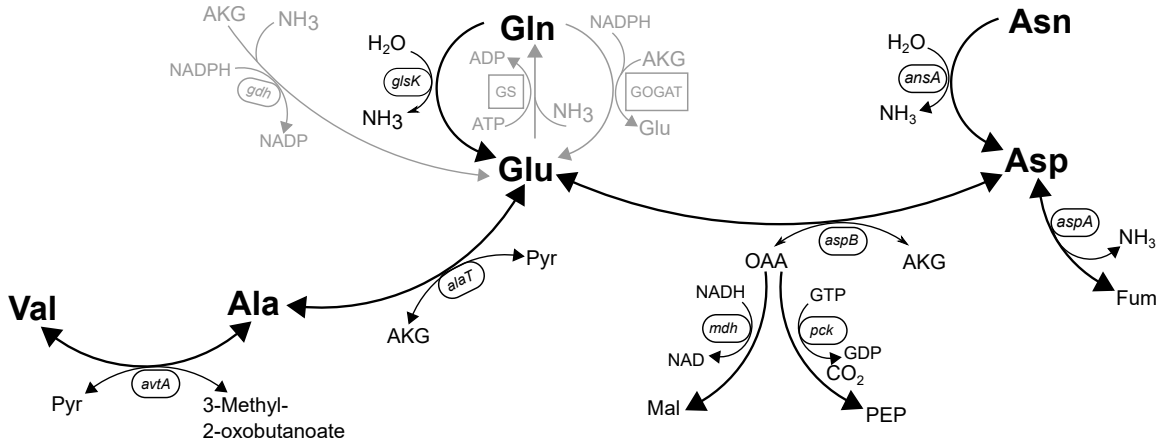

Figure 4.1.: Simplified overview of the transaminase network and its protagonists glutamate (Glu), glutamine (Gln), aspartate (Asp), and asparagine (Ans) in *C. glutamicum*. Related genes (printed in italic) of this network encode the following enzymes. *alaT*: alanine aminotransferase; *ansA*: L-asparaginase; *aspA*: aspartate ammonia-lyase; *aspB*: aspartate aminotransferase; *avtA*: valine aminotransferase; *gdh*: NADP-specific glutamate dehydrogenase; *glsK*: putative glutaminase; *mdh*: malate dehydrogenase; *pck*: PEP carboxykinase. GS: glutamine synthase, GOGAT: glutamine oxoglutarate aminotransferase

This complex interplay of amino acids within *C. glutamicum*'s transaminase network was also observed in the *in silico* investigations. Sensitivity studies revealed that amino acids of the second or third group did not influence growth profoundly if they were supplemented in restricted amounts in addition to glucose as only other carbon source. However, in the reverse scenario where the *in silico* cell was allowed to consume unlimited amounts of each amino acid, again the protagonists of the transaminase network were taken up non-proportional withregard to the biomass composition of the network model.

The only phenotypes of the second and third group that could not be explained by the transaminase network were the over-consumption of Pro and the under-consumption of Gly. Threefold higher amounts of Pro as expected were consumed by the cell, suggesting that Pro was used as additional carbon source facilitated by Pro dehydrogenause PutA (Ling et al., 1994). However, contradictory studies exist either observing Pro uptake (Bott & Niebisch, 2003) or dismissing it (Jensen & Wendisch, 2013). *In vivo* Gly consumption only covered 14 % of the cell's Gly demand, whilst *in silico* consumption resulted in 60 % coverage when Gly was supplied in abundance together with (limited amounts of) glucose. Since Gly is a byproduct of MTHF synthesis which requires Ser as precursor (Simic et al., 2001), tight regulation of this pathway might have limited *in vivo* as well as *in silico* uptake.

4.3. Transcriptional response to media supplementation

The physiological response of *C. glutamicum* to varying nutrient environments, summarized in section 4.1.1 and given in detail in Graf et al. (2018) (cf. section A), was expanded by transcript analyses. The supplement and growth related transcriptional response of the strain induced by varying additives [(1–37) g L^{-1} BHI, 10 mg L^{-1} PCA] in CGXII (20 g L^{-1} glucose) was studied. Transcriptome samples were withdrawn during the mid-exponential growth phase of reference, BHI- and PCA-supplemented batch cultivations exhibiting growth rates from 0.32 h^{-1} to 0.67 h^{-1} (cf. table 4.2). The samples were further processed as described in section 3.12.1 and deduced raw read counts were analyzed for differentially expressed genes (DEGs) as described in section 3.12.2. A DEG is a gene with an expression level that is significantly elevated or decreased in comparison to its expression under control conditions. Thus, the supplement-impact of PCA and 37 g L^{-1} BHI was preliminary examined on *C. glutamicum*'s transcriptional level to derive potential growth limitations in non-supplemented CGXII minimal medium. Based on the broad growth rate range induced by the different supplements [(0.32–0.67) h^{-1}], strict growth rate dependent gene expression patterns were identified next. If not otherwise stated, the gene products of discussed genes were retrieved from the CoryneRegNet database (Pauling et al., 2012).

Table 4.2.: Determined growth (μ) and glucose consumption (q_{Glc}) rates of *C. glutamicum* wild type (WT) determined from bioreactor cultivations in standard CGXII minimal medium with 20 g L^{-1} glucose (denoted as reference) and supplemented with (1–37) g L^{-1} brain-heart-infusion (BHI, abbr. to 1–37 BHI) or 0.1 mmol L^{-1} protocatechuate (PCA). Values represent means with standard deviation from biological triplicates.

Supplement	μ, h^{-1}	q_{Glc}, g g^{-1} h^{-1}
reference	0.32 ± 0.02	0.64 ± 0.05
1 BHI	0.44 ± 0.01	0.81 ± 0.04
PCA	0.45 ± 0.01	0.83 ± 0.05
5 BHI	0.54 ± 0.02	0.82 ± 0.04
10 BHI	0.50 ± 0.01	0.79 ± 0.02
37 BHI	0.67 ± 0.03	0.57 ± 0.06

4.3.1. Transcriptional response to PCA supplementation

The supplement PCA was described to have growth stimulating effects on *C. glutamicum* (Grünberger et al., 2013; Liebl et al., 1989; Unthan et al., 2013). Hence, the transcriptome

analysis of corresponding PCA supplementation experiments and reference experiments are contrasted here to potentially unravel growth limiting factors in the CGXII minimal reference. Recently, Unthan et al. (2013) investigated how the transcriptional repertoire of *C. glutamicum* changed during the course of a batch cultivation from PCA-rich to PCA-depleted CGXII minimal medium. In contrast to Unthan et al. (2013), this study compared the transcriptional response between individual cultures grown with or without PCA in biologically-independent experiments. Transcript analysis revealed 164 genes with significantly increased or decreased gene expression compared to the reference (cf. table C.1). 84 genes exhibited decreased expressions with log fold changes (M-values) of -2 to -9 and a similar number of 80 genes revealed enhanced expression levels (M = 1.9–6.7).

One of the most interesting observations was the iron-related transcriptional response of the microogranism to PCA. *ripA* encoding the regulator of iron proteins A (Wennerhold et al., 2005) was severely down-regulated (M = -4). This gene is exclusively controlled by the global iron-dependent regulator DtxR that represses the gene under iron-exceeding conditions (Wennerhold et al., 2005). Due the observed decreased expression level of *ripA*, it is assumed that the intracellular amount of iron in the PCA experiments was higher than under reference conditions. This theory is confirmed by significantly increased expression of RipA's targets genes *ackA*, *acn*, *catA*, *katA*, *narKGHJI*, *pta*, and *sdhCDAB* showing log-fold changes of up to 5. These target genes are only de-repressed of RipA-control under non-limiting iron conditions (Wennerhold et al., 2005). Additionally, 36 other target genes of DtxR that are involved in (siderophore-assisted) iron acquisition [c.f. table C.1, Wennerhold & Bott (2006)] were pronouncedly down-regulated. Likewise but not under DtxR-control, genes cg1832, cg1833, and cg1832 encoding an ABC-type putative iron-siderophore transporter were similarly repressed (M = -3). This could indicate that the intracellular amount of iron was sufficient during the mid-exponential growth phase and no further iron transport was needed. Apart from being released from RipA-repression, the up-regulation of succinate dehydrogenase genes *sdhCDAB* could also be the direct consequence of DtxR-activation under iron excess as suspected by Wennerhold & Bott (2006). Moreover, vast amounts of 'free' intracellular iron are a signal for potential oxidative stress of cells: free iron atoms promote the Fenton reaction that produces reactive oxygen species such as H_2O_2 (Touati, 2000). *C. glutamicum* perceives oxidative stress via the regulator OxyR that de-represses its target genes in the presence of H_2O_2 to prevent cellular damage (Milse et al., 2014). Here, OxyR's targets *katA* and the *cyd*-operon were significantly expressed (M = 2.2–2.7) hinting at an oxidative stress

response under PCA-supplemented conditions. This could also explain the increased expression of *uspA2* encoding an universal stress response protein. Simultaneously, H_2O_2 induces genes of the DtxR regulon independently from OxyR (Brune et al., 2006; Wennerhold & Bott, 2006). In conclusion, the presented transcriptional responses all hint at a higher intracellular iron availability for *C. glutamicum* when PCA is added to the medium. Liebl et al. (1989) support this by stating that *C. glutamicum* requires an iron-complexing compound (such as PCA) as growth factor since the strain might be a siderophore-auxotroph. Hence, the corresponding 40 %-increased growth performance of the microorganism could be due to sufficient iron environments rather than using PCA as TCA-fueling substrate as proposed by Unthan et al. (2013).

Another transcriptional response to the presence of PCA was related to genes of the β-ketoadipate pathway that is employed by *C. glutamicum* for degradation of aromatic compounds. Similar to the results of Unthan et al. (2013), up-regulation of genes *catA* and *pcaH* (M = 2.7) was observed which encode enzymes of said β-ketoadipate pathway (Brinkrolf et al., 2006). Besides, genes related to degradation pathways of other aromatics [summarized by Shen et al. (2012)] also revealed higher expression levels: cg2966 encoding a putative phenol 2-monooxygenase and *vanA* coding for putative vanillate demethylase [catalyzes the conversion of vanillate to PCA, Kalinowski et al. (2003)] showed log-fold changes of about 2. Contrary to our *vanA* findings, Merkens et al. (2005) did not detect a positive influence of PCA on the gene's expression. Nevertheless, the additional activation of genes apart from the PCA-pathways shows a more global transcriptional response of *C. glutamicum* to substrates from its native habitat. Accordingly, the up-regulation of genes involved in gluconate transport (*gntP*) or degradation of propionate (*prpD2B2C2*), compounds that are also found in soil, support this assumption.

Besides iron-, aromats-, and soil compound-related transcriptional responses, genes encoding the uptake and assimilation of nutrients were also significantly expressed. For instance, sugar transport via PTS-specific transporters for glucose (*ptsG*), fructose (*ptsF*), and *ptsI* encoding the general Enzyme I of PTS exhibited log-fold changes of around 2. Moreover, alternative (putative) sugar uptake systems like *iolT1* (Ikeda et al., 2011), cg0340, and *msiK1* showed similar high expression levels. Possibly, the increased glucose consumption rate under PCA-supplementation [$q_{Glc} = (0.83 \pm 0.05)\,\mathrm{g\,g^{-1}\,h^{-1}}$] in comparison to the reference [$q_{Glc} = (0.64 \pm 0.05)\,\mathrm{g\,g^{-1}\,h^{-1}}$, cf. table 4.2] could have been facilitated not only by PtsG, but also by the other mentioned transporters. Apart from enhanced sugar transport expression, several oligopeptide transporters (cg2181, cg2182, cg2183, cg2184; cg2937, cg2939, cg2940) exhibited higher expression levels as well, which

fitted the data of Unthan et al. (2013). *amtA* and *amtB*, coding for putative ammonium transport proteins (Walter et al., 2008), and *ssuA*, *ssuD1* and *ssuD2*, encoding enzymes for sulfonate-sulfur utilization (Koch et al., 2005), were significantly down-regulated (M-values about -2 and -3, respectively). Possibly, nitrogen- and sulfur-sources were more readily available for the cell under PCA-environments whereby corresponding transporter protein genes were repressed. Astonishingly, down-regulation (M = -2) of arginine biosynthesis genes *argCJBDF* was also observed. Normally, this operon is under the control of ArgR, repressing transcription of the genes in the presence of arginine (Yim et al., 2011), and of FarR which is a putative regulator of amino acid metabolism and is triggered by still unknown effector molecules (Hänssler et al., 2007). Arg was not supplemented in addition to PCA and therefore expression of *argR* was correspondingly decreased. Thus, the down-regulation of *argCJBDF* might be caused by FarR.

The study of Unthan et al. (2013) revealed that PCA was used by *C. glutamicum* as additional carbon and energy source next to glucose. The authors proposed that by fueling the strain's TCA cycle via previous degradation in the β-ketoadipate pathway, PCA most likely improves *C. glutamicum*'s growth performance. However, the authors could not rule out that apart from its effect on catabolism, PCA might influence iron transport as well. Whilst our transcript analysis confirmed the employment of the β-ketoadipate pathway, we also distinctly observed an iron-related response to PCA indicating that iron-availability for the cell could have been more advantageous in PCA-supplemented than in PCA-devoid environments. These results clearly support the physiological observations by Liebl et al. (1989) assigning PCA an iron-related growth enhancing role. Moreover, the stimulation of genes involved in the uptake and assimilation of elemental nutrients like carbon, sulfur, and nitrogen might additionally hint at a regulatory function of the compound that ultimately influences basic cellular demands and thereby μ. The results of the adaptive evolution growth investigation also supports this thesis [cf. section 4.8.3 and Graf et al. (2019), section B].

4.3.2. Transcriptional response to BHI supplementation

The transcriptional response of *C. glutamicum* to complex media was not investigated in literature yet. To identify potential shortcomings in the composition of minimal medium CGXII regarding its growth stimulating properties, corresponding transcript results of *C. glutamicum* are contrasted to the ones recorded for $37\,\mathrm{g\,L^{-1}}$ BHI supplementation. In this rich growth environment, 167 DEGs were identified of which the majority (122

genes) revealed decreasing and only 45 genes increasing gene expression in comparison to the CGXII control experiment (cf. table C.2).

As observed under PCA supplemented conditions, supplementation with BHI provoked an iron response in the transcriptome of *C. glutamicum*: *ripA* encoding the regulator of iron proteins A, genes coding for (siderophore-assisted) iron transport (operons *cg0466*, *cg0589*, *cg0767*, *cg0921*, *cg0926*), and heme degradation [*hmuO*, Frunzke et al. (2011)] were significantly decreased in expression (M-values up to -5). Simultaneously, several of RipA's targets (*catA*, *katA*, *narKGHJI*, *sdhAB*) were up-regulated most likely due to de-repression of RipA control (cf. section 4.3.1). Therefore, it was assumed that the complex BHI medium contained PCA-like compounds, e.g. other siderophores like citrate (Liebl et al., 1989), that facilitated iron transport and thereby provided the cell with a higher amount of intracellular iron than under reference conditions. Comparable to the iron response, sufficient amounts of intracellular cobalt might have been available in the mid-exponential growth phase since expression of operon cg1227 encoding a cobalt transporter was severely decreased (M = -10).

Down-regulation of the Arg operon *argCJBDFR* (Yim et al., 2011) was more pronounced than under PCA supplementation (M-values: -3.5 vs. -2). In contrast to the PCA condition, decreasing expression of amino acid biosynthesis, and therefore Arg-encoding genes, was expected because BHI contains (oligo)peptides and free amino acids making *de novo* synthesis of amino acids unnecessary. Fittingly, peptide transporters were up-regulated (operon cg2181 and gene cg2610), whilst genes encoding other amino acid biosynthesis pathways showed diminished expression. For instance, Met synthesis genes *metQ*, *metX*, *metY*, *metE*, *metH*, *metK*, and *metB*, which are scattered in the genome (Qin et al., 2015), showed log-fold changes of up to -7. Glu synthesis was also reduced by down-regulation of *gltB* and *gltD* (M-values: -4 and -2) that could also be a side effect of sufficient ammonium supply (see below). Expression of *aroF* coding for 3-deoxy-D-arabino-heptulosonate 7-phosphate (3DDAH7-P) synthase, which is the first enzyme in the shikimate pathway (Liu et al., 2008), was also down-regulated (M-value: -3.5). As a result, biosynthesis of aromatic amino acids Trp, Phe, and Tyr depending on 3DDAH7-P as precursor could have been repressed since corresponding pathway genes were non-significantly, but nevertheless decreasingly expressed. Likewise, genes *lysC* and *asd*, encoding the first enzymes of the pathway leading to amino acids of the Asp-family (Kalinowski et al., 1991; Kalinowski et al., 1990), *ilvBN*, coding for the first step of Val and Leu synthesis (Keilhauer et al., 1993), and *hisG*, starting His synthesis (Kwon et al., 2000), exhibited not-significantly but decreased expression. In sum, *C. glutamicum*

apparently reduced the expression of genes from at least 13 amino acid biosynthesis pathways. Equal observations regarding expression of amino acid synthesis genes were made by Tao et al. (1999) who investigated the transcriptional response of *E. coli* grown in minimal and rich LB medium.

Considering that peptides and amino acids provide cells with the elemental compounds nitrogen and sulfur, the diminished expression of genes encoding transport of ammonium (*amtA*, *amtB*) and transport or utilization of sulfonate/sulfur [*ssuA*-operon, *ssuD2*, *ssuI*, *ssuR*, *seuAB*; sulfate reduction via *fpr2*, Rückert et al. (2005)] was expected. Again, similar observations were made for *E. coli* (Tao et al., 1999). For the same reason, ammonium assimilation via the GOGAT-mechanism represented by genes *gltB* and *gltD* (Beckers et al., 2001) was possibly reduced, hinting at sufficient intracellular ammonium concentrations (Beckers et al., 2001; Tesch et al., 1999). Besides, repression of *gltB*, *gltD*, *amtA*, and *amtB* might have been mediated by the global nitrogen regulator AmtR (Beckers et al., 2005) even though *amtR* was not differentially expressed. In this context, increased expression of the nitrate transporter and nitrate/nitrit reductase operon *narKGHJI* (M-values about 3) was astonishing. The *nar* genes are involved in nitrate utilization and are normally only expressed under anaerobic conditions (Nishimura et al., 2007) and repressed by ArnR in aerobic conditions (Nishimura et al., 2008). Since oxygen saturation was sufficient in all experiments, it is more likely that the enhanced expression of the *nar* operon was a result of de-repression from RipA (as previously discussed in section 4.3.1) rather than a response to anaerobic environments.

In the preceding presentation of *C. glutamicum*'s physiological response to different concentrations of BHI [section 4.1 and Graf et al. (2018), cf. section A], the theory was formulated that the ATP-demand of cells grown in high dosages of BHI was reduced due to the presence of fatty acids and nucleotides providing the microogranisms with an ATP-benefit. Accordingly, the transcript data set was revised for genes involved in these synthesis pathways and ultimately could confirmed the theory. Previously, Irzik et al. (2014) investigated the response of *C. glutamicum* to fatty acids by supplementing oleate to minimal growth medium and detected decreased mRNA leveles of *accD1* and *fasA* encoding fatty acid synthases. Even though not differentially expressed, *accD1* and *fasA* exhibited decreased expression (M-values of -1.6 and -0.7, respectively) in our study as well, indicating the presence of this fatty acid. Regarding nucleotides, genes of purine (*pur* genes) and pyrimidine (*pyr* genes, *carA*, *carB*) synthesis, required for *de novo* nucleotide synthesis, were not differentially expressed. However, genes encoding purine salvage pathways (e.g. *adk*, *apt*, *hpt*, *gmk*), revealed increased log-fold changes of

up to 0.9. Up-regulation of salvage pathway genes and reference-like expression of *de novo* synthesis genes fitted with the *E. coli*-observations of Tao et al. (1999). The authors proposed that this behavior was due to availability of nucleotides in rich medium and thus again confirmed the assumption from the physiological analysis.

In the CCM, genes of glycolysis did not show differentially expressed genes. Possibly, this was due to very similar glucose consumption under $37\,\mathrm{g\,L^{-1}}$ BHI [$q_{Glc} = (0.57 \pm 0.06)\,\mathrm{g\,g^{-1}\,h^{-1}}$] and reference conditions [$q_{Glc} = (0.64 \pm 0.05)\,\mathrm{g\,g^{-1}\,h^{-1}}$; table 4.2] leading to a comparable expression of glycolytic genes. Results from the *E. coli* LB-medium studies again were in line (Tao et al., 1999). However, some of the TCA genes revealed significant expression changes: genes *aceA* and *aceB* showed decreased expressions (M = -3) indicating a closed glyoxylate shunt and the absence of acetate (Cramer et al., 2006). In contrast, *sucCD* and *sdhAB* showed increased gene expressions with log-fold changes of about 3, potentially due to de-repression from RipA control. Alternatively, compounds directly fueling the TCA cycle could have been present in $37\,\mathrm{g\,L^{-1}}$ BHI impacting expression of named TCA genes. For example, one of the two genes coding for myo-inositol transport (*iolT1*) and genes encoding its degradation [*idhA1*, *idhA2*, *iolC*, cg0198, *iolABDEGH*; Krings et al. (2006)] exhibited elevated log-fold changes of up to 6. Metabolization of myo-inositol requires one molecule of ATP but feeds TCA via acetyl-CoA formation and simultaneously produces two molecules of NADH (Krings et al., 2006). Recently, Brüsseler et al. (2018) showed that transporter IolT1 is also able to take up D-xylose in the absence of repressor IolR which qualifies D-xylose as potential compound in BHI, too.

The last striking observation amongst the DEGs of the $37\,\mathrm{g\,L^{-1}}$ BHI environment was the down-regulation of genes encoding thiamin synthesis (*thiC*, *thiD1* , *thiM*, *thiEFGOS*) revealing log-fold changes between -4 and -10. Similar observations for this vitamin and others (porphyrin, tetrahydrofolate, glutathione) were made by Tao et al. (1999) for *E. coli*. DNA microarray results of Lee et al. (2001) revealed that supplementation of vitamins to defined mineral medium down-regulated expression of *Bacillus subtilis* genes involved in corresponding biosynthesis pathways. Deduced from these publications, our results indicated that thiamin could be a (growth-boosting) component of BHI. This hypothesis was tested in duplicate bioreactor batch studies by supplementing $0.2\,\mathrm{mg\,L^{-1}}$ (matching the concentration of the standard CGXII vitamin biotin) to CGXII minimal medium ($20\,\mathrm{g\,L^{-1}}$ glucose). In comparison to the reference [$\mu = (0.32 \pm 0.02)\,\mathrm{h^{-1}}$, $q_{Glc} = (0.64 \pm 0.05)\,\mathrm{g\,g^{-1}\,h^{-1}}$] growth rate and glucose consumption rate were increased by 20 %. Since thiamin biosynthesis is ATP-costly, external thiamin supplementation might be

beneficial for *C. glutamicum* in terms of ATP saving.

Deduced from this transcript analysis, several theories from the physiological and energetic growth investigation (c.f. section 4.1) regarding the composition of BHI could be affirmed. Thus, a transcriptional response towards amino acids, peptides, fatty acids, and nucleotides was observed, that most likely provided the strain with the suggested ATP benefit if supplied in higher dosages of BHI. These commodities simultaneously could have supplied *C. glutamicum* with sufficient amounts of elemental compounds (e.g. sulfur) making energy intensive assimilation and transport mechanisms unnecessary. Regarding the growth stimulating properties of even low concentrations of BHI, the presence of compounds facilitating metal transport and vitamins like thiamin could be the reason. In summary, relieving *C. glutamicum* of the biosynthesis of ATP-costly compounds and supplying it with specific trace elements most likely increased μ under the tested experimental conditions.

4.3.3. Growth rate dependent gene expression

Supplementation of CGXII minimal medium with various supplements (PCA, 1, 5, 10, and 37 g L^{-1} BHI) resulted in *C. glutamicum* cultures exhibiting a broad range of growth rates [(0.32–0.67) h^{-1}]. Hence, apart from identifying media dependent transcript responses of *C. glutamicum* (cf. section 4.3.1 and section 4.3.2), growth rate dependent gene expression levels could be studied as well. Therefore, genes classified as DEGs from named growth experiments were compared. 38 genes were significantly expressed in cultures of all the tested supplements (cf. table C.3) and therefore qualified for further identification of growth rate dependent expression. Therefore, the filtering method described in cf. section 3.12.2 was applied and 14 genes were obtained that exhibited significant μ-dependent expression levels with confidence levels between 90 % and 100 %: cg1296, *ssuD1*, *ssuA*, *thiC*, *argB*, *argD*, *argF*, *amtA*, *amtB*, cg3329, cg3372, cg3374, *rpf1*, and cg2546. The corresponding gene profiles are pictured in figure 4.2 and figure 4.3 versus the growth rate.

Since the ultimate aim of this investigation was to identify genes whose expression level might influence the growth rate of *C. glutamicum*, corresponding mutant strains were constructed featuring alterations in corresponding genes. Thus, genes potentially having a growth-regulating role in *C. glutamicum* should be either over-expressed in the mutant strain if it had previously shown increased expression over μ. On the contrary, genes with decreasing expression over μ should be deleted from the genome to potentially

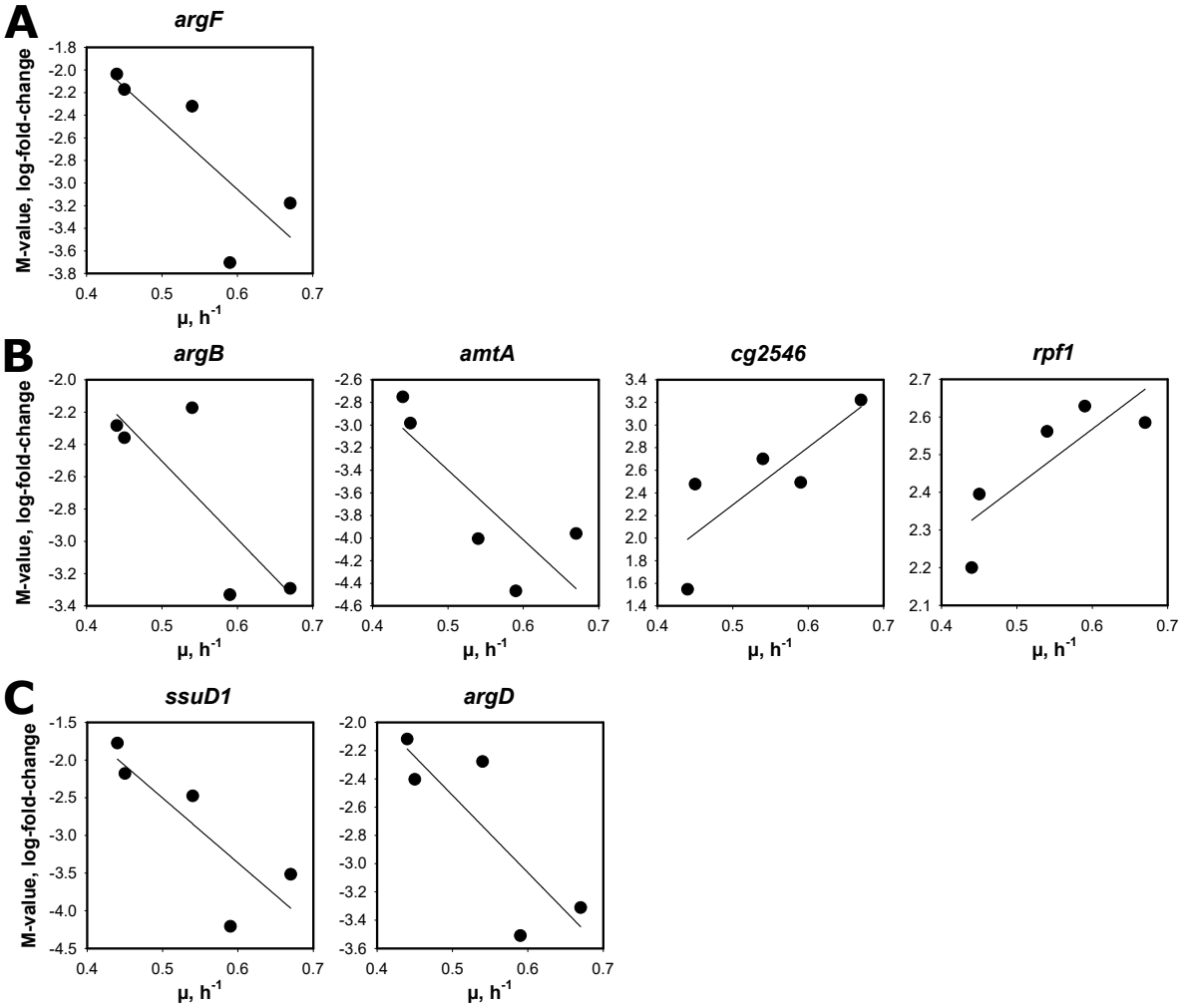

Figure 4.2.: Relation between gene expression level (M-value, log-fold-change) and the exponential growth rate μ of common genes found to be differentially expressed under supplemented conditions (1–37) $\mathrm{g\,L^{-1}}$ brain-heart-infusion and 0.1 $\mathrm{mmol\,L^{-1}}$ protocatechuate. According to a two-tailed t-test applied to Pearson correlation factors of the illustrated genes and their respective expression levels over μ, the correlation is significant with a confidence level of 90 % (A), 91 % (B), and 92 % (C).

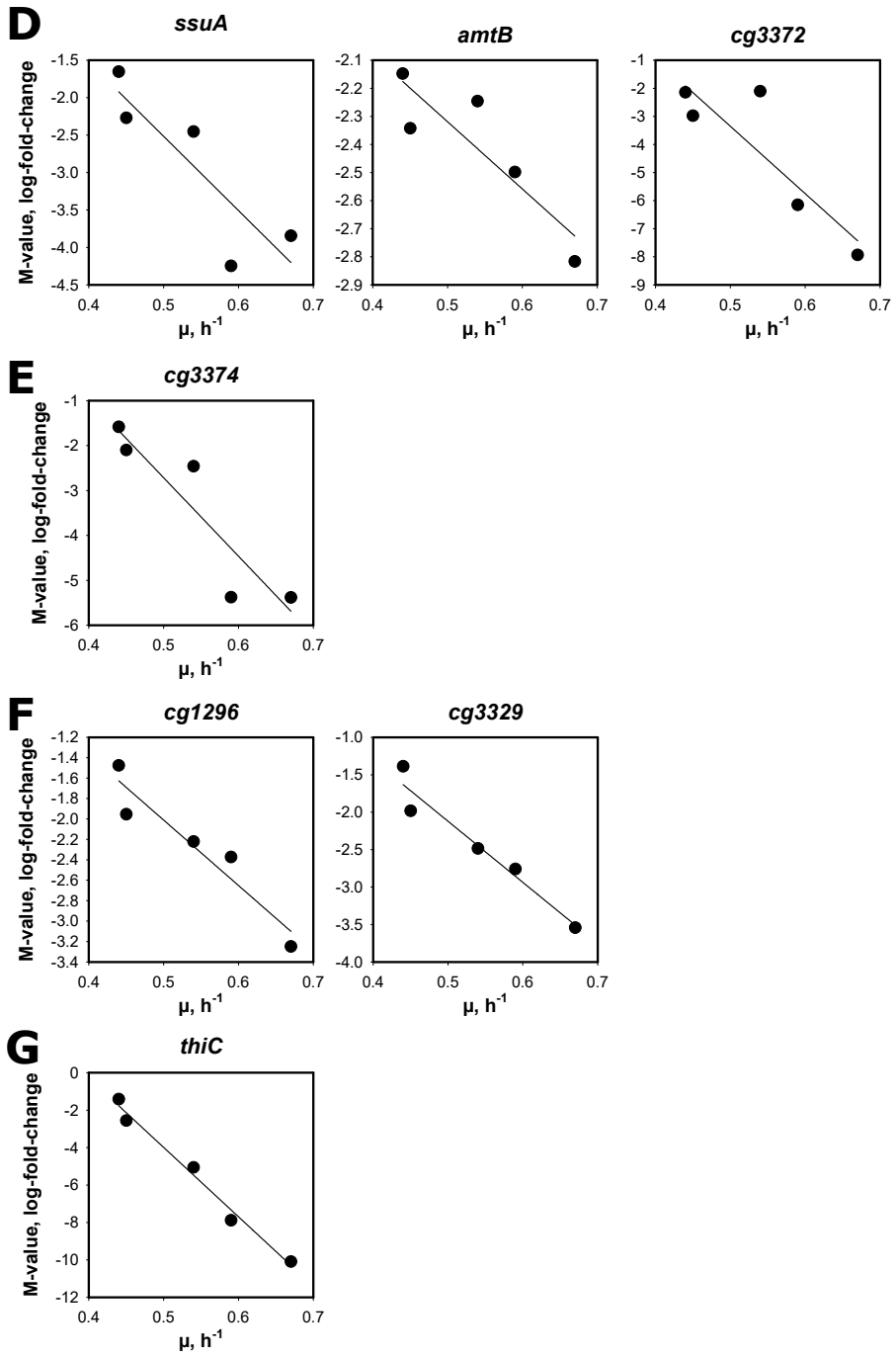

Figure 4.3.: Relation between the gene expression level (M-value, log-fold-change) and the exponential growth rate μ of common genes found to be differentially expressed under supplemented conditions (1–37) g L^{-1} brain-heart-infusion and 0.1 mmol L^{-1} protocatechuate. According to a two-tailed t-test applied to Pearson correlation factors of the illustrated genes and their respective expression levels over μ, the correlation is significant with a confidence level of 95 % (D), 97 % (E), 99 % (F), and 100 % (G).

enhance growth. However, not all of the 14 DEGs that revealed μ dependent expression patterns were modified in the WT strain. Only the genes encoding promising proteins based on their cellular function(s) were chosen.

Three genes of the Arg biosynthesis operon (*argB*, *argD*, and *argF*) were gradually down-regulated with log-fold changes between -2 and -4 (cf. figure 4 .2). Since deletion of these genes would most likely result in an Arg-auxotroph strain unable to grow without the amino acid, *argB*, *argD*, and *argF* were not considered as manipulating-options. Genes encoding proteins involved in macroelement transport (ammonia uptake: *amtA*, *amtB*; sulfonate/sulfur utilization: *ssuA*, *ssuD1*) were also ruled out, because their down-regulated expression patterns were most likely the result from the nutrient-rich BHI medium and not a growth-related response (cf. section 4.3.2). cg2546, a putative secondary C_4-dicarboxylate transporter exchanging species like aspartate, succinate, fumarate, and malate (Janausch et al., 2002), was up-regulated over μ. Again, the rich composition of the BHI might be responsible for this behavior, even though an M-value of 2.4 was determined under PCA-supplementation as well. Gene cg3372 encodes a hypothetical protein and was also not considered because BLAST search of its corresponding protein sequence lead to no further insights of the protein's function. Even though *thiC* showed the expression pattern with the highest growth dependency (confidence level of 100 %), deletion was ruled out to avoid a thiamin-auxotroph strain. As a result, genes *rpf1*, cg3374, cg3329, and cg1296 were left as targets due to their respective functions:

rpf1 This gene encodes one of the two resuscitation promoting factors (Rpf1, Rpf2) in *C. glutamicum* (Hartmann et al., 2004). In *Micrococcus luteus*, *rpf* is essential and stimulates growth of dormant *Mic. luteus* cells. Therefore, Rpf proteins are destined to be growth stimulating factors in Gram-positive bacteria with high GC-amounts. However, Hartmann et al. (2004) showed that deletion of *rpf1* and/or *rpf2* induced no impaired growth in complex or minimal medium indicating that the genes are not essential for *C. glutamicum*. Nevertheless, deletion of one of the *rpf* genes in combination with inoculation from a prolonged stationary pre-culture phase induced longer lag-phases in the main culture, which could be again reduced by adding supernatants from exponentially growing *C. glutamicum* WT or of overexpressing *rpf1* or *rpf2* mutants, respectively. Ultimately, the authors found that another molecule besides the Rpf proteins seems to have a growth promoting effect on *C. glutamicum*, but only in combination with Rpf1 or Rpf2. Besides, Hartmann et al. (2004) showed that enhancing or deleting *rpf2* had

no effect on μ. Since *rpf1* exhibited increasing expression over μ and the other authors exclusively investigated the role of *rpf2*, *rpf1* was over-expressed in this study in strain *C. glutamicum* ATCC 13032 pVWEx1-cg0936.

cg3374 This gene encodes a putative NADH-dependent flavin oxidoreductase catalyzing the reduction of flavin species (e.g. riboflavin, FMN, FAD) and simultaneous oxidation of NADH: $\text{Flavin}_{\text{ox}} + \text{NADH} \xrightarrow{H+} \text{Flavin}_{\text{red}} + \text{NAD}^+$. The reduced flavin-species in turn can be involved in (i) the reduction of ferrisiderophores (iron metabolism), (ii) the activation of ribonucleotide reductases, (iii) the reduction of methemoglobin, (iv) in biomluminescence reactions, and (v) in the activation of oxygen (Fieschi et al., 1995). Besides, cg3374 is the first gene of a predicted operon with cg3375 (encoding a predicted nucleoside-diphosphate-sugar epimerase). Both genes showed decreasing expression over μ, but only cg3374 was differentially expressed in comparison to the reference. Thus, the gene was deleted in mutant strain *C. glutamicum* ATCC 13032 Δcg3374 to possibly increase growth.

cg3329 This gene encodes a conserved hypothetical protein. BLAST search of the corresponding protein sequence showed similarities to the RtcB protein of *E. coli* that is a RNA ligase involved in splicing and repair of tRNA (Chakravarty et al., 2012). According to the later, RtcB is indifferent to the presence of ATP and stimulated by GTP. In the supplementation experiments, the expression of cg3329 was decreased over μ and therefore deleted in strain *C. glutamicum* ATCC 13032 Δcg3329.

cg1296 This gene encodes a putative non-ribosomal peptide synthetase module. Additionally, BLAST search of the corresponding protein sequence revealed a 99 % query recovery with an N-acetlytransferase of *Rhodococcus triatomae* that is of the same class of bacteria as *C. glutamicum* (Yassin, 2005). Nguyen et al. (2015) deleted several putative acetlytransferases of *C. glutamicum*, amongst them cg1138, cg1417, and cg2835*, but with no obvious impact on μ. In contrast, deletion cg1581 encoding glutamate N-acetlytransferase (*argJ*), revealed that mutant PUT21Δcg1581 was not able to grow (Nguyen et al., 2015). Consequently, both deletion (*C. glutamicum* ATCC 13032 Δcg1296) and overexpression (*C. glutamicum* ATCC 13032 pVWEx1-cg1296) of cg1296 was performed in this study to test the impact on growth.

*These genes were down regulated over μ in our analysis as well, but not significantly (data not shown).

Deletion strains *C. glutamicum* Δcg1296, Δcg3329, and Δcg3374 were cultivated in CGXII standard minimal medium with $20\,g\,L^{-1}$ glucose and optional addition of $37\,g\,L^{-1}$ BHI in the triple reactor system (one biological replicate respectively) and compared to the WT (cf. table 4.3). In the rich medium, all strains showed the same growth behavior as the WT control [$(0.66–0.69)\,h^{-1}$], whilst only Δcg1296 revealed diminished growth of $0.27\,h^{-1}$ in minimal medium [WT: $(0.32 \pm 0.02)\,h^{-1}$]. Thus, deletion of any gene that revealed a decreasing expression pattern with rising μ did not enhance the growth performance of *C. glutamicum*. On the contrary, deletion of cg1296 further reduced growth under minimal media conditions.

Table 4.3.: Determined growth rates of *C. glutamicum* wild type (WT) and deletion mutants Δcg1296, Δcg3329, and Δcg3374 determined from bioreactor cultivations in standard CGXII minimal medium with $20\,g\,L^{-1}$ glucose (denoted as 'CGXII') and supplemented with $37\,g\,L^{-1}$ BHI-medium (denoted as 'BHI'). Values of mutant cultivations are derived from one biological experiment, whilst WT data derives from three biological replicates ± SD.

	μ, h^{-1}	
Strain	CGXII	BHI
WT	0.32 ± 0.02	0.67 ± 0.03
Δcg1296	0.27	0.68
Δcg3329	0.31	0.66
Δcg3374	0.32	0.69

Over-expression strains *C. glutamicum* pVWEx1-cg1296 and pVWEx1-rpf1 were cultivated in two independent shaking flask cultivations in CGXII minimal medium ($10\,g\,L^{-1}$ glucose, $50\,\mu g\,mL^{-1}$ kanamycin, 1 mM IPTG for induction) with optionally added $37\,g\,L^{-1}$ BHI. Overexpression of cg1296 lead to diminished growth rates in CGXII ($0.19\,h^{-1}$, WT: μ = $0.36\,h^{-1}$) whilst growth in BHI was only slightly reduced ($0.60\,h^{-1}$, WT: $0.65\,h^{-1}$, cf. table 4.4). Likewise, over-expression of *rpf1* led to slightly smaller μ in both tested media (CGXII: $0.32\,h^{-1}$; $37\,g\,L^{-1}$ BHI: $0.61\,h^{-1}$).

In general, additional protein expression from plasmids and the selection pressure from antibiotic supplementation burden can lead to impaired growth. To quantify the impact of plasmid expression on μ, control experiments with a *C. glutamicum* strain harboring an empty plasmid should be performed, but was not tested here. Nevertheless, both influences most likely were the reason for slightly smaller μ of the *rpf1* over-expression mutant in CGXII and BHI-supplemented media and for the cg1296 mutant in BHI compared to the reference. However, the about 50 %- and 20 %-diminished growth performance of *C. glutamicum* ATCC 13032 pVWEx1-cg1296 and *C. glutamicum*

Table 4.4.: Determined growth rates of *C. glutamicum* wild type (WT) and over-expression mutants *C. glutamicum* pVWEx1-cg1296 and pVWEx1-rpf1 determined from cultivations on standard CGXII minimal medium with $10\,g\,L^{-1}$ glucose (denoted as 'CGXII') and supplemented with $37\,g\,L^{-1}$ BHI-medium (denoted as 'BHI') in shaking flask cultivations. Growth media of plasmid-bearing strains contained $50\,\mu g\,mL^{-1}$ kanamycin and 1 mM IPTG for induction. Values are the mean from two biologically independent experiments.

	μ, h^{-1}	
Strain	CGXII	BHI
WT	0.36	0.65
pVWEx1-cg1296	0.19	0.60
pVWEx1-rpf1	0.32	0.61

Δcg1296 cultivated in minimal medium indicated that the (putative) N-acetyl transferase encoded by cg1296 is crucial for the strain in sparse growth environments. This finding was comparable to the results of Nguyen et al. (2015) for the deletion of gene *argJ* that encodes a glutamate n-acetyl transferase.

In conclusion, the mutant studies could not classify genes *rpf1*, cg3374, and cg3329 as growth-influencing for *C. glutamicum* under the tested experimental conditions, and altering the expression of cg1296 had in either case detrimental effects on μ. Since all of the genes apart from cg3329 are under the control of global regulatory proteins [*rpf1*: GlxR, Kohl et al. (2008); cg3374: CysR, Rückert et al. (2008); cg1296: AmtR, Beckers et al. (2005)], it might be worth to further investigate their role as potential growth influencing factors in *C. glutamicum*.

PART II

Growth under metabolic stationary conditions

Another focus of this thesis was to investigate growth of *C. glutamicum* under stationary metabolic conditions by studying its physiological response. Therefore, a continuous bioreactor was employed to install varying growth rates and constant environmental process conditions. After characterizing metabolic steady states based on kinetic parameters, *C. glutamicum*'s intracellular response was more closely studied by means of OMIC techniques. Thus, intracellular metabolite pools and their response to increasing growth rates as well as the transcriptional responses were analyzed. Lastly, a stationary isotopic ^{13}C-labeling experiment in continuous mode was performed to determine the fluxome of *C. glutamicum* at μ = 0.4 h^{-1}.

4.4. Physiology and growth kinetics

4.4.1. Process parameters

Three biologically independent continuous bioreactor cultivations were conducted in chemostat mode employing CGXII minimal medium supplemented with 12 g L^{-1} glucose and 30 mg L^{-1} PCA. The later compound was added since preliminary studies without it lead to wash out of the culture at growth rates above 0.3 h^{-1} (data not shown). The following process parameters of the experiments (A, B, C) at μ = 0.2 h^{-1}, 0.3 h^{-1} and 0.4 h^{-1} are illustrated in figure 4.4: pO$_2$-signal, molar oxygen (y_{O_2}) and carbon dioxide (y_{CO_2}) concentrations in the off-gas, biomass concentrations determined via CDW measurements, and the dynamic wash-out phase at dilution rates above μ_{max}. Differences in biomass concentrations at the same dilution rate were due to slightly varying amounts of glucose [$c_{Glc,F}$ = (12.47 ± 0.35) g L^{-1}] in the feed media of the three processes. Most likely, this was also the reason for the small deviations in the absolute values of pO$_2$, y_{O_2}, and y_{CO_2} in between biological replicates. By maintaining constant stirrer speeds of 700 min^{-1} and aeration rates of 0.67 vvm independent from set dilution rates, progression towards stable cellular metabolic steady states could be easily deduced from constant pO$_2$ and exhaust gas signals. Likewise, any shift from the established steady state would have been detected fast. After about 7.5 h of each preliminary batch phase [μ = (0.44 ± 0.01) h^{-1}], the continuous processes were started (process time 0 h) with D = 0.2 h^{-1} and subsequently increased to 0.3 h^{-1} (≈ 28 h) and D = 0.4 h^{-1} (≈ 49 h).

Irrelevant of D, stable online parameters (pO_2, y_{O_2}, y_{CO_2}) were already observed after 4 RTs indicating metabolic steady states. Nevertheless, OD, CDW, filtrate TC/TIC, metabolome, and transcriptome samples were withdrawn after 5 RT for three times in 1.5 h-intervals. To determine μ_{max} of *C. glutamicum* in a continuous growth environment with PCA-supplemented CGXII mineral medium, each chemostat process was terminated with a dynamic wash-out phase (cf. figure 4.4). Therefore, dilution rates were set between $0.56\,h^{-1}$ and $0.6\,h^{-1}$, that equaled the strain's μ_{max} under highly diluted growth conditions (Grünberger et al., 2013; Unthan et al., 2013), but was never observed under standard batch process conditions [$0.45\,h^{-1}$, cf. section 4.1.1 ; Grünberger et al. (2013),Unthan et al. (2013)]. The wash out behavior was followed online by declining respiratory signals (cf. figure 4.4) and recorded offline by withdrawing samples for CDW measurements hourly for 7 h.

4.4.2. Kinetic parameters

In each process, biomass concentrations elevated slightly from $(5.87 \pm 0.13)\,g\,L^{-1}$ to $(6.43 \pm 0.18)\,g\,L^{-1}$ with rising D leading to a 10 %-increase of the biomass substrate yield from $(0.47 \pm 0.01)\,g\,g^{-1}$ to $(0.52 \pm 0.00)\,g\,g^{-1}$ (cf. table 4.5). Glucose concentrations in all samples were below the detectable limit. Derived biomass-specific kinetic parameters (q_{Glc}, q_{O_2}, q_{CO_2}) from each process at the same growth rate were in very good agreement, but non-proportional with μ due to the increase of Y_{XS}. Respiratory quotients (RQ) calculated from oxygen uptake and carbon dioxide evolution rates ranged around 1. Closed carbon balances of (99 ± 1) %, (98 ± 2) %, and (96 ± 3) % were determined for μ = $0.2\,h^{-1}$, $0.3\,h^{-1}$ and $0.4\,h^{-1}$ (cf. figure 4.5), respectively, indicating that glucose was either transformed to biomass or CO_2. No by-products such as acetate or Pyr (Han et al., 2008; Yokota & Lindley, 2005), lactate or alanine (Blombach et al., 2013) were detectable in biomass-free filtrates analyzed via mass spectronomy (LC-MS QTOF). Based on half-logarithmic linear regression of biomass-time courses from the wash-out phase of each experiment, μ_{max} was determined as described in section 3.10.2 and pictured in figure D.1 in the appendix resulting in $(0.47 \pm 0.00)\,h^{-1}$.

To evaluate the obtained data from the continuous processes, the experimentally determined biomass concentrations for growth rates $\mu = 0.2\,h^{-1}$, $0.3\,h^{-1}$ and $0.4\,h^{-1}$ were compared to theoretical metabolic steady state biomass concentrations $\tilde{c_x}$. Therefore, the mass balances derived in section 3.10.2 were employed as summarized in Eq. 35. Hence, theoretical substrate concentrations $\tilde{c_s}$ at metabolic stationarity were simulated for D =

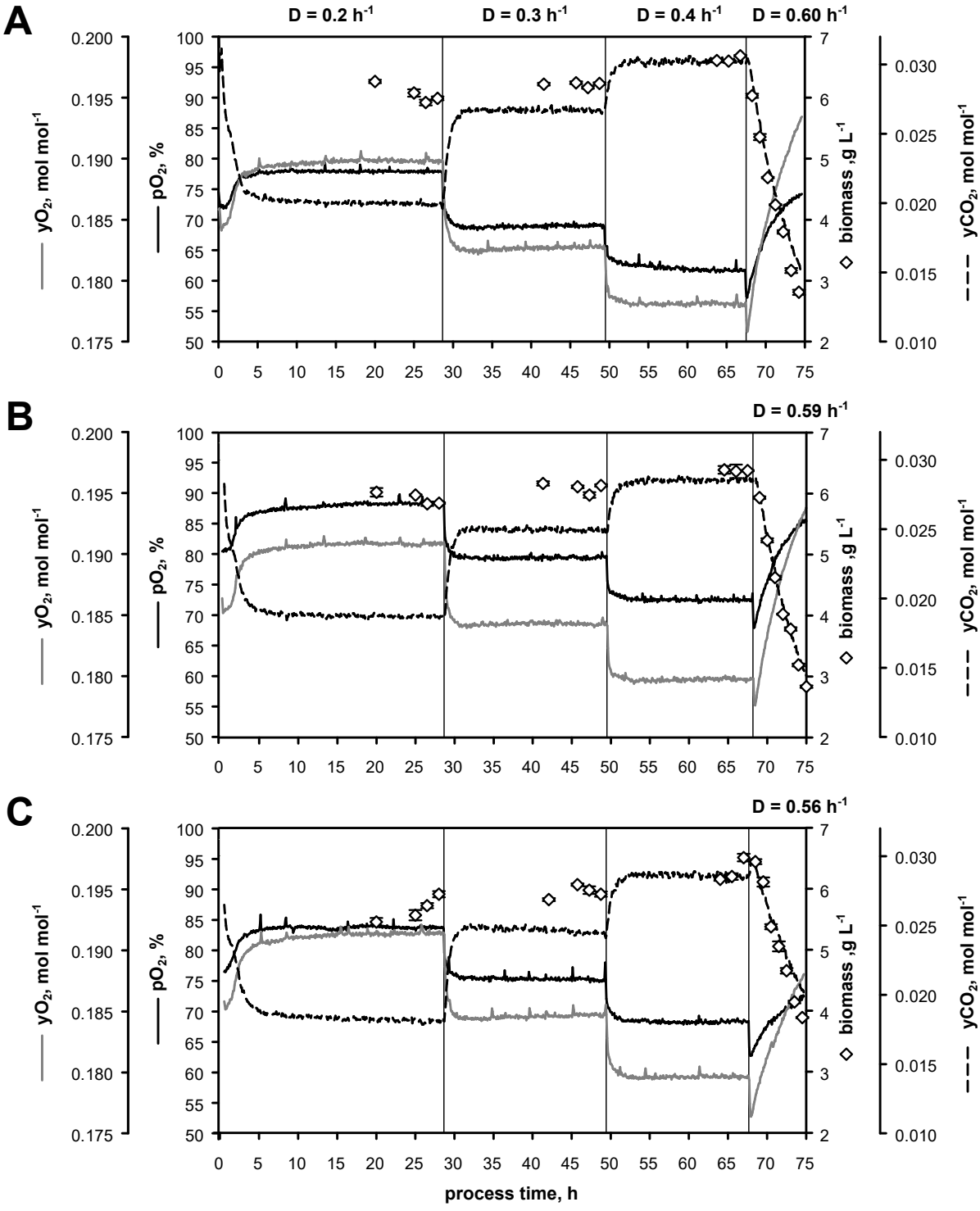

Figure 4.4.: Illustration of oxygen saturation (pO_2), molar oxygen (y_{O_2}) and carbon dioxide (y_{CO_2}) in the off-gas, and biomass concentrations (black diamonds) of three (A, B, C) chemostat processes with dilution rates D =0.2 h^{-1}, 0.3 h^{-1} and 0.4 h^{-1} and subsequent dynamic wash-out at D =(0.56–0.6) h^{-1}. *C. glutamicum* was cultivated in CGXII minimal medium supplemented with (12.47 ± 0.35) g L^{-1} glucose and 30 mg L^{-1} PCA. Given standard deviations of biomass measurements are calculated from three technical replicates.

Table 4.5.: Listing of kinetic process parameters ± standard deviation calculated from three individual chemostat processes with *C. glutamicum* cultivated in CGXII medium supplemented with $(12.47 \pm 0.35)\,\mathrm{g\,L^{-1}}$ glucose and $30\,\mathrm{mg\,L^{-1}}$ protocatechuate. c_x: biomass concentration, q_{Glc}: biomass specific glucose uptake rate, Y_{xGlc}: biomass-glucose-yield, $q_{\mathrm{O_2}}$: biomass specific oxygen uptake rate, $q_{\mathrm{CO_2}}$: carbon dioxide evolution rate, RQ: respiratory quotient.

D, $\mathrm{h^{-1}}$	c_x, $\mathrm{g\,L^{-1}}$	q_{Glc}, $\mathrm{g\,g^{-1}\,h^{-1}}$	Y_{xGlc}, $\mathrm{g\,g^{-1}}$	$q_{\mathrm{O_2}}$, $\mathrm{mmol\,g^{-1}\,h^{-1}}$	$q_{\mathrm{CO_2}}$, $\mathrm{mmol\,g^{-1}\,h^{-1}}$	RQ, $\mathrm{mol\,mol^{-1}}$
0.20 ± 0.01	5.87 ± 0.13	0.42 ± 0.01	0.47 ± 0.01	5.36 ± 0.10	5.64 ± 0.14	1.05 ± 0.01
0.30 ± 0.01	6.09 ± 0.12	0.62 ± 0.01	0.49 ± 0.01	7.16 ± 0.14	7.30 ± 0.18	1.02 ± 0.01
0.40 ± 0.01	6.43 ± 0.18	0.77 ± 0.01	0.52 ± 0.01	8.15 ± 0.15	7.94 ± 0.10	0.97 ± 0.01

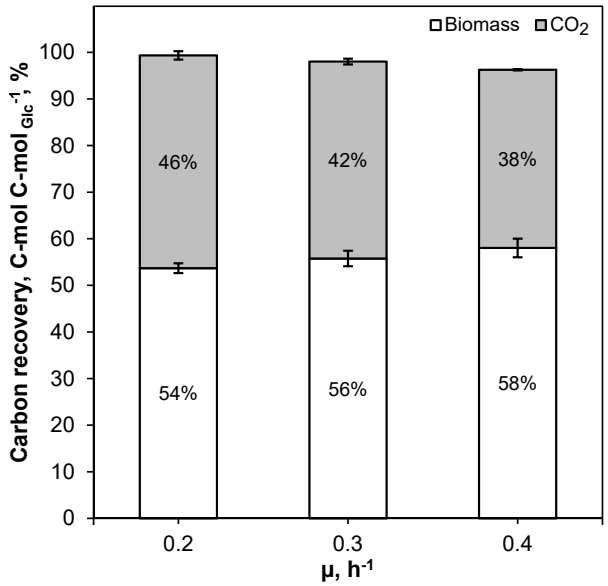

Figure 4.5.: Elemental carbon balance showing the mean C-recovery ± standard deviation from three continuous processes A, B, C with *C. glutamicum* cultivated at $\mu = 0.2\,\mathrm{h^{-1}}$, $0.3\,\mathrm{h^{-1}}$ and $0.4\,\mathrm{h^{-1}}$.

$0.2\,h^{-1}$, $0.3\,h^{-1}$ and $0.4\,h^{-1}$ by assuming Monod-type growth and making use of existing *C. glutamicum* literature values for $K_S = 14\,\mu mol\,L^{-1}$ (Lindner et al., 2011) and $\mu_{max} = 0.62\,h^{-1}$ (Grünberger et al., 2013). Further using the definition for cellular maintenance after Pirt (1982) (cf. Eq. 49) and corresponding values for growth independent (m_S) and growth dependent ($1/Y_{xs}^{real}$) maintenance parameters determined by Koch-Koerfges et al. (2013) for *C. glutamicum* WT, $\tilde{c_x}$ became a simple function of the experimentally set dilution rate D and employed substrate feed concentration $c_{s,in}$. Thus, in accordance with the experiments, $D = 0.2\,h^{-1}$, $0.3\,h^{-1}$ and $0.4\,h^{-1}$ and three slightly varying values for $c_{s,in} = 12.87\,g\,L^{-1}$, $12.36\,g\,L^{-1}$ and $12.19\,g\,L^{-1}$ were inserted. The simulated results are exemplarily illustrated for continuous process A in figure 4.6 (and listed in table D.4) together with corresponding experimental data. The experimentally determined biomass concentrations represent the mean of at least three technical replicates ± standard deviations for each installed D.

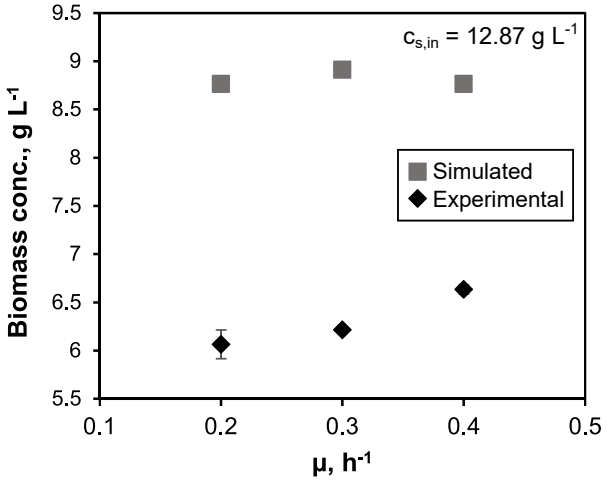

Figure 4.6.: Illustration of experimental biomass concentration from chemostat process A and theoretical simulated biomass steady-state concentrations. The latter were derived from mass balances of the continuous bioreactor, assuming Monod type growth [$\mu_{max} = 0.62\,h^{-1}$, Grünberger et al. (2013); $K_S = 14\,\mu mol\,L^{-1}$; Lindner et al. (2011)], and maintenance parameters [m_s: $(0.08 \pm 0.02)\,mmol\,g^{-1}\,h^{-1}$; $1/Y_{XS}^{real}$: $(7.74 \pm 0.16)\,mmol\,g^{-1}$; Koch-Koerfges et al. (2013)].

A clear discrepancy between theoretically predicted and experimentally observed biomass concentration over the installed growth rate was assessed. Since simulated $\tilde{c_s}$ and $\tilde{c_x}$ based on equations comprising literature data on *C. glutamicum* such as its maximum growth rate and cellular maintenance, corresponding parameters were derived from the presented chemostat processes to find out if this could explain the off-set. Thereby, the maximum growth rate determined during the wash out phase of each process yielded $\mu_{max} = (0.47 \pm 0.00)\,h^{-1}$ which was in stark contrast to $\mu_{max} =$

$(0.62 \pm 0.02)\,\mathrm{h}^{-1}$ determined by Grünberger et al. (2013). Most likely, this was due to differences in the experimental setups employed to determine μ_{max}, even though the growth medium was identical (CGXII medium supplemented with PCA and glucose). Grünberger et al. (2013) made use of a continuous micro-scale bioreactor enabling single cells to grow in highly diluted turbidostat conditions (Grünberger et al., 2014) which was shown to have a beneficial impact on growth of *C. glutamicum* if PCA is supplemented. With regard to the simulation, however, the absolute magnitude of μ_{max} had only a minor impact on predicted $\tilde{c_x}$ (cf. Eq. 36). Based on the extreme low value of K_S, the in turn simulated $\tilde{c_s}$ was negligible small compared to $c_{s,in}$ (cf. table D.4) and therefore impacted the resulting $\tilde{c_x}$ only very slightly.

Consequently, the employed growth (in)dependent maintenance parameters, that ultimately influence the theoretical glucose consumption rate of the cell, should be able to explain the difference between simulated and experimental data. Hence, cellular maintenance parameters were derived from the experimental q_s-μ pairs as illustrated in figure 4.7. Using this concept, $m_s = (0.44 \pm 0.04)\,\mathrm{mmol\,g^{-1}\,h^{-1}}$ and $1/Y_{XS}^{real} = (9.73 \pm 0.08)\,\mathrm{mmol\,g^{-1}}$

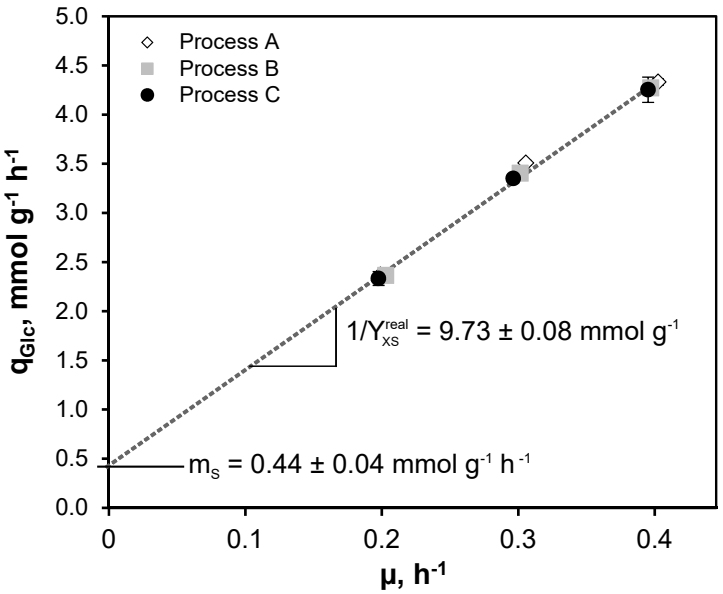

Figure 4.7.: Determination of non- and growth rate associated maintenance parameters m_S and $1/Y_{xs}^{real}$ after Pirt (1982). Mean values ± standard deviations are deduced from the three chemostat experiments A, B, C.

were obtained that were about five times and 25 % higher, respectively, than respective values determined by Koch-Koerfges et al. (2013) [m_s: $(0.08 \pm 0.02)\,\mathrm{mmol\,g^{-1}\,h^{-1}}$; $1/Y_{XS}^{real}$: $(7.74 \pm 0.16)\,\mathrm{mmol\,g^{-1}}$]. The discrepancy between these maintenance parameters was due to the approx. 20 % higher biomass yield observed by Koch-Koerfges et al. (2013)

($Y_{XS} = 0.6\,\mathrm{g\,g^{-1}}$) than in this investigation [(0.47–0.52) $\mathrm{g\,g^{-1}}$; cf. table 4.5], resulting in lower glucose consumption rates for growth rates between (0.05–0.3) $\mathrm{h^{-1}}$ in the latter publication. Potentially, differences in the continuous bioreactor setups employed in both studies were the cause for the varying kinetic process parameters. A smaller reactor scale (200 mL vs. 1.5 L) and different dilution rate control was employed in the work of Koch-Koerfges et al. (2013), and metabolic steady states were presumed to be achieved after 3.5 RT vs. 5 RT in our experiments. Consequently, the metabolic steady states established and/or analyzed by Koch-Koerfges et al. (2013) and in this work might have differed resulting in different kinetic parameters and ultimately in different maintenance values. One example that might support this hypothesis is the study of Cocaign-Bousquet et al. (1996) for *C. glutamicum* WT ATCC 17965 cultivated in a 3.5 L chemostat setup. This experimental setup featured a comparable dilution rate control as in this work and kinetic parameters were very comparable to ours.

In sum, the discrepancy between predicted metabolic steady state concentrations and experimentally observed data was traced back to kinetic growth parameters (q_s) that in turn built the basis for mathematical constructs describing cellular maintenance. However, such 'maintenance equations' were previously hotly discussed since especially the derivation of growth independent parameters is problematic (Bodegom, 2007). Hence, it might be worth to gather a larger data set of growth parameters from continuous processes with *C. glutamicum*, especially at very low growth rates ($\mu < 0.05\,\mathrm{h^{-1}}$, to potentially formulate an alternative description of maintenance. This could ultimately improve the prediction of steady state biomass concentrations as preliminary performed in this work.

4.5. Quantification of intracellular metabolite pools

As prerequisite to investigate intracellular metabolite pool sizes as a function of the growth rate and as mandatory input for non-stationary flux simulations, suitable quenching and extraction techniques were tested and validated to determine accurate metabolite pool sizes of *C. glutamicum*. For this purpose, a continuous process at $D = 0.4\,\mathrm{h^{-1}}$ was performed and different quenching-extraction combinations were tested. Based on these results, metabolome samples were withdrawn from continuous cultivations at $D = 0.2\,\mathrm{h^{-1}}$, $0.3\,\mathrm{h^{-1}}$ and $0.4\,\mathrm{h^{-1}}$.

4.5.1. Identification of best-suited quenching/extraction technique

For the quantification of *C. glutamicum*'s intracellular CCM metabolite and amino acid pool sizes, two different quenching and extraction techniques were tested, respectively. The combination yielding the greatest number of quantifiable metabolites with the highest metabolite concentration should be found and later employed to determine potential μ-dependent pool sizes (cf. section 4.6) and as a prerequisite for non-stationary ^{13}C-flux analysis (cf. section 4.7). Another requirement was that the extraction method should be performable in one single step. Thereby, differential measurements of quenching-supernatants are omitted which otherwise have to be performed to account for leaked intracellular metabolites (Paczia et al., 2012).

Four independent metabolome samples from a continuous process at $D = 0.4\,\mathrm{h}^{-1}$ were taken in 1.5 h intervals in the metabolic stationary phase after at least 5 RT. Classical cold-methanol quenching [MQ, Koning & van Dam (1992)] or an adapted version (Teleki, 2016) of FCT (Plassmeier et al., 2007) were used as quenching methods for 2 mL biosuspension. Chloroform-methanol extraction [CE, Koning & van Dam (1992)] and hot-water-extraction [HWE, Bolten et al. (2007)] were applied to extract metabolites from the resulting biomass pellets (cf. section 3.11.1). Both quenching methods were combined with either of the extraction techniques resulting in four sample pairs: MQ-HWE, MQ-CE, FCT-HWE, and FCT-CE. To ensure comparability of the measured metabolite concentrations obtained from each pair, the same amount of extraction solution was used for either method. Metabolite extracts were then analyzed with an LC-MS QQQ device and subsequently quantified as described in section 3.11.3. The results of this analysis is illustrated in figure 4.8 for CCM metabolites and in figure 4.9 for amino acids showing the performance of each sample pair with standard deviations from the four replicates. In table 4.6, the 30 detected metabolites were assigned to one of the quenching-extraction combinations yielding the best result.

Regarding the spread of peak area measurements of a single metabolite, MQ-HWE and MQ-CE showed the highest deviations with an average standard error of about 20 %. In contrast, FCT-CE showed a mean error of 9 % and FCT-HWE of 6 %. Considering the smaller errors of the FCT-methods, a biological deviation in between samples was excluded which was further confirmed by equal kinetic parameters determined for each sampling point (data not shown). Hence, the high deviation was most likely a consequence of the MQ-technique showing high errors with either HWE or CE. In addition to the small deviations observed for FCT-HWE samples, the combination yielded the highest peak

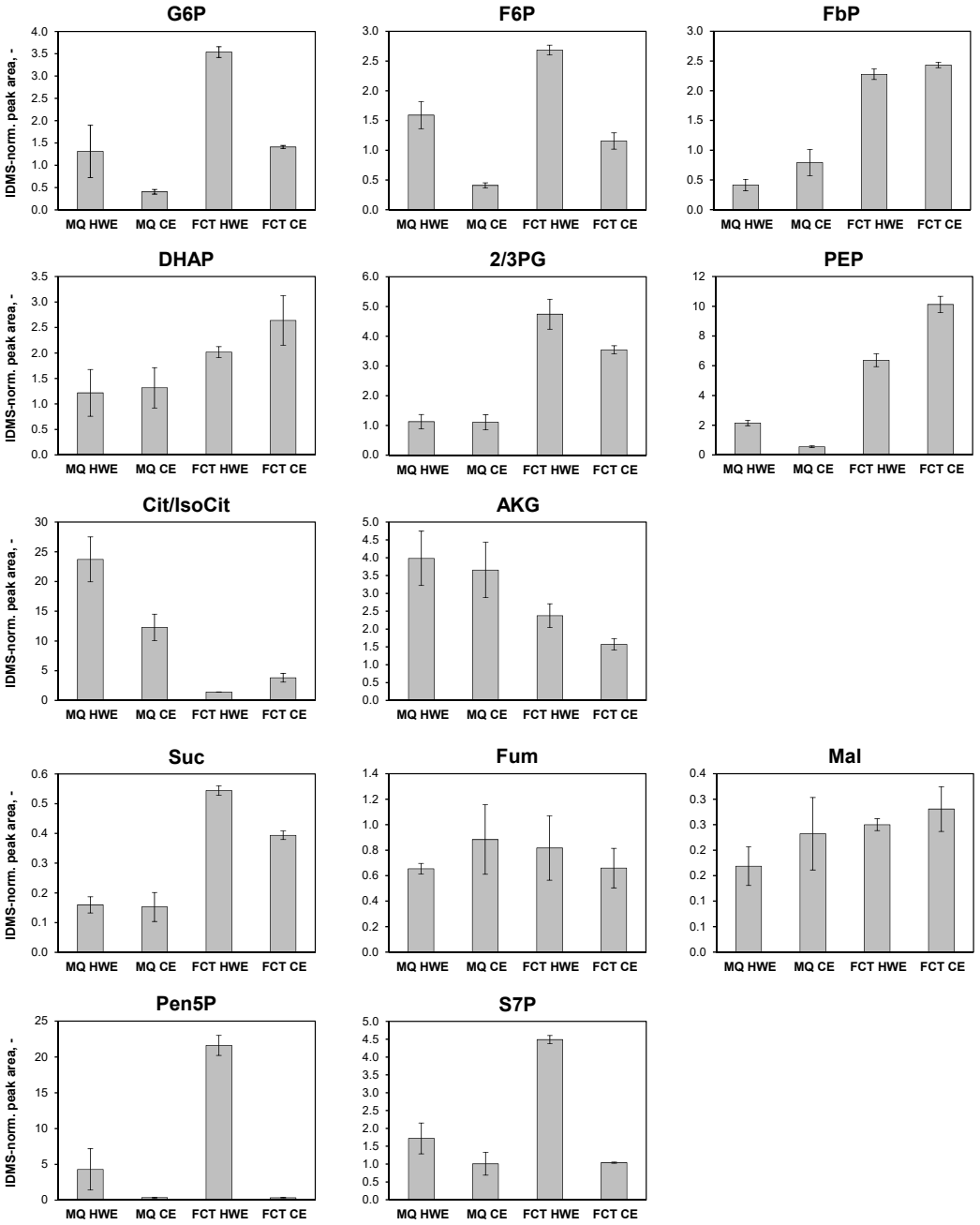

Figure 4.8.: Illustration of IDMS-normalized peak areas of intracellular metabolites of *C. glutamicum*'s central carbon metabolism. *C. glutamicum* was cultivated in a chemostat process at $\mu = 0.4\,\mathrm{h}^{-1}$. Cold methanol-quenching (MQ) or fast centrifugation treatment (FCT) were employed as quenching techniques in combination with cold methanol (CE) or hot-water-extraction (HWE). Mean peak areas ± standard deviations are based on peak areas of four individual biomass samples withdrawn during the course of the experiment.

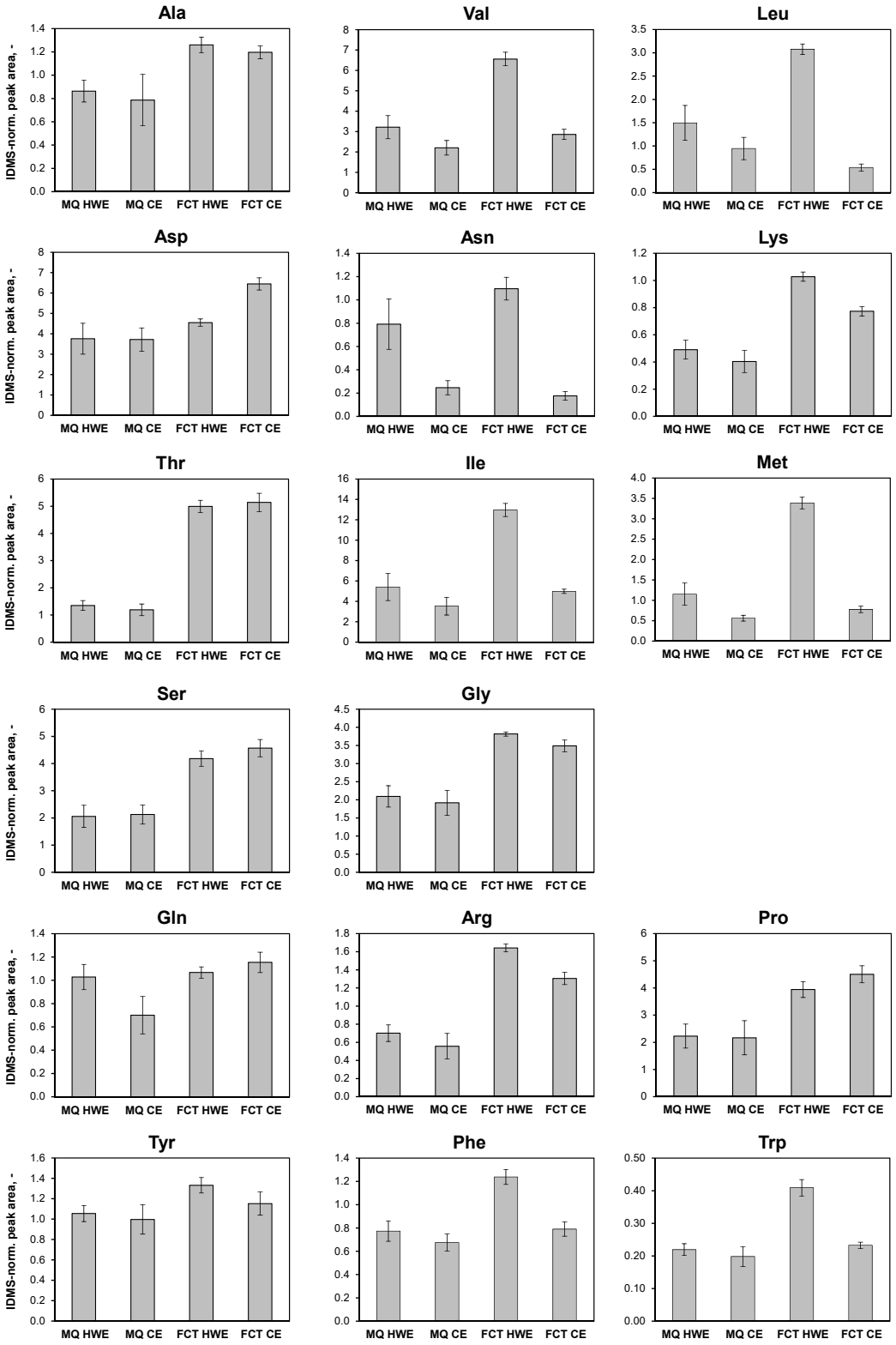

Figure 4.9.: Illustration of IDMS-normalized peak areas of intracellular amino acids from *C. glutamicum* cultivated in a chemostat process at $\mu = 0.4\,\mathrm{h}^{-1}$. MQ: cold methanol-quenching, FCT: fast centrifugation treatment, CE: cold methanol extraction, HWE: hot-water-extraction (HWE).

Table 4.6.: Ranking of quenching-extraction combinations according to metabolites showing the highest IDMS-normalized peak areas with respective methods. MQ: methanol-quenching, FCT: fast centrifugation treatment, HWE: hot-water extraction, CE: cold-methanol extraction.

MQ-HWE	MQ-CE	FCT-HWE	FCT-CE
Cit/IsoCit	Fum	G6P	FbP
AKG		F6P	DHAP
		2/3PG	PEP
		Pen5P	Mal
		S7P	Asp
		Suc	Thr
		Ala	Ser
		Leu	Gln
		Val	Pro
		Asn	
		Ile	
		Lys	
		Met	
		Gly	
		Arg	
		Tyr	
		Phe	
		Trp	

areas for most metabolites. Since MQ-CE is still the standard method for metabolome pool quantification of many organisms (Zhang et al., 2018), corresponding results were used as bench mark for the other quenching/extraction combinations in the following. Regarding metabolites of glycolysis (cf. figure 4.8), peak areas of sugar phosphates G6P and F6P, and 2/3PG were in average seven-fold greater for FCT-HWE than for MQ-CE. FCT-CE yielded the highest area for FbP, DHAP, and PEP (3.1 ×, 2.0 ×, 18.5 × MQ-CE). However, the standard deviation for FbP using this method was within the range of FCT-HWE. FCT-HWE offered the highest areas for the PPP metabolites (Pen5P: 59 ×, S7P: 4.5 × MQ-CE), and Suc (3.6 × MQ-CE). Fum and Mal showed the highest quantity with MQ-CE and FCT-CE (1.2 × MQ-CE), respectively, that were both within the range of the FCT-HWE results. MQ-HWE was the best option for the other TCA players Cit/IsoCit and AKG (1.9 ×, 1.2 × MQ-CE). All detectable amino acids* revealed the highest peak areas with a FCT-combination (cf. figure 4.9). Asp showed the best result with FCT-CE (1.7 × MQ-CE), whilst Thr, Ser, Gln, and Pro quantities of FCT-CE samples were within the range of the ones obtained from FCT-HWE. The residual amino acids were all captured in the highest quantities with FCT-HWE giving a

*Glutamate was abundant in all samples exceeding the calibration range and was therefore not considered in deciding on the most-suitable quenching-extraction technique.

mean of 2.9 × peak area of MQ-CE. In summary, the standard procedure MQ-CE only proved to be the best option for Fum and MQ-HWE was equally seldom the option of choice (Cit/IsoCit, AKG). FCT-HWE was the best combination for 18 and FCT-CE for nine metabolites, whereof five (FbP, Thr, Ser, Gln, Pro) showed similar high peak areas with FCT-HWE.

As already suspected from the high MQ-sample deviations, quenching with cold methanol most likely caused metabolite loss from quenched biomass samples. The same observation was made by Wittmann et al. (2004) who discovered that cold shock induced by cold methanol causes leaky *C. glutamicum* cells. The authors registered severe losses of intracellular amino acid pools which mirrors our results. This qualifed either FCT-HWE or FCT-CE as the methods of choice to quantify intracellular amino acids. Bolten et al. (2007) and Spura et al. (2009) detected losses of a wide range of metabolites (i.e. amino acids, phosphorylated compounds, and organic acids) from methanol-quenched samples in contrast to non-quenched samples obtained by an FCT-like approach. Since the majority of metabolites except for AKG, Cit/IsoCit, and Fum were lost in our MQ-samples as well, it could be possible that these compounds stuck to the cell debris after quenching with cold methanol and therefore did not leak from the cell prior to extraction. Based on the generally higher peak areas of most metabolites quenched with FCT, less cell leakage as in MQ-samples seemed plausible and was conform with the results of Plassmeier et al. (2007). Nevertheless, using FCT delayed quenching of the biomass sample for at least 30 s which is a severe drawback of the method (Gulik, 2010; Plassmeier et al., 2007). Due to the high turn-over rates of *in vivo* intracellular metabolite pools, a shift of metabolite pools in this time period has to be expected (Oldiges et al., 2007). Hence, differences in peak areas of MQ- and FCT-quenched cells could represent another metabolic state of the cell. On that account, a smaller concentration of pools from upper glycolysis (G6P, F6P) should be observable in FCT samples, using the turnover rate of $1\,\mathrm{mmol\,L^{-1}\,s^{-1}}$ for cytosolic glucose determined in yeast cultures as guideline (Koning & van Dam, 1992). However, comparing FCT- to MQ-samples revealed seven-fold higher concentrations of the hexose phosphate sugars with FCT, making it impossible to quantify a 'loss' due to metabolic turnover. This observation was reverse to the findings of Bolten et al. (2007) who measured declining levels of upper glycolysis metabolites retrieved from fast filtration samples that were also afflicted with a delay time. In this case, however, biomass samples were withdrawn from substrate unlimited batch cultivations. *Vice versa*, the (unexpectedly) high pools of phosphate sugars in FCT-biomass observed here (see also section 4.5.2) were withdrawn from a glucose-limited growth environment in

which extracellular glucose concentrations should range around the K_S value of the active glucose transporter(s) [e.g. PTS: 14 µmol L^{-1}, Lindner et al. (2011)]. Thus, during the delay between sampling and quenching of cells with FCT (contrasted to the immediate quenching with MQ) the cell's extracellular environment did not alter drastically: glucose was still limiting and oxygen deprivation should not have set in this fast considering oxygen saturation of at least 70 % in the bioreactor (data not shown). As a result, the metabolic state recorded in substrate-limited chemostat samples might not be disturbed by prolonged time until quenching as generally suspected. The high similarity between metabolite pool concentrations of phosphate sugars determined from differentially measured MQ-samples at $D = 0.2\,h^{-1}$ of Pfelzer (2016) and our FCT-results affirmed this hypothesis (cf. section 4.5.2).

A disadvantage of both tested quenching techniques is the potential carryover of extracellular metabolites from the unwashed biomass samples that potentially bias the intracellular quantification as shown by Persicke et al. (2011) and Paczia et al. (2012). However, in contrast to the later studies where samples were withdrawn from *C. glutamicum* batch cultivations with substrate excess, again the substrate-limited conditions in chemostats were advantageous. Previously, an *E. coli* chemostat study showed that amounts of extracellular metabolites were insignificantly small compared to intracellular metabolite pool concentrations (Paczia et al., 2012). In our processes, no by-products or typical intracellular metabolites were detectable in filtrates of continuous process samples analyzed with LC-MS QTOF. Nevertheless, biased intracellular metabolite pools by carryover from extracellular compounds is not only a valid point for quenching samples from batch cultivations, but also for investigations with producer strains since they excrete intracellular metabolites as products. Under such circumstances isotonic washing should be incorporated in the quenching-extraction procedure to deprive the intercellular room of extracellular metabolites (Bolten et al., 2007; Teleki, 2016). Irrespective of the applied quenching method, water proved to be the extracting agent of choice for most metabolites. Comparing the results of MQ-HWE with MQ-CE and FCT-HWE with FCT-CE, respectively, higher concentrations of upper glycolysis-, PPP-, most TCA-metabolites, and most amino acids were obtained with sole water than with methanol-water solution. A more detailed analysis regarding the causes of this observation was not performed since it would exceed the scope of this thesis.

Summary and interim conclusion

In summary, the different combinations of quenching and extraction techniques resulted in

varying peak areas for the same metabolite. Consequently, determination of intracellular metabolite pool concentration does not only depend on accurate measurements of the cell volume (which was not part of this work), but also on the chosen quenching-extraction methods. Deduced from these results, there is no single-best option for all metabolites to reliably determine intracellular pool sizes. For instance, FCT-HWE showed the highest peak areas for hexose phosphate sugars G6P and F6P whilst TCA-players citrate and AKG were best captured with MQ-HWE. The ideal quenching-extraction procedure would look as the following: one quenching technique is applied to record one specific metabolic steady state of the cell. Biomass samples are then extracted using a variety of extraction methods that are ideal for the target metabolites which allows determination of accurate pool concentrations. Zhang et al. (2018) came to the same conclusion for batch-grown *C. glutamicum* cultures. They showed that 33 % (v/v) boiling ethanol solution was the best extraction method for organic acids and amino acids (especially Val, Ser), whilst 50 % (v/v) acidic acetonitrile solution [with 0.1 %(v/v) formic acid] at −20 °C was best for sugar phosphates and other amino acids (e.g. Asp, Tyr). With regard to quenching, they furthermore found that the low temperature of −70 °C and high concentration of methanol [60 % (v/v)] in the standard MQ-procedure (Koning & van Dam, 1992) were responsible for severe cell damage and leakage of intracellular metabolites. Consequently, they adjusted the original method using 40 % (v/v) methanol-solution and operating at −20 °C which delivered intact quenched *C. glutamicum* cells exhibiting no leakage. Because this latter study was published after the presented analytical investigations were performed in the scope of this thesis, results of Zhang et al. (2018) were not employed in this work.

Based on the presented investigation of different quenching and extraction techniques, several conclusions were drawn for the aims of this thesis. Firstly, absolute quantification of intracellular metabolite concentrations cannot be performed with only one quenching-extraction combination and needs further optimization. Only a preliminary estimation on absolute intracellular pool sizes can be given. To nevertheless investigate pool size changes in relation to growth rate changes, relative measurements will be performed employing one single quenching-extraction combination for all samples and metabolites. Thereby, leakage or insufficient extraction effects are accounted for allowing statements about pool size changes due to growth rate changes. In this sense, FCT-HWE was chosen as method of choice because it provided the highest peak areas for most metabolites and the smallest standard deviations. Besides, this combination provided the shortest quenching and extraction procedures. Secondly, to determine intracellular fluxes at μ

$= 0.4\,h^{-1}$ in continuous cultivation mode, a stationary ^{13}C-labeling experiment will be performed since no metabolite pool sizes are required for corresponding stationary MFA simulations.

4.5.2. Biomass specific metabolic pool sizes

Based on the investigation presented in the previous section, metabolome samples withdrawn during continuous processes at growth rates of $0.2\,h^{-1}$, $0.3\,h^{-1}$ and $0.4\,h^{-1}$ (cf. section 4.4) were quenched with the FCT method and intracellular metabolites were extracted with HWE. To account for the slightly increasing biomass concentrations observed with increase of μ (cf. table 4.5 and figure 4.4), the amount of extraction buffer was adjusted to yield the same biomass extraction concentration. Subsequently, extracts were analyzed with LC-MS QQQ as described before (cf. section 3.11.3). Each growth rate of the three processes was sampled for three times in 1.5 h intervals whereof mean values and standard deviations were calculated as listed in table D.5. In addition, average biomass specific metabolite pool concentrations for one growth rate was calculated from all biological replicates and are given in table 4.7. Biomass specific pools ranged between minimal values of $0.01\,\mu mol\,g^{-1}{}_{CDW}$ (Asn) and maximum values of $250\,\mu mol\,g^{-1}{}_{CDW}$ (Glu). Pool sizes measured at the same growth rate of the three biological replicate processes exhibited very good reproducibility with standard errors between 2 and 8 %. This matched the results of the quenching-extraction-investigation that qualified FCT-HWE as method with the lowest standard deviation between technical replicates (cf. section 4.5.1). Moreover, this indicated that the sampled metabolic steady states of biological replicates at equal growth rates were the same, as previously shown by agreeing kinetic parameters presented in section 4.4.2. However, Cit/Isocit and Pro pools revealed standard errors of 13 % and 25 % at $\mu = 0.2\,h^{-1}$, respectively. The former result was most likely due to the very low amounts of Cit/Isocit measured [(3–10) $nmol\,g^{-1}{}_{CDW}$] as a consequence of using FCT-HWE (section 4.5.1). An interesting observation was that pool concentrations for nearly all analyzed metabolites changed in a growth rate dependent manner, e.g. the G6P pool increased from $(1.32 \pm 0.04)\,\mu mol\,g^{-1}{}_{CDW}$ at $\mu = 0.2\,h^{-1}$ to $(6.65 \pm 0.29)\,\mu mol\,g^{-1}{}_{CDW}$ at $\mu = 0.4\,h^{-1}$, which will be further discussed in section 4.6.

Normally, the accurate unit of measure for metabolite pool sizes is $\mu mol\,L^{-1}$ or $mmol\,L^{-1}$, e.g. to analyze the influence of the metabolite concentration on enzyme activities by comparison to saturation or inhibition concentrations. However, data

presented here (cf. table 4.7) is based on the mass of biomass ($\mu mol\,g^{-1}_{CDW}$) since the cell volume was not determined in this work. Knowledge of the cell volume is crucial to calculate correct intracellular pool concentrations in $mmol\,L^{-1}$. A study has shown that the cell length of *C. glutamicum* can vary with the growth rate (Unthan et al., 2013) which can influence the cell volume and ultimately the pool concentration. Therefore, the measured metabolite pools were not normalized to an assumed cell volume as often done in literature to prevent false interpretation.

4.6. Metabolic and transcriptional response to increasing growth rates

After characterizing the growth physiology of *C. glutamicum* at different metabolic steady states ($\mu = 0.2\,h^{-1}$, $0.3\,h^{-1}$ and $0.4\,h^{-1}$) from an extracellular point of view (section 4.4), a detailed look is taken on intracellular metabolome and transcriptome levels in this section. Based on the results of previous section 4.5, changes of metabolite pools at growth rates $0.3\,h^{-1}$ and $0.4\,h^{-1}$ are discussed in relation to the pool sizes of $\mu = 0.2\,h^{-1}$ and not quantitatively. Thereby, a potential bias in the respective pools sizes originating from the chosen quenching-extraction technique FCT-HWE was avoided. Transcriptome samples were withdrawn once at each μ and from each process and were further processed as stated in section 3.12.3. Comparable to the presentation of metabolite pool size changes, gene expression changes of differentially expressed genes (DEGs) determined at $\mu = 0.3\,h^{-1}$ and $0.4\,h^{-1}$ are based on gene expressions determined at $\mu = 0.2\,h^{-1}$ and are given as log-fold changes (FCs). The analysis revealed a total of 547 DEGs that were distinguished in two clusters as pictured in figure 4.10. Cluster 1 contained 257 genes showing increasing expression over the growth rate (cf. table D.6), whilst cluster 2 comprised the residual 290 genes with strictly decreasing expression over μ (cf. table D.7). Due to their nearly proportional expression over μ (cf. figure 4.10), given FCs in the following paragraphs always refer to the maximum FC change determined for $\mu = 0.4\,h^{-1}$. Gene products of discussed genes were retrieved from the CoryneRegNet database (Pauling et al., 2012) if not otherwise stated. The intracellular metabolome analysis only covered intermediates of the CCM and intracellular amino acids. Therefore, results of the metabolome analysis are firstly discussed together with corresponding data of the transcript analysis. Afterwards, growth rate dependent gene expression patterns of other cellular functions are presented.

Table 4.7.: Biomass specific metabolite pool concentrations obtained with the fast-centrifugation-treatment and hot-water-extraction from three biological replicates of *C. glutamicum* cultures cultivated in chemostat mode (processes A, B, C) at growth rates of $0.2\,h^{-1}$, $0.3\,h^{-1}$ and $0.4\,h^{-1}$. Values represent means ± standard deviations of the biological triplicates.

Metabolite	Pool size, µmol g^{-1}_{CDW}		
	$\mu = 0.2\,h^{-1}$	$\mu = 0.3\,h^{-1}$	$\mu = 0.4\,h^{-1}$
G6P	1.32 ± 0.04	4.32 ± 0.16	6.65 ± 0.29
F6P	0.64 ± 0.03	2.16 ± 0.06	3.24 ± 0.08
FbP	0.85 ± 0.07	4.54 ± 0.09	9.33 ± 0.64
DHAP	0.16 ± 0.02	0.52 ± 0.03	0.63 ± 0.04
2/3PG	1.05 ± 0.04	0.96 ± 0.07	0.65 ± 0.02
PEP	1.48 ± 0.04	1.27 ± 0.04	0.90 ± 0.03
Cit/IsoCit	0.00 ± 0.00	0.01 ± 0.01	0.01 ± 0.00
AKG	0.75 ± 0.05	0.58 ± 0.01	0.58 ± 0.02
Suc	7.12 ± 0.53	9.27 ± 0.14	8.71 ± 0.52
Fum	0.06 ± 0.00	0.09 ± 0.00	0.11 ± 0.00
Mal	0.34 ± 0.01	0.60 ± 0.01	0.75 ± 0.03
Pen5P	0.89 ± 0.02	0.82 ± 0.03	1.00 ± 0.04
S7P	0.44 ± 0.03	0.76 ± 0.02	0.83 ± 0.02
Ala	5.19 ± 0.41	5.59 ± 0.23	6.37 ± 0.81
Leu	0.66 ± 0.03	0.64 ± 0.01	0.41 ± 0.01
Val	2.25 ± 0.01	3.04 ± 0.07	2.63 ± 0.05
Asp	5.44 ± 0.25	4.87 ± 0.20	5.86 ± 0.12
Asn	0.01 ± 0.00	0.01 ± 0.00	0.01 ± 0.00
Lys	0.78 ± 0.06	1.20 ± 0.06	1.45 ± 0.12
Thr	0.86 ± 0.02	1.11 ± 0.02	1.35 ± 0.02
Ile	0.50 ± 0.03	0.73 ± 0.02	0.64 ± 0.01
Met	0.61 ± 0.03	0.48 ± 0.01	0.31 ± 0.00
Ser	0.99 ± 0.03	1.46 ± 0.04	1.61 ± 0.04
Gly	1.43 ± 0.04	1.98 ± 0.05	3.13 ± 0.06
Glu	255.35 ± 4.06	253.23 ± 5.02	248.58 ± 3.98
Gln	6.22 ± 0.16	6.79 ± 0.14	10.13 ± 0.15
Arg	0.24 ± 0.01	0.25 ± 0.00	0.28 ± 0.00
Pro	0.73 ± 0.19	1.09 ± 0.01	3.89 ± 0.08
Tyr	0.03 ± 0.00	0.06 ± 0.00	0.09 ± 0.00
Phe	0.05 ± 0.00	0.08 ± 0.00	0.13 ± 0.00
Trp	0.02 ± 0.00	0.03 ± 0.00	0.03 ± 0.00

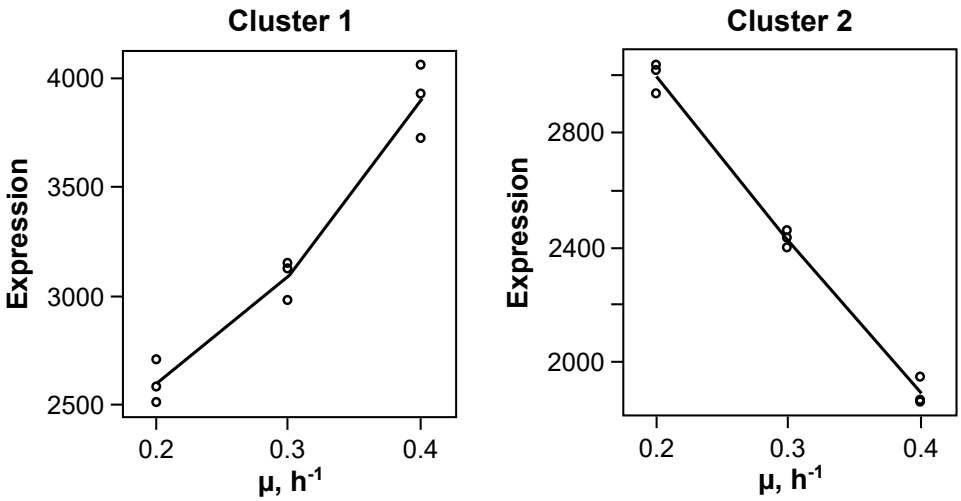

Figure 4.10.: Median expression profile of differentially expressed genes obtained from transcriptome analysis of *C. glutamicum* cells grown in chemostat cultures ($\mu = 0.2\,h^{-1}$, $0.3\,h^{-1}$ and $0.4\,h^{-1}$). 257 genes were grouped in cluster 1 and 290 genes in cluster 2.

4.6.1. Central carbon metabolism and amino acid biosynthesis

In figure 4.11 and figure 4.12, $\mu = 0.2\,h^{-1}$ normalized poolsizes of CCM metabolites and amino acids are illustrated. Each of the three data points at $\mu = 0.2\,h^{-1}$, $0.3\,h^{-1}$ and $0.4\,h^{-1}$ represents the average value of three samples withdrawn during one continuous process as listed in table D.5. The majority of metabolite pools increased with the growth rate resulting in 1.2 to 11 times higher concentrations at $\mu = 0.4\,h^{-1}$ compared to $\mu = 0.2\,h^{-1}$. AKG, Asp, and Glu revealed approximately constant pools at each tested growth rate. 2/3PG, PEP, Leu, and Met were the only compounds showing significantly decreasing pools that were down to half the concentration measured at $\mu = 0.2\,h^{-1}$. 32 of the 547 genes exhibiting significant expression changes with μ encoded enzymes of CCM and amino acid biosynthesis. 20 genes showed increasing and 12 genes diminished expression with moderate FCs of 1.4 as maximum and -1.6 as minimum value, respectively, compared to the expression at $\mu = 0.2\,h^{-1}$.

In glycolysis, metabolite pools of the upper part (G6P, F6P, FbP, DHAP) linearly increased five- to 11-fold from $\mu = 0.2\,h^{-1}$ to $0.4\,h^{-1}$ which is contrasted by representatives of lower glycolysis (2/3PG, PEP) decreasing about 40 % in pool size. Interestingly, transcript data revealed two genes related to glucose uptake and only one gene of glycolysis being differentially expressed with the growth increase. *ptsI* and *ptsS* encoding enzyme I and the sucrose-specific enzyme II of the PTS revealed FCs of up to 0.5 and 1.1, respectively, fitting the enhanced glucose consumption rates with rising μ (cf. table 4.5).

However, *pgi* encoding glucose 6-phosphate isomerase (G6PI), catalyzing the very first step towards glycolysis, was slightly decreased in its expression (FC = -0.3).

In PPP, the summed pool of Pen5P sugars showed a 10 % decrease at $\mu = 0.3\,h^{-1}$ compared to the $\mu = 0.2\,h^{-1}$ pool, which again slightly increased to 1.1-fold at $\mu = 0.4\,h^{-1}$. S7P showed a steady increase to twofold the pool size of $\mu = 0.2\,h^{-1}$ at $0.4\,h^{-1}$. No growth-dependent transcriptional response was detected for any of the PPP-related genes.

Regarding pool changes of TCA-metabolites, the summed pool of Cit/IsoCit rose about five times the quantity of the pool at $\mu = 0.2\,h^{-1}$. However, Cit/IsoCit pools were exceptionally small compared with other metabolites (cf. table 4.7) as a consequence of the FCT-HWE method. Further downstream, AKG revealed slightly decreasing pool sizes with rising μ, but rather high deviations were observed that were within the $\mu = 0.2\,h^{-1}$ range for the $\mu = 0.3\,h^{-1}$ and $0.4\,h^{-1}$ data points. Increasing μ from $0.2\,h^{-1}$ to $0.3\,h^{-1}$ resulted in 1.4 × higher Suc pools remaining at this size at $\mu = 0.4\,h^{-1}$. In contrast, Fum and Mal showed linear increases between 1.5- and twofold over μ. Transcriptome analysis yielded ten TCA-related DEGs. In total, four showed enhanced expression over μ of which three encode enzymes that catalyze reactions fueling TCA via acetate (*ackA* and *pta*, both with FC = 0.9) or via AceCoA (*gltA*, FC = 0.6). *lpdA* (cg0790) coding for a lipoamide dehydrogenase (LPD), in addition or as alternative (Eikmanns, 2005) to gene *lpd* [cg0441, (Schwinde et al., 2001)], exhibited enlarged expression over μ (FC = 0.4). Since this enzyme is part of the Pyr dehydrogenase and 2-oxoglutarate dehydrogenase complex (PDHC, ODHC), its differential expression might be relevant for glycolysis- and TCA-control by fueling AceCoA or SucCoa formation, respectively. However, genes encoding the other subunits of the dehydrogenases (PDHC: *aceE*, *aceF*; ODHC: *odhA*, *aceF*) were not significantly expressed. Genes *ldh* and *pqo*, encoding lactate dehydrogenase and pyruvate:quinone oxidoreductase, showed decreasing expression levels with log-fold changes of -0.3 and -0.9, respectively. Likewise, *sucC* and *sucD* encoding the α- and β-subunits of the succinyl-CoA synthetase (FC = -1.6 and -1.7), *aceB* coding for malate synthase in the glyoxylate shunt (FC = -0.5), *mdh* coding for malate dehydrogenase (FC = -0.7), and *pck* representing PEP carboxykinase (FC = -1.0), all revealed decreasing expression with rising growth rate.

Varying pool profiles of the Pyr family amino acids were observed as Ala and Val linearly rose up to 1.4-fold at $\mu = 0.4\,h^{-1}$, but the Leu pool had dropped by 40 % at $\mu = 0.4\,h^{-1}$. The branch-chained amino acids Val and Ile share enzymes encoded by *ilvBNCDE* for their respective biosynthesis pathways [summarized in Pátek (2007)]. For

Val synthesis, 2-ketoisovalerate is the final and simultaneously the first precursor in the Leu pathway. In this context, *ilvC* encoding the NADPH-dependent reaction from acetolactate to 2,3-dihydroxy-ketoisovalerate in the Val pathway revealed an increased expression level with a log-fold change of 0.8. In Leu synthesis, expressions of genes *leuA* (FC = 0.4), *leuC* and *leuD* were increased. The later two encode the subunits of 3-isopropylmalate dehydratase and showed the highest gene expressions amongst the CCM and amino acid biosynthesis related DEGs (FC = 1.4). Astonishingly, *ltbR* encoding regulatory protein LtbR that directly controls the biosynthesis of Leu via repression of *leuB leuC*, and *leuD*, and of Trp synthesis (Brune et al., 2007), was increasingly expressed as well.

Amongst the Asp family amino acids, Lys and Thr showed linear pool increases by two- and 1.6-fold, respectively, whilst Asp revealed a decline of about 10 % at $\mu = 0.3\,h^{-1}$ and rose only slightly to about 1.1-fold at $0.4\,h^{-1}$. An inverse behavior was observed for Asn and Ile, showing initial increases (1.2- and 1.4-fold, respectively) and then moderate decreasing sizes at $0.4\,h^{-1}$ by 10 % and 20 %, respectively. On the contrary, the Met pool linearly decreased over the growth rate yielding only 40 % of the $\mu = 0.2\,h^{-1}$ pool size at $\mu = 0.4\,h^{-1}$. The Asp building reaction via Fum encoded by *aspA* showed a decreased expression over μ (FC = -0.5), but the other seven Asp family-related DEGs were increasingly expressed: the key reaction into the Asp branch catalyzed by *asd* (FC = 0.4), the (potential) Ans building reaction encoded by *ltsA* (FC = 0.4), *dapB* of Lys synthesis (FC = 0.5), *thrC* encoding the final step in Thr formation (FC = 0.4), *ilvC* of Ile/Val synthesis (FC = 0.8), and two genes of the Met pathway (*metB*: FC = 0.7, *metE*: FC = 0.8).

Amino acid pools of the Ser family (Gly, Ser) rose proportionally with μ, whilst Cys was not analyzable with the applied analytical methods (cf. section 3.11.3). Interestingly, Gly showed higher pool changes (2.5×) in comparison to Ser (1.75×). *serC* encoding the transaminase reaction towards phosphoserine and *cysE* coding for serine O-acetyltransferase were the only DEGs in this amino acid family showing increased expression over μ (FC = 0.3 and 0.4, respectively). Besides, *sdaA* encoding the degradation of Ser to Pyr (Netzer et al., 2004) revealed diminished expression with increasing μ (FC = -0.7).

Likewise to AKG, Glu pools were constant over μ, but Gln and Arg showed straight proportionality of up to 1.6- and 1.2-fold, respectively. Pro revealed enhanced sizes at $0.4\,h^{-1}$ that were up to six times the value of $\mu = 0.2\,h^{-1}$, but with high deviations between biological replicates due to varying pool sizes at $\mu = 0.2\,h^{-1}$ (cf. section 4.5.2).

With regard to the whole Glu amino acid family, only *glnA2*, the second gene encoding glutamine synthetase next to *glnA* exhibited decreasing fold changes of -0.3. The function of *glnA2* in Gln synthesis is still unclear (Rehm & Burkovski, 2011).

Aromatic amino acids revealed strictly increasing pools with increasing growth rate. Whilst Tyr- and Phe-concentrations were similarly enhanced to about threefold the value of $\mu = 0.2\,h^{-1}$ at $0.4\,h^{-1}$, Trp showed a smaller increase by 1.4-fold. Transcript analysis did not yield DEGs related to the individual biosynthesis pathways of Tyr, Phe, or Trp, but revealed two genes of the shikimate pathway that were either increased (*qsuC*: FC = 0.5) or decreased (*aroE1*: FC = -0.2) in expression. Besides Cys, His was the other amino acid whose pool could not be determined with the used analytical methods. Nevertheless and in accordance to the other DEGs related to amino acid biosynthesis presented, expression of gene *hisG* was elevated with a log-fold change of 0.5.

Merging metabolome, transcriptome, and proteome data

Since this investigation did not cover the proteomic response of *C. glutamicum* to increasing growth rates in carbon-limited environments, the recent study of Noack et al. (2017) might give further input to interpret the observed metabolic and transcriptional responses. Noack et al. (2017) conducted chemostat cultivations at growth rates of $0.05\,h^{-1}$, $0.1\,h^{-1}$, $0.2\,h^{-1}$ and $0.35\,h^{-1}$ and found that concentrations of detectable CCM enzymes were constant at all μ. They concluded that under the tested conditions, metabolic fluxes are likely more affected by concentrations of local substrates and allosteric metabolite effectors than by the concentration of enzymes (Noack et al., 2017). Considering the highly comparable experimental setup and identical growth medium as used in this study, it was assumed that enzymes whose genes were not differentially expressed over μ in this investigation mirrored the results of Noack et al. (2017) and most likely had constant concentrations in this work as well. However, potential post-translational modifications influencing the enzyme activity are neglected in these considerations. Besides, the transcriptome study of my colleague Thorsten Haas is of great interest for comparison. In the corresponding paper, genes representing the growth modulon of *C. glutamicum* were identified for growth rate transitions in glucose-unlimited batch cultivations (Haas et al., 2019). Since the same growth medium as employed in the presented chemostat studies was used by Haas et al. (2019) (CGXII minimal medium supplemented with glucose and PCA), growth medium independent conclusions regarding μ ranges between $(0–0.4)\,h^{-1}$ could be derived. Together with the previous presentation of growth rate dependent gene expression from the supplementation studies (cf. section 4.3), control strategies

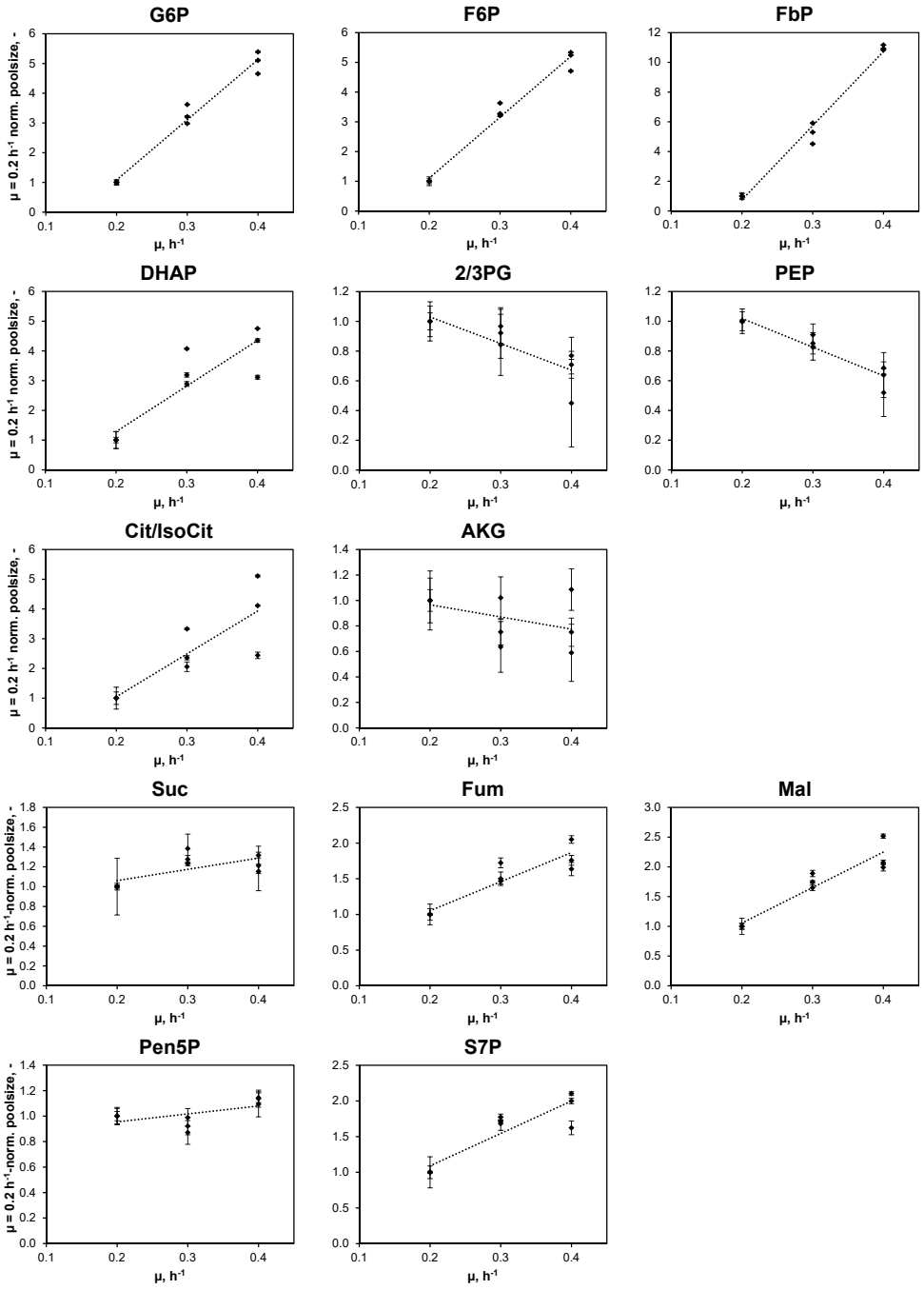

Figure 4.11.: Illustration of relative intracellular pool size changes of metabolites from central carbon metabolism. Pool sizes determined at $\mu = 0.3\,\mathrm{h}^{-1}$ and $0.4\,\mathrm{h}^{-1}$ were normalized to respective metabolite concentrations determined at $\mu = 0.2\,\mathrm{h}^{-1}$. Values represent the mean of three technical replicates ± standard deviation.

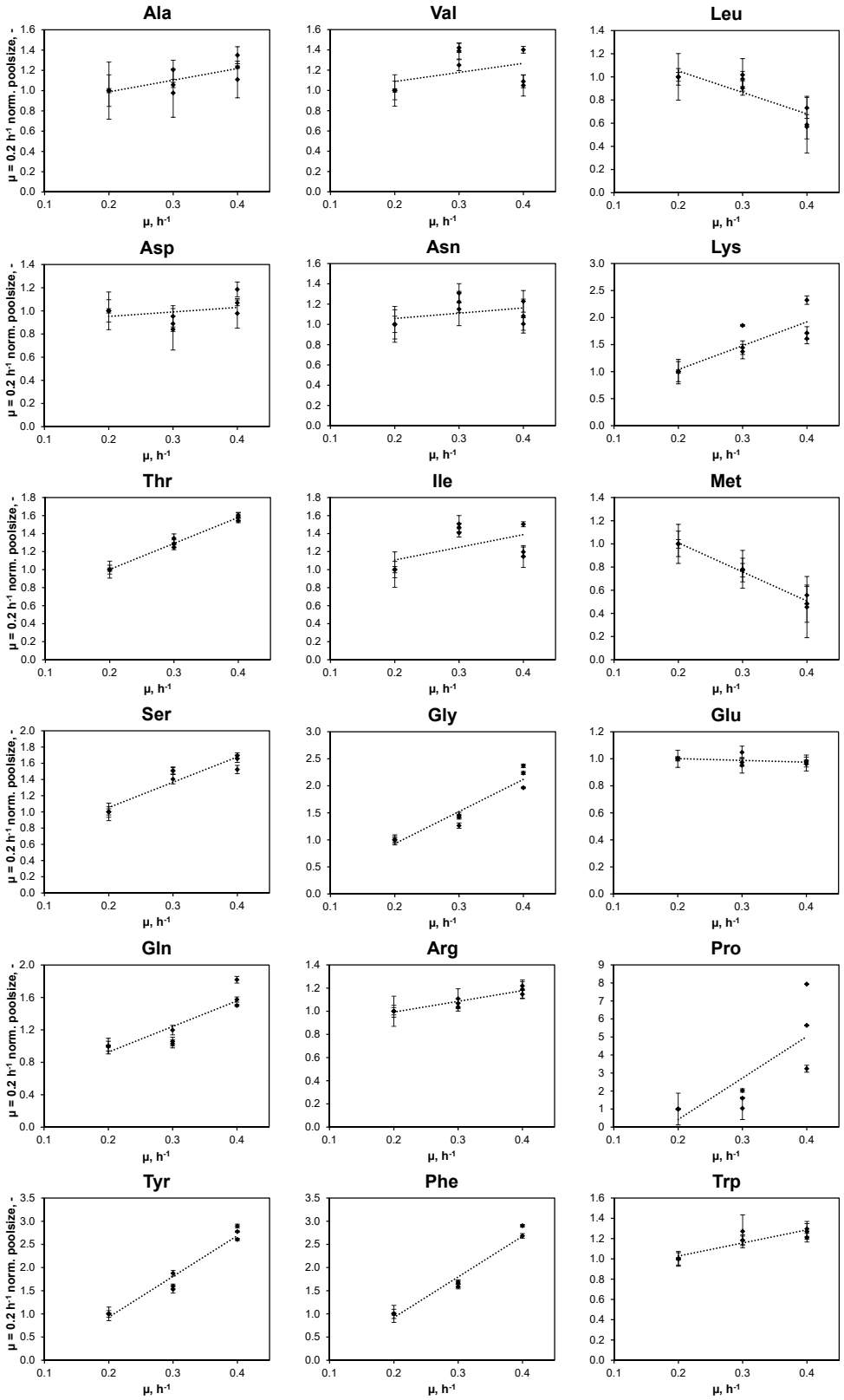

Figure 4.12.: Illustration of relative intracellular pool size changes of amino acids. Pool sizes determined at $\mu = 0.3\,\mathrm{h}^{-1}$ and $0.4\,\mathrm{h}^{-1}$ were normalized to respective amino acid concentrations determined at $\mu = 0.2\,\mathrm{h}^{-1}$. Values represent the mean of three technical replicates ± standard deviation.

governing growth of *C. glutamicum* and potential limitations in metabolic steady state growth could be identified.

Glucose uptake Genes encoding the general enzyme I of the PTS (*ptsI*) and the PTS-specific transporter for sucrose (*ptsS*) were significantly increased over μ. Since no proteome data was available for these enzymes (Noack et al., 2017), our transcriptome results suggested that the transport system was transcriptionally controlled. Findings of Engels & Wendisch (2007), Gaigalat et al. (2007), and Tanaka et al. (2008b) support this theory revealing that the presence of PTS sugars control *ptsI* expression mainly on the transcript level. Consequently, the increasing availability of glucose at rising growth rates most likely enhanced expression of *ptsI*. However, it is peculiar that *ptsS* was amongst the DEGs because it was reported that only fructose and sucrose enhance the expression of this gene (Tanaka et al., 2008b), but neither of the sugars was in the growth medium. Thus, the increased expression of *ptsS* could have resulted from de-repression of the master regulator of carbon metabolism SugR (Gaigalat et al., 2007). *sugR* showed diminished expression over μ (FC = -0.4). Normally, the regulator represses expression of PTS genes *ptsI*, *ptsH*, *ptsG*, *ptsF*, and *ptsS* in the absence of phosphorylated PTS sugars (Dietrich et al., 2009; Engels & Wendisch, 2007; Engels et al., 2008; Gaigalat et al., 2007; Tanaka et al., 2008a). Hence, under the tested chemostat conditions, SugR should not bind to the promoter region of its 43 target genes, which could explain why *ptsI* and *ptsS* revealed increased expression. Besides, Mori & Shiio (1987) and Parche et al. (2001) measured constitutive high glucose-PTS activity in *C. glutamicum* whether glucose was absent or present in the growth medium. This would explain why de-repression from SugR was not visible in the expression of *ptsG* but only in *ptsS* and *ptsI*.

Comparable observations were made in the transient batch cultivation study of Haas et al. (2019) finding increased expressions of *ptsI* and *ptsG* with rising μ. Consequently, expression of glucose uptake via PTS seems to be under transcriptional control whether *C. glutamicum* is grown in glucose-limited chemostat or glucose-abundant batch environments.

Glycolysis, PPP, and TCA *pgi* encoding glucose-6-phosphate isomerase (GPI) was the only glycolytic gene that showed a significant expression change with rising μ (cf. figure 4.13). Unfortunately, no proteome data is available for GPI (Noack et al., 2017). GPI is situated in the intersection of glycolysis and PPP and was shown to be strongly inhibited by E4P in *C. glutamicum* ATCC 14067 (Sugimoto & Shiio, 1987), most likely to

prevent E4P overproduction. Moreover, it is believed that GPI has no significant control over the carbon flux in glycolysis because the enzyme worked close to its thermodynamic equilibrium when *C. glutamicum* ATCC 17965 was cultivated in substrate-unlimited batch environments (Dominguez et al., 1998; Gourdon & Lindley, 1999). However, the role of GPI under glucose-limited growth environments was not investigated yet. Hence, if the observed decreasing transcriptional expression of corresponding gene *pgi* indeed mirrored a reduced activity of GPI or even represented a form of transcriptional control, this would imply that flux towards glycolysis was diminished with rising growth rates under the tested experimental conditions.

Apart from *pgi*, no genes of glycolysis revealed significant expression levels over μ and apparently, the de-repression of SugR-control did not influence the expression of its other target genes, e.g. *pfkA*, *fba*, *gapA*, or *pyk* (Engels et al., 2008). This non-existent transcriptional response corroborated the constant CCM-enzyme concentrations measured in the proteome study of Noack et al. (2017) which meant that carbon flux through glycolysis was very likely under metabolic control. Surprisingly, this result was in stark contrast to the elevated and μ-proportional expression of glycolytic genes in the batch investigation of Haas et al. (2019).

Based on the non-existent transcriptional response of PPP-genes [proteome data was not available from Noack et al. (2017)], one could assume that PPP-enzymes were expressed with constant concentrations over μ, mirroring the behavior of glycolytic proteins. Consequently, flux control would be on the metabolic level under the tested conditions, which is in agreement with studies of Moritz et al. (2000) and Haas et al. (2019).

Significant expression changes of several TCA genes were observed revealing both up- and down-regulated genes as illustrated in figure 4.14. Genes representing the entryway into TCA via Pyr revealed increased expression over μ (*lpdA*, *gltA*), as did genes encoding enzymes fueling TCA cycle via acetate activation (*ackA*, *pta*). Curiously, gene *pqo* encoding acetate synthesis via pyruvate:quinone oxidoreductase as well as *ldh* coding for lactate dehydrogenase were down regulated. A similar result was found in the transcript analysis of transient batch cultivations (Haas et al., 2019), however only for low growth rates. Also, *sucCD* revealed decreasing expression under glucose-limited but increased expression during the glucose-unlimited batch experiment (Haas et al., 2019). Noack et al. (2017) did not measure altered enzyme concentrations of any corresponding TCA enzymes (i.e. citrate synthase, fumarase, malate dehydrogenase, malate synthase, PEP carboxykinase) in chemostat conditions which speaks for a metabolic regulation of TCA.

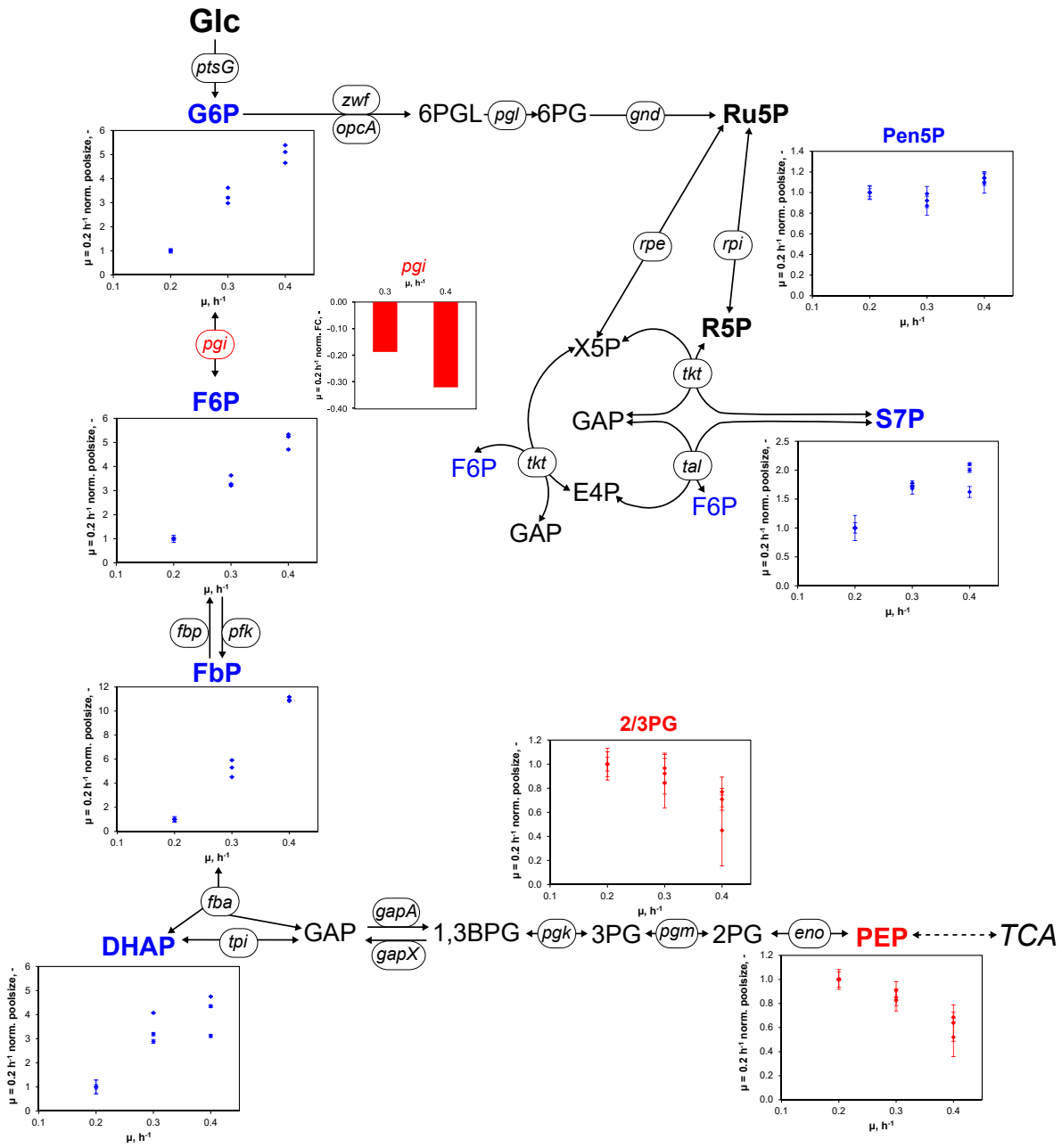

Figure 4.13.: Illustration of relative growth rate dependent intracellular metabolite pools and gene expression of glycolysis and pentose phosphate pathway. Intracellular metabolite pools were normalized to respective values determined at $\mu = 0.2\,\mathrm{h}^{-1}$ and values represent the mean of three technical replicates ± standard deviation. Gene expression was normalized to the expression at $\mu = 0.2\,\mathrm{h}^{-1}$ and is depicted as log fold change (FC). Color coding: red = decreasing pool/expression; blue: increasing pool/expression.

Nevertheless, post-translational modifications on TCA enzymes cannot be excluded, which in turn could trigger a corresponding response on the transcriptional level as observed in this work.

Summarizing, PPP was apparently under metabolic control regardless of glucose being supplied limited (chemostat cultivation) or in abundance [batch cultivation, Haas et al. (2019)]. Concerning PPP, increasing metabolite pool concentrations of Pen5P and S7P observed with rising μ from 0.2 to 0.4 h^{-1} in the chemostats were the representation of this metabolic control. Regarding control of glycolysis, growth environments in glucose-limited chemostat experiments induced a metabolic control scheme of glycolytic genes, whilst transcriptional control was observed in transient batch cultures with glucose abundance (Haas et al., 2019). The first conclusion from this observation is that the process mode of cultivation ultimately dictated whether glycolysis was controlled metabolically or transcriptionally. More precisely, the availability of extracellular glucose seemed to be the crucial switch between metabolic and transcriptional control for *C. glutamicum*. The second conclusion is that the pool profiles from CCM metabolites (cf. figure 4.11) were an illustration of the current metabolic control strategy of the cell in response to increasing growth rates installed in glucose-limited environments. Thereof, potential bottlenecks on the metabolic level limiting growth of *C. glutamicum* under glucose-limited conditions might be derived as described in the subsequent paragraphs. Lastly, depending on whether TCA enzymes bared post-translational modifications, control could be either on the metabolome or transcriptome level under glucose-limited environments.

Potential bottleneck in glycolysis Under the assumption that metabolic regulation is the predominant control of carbon flux through *C. glutamicum*'s glycolysis under glucose-limited growth environments, the differing metabolic pool profiles of upper and lower glycolysis from $\mu = 0.2\,h^{-1}$ to $0.4\,h^{-1}$ were of great interest. The former pools showed increases of up to 11-fold (FbP) and, according to the law of mass action and assuming simple Michaelis-Menten kinetics, flux through this part could have enhanced over μ by increased activity of 6-phosphofructokinase based on K_M for F6P of 2.4 mmol L^{-1} (Sugimoto & Shiio, 1989) and estimated F6P metabolite pools below K_M between (0.33–1.68) mmol L^{-1}* for $\mu = (0.2–0.4)\,h^{-1}$. Simultaneously, rising pools might also indicate (a) limiting reaction rate(s) in lower glycolysis causing accumulation of upstream metabolites. This explanation seems plausible with regard to 40 % decreased

*Values are based on the biomass specific pool sizes from table 4.7 and an estimated cell volume of 1.93 mL g^{-1}_{CDW} (Rönsch et al., 2003).

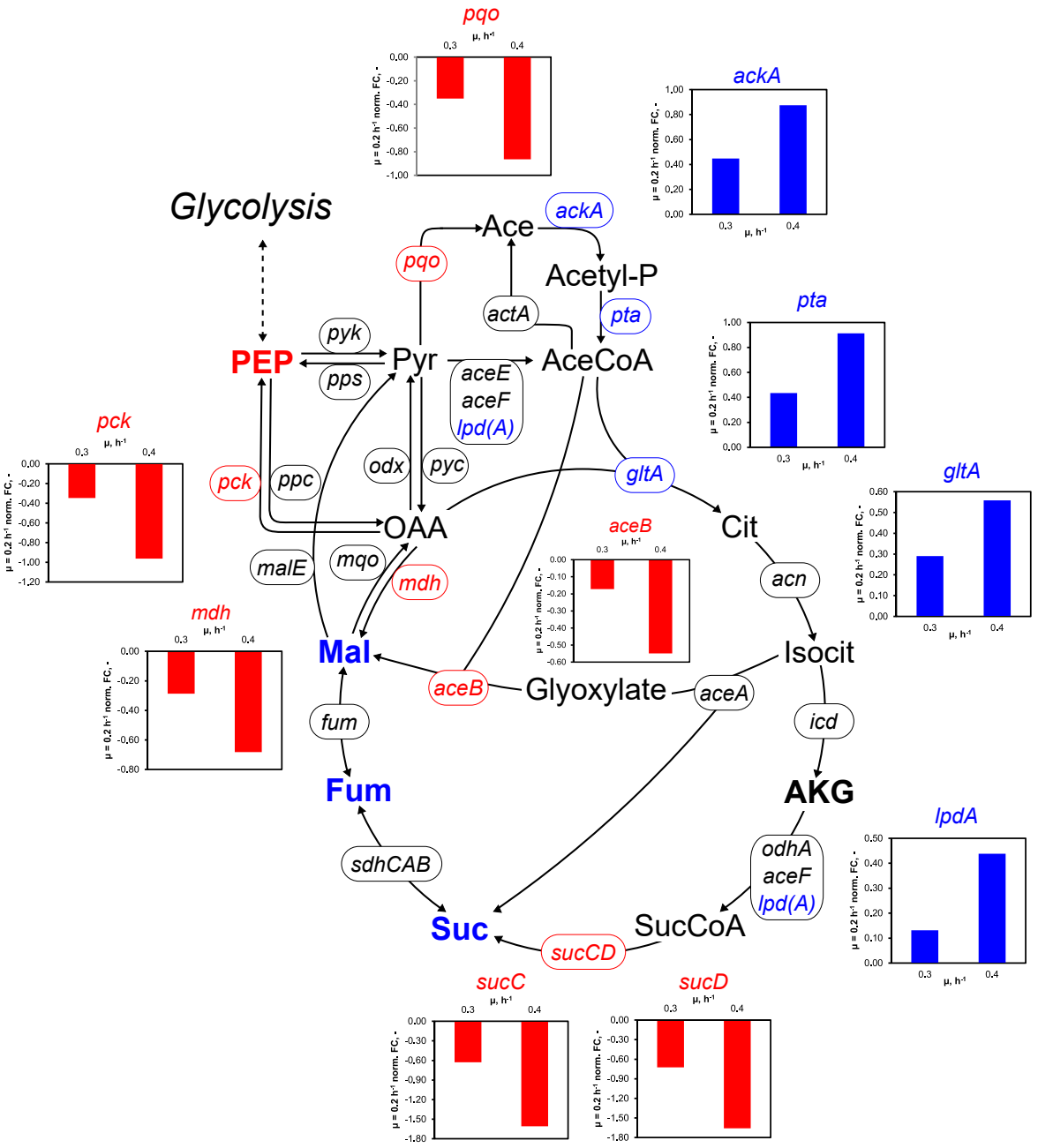

Figure 4.14.: Illustration of relative growth rate dependent intracellular metabolite pools and gene expression of the TCA cycle. Intracellular metabolite pools normalized to respective values determined at $\mu = 0.2\,\mathrm{h}^{-1}$ for the three biological replicates are pictured in figure 4.11 and color coded in this illustration. Gene expression was normalized to the expression at $\mu = 0.2\,\mathrm{h}^{-1}$ and is depicted as log fold change (FC). Color coding: red = decreasing pool/expression; blue: increasing pool/expression.

pools of lower glycolysis intermediates 2/3PG and PEP. Possibly, these diminished pools were the consequence of slow reactions yielding 2/3PG (via phosphoglycerate kinase and phosphoglycerate mutase) and PEP (via enolase) as products, but rapid following reactions using these metabolites as substrates, i.e. fueling Ser-synthesis and TCA, shikimate, or anaplerotic reactions. A similar observation was made by Dominguez et al. (1998) for fructose-grown *C. glutamicum* ATCC 17965 cultures revealing elevated upper glycolysis and decreased lower glycolysis pool sizes when contrasted to pool sizes of glucose-grown pendants. They reasoned that the reaction from GAP to 1,3BG, catalyzed by glyceraldehyde-3-phosphate dehydrogenase GapA, could be the critical factor. Even though 1,3BG was not analyzed in this study, the decreased pools of 2/3PG and PEP might represent the same circumstance. GapA requires NAD^+ as cofactor for the formation of GAP and the enzyme's activity is very sensitive to the installed $NADH/NAD^+$-ratio (Dominguez et al., 1998). GapA was inhibited by 85 % in fructose-grown cells with a $NADH/NAD^+$-ratio of 0.34, which was smaller for glucose-grown cell's (0.21) and correspondingly led to a milder inhibition of 65 %. If a growth increase under glucose-limited continuous conditions also resulted in an unfavorable $NADH/NAD^+$-ratio in *C. glutamicum* ATCC 13032, GapA could have been partially inhibited which could have led to accumulation of upper glycolysis pools and draining of 2/3 PG and PEP supplies if demand of these metabolites increased proportional to μ. Hence, an unfortunate $NADH/NAD^+$-ratio could have slowed down the carbon flux towards lower glycolysis which ultimately could have reduced the flux towards TCA. Based on this unbalance between fluxes of glycolysis and TCA, the supply of anabolic precursors could have become non-proportional with rising μ ultimately limiting *C. glutamicum* to grow faster. The results of our *C. glutamicum* ALE experiments point in a similar direction as discussed in section 4.8.3.

Potential bottlenecks in MTHF- and/or SAM-synthesis Another metabolic bottleneck preventing faster growth of *C. glutamicum* could be the supply of the activated C-1 compound 5,10-methylenetetrahydrofolate (5,10-MTHF) and/or the related cosubstrate S-adenosyl methionine (SAM). MTHF is a crucial cofactor in purine-, pyrimidine, and Met-biosynthesis. In turn, Met serves as precursor for SAM that is required for methylation of newly synthesized RNA- and DNA-strands which is especially relevant for fast-growing strains (Rückert & Kalinowski, 2008). 5,10-MTHF is synthesized via serine hydroxymethyltransferase (GlyA) using Ser and tetrahydrofolate (THF) as substrates and releasing Gly as by-product (Simic et al., 2002). The relationship between Ser-, MTHF-,

Met-, and SAM-synthesis pathways is illustrated in figure 4.15. The metabolome analysis

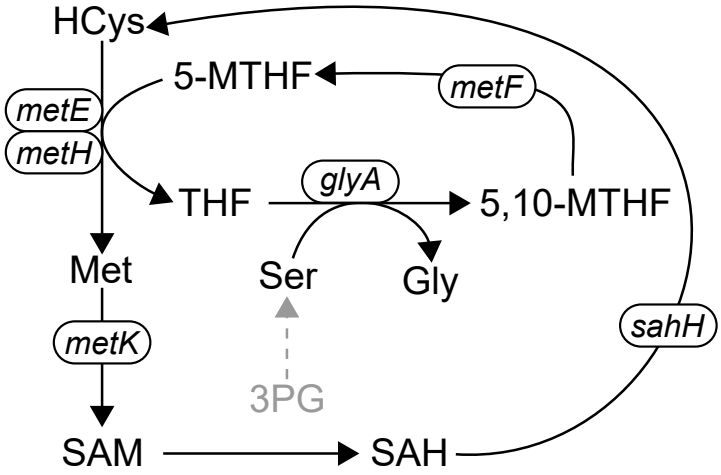

Figure 4.15.: Simplified illustration of *C. glutamicum*'s S-adenosyl methionine (SAM) synthesis cycle, adapted from Rückert & Kalinowski (2008). Genes of this cycle encode the following enzymes: *glyA*: serine hydroxymethyltransferase; *metE*: momocysteine methyltransferase; *metF*: 5,10-methylenetetrahydrofolate reductase; *metH*: homocysteine methyltransferase; *metK*: S-adenosylmethionine aynthetase; *sahH*: adenosylhomocysteinase. 5(,10)-MTHF: 5(,10)-methylenetetrahydrofolate; Gly: glycine; HCys: homocysteine; Met: methionine; SAH: S-adenosyl homocysteine; Ser: serine; THF: tetrahydrofolate

revealed that 3PG, the CCM precursor for Ser, together with 2PG exhibited decreasing pool sizes over μ (cf. figure 4.11). If formation of 3PG was somehow limited, e.g. by an unfortunate NADH/NAD^+-ratio as outlined above, the potentially faster reactions towards Ser-synthesis might have drained the 3PG pool. To satisfy the cell's demand for activated C-1 compounds, about 15 % of the glycolytic flux is diverted towards Ser during growth on glucose (Simic et al., 2002). Interestingly, the Ser-pool increased 1.7-fold with rising μ, which was significantly less than the increase of the intracellular Gly concentration (2.5-fold). Possibly, the cellular need for Gly, which is built in equimolar amounts with 5,10-MTHF, was non-proportional to the Ser-requirement of the cell. Otherwise, Ser and Gly pools would have exhibited comparable increased pool sizes. Besides, *C. glutamicum* does not possess a glycine cleavage system [GCV; Krömer et al. (2006)] which fuels 5,10-MTHF-synthesis by degradation of Gly to 5,10-MTHF, CO_2 and NH_4^+ in *E. coli* (Okamura-Ikeda et al., 1993). Consequently, a heightened demand for MTHF with rising μ might lead to accumulation of Gly as by-product. According to the law of mass action, this could ultimately slow down 5,10-MTHF-synthesis and in turn increase the Ser-pool, if further usage of Ser for other purposes than 5,10-MTHF-synthesis was slower than Ser formation. Accumulation of intracellular Ser has previously caused impaired growth of a *C. glutamicum* Ser-producer strain, most likely as a consequence of perturbing the

C1-metabolism (Peters-Wendisch et al., 2005). Considering that Ser is the only resource for 5,10-MTHF-synthesis in *C. glutamicum*, the enhanced transcriptional expression of *serC* in the Ser biosynthesis pathway and the concurrent decreasing expression of Ser degradation gene *sdaA* furthermore stresses that Ser seems to be more important as precursor of 5,10-MTHF than fueling lower glycolysis via Pyr.

In addition to being a cofactor in purine and pyrimidine biosynthesis, 5-MTHF is required in the final methylation step of Met synthesis catalyzed by methionine synthase. If the 5,10-MTHF supply was limited as hypothesized, purine/pyrimidine and Met synthesis might had to compete for the activated C1-compound. If this indeed was the case and Met synthesis was not favored, the observed decreasing intracellular Met pools over μ (cf. figure 4.12) could imply that the cell formed less of the amino acid but more purine/pyrimidin over rising μ. In contrast, if Met- and therefore SAM-synthesis were favored, the declining Met pools could also indicate faster SAM synthesis than re-supply of Met. After SAM has released its methyl group, e.g. to methylate RNA or DNA strands, S-adenosyl-homocysteine (SAH) is left which, in turn, serves as precursor for homocysteine. Together with 5-MTHF, homocysteine again serves as direct precursor for Met synthesis in the so-called SAM-cycle (cf. figure 4.15). High SAH pools inactivate the master regulator of sulfur metabolism (McbR) whereby its target *cysR*, encoding a dual transcriptional regulator that controls sulfide production, is de-repressed (Rückert et al., 2008). Indeed, gene expression of *cysR* enhanced with rising growth rates (*mcbR* was not amongst DEGs) which could be an indicator for increasing SAH pools with rising μ. On the other hand, if the SAM concentration becomes to high in *C. glutamicum*, it inhibits the expression of Met- and Cys-synthesis genes *metB* and *cysE*, stopping synthesis of its direct precusor Met and of Met's precursor Cys. In contrast to this, *metB* and *cysE* exhibited enhanced expression over μ in this work declining a potential accumulation of SAM.

In summary, 5,10-MTHF synthesis ultimately could be a limitation at high growth rates that could further hamper SAM-synthesis. To resolve this potential bottleneck, heterologous introduction of the GCV into *C. glutamicum* could be performed. Thereby, additional C1-compounds are provided by degrading excess Gly that finally could enable the strain to grow faster. Recently, Zhang et al. (2018) showed that growth of a *C. glutamicum* mutant strain with attenuated *glyA* can be restored by incorporating the *E. coli* GCV. Nevertheless, shifting of corresponding Ser, THF, Gly and MTHF pools might have unknown effects due to the tight regulation of this node (Simic et al., 2002).

4.6.2. Transcriptional response of other cellular functions

Translation

Several genes related to translation processes were differentially expressed with rising μ (cf. table D.6). More than half of the total 53 genes involved in expressing ribosomal proteins (30S and 50S subunits) revealed an increase in expression with elevated growth rates. Accordingly, genes *infA* and *infC* encoding translation initiation factors IF-1 and IF-3, and *pheS* and *trpS* coding for tRNA synthases showed elevated expression as well. Interestingly, genes inscribing elongation factors were not amongst the DEGs. *rbfA* encoding ribosome binding factor A was the only translation-related gene with decreasing expression over rising μ. This observation was contrary to the batch transcriptional response detected by Haas et al. (2019), but in accordance with data from the nitrogen-limited chemostat study of Silberbach et al. (2005). The chemostat-derived results are in line with the general assumption that fast-growing cells have a higher number of ribosomes enabling a higher throughput of translational mechanisms than slow growing cells (Grunberg-Manago, 1996; Keener & Nomura, 1996). Moreover, enhanced expression of genes encoding enzymes of nearly all essential amino acid pathways was observed with rising growth rates. This corroborated the increased expression of translational genes since amino acids are crucial building blocks in biomass and ribosome formation, and to charge tRNAs for protein assembly. Hence, translational processes were most likely controlled on the transcript level under the tested conditions.

Sigma factors

Sigma factors B and E were amongst the DEGs revealing decreasing expression with rising μ. σ^B is a nonessential primary-like sigma factor and is involved in responses to environmental stress (Schröder & Tauch, 2010). It was previously shown that its transcription level increases when *C. glutamicum* approaches the transition phase, whilst the expression level of the house-keeping σ^A concomitantly decreased [reviewed in (Schröder & Tauch, 2010)]. The growth rate dependent response derived from the glucose-limited chemostat experiments was in accordance with the transcriptome and proteome results of Silberbach et al. (2005) from nitrogen-limited chemostats and from Haas et al. (2019). Furthermore, the latter assumed that genes of σ^B's currently predicted regulon were enriched due to de-repression from σ^B control. *sigE* encodes the sigma factor σ^E with extracytoplasmic function. It is involved in responses to cell surface stresses and interacts with anti-sigma factor CseE, e.g. upon heat stress (Park et al.,

2008). Under normal growth conditions installed by the latter authors, the operon was only expressed at low levels. Under the tested chemostat conditions presented here, the diminished expression of both sigma factors could imply that the cell somehow experienced less stress when the growth rate was elevated.

Inositol transport, degradation, and synthesis

iolT1 encoding the inositol transporter IolT1, that is capable of glucose transport (Lindner et al., 2011), exhibited increased expression over μ. Since glucose is usually transported and simultaneously phosphorylated via the glucose specific PTS encoded by *ptsG*, this result could imply that glucose might have been additionally transported via IolT1 under glucose-limited conditions. However, IolT1 revealed lower affinity for glucose than the glucose-specific PTS [$K_S = 2.8\,\mathrm{mmol\,L^{-1}}$ vs. $14\,\mu\mathrm{mol\,L^{-1}}$, Lindner et al. (2011)]. Besides, if this transporter would have been employed, additional glucokinase activity was required for the phosphorylation step, but *glk* and *ppgK* encoding glucokinases were not differentially expressed. Simultaneously, expression of genes involved in inositol degradation (*iolC*, cg0198, *iolC*) increased with rising μ, whilst genes coding for myo-inositol synthesis (*suhB*, *idhA1*) revealed decreasing expression levels. Interestingly, a similar inositol-related transcriptional response was observed by Haas et al. (2019) in transient batch cultivations with glucose abundancy, and additionally, genes encoding glucokinases were increased in expression as well. Moreover, the transcript analyses from the BHI- and PCA-supplemented batch conditions (cf. section 4.3) also identified significant expression of *iol* genes with rising μ. Taken together, transcriptional activation of inositol transport and degradation pathways could be a general response of *C. glutamicum* to increased growth rates and not to varying growth supplements as previously suggested in section 4.3. However, in case of Haas et al. (2019), glucose transport via IolT1 cannot be excluded since glucokinases might have been active to phosphorlyate transported glucose to G6P.

Growth rate-dependent genes in batch and chemostat studies

Several genes that were identified as μ-dependent DEGs in the supplementation studies (cf. section 4.3.3) also revealed a growth rate-dependent expression pattern in the chemostat experiments. For instance, *rpf1* encoding the resusciation promoting factor Rpf1 (Hartmann et al., 2004) showed an increasing expression with rising μ in both experimental setups. However, over-expression of *rpf1* in the *C. glutamicum* WT background did not further boost the growth rate of *C. glutamicum* ATCC 13032 (pFEM18)

(cf. table 4.4). Possibly, the μ-dependent expression of this gene is a side-effect of being under the control of the global transcription regulator GlxR (Jungwirth et al., 2008). Since GlxR influences 14 % of the annotated *C. glutamicum* genes involved in, e.g. central carbohydrate metabolism and aromatic compound degradation (Kohl & Tauch, 2009), growth increases as a result of different carbon supplies (supplement experiments) or rising carbon supply (chemostats) most likely trigger the cAMP-sensing regulator, even though its own expression was not significantly expressed. Nevertheless, Haas et al. (2019) observed a growth rate dependent response of several genes of the GlxR modulon in their transcript data set. cg2546 also exhibited increased and μ-dependent expression in the supplement and chemostat studies. This gene was not over-expressed in the previous experiments since a growth controlling function of the inscribed putative secondary C4-dicarboxylate transporter (Janausch et al., 2002) was excluded. However, based on the chemostat results, it might be worthwhile to further look into this gene. Gene cg3374 coding for a putative NADH-dependent flavin oxidoreductase revealed a μ-dependent decrease in expression in the supplement studies and the corresponding deletion mutant did not reveal an enhanced growth performance (table 4.3). In the chemostat experiments, the gene showed the inverse expression pattern. Hence, construction of an over-expressing mutant would be an interesting option to test for elevated growth. A similar behavior was observed for representatives of the thiamin operon. Whilst the operon was severely decreased in expression in the supplement experiments (cf. section 4.3.3), *thiG* and *thiD2* revealed an increased gene expression in the chemostats. Deduced from the decreased expression in the batch cultivations, we concluded and proved that thiamin is a growth-boosting compound (cf. section 4.3.2). In turn, it seems possible that a rising amount of thiamin is required and synthesized by *C. glutamicum* at elevated growth rates when the vitamin is not added as supplement to the growth medium. Thus, both experimental setups indicate that sufficient supply of thiamin might be a limiting factor for fast growth of *C. glutamicum*.

4.6.3. Interim summary

The combined OMICs data from *C. glutamicum* chemostat cultivations of this work and of Noack et al. (2017) from different growth rates revealed that glucose uptake via PTS was likely under transcriptional control, whilst glycolysis and PPP were likely controlled on the metabolome level. Hence, under the tested conditions, the metabolic flux in these parts of the CCM was modulated via the observed increasing or decreasing intracellular

metabolite concentrations ultimately influencing enzyme activities. However, the control level orchestrating fluxes in the TCA could not be identified. Comparing transcriptome data from substrate-limited with substrate-unlimited growth conditions (Haas et al., 2019) revealed the same results apart from glycolysis. The latter study clearly identified control to be on the transcript level. Thus, the availability of extracellular glucose seems to the trigger between metabolic and transcriptional control of glycolysis in *C. glutamicum*.

Regarding potential growth limitations, enhanced pool sizes of upper and diminished pools of lower glycolysis metabolites might point at an unfortunate NADH/NAD^+-ratio with increasing growth rate. Moreover, unbalanced pool size increases of Ser and Gly, a decreasing metabolites pool of Met with rising μ, and corresponding transcriptional responses of genes involved in sulfur metabolism, Met and Cys biosynthesis could be signs for shortcomings in supplying 5,10-MTHF and/or SAM at higher growth rates.

Several genes or gene families that were previously identified in the transcript analysis of the batch supplement studies re-appeared in the chemostat transcript analysis. Hence, the increased expression of genes involved in inositol uptake and degradation could be a growth-related response of *C. glutamicum* to enhanced growth rates, as was confirmed by the data of Haas et al. (2019). Besides, several genes (*rpf1*, cg2546, cg3374) exhibited growth rate dependent expression patterns in the supplement and chemostat experiments and therefore might be interesting targets for future mutant studies. Lastly, sufficient supply of thiamin could be another bottleneck for fast growth of *C. glutamicum*.

4.7. (Non-)stationary ^{13}C-labeling experiment

Based on the observations regarding intracellular metabolite pool sizes of *C. glutamicum* (cf. section 4.5.1), a stationary instead of a non-stationary ^{13}C-labeling experiment in chemostat mode was performed to determine intracellular fluxes of *C. glutamicum*'s CCM at $\mu = 0.4\,h^{-1}$. Even though this experimental type does not require fast sampling when the ^{13}C-tracer is introduced (cf. section 2.3.4), it was nevertheless conducted to test whether the designed experimental setup would in principle be able to capture dynamic isotopolouge patterns in CCM metabolites occurring within the first seconds of ^{13}C-labeling. After 4 RT, sampling was repeated to obtain stationary isotopologue distributions for subsequent stationary MFA. The results of this expanded stationary ^{13}C-process is described in this section.

4.7.1. Process overview

The labeling experiment was initiated with a batch cultivation supplying $12\,g\,L^{-1}$ glucose in CGXII minimal medium supplemented with $30\,mg\,L^{-1}$ PCA. After glucose was consumed, indicated by a sharp rise of the pO_2 signal, the continuous process was started with $D = 0.4\,h^{-1}$ (cf. figure 4.16) feeding the same medium. Stirrer speed $N = 600\,min^{-1}$ and aeration rate $V_g = 0.8\,L\,min^{-1}$ were kept constant to observe a possible shift from the metabolic steady state. The semi-automatic sampling device introduced in section 3.8 was employed for rapid metabolome sampling. In contrast to previous chemostat processes, the antifoam feed rate was slightly higher ($200\,\mu L\,h^{-1}$ vs. $160\,\mu L\,h^{-1}$) to ensure precise sample volumes of 1 mL facilitated by the sampling device. After at least five RTs (12.5 h), a metabolic steady state was reached indicated by stable biomass concentrations of about $6\,g\,L^{-1}$, $pO_2 = 67\,\%$ and steady off-gas signals ($y_{O_2} = 0.18\,mol\,mol^{-1}$, $y_{CO_2} = 0.03\,mol\,mol^{-1}$) as illustrated in figure 4.16. As basis for the subsequent MFA requiring experimental kinetic rates as input, the following samples were withdrawn four times in 2.5 h-intervals equaling one residence time: OD, CDW measurement, filtrates of biosuspension, TC and TIC determination of biosuspension and pure biomass samples. Measurement of the glucose concentration in the ^{12}C-feed revealed a slightly smaller

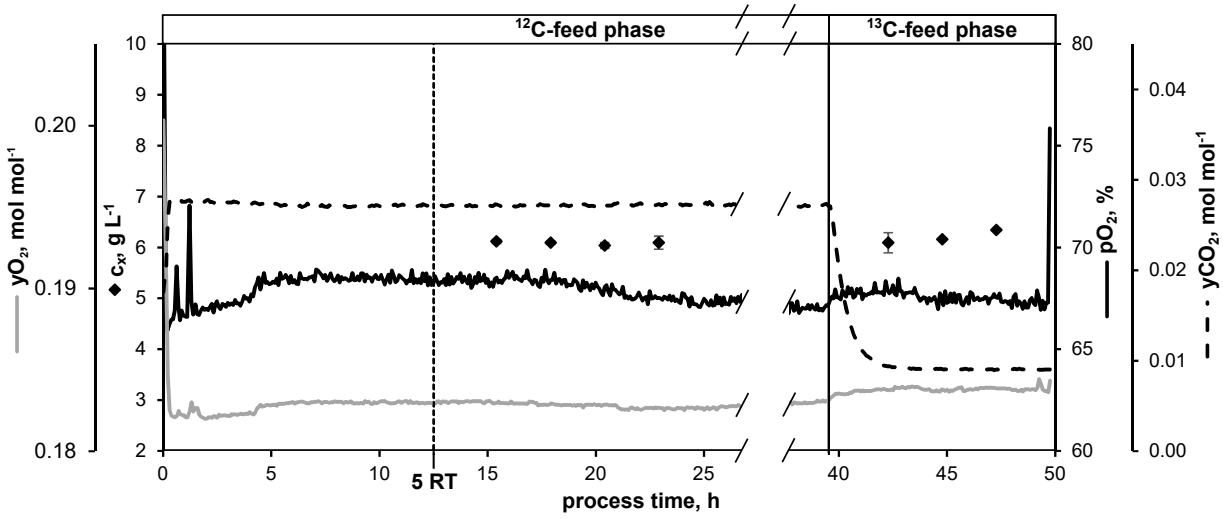

Figure 4.16.: Illustration of the stationary ^{13}C-labeling experiment using CGXII minimal medium supplemented with $12\,g\,L^{-1}$ glucose and $30\,mg\,L^{-1}$ protocatechuate at a $\mu = 0.4\,h^{-1}$. Sampling in the ^{12}C-phase was started after 5 residence times (RT, 12.5 h). After 39.5 h, the feed was switched to labeled CGXII medium containing a $12\,g\,L^{-1}$ glucose mixture of 67 % uniformly and 33 % 1-^{13}C glucose.

value of $(11.32 \pm 0.10)\,g\,L^{-1}$ than the aimed for $12\,g\,L^{-1}$. Deduced from biomass and glucose concentrations, the glucose consumption rate was $(0.74 \pm 0.01)\,g\,g^{-1}\,h^{-1}$ and

the biomass substrate yield was $(0.54 \pm 0.01)\,\mathrm{g\,g^{-1}}$ (cf. table 4.8). Both parameters lay within the range of previous results from chemostats at D =0.4 $\mathrm{h^{-1}}$ (cf. table 4.5). Respiratory rates deduced from the exhaust gas measurement and TIC analysis to account for dissolved CO_2-species revealed q_{O_2} = $(9.26 \pm 0.09)\,\mathrm{mmol\,g^{-1}\,h^{-1}}$ and q_{CO_2} = $(9.86 \pm 0.10)\,\mathrm{mmol\,g^{-1}\,h^{-1}}$, whereby the respiratory quotient (RQ) was 1.07. These respiratory rates were slightly higher than in the former chemostats (cf. table 4.5). Nevertheless, the total carbon balance was closed to 100 % and the fed carbon distributed to 60 % biomass and 40 % CO_2 which was reproducible to the previous chemostat study. By-product formation was again not observed.

In figure 4.16, the switch from ^{12}C-feed to ^{13}C-labeled feed is indicated at ca. 39.5 h and was performed as described in section 3.8, whilst process parameters were kept as in the ^{12}C-phase. Based on the results of the tracer experiments and the experimental design study (EDS, cf. section 3.8.2), a sampling plan designed for isotopic non-stationary and stationary sampling was employed (cf. table D.8). To capture the dynamic labeling patterns, metabolome samples were withdrawn every 4 s in the first minute after the switch. Subsequently, sampling intervals were exponentially increased until the labeling time reached 1 RT (2.5 h) after which samples were withdrawn in RT-intervals. Approximating the end of the labeling phase at 4 RTs (10 h), sampling intervals were again increased after 3.8 RTs (9.5 h) in 10 min steps to resolve the time of expected isotopologue stationarity. All metabolome samples were immediately quenched in cold MeOH-solution to ensure frozen metabolic states. Standard samples (OD, CDW, filtrates, TIC/TC) were withdrawn after each RT. During the ^{13}C-phase, a slight increase of the biomass concentration to 6.2 $\mathrm{g\,L^{-1}}$ was observed (cf. figure 4.16). Determination of the glucose concentration of the labeled feed yielded $(11.88 \pm 0.20)\,\mathrm{g\,L^{-1}}$ which was slightly higher than in the ^{12}C-phase, explaining the small increase in biomass concentration compared to the ^{12}C-phase. A sharp drop of y_{CO_2} was detected indicating the fast production of isotopic CO_2 that could not be detected by the near-infrared (NIR) measurement of the exhaust gas analytics*. Despite these small differences, kinetic parameters determined in this phase were comparable to the previous ^{12}C-phase (cf. table 4.8).

4.7.2. Intracellular ^{13}C-labeling progress

Isotopologues of 33 intracellular metabolites extracted from 25 metabolome samples withdrawn in the labeling phase were analyzed with LC-MS QTOF as described in

*The wavelength of the NIR was calibrated by the manufacturer such to capture only ^{12}C-CO_2.

Table 4.8.: Kinetic parameters determined from the stationary ^{13}C-labeling experiment using CGXII minimal medium supplemented with $12\,g\,L^{-1}$ glucose and $30\,mg\,L^{-1}$ protocatechuate at a dilution rate of $0.4\,h^{-1}$. Results are the means of four (^{12}C-phase) or three (^{13}C-phase) technical replicates.

Phase	mean c_X, $g\,L^{-1}$	$c_{S,F}$, $g\,L^{-1}$	q_s, $g\,g^{-1}\,h^{-1}$	q_{O_2}, $mmol\,g^{-1}\,h^{-1}$	q_{CO_2}, $mmol\,g^{-1}\,h^{-1}$
^{12}C-feed	6.09 ± 0.03	11.32 ± 0.10	0.744 ± 0.004	9.26 ± 0.09	9.86 ± 0.10
^{13}C-feed	6.20 ± 0.11	11.88 ± 0.20	0.767 ± 0.016	9.77 ± 0.14	n.d.

section 3.11.4 and corresponding isotopologue distribtuions are lsited in table D.9. In contrast to previous LC-MS QQQ analyses, isotopologues of additional metabolites (Pyr, AceCoA, Cit, IsoCit) could be retrieved and distinguished from the complex sample matrix due to the higher sensitivity of the QTOF device (Feith et al., 2019), however Trp could not be analyzed. Resulting chromatograms were further processed with MassHunter software enabling determination of relative amounts of $m+1 \ldots m+n$ isotopologues.

Based on this information, the first interesting observation was the high dynamics in isotopologue distributions of all glycolytic and PPP metabolites observed after switching from unlabeled to labeled feed. After 16 s of steadily increasing labeling information, an abrupt decrease of ^{13}C-signal was detected that was accompanied by simultaneously rising amounts of unlabeled $m+0$ -species (cf. figure 4.17 and figure D.2). The same pattern repeated after 40 s and 80 s. In contrast to glycolysis and PPP metabolites, only TCA metabolites Fum, Mal, and Suc (cf. figure 4.18 and figure D.3) showed slight excursions at named time points resembling the pattern of PEP and Pyr. This could be explained by anaplerotic reactions channeling carbon from PEP via PEP carboxylase towards OAA, or from Pyr towards OAA via Pyr carboxylase. All other metabolites did not show significant labeling fluctuations during the first 180 s (cf. figure D.4 and figure D.5).

Based on these findings, we hypothesize that the labeling enrichment in the first 80 s of introducing ^{13}C- glucose was somehow diluted by unlabeled carbon channeling into glycolysis and PPP. Similar observations were made by Pfelzer (2016) who detected increasing $m+0$ traces after the first 5 s of introducing labeled glucose in a non-stationary labeling process of *C. glutamicum* Δ*ilvA*- and Δ*ilvA* Δ*glcC* chemostat cultures. Pfelzer proposed that unlabeled degradation products of storage/buffer metabolites such as glycogen or trehalose might have channeled $m+0$ species into said pathways.

The second interesting observation was that the accumulation of labeling information in metabolites of lower glycolysis (FbP, 2/3PG, PEP, Pyr), PPP, and all TCA-metabolites

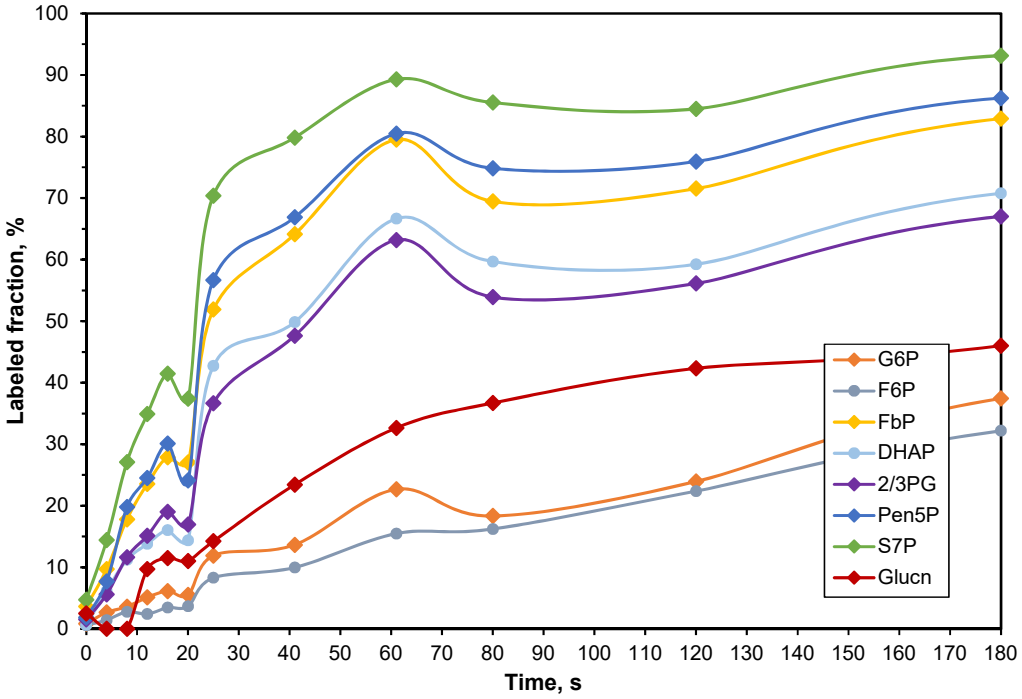

Figure 4.17.: Progress of the total labeling fraction in metabolites of upper glycolysis and pentose phosphate pathway and gluconate (Glucn) in the first 180 s after switching from ^{12}C- to ^{13}C-feed in the stationary ^{13}C-labeling experiment $\mu = 0.4\,h^{-1}$.

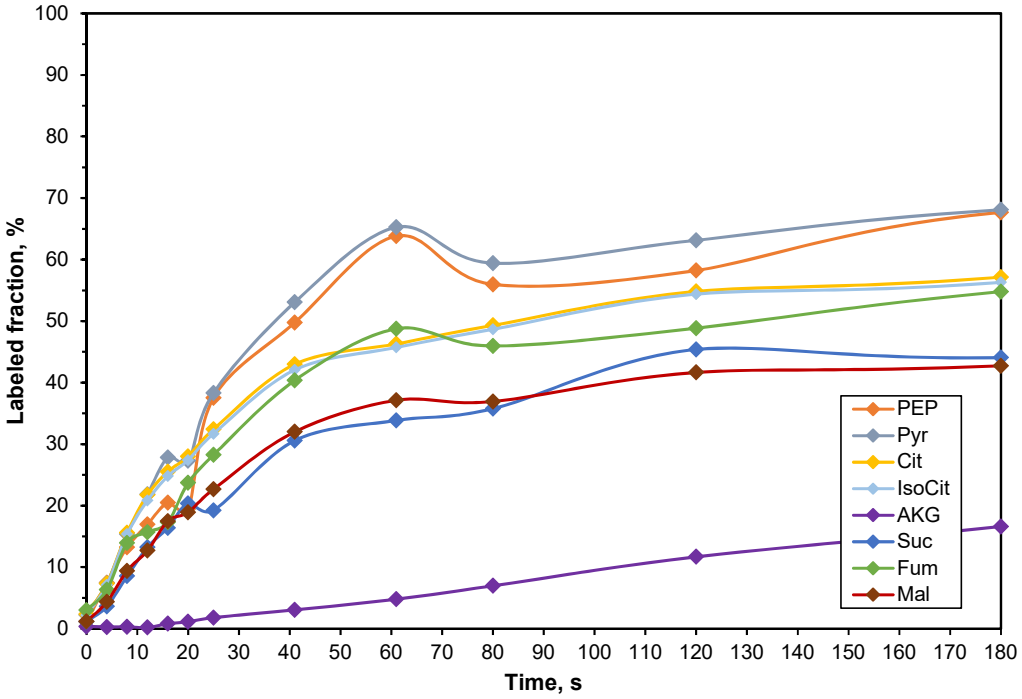

Figure 4.18.: Progress of the total labeling fraction in metabolites of lower glycolysis and TCA cycle in the first 180 s after switching from ^{12}C- to ^{13}C-feed in the stationary ^{13}C-labeling experiment $\mu = 0.4\,h^{-1}$.

except AKG was faster than in G6P and F6P (cf. figure 4.17 and figure 4.18). This was especially surprising for G6P because it is the direct product of labeled glucose being transported into the cell and simultaneously phosphorylated via glucose-specific PTS. To test if labeled glucose exclusively followed this linear path from G6P towards lower glycolysis, a balance of summed ^{13}C-portions detected in G6P, F6P, and FbP was performed neglecting gluconeogenic reversible reactions, the branch off at G6P towards PPP, and influx of labeled F6P redirected from PPP (cf. figure 4.19). Based on this simplified pathway, the maximum amount of labeled carbon from G6P should be passed on to F6P and FbP. Balancing was based on data retrieved at sampling time 120 s due to high dynamics in isotopologue patterns before this time point. The mass of labeled carbon in G6P, F6P, and FbP was determined by multiplication of the total fraction of labeled carbon (G6P: 22.5 %, F6P: 25 %, FbP: 72 %) with the respective presumably correct (cf. section 4.5.2) pool sizes previously determined at $\mu = 0.4\,\mathrm{h}^{-1}$ (cf. table 4.7). As a result, about 1.46 µmol g^{-1}_{CDW} of labeled G6P, 0.8 µmol g^{-1}_{CDW} of F6P, and 6.7 µmol g^{-1}_{CDW} of FbP were obtained as proportionally illustrated in figure 4.19. This simple calculation indicated that labeling information of G6P covered half the amount of F6P which is in accordance with typically observed glycolysis-PPP split ratios of 50 % (cf. section 4.7.3). However, the 0.8 µmol g^{-1}_{CDW} of labeled carbon from F6P only accounted for roughly an eighth of the labeled portion in FbP. Based on this, it seemed likely that under the tested process conditions, carbon channeled into glycolysis through a second path besides the linear pathway via G6P.

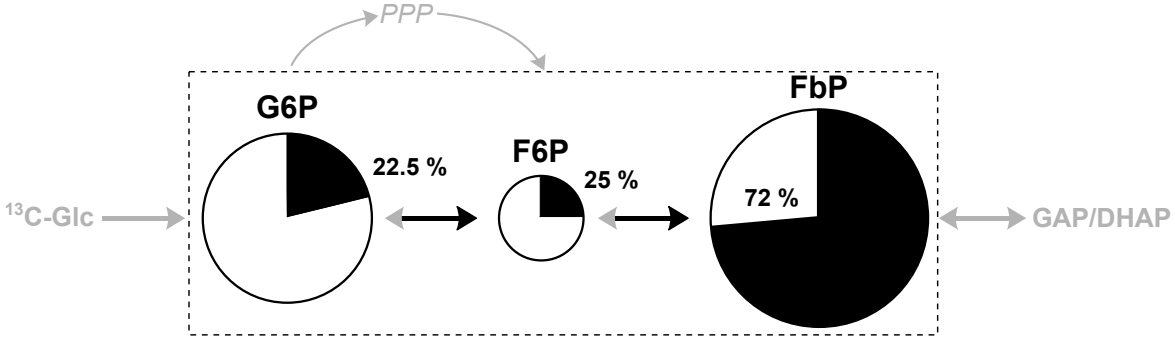

Figure 4.19.: Illustration of a simplified ^{13}C-mass balance for intracellular metabolite pools of glucose 6-phosphate (G6P), fructose 6-phosphate (F6P), and fructose 1,6-bisphosphate (FbP) at t = 120 s after switching to ^{13}C-labeled feed. ^{13}C-labeled portions are shown in black and ^{12}C-portions are illustrated in white. Neglected fluxes of the balance are shown in gray. DHAP: dihydroxyacetone phosphate; GAP: glyceraldehyde-3-phosphate; Glc: glucose; PPP: pentose phosphate pathway.

Cocaign-Bousquet et al. (1996) came to a similar conclusion based on growth and enzyme kinetic studies in chemostat experiments with *C. glutamicum* WT ATCC 17965.

They proposed that a secondary transport system for glucose of the low affinity type is active at $\mu > 0.33\,h^{-1}$ which was confirmed by Lindner et al. (2011). The latter found that in the absence of the PTS, overexpression of a glucokinase in combination with inositol permease IolT1 enabled glucose transport into the cell. The transcriptome study introduced in section 4.6.2 revealed enhanced expression of both corresponding genes *iolT1* and *iolT2*, but no growth-dependent expression of glucokinase genes. The low affinity of the inositol transporter for glucose [$K_S = 2.8\,mmol\,L^{-1}$, Lindner et al. (2011)] also speaks against an involvement of IolT1 under the tested conditions, since no residual glucose could be determined in filtrate samples of this ^{13}C-process.

Nevertheless, we propose that the inflow of labeled glucose into the cell might have partially by-passed G6P (at least in the first 120 s) and additionally took a second route. The isotopologue traces of G6P, F6P, and FbP support this thesis. If the main route of labeled carbon had passed exclusively via G6P towards FbP, $m+1$ and $m+6$ fractions of FbP would have had the greatest share as observed in G6P and F6P due to the fed ^{13}C-substrate mixture of 33 % $^{13}C_1$- and 67 % U-^{13}C-labeled glucose. However, until 120 s, FbP's fraction of $m+1$ species was only about 11 % and that of $m+6$ about 20 %, as was the share of $m+3$ species (cf. figure 4.20). Regarding this 20 % share of $m+3$ species in FbP, the potential second glucose route might have led through PPP. Remarkably, the fastest labeling enrichment of all metabolites was observed for S7P, and nearly identical total labeling patterns as in FbP (cf. figure 4.17) were obtained for Pen5P and S7P. Possibly, the high portion of $m+3$ species in FbP could therefore have been caused by labeled substrate entering the PPP and being gluconeogenicly redirected to FbP and lower glycolysis.

Hence, an alternative non-phosphorylating pathway could have been employed by the cell to facilitate inflow of glucose via PPP in addition to PTS. For instance, in the non-phosphorylating Entner-Doudoroff pathway*, glucose is firstly transformed to gluconate via glucose dehydrogenase [EC:1.1.1.360] and gluconolactonase [EC:3.1.1.17] instead of being phosphorylated (cf. figure 4.21). In turn, gluconate is phosphorylated and gluconate-6P can be transformed into hexoses in PPP reactions or transformed via phosphogluconate dehydratase [EC:4.2.1.12] to 2-dehydro-3-deoxy-D-gluconate-6P, finally leading to GAP and Pyr (catalyzed by an aldolase reaction) amongst other ED-specific pathways. Consequently, such a pathway would explain the fast labeling of lower glycolysis metabolites if the labeled substrate was channeled via GAP and/or Pyr into

*The following information was retrieved from the KEGG reference pathway database: `https://www.kegg.jp/kegg-bin/show_pathway?map00030`.

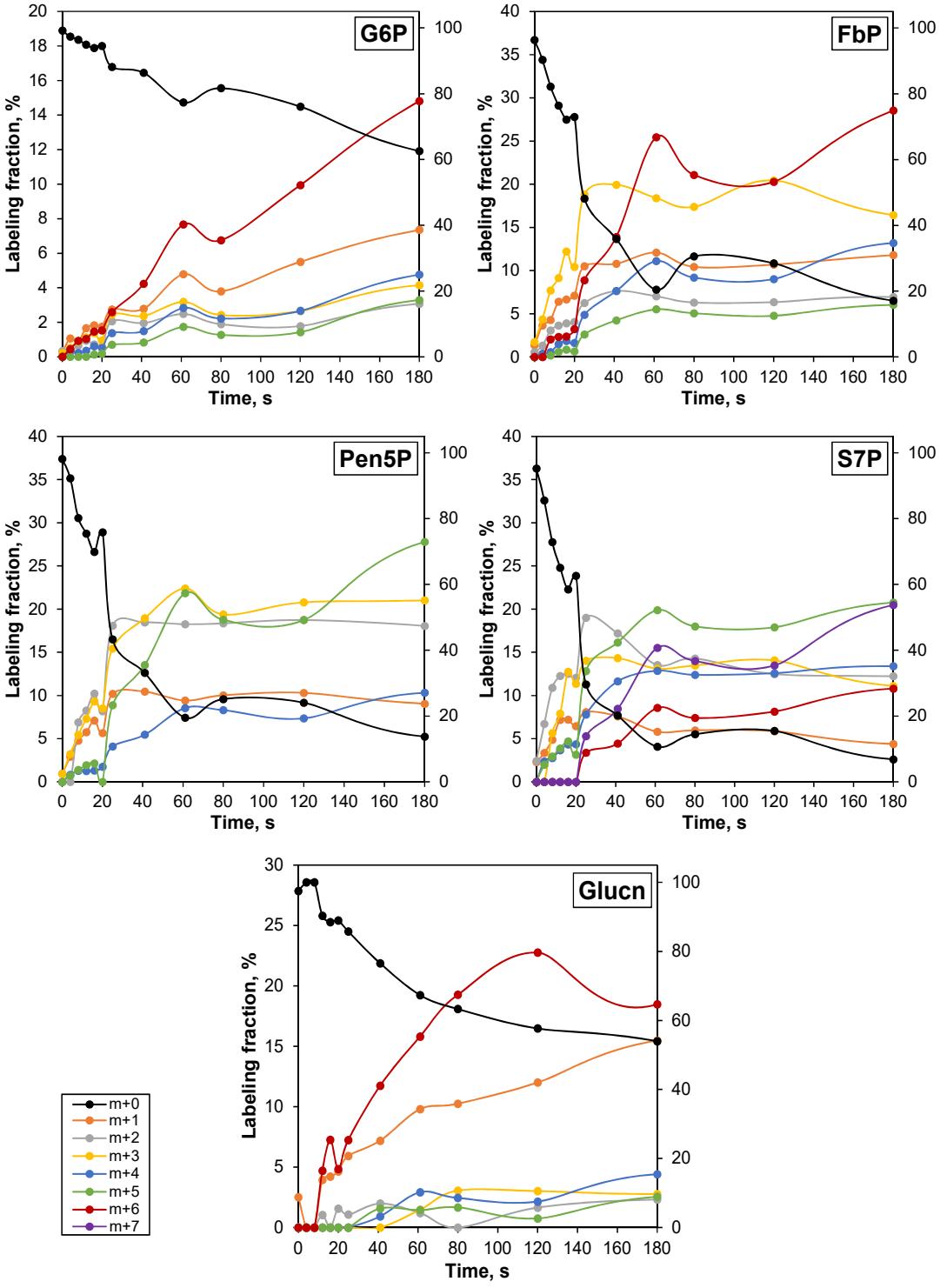

Figure 4.20.: Illustration of the labeling progress in $m+1...m+n$ isotopologues of glucose 6-phosphate (G6P), fructose 1,6-bisphosphate (FbP), pentose 5-phosphates (pool of rib(ul)ose 5-phosphate, Pen5P), sedoheptulose 7-phosphate (S7P), and gluconate (Glucn) in the first 180 s after switching from unlabeled ^{12}C- to labeled ^{13}C-feed in the chemostat process performed at $D = 0.4\,\mathrm{h}^{-1}$.

glycolysis. Even though *C. glutamicum* is able to metabolize gluconate as sole carbon source and channel the carbon via PPP reactions towards glycolysis (Frunzke et al., 2008; Lee et al., 1998), the pathway via phosphogluconate dehydratase and the initial steps of glucose being transformed into gluconate were not confirmed (Vallino & Stephanopoulos, 1994). However, the latter authors exclusively cultivated the strain in substrate-sufficient batch environments, but the presence of ED was never investigated for *C. glutamicum* cultivated in chemostat processes. Thus, the glucose-limited condition as applied in this study could have potentially triggered additional glucose metabolization pathways such as the ED.

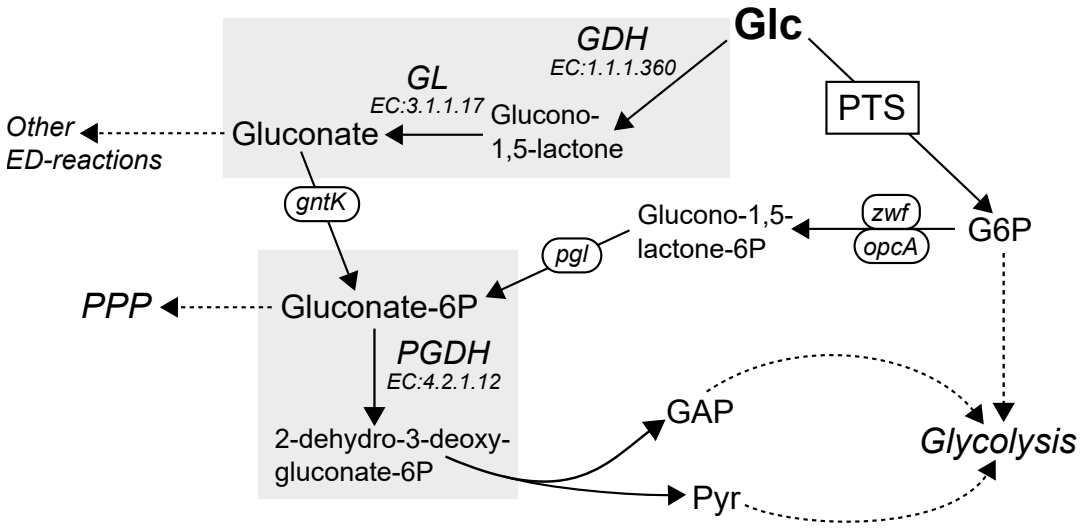

Figure 4.21.: Schematic illustration of pentose phosphate pathway (PPP) and Entner-Doudoroff (ED) pathway. Enzymes/pathways that were not confirmed for *C. glutamicum* are shown with a gray background. *C. glutamicum*-specific genes being part of the pictured pathways are given if annotated for the strain: *gntK*: putative gluconokinase; *pgl*: putative 6-phosphogluconolactonase; *opcA*, *zwf*: glucose 6-phosphate dehydrogenase. G6P: glucose 6-phosphate; GAP: glyceraldehyde-3-phosphate; GDH: glucose dehydrogenase; GL: gluconolactonase; Glc: glucose; PGDH: phosphogluconate dehydratase; PTS: phosphotransferase system; Pyr: pyruvate

In a first attempt to evaluate this thesis, the recorded mass spectra were checked for the presence of gluconate. Indeed, the metabolite was found in the spectra (cf. figure 4.20), revealing exceptionally high portions of labeled $m+1$ and $m+6$ isotopologue species fitting the composition of the ^{13}C-glucose mixture. Since gluconate was identified as intracellular metabolite in *C. glutamicum*'s metabolism only after the experiments were performed, no metabolite pool measurements could be performed retrospectively. Therefore, we cannot give a clear answer yet whether *C. glutamicum* employed a potential gluconate pathway under the tested conditions. Nevertheless, it is notable that ED is the

most frequent biochemical device found in free-living bacteria and Archaea for glucose utilization (Nikel et al., 2015). Besides, several bacteria such as the soil bacterium *Pseudomonas putida* (Nikel et al., 2015) and other organisms (Ahmed et al., 2004; Hanke et al., 2013; Schatschneider et al., 2014) are able to use ED and glycolysis in parallel. In this context, it seems plausible that *C. glutamicum* does possess other resources to accumulate and metabolize glucose as well. Subsequent and comparable labeling experiments could focus on determining metabolites of the ED to prove or reject this hypothesis.

4.7.3. Stationary metabolic flux analysis at $\mu = 0.4\,h^{-1}$

Metabolome samples withdrawn after 10 h (representing 4 RT) after switching from ^{12}C- to ^{13}C-glucose feed provided stable isotopic ^{13}C-patterns in each metabolite (cf. table D.9) as basis for stationary flux simulations. The MFA was kindly performed by our project partners Martin Cerff and Katharina Nöh (FZJ) as briefly described in section 3.13. The simulated carbon fluxes towards glycolysis, PPP, and TCA representing the best fit of the MFA are pictured in figure 4.22*. All depicted fluxes were normalized to the biomass specific glucose consumption rate of 4.13 mmol L^{-1} g^{-1} h^{-1}. As illustrated, about 44.9 % of consumed glucose was channeled into glycolysis (reaction **pgi**), whilst 53.3 % replenished the PPP (reaction **gnd**). Since only labeling information of two PPP metabolites (combined labeling signal of R5P and Ru5P, S7P) was available, comparable high confidence intervals in the reactions of **tkt1**, **tkt2**, and **tal** were obtained (cf. table D.10.). Due to inflow from the PPP, flux through glycolysis downstream of G6P increased to 73.7 % (reactions **pfk**, **fda**). Based one the following reaction to form GAP and DHAP, the flux roughly doubled towards phosphoglycerate (PGA, reaction **gapA**: 159.7 %). After the branch off towards Ser biosynthesis at PGA, the downstream flux was 146.8 % (reaction **eno**) that further diminished to 82.3 % (reaction **pyk**) due to the branch off towards anaplerotic reactions. In turn, influx from said reactions could have increased the following flux to 92.5 % (reaction **pdh**). Carbon flux into the TCA was 66.1 % (reactions **gltA**, **acnA**, **acnB**, **icd**), until the pathway towards glutamate synthesis reduced the downstream flux towards OAA to 44.3 % (**odh**, **sdh**, **fum**). Fluxes around the anaplerotic knot could not be accurately predicted and remain undetermined as previously shown by Kappelmann et al. (2015) and were therefore not further discussed.

*Fluxes through all reactions of the simulation model are listed in table D.10.

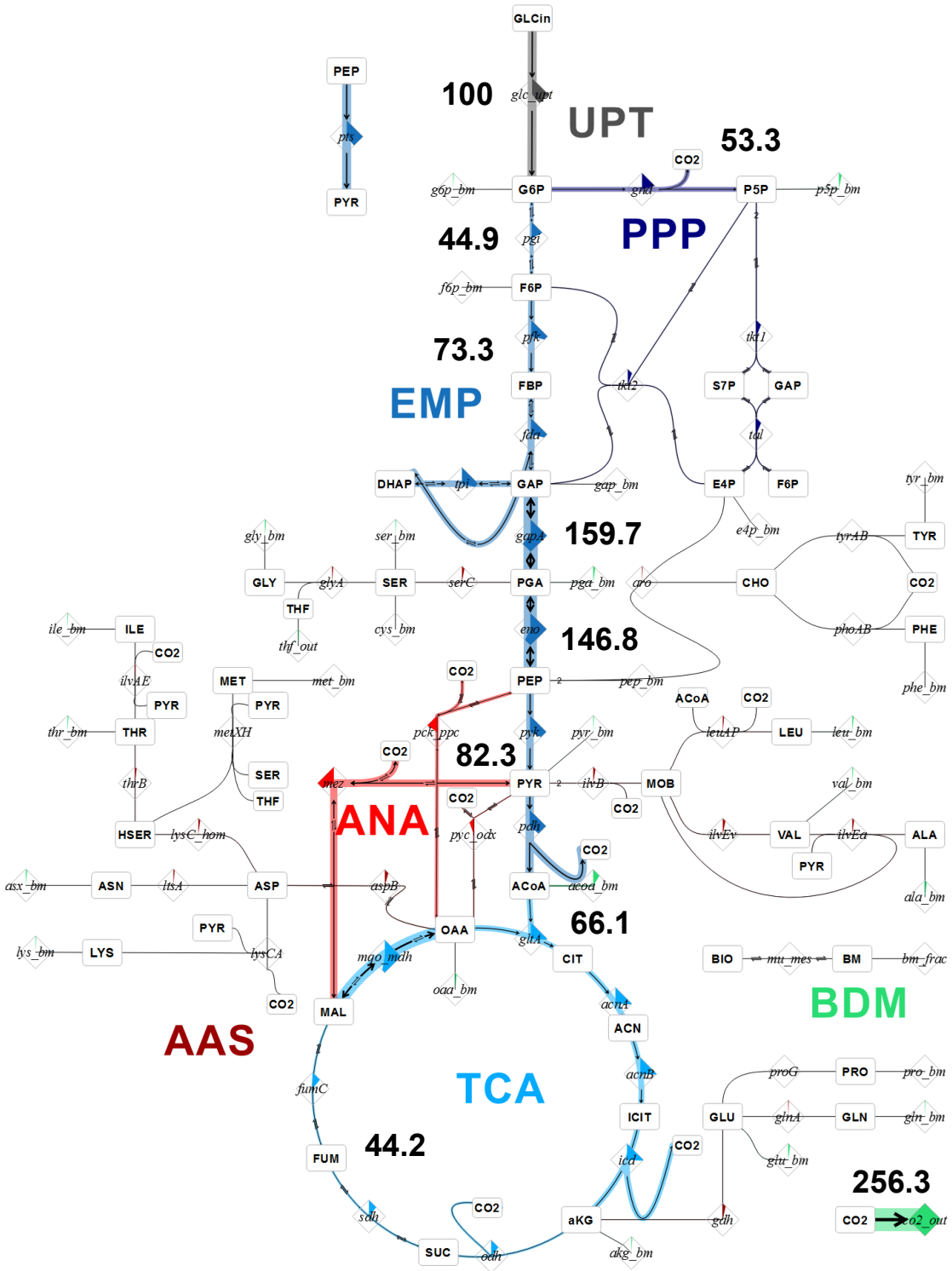

Figure 4.22.: Carbon flux distribution in the central carbon metabolism of *C. glutamicum* WT cultivated in a chemostat process at $\mu = 0.4\,h^{-1}$. Flux simulations are based on ^{13}C-labeling data of intracellular metabolites extracted from quenched biomass samples at process time 10 h and derived paramters from the ^{12}C-phase (cf. table 4.8). Illustrated fluxes are given in % in relation to the glucose consumption rate of $4.13\,mmol\,g^{-1}\,L^{-1}$. ANA: anaplerosis, AAS: amino acid synthesis, BDM: biomass formation, EMP: glycolysis, PPP: pentose phosphate pathway, TCA: tricarboxyl cycle, UPT: glucose uptake

To identify potential growth bottlenecks in the CCM of *C. glutamicum*, the presented fluxes were compared to published flux distributions determined from labeling experiments at other growth rates as summarized in table 4.9. In all listed publications, stationary labeling experiments were conducted. The majority employed chemostat processes, whilst four experiments were performed in batch mode employing bioreactors (Bartek et al., 2011; Shirai et al., 2007) or shaking flasks (Rollin et al., 1995; Sonntag et al., 1995). Studies were done with either *C. glutamicum* WT strains ATCC 13032 (Bartek et al., 2011; Miebach, 2011; Pfelzer, 2016; Sonntag et al., 1995), ATCC 13869 (Shirai et al., 2007), or ATCC 17965 (Rollin et al., 1995). Compared to the physiology of ATCC 13032, strain ATCC 17965 previously revealed comparable kinetic parameters (cf. section 4.4). Tested growth rates ranged from $0.05\,h^{-1}$ (Miebach, 2011) to a maximum of $0.55\,h^{-1}$ (Rollin et al., 1995). No specific growth rate was stated by Sonntag et al. (1995) and was therefore calculated from the glucose consumption rate and the biomass glucose yield to be approx. $0.25\,h^{-1}$. Miebach (2011) performed several labeling experiments in small-scale chemostats covering growth rates between $(0.05–0.2)\,h^{-1}$ in biological quadruplicates. However, the author states that 7 of 16 resulting flux patterns lead to high variances in the flux distribution due to analytical measurement flaws. Thus, only corresponding cultivations remarked as 'reliable' by Miebach were considered in the following.

Deduced from the listed fluxes towards glycolysis, PPP, and TCA, a rough trend could be observed: growth rates $\leq 0.10\,h^{-1}$ determined glycolytic fluxes between (63–86) % of respective glucose consumption rates and accordingly, smaller portions towards PPP [(13–36) %], whilst fluxes towards TCA ranged between (91–119) %. Higher growth rates between $(0.15–0.55)\,h^{-1}$ revealed nearly identical flux distributions in all publications, with the exception of data from Miebach (2011) for $0.2\,h^{-1}$ most likely due to mentioned analytical issues*, and for the batch cultivation of Bartek et al. (2011) most likely due to experimental shortcomings†. All other studies determined glycolytic fluxes between (46–57) %, PPP fluxes ranging from (40–55) %, and TCA fluxes between (66–83) %. The fluxes determined by Wittmann & Heinzle (2002) (cf. table 4.9) for shaking flask cultures of ATCC 13032 also fitted nicely within these ranges, but unfortunately, no growth rate was stated and could not be reliably determined from the given data.

*Only one experiment out of four at $\mu = 0.2\,h^{-1}$ showed an explicit optimum of the flux distribution (Miebach, 2011).

†No stationary patterns where reached in TCA metabolites due to too short labeling duration (Bartek et al., 2011).

Table 4.9.: Summary of carbon flux distributions for *C. glutamicum* at different growth rates. The calculation of generated NADHP was based on the respective μ and listed flux distributions assuming that 2 NADPH/molecule glucose and 1 NADPH/glucose are produced in PPP and TCA, respectively. n.d.a.: no data available; n.c.: not calculated

μ, h^{-1}	Glycolysis, %	PPP, %	TCA, %	Calc. NADPH g^{-1}_{CDW}	Reference
0.05	63–76	23–36	96–119	15.5	Miebach (2011)
0.10	73	26	n.d.a.	n.c.	Petersen et al. (2000)
0.10	75–86	13–24	91–106	12.6	Miebach (2011)
0.15	51–69	47–55	94–101	19	Miebach (2011)
0.15	46.2	52.1	74.8	21.2	Pfelzer (2016)
0.20	10–37	60–90	91–104	n.c.	Miebach (2011)
0.25	58	40	108	28.6	Sonntag et al. (1995)
0.25	57	40	100	22.0	Shirai et al. (2007)
0.40	44.9	53.3	66.1	18.5	This work
0.43	27.6	69	n.d.a.	n.c	Bartek et al. (2011)
0.55	55	45	n.d.a.	n.c	Rollin et al. (1995)
n.d.a.	46.5	51.2	82.7	n.c.	Wittmann & Heinzle (2002)

In general, a total amount of 5 molecules NADH per consumed molecule of glucose is obtained in the CCM (i.e. 2 NADH/glucose in glycolysis, 2 NADH/glucose at the entryway towards TCA (Pyr dehydrogenase reaction), 1 NADH/glucose in TCA). This value remains constant if carbon is channeled towards PPP and again redirected towards glycolysis via F6P or GAP. However, the total amount of NADPH greatly depends on whether G6P is directed towards PPP or glycolysis. In the first case, 2 NADPH per molecule glucose are obtained via G6P dehydrogenase and 6PG dehydrogenase and only 1 additional NADPH/glucose is produced in the TCA catalyzed by IsoCit dehydrogenase (Eikmanns et al., 1995). Since *C. glutamicum* does not possess a NADH:NADPH transhydrogenase (Vallino & Stephanopoulos, 1994), the major supply of NADPH is hence provided by the PPP. Considering the increase of carbon flux towards PPP at $\mu \geq 0.15\,h^{-1}$ (cf. table 4.9), the produced amount of NADPH should consequently increase, too. Therefore, the known fluxes towards PPP and TCA from table 4.9 were used (if determined in respective publications) to estimate produced amounts of NADPH for several growth rates (cf. table 4.9). The obtained values were then compared to *C. glutamicum*'s demand of 16.4 NADPH to form 1 g of biomass (Wittmann & de Graaf, 2005). As a result, growth rates $0.05\,h^{-1}$ and $0.10\,h^{-1}$ with smaller fluxes through PPP revealed NAPDH supplies of 15.5 and 12.6 mmol per g biomass, respectively, which was in the range of the cell's NADPH demand. In contrast, at $\mu = 0.15\,h^{-1}$, $0.25\,h^{-1}$ and $0.4\,h^{-1}$ the average PPP fluxes were about 50 % and exceeded the 16.4 mmol NADPH per

g biomass with values of 19–21.2 ($\mu = 0.15\,h^{-1}$), 22–28.6 ($\mu = 0.25\,h^{-1}$), and 18.5 mmol NADPH per g biomass ($\mu = 0.4\,h^{-1}$), respectively. Deduced from this rough estimate, it seems that *C. glutamicum* produces a higher amount of NADPH than required to form 1 gram biomass if $\mu \geq 0.15\,h^{-1}$.

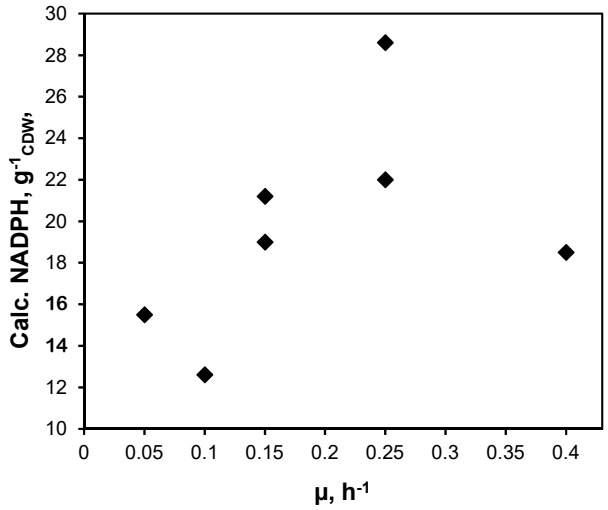

Figure 4.23.: Illustration of theoretically produced amounts of NAPDH (cf. table 4.9) at different growth rates.

As summarized in Wittmann & Heinzle (2008), it was previously shown that *C. glutamicum* has a highly flexible NADPH metabolism depending on the nutrient and whether it was genetically modified to produce amino acids like Glu, Lys, Met, or Trp that partially require high amounts of NADPH for their respective biosynthesis routes. Derived from the outlined studies, Wittmann & Heinzle (2008) concluded that in most of the cases, the strain produced excessive amounts of NADPH exceeding the demand for biomass formation. Apparently, this NADPH surplus increased with decreasing NADPH oxidation. Hence, it was assumed that NADPH supply and demand in *C. glutamicum* is imbalanced due to the interplay of unassigned NADPH consuming or producing reactions, e.g. via NAPDH oxidase (Matsushita et al., 2001) and via the formation of a futile cycle in the Pyr node facilitated by malic enzyme (Graaf, 2000; Petersen et al., 2000). With regard to a potential growth rate dependent NADPH supply shifting from sufficient to exceeding amounts, the same reasoning might apply. Besides, it could be possible that the cellular composition of *C. glutamicum* alters with rising growth rates whereby the NADPH supply accordingly increases above 16.4 $NADPHg^{-1}{}_{CDW}$ as previously determined by Wittmann & de Graaf (2005). To test whether one of these hypothesis is feasible, future ^{13}C-labeling experiments should include intracellular measurements

of NADPH. Furthermore, the cellular composition should be analyzed with regard to the growth rate and cultivation system (e.g. substrate-unlimited batch cultivation vs. substrate limited continuous process) and be incorporated into the SNM employed for the flux simulation.

Concluding from this fluxome analysis, no growth-limiting factor in the CCM of *C. glutamicum* could be identified *per se*. However, the assumed shift from NADPH-sufficient conditions at smaller growth rates to NADPH-exceeding conditions at higher growth rates might be worth to look further into, since a growth rate-dependent NADPH supply for *C. glutamicum* was not previously described and should be considered in the design of NAPDH-intensive production processes.

PART III
Adaptive laboratory continuous evolution

4.8. Evolution studies with *C. glutamicum*

In the first two parts of this thesis, growth limitations were investigated from a systems biology viewpoint focusing on the transcriptome, metabolome, and fluxome of *C. glutamicum* facing (pseudo-)stationary growth environments. In this third part, growth limitations were elucidated from a more traditional perspective by cultivating the strain in an ALE setup. Thereby obtained evolved strain EVO5 exhibiting an enhanced growth performance in comparison to the parental strain was analyzed with WGS and characterized in batch cultivation studies. Thereupon, growth beneficial mutations were discussed. For more details, the reader is kindly referred to the submitted contribution Graf et al. (2019) in the appendix of this thesis (cf. section B).

4.8.1. Design of the continuous ALE experiment

In this investigation, *C. glutamicum* ATCC 13032 WT was cultivated under controlled but challenging growth environments for prolonged periods of time. Thereby, we aimed for natural adaption processes that ultimately selected the fastest growing subpopulation with superior growth performance over the parental WT strain (Dettman et al., 2012; Ryall et al., 2012). During the time these experiments were performed in our laboratory, two other *C. glutamicum* ALE investigations were published with the same aim. Both studies employed repetitive batch cultivations in well plates (Pfeifer et al., 2017) or shaking flasks (Wang et al., 2018b) to cultivate the *C. glutamicum* WT for a prolonged time period in minimal growth medium supplemented with the siderophores PCA (Pfeifer et al., 2017) or catechol (Wang et al., 2018b) and glucose as sole carbon source. Subsequently, both working groups performed WGS of potentially mutated strains, re-engineered the most promising mutations in the WT, and conducted characterization studies with the mutants. Besides, Wang et al. (2018b) analyzed the transcriptome and fluxome of two mutant strains.

The study presented here followed a different experimental concept. Firstly, a continuous experimental bioreactor setup was chosen in which the organism was repetitively cultivated near its maximum growth rate by setting high dilution rates. Therefore, an advanced chemostat controller concept was employed as described in Graf et al. (2019) (cf.

section B) enabling a dilution rate resolution of 0.01 h^{-1} and simultaneously maintaining a constant bioreactor volume of 1.2 L. Secondly, the growth medium varied from the other two studies. Preliminary, a rich growth medium comprising CGXII minimal medium without PCA (Buchholz et al., 2014b), 10 g L^{-1} glucose, and 10 g L^{-1} YE was applied. Over the course of cultivations, however, the richness of the medium was continuously decreased by stepwise reduction of YE until the complex compound was totally omitted during the last process. Summarizing, the technical execution of the repetitive ALE experiments as well as the selection pressures differed greatly from the other two ALE experiments. Hence, the employed growth medium in combination with installing high dilution rates should potentially guide cellular adaption towards different mutation sets than previously observed by Pfeifer et al. (2017) and Wang et al. (2018b).

4.8.2. Advantages of continuous ALE experiments

In total, five continuous ALE processes were performed which were run between 2-3 weeks, respectively. All cultivations were started by employing the standard seed train described in section 3.6 and initiated with a batch cultivation (c.f. section 3.7.4) using the same medium as in the subsequent continuous phase. Finally, before one ALE experiment was stopped, glycerol cultures were prepared from the biosuspension to preserve the potentially evolved strain and used to inoculate the next continuous ALE process. Also, the growth conditions installed at the end of one process, e.g. final dilution rate and amount of YE, were set as starting conditions for the following experiment. Biomass formation was followed daily by measuring the OD of the biosuspension. During the course of one process, the dilution rate was steadily increased whenever a metabolic steady state was reached which was derived from stable respiratory oxygen and carbon dioxide signals in the off gas. Moreover, the concentration of YE in the growth medium was reduced at least once in every cultivation while maintaining a high D. Whenever a potential wash out of the culture was assumed, indicated by decreasing biomass levels over the time, D was slightly lowered. A summary of all processes is illustrated in figure 1 of Graf et al. (2019) (cf. section B) showing the dilution rate and concentration of YE over the summed process time/number of *C. glutamicum* generations.

In the first ALE experiment, a maximum D of 0.72 h^{-1} and an initial amount of 10 g L^{-1} YE were installed. During the process, the YE concentration was halved but D could be maintained. YE was further reduced to 2.5 g L^{-1} in the following run and the dilution rate could ultimately be increased to 0.75 h^{-1}. Further reducing YE to 1.25 g L^{-1}

required a small decrease of D to $0.74\,h^{-1}$ in the third process. In the fourth run, YE was successively reduced in small steps from $1.25\,g\,L^{-1}$ to $0.25\,g\,L^{-1}$ which also required stepwise lowering of D to $0.68\,h^{-1}$ to avoid a wash out. Finally in the last process, YE was completely omitted as compound in the minimal CGXII medium and a dilution rate of $0.52\,h^{-1}$ was achieved. In sum, the total process time of the five successive ALE cultivations was 74 days with 1,700 generations of *C. glutamicum*. The *C. glutamicum* strain that was withdrawn after the last run was called EVO5. WGS was performed to identify alterations in the genome of EVO5. Simultaneously, the evolved strain was characterized in bioreactor batch studies to determine growth kinetics.

The ALE experiments of Pfeifer et al. (2017) and Wang et al. (2018b) targeted at growth improvements of *C. glutamicum* in minimal growth medium by cultivating the cell for prolonged times in repetitive batch cultivations. The ultimate goal of this contribution was the same but clearly differed from the other approaches by (i) performing the study in a controlled continuous bioreactor; (ii) challenging *C. glutamicum* with installed dilution rates near its maximum growth rate; and (iii) by initiating the experiments with a rich growth medium that was successively reduced in its complexity to finally yield minimal growth medium. Consequently, the growth environment faced by the organism in the batch ALE cultivations of Pfeifer et al. (2017) and Wang et al. (2018b) were highly dynamic over the process time as characterized by increasing biomass, decreasing substrate, and varying pO_2 and pH. Such growth conditions can promote the formation of by-products as a result of overflow metabolism (Paczia et al., 2012) or oxygen limitation (Lange et al., 2018) and ultimately become additional selection pressures. In turn, this could trigger unwanted side-mutations that are not beneficial for an improvement of the growth performance. In contrast, employing a chemostat process ensuring a stable growth environment and continuous dilution of potential by-products might minimize the risks for growth-irrelevant side mutations. Likewise, slow-growing subpopulations are washed out whereby faster growing subpopulations do not have to compete for nutrients (Gostomski et al., 1994). Eventually, this makes a continuous process operated at high dilution rates the perfect tool for selecting fast-growing subpopulations (Bull, 2010). Regarding the operation time of an ALE experiment, the continuous process setup also proofs to be advantageous. In repetitive batch approaches, cell passaging is often performed after the culture entered the stationary phase. These time periods, in which the cells cannot grow exponentially and experience stationary conditions, artificially prolong the time of a batch ALE experiment and moreover might trigger additional side-mutations (Zambrano et al., 1993). In contrast, the cells proliferate exponentially in

the continuous setup whereby the number of cell generations per experiment are higher in a chemostat setup. Thereby 1,700 generations where obtained in 2.5 months in this study, whilst Wang et al. (2018b) cultivated 1,500 in about 7 months. Hence, if the aim of an ALE process is to produce potential mutant strains in a fast fashion, the employment of a continuous process is the option of choice.

4.8.3. Evolved strain EVO5 and mutations impacting growth

Subsequent to the last ALE experiment, the genome of evolved strain EVO5 was sequenced whereby ten mutations compared to the parental WT strain were identified [cf. table 1 in Graf et al. (2019); section B]. Point mutations in genes cg2069 (*psp1*; P511, CCT → CCG), cg2504 (R265, CGT → CGC), and cg2935 (*nanP*; A265, GCC → GCT) had no impact on the encoded amino acid, respectively. A deletion of guanine occurred at position 3168391 in an intergenic region placing it 28 bp ahead of the cg3285 (*copR*) start codon. Another deletion was detected in gene cg2293 causing a frameshift and consequent stop codon (T nt 139 → amino acid 55 stop). The other five point mutations in cg2067 (L91V TTG → GTG), cg2468 (N97D, AAC → GAC), cg0655 (*rpoA*; S280F, GGA → GAA), cg2103 (*dtxR*; R103H, CGC → CAC), and cg2831 (*ramA*; S101C, CGA → GCA) caused an amino acid exchange in the respective genes. Since Wang et al. (2018b) also observed a point mutation in the latter gene encoding the global carbon regulator RamA, the S101C point mutation was re-engineered into the ATCC 13032 WT strain.

The corresponding mutant was named Cg reRamA and characterized together with the WT and EVO5 in triplicate batch bioreactor experiments. 1.5 L CGXII minimal medium (without PCA) supplemented with $20\,\mathrm{g\,L^{-1}}$ glucose was used as growth medium and all strains were cultivated at constant conditions (30 °C, 1.5 bar, pH 7.4, $p\mathrm{O_2} > 30\,\%$). Cg reRamA and EVO5 revealed an 8 % and 58 % enhanced growth rate, respectively, in comparison to the WT strain [$\mu = (0.34 \pm 0.03)\,\mathrm{h^{-1}}$, table 2 in Graf et al. (2019); cf. section B]. Interestingly, Cg reRamA showed a smaller biomass-substrate yield than the WT [$(0.49 \pm 0.01)\,\mathrm{g\,g^{-1}}$ vs. $(0.53 \pm 0.01)\,\mathrm{g\,g^{-1}}$] and EVO5 [$(0.52 \pm 0.01)\,\mathrm{g\,g^{-1}}$]. Concomitantly, the glucose consumption rate of Cg reRamA was non-proportional to μ [$q_{Glc} = (0.77 \pm 0.04)\,\mathrm{g\,g^{-1}\,h^{-1}}$] in contrast to EVO5 [$q_{Glc} = (1.03 \pm 0.01)\,\mathrm{g\,g^{-1}\,h^{-1}}$]. Respiratory rates were proportionally increased with μ for both strains [Cg reRamA: $q_{O_2} = (7.04 \pm 0.56)\,\mathrm{mmol\,g^{-1}\,h^{-1}}$, $q_{CO_2} = (6.93 \pm 0.55)\,\mathrm{mmol\,g^{-1}\,h^{-1}}$; EVO5: $q_{O_2} = (9.14 \pm 0.31)\,\mathrm{mmol\,g^{-1}\,h^{-1}}$, $q_{CO_2} = (9.70 \pm 0.18)\,\mathrm{mmol\,g^{-1}\,h^{-1}}$]. Under the tested conditions, all strains produced Pyr as by-product. The WT accumulated up to

60 mg L^{-1}, whilst EVO5 produced only 23 mg L^{-1} Pyr. Both strains re-consumed the organic acid by the end of the respective processes. In contrast, Cg reRamA accumulated up to 120 mg L^{-1} Pyr which was not totally consumed at the end of the exponential growth phase.

Apart from the experimental setup, the chosen selection pressures in this investigation also varied from the previous studies of Pfeifer et al. (2017) and Wang et al. (2018b). The presented ALE experiments of this work were designed in a way to impose a double selection pressure on *C. glutamicum* WT: firstly by setting the dilution rate near the strain's maximum growth rate that is achievable by the cell with the employed growth medium; secondly by steadily decreasing the richness of the growth medium, namely the amount of YE, whereby the cell was provided with less and less building blocks such as amino acids over the consecutive processes. In part I of this dissertation it was shown that *C. glutamicum* possesses a maximum catabolic capacity to metabolize glucose to provide precursors for amino acid formation (cf. section 4.1.2). This potential bottleneck was targeted with the chosen selection pressures. During the beginning of the ALE experiments, when the amount of YE was still high in the growth medium, evolution was directed towards targets controlling usage of extracellularly supplied amino acids. Thus, mutations in basic regulatory functions might have been triggered. By continuously decreasing the supply of amino acids (YE), but simultaneously keeping dilution rates high, evolution was then guided towards genes of the CCM and to related regulons that ultimately affect the supply of precursors for amino acid biosynthesis.

As outcome of the continuous ALE series, evolved strain EVO5 revealed a superior growth performance (58 % increased μ) and a proportionally elevated glucose consumption rate over the WT. Consequently, this increase in fitness has to be rooted in the identified mutations. On the one hand, the point mutations observed in *psp1*, cg2504, and *nanP* most likely had no impact on the growth phenotype of EVO5 since the encoded amino acid sequences were not altered. Even though the point mutation in cg2468 altered the encoded amino acid, a growth influencing impact is not expected in minimal medium because the gene encodes the permease component of a branched-chain amino acid (BCA) ABC-type transporter. Hence, a potential influence of this mutation on μ might only be observed in complex medium containing amino acids. Besides, this mutation could have occurred during the first ALE experiment phase where evolution was guided towards targets of amino acid uptake. On the other hand, the residual six mutations might have influenced the cell's growth in minimal medium. Even though the deletion upstream of

copR did not impact the binding site of CopR* encoding a response regulator that is part of the key regulatory system in *C. glutamicum* against copper ion resistance [CopRS; Schelder et al. (2011)], it might influence the transcriptional starting site of *copR* which was not detected yet (Pfeifer-Sancar et al., 2013; Schelder et al., 2011). Furthermore, the deletion in gene cg2293, coding for a putative indole-3-glycerol phosphate synthase, most likely makes this protein non-functional as the resulting frameshift caused a stop codon at the beginning of the protein sequence. The point mutation in cg2067 encoding a hypothetical protein might influence the cell's growth performance as well.

Above all, the point mutations detected in *rpoA*, *dtxR*, and *ramA* were the most promising ones considering that their gene products have regulatory functions in *C. glutamicum*. *rpoA* encodes the alpha subunit of th DNA-directed RNA polymerase (RpoA) of *C. glutamicum* and the corresponding point mutation was detected near the alpha C-terminal domain. This domain interacts with transcriptional regulators and promoter DNA to regulate transcription (Browning & Busby, 2004; Busby & Ebright, 1999). Therefore, it is considered as interesting target to introduce global transcriptional changes in a strain (Klein-Marcuschamer et al., 2009). Besides, an *E. coli* ALE investigation identified several μ-influencing mutations in the beta-subunit of the RNA polymerase (LaCroix et al., 2015).

dtxR encodes the master regulator of iron-dependent gene expression (Wennerhold & Bott, 2006). Possibly, the observed point mutation was a result of improving the cell's iron availability as suggested by Rolfe et al. (2012). Also, DtxR and RamA both influence the control of the succinate dehydrogenase operon in *C. glutamicum* under standard growth conditions (Auchter et al., 2011; Brune et al., 2006; Bussmann et al., 2009).

In contrast to the other mutations, the mutation in *ramA* encoding the global regulator of carbon metabolism (Cramer et al., 2006) was re-engineered in the WT to test if a similar growth enhancing effect could be observed as in the study of Wang et al. (2018b). Indeed, a 8 %-increased μ was determined for Cg reRamA compared to the WT, but was remarkably smaller than the 20 %-growth enhancement of the re-engineered strain of Wang et al. (2018b). Another difference to this latter study was the decreased biomass substrate yield of Cg reRamA resulting in a non-proportional increase of q_{Glc} with μ. Simultaneously, Cg reRamA produced twice as much Pyr as the WT and did not completely re-consume it. Apparently, this finding represents an unbalance between

*The binding site is located -59 and -78 bp upstream of the *copR* start codon

increased fluxes of glycolysis as a result of increased glucose uptake, but non-adjusted TCA-fluxes. Metabolic flux studies and transcriptome analysis performed by Wang et al. (2018b) with their re-engineered RamA-mutant revealed an up-regulation of glycolytic genes and a slight decrease in TCA activity fitting nicely with the observations of this study. Furthermore, these results are in line with the hypothesis formulated in section 4.6.1 suggesting that upper glycolysis might be a bottleneck in the CCM of *C. glutamicum*. Summarizing, the identified mutations in EVO5 differed from the findings of Pfeifer et al. (2017) who detected mutations in the CCM genes *pyk* encoding pyurvate kinase and *fruK* coding for 1-phosphofructikinase.

The omission of an iron chelating compound in the applied basis medium CGXII represented a third selection pressure on the *C. glutamicum* WT strain in this ALE study and was another difference to investigations of Pfeifer et al. (2017) and Wang et al. (2018b). PCA and catechol, employed in the respective mineral media of the latter, are reported to have a positive influence on growth. This could be due to facilitating cellular iron acquisition (Liebl et al., 1989) or by degradation products of PCA/catechol fueling the TCA cycle (Shen et al., 2012; Unthan et al., 2013). Interestingly, the final strain EVO5 did not reveal a further growth boost in a comparative batch cultivation with CGXII medium supplemented with PCA [cf. supplementary figure 3 in Graf et al. (2019)]. Consequently, the intrinsic growth rate of EVO5 was still 20 % higher than that of the WT cultivated in PCA- or catechol-containing CGXII minimal medium (cf. section 4.1.1). This result suggest an alternative hypothesis regarding the role of PCA in growth medium compared to the previous assumptions by Liebl et al. (1989) and Unthan et al. (2013). Rather than influencing iron acquisition or fueling TCA, PCA might have an (additionally) regulatory function on the growth of *C. glutamicum* as was shown for other siderophores with other organisms (Johnstone & Nolan, 2015).

CHAPTER 5

Conclusion and Outlook

Growth under metabolic pseudo-stationary conditions

In the first part of this thesis, pseudo-stationary growth conditions of *C. glutamicum* were investigated to reveal potential growth bottlenecks. Therefore, macroscopic phenotype studies were expanded by systems biology tools such as employing a SNM of *C. glutamicum* and conducting transcriptome analysis.

C. glutamicum was cultivated in bioreactor batch processes in minimal medium CGXII with glucose as sole carbon source serving as control experiments ($\mu = 0.32\,\mathrm{h}^{-1}$). Thereupon, the medium was supplemented with either (1–37) $\mathrm{g\,L}^{-1}$ BHI, a mixture of 18 amino acids with concentrations of $5\,\mathrm{mmol\,L}^{-1}$, respectively, $0.1\,\mathrm{mmol\,L}^{-1}$ PCA, or $0.2\,\mathrm{mg\,L}^{-1}$ thiamin.

Firstly, the impact of named supplements on growth rate, glucose and total carbon consumption was assessed, revealing that each supplement stimulated *C. glutamicum*'s growth rate. (1–37) $\mathrm{g\,L}^{-1}$ BHI produced a growth rate range of $\mu = (0.44\text{–}0.67)\,\mathrm{h}^{-1}$ in a Monod-like saturation curve ($K_{BHI} = 2.37\,\mathrm{g\,L}^{-1}$). However, amino acids in the complex BHI medium were not solely responsible for this enhancement since their supplementation resulted in a comparably moderate growth increase of $\mu = 0.47\,\mathrm{h}^{-1}$. Subsequently performed energetic analysis revealed that the growth stimulating effect of extracellularly fed amino acids can be traced back to releasing the cell of amino acid biosynthesis costs (4 ATP g_{CDW}^{-1}) and additionally supplying precursors for translation

processes. This also indicated that ATP-costly compounds like fatty acids and nucleotides, provided in larger concentrations of BHI, facilitate fast growth of *C. glutamicum* up to the apparent maximum of $\mu = 0.67\,\mathrm{h}^{-1}$. Besides, trace elements such as PCA and thiamin were revealed as growth stimulants as well ($\mu = 0.45\,\mathrm{h}^{-1}$).

Apart from influencing the growth rate, glucose consumption and total carbon consumption were also impacted by supplementation. Glucose consumption was initially stimulated by mere amounts of $1\,\mathrm{g\,L}^{-1}$ BHI ($q_{Glc} = 0.0277$ C-mol $\mathrm{L}^{-1}\,\mathrm{g}^{-1}\,\mathrm{h}^{-1}$; reference: 0.0214 C-mol $\mathrm{L}^{-1}\,\mathrm{g}^{-1}\,\mathrm{h}^{-1}$), but steadily decreased from this plateau with rising BHI portions. In contrast, every supplemented compound induced total carbon consumption rates strictly proportional to the respective growth rate, resulting in a constant biomass carbon yield of about $18\,\mathrm{g}_{CDW}$ C-mol^{-1} irrespective of the supplement type. Apparently, this value represents the strain's maximum capacity of processing carbon and nitrogen.

Secondly, the role of amino acid supplementation with regard to growth was analyzed in more detail. The preliminary supplementation study covered investigations on adding a mixture of amino acids, whereby 18 corresponding consumption rates were experimentally determined. This was extended by *in silico* investigations with the SNM *iMG481* of *C. glutamicum* that was curated and expanded from an existing model with regard to amino acid biosynthesis and uptake, facilitating dry-lab individual amino acid consumption studies. Deduced from *in vivo* observations, three amino acid consumption phenotypes were distinguished by comparison with the average *C. glutamicum* amino acid biomass composition. Additional FBAs and sensitivity analyses with *iMG481* further characterized these three groups. Combining *in vivo* and *in silico* techniques could thus reveal that amino acids of the first group (Arg, His, Ile, Leu, Met, Phe, Ser, Thr, Trp) were consumed according to the amino acid biomass composition of the cell since they predominantly serve biomass formation purposes. Besides, supplementation of individual amino acids from this group is advantageous for growth since their ATP-intensive biosynthesis is omitted. The residual amino acids were categorized to be either over-consumed (Asn, Gln, Pro) or under-consumed (Ala, Asp, Glu, Gly, Lys, Val) regarding the amino acid biomass composition. A complex interplay within the cell's transaminase network was identified as cause with Gln and Asn playing crucial roles as precursor or amino group donor for other amino acids.

The presented physiological and *in silico* results offer a broad range of targets to improve growth and nutrient consumption of *C. glutamicum* in an industrial context. Especially growth coupled bioprocesses might benefit by incorporating growth boosters like thiamin and ATP-intensive species such as fatty acids, nucleotides, and certain

amino acids (e.g. Met, Arg, His) into standard growth media. Based on their crucial role in the transaminase network of *C. glutamicum*, Gln and Asn are valuable additives as well, making supplementation of several other amino acids (e.g. Glu, Asp, Ala, Val) unnecessary. Consequently, an optimized growth medium for *C. glutamicum* can be designed on the basis of these investigations.

Apart from optimizing the extracellular growth environment of *C. glutamicum*, the strain itself might be improved. In this context, first interesting targets for strain engineering approaches were identified by conduction transcriptome analysis in the presented growth supplement studies featuring (1–37) $g\,L^{-1}$ BHI and 0.1 $mmol\,L^{-1}$ PCA.

As starting point, the transcriptional response of *C. glutamicum* towards PCA- and BHI-supplemented media was studied. In the case of PCA, this was done to shed light into the growth accelerating properties of PCA supporting a growth increase by ca. 40 % compared to reference conditions. Literature offers two possible reasons for this: the compound facilitates iron acquisition and/or is used as carbon source fueling the TCA cycle. Based on the expression of corresponding genes, the analysis could confirm that the availability of intracellular iron could have been higher and that PCA was degraded. Additionally, a new aspect was unraveled as well. The increased expression of genes involved in the uptake and assimilation of elemental nutrients like carbon, sulfur, and nitrogen might additionally hint at a regulatory function of PCA which therefore could influence basic cellular needs. Consequently, further supplement studies might employ similar compounds as PCA, potentially from the natural soil habitat of *C. glutamicum*, to assess whether such substances have in general a positive impact on growth and thus might serves as alternative growth supplements.

The transcriptional response of *C. glutamicum* to complex growth media like BHI was assessed for the first time in literature and was employed as tool to investigate its μ-increasing supplements. Thereby, the results could firstly confirm the theoretically characterized growth enhancing compounds from the presented physiological investigation. Thus, decreased expression of amino acid biosynthesis genes indicated the presence of amino acids in BHI, upregulation of genes encoding transporters for (oligo)peptides that of peptides, reduced expression of fatty acid synthase genes that of fatty acids, and increased expression of purine salvage pathway genes that of nucleotides. Apart from these ATP-intensive compounds, BHI most likely contained further compounds that made ATP-costly assimilation or transport of elemental compounds (e.g. sulfur) unnecessary as well, providing the strain with yet another energy advantage. Severe down-regulation of the complete thiamin biosynthesis operon was the reason for previously testing this

supplement as potential growth booster which could be positively confirmed. Moreover, a similar iron response as in the PCA transcript analysis was detected potentially indicating the presence of iron chelators like PCA. Consequently, transcriptome analysis can be employed as tool to investigate potential growth increasing supplements. Based on these results, the transcriptional response of the strain to other complex medium compounds such as corn-steep liquor or molasses usually employed in industrial processes might reveal additional growth stimulating compounds. Such components might then be added to industrial minimal media making the usage of undefined complex media unnecessary.

Apart from studying the strain's response to single media supplementation, differentially expressed genes detected in all supplemented cultivations [(1–37) $g\,L^{-1}$ BHI, 0.1 $mmol\,L^{-1}$ PCA] were analyzed. Thereby, genes with potential transcriptional control over the growth rate were assessed. Corresponding candidate genes for modified *C. glutamicum* strains were derived potentially exhibiting an increased μ upon gene over-expression or deletion as result of altered expression levels. Since the supplements induced a broad μ-range of (0.44–0.67) h^{-1}, common DEGs obtained from the varying nutrient supplement conditions were exclusively scanned for strict growth rate dependent expression patterns. Thereof, 14 genes were identified of which four (*rpf1*, cg3374, cg3329, cg1296) were the most promising ones according to respective encoded protein functions. However, construction of corresponding mutant strains and characterization studies in CGXII minimal medium optionally supplemented with 37 $g\,L^{-1}$ BHI had no positive impact on μ. Concluding from this, the gene expression status of named genes does not transcriptionally influence the growth rate of *C. glutamicum*. Hence, future studies might aim at altering the expression of their subordinate regulators, i.e. GlxR, CysR, or AmtR.

Growth under metabolic stationary conditions

In the second pat of this thesis, potential growth limitations of *C. glutamicum* cultivated under metabolic stationary conditions were investigated. To establish metabolic steady-states in the cell, continuous chemostat cultivations were conducted to install different growth rates independent of the growth medium. On this basis, the cellular growth phenotype was elucidated by making use of the systems biology tools metabolomics and transcriptomics. Additionally, the fluxome was investigated at $\mu = 0.4\,h^{-1}$ with an isotopic ^{13}C-labeling experiment.

Three biologically independent chemostat cultivations were performed at $\mu = 0.2\,h^{-1}$,

$0.3\,h^{-1}$ and $0.4\,h^{-1}$ employing CGXII minimal medium supplemented with $12\,g\,L^{-1}$ glucose and $30\,mg\,L^{-1}$ PCA. As basis for the metabolome and transcriptome analysis, kinetic parameters (q_{Glc}, q_{O_2}, q_{CO_2}) were determined for each growth rate. Experimentally derived steady state biomass concentrations were compared to corresponding simulated values obtained by employing continuous mass balances, Monod-kinetics, and maintenance equations after Pirt. However, the experimental and predicted data sets did not coincide which was traced back to the theoretical formulation of cellular maintenance. Hence, further research could focus on determining a solid data set on kinetic parameters of *C. glutamicum* for a broader range of growth rates (especially at low μ), whereby alternative maintenance formulations could be derived that ultimately improve macrokinetic models as employed in this work.

As prerequisite to study the metabolic response of *C. glutamicum* to different μ and as necessary input for non-stationary ^{13}C-MFA, first steps towards an accurate quantification of the strain's intracellular metabolite pools from CCM metabolites and amino acids were made. A comparison between two quenching and two extraction techniques was performed for metabolome samples retrieved from a continuous process at $\mu = 0.4\,h^{-1}$. Analysis via LC-MS QQQ revealed FCT-HWE as the combination of choice capturing the highest pool concentrations for 18 out of 30 metabolites and showing equally good performance as other combinations for five further metabolites. However, quenching with FCT is afflicted with a time delay potentially distorting the sampled metabolic state of the cell. Nevertheless, equally high intracellular pool sizes of sugar 6-phosphates, that exhibit high metabolic turn-over rates, obtained via FCT-HWE and differential MQ-CE measurements (literature value) revealed nearly identical values. This implies that the 30 s delay until quenching is completed with FCT has no influence on intracellular metabolite pools in glucose-limited growth environments as facilitated in a chemostat. A future comparative metabolome study between glucose-unlimited batch cultivations and glucose-limited chemostat conditions could further investigate this hypothesis. In this sense, it would be expected that a prolonged delay until quenching of metabolome samples from the batch cultivation is visible in metabolome pools of 6-phosphate sugars due to remaining extracellular glucose. Another important finding was that there is no single best extraction method for the entity of CCM metabolites and amino acids. Consequently, the best way to accurately quantify intracellular metabolites would be to employ one quenching technique that ensures that the same metabolic state is captured. Extraction would than be performed with a variety of methods tailored for optimal extraction of individual intracellular metabolites.

These results had consequences for the further steps in this work. Since no accurate metabolite pool concentrations could be reliably determined, the metabolic response to varying growth rates was not based on absolute but relative pool size measurements. Furthermore, a stationary ^{13}C-MFA was performed that required no information on intracellular pool sizes opposed to the non-stationary MFA variant.

In light of the physiological metabolic steady state determination, intracellular investigations of *C. glutamicum* cultivated at $\mu = 0.2\,h^{-1}$, $0.3\,h^{-1}$ and $0.4\,h^{-1}$ were performed with the help of metabolome and transcriptome analysis. Relative pool size changes proportional to the growth rate were assessed for nearly all analyzed CCM metabolites and amino acids and the majority of compounds revealed enhanced pools with rising μ. Identification of growth rate dependent and significant gene expression resulted in two clusters that distinguished 257 genes with rising and 290 genes with decreasing expression with elevated μ.

Thereby, potential control strategies of the CCM in *C. glutamicum* cultivated under glucose-limited conditions were revealed by bringing together the assessed metabolome and transcriptome data with a proteome analysis described in literature, that was performed under nearly identical conditions as in this study. As result, glucose uptake via PTS was under transcriptional control, glycolysis and PPP were under metabolic control, but no distinct scheme could be assessed for control of the TCA cycle.

Two potential bottlenecks limiting growth of *C. glutamicum* under the tested conditions could be derived from the combined metabolome and transcritpome responses. The first bottleneck could be located in glycolysis. Contrary metabolite profiles of upper and lower glycolysis metabolites hint at an unfortunate NADH/NAD^+-ratio with increasing growth rates, which could result in an unbalance between glycolytic flux and flux through the TCA cycle. Ultimately, this might result in a non-proportionality between the growth rate and anabolic precursors supplied by the TCA cycle for biomass formation. The second bottleneck could be located in the Met-SAM-cycle based on metabolic and transcriptional responses of the protagonists Ser, Met, and SAM. On the one hand, non-proportional increases of Ser and Gly pools, enhanced expression of Ser biosynthesis (*serC*) but decreased expression of its degradation gene *sdaA* signaled a rising demand of this 5,10-MTHF-precursor over μ. If accumulation of intracellular Gly slowed down the Ser hydroxymethyltransferase reaction, 5,10-MTHF- and thereby Met-synthesis, which showed enhanced expression levels (*metB*, *metE*, *cysE*), could have been hampered with increasing growth rates as indicated by a strictly decreasing intracellular pool size. In turn, SAM synthesis could have suffered employing Met as precursor. As a result,

sufficient supply of 5,10-MTHF and SAM might become growth limiting in the strain at increased μ. In sum, deduced from the metabolic and transcriptome trends observed in both cases, higher growth rates of *C. glutamicum* might ultimately be prevented by the identified bottlenecks. Consequently, to prove if the NADH/NAD^+ ratio indeed is responsible for a growth limitation, further chemostat investigations should analytically determine intracellular NADH and NAD^+ pools for different growth rates. Also, to open the potential bottleneck around the Met-SAM-cycle, heterologous introduction of the GCV into the genome of *C. glutamicum* could be performed to provide additional 5,10-MTHF from Gly.

CCM transcript results were contrasted with transcriptome data of a batch experiment investigating growth rate transitions within the range $\mu = (0–0.4)\,h^{-1}$. Based on this, it seems that the process mode of the cultivation ultimately dictates whether glycolysis is controlled metabolically or transcriptionally in *C. glutamicum*. Thus, in glucose-limited environments, glycolysis was controlled metabolically whilst glucose-rich environments in batch cultivations induced transcriptional control. As a result, the availability of extracellular glucose could be the switch between the two control strategies. This implies that modifying the gene expression of glycolysis-related genes might only prove fruitful if the resulting engineered strain is cultivated under glucose-unlimited conditions. *Vice versa*, glucose limited conditions set in continuous or fed-batch cultivations should influence engineered strains with altered intracellular glycolytic metabolite pools. In contrast to the transient batch results, translational processes appear to be controlled on the transcriptional level in glucose-limited chemostat cultivations based on increased expression of genes encoding ribosmal proteins, translation initiation factors, and tRNA synthases with elevated μ. Fittingly, expression of genes coding for enzymes involved in amino acid biosynthesis were likewise increased to supply a larger amount of amino acids for protein formation. Hence, exclusively under glucose-limited conditions, overexpression of said genes involved in the translational process might prove to be beneficial.

Besides, increased expression of genes encoding inositol transport and degradation was recorded in transcripts from transient batch and chemostat cultivations with rising μ. This also corroborated the transcript analysis from the batch supplementation studies. Consequently, the inositol-related response seems to be independent from the growth medium, glucose or inositol availability and could thus be a general growth-dependent response of the cell. This is even more interesting when considering that transporter IolT1, which has only a low affinity for glucose, is able to take up glucose in the absence of PTS. Hence, it might be of interest to further investigate the role of this transporter

and degradation pathway with regard to a potential growth acceleration.

Finally, genes *rpf1* and cg3374 reappeared as growth dependent DEGs under chemostat conditions as previously documented for the supplemented batch conditions. Since overexpression of *rpf1* or deletion of cg3374 did not influence the growth rate, the growth rate dependent expression was most likely an effect of regulation by GlxR and CysR, respectively, even though these global regulators were not significantly expressed in either study. Hence, it might be of interest to further investigate the role of these regulators in influencing *C. glutamicum*'s growth rate. Again comparable to the supplementation studies, a transcriptional response of thiamin biosynthesis genes was assessed under chemostat conditions. However, expression under substrate limited conditions was increased instead which signals an apparent importance of this vitamin for fast growth.

A ^{13}C-labeling experiment in chemostat mode was performed to determine intracellular carbon fluxes in the CCM of *C. glutamicum* at $\mu = 0.4\,\mathrm{h}^{-1}$. Initially, it was planned to perform this experiment in a non-stationary fashion which generates non-stationary labeling patterns in the isotopologue traces of metabolites. Therefore, the continuous bioreactor setup was expanded by a feed-switch and a device for rapid sampling. However, non-stationary ^{13}C-MFA simulations also require accurate absolute intracellular metabolite pool sizes. Since this could not be guaranteed as previously described, a stationary ^{13}C-experiment was conducted instead. Nevertheless, the rapid sampling scheme originally designed for the non-stationary experiment was employed to test the functionality of the established experimental setup for future non-stationary experiments in chemostat mode. Moreover, rapid sampling of a stationary chemostat labeling experiment was not yet described in literature.

Kinetic growth parameters derived from the ^{12}C-feed phase were in accordance with values from the previous chemostat experiments conducted at the same growth rate. Moreover, the established experimental setup proved to be applicable for non-stationary labeling purposes as dynamic ^{13}C-patterns were recorded in all of the analyzed metabolites from CCM and in amino acids. Derived from the non-stationary labeling patterns of CCM metabolites, two interesting observations were made. Firstly, fluctuations in the total labeling fraction of nearly all CCM metabolites were revealed within the first 80 s of labeling showing periodically increases of unlabeled $m+0$ traces. Most likely, unlabeled carbon was channeled into glycolysis from buffer or storage compounds distorting the labeling enrichment. Secondly, a faster ^{13}C-labeling progress in lower glycolysis- and PPP-metabolites was observed than in G6P and F6P. A simplified ^{13}C-balance showed that the high labeling fraction of FbP could not solely originate from G6P. Additionally,

the high portion of $m+3$ isotopologues in FbP indicated gluconeogenic fluxes. This hinted at an alternative second route for glucose to channel into glycolysis. Thus, the presence of ^{13}C-labeled gluconate was retrospectively identified which could be an indicator for an Entner-Doudoroff-like pathway in *C. glutamicum*, that might be only employed by the strain under glucose-limited conditions. Moreover, this could indicate a possible limitation in glucose uptake via PTS under the tested conditions. Consequently, it would be of great interest to investigate this topic further in comparable chemostat studies by screening the intracellular metabolite spectrum of *C. glutamicum* for representatives of an potential alternative glucose pathway.

With the help of the employed experimental setup, stationary labeling patterns were determined after about four residence times (= 10 h) at $D = 0.4\,\mathrm{h}^{-1}$ in all analyzed metabolites. Together with derived isotopologue patterns, kinetic growth parameters from the ^{12}C-phase served as input data for subsequent stationary ^{13}C-MFA. Thereby, intracellular metabolite fluxes in the CCM at $\mu = 0.4\,\mathrm{h}^{-1}$ were derived. 54 % of the consumed glucose was channeled towards PPP, whilst 45 % was channeled to glycolysis, and 66 % towards the TCA cycle. Comparison with flux distributions obtained from other stationary ^{13}C-experiments for $\mu < 0.4\,\mathrm{h}^{-1}$ described in literature served to identify potential growth limitations of the strain. Thereof, the produced amount of NADPH was derived for growth rates (0.05–0.4) h^{-1}, revealing a slight increase of produced NADPH for $\mu \geq 0.15\,\mathrm{h}^{-1}$. This increase surpassed the NADPH requirement for biomass formation, but was not described for *C. glutamicum* with regard to a growth rate dependency before. Since the production of NADPH-intensive products such as Lys would potentially benefit from the NADPH surplus assessed at $\mu \geq 0.15\,\mathrm{h}^{-1}$, the installed growth rate during such productions processes becomes relevant. Consequently, future research might aim at investigating this potential surplus further by analyzing potential growth rate dependent intracellular NAPDH pools.

Adaptive laboratory continuous evolution

In the third part of this thesis, five repetitive ALE experiments were performed to evolve *C. glutamicum* towards higher growth rates by means of natural selection processes. Thus, growth limitations of the WT strain could be revealed in retrospect by comparison with evolved mutant strain EVO5.

For this ALE investigation, a continuous bioreactor setup was employed that featured an advanced chemostat controller setup to precisely control the set dilution rate. Thereby,

dilution rates near the maximum growth rate of *C. glutamicum* could be installed which served as the first selection pressure of this ALE concept. The second selection pressure targeted the strain's maximum catabolic capacity to metabolize glucose identified in the first part of this work to provide precursors for amino acid formation. Therefore, the richness of the employed growth medium was gradually decreased over the ALE experiments by reducing the amount of supplemented YE in glucose-containing CGXII minimal medium, until the ALE process was finally performed in sole minimal medium. Consequently, when the richness of the growth medium was high, evolution was guided toward targets controlling usage of extracellularly supplied amino acids potentially triggering mutations in basic regulatory functions of the cell. When YE was gradually decreased and finally omitted from the medium, evolution was guided toward targets in CCM and to related regulons that ultimately affect the supply of precursors for amino acid biosynthesis. The third selection pressure was the omission of PCA which is a standard component in CGXII growth medium. Besides, the otherwise constant growth parameters, enabled by the employment of the continuous bioreactor, reduced the risks of unwanted 'side mutations' that might be triggered in dynamic growth environments.

In sum, five consecutive continuous processes were performed within 2.5 months starting with the *C. glutamicum* WT. Potentially evolved strains at the end of one process were preserved and employed to inoculate the subsequent ALE experiment. Thus, evolved strain EVO5 was obtained after 1,700 generations at the end of the fifth process cultivated in YE-free growth medium. EVO5 was further investigated in triplicate batch cultivations and revealed a promising increase in μ from $0.34\,h^{-1}$ to $0.54\,h^{-1}$ in PCA-free CGXII minimal medium and a proportionally increased glucose consumption rate compared to the WT. Besides, supplementation of PCA in CGXII did not influence the growth rate of EVO5 under the tested bioreactor batch conditions. This observation could indicate that PCA might have a regulatory function on growth of *C. glutamicum* WT in addition to its hitherto described attributes as iron acquisition facilitating or TCA-fueling compound. Otherwise, addition of PCA to the growth medium would have boosted μ of EVO5 even further.

The genome of EVO5 was sequenced and ten mutations were revealed compared to the parental WT strain. Out of the ten mutations, six mutations could be responsible for the improved growth rate of EVO5. Amongst them the most promising ones occurred in genes encoding the global carbon regulator RamA, the iron regulator DtxR, and the alpha subunit of the DNA-directed RNA polymerase. The RamA point mutation S101C was re-engineered in the WT strain and the resulting mutant was named Cg

ReRamA. Growth characterization in triplicate bioreactor batch cultivations in CGXII minimal medium revealed a growth increase of 8 % over the WT and a non-proportionally increased glucose consumption rate of 25 %. The thereby reduced biomass substrate yield could be attributed to the formation of Pyr. Since Pyr represents the intersection between glycolysis and TCA cycle, an unbalance between glycolytic flux and TCA flux seems likely. With regard to the predicted bottleneck in glycolysis previously identified from the chemostat data of this work, the manifested mutation in RamA, triggered by the successive ALE experiments, could have opened this bottleneck. In turn, an increase of the glucose consumption rate and enhanced activity in glycolysis were obtained, but not (yet) matched by the TCA cycle performance. Since the point mutation in RamA did only partially contribute to the growth increase of EVO5, the residual mutations might have led to an adjustment of the TCA flux. Hence, the rising demand for anabolic precursors could be provided by an equally accelerated TCA flux, whereby the biomass substrate yield of EVO5 again reached the WT value and Pyr was no longer detected as metabolic overflow by-product. Considering that the mutation in *rpoA* likely has an impact on the interaction with transcriptional regulators and DNA promoters, re-engineering of this mutation in the WT and Cg reRamA is expected to be very promising in terms of an additional growth increase. Consequently, all mutant strains with enhanced growth performance that will be derived from this ALE investigation are of utmost interest for industrial applications, especially for growth-coupled processes.

References

Agrawal, P. & H.C. Lim. Analyses of various control schemes for continuous bioreactors. In: *Bioprocess Parameter Control*. Vol. 30. Advances in Biochemical Engineering/Biotechnology. Springer Berlin Heidelberg, 1984, 61–90.

Ahmed, H., B. Tjaden, R. Hensel & B. Siebers. Embden–Meyerhof–Parnas and Entner–Doudoroff pathways in *Thermoproteus tenax*: metabolic parallelism or specific adaptation? In: *Biochemical Society Transactions* 32.2 (2004), 303–304.

Antoniewicz, M.R. Methods and advances in metabolic flux analysis: a mini-review. In: *Journal of industrial microbiology & biotechnology* 42.3 (2015), 317–325.

Arndt, A. & B.J. Eikmanns. Regulation of Carbon Metabolism in *Corynebacterium glutamicum*. In: *Corynebacteria*. Ed. by **Burkovski, A.** Wymondham: Caister Academic, 2008, 155–182.

Auchter, M. et al. RamA and RamB are global transcriptional regulators in *Corynebacterium glutamicum* and control genes for enzymes of the central metabolism. In: *Journal of Biotechnology* 154.2-3 (2011), 126–139.

Barrick, J.E. et al. Genome evolution and adaptation in a long-term experiment with *Escherichia coli*. In: *Nature* 461.7268 (2009), 1243–1247.

Bartek, T. et al. Comparative ^{13}C metabolic flux analysis of pyruvate dehydrogenase complex-deficient, L-valine-producing *Corynebacterium glutamicum*. In: *Applied and environmental microbiology* 77.18 (2011), 6644–6652.

Bäumchen, C. et al. Effect of elevated dissolved carbon dioxide concentrations on growth of *Corynebacterium glutamicum* on D-glucose and L-lactate. In: *Journal of Biotechnology* 128.4 (2007), 868–874.

Becker, J. & C. Wittmann. Bio-based production of chemicals, materials and fuels - *Corynebacterium glutamicum* as versatile cell factory. In: *Current Opinion in Biotechnology* 23.4 (2012), 631–640.

Becker, J., N. Buschke, R. Bücker & C. Wittmann. Systems level engineering of *Corynebacterium glutamicum* - Reprogramming translational efficiency for superior production. In: *Engineering in Life Sciences* 10.5 (2010), 430–438.

Beckers, G., L. Nolden & A. Burkovski. Glutamate synthase of *Corynebacterium glutamicum* is not essential for glutamate synthesis and is regulated by the nitrogen status. In: *Microbiology (Reading, England)* 147.Pt 11 (2001), 2961–2970.

Beckers, G. et al. Regulation of AmtR-controlled gene expression in *Corynebacterium glutamicum*: mechanism and characterization of the AmtR regulon. In: *Molecular microbiology* 58.2 (2005), 580–595.

Blombach, B., J. Buchholz, T. Busche, J. Kalinowski & R. Takors. Impact of different CO_2/HCO_3^- levels on metabolism and regulation in *Corynebacterium glutamicum*. In: *Journal of Biotechnology* 168.4 (2013), 331–340.

Blombach, B. et al. *Corynebacterium glutamicum* tailored for efficient isobutanol production. In: *Applied and environmental microbiology* 77.10 (2011), 3300–3310.

Bodegom, P. van. Microbial maintenance: a critical review on its quantification. In: *Microbial ecology* 53.4 (2007), 513–523.

Bolten, C.J., P. Kiefer, F. Letisse, J.-C. Portais & C. Wittmann. Sampling for metabolome analysis of microorganisms. In: *Analytical chemistry* 79.10 (2007), 3843–3849.

Bott, M. & A. Niebisch. The respiratory chain of *Corynebacterium glutamicum*. In: *Journal of Biotechnology* 104.1-3 (2003), 129–153.

Brinkrolf, K., I. Brune & A. Tauch. The transcriptional regulatory network of the amino acid producer *Corynebacterium glutamicum*. In: *Journal of Biotechnology* 129.2 (2007), 191–211.

Brinkrolf, K., J. Schröder, A. Pühler & A. Tauch. The transcriptional regulatory repertoire of *Corynebacterium glutamicum*: reconstruction of the network controlling pathways involved in lysine and glutamate production. In: *Journal of Biotechnology* 149.3 (2010), 173–182.

Brinkrolf, K., I. Brune & A. Tauch. Transcriptional regulation of catabolic pathways for aromatic compounds in *Corynebacterium glutamicum*. In: *Genetics and Molecular Research* 5.4 (2006), 773–789.

Bröer, S. & R. Krämer. Lysine uptake and exchange in *Corynebacterium glutamicum*. In: *Journal of bacteriology* 172.12 (1990), 7241–7248.

Browning, D.F. & S.J. Busby. The regulation of bacterial transcription initiation. In: *Nature reviews. Microbiology* 2.1 (2004), 57–65.

Brune, I., H. Werner, A.T. Hüser, J. Kalinowski, A. Pühler & A. Tauch. The DtxR protein acting as dual transcriptional regulator directs a global regulatory network involved in iron metabolism of *Corynebacterium glutamicum*. In: *BMC genomics* 7 (2006), 21.

Brune, I. et al. The IclR-type transcriptional repressor LtbR regulates the expression of leucine and tryptophan biosynthesis genes in the amino acid producer *Corynebacterium glutamicum*. In: *Journal of bacteriology* 189.7 (2007), 2720–2733.

Brüsseler, C., A. Radek, N. Tenhaef, K. Krumbach, S. Noack & J. Marienhagen. The myo-inositol/proton symporter IolT1 contributes to D-xylose uptake in *Corynebacterium glutamicum*. In: *Bioresource technology* 249 (2018), 953–961.

Buchholz, J. et al. CO_2/HCO_3^- perturbations of simulated large scale gradients in a scale-down device cause fast transcriptional responses in *Corynebacterium glutamicum*. In: *Applied Microbiology and Biotechnology* (2014), 1–10.

Buchholz, J., M. Graf, B. Blombach & R. Takors. Improving the carbon balance of fermentations by total carbon analyses. In: *Biochemical Engineering Journal* (2014).

Buerger, J., N. Rehm, L. Grebenstein & A. Burkovski. Glutamine metabolism of *Corynebacterium glutamicum*: role of the glutaminase GlsK. In: *FEMS Microbiology Letters* 363.20 (2016).

Bull, A.T. The renaissance of continuous culture in the post-genomics age. In: *Journal of industrial microbiology & biotechnology* 37.10 (2010), 993–1021.

Burkovski, A., B. Weil & R. Krämer. Characterization of a secondary uptake system for L-glutamate in *Corynebacterium glutamicum*. In: *FEMS Microbiology Letters* 136.2 (1996), 169–173.

Busby, S. & R.H. Ebright. Transcription activation by catabolite activator protein (CAP). In: *Journal of Molecular Biology* 293.2 (1999), 199–213.

Bussmann, M., D. Emer, S. Hasenbein, S. Degraf, B.J. Eikmanns & M. Bott. Transcriptional control of the succinate dehydrogenase operon *sdhCAB* of *Corynebacterium glutamicum* by the cAMP-dependent regulator GlxR and the LuxR-type regulator RamA. In: *Journal of Biotechnology* 143.3 (2009), 173–182.

Chakravarty, A.K., R. Subbotin, B.T. Chait & S. Shuman. RNA ligase RtcB splices 3'-phosphate and 5'-OH ends via covalent RtcB-(histidinyl)-GMP and polynucleotide-(3')pp(5')G intermediates. In: *Proceedings of the National Academy of Sciences of the United States of America* 109.16 (2012), 6072–6077.

Choi, J.W., S.S. Yim & K.J. Jeong. Development of a high-copy-number plasmid via adaptive laboratory evolution of *Corynebacterium glutamicum*. In: *Applied microbiology and biotechnology* 102.2 (2018), 873–883.

Cocaign-Bousquet, M., A. Guyonvarch & N.D. Lindley. Growth Rate-Dependent Modulation of Carbon Flux through Central Metabolism and the Kinetic Consequences for Glucose-Limited Chemostat Cultures of *Corynebacterium glutamicum*. In: *Applied and environmental microbiology* 62.2 (1996), 429–436.

Cocaign, M., C. Monnet & N.D. Lindley. Batch kinetics of *Corynebacterium glutamicum* during growth on various carbon substrates: use of substrate mixtures to localise metabolic bottlenecks. In: *Applied Microbiology and Biotechnology* 40.4 (1993), 526–530.

Cox, R.A. Quantitative relationships for specific growth rates and macromolecular compositions of *Mycobacterium tuberculosis*, *Streptomyces coelicolor* A3(2) and *Escherichia coli* B/r: an integrative theoretical approach. In: *Microbiology* 150.5 (2004), 1413–1426.

Cramer, A., R. Gerstmeir, S. Schaffer, M. Bott & B.J. Eikmanns. Identification of RamA, a novel LuxR-type transcriptional regulator of genes involved in acetate metabolism of *Corynebacterium glutamicum*. In: *Journal of bacteriology* 188.7 (2006), 2554–2567.

Davey, H.M., C.L. Davey, A.M. Woodward, A.N. Edmonds, A.W. Lee & D.B. Kell. Oscillatory, stochastic and chaotic growth rate fluctuations in permittistatically controlled yeast cultures. In: *Biosystems* 39.1 (1996), 43–61.

Dettman, J.R., N. Rodrigue, A.H. Melnyk, A. Wong, S.F. Bailey & R. Kassen. Evolutionary insight from whole-genome sequencing of experimentally evolved microbes. In: *Molecular ecology* 21.9 (2012), 2058–2077.

Dietrich, C., A. Nato, B. Bost, P. Le Maréchal & A. Guyonvarch. Regulation of *ldh* expression during biotin-limited growth of *Corynebacterium glutamicum*. In: *Microbiology (Reading, England)* 155.Pt 4 (2009), 1360–1375.

Dominguez, H., C. Rollin, A. Guyonvarch, J.L. Guerquin-Kern, M. Cocaign-Bousquet & N.D. Lindley. Carbon flux distribution in the central metabolic pathways of *Corynebacterium*

glutamicum during growth on fructose. In: *European journal of biochemistry / FEBS* 254.1 (1998), 96–102.

Dominguez, H., C. Nezondet, N.D. Lindley & M. Cocaign. Modified carbon flux during oxygen limited growth of *Corynebacterium glutamicum* and the consequences for amino acid overproduction. In: *Biotechnology Letters* 15.5 (1993), 449–454.

Dominguez, H., M. Cocaign-Bousquet & N.D. Lindley. Simultaneous consumption of glucose and fructose from sugar mixtures during batch growth of *Corynebacterium glutamicum*. In: *Applied Microbiology and Biotechnology* 47.5 (1997), 600–603.

Dower, W.J., J.F. Miller & C.W. Ragsdale. High efficiency transformation of *E. coli* by high voltage electroporation. In: *Nucleic acids research* 16.13 (1988), 6127–6145.

Dragosits, M. & D. Mattanovich. Adaptive laboratory evolution – principles and applications for biotechnology. In: *Microbial cell factories* 12 (2013), 64.

Dunn, W.B., N.J.C. Bailey & H.E. Johnson. Measuring the metabolome: current analytical technologies. In: *The Analyst* 130.5 (2005), 606–625.

Ebbighausen, H., B. Weil & R. Krämer. Transport of branched-chain amino acids in *Corynebacterium glutamicum*. In: *Archives of Microbiology* 151.3 (1989), 238–244.

Eikmanns, B.J., D. Rittmann & H. Sahm. Cloning, sequence analysis, expression, and inactivation of the *Corynebacterium glutamicum icd* gene encoding isocitrate dehydrogenase and biochemical characterization of the enzyme. In: *Journal of Bacteriology* 177.3 (1995), 774–782.

Eikmanns, B. Central Metabolism: Tricarboxylic Acid Cycle and Anaplerotic Reactions. In: *Handbook of Corynebacterium glutamicum*. Ed. by **Eggeling, L. & Bott, M.** Boca Raton: Taylor & Francis, 2005, 244–278.

Eikmanns, B., M. Metzger, D. Reinscheid, M. Kircher & H. Sahm. Amplification of three threonine biosynthesis genes in *Corynebacterium glutamicum* and its influence on carbon flux in different strains. In: *Applied Microbiology and Biotechnology* 34.5 (1991), 617–622.

Ellis, D.I., W.B. Dunn, J.L. Griffin, J.W. Allwood & R. Goodacre. Metabolic fingerprinting as a diagnostic tool. In: *Pharmacogenomics* 8.9 (2007), 1243–1266.

Engels, V. & V.F. Wendisch. The DeoR-type regulator SugR represses expression of *ptsG* in *Corynebacterium glutamicum*. In: *Journal of bacteriology* 189.8 (2007), 2955–2966.

Engels, V., S.N. Lindner & V.F. Wendisch. The global repressor SugR controls expression of genes of glycolysis and of the L-lactate dehydrogenase LdhA in *Corynebacterium glutamicum*. In: *Journal of bacteriology* 190.24 (2008), 8033–8044.

Esener, A.A., J.A. Roels, Kossen, N. W. F. & Roozenburg, J. W. H. Description of microbial growth behaviour during the wash-out phase; determination of the maximum specific growth rate. In: *European journal of applied microbiology and biotechnology* 13.3 (1981), 141–144.

Feist, A.M., D.C. Zielinski, J.D. Orth, J. Schellenberger, M.J. Herrgard & B.Ø. Palsson. Model-driven evaluation of the production potential for growth-coupled products of *Escherichia coli*. In: *Metabolic engineering* 12.3 (2010), 173–186.

Feith, A., A. Teleki, M. Graf, L. Favilli & R. Takors. HILIC-Enabled ^{13}C Metabolomics Strategies: Comparing Quantitative Precision and Spectral Accuracy of QTOF High- and QQQ Low-Resolution Mass Spectrometry. In: *Metabolites* 9.4 (2019).

Festel, G., C. Detzel & R. Maas. Industrial biotechnology–Markets and industry structure. In: *Journal of Commercial Biotechnology* 18.1 (2012).

Fiehn, O. Combining genomics, metabolome analysis, and biochemical modelling to understand metabolic networks. In: *Comparative and functional genomics* 2.3 (2001), 155–168.

Fieschi, F., V. Nivière, C. Frier, J.-L. Décout & M. Fontecave. The mechanism and substrate specificity of the NADPH: flavin oxidoreductase from *Escherichia coli*. In: *Journal of Biological Chemistry* 270.51 (1995), 30392–30400.

Follmann, M. et al. Functional genomics of pH homeostasis in *Corynebacterium glutamicum* revealed novel links between pH response, oxidative stress, iron homeostasis and methionine synthesis. In: *BMC genomics* 10 (2009), 621.

Freudl, R. Beyond amino acids: Use of the *Corynebacterium glutamicum* cell factory for the secretion of heterologous proteins. In: *Journal of Biotechnology* 258 (2017), 101–109.

Frunzke, J., V. Engels, S. Hasenbein, C. Gätgens & M. Bott. Co-ordinated regulation of gluconate catabolism and glucose uptake in *Corynebacterium glutamicum* by two functionally equivalent transcriptional regulators, GntR1 and GntR2. In: *Molecular microbiology* 67.2 (2008), 305–322.

Frunzke, J., C. Gätgens, M. Brocker & M. Bott. Control of heme homeostasis in *Corynebacterium glutamicum* by the two-component system HrrSA. In: *Journal of bacteriology* 193.5 (2011), 1212–1221.

Gaigalat, L. et al. The DeoR-type transcriptional regulator SugR acts as a repressor for genes encoding the phosphoenolpyruvate:sugar phosphotransferase system (PTS) in *Corynebacterium glutamicum*. In: *BMC molecular biology* 8 (2007), 104.

Gibson, D.G. Enzymatic assembly of overlapping DNA fragments. In: *Methods in Enzymology* 498 (2011), 349–361.

Gong, S., H. Richard & J.W. Foster. YjdE (AdiC) Is the Arginine:Agmatine Antiporter Essential for Arginine-Dependent Acid Resistance in *Escherichia coli*. In: *Journal of bacteriology* 185.15 (2003), 4402–4409.

Gopal, G.J. & A. Kumar. Strategies for the production of recombinant protein in *Escherichia coli*. In: *The protein journal* 32.6 (2013), 419–425.

Gostomski, P., M. Mühlemann, Y.-H. Lin, R. Mormino & H. Bungay. Auxostats for continuous culture research. In: *Journal of Biotechnology* 37.2 (1994), 167–177.

Gourdon, P. & N.D. Lindley. Metabolic analysis of glutamate production by *Corynebacterium glutamicum*. In: *Metabolic engineering* 1.3 (1999), 224–231.

Gourdon, P., M. Raherimandimby, H. Dominguez, M. Cocaign-Bousquet & N.D. Lindley. Osmotic stress, glucose transport capacity and consequences for glutamate overproduction in *Corynebacterium glutamicum*. In: *Journal of Biotechnology* 104.1-3 (2003), 77–85.

Graaf, A.A. de. Metabolic flux analysis of *Corynebacterium glutamicum*. In: *Bioreaction Engineering*. Springer, 2000, 506–555.

Graf, M. et al. Continuous Adaptive Evolution of a Fast-Growing Corynebacterium glutamicum Strain Independent of Protocatechuate. In: *Frontiers in microbiology* 10 (2019), 1648.

Graf, M., J. Zieringer, T. Haas, A. Nieß, B. Blombach & R. Takors. Physiological Response of *Corynebacterium glutamicum* to Increasingly Nutrient-Rich Growth Conditions. In: *Frontiers in microbiology* 9 (2018), 2058.

Grunberg-Manago, M. Regulation of the expression of aminoacyl-tRNA synthetases and translation factors. In: *Escherichia coli and Salmonella: cellular and molecular biology*. Ed. by **Neidhardt, F.C.** Washington, D.C: American Society for Microbiology, 1996, 1432–1457.

Grünberger, A. et al. Beyond growth rate 0.6: *Corynebacterium glutamicum* cultivated in highly diluted environments. In: *Biotechnology and Bioengineering* 110.1 (2013), 220–228.

Grünberger, A., W. Wiechert & D. Kohlheyer. Single-cell microfluidics: opportunity for bioprocess development. In: *Current Opinion in Biotechnology* 29 (2014), 15–23.

Gulik, W.M. van. Fast sampling for quantitative microbial metabolomics. In: *Current Opinion in Biotechnology* 21.1 (2010), 27–34.

Haas, T. et al. Identifying the Growth Modulon of *Corynebacterium glutamicum*. In: *Frontiers in Microbiology* 10 (2019), 974.

Han, S.O., M. Inui & H. Yukawa. Effect of carbon source availability and growth phase on expression of *Corynebacterium glutamicum* genes involved in the tricarboxylic acid cycle and glyoxylate bypass. In: *Microbiology (Reading, England)* 154.Pt 10 (2008), 3073–3083.

Hanahan, D. Studies on transformation of *Escherichia coli* with plasmids. In: *Journal of Molecular Biology* 166.4 (1983), 557–580.

Hanke, T. et al. Combined fluxomics and transcriptomics analysis of glucose catabolism via a partially cyclic pentose phosphate pathway in *Gluconobacter oxydans* 621H. In: *Applied and environmental microbiology* 79.7 (2013), 2336–2348.

Hänssler, E. et al. FarR, a putative regulator of amino acid metabolism in *Corynebacterium glutamicum*. In: *Applied microbiology and biotechnology* 76.3 (2007), 625–632.

Hartmann, M., A. Barsch, K. Niehaus, A. Pühler, A. Tauch & J. Kalinowski. The glycosylated cell surface protein Rpf2, containing a resuscitation-promoting factor motif, is involved in intercellular communication of *Corynebacterium glutamicum*. In: *Archives of Microbiology* 182.4 (2004), 299–312.

Heijnen, J.J. Impact of thermodynamic principles in systems biology. In: *Advances in biochemical engineering/biotechnology* 121 (2010), 139–162.

Herbert, D., R. Elsworth & R.C. Telling. The Continuous Culture of Bacteria; a Theoretical and Experimental Study. In: *Journal of General Microbiology* 14.3 (1956), 601–622.

Hermann, T. Industrial production of amino acids by coryneform bacteria. In: *Journal of Biotechnology* 104.1-3 (2003), 155–172.

Hoffart, E. et al. High Substrate Uptake Rates Empower *Vibrio natriegens* as Production Host for Industrial Biotechnology. In: *Applied and environmental microbiology* 83.22 (2017).

Hoskisson, P.A. & G. Hobbs. Continuous culture–making a comeback? In: *Microbiology* 151.Pt 10 (2005), 3153–3159.

Ibarra, R.U., J.S. Edwards & B.O. Palsson. *Escherichia coli* K-12 undergoes adaptive evolution to achieve *in silico* predicted optimal growth. In: *Nature* 420.6912 (2002), 186–189.

Ikeda, M. & S. Nakagawa. The *Corynebacterium glutamicum* genome: features and impacts on biotechnological processes. In: *Applied Microbiology and Biotechnology* 62.2-3 (2003), 99–109.

Ikeda, M. Sugar transport systems in *Corynebacterium glutamicum*: features and applications to strain development. In: *Applied Microbiology and Biotechnology* 96.5 (2012), 1191–1200.

Ikeda, M., Y. Mizuno, S.-i. Awane, M. Hayashi, S. Mitsuhashi & S. Takeno. Identification and application of a different glucose uptake system that functions as an alternative to the phosphotransferase system in *Corynebacterium glutamicum*. In: *Applied Microbiology and Biotechnology* 90.4 (2011), 1443–1451.

Ingraham, J.L., O. Maaløe & F.C. Neidhardt. *Growth of the bacterial cell*. Sinauer Associates, 1983.

Inui, M., H. Kawaguchi, S. Murakami, A.A. Vertès & H. Yukawa. Metabolic Engineering of *Corynebacterium glutamicum* for Fuel Ethanol Production under Oxygen-Deprivation Conditions. In: *Journal of Molecular Microbiology and Biotechnology* 8.4 (2004), 243–254.

Irzik, K., J. van Ooyen, J. Gätgens, K. Krumbach, M. Bott & L. Eggeling. Acyl-CoA sensing by FasR to adjust fatty acid synthesis in *Corynebacterium glutamicum*. In: *Journal of Biotechnology* 192 Pt A (2014), 96–101.

Ishii, N. et al. Multiple high-throughput analyses monitor the response of *E. coli* to perturbations. In: *Science (New York, N.Y.)* 316.5824 (2007), 593–597.

Janausch, I., E. Zientz, Q. Tran, A. Kröger & G. Unden. C_4-dicarboxylate carriers and sensors in bacteria. In: *Biochimica et Biophysica Acta (BBA) - Bioenergetics* 1553.1-2 (2002), 39–56.

Jensen, J.V.K. & V.F. Wendisch. Ornithine cyclodeaminase-based proline production by *Corynebacterium glutamicum*. In: *Microbial cell factories* 12.1 (2013), 63.

Johnstone, T.C. & E.M. Nolan. Beyond iron: non-classical biological functions of bacterial siderophores. In: *Dalton transactions (Cambridge, England : 2003)* 44.14 (2015), 6320–6339.

Jungwirth, B. et al. Triple transcriptional control of the resuscitation promoting factor 2 (*rpf2*) gene of *Corynebacterium glutamicum* by the regulators of acetate metabolism RamA and RamB and the cAMP-dependent regulator GlxR. In: *FEMS Microbiology Letters* 281.2 (2008), 190–197.

Kabus, A., T. Georgi, V.F. Wendisch & M. Bott. Expression of the *Escherichia coli pntAB* genes encoding a membrane-bound transhydrogenase in *Corynebacterium glutamicum* improves L-lysine formation. In: *Applied microbiology and biotechnology* 75.1 (2007), 47–53.

Kaleta, C., S. Schäuble, U. Rinas & S. Schuster. Metabolic costs of amino acid and protein production in *Escherichia coli*. In: *Biotechnology journal* 8.9 (2013), 1105–1114.

Kalinowski, J., J. Cremer., B. Bachmann, L. Eggeling, H. Sahm & A. Pühler. Genetic and biochemical analysis of the aspartokinase from *Corynebacterium glutamicum*. In: *Molecular Microbiology* 5.5 (1991), 1197–1204.

Kalinowski, J., D. Wolters & A. Poetsch. Proteomics of *Corynebacterium glutamicum* and Other *Corynebacteria*. In: *Corynebacteria*. Ed. by **Burkovski, A.** Wymondham: Caister Academic, 2008, 55–78.

Kalinowski, J. et al. The complete *Corynebacterium glutamicum* ATCC 13032 genome sequence and its impact on the production of L-aspartate-derived amino acids and vitamins. In: *Journal of Biotechnology* 104.1-3 (2003), 5–25.

Kalinowski, J., B. Bachmann, G. Thierbach & A. Phler. Aspartokinase genes *lysC*-alpha and *lysC*-beta overlap and are adjacent to the aspartate beta-semialdehyde dehydrogenase gene *asd* in *Corynebacterium glutamicum*. In: *MGG Molecular & General Genetics* 224.3 (1990).

Kappelmann, J., W. Wiechert & S. Noack. Cutting the Gordian Knot: Identifiability of anaplerotic reactions in *Corynebacterium glutamicum* by means of ^{13}C-metabolic flux analysis. In: *Biotechnology and Bioengineering* 113.3 (2015), 661–674.

Käß, F. et al. Assessment of robustness against dissolved oxygen/substrate oscillations for *C. glutamicum* DM1933 in two-compartment bioreactor. In: *Bioprocess and biosystems engineering* 37.6 (2014), 1151–1162.

Käß, F., S. Junne, P. Neubauer, W. Wiechert & M. Oldiges. Process inhomogeneity leads to rapid side product turnover in cultivation of *Corynebacterium glutamicum*. In: *Microbial cell factories* 13 (2014), 6.

Keener, J. & M. Nomura. Regulation of ribosome synthesis. In: *Escherichia coli and Salmonella: cellular and molecular biology*. Ed. by **Neidhardt, F.C.** Washington, D.C: American Society for Microbiology, 1996, 1417–1431.

Keilhauer, C., L. Eggeling & H. Sahm. Isoleucine synthesis in *Corynebacterium glutamicum*: molecular analysis of the *ilvB-ilvN-ilvC* operon. In: *Journal of bacteriology* 175.17 (1993), 5595–5603.

Kimura, K. The effect of biotin on the amino acid biosynthesis by *Micrococcus glutamicus*. In: *The Journal of General and Applied Microbiology* 9.2 (1963), 205–212.

Kind, S., W.K. Jeong, H. Schröder, O. Zelder & C. Wittmann. Identification and elimination of the competing N-acetyldiaminopentane pathway for improved production of diaminopentane by *Corynebacterium glutamicum*. In: *Applied and environmental microbiology* 76.15 (2010), 5175–5180.

Kinoshita, S. A Short History of the Birth of the Amino Acid Industry in Japan. In: *Handbook of Corynebacterium glutamicum*. Ed. by **Eggeling, L. & Bott, M.** Boca Raton: Taylor & Francis, 2005, 3–5.

Kinoshita, S., S. Udaka & M. Shimono. Studies on the Amino Acid Fermentation. In: *The Journal of General and Applied Microbiology* 3.3 (1957), 193–205.

Kirchner, O. & A. Tauch. Tools for genetic engineering in the amino acid-producing bacterium *Corynebacterium glutamicum*. In: *Journal of Biotechnology* 104.1-3 (2003), 287–299.

Kitano, H. Systems biology: a brief overview. In: *Science (New York, N.Y.)* 295.5560 (2002), 1662–1664.

Kjeldsen, K.R. & J. Nielsen. *In silico* genome-scale reconstruction and validation of the *Corynebacterium glutamicum* metabolic network. In: *Biotechnology and Bioengineering* 102.2 (2009), 583–597.

Klein-Marcuschamer, D., C.N.S. Santos, H. Yu & G. Stephanopoulos. Mutagenesis of the bacterial RNA polymerase alpha subunit for improvement of complex phenotypes. In: *Applied and environmental microbiology* 75.9 (2009), 2705–2711.

Klein, S. & E. Heinzle. Isotope labeling experiments in metabolomics and fluxomics. In: *Wiley interdisciplinary reviews. Systems biology and medicine* 4.3 (2012), 261–272.

Knöppel, A. et al. Genetic Adaptation to Growth Under Laboratory Conditions in *Escherichia coli* and *Salmonella enterica*. In: *Frontiers in microbiology* 9 (2018), 756.

Koch-Koerfges, A., N. Pfelzer, L. Platzen, M. Oldiges & M. Bott. Conversion of *Corynebacterium glutamicum* from an aerobic respiring to an aerobic fermenting bacterium by inactivation of the respiratory chain. In: *Biochimica et biophysica acta* 1827.6 (2013), 699–708.

Koch-Koerfges, A., A. Kabus, I. Ochrombel, K. Marin & M. Bott. Physiology and global gene expression of a *Corynebacterium glutamicum* DeltaF_1F_0-ATP synthase mutant devoid of oxidative phosphorylation. In: *Biochimica et biophysica acta* 1817.2 (2012), 370–380.

Koch, D.J., C. Rückert, D.A. Rey, A. Mix, A. Pühler & J. Kalinowski. Role of the *ssu* and *seu* genes of *Corynebacterium glutamicum* ATCC 13032 in utilization of sulfonates and sulfonate esters as sulfur sources. In: *Applied and environmental microbiology* 71.10 (2005), 6104–6114.

Kohl, T.A. & A. Tauch. The GlxR regulon of the amino acid producer *Corynebacterium glutamicum*: Detection of the corynebacterial core regulon and integration into the transcriptional regulatory network model. In: *Journal of Biotechnology* 143.4 (2009), 239–246.

Kohl, T.A., J. Baumbach, B. Jungwirth, A. Pühler & A. Tauch. The GlxR regulon of the amino acid producer *Corynebacterium glutamicum*: *in silico* and *in vitro* detection of DNA binding sites of a global transcription regulator. In: *Journal of Biotechnology* 135.4 (2008), 340–350.

Koning, W. de & K. van Dam. A method for the determination of changes of glycolytic metabolites in yeast on a subsecond time scale using extraction at neutral pH. In: *Analytical biochemistry* 204.1 (1992), 118–123.

Krämer, R. & C. Lambert. Uptake of glutamate in *Corynebacterium glutamicum*. 2. Evidence for a primary active transport system. In: *European Journal of Biochemistry* 194.3 (1990), 937–944.

Krämer, R., C. Lambert, C. Hoischen & H. Ebbighausen. Uptake of glutamate in *Corynebacterium glutamicum*. 1. Kinetic properties and regulation by internal pH and potassium. In: *European Journal of Biochemistry* 194.3 (1990), 929–935.

Krause, F.S., A. Henrich, B. Blombach, R. Krämer, B.J. Eikmanns & G.M. Seibold. Increased glucose utilization in *Corynebacterium glutamicum* by use of maltose, and its application for the improvement of L-valine productivity. In: *Applied and environmental microbiology* 76.1 (2010), 370–374.

Krings, E. et al. Characterization of myo-inositol utilization by *Corynebacterium glutamicum*: the stimulon, identification of transporters, and influence on L-lysine formation. In: *Journal of bacteriology* 188.23 (2006), 8054–8061.

Krömer, J.O., C. Wittmann, H. Schröder & E. Heinzle. Metabolic pathway analysis for rational design of L-methionine production by *Escherichia coli* and *Corynebacterium glutamicum*. In: *Metabolic engineering* 8.4 (2006), 353–369.

Kronemeyer, W., N. Peekhaus, R. Krämer, H. Sahm & L. Eggeling. Structure of the *gluABCD* cluster encoding the glutamate uptake system of *Corynebacterium glutamicum*. In: *Journal of bacteriology* 177.5 (1995), 1152–1158.

Kulis-Horn, R.K., M. Persicke & J. Kalinowski. Histidine biosynthesis, its regulation and biotechnological application in *Corynebacterium glutamicum*. In: *Microbial biotechnology* 7.1 (2014), 5–25.

Kwon, J.H. et al. Cloning of the histidine biosynthetic genes from *Corynebacterium glutamicum*: organization and analysis of the *hisG* and *hisE* genes. In: *Canadian journal of microbiology* 46.9 (2000), 848–855.

LaCroix, R.A. et al. Use of adaptive laboratory evolution to discover key mutations enabling rapid growth of *Escherichia coli* K-12 MG1655 on glucose minimal medium. In: *Applied and environmental microbiology* 81.1 (2015), 17–30.

Lange, C., D. Rittmann, V.F. Wendisch, M. Bott & H. Sahm. Global Expression Profiling and Physiological Characterization of *Corynebacterium glutamicum* Grown in the Presence of L-Valine. In: *Applied and environmental microbiology* 69.5 (2003), 2521–2532.

Lange, J. et al. Deciphering the Adaptation of *Corynebacterium glutamicum* in Transition from Aerobiosis via Microaerobiosis to Anaerobiosis. In: *Genes* 9.6 (2018).

Lange, J., F. Müller, K. Bernecker, N. Dahmen, R. Takors & B. Blombach. Valorization of pyrolysis water: a biorefinery side stream, for 1,2-propanediol production with engineered *Corynebacterium glutamicum*. In: *Biotechnology for biofuels* 10 (2017), 277.

Larsson, G., S.-O. Enfors & H. Pham. The pH-auxostat as a tool for studying microbial dynamics in continuous fermentation. In: *Biotechnology and Bioengineering* 36.3 (1990), 224–232.

Lee, H.-W., J.-G. Pan & J.-M. Lebeault. Enhanced L-lysine production in threonine-limited continuous culture of *Corynebacterium glutamicum* by using gluconate as a secondary carbon source with glucose. In: *Applied microbiology and biotechnology* 49.1 (1998), 9–15.

Lee, J.M., S. Zhang, S. Saha, S. Santa Anna, C. Jiang & J. Perkins. RNA expression analysis using an antisense *Bacillus subtilis* genome array. In: *Journal of bacteriology* 183.24 (2001), 7371–7380.

Lehmann, K.B. & R. Neumann. *Atlas und Grundriss der Bakteriologie und Lehrbuch der speziellen bakteriologischen Diagnostik*. München: J. F. Lehmann, 1896.

Lenski, R.E., M.R. Rose, S.C. Simpson & S.C. Tadler. Long-Term Experimental Evolution in *Escherichia coli*. I. Adaptation and Divergence During 2,000 Generations. In: *The American Naturalist* 138.6 (1991), 1315–1341.

Leuchtenberger, W., K. Huthmacher & K. Drauz. Biotechnological production of amino acids and derivatives: current status and prospects. In: *Applied Microbiology and Biotechnology* 69.1 (2005), 1–8.

Li, Z., Y.-P. Shen, X.-L. Jiang, L.-S. Feng & J.-Z. Liu. Metabolic evolution and a comparative omics analysis of *Corynebacterium glutamicum* for putrescine production. In: *Journal of industrial microbiology & biotechnology* 45.2 (2018), 123–139.

Liebl, W. Corynebacterium-Nonmedical. In: *The prokaryotes*. Ed. by **Dworkin, M. & Falkow, S.** New York: Springer, 2006, 796–818.

Liebl, W., R. Klamer & K.-H. Schleifer. Requirement of chelating compounds for the growth of *Corynebacterium glutamicum* in synthetic media. In: *Applied Microbiology and Biotechnology* 32.2 (1989), 205–210.

Lindner, S.N., G.M. Seibold, A. Henrich, R. Kramer & V.F. Wendisch. Phosphotransferase System-Independent Glucose Utilization in *Corynebacterium glutamicum* by Inositol Permeases and Glucokinases. In: *Applied and environmental microbiology* 77.11 (2011), 3571–3581.

Ling, M., S.W. Allen & J.M. Wood. Sequence analysis identifies the proline dehydrogenase and delta 1-pyrroline-5-carboxylate dehydrogenase domains of the multifunctional *Escherichia coli* PutA protein. In: *Journal of Molecular Biology* 243.5 (1994), 950–956.

Liu, Y.-J. et al. *Corynebacterium glutamicum* contains 3-deoxy-D-arabino-heptulosonate 7-phosphate synthases that display novel biochemical features. In: *Applied and environmental microbiology* 74.17 (2008), 5497–5503.

Love, M.I., W. Huber & S. Anders. Moderated estimation of fold change and dispersion for RNA-seq data with DESeq2. In: *Genome biology* 15.12 (2014), 550.

Mahr, R., C. Gätgens, J. Gätgens, T. Polen, J. Kalinowski & J. Frunzke. Biosensor-driven adaptive laboratory evolution of L-valine production in *Corynebacterium glutamicum*. In: *Metabolic engineering* 32 (2015), 184–194.

Malin, G.M. & G.I. Bourd. Phosphotransferase-dependent glucose transport in *Corynebacterium glutamicum*. In: *Journal of Applied Bacteriology* 71.6 (1991), 517–523.

Marienhagen, J. & L. Eggeling. Metabolic function of *Corynebacterium glutamicum* aminotransferases AlaT and AvtA and impact on L-valine production. In: *Applied and environmental microbiology* 74.24 (2008), 7457–7462.

Marin, K. & R. Krämer. Amino Acid Transport Systems in Biotechnologically Relevant Bacteria. In: *Amino Acid Biosynthesis - Pathways, Regulation and Metabolic Engineering*. Ed. by **Wendisch, V.F.** Vol. 5. Berlin, Heidelberg: Springer Berlin Heidelberg, 2007, 289–325.

Martin, G. & W. Hempfling. A method for the regulation of microbial population density during continuous culture at high growth rates. In: *Archives of Microbiology* 107.1 (1976), 41–47.

Marx, A., de Graaf, Albert A., W. Wiechert, L. Eggeling & H. Sahm. Determination of the fluxes in the central metabolism of *Corynebacterium glutamicum* by nuclear magnetic resonance spectroscopy combined with metabolite balancing. In: *Biotechnology and Bioengineering* 49.2 (1996), 111–129.

Matsushita, K., A. Otofuji, M. Iwahashi, H. Toyama & O. Adachi. NADH dehydrogenase of *Corynebacterium glutamicum*. Purification of an NADH dehydrogenase II homolog able to oxidize NADPH. In: *FEMS Microbiology Letters* 204.2 (2001), 271–276.

McCloskey, D. et al. Adaptation to the coupling of glycolysis to toxic methylglyoxal production in *tpiA* deletion strains of *Escherichia coli* requires synchronized and counterintuitive genetic changes. In: *Metabolic engineering* 48 (2018), 82–93.

Mentz, A., A. Neshat, K. Pfeifer-Sancar, A. Pühler, C. Rückert & J. Kalinowski. Comprehensive discovery and characterization of small RNAs in *Corynebacterium glutamicum* ATCC 13032. In: *BMC genomics* 14 (2013), 714.

Merkens, H., G. Beckers, A. Wirtz & A. Burkovski. Vanillate metabolism in *Corynebacterium glutamicum*. In: *Current microbiology* 51.1 (2005), 59–65.

Mesas, J.M., J.A. Gil & J.F. Martín. Characterization and partial purification of L-asparaginase from *Corynebacterium glutamicum*. In: *Journal of General Microbiology* 136.3 (1990), 515–519.

Michel, A., A. Koch-Koerfges, K. Krumbach, M. Brocker & M. Bott. Anaerobic Growth of *Corynebacterium glutamicum* via Mixed-Acid Fermentation. In: *Applied and environmental microbiology* 81.21 (2015), 7496–7508.

Miebach, S. *Charakterisierung und Validierung der ^{13}C-Stoffflussanalyse im Parallelansatz*. Dissertation. Bielefeld: Universität Bielefeld, 2011.

Milse, J., K. Petri, C. Rückert & J. Kalinowski. Transcriptional response of *Corynebacterium glutamicum* ATCC 13032 to hydrogen peroxide stress and characterization of the OxyR regulon. In: *Journal of Biotechnology* 190 (2014), 40–54.

Mohamed, E.T. et al. Generation of a platform strain for ionic liquid tolerance using adaptive laboratory evolution. In: *Microbial cell factories* 16.1 (2017), 204.

Monod, J. La technique de culture continue: Théorie et applications. In: *Ann. Inst. Pasteur* 79 (1950), 390–410.

— The growth of bacterial cultures. In: *Annual Reviews in Microbiology* 3.1 (1949), 371–394.

Mori, M. & I. Shiio. Phosphoenolpyruvate: Sugar Phosphotransferase Systems and Sugar Metabolism in *Brevibacterium flavum*. In: *Agricultural and Biological Chemistry* 51.10 (1987), 2671–2678.

Moritz, B., K. Striegel, A.A. de Graaf & H. Sahm. Kinetic properties of the glucose-6-phosphate and 6 phosphogluconate dehydrogenases from *Corynebacterium glutamicum* and their application for predicting pentose phosphate pathway flux *in vivo*. In: *European Journal of Biochemistry* 267.12 (2000), 3442–3452.

Moser, J.W. et al. Implications of evolutionary engineering for growth and recombinant protein production in methanol-based growth media in the yeast *Pichia pastoris*. In: *Microbial cell factories* 16.1 (2017), 49.

Netzer, R., P. Peters-Wendisch, L. Eggeling & H. Sahm. Cometabolism of a nongrowth substrate: L-serine utilization by *Corynebacterium glutamicum*. In: *Applied and environmental microbiology* 70.12 (2004), 7148–7155.

Nguyen, A.Q.D., J. Schneider & V.F. Wendisch. Elimination of polyamine N-acetylation and regulatory engineering improved putrescine production by *Corynebacterium glutamicum*. In: *Journal of Biotechnology* 201 (2015), 75–85.

Niedenführ, S., W. Wiechert & K. Nöh. How to measure metabolic fluxes: a taxonomic guide for ^{13}C fluxomics. In: *Systems Biology Nanobiotechnology* 34.0 (2015), 82–90.

Nieß, A., J. Failmezger, M. Kuschel, M. Siemann-Herzberg & R. Takors. Experimentally Validated Model Enables Debottlenecking of in Vitro Protein Synthesis and Identifies a Control Shift under *in Vivo* Conditions. In: *ACS synthetic biology* 6.10 (2017), 1913–1921.

Nikel, P.I., M. Chavarría, T. Fuhrer, U. Sauer & V. de Lorenzo. *Pseudomonas putida* KT2440 Strain Metabolizes Glucose through a Cycle Formed by Enzymes of the Entner-Doudoroff, Embden-Meyerhof-Parnas, and Pentose Phosphate Pathways. In: *The Journal of biological chemistry* 290.43 (2015), 25920–25932.

Nishimura, T., A.A. Vertès, Y. Shinoda, M. Inui & H. Yukawa. Anaerobic growth of *Corynebacterium glutamicum* using nitrate as a terminal electron acceptor. In: *Applied Microbiology and Biotechnology* 75.4 (2007), 889–897.

Nishimura, T., H. Teramoto, A.A. Vertès, M. Inui & H. Yukawa. ArnR, a novel transcriptional regulator, represses expression of the *narKGHJI* operon in *Corynebacterium glutamicum*. In: *Journal of Bacteriology* 190.9 (2008), 3264–3273.

Noack, S., R. Voges, J. Gätgens & W. Wiechert. The linkage between nutrient supply, intracellular enzyme abundances and bacterial growth: New evidences from the central carbon metabolism of *Corynebacterium glutamicum*. In: *Journal of Biotechnology* (2017).

Nöh, K. & W. Wiechert. Experimental design principles for isotopically instationary ^{13}C labeling experiments. In: *Biotechnology and Bioengineering* 94.2 (2006), 234–251.

Novick, A. & L. Szilard. Description of the Chemostat. In: *Science* 112.2920 (1950), 715–716.

Nueda, M.J., S. Tarazona & A. Conesa. Next maSigPro: updating maSigPro bioconductor package for RNA-seq time series. In: *Bioinformatics (Oxford, England)* 30.18 (2014), 2598–2602.

Oide, S. et al. Thermal and solvent stress cross-tolerance conferred to *Corynebacterium glutamicum* by adaptive laboratory evolution. In: *Applied and environmental microbiology* 81.7 (2015), 2284–2298.

Oikawa, T. Alanine, Aspartate, and Asparagine Metabolism in Microorganisms. In: *Amino Acid Biosynthesis - Pathways, Regulation and Metabolic Engineering*. Ed. by **Wendisch, V.F.** Vol. 5. Berlin, Heidelberg: Springer Berlin Heidelberg, 2007, 273–288.

Okamura-Ikeda, K., Y. Ohmura, K. Fujiwara & Y. Motokawa. Cloning and nucleotide sequence of the *gcv* operon encoding the *Escherichia coli* glycine-cleavage system. In: *European Journal of Biochemistry* 216.2 (1993), 539–548.

Okino, S., M. Inui & H. Yukawa. Production of organic acids by *Corynebacterium glutamicum* under oxygen deprivation. In: *Applied Microbiology and Biotechnology* 68.4 (2005), 475–480.

Oldiges, M., S. Lütz, S. Pflug, K. Schroer, N. Stein & C. Wiendahl. Metabolomics: current state and evolving methodologies and tools. In: *Applied Microbiology and Biotechnology* 76.3 (2007), 495–511.

Paczia, N., A. Nilgen, T. Lehmann, J. Gätgens, W. Wiechert & S. Noack. Extensive exometabolome analysis reveals extended overflow metabolism in various microorganisms. In: *Microbial cell factories* 11 (2012), 122.

Palmieri, L., D. Berns, R. Krämer & M. Eikmanns. Threonine diffusion and threonine transport in *Corynebacterium glutamicum* and their role in threonine production. In: *Archives of Microbiology* 165.1 (1996), 48–54.

Parche, S., A. Burkovski, G.A. Sprenger, B. Weil, R. Krämer & F. Titgemeyer. *Corynebacterium glutamicum*: a dissection of the PTS. In: *Journal of molecular microbiology and biotechnology* 3.3 (2001), 423–428.

Park, S.-D., J.-W. Youn, Y.-J. Kim, S.-M. Lee, Y. Kim & H.-S. Lee. *Corynebacterium glutamicum* SigmaE is involved in responses to cell surface stresses and its activity is controlled by the anti-sigma factor CseE. In: *Microbiology* 154.3 (2008), 915–923.

Pátek, M. Branched-Chain Amino Acids. In: *Amino Acid Biosynthesis - Pathways, Regulation and Metabolic Engineering*. Ed. by **Wendisch, V.F.** Vol. 5. Berlin, Heidelberg: Springer Berlin Heidelberg, 2007, 129–162.

Patti, G.J., O. Yanes & G. Siuzdak. Metabolomics: the apogee of the omics trilogy. In: *Nature Reviews Molecular Cell Biology* 13 (2012), 263 EP.

Pauling, J., R. Röttger, A. Tauch, V. Azevedo & J. Baumbach. CoryneRegNet 6.0–Updated database content, new analysis methods and novel features focusing on community demands. In: *Nucleic acids research* 40.Database issue (2012), D610–4.

Persicke, M., J. Plassmeier, H. Neuweger, C. Rückert, A. Pühler & J. Kalinowski. Size exclusion chromatography: an improved method to harvest *Corynebacterium glutamicum* cells for the analysis of cytosolic metabolites. In: *Journal of Biotechnology* 154.2-3 (2011), 171–178.

Peter, H., A. Bader, A. Burkovski, C. Lambert & R. Krämer. Isolation of the *putP* gene of *Corynebacterium glutamicum* and characterization of a low-affinity uptake system for compatible solutes. In: *Archives of Microbiology* 168.2 (1997), 143–151.

Peters-Wendisch, P., R. Netzer, L. Eggeling & H. Sahm. 3-Phosphoglycerate dehydrogenase from *Corynebacterium glutamicum*: the C-terminal domain is not essential for activity but is required for inhibition by L-serine. In: *Applied microbiology and biotechnology* 60.4 (2002), 437–441.

Peters-Wendisch, P., M. Stolz, H. Etterich, N. Kennerknecht, H. Sahm & L. Eggeling. Metabolic engineering of *Corynebacterium glutamicum* for L-serine production. In: *Applied and environmental microbiology* 71.11 (2005), 7139–7144.

Petersen, S., de Graaf, A A, L. Eggeling, M. Möllney, W. Wiechert & H. Sahm. *In vivo* quantification of parallel and bidirectional fluxes in the anaplerosis of *Corynebacterium glutamicum*. In: *The Journal of biological chemistry* 275.46 (2000), 35932–35941.

Pfeifer-Sancar, K., A. Mentz, C. Rückert & J. Kalinowski. Comprehensive analysis of the *Corynebacterium glutamicum* transcriptome using an improved RNAseq technique. In: *BMC genomics* 14 (2013), 888.

Pfeifer, E., C. Gätgens, T. Polen & J. Frunzke. Adaptive laboratory evolution of *Corynebacterium glutamicum* towards higher growth rates on glucose minimal medium. In: *Scientific Reports* 7.1 (2017), 1243.

Pfelzer, N. *Experimentelle Bestimmung zellulärer Energiezustände und Analyse des Glykogenstoffwechsels in Corynebacterium glutamicum*. Dissertation. Aachen: RWTH, 2016.

Pir, P. et al. The genetic control of growth rate: a systems biology study in yeast. In: *BMC systems biology* 6 (2012), 4.

Pirt, S.J. Maintenance energy: a general model for energy-limited and energy-sufficient growth. In: *Archives of Microbiology* 133.4 (1982), 300–302.

Pirt, S.J. & D.S. Callow. Studies of the growth of *Penicillium chrysogenum* in continuous flow culture with reference to penicillin production. In: *Journal of Applied Bacteriology* 23.1 (1960), 87–98.

Plassmeier, J., A. Barsch, M. Persicke, K. Niehaus & J. Kalinowski. Investigation of central carbon metabolism and the 2-methylcitrate cycle in *Corynebacterium glutamicum* by metabolic profiling using gas chromatography-mass spectrometry. In: *Journal of Biotechnology* 130.4 (2007), 354–363.

Potrykus, K., H. Murphy, N. Philippe & M. Cashel. ppGpp is the major source of growth rate control in *E. coli*. In: *Environmental Microbiology* 13.3 (2011), 563–575.

Qin, T., X. Hu, J. Hu & X. Wang. Metabolic engineering of *Corynebacterium glutamicum* strain ATCC13032 to produce L-methionine. In: *Biotechnology and applied biochemistry* 62.4 (2015), 563–573.

Radek, A. et al. Miniaturized and automated adaptive laboratory evolution: Evolving *Corynebacterium glutamicum* towards an improved D-xylose utilization. In: *Bioresource technology* 245.Pt B (2017), 1377–1385.

Rehm, N. & A. Burkovski. Engineering of nitrogen metabolism and its regulation in *Corynebacterium glutamicum*: influence on amino acid pools and production. In: *Applied Microbiology and Biotechnology* 89.2 (2011), 239–248.

Rehm, N. et al. L-Glutamine as a nitrogen source for *Corynebacterium glutamicum*: derepression of the AmtR regulon and implications for nitrogen sensing. In: *Microbiology* 156.10 (2010), 3180–3193.

Rodionov, D.A. et al. Transcriptional regulation of NAD metabolism in bacteria: NrtR family of Nudix-related regulators. In: *Nucleic acids research* 36.6 (2008), 2047–2059.

Rolfe, M.D. et al. Lag phase is a distinct growth phase that prepares bacteria for exponential growth and involves transient metal accumulation. In: *Journal of bacteriology* 194.3 (2012), 686–701.

Rollin, C., V. Morgant, A. Guyonvarch & J.-L. Guerquin-Kern. *13*C-NMR Studies of *Corynebacterium melassecola* Metabolic Pathways. In: *European Journal of Biochemistry* 227.1-2 (1995), 488–493.

Rönsch, H., R. Krämer & S. Morbach. Impact of osmotic stress on volume regulation, cytoplasmic solute composition and lysine production in *Corynebacterium glutamicum* MH20-22B. In: *Journal of Biotechnology* 104.1-3 (2003), 87–97.

Rückert, C. & J. Kalinowski. Sulfur Metabolism in *Corynebacterium glutamicum*. In: *Corynebacteria*. Ed. by **Burkovski, A.** Wymondham: Caister Academic, 2008.

Rückert, C. et al. Functional genomics and expression analysis of the Corynebacterium *glutamicum fpr2-cysIXHDNYZ* gene cluster involved in assimilatory sulphate reduction. In: *BMC genomics* 6 (2005), 121.

Rückert, C., J. Milse, A. Albersmeier, D.J. Koch, A. Pühler & J. Kalinowski. The dual transcriptional regulator CysR in *Corynebacterium glutamicum* ATCC 13032 controls a subset of genes of the McbR regulon in response to the availability of sulphide acceptor molecules. In: *BMC genomics* 9 (2008), 483.

Rugbjerg, P., A.M. Feist & M.O.A. Sommer. Enhanced Metabolite Productivity of *Escherichia coli* Adapted to Glucose M9 Minimal Medium. In: *Frontiers in bioengineering and biotechnology* 6 (2018), 166.

Ryall, B., G. Eydallin & T. Ferenci. Culture history and population heterogeneity as determinants of bacterial adaptation: the adaptomics of a single environmental transition. In: *Microbiology and molecular biology reviews : MMBR* 76.3 (2012), 597–625.

Sakanyan, V. et al. Genes and enzymes of the acetyl cycle of arginine biosynthesis in *Corynebacterium glutamicum*: enzyme evolution in the early steps of the arginine pathway. In: *Microbiology* 142.1 (1996), 99–108.

Sambrook, J. & D.W. Russell. *Molecular cloning: a laboratory manual. 2001*. 2001.

San, K.-Y., G.N. Bennett, A.A. Aristidou & C.-H. Chou. Strategies in High-Level Expression of Recombinant Protein in *Escherichia coli*. In: *Annals of the New York Academy of Sciences* 721.1 Recombinant D (1994), 257–267.

Sandberg, T.E., C.P. Long, J.E. Gonzalez, A.M. Feist, M.R. Antoniewicz & B.O. Palsson. Evolution of *E. coli* on U-13C Glucose Reveals a Negligible Isotopic Influence on Metabolism and Physiology. In: *PLoS ONE* 11.3 (2016), e0151130.

Sauer, U. Metabolic networks in motion: ^{13}C-based flux analysis. In: *Molecular systems biology* 2 (2006), 62.

Sauer, U., F. Canonaco, S. Heri, A. Perrenoud & E. Fischer. The soluble and membrane-bound transhydrogenases UdhA and PntAB have divergent functions in NADPH metabolism of *Escherichia coli*. In: *The Journal of biological chemistry* 279.8 (2004), 6613–6619.

Schäfer, A., A. Tauch, W. Jäger, J. Kalinowski, G. Thierbach & A. Pühler. Small mobilizable multi-purpose cloning vectors derived from the *Escherichia coli* plasmids pK18 and pK19: selection of defined deletions in the chromosome of *Corynebacterium glutamicum*. In: *Gene* 145 (1994), 69–73.

Schatschneider, S. et al. Metabolic flux pattern of glucose utilization by *Xanthomonas campestris* pv. campestris: prevalent role of the Entner-Doudoroff pathway and minor fluxes through the pentose phosphate pathway and glycolysis. In: *Molecular bioSystems* 10.10 (2014), 2663–2676.

Scheele, S. et al. Secretory production of an FAD cofactor-containing cytosolic enzyme (sorbitol-xylitol oxidase from *Streptomyces coelicolor*) using the twin-arginine translocation (Tat) pathway of *Corynebacterium glutamicum*. In: *Microbial biotechnology* 6.2 (2013), 202–206.

Schelder, S., D. Zaade, B. Litsanov, M. Bott & M. Brocker. The two-component signal transduction system CopRS of *Corynebacterium glutamicum* is required for adaptation to copper-excess stress. In: *PLoS ONE* 6.7 (2011), e22143.

Schröder, J. & A. Tauch. The Transcriptional Regulatory Network of *Corynebacterium glutamicum*. In: *Corynebacterium glutamicum*. Ed. by **Yukawa, H. & Inui, M.** Berlin, Heidelberg: Springer Berlin Heidelberg, 2013.

— Transcriptional regulation of gene expression in *Corynebacterium glutamicum*: the role of global, master and local regulators in the modular and hierarchical gene regulatory network. In: *FEMS Microbiology Reviews* 34.5 (2010), 685–737.

Schwinde, J.W., P.F. Hertz, H. Sahm, B.J. Eikmanns & A. Guyonvarch. Lipoamide dehydrogenase from *Corynebacterium glutamicum*: molecular and physiological analysis of the *lpd* gene and characterization of the enzyme. In: *Microbiology* 147.8 (2001), 2223–2231.

Seep-Feldhaus, A.H., J. Kalinowski & A. Pühler. Molecular analysis of the *Corynebacterium glutamicum* gene involved in lysine uptake. In: *Molecular microbiology* 5.12 (1991), 2995–3005.

Shang, X. et al. Characterization and molecular mechanism of AroP as an aromatic amino acid and histidine transporter in *Corynebacterium glutamicum*. In: *Journal of bacteriology* 195.23 (2013), 5334–5342.

Shen, X.-H., N.-Y. Zhou & S.-J. Liu. Degradation and assimilation of aromatic compounds by *Corynebacterium glutamicum*: another potential for applications for this bacterium? In: *Applied Microbiology and Biotechnology* 95.1 (2012), 77–89.

Shimizu, H. & T. Hirasawa. Production of Glutamate and Glutamate-Related Amino Acids: Molecular Mechanism Analysis and Metabolic Engineering. In: *Amino Acid Biosynthesis - Pathways, Regulation and Metabolic Engineering*. Ed. by **Wendisch, V.F.** Berlin, Heidelberg: Springer Berlin Heidelberg, 2007, 1–38.

Shinfuku, Y., N. Sorpitiporn, M. Sono, C. Furusawa, T. Hirasawa & H. Shimizu. Development and experimental verification of a genome-scale metabolic model for *Corynebacterium glutamicum*. In: *Microb Cell Fact* 8.1 (2009), 43.

Shirai, T., K. Fujimura, C. Furusawa, K. Nagahisa, S. Shioya & H. Shimizu. Study on roles of anaplerotic pathways in glutamate overproduction of *Corynebacterium glutamicum* by metabolic flux analysis. In: *Microbial cell factories* 6 (2007), 19.

Siewe, R.M., B. Weil & R. Krämer. Glutamine uptake by a sodium-dependent secondary transport system in *Corynebacterium glutamicum*. In: *Archives of Microbiology* 164.2 (1995), 98–103.

Silberbach, M. et al. Adaptation of *Corynebacterium glutamicum* to ammonium limitation: a global analysis using transcriptome and proteome techniques. In: *Applied and environmental microbiology* 71.5 (2005), 2391–2402.

Simic, P., J. Willuhn, H. Sahm & L. Eggeling. Identification of *glyA* (Encoding Serine Hydroxymethyltransferase) and Its Use Together with the Exporter ThrE To Increase L-Threonine Accumulation by *Corynebacterium glutamicum*. In: *Applied and environmental microbiology* 68.7 (2002), 3321–3327.

Simic, P., H. Sahm & L. Eggeling. L-Threonine Export: Use of Peptides To Identify a New Translocator from *Corynebacterium glutamicum*. In: *Journal of bacteriology* 183.18 (2001), 5317–5324.

Sinumvayo, J.P., C. Zhao & P. Tuyishime. Recent advances and future trends of riboswitches: attractive regulatory tools. In: *World journal of microbiology & biotechnology* 34.11 (2018), 171.

Sonntag, K., L. Eggeling, A.A. de Graaf & H. Sahm. Flux partitioning in the split pathway of lysine synthesis in *Corynebacterium glutamicum*. Quantification by ^{13}C- and 1H-NMR spectroscopy. In: *European journal of biochemistry / FEBS* 213.3 (1993), 1325–1331.

Sonntag, K. et al. ^{13}C NMR studies of the fluxes in the central metabolism of *Corynebacterium glutamicum* during growth and overproduction of amino acids in batch cultures. In: *Applied microbiology and biotechnology* 44.3-4 (1995), 489–495.

Sprenger, G.A. Aromatic Amino Acids. In: *Amino Acid Biosynthesis - Pathways, Regulation and Metabolic Engineering*. Ed. by **Wendisch, V.F.** Vol. 5. Berlin, Heidelberg: Springer Berlin Heidelberg, 2007, 93–127.

Spura, J., L.C. Reimer, P. Wieloch, K. Schreiber, S. Buchinger & D. Schomburg. A method for enzyme quenching in microbial metabolome analysis successfully applied to gram-positive and gram-negative bacteria and yeast. In: *Analytical biochemistry* 394.2 (2009), 192–201.

Stella, R.G., J. Wiechert, S. Noack & J. Frunzke. Evolutionary engineering of *Corynebacterium glutamicum*. In: *Biotechnology journal* (2019), e1800444.

Stephanopoulos, G., A.A. Aristidou & J. Nielsen. *Metabolic engineering: principles and methodologies*. Elsevier, 1998.

Sugimoto, S.-i. & I. Shiio. Fructose Metabolism and Regulation of 1-Phosphofructokinase and 6-Phosphofructokinase in *Brevibacterium flavum*. In: *Agricultural and Biological Chemistry* 53.5 (1989), 1261–1268.

— Regulation of glucose-6-phosphate dehydrogenase in *Brevibacterium flavum*. In: *Agricultural and Biological Chemistry* 51.1 (1987), 101–108.

Takors, R., B. Bathe, M. Rieping, S. Hans, R. Kelle & K. Huthmacher. Systems biology for industrial strains and fermentation processes - Example: Amino acids. In: *Molecular systems biology* 129.2 (2007), 181–190.

Tanaka, Y., H. Teramoto, M. Inui & H. Yukawa. Regulation of expression of general components of the phosphoenolpyruvate: carbohydrate phosphotransferase system (PTS) by the global regulator SugR in Corynebacterium glutamicum. In: *Applied microbiology and biotechnology* 78.2 (2008), 309–318.

Tanaka, Y., N. Okai, H. Teramoto, M. Inui & H. Yukawa. Regulation of the expression of phosphoenolpyruvate: carbohydrate phosphotransferase system (PTS) genes in *Corynebacterium glutamicum* R. In: *Microbiology (Reading, England)* 154.Pt 1 (2008), 264–274.

Tao, H., C. Bausch, C. Richmond, F.R. Blattner & T. Conway. Functional genomics: expression analysis of *Escherichia coli* growing on minimal and rich media. In: *Journal of bacteriology* 181.20 (1999), 6425–6440.

Tauch, A., T. Hermann, A. Burkovski, R. Krämer, A. Pühler & J. Kalinowski. Isoleucine uptake in *Corynebacterium glutamicum* ATCC 13032 is directed by the *brnQ* gene product. In: *Archives of Microbiology* 169.4 (1998), 303–312.

Teleki, A. *Systembiologische Untersuchungen zur Optimierung mikrobieller Produzenten schwefelhaltiger Aminosäuren*. Dissertation. Stuttgart: Universität Stuttgart, 2016.

Teleki, A., A. Sánchez-Kopper & R. Takors. Alkaline conditions in hydrophilic interaction liquid chromatography for intracellular metabolite quantification using tandem mass spectrometry. In: *Analytical biochemistry* 475 (2015), 4–13.

Terzer, M., N.D. Maynard, M.W. Covert & J. Stelling. Genome-scale metabolic networks. In: *Wiley interdisciplinary reviews: Systems biology and medicine* 1.3 (2009), 285–297.

Tesch, M., A.A. de Graaf & H. Sahm. In vivo fluxes in the ammonium-assimilatory pathways in *Corynebacterium glutamicum* studied by ^{15}N nuclear magnetic resonance. In: *Applied and environmental microbiology* 65.3 (1999), 1099–1109.

Teusink, B., A. Wiersma, L. Jacobs, R.A. Notebaart & E.J. Smid. Understanding the adaptive growth strategy of *Lactobacillus plantarum* by *in silico* optimisation. In: *PLoS computational biology* 5.6 (2009), e1000410.

Theorell, A., S. Leweke, W. Wiechert & K. Nöh. To be certain about the uncertainty: Bayesian statistics for ^{13}C metabolic flux analysis. In: *Biotechnology and bioengineering* 114.11 (2017), 2668–2684.

Touati, D. Iron and oxidative stress in bacteria. In: *Archives of biochemistry and biophysics* 373.1 (2000), 1–6.

Toyoda, K. & M. Inui. Regulons of global transcription factors in *Corynebacterium glutamicum*. In: *Applied Microbiology and Biotechnology* (2015).

Tremblay, P.-L., D. Höglund, A. Koza, I. Bonde & T. Zhang. Adaptation of the autotrophic acetogen *Sporomusa ovata* to methanol accelerates the conversion of CO_2 to organic products. In: *Scientific reports* 5 (2015), 16168.

Trötschel, C. *Methioninaufnahme und -export in Corynebacterium glutamicum*. Dissertation. Köln: Universität zu Köln, 2005.

Trötschel, C. et al. Methionine uptake in *Corynebacterium glutamicum* by MetQNI and by MetPS, a novel methionine and alanine importer of the NSS neurotransmitter transporter family. In: *Biochemistry* 47.48 (2008), 12698–12709.

Udaka, S. The Discovery of *Corynebacterium glutamicum* and Birth of Amino Acid Fermentation Industry in Japan. In: *Corynebacteria*. Ed. by **Burkovski, A.** Wymondham: Caister Academic, 2008, 1–6.

Unthan, S. et al. Beyond growth rate 0.6: What drives *Corynebacterium glutamicum* to higher growth rates in defined medium. In: *Biotechnology and Bioengineering* (2013).

Vallino, J.J. & G. Stephanopoulos. Carbon flux distributions at the glucose 6–phosphate branch point in *Corynebacterium glutamicum* during lysine overproduction. In: *Biotechnology progress* 10.3 (1994), 327–334.

van der Rest, M.E., C. Lange & D. Molenaar. A heat shock following electroporation induces highly efficient transformation of *Corynebacterium glutamicum* with xenogeneic plasmid DNA. In: *Applied Microbiology and Biotechnology* 52 (1999), 541–545.

van Gulik, W.M. & J.J. Heijnen. A metabolic network stoichiometry analysis of microbial growth and product formation. In: *Biotechnology and Bioengineering* 48.6 (1995), 681–698.

Vertès, A.A., M. Inui & H. Yukawa. Postgenomic approaches to using corynebacteria as biocatalysts. In: *Annual review of microbiology* 66 (2012), 521–550.

— The Biotechnological Potential of *Corynebacterium glutamicum*, from Umami to Chemurgy. In: *Corynebacterium glutamicum*. Ed. by **Yukawa, H. & Inui, M.** Berlin, Heidelberg: Springer Berlin Heidelberg, 2013, 1–49.

Wada, M. & H. Takagi. Metabolic pathways and biotechnological production of L-cysteine. In: *Applied Microbiology and Biotechnology* 73.1 (2006), 48–54.

Walter, B., M. Küspert, D. Ansorge, R. Krämer & A. Burkovski. Dissection of ammonium uptake systems in *Corynebacterium glutamicum*: mechanism of action and energetics of AmtA and AmtB. In: *Journal of bacteriology* 190.7 (2008), 2611–2614.

Wang, X., I. Khushk, Y. Xiao, Q. Gao & J. Bao. Tolerance improvement of *Corynebacterium glutamicum* on lignocellulose derived inhibitors by adaptive evolution. In: *Applied microbiology and biotechnology* 102.1 (2018), 377–388.

Wang, Z., J. Liu, L. Chen, A.-P. Zeng, C. Solem & P.R. Jensen. Alterations in the transcription factors GntR1 and RamA enhance the growth and central metabolism of *Corynebacterium glutamicum*. In: *Metabolic engineering* 48 (2018), 1–12.

Wang, Z., M. Gerstein & M. Snyder. RNA-Seq: a revolutionary tool for transcriptomics. In: *Nature reviews genetics* 10.1 (2009), 57.

Wehrmann, A., S. Morakkabati, R. Krämer, H. Sahm & L. Eggeling. Functional analysis of sequences adjacent to *dapE* of *Corynebacterium glutamicum* reveals the presence of *aroP*, which encodes the aromatic amino acid transporter. In: *Journal of bacteriology* 177.20 (1995), 5991–5993.

Weinand, M., R. Krämer & S. Morbach. Characterization of compatible solute transporter multiplicity in *Corynebacterium glutamicum*. In: *Applied Microbiology and Biotechnology* 76.3 (2007), 701–708.

Wendisch, V.F., de Graaf, A. A., H. Sahm & B.J. Eikmanns. Quantitative Determination of Metabolic Fluxes during Coutilization of Two Carbon Sources: Comparative Analyses with *Corynebacterium glutamicum* during Growth on Acetate and/or Glucose. In: *Journal of bacteriology* 182.11 (2000), 3088–3096.

Wendisch, V.F., M. Mindt & F. Pérez-García. Biotechnological production of mono- and diamines using bacteria: recent progress, applications, and perspectives. In: *Applied microbiology and biotechnology* 102.8 (2018), 3583–3594.

Wendisch, V.F., M. Bott, J. Kalinowski, M. Oldiges & W. Wiechert. Emerging *Corynebacterium glutamicum* systems biology. In: *Journal of Biotechnology* 124.1 (2006), 74–92.

Wendisch, V.F., M. Bott & B.J. Eikmanns. Metabolic engineering of *Escherichia coli* and *Corynebacterium glutamicum* for biotechnological production of organic acids and amino acids. In: *Current Opinion in Microbiology* 9.3 (2006), 268–274.

Wennerhold, J. & M. Bott. The DtxR regulon of *Corynebacterium glutamicum*. In: *Journal of bacteriology* 188.8 (2006), 2907–2918.

Wennerhold, J., A. Krug & M. Bott. The AraC-type regulator RipA represses aconitase and other iron proteins from *Corynebacterium* under iron limitation and is itself repressed by DtxR. In: *The Journal of biological chemistry* 280.49 (2005), 40500–40508.

Wiechert, W. & K. Nöh. From Stationary to Instationary Metabolic Flux Analysis. In: *Technology Transfer in Biotechnology*. Ed. by **Kragl, U.** Vol. 92. Advances in Biochemical Engineering. Springer Berlin Heidelberg, 2005, 145–172.

— Isotopically non-stationary metabolic flux analysis: complex yet highly informative. In: *Current Opinion in Biotechnology* 24.6 (2013), 979–986.

Wieschalka, S., B. Blombach & B. Eikmanns. Engineering *Corynebacterium glutamicum* for the production of pyruvate. In: *Applied Microbiology and Biotechnology* 94.2 (2012), 449–459.

Winder, C.L. et al. Global metabolic profiling of *Escherichia coli* cultures: an evaluation of methods for quenching and extraction of intracellular metabolites. In: *Analytical chemistry* 80.8 (2008), 2939–2948.

Winkler, J., L.H. Reyes & K.C. Kao. Adaptive laboratory evolution for strain engineering. In: *Methods in molecular biology (Clifton, N.J.)* 985 (2013), 211–222.

Winter, G. & J.O. Krömer. Fluxomics - connecting 'omics analysis and phenotypes. In: *Environmental Microbiology* 15.7 (2013), 1901–1916.

Wittmann, C. & A. de Graaf. Metabolic flux analysis in *Corynebacterium glutamicum*. In: *Handbook of Corynebacterium glutamicum*. Ed. by **Eggeling, L. & Bott, M.** Boca Raton: Taylor & Francis, 2005, 277–304.

Wittmann, C. & E. Heinzle. Genealogy Profiling through Strain Improvement by Using Metabolic Network Analysis: Metabolic Flux Genealogy of Several Generations of Lysine-Producing Corynebacteria. In: *Applied and environmental microbiology* 68.12 (2002), 5843–5859.

Wittmann, C. & J. Becker. The L-Lysine Story: From Metabolic Pathways to Industrial Production. In: *Amino Acid Biosynthesis - Pathways, Regulation and Metabolic Engineering*. Ed. by **Wendisch, V.F.** Vol. 5. Berlin, Heidelberg: Springer Berlin Heidelberg, 2007, 39–70.

Wittmann, C. & E. Heinzle. Metabolic Network Analysis and Design in *Corynebacterium glutamicum*. In: *Corynebacteria*. Ed. by **Burkovski, A.** Wymondham: Caister Academic, 2008.

Wittmann, C., P. Kiefer & O. Zelder. Metabolic fluxes in *Corynebacterium glutamicum* during lysine production with sucrose as carbon source. In: *Applied and environmental microbiology* 70.12 (2004), 7277–7287.

Xu, N. et al. Impaired oxidative stress and sulfur assimilation contribute to acid tolerance of *Corynebacterium glutamicum*. In: *Applied microbiology and biotechnology* 103.4 (2019), 1877–1891.

Yassin, A.F. *Rhodococcus triatomae* sp. nov., isolated from a blood-sucking bug. In: *International journal of systematic and evolutionary microbiology* 55.Pt 4 (2005), 1575–1579.

Yim, S.-H. et al. Purification and characterization of an arginine regulatory protein, ArgR, in *Corynebacterium glutamicum*. In: *Journal of industrial microbiology & biotechnology* 38.12 (2011), 1911–1920.

Yokota, A. & N.D. Lindley. Central Metabolism: Sugar Uptake and Conversion. In: *Handbook of Corynebacterium glutamicum*. Ed. by **Eggeling, L. & Bott, M.** Boca Raton: Taylor & Francis, 2005, 215–242.

Zamboni, N., S.-M. Fendt, M. Rühl & U. Sauer. ^{13}C-based metabolic flux analysis. In: *Nature protocols* 4.6 (2009), 878–892.

Zambrano, M.M., D.A. Siegele, M. Almirón, A. Tormo & R. Kolter. Microbial competition: *Escherichia coli* mutants that take over stationary phase cultures. In: *Science* 259.5102 (1993), 1757–1760.

Zelle, E., K. Nöh & W. Wiechert. Growth and production capabilities of *Corynebacterium glutamicum*: interrogating a genome-scale metabolic network model. In: *Corynebacterium glutamicum: from systems biology to biotechnological applications*. Ed. by **Andreas Burkovski**. Norfolk: Caister Academic Press, 2015, 39–54.

Zhang, Q. et al. Comprehensive optimization of the metabolomic methodology for metabolite profiling of *Corynebacterium glutamicum*. In: *Applied microbiology and biotechnology* (2018).

Zhang, Y. et al. A new genome-scale metabolic model of *Corynebacterium glutamicum* and its application. In: *Biotechnology for biofuels* 10 (2017), 169.

Zhao, Y. & S. Skogestad. Comparison of Various Control Configurations for Continuous Bioreactors. In: *Industrial & Engineering Chemistry Research* 36.3 (1997), 697–705.

Zhao, Y. & Y.-H. Lin. Flux distribution and partitioning in *Corynebacterium glutamicum* grown at different specific growth rates. In: *Process Biochemistry* 37.7 (2002), 775–785.

Zhao, Z., J.-Y. Ding, T. Li, N.-Y. Zhou & S.-J. Liu. The ncgl1108 (PheP (Cg)) gene encodes a new L-Phe transporter in *Corynebacterium glutamicum*. In: *Applied Microbiology and Biotechnology* 90.6 (2011), 2005–2013.

Ziert, C. *Metabolic engineering of Corynebacterium glutamicum for the production of L-aspartate and its derivatives beta-alanine and ectoine*. Dissertation. Bielefeld: Universität Bielefeld, 2014.

Appendices

A. Manuscript 1

'Physiological Response of *C. glutamicum* to Increasingly Nutrient-Rich Growth Conditions'

frontiers in Microbiology

ORIGINAL RESEARCH
published: 29 August 2018
doi: 10.3389/fmicb.2018.02058

Physiological Response of *Corynebacterium glutamicum* to Increasingly Nutrient-Rich Growth Conditions

*Michaela Graf, Julia Zieringer, Thorsten Haas, Alexander Nieß, Bastian Blombach and Ralf Takors**

Institute of Biochemical Engineering, University of Stuttgart, Stuttgart, Germany

OPEN ACCESS

Edited by:
Dimitris G. Hatzinikolaou, National and Kapodistrian University of Athens, Greece

Reviewed by:
Stefan Junne, Technische Universität Berlin, Germany
Armen Trchounian, Yerevan State University, Armenia

****Correspondence:***
Ralf Takors
takors@ibvt.uni-stuttgart.de

Specialty section:
This article was submitted to Systems Microbiology, a section of the journal Frontiers in Microbiology

Received: *29 May 2018*
Accepted: *13 August 2018*
Published: *29 August 2018*

Citation:
Graf M, Zieringer J, Haas T, Nieß A, Blombach B and Takors R (2018) Physiological Response of Corynebacterium glutamicum to Increasingly Nutrient-Rich Growth Conditions. Front. Microbiol. 9:2058. doi: 10.3389/fmicb.2018.02058

To ensure economic competitiveness, bioprocesses should achieve maximum productivities enabled by high growth rates (μ) and equally high substrate consumption rates (q_S) as a prerequisite of sufficient carbon-to-product conversion. Both traits were investigated and improved via bioprocess engineering approaches studying the industrial work horse *Corynebacterium glutamicum*. Standard minimal medium CGXII with glucose as sole carbon source was supplemented with complex brain-heart-infusion (BHI) or amino acid (AA) cocktails. Maximum μ of 0.67 h^{-1} was exclusively observed in 37 g BHI L^{-1} whereas only minor growth stimulation was found after AA supplementation (μ = 0.468 h^{-1}). Increasing glucose consumption rates (q_{Glc}) were solely observed in certain dosages of BHI (1–10 g L^{-1}), while 37 g BHI L^{-1} and AA addition revealed q_{Glc} below the reference experiments. Moreover, BHI supplementation revealed Monod-type saturation kinetics of μ (K_{BHI} = 2.73 g BHI L^{-1}) referring to the preference of non-AAs as key boosting nutrients. ATP-demands under reference, 1 g BHI L^{-1}, and AA conditions were nearly constant but halved in BHI concentrations above 5 g L^{-1} reflecting the energetic advantage of consuming complex nutrient components in addition to "simple" building blocks such as AAs. Furthermore, *C. glutamicum* revealed maximum biomass per carbon yields of about 18 g_{CDW} C-mol^{-1} irrespective of the medium. In AA supplementation experiments, simultaneous uptake of 17 AAs was observed, maximum individual consumption rates determined, and L-asparagine and L-glutamine were distinguished as compounds with the highest consumption rates. Employment of the expanded stoichiometric model *iMG481* successfully reproduced experimental results and revealed the importance of *C. glutamicum*'s transaminase network to compensate needs of limiting AA supply. Model-based sensitivity studies attributed the highest impact on μ to AAs with high ATP and NADPH demands such as L-tryptophan or L-phenylalanine.

Keywords: *Corynebacterium glutamicum*, growth rate, substrate consumption, carbon and nitrogen consumption, amino acid uptake, stoichiometric network model *iMG481*, sensitivity analyses

INTRODUCTION AND MOTIVATION

Corynebacterium glutamicum is a Gram-positive, non-sporulating, facultative anaerobic prokaryote (Liebl, 2006; Nishimura et al., 2007), generally recognized as safe (GRAS), and best known for its production of L-glutamate (Kinoshita et al., 1957). Revelation of the *C. glutamicum* ATCC 13032 wild type (WT) genome by Ikeda and Nakagawa (2003) and Kalinowski et al. (2003) enabled application of metabolic engineering techniques and the construction of genome scale metabolic models (Kjeldsen and Nielsen, 2009; Shinfuku et al., 2009). Thereby, targeted modification of the strain's genome, often predicted by said *in silico* models, enhanced *C. glutamicum*'s abilities to produce lactate, succinate, and pyruvate (Dominguez et al., 1993; Okino et al., 2005; Wendisch et al., 2006; Wieschalka et al., 2012), to form non-natural compounds such as diamins (Kind et al., 2010) or heterologous proteins (Scheele et al., 2013), and to emerge in the field of bio-based chemicals, materials, and fuels (Becker and Wittmann, 2012). Besides, the advantageous physiological properties, summarized by Vertès et al. (2012), further empower the microorganism to endure harsh production conditions as simulated and investigated in several scale-down studies mimicking production-like environments (Buchholz et al., 2014b; Käß et al., 2014a,b). Accordingly, the strain is well accepted as industrial platform and predominately employed for the production of the amino acids (AAs) L-glutamate, L-lysine, and L-valine (Hermann, 2003) serving demands of food, feed, cosmetic, and pharmaceutical markets (Takors et al., 2007). More than 2 million tons per year of L-glutamate (Becker and Wittmann, 2012) are likely to be produced by the strain in large scale bioreactors reaching volumes of 500 m^3 and more.

Regarding industrial AA production, *C. glutamicum* competes with *Escherichia coli*. Whereas the first offers advantages in robustness also including minimized phage contamination vulnerability, *E. coli* naturally possesses transhydrogenases which allow quick equilibration of NADH/NAD^+ and NADPH/$NADP^+$ pools (Sauer et al., 2004). The latter is of particular importance to engineer top producers of NADPH demanding compounds such as L-lysine requiring 4 mol NADPH in the synthesis of 1 mol L-lysine (Marx et al., 1997). Besides, *C. glutamicum* reveals only second-best properties in terms of growth kinetics: maximum growth rates of about 0.58 h^{-1} have been measured for *C. glutamicum* strain ATCC 17965 in batch and continuous cultivations with minimal medium containing glucose (Cocaign-Bousquet et al., 1996; Gourdon et al., 2003) and in turbidostatic processes using *C. glutamicum* ATCC 13032 (Bäumchen et al., 2007). Grünberger et al. (2013) achieved even slightly faster growth rates of 0.60–0.64 h^{-1} in highly diluted microliter-scale conditions using CGXII minimal medium with glucose as sole carbon source. However, the same medium only shows approximately 0.4 h^{-1} in conventional bioreactor setups (Blombach et al., 2013; Grünberger et al., 2013). On the contrary, *E. coli* achieves maximum growth rates of up to 1.04 h^{-1} in glucose supplemented minimal medium and 1.73 h^{-1} in complex broth (Cox, 2004). In general, low growth rates inherently limit the productivity of the production process: first by achieving the desired biomass concentration, second by limiting product formation in growth coupled kinetics. By analogy, low biomass specific glucose uptake rates represent an intrinsic disadvantage of the producing cell as they may cause low biomass specific productivities, too.

Consequently, to increase the attraction of *C. glutamicum* for industrial application, improvement of fundamental kinetics would be highly appreciated. Strain and process engineering measures could be applied. The first, however, is beyond the scope of this contribution. Instead, properly applied medium supplements may improve productivities of existing production processes without necessary strain engineering. Accordingly, our contribution investigates process engineering means, in particular medium supplementation, for increasing growth and glucose consumption rates of *C. glutamicum* WT as a prerequisite of improving volumetric productivities. Industrial bioprocess development aims at reducing complex media such as yeast extract or corn steep liquor to reduce medium costs and variabilities. Of course, key performance criteria of the fermentation should still be achieved. Accordingly, the identification of so-called "goodies" of medium constituents is welcomed. However, the general physiological response of *C. glutamicum* to complex medium (compounds) was not studied yet. To date, supplementation investigations with the strain mostly aimed at media optimization (Coello et al., 2002; Jeon et al., 2013) or usage of alternative carbon and/or nitrogen sources (Lee et al., 2014; Wendisch et al., 2016; Lange et al., 2017). For *E. coli*, in contrast, profound knowledge exists based on physiological investigations in Luria–Bertani (LB) broth (Sezonov et al., 2007) and due to comparable transcriptional expression analyses of late-exponential *E. coli* cultures grown in minimal and LB medium (Tao et al., 1999). This approach was further expanded in a broad gene expression study analyzing the different growth phases of the enterobacterium grown in the same complex medium (Baev et al., 2006a,b,c).

Thus, we performed a two-staged analysis to study how supplementation of standard growth minimal medium CGXII impacts the physiology of *C. glutamicum* WT in bioreactor batch cultivations. In the first part, complex brain-heart-infusion (BHI) was added to CGXII to investigate and identify the maximum metabolic capacity of the cell regarding growth. As a step toward the identification of optimum synthetic growth medium, AA supplementation was studied in the second part which also allows the analysis of theoretical impacts via stoichiometric modeling. Until now, AA consumption was only investigated in transporter characterization studies (e.g., Burkovski et al., 1996; Trötschel et al., 2008; Shang et al., 2013) or under anaerobic conditions (Michel et al., 2015). In summary, the manuscript focuses on process engineering approaches to accelerate growth of *C. glutamicum*.

MATERIALS AND METHODS

Experimental Setup

Preculture Cultivation

Corynebacterium glutamicum ATCC 13032 WT cells from working cell bank glycerol stocks were spread on 2 x

tryptone-yeast extract (2 x TY) medium (Sambrook, 2001) agar plates and incubated for 48–60 h at 30°C. Colonies were used to inoculate 5 mL of 2 x TY medium in glass reaction tubes which were incubated for 8 h at 30°C and 120 rpm on a bench-top rotary shaker (Infors HT, Bottmingen, Switzerland). The content of one glass reaction tube was used to inoculate 50 mL modified CGXII minimal medium (Buchholz et al., 2014a) supplemented with 4% (w/v) glucose. The shaking flask precultures were incubated overnight at 30°C and 120 rpm.

Cultivation in Bioreactors

Bioreactor cultivations were carried out in two different bioreactor systems. Experiments with BHI-supplementation were conducted in biological triplicates in a parallel triplex glass bioreactor system (HWS Labortechnik, Mainz, Germany) with a working volume of 250 mL. CGXII minimal medium (Buchholz et al., 2014a) was supplemented with 2% (w/v) glucose (reference) and optionally 1, 5, 10, or 37 g BHI (1, 5, 10, 37 BHI) medium per liter. Culture broth from preculture shaking flasks was harvested, centrifuged at 4°C for 10 min at 4000 × *g* (5430 R, Eppendorf, Hamburg, Germany) and resuspendend in sterile 0.9% (w/v) NaCl-solution. The differently supplemented CGXII media were inoculated with the washed preculture installing initial optical densities (OD_{600}) of 1 in 200 mL reaction volume. The parallel reactor system was equipped with dissolved oxygen (pO_2)- and pH-probes (Mettler Toledo GmbH, Albstadt, Germany). The temperature was kept constant at 30°C, pO_2 was kept >30% by increasing the impeller speed by 50 rpm (initial speed: 200 rpm) and the aeration rate by 20 mL min^{-1} (initial rate: 20 mL min^{-1}) in a cascadic fashion. pH was kept constant by adding 25% (v/v) NH_4OH. Antifoam agent (Struktol® J 647, Schill + Seilacher, Hamburg, Germany) was added manually when needed.

For AA supplementation experiments, biological triplicates were conducted in a 3 L steel-tank bioreactor (Bioengineering, Wald, Switzerland) ensuring high cell densities and enabling off-gas analysis. CGXII minimal cultivation media supplemented with 4% (w/v) glucose and optionally 5 mmol of the following AAs per liter were used: L-alanine (Ala), L-asparagine (Asn), L-aspartate (Asp), L-arginine (Arg), L-glutamine (Gln), L-glutamate (Glu), glycine (Gly), L-histidine (His), L-isoleucine (Ile), L-leucine (Leu), L-lysine (Lys), L-methionine (Met), L-phenylalanine (Phe), L-proline (Pro), L-serine (Ser), L-threonine (Thr), L-tryptophan (Trp), and L-valine (Val); 100 mL washed shaking flask preculture was used to inoculate supplemented CGXII media to give a starting OD_{600} of 3 and a total of 1.5 L reaction volume. The bioreactor was equipped with a six-blade Rushton impeller, a pO_2-, and pH-probe and operated at a total pressure of 1.5 bar at 30°C. pO_2 was kept > 30% by increasing the impeller speed by 50 rpm (initial speed: 250 rpm) and the aeration rate by 0.3 L min^{-1} (initial rate: 0.3 L min^{-1}) in a cascadic fashion. pH was kept constant by adding 25% (v/v) NH_4OH. Exhaust gas analysis of molar O_2- and CO_2-fractions was performed with non-dispersive (photometric) infrared gas analyzers (BCPO2 and BCPCO2, BlueSens, Herten, Germany). Antifoam agent was added manually when needed.

Analytical Methods

During the BHI-supplementation experiments, biosuspension samples were withdrawn hourly to measure the biomass concentration and to obtain cell-free samples. Determination of biomass was performed in technical replicates by following the optical density (OD_{600}) of the cell suspension with a spectrophotometer (DR 3900, Dr. Lange, Berlin, Germany) at 600 nm. During the AA supplementation experiments, biomass was additionally measured gravimetrically: 1 mL biosuspension was centrifuged at 20,173 × *g* and 4°C for 2 min (5430 R, Eppendorf, Hamburg, Germany), washed twice with deionized water, and dried at 105°C for at least 24 h in a convection oven (Heraeus, Hanau, Germany). Correlating the OD_{600} and cell-dry-weight (CDW) measurements resulted in a correlation factor of 0.27 g biomass L^{-1}. Cell-free samples were obtained by applying syringe filters with 0.2 μm pore size (Rotilabo®, Carl Roth, Karlsruhe, Germany) and storing the filtrates at −20°C until glucose-, total organic carbon- (TOC), and AA-quantification was performed. Glucose concentration was determined with an enzymatic assay following the instructions of the manufacturer (R-biopharma, Darmstadt, Germany). Following the protocols given by Buchholz et al. (2014a), AA concentrations were determined by means of high-pressure liquid chromatography, and total inorganic carbon (TIC)-, and TOC-amounts in biosuspension samples, cell-free filtrates, and biomass samples were measured with total carbon (TC) analysis. Therefore, a TC analyzer (Multi N/C 2100s, Analytik Jena, Jena, Germany) was employed to analyze samples regarding (i) the TIC content by acidification with 10% *ortho*-phosphoric acid to free carbonate-derived CO_2 and (ii) the TC content by total combustion of organic and inorganic carbon species to CO_2 at 750°C in a furnace system. TOC amounts were obtained with the differential detection mode of the device (TOC = TC – TIC). In the AA supplementation experiments, harvesting frequency was doubled after 4 h, and additional sampling enabled measuring of TOC and TIC values to check CO_2 exhaust-gas analysis as proposed by Buchholz et al. (2014a).

Determination of Kinetic Parameters

Exponential Growth Rate

Exponential growth rates (μ) were determined using linear regression of logarithmic biomass concentration curves over the process time as described by Grünberger et al. (2013) for batch cultivations.

Consumption Rates and Yields

Biomass-specific glucose, AA, and TOC consumption rates (q_{Glc}, q_{AA}, q_C) were determined by dividing the exponential growth rate (μ) by the biomass substrate yield (Y_{XS}) previously calculated by linear regression of substrate (S, representing glucose or carbon) concentrations curves over the biomass (X) concentration.

$$q_S = \frac{\mu}{Y_{XS}} \quad (1)$$

Respiratory Rates in Amino Acid Supplementation Experiments

Biomass-specific respiratory rates (q_{O2}, q_{CO2}) from AA supplementation experiments were determined by dividing the volumetric oxygen consumption or carbon dioxide emission rate by the biomass concentration. q_{CO2} deduced from the off-gas analysis was corrected by accounting for dissolved carbon species in the liquid volume (TIC) in the early growth phase (Buchholz et al., 2014a).

Estimation of Respiratory Rates and ATP-Biomass Yield in BHI Supplementation Experiments

To estimate the produced CO_2 during the BHI-supplementation experiments, molar (n) carbon (C) balancing was performed assuming that the consumed molar amount of TOC ($n_{C(TOC)}$) in the time frame of the exponential growth phase was either converted to biomass or to CO_2 neglecting TIC species accumulating in the fermentation broth in the early growth phase

$$\Delta n_{C(CO_2)} = \Delta n_{C(TOC)} - \Delta n_{C(biomass)} \quad (2)$$

Determination of TOC in biomass and cell-free samples by TC-analysis allowed calculation of the theoretically produced amount of CO_2. Thereof, the CO_2-biomass yield was obtained and converted to $q_{CO2,est}$ by multiplication with μ. The corresponding oxygen consumption rate $q_{O2,est}$ was deduced from $q_{CO2,est}$ by assuming a respiratory quotient (RQ) of 1, which was supported by the experimental rates of the reference and AA-supplementation experiments (c.f. **Tables 1**, **2**) in the steel-tank bioreactor

$$q_{O_2,est} = RQ \cdot q_{CO_2,est} \quad (3)$$

ATP production and consumption were assumed to be equilibrated. The first was deduced from $q_{O2,est}$ assuming a P/O-ratio of 1.2 as a conservative estimate. Accordingly, the biomass-specific ATP production rate (q_{ATP}) could be calculated as

$$q_{ATP} = P/O \cdot q_{O_2,est} \quad (4)$$

In turn, division of q_{ATP} by μ resulted in the ATP-biomass yield Y_{ATPX}. Standard deviations (SDs) for C-balancing are based on experimental results (biological triplicates) of carbon measurement of biomass and TOC, while SDs in all further calculation steps (cf. Eqs 3 and 4) were calculated by Gaussian error propagation.

Fitting of Monod-Type Parameters

The exponential growth rate μ of a microorganism can be calculated based on Monod-type kinetics (Monod, 1949)

$$\mu = \mu_{max} \frac{c_S}{c_S + K_S} \quad (5)$$

where c_S is the substrate concentration of the only growth limiting substrate, K_S is the half-saturation constant (which equals the substrate concentration leading to the half maximum growth rate), and μ_{max} is the maximum growth rate observed for the used substrate. In this study, Monod-kinetics were applied to examine the effect of different BHI concentrations (1–37 g L^{-1}) on the corresponding growth rate (μ_{BHI}) by calculating the difference ($\Delta\mu$) between growth rates obtained from experiments without BHI [μ_{Ref}, 2% (w/v) glucose as only carbon source] and μ_{BHI}

$$\Delta\mu = \mu_{BHI} - \mu_{Ref} \quad (6)$$

Inserting Eq. (6) into Eq. (5) depicted the influence of BHI-concentration (c_{BHI}) on the resulting growth difference

$$\Delta\mu = \Delta\mu_{max} \frac{c_{BHI}}{c_{BHI} + K_{BHI}} \quad (7)$$

To determine the unknown parameters $\Delta\mu_{max}$, that is the difference between the reference growth rate and the maximum growth rate observed under 37 g BHI L^{-1}, and the saturation constant of BHI (K_{BHI}), which is the BHI-concentration leading to half-maximum growth, the Curve Fitting Toolbox of Matlab (MATLAB Release 2014a, The MathWorks, Inc., Natick, MA, United States) was used. Thereby, non-linear least squares fitting to the experimental data based on the Monod-equation (7) were performed making use of the Levenberg–Marquadt algorithm and setting the confidence level to 90%.

Simulations With Stoichiometric Network Model *iMG481*

Curation of Model *iEZ475* and Expansion to *iMG481*

The stoichiometric model curated and expanded in this work is based on model *iEZ475* of Zelle et al. (2015). Recently, another *C. glutamicum* reconstruction was crafted by Zhang

TABLE 1 | Summary of kinetic parameters determined and estimated (index est) for *C. glutamicum* ATCC 13032 grown in modified CGXII minimal medium supplemented with 2% (w/v) glucose (Glc, reference) and additionally 1, 5, 10, or 37 g BHI L^{-1} (abbr. to 1, 5, 10, 37 BHI).

Supp.	μ, h^{-1}	q_{Glc}, C-mol g^{-1} h^{-1}	q_C, C-mol g^{-1} h^{-1}	Y_{XC} g C-mol^{-1}	$q_{CO2,est}$; q^*_{O2est}, mmol g^{-1} h^{-1}	q_{ATP}, mmol g^{-1} h^{-1}	Y_{ATPX}, mmol g^{-1}
Glc	0.32 ± 0.02	0.0214 ± 0.0015	0.0216 ± 0.0016	14.84 ± 0.33	6.94 ± 0.28	8.33 ± 0.34	26.03 ± 2.08
+1 BHI	0.44 ± 0.01	0.0277 ± 0.0016	0.0255 ± 0.0021	17.29 ± 1.34	8.79 ± 1.09	10.55 ± 1.31	23.90 ± 3.04
+5 BHI	0.54 ± 0.02	0.0272 ± 0.0014	0.0281 ± 0.0027	19.18 ± 1.64	5.48 ± 1.13	6.58 ± 1.35	12.22 ± 2.56
+10 BHI	0.59 ± 0.01	0.0264 ± 0.0007	0.0325 ± 0.0015	18.16 ± 0.73	6.32 ± 1.63	7.59 ± 1.95	12.87 ± 3.33
+37 BHI	0.67 ± 0.03	0.0191 ± 0.0019	0.0368 ± 0.0003	17.61 ± 1.61	8.13 ± 0.46	9.76 ± 0.56	14.67 ± 1.01

Bioreactor batch cultivations were performed at 30°C and pH 7.4 in biological triplicates. Values represent the statistical mean ± standard deviation.
**Estimated rates for oxygen consumption ($q_{O2,est}$) and carbon dioxide emission ($q_{CO2,est}$) are identical due to assumed respiratory quotient (RQ) of 1.*

TABLE 2 | Summary of kinetic parameters determined for *C. glutamicum* grown in modified CGXII minimal medium supplemented with 4% (w/v) glucose (Glc) or additionally 5 mmol of 18 amino acids (AAs) per L (abbr. to 5 AA).

Supp.	μ, h^{-1}	q_{Glc}, C-mol g^{-1} h^{-1}	q_C, C-mol g^{-1} h^{-1}	Y_{XC} g C-mol^{-1}	q_{O2}, mmol g^{-1} h^{-1}	q_{CO2}, mmol g^{-1} h^{-1}
Glc	0.337 ± 0.033	0.0213 ± 0.0020	0.0213 ± 0.0020	15.82 ± 0.03	6.06 ± 0.48	6.17 ± 0.65
+5 AA	0.468 ± 0.003	0.0205 ± 0.0006	0.0257 ± 0.0006	18.00 ± 0.52	9.49 ± 0.85	8.92 ± 0.09

Individual AA consumption rates are given in ***Table 3****. Bioreactor batch cultivations were performed at 30°C, 1.5 bar, and pH 7.4 in biological triplicates. Values represent the statistical mean ± standard deviation.*

et al. (2017), but was not considered in this investigation. After examination of AA biosynthesis and transporter reactions in *iEZ475*, the following alterations and expansions were performed according to published knowledge on the topics. *iMG481* is attached in the **Supplementary Material** as sbml- and Excel-file.

Regarding AA biosynthesis, the main route for Ala synthesis via alanine-transferase AlaT (Marienhagen and Eggeling, 2008) using pyruvate (Pyr) and Glu as precursors was added as reaction "alaT" yielding Ala and oxo-glutarate as products. Recently, Buerger et al. (2016) annotated gene *glsK* (*cg2728*) encoding the only known glutaminase in *C. glutamicum*. The corresponding hydrolyzation of Gln to Glu and NH_3 was added as irreversible reaction "glsK." Concerning the transport of AAs into the *in silico* cell, the direction of already implemented reactions "SER_t_NA" and "THR_t_NA," formerly used for export of the AAs, was reversed to enable Ser and Thr import with Na^+-symport (Palmieri et al., 1996) since the export of both AAs is independent of sodium ions (Palmieri et al., 1996). The Na^+-flux, formerly in antiport with Gln, was reversed in reaction "GLN_t_NA" according to Siewe et al. (1995). Lys import can be facilitated by antiport with Ala, Ile, and Val (Bröer and Krämer, 1990) and reaction "LYS_t_LEU" which falsely uses Leu was corrected to "LYS_t_ILE" transporting Ile.

Incorporating *C. glutamicum*-specific information on AA transporters, several reactions were added: (i) Asn transport, hitherto only possible via diffusion, was expanded by a Na^+-symporter ("ASN_t_NA") making use of (supposedly) the same transporter as for Gln (Siewe et al., 1995); (ii) Asp uptake was expanded by ATP-dependency ("ASP_t_ATP") mirroring the same transporter type as for Glu uptake (Krämer et al., 1990; Marin and Krämer, 2007); and (iii) Met transport facilitated by Na^+-symport (Trötschel et al., 2008) was added ("MET_t_NA") to the existing ATP-dependent system. No Arg-transporter was implemented in model *iEZ475* because Arg transport or a specific Arg transporter is not yet characterized or validated for *C. glutamicum*. However, Arg consumption was observed during the experiments (cf. section "Amino Acid Consumption and Amino Acid-Biomass Yield"), and therefore an ATP-dependent importer ("ARG_t_ATP") was added based on experimental evidence for *E. coli* (Gong et al., 2003).

Flux Balance Analysis

Growth rates, AA consumption rates, and metabolic flux distributions of the *in silico* cell were calculated using the *optimizeCbModel* function of "The COBRA Toolbox" (Heirendt et al., 2017) with solver set "glpk" and Matlab software. Biomass production was set as objective function, while experimentally determined glucose consumption rates (q_{Glc}), AA consumption rates (q_{AA}), and respiratory rates (q_{O2}, q_{CO2}) were used as constraints. To simulate abundant AA supply, AA uptake was unconstrained by setting the upper flux bound to 1000.

Sensitivity Analysis

To study the impact of AA supplementation on the growth rate of the *in silico* cell, sensitivity analyses were performed. Thus, FBAs were conducted where the glucose uptake rate was constrained to 3.5 mmol g^{-1} h^{-1}, representing the operation mode of exponential growth (cf. section "Amino Acid Consumption and Amino Acid-Biomass Yield"), and that of one single AA (q_{AA}) to 3.5 nmol g^{-1} h^{-1} with the objective to maximize growth (μ_{Sim}). FBA with only glucose uptake and without AA uptake yielded the reference growth rate μ_{Ref}. The sensitivity of each AA was thus calculated as:

$$Sensitivity = \frac{\mu_{sim} - \mu_{ref}}{q_{AA}} \quad (8)$$

RESULTS

BHI Supplementation Experiments

Kinetic Parameters

The impact of BHI medium on growth behavior and kinetic parameters of *C. glutamicum* ATCC 13032 was studied in triplicate bioreactor cultivations. Therefore, 1, 5, 10, or 37 g BHI L^{-1} (1, 5, 10, 37 BHI) was added to modified CGXII minimal medium [2% (w/v) glucose] and the determined kinetic properties were compared to reference cultivations with glucose as sole carbon source. Calculated exponential growth rates μ obtained from each condition showed an increase of μ with increasing BHI amounts (μ = 0.44–0.67 h^{-1}; **Table 1**). Under reference conditions, μ = 0.32 ± 0.02 h^{-1} was observed and a maximum rate of 0.67 ± 0.03 h^{-1} in 37 BHI. Pairwise *t*-tests between conditions with the most similar μ confirmed significant differences in growth mirroring the different BHI supplements. Besides, BHI stimulated the glucose consumption under 1–10 BHI conditions, revealing q_{Glc} of 0.0277 ± 0.0016 C-mol g^{-1} h^{-1} in 1 BHI, which was 29% higher than the reference. However, a decline of q_{Glc} with increasing growth rate promoted by increasing BHI amounts was observed (**Figure 1**, open circles), finally reaching a value of 0.0191 ± 0.0019 C-mol g^{-1} h^{-1} in 37 BHI that was 11% smaller than in reference conditions. In contrast to glucose consumption, the TC consumption rate q_C increased proportionally with μ as illustrated in **Figure 1** (filled

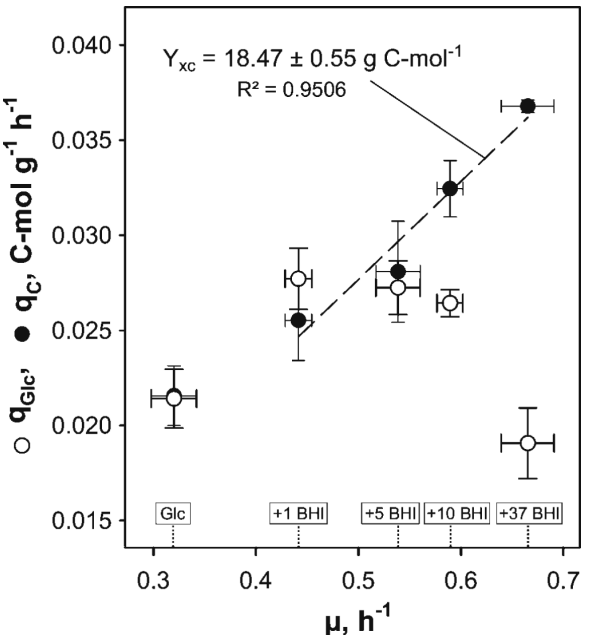

FIGURE 1 | Illustration of biomass-specific glucose (q_{Glc}) and total organic carbon (q_C) consumption rates obtained in experiments with *C. glutamicum* WT grown in modified CGXII minimal medium with 2% (w/v) glucose (Glc) and brain-heart-infusion (BHI)-supplemented media (1, 5, 10, or 37 g BHI L^{-1}) over the corresponding exponential growth rate (μ). A proportional increase of q_C in BHI-supplemented conditions with μ indicated a constant biomass-organic carbon yield (Y_{XC}, cf. **Table 1**). Values are deduced from three biological replicates ± standard deviation.

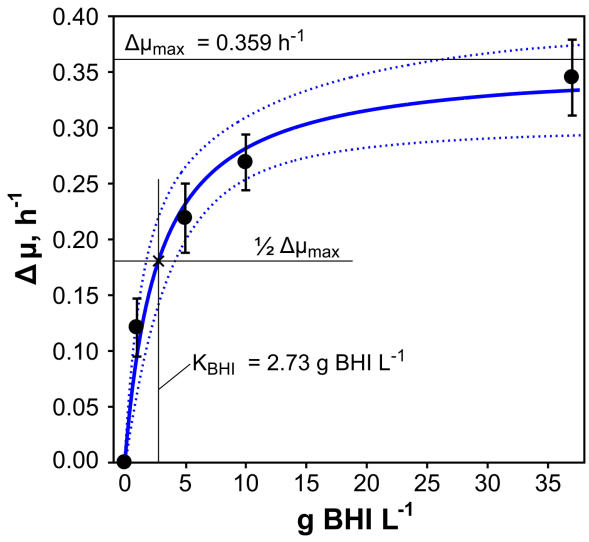

FIGURE 2 | Exponential growth rate differences ($\Delta\mu$) were calculated for *C. glutamicum* WT grown in modified CGXII minimal medium supplemented with 2% (w/v) glucose and with additional 1, 5, 10, or 37 g brain-heart-infusion (BHI) L^{-1} medium (three biological replicates ± standard deviation). Illustration of $\Delta\mu$ over the corresponding amount of BHI revealed a Monod-like saturation curve. The half-velocity constant for BHI (K_{BHI}) and the maximum growth rate difference ($\Delta\mu_{max}$) given in the figure were deduced from non-linear least-squares fitting (blue solid line) with a confidence level of 90% (blue dotted lines).

black circles). Thereby, a constant biomass-carbon yield (Y_{XC}) of 18.47 ± 0.55 g C-mol^{-1} could be calculated by linear regression of biomass production versus carbon consumption.

Monod-Like Kinetics

The supplementation of CGXII minimal medium with different amounts of BHI induced a diversification of the growth rate of *C. glutamicum* which motivated us to investigate the influence of BHI concentration on μ. Therefore, differences in growth ($\Delta\mu$) of BHI-supplemented and non-supplemented conditions (reference) were calculated (Eq. 6) and plotted against related BHI concentrations (1–37 g BHI L^{-1}), illustrated in **Figure 2** (filled black circles). A Monod-like saturation curve was observed with a steep increase of $\Delta\mu$ for low BHI additions (1–5 g BHI L^{-1}) leveling out at BHI-concentrations above 10 g L^{-1} and approximating the maximal growth rate difference ($\Delta\mu_{max}$). Therefore, non-linear least squares fitting of the experimental data was performed, using the Monod-type equation (7) with 90% confidence level of the fit. $\Delta\mu_{max}$ and the saturation constant of BHI (K_{BHI}), that is the BHI concentration leading to half-$\Delta\mu_{max}$, were thus estimated with 0.359 h^{-1} and 2.73 g BHI L^{-1}, respectively. Plugging both values into Eq. 7 results in the estimation curve (blue solid line) pictured in **Figure 2** with the dotted curves above and below as a measure for the confidence level.

Estimated ATP-Biomass Yield

The ATP consumption of *C. glutamicum* cultivated in supplemented CGXII media was estimated to evaluate the energy demand of the cell under minimal and increasingly rich conditions. Since no intracellular ATP pools were measured, the theoretical amount of ATP produced and consumed by the strain was estimated as given in Eqs 2–4. Therefore, carbon balancing was performed to estimate the produced molar amount of CO_2 which was converted to the (estimated) carbon emission rate $q_{CO2,est}$ (**Table 1**). Assuming a RQ of 1 led to the corresponding oxygen consumption rate $q_{O2,est}$, which was then used to calculated the ATP consumption rate by assuming a P/O ratio of 1.2. The resulting ATP-biomass yield Y_{ATPX} is plotted against growth rates in **Figure 3**. Under reference conditions (glucose as sole carbon source), the highest ATP-yield of 26.03 ± 2.08 mmol g^{-1} was observed, whereas the yield with 1 g BHI L^{-1} was in the same range (23.9 ± 3.04 mmol g^{-1}). However, elevation of BHI-amounts above 1 g L^{-1} lead to a new ATP-level of around 14 mmol g^{-1} considering the SDs of the respective conditions (5, 10, and 37 BHI). This equals a drop of the ATP-biomass yield by ca. 46% in comparison to reference conditions.

Amino Acid Supplementation Experiments

Kinetic Parameters

To unravel whether the stimulative effect of BHI on growth rate and TC consumption of *C. glutamicum* WT was due to AAs, which are components of BHI in free or peptide-bound form, AA

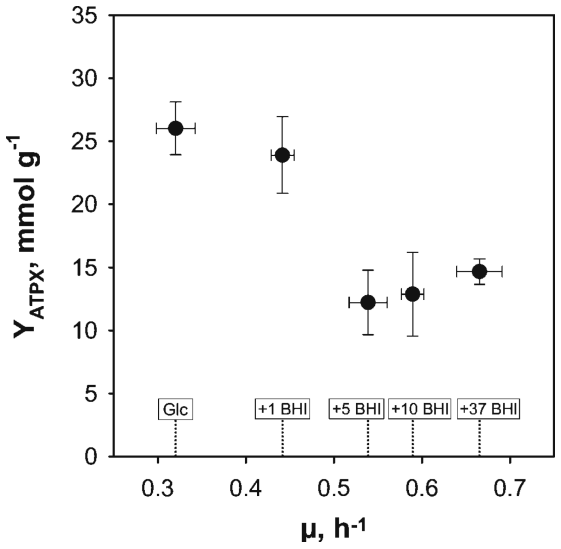

FIGURE 3 | Illustration of estimated ATP-biomass yields (Y_{ATPX}) over exponential growth rates (μ) from BHI-supplementation experiments with *C. glutamicum* WT grown in modified CGXII minimal medium with 2% (w/v) glucose (Glc) and brain-heart-infusion (BHI)-supplemented media (1, 5, 10, or 37 g BHI L^{-1}). Y_{ATPX}-estimation was based on carbon balancing to calculate the theoretical respiratory rates and assuming a P/O-ratio of 1.2 (cf. Eqs 2–4 and **Table 1**). Values are deduced from three biological replicates and error propagation was used to determine corresponding standard deviations pictured as error bars in the figure.

supplementation fermentations were performed. Thus, 5 mM of all essential AAs (except for L-cysteine and L-tyrosine) were added to modified CGXII minimal medium [4% (w/v) glucose] to comparably study the kinetic properties of the strain cultivated in the "simulated" complex medium. Impacts of elevated biomass concentrations were studied in the pressurized bioreactor to prevent oxygen limitation. To ensure comparability, reference cultivations with glucose as only carbon source were repeated in this bioreactor. Deduced kinetic parameters (**Table 2**) showed good conformity with corresponding values obtained in the previous system (**Table 1**). Accordingly, all results can be discussed irrespective of the reactor system. Addition of AAs to CGXII minimal medium increased μ by about 40% from 0.337 ± 0.033 (reference) to 0.468 ± 0.003 h^{-1} (**Table 2**) which was within the range of 1–5 BHI supplementation (μ = 0.44–0.54 h^{-1}; **Table 1**). Interestingly, the maximum observed growth rate (0.67 ± 0.03 h^{-1}) in 37 BHI was not reached by AA supplementation. As previously observed in 37 BHI, q_{Glc} determined under AA-supplemented conditions was within the range of the reference considering the deviance (AA: 0.0205 ± 0.0006 C-mol g^{-1} h^{-1}; reference: 0.0213 ± 0.0020 C-mol g^{-1} h^{-1}). In contrast, TC consumption was about 21% higher (0.0257 ± 0.0006 C-mol g^{-1} h^{-1}) making it comparable to the values observed in 1 BHI (0.0255 ± 0.0021 C-mol g^{-1} h^{-1}). Determination of the biomass-carbon yield Y_{XC} in AA supplementation revealed a value of 18.00 ± 0.52 g C-mol^{-1} which fits to the linear regression of Y_{XC} from the BHI-experiments (18.47 ± 0.55 g C-mol^{-1}). Calculation of respiratory rates deduced from exhaust gas analysis displayed an increase of about 45% compared to the reference (q_{O2} = 6.06 ± 0.48 mmol g^{-1} h^{-1}; q_{CO2} = 6.17 ± 0.65 mmol g^{-1} h^{-1}) which equals the increase of growth (about 40%).

Amino Acid Consumption and Amino Acid-Biomass Yield

Regarding the consumption of the 18 added AAs in the AA supplementation experiments, all AAs except for Asp were consumed (cf. **Supplementary Figure S1**) by *C. glutamicum* WT. Simultaneous decrease of AA concentrations in cell-free filtrates was observed but for Asn which was consumed only after Gln was nearly depleted (3–4 h, **Supplementary Figure S1**). Related AA consumption rates were calculated for each AA and are summarized in **Table 3**. The highest rate of 0.694 ± 0.005 mmol g^{-1} h^{-1} was obtained for Gln, whereas Trp was consumed with the smallest rate (0.022 ± 0.001 mmol g^{-1} h^{-1}). Next, AA-biomass yields (Y_{AA}) were determined and compared to three biomass AA-compositions of different *C. glutamicum* species (**Table 4**): *Micrococcus glutamicus* No. 541 (*C. glutamicum* ATCC 13058, Kimura, 1963), *C. glutamicum* ATCC 17965 (Cocaign-Bousquet et al., 1996), and *C. glutamicum* MH20-22B (lysine producer based on *C. glutamicum* ATCC 13032, Marx et al., 1996). Mean biomass compositions were derived to check whether experimental Y_{AA} mirror the apparent needs for biomass build-up (last column in **Table 4**). Thereby, three groups could be identified: (i) AAs fitting well with the reference data (Arg, His, Ile, Leu, Met, Phe, Ser, Thr, Trp), (ii) AAs taken up in higher (Gln, Asn, Pro), or (iii) in lower amounts (Ala, Glu,

TABLE 3 | Amino acid (AA) consumption rates (q_{AA}) of *C. glutamicum* cultivated in CGXII minimal medium supplemented with 4% (w/v) glucose and 5 mM of all AAs except L-cysteine and L-tyrosine.

AA	q_{AA}, mmol g^{-1} h^{-1}
Gln	0.694 ± 0.005
Asn	0.302 ± 0.003
Pro	0.218 ± 0.010
Ser	0.134 ± 0.003
Thr	0.118 ± 0.001
Glu	0.117 ± 0.001
Leu	0.112 ± 0.002
Ile	0.108 ± 0.002
Arg	0.093 ± 0.003
Ala	0.083 ± 0.002
Phe	0.066 ± 0.002
Val	0.051 ± 0.008
Met	0.046 ± 0.002
His	0.031 ± 0.002
Gly	0.025 ± 0.006
Lys	0.025 ± 0.001
Trp	0.022 ± 0.001
Asp	n. c. d.

Table is ordered according to the magnitude of q_{AA}. Values represent the statistical mean ± standard deviation of three individual bioprocesses. n.c.d., no consumption detected.

TABLE 4 | Comparison of published amino acid (AA)-compositions of different *C. glutamicum* strains determined by (A) Kimura, 1963, (B) Cocaign-Bousquet et al., 1996, (C) Marx et al., 1996, and experimentally determined AA-yields (Y_{AA}).

AA	AA compositions of *C. glutamicum* $\mu mol\ g_{CDW}^{-1}$			Mean or range of A, B, C M ± SD, $\mu mol\ g_{CDW}^{-1}$	Experimental yield Y_{AA}, $\mu mol\ g_{CDW}^{-1}$	Y_{AA}/M, %
	A	B	C			
Ala	802	725	606	711 ± 99	177 ± 5	25
Arg	196	190	189	192 ± 4	198 ± 8	103
Asn	n.v.	187	200	187–200 (194)	646 ± 4	334
Asp	434	187	200	187–200 (194)	n.c.d.	n.c.d.
Glu	569	486	403	486 ± 83	1482 ± 3	52
Gln	n.v.	486	403	403–486 (445)	251 ± 2	333
Gly	411	344	361	372 ± 35	51 ± 13	14
His	135	63	71	63–71 (67)	66 ± 5	99
Ile	535	175	202	175–202 (189)	231 ± 5	123
Leu	354	262	0	262–354 (308)	239 ± 6	78
Lys	260	171	202	211 ± 45	54 ± 3	26
Met	72	5	146	72–146 (109)	99 ± 4	91
Phe	148	123	133	135 ± 13	140 ± 5	104
Pro	163	148	170	160 ± 11	466 ± 23	290
Ser	326	265	225	272 ± 51	285 ± 7	105
Thr	252	270	275	266 ± 12	251 ± 1	95
Trp	n.v.	1	54	54	47 ± 3	86
Val	353	262	284	300 ± 47	107 ± 18	36

For better comparison, the percentage of Y_{AA} in relation to the mean value (M) or value range (M in brackets) of A, B, and C ± standard deviation was calculated. Y_{AA}-values represent the statistical mean ± standard deviation of three biological triplicates. n.v., no value available; n.c.d., no consumption detected.

Gly, Lys, Val, Asp) than expected from composition. **Figure 4A** illustrates the observation by color-coding AAs of group (i) in white, AAs of group (ii) in yellow, and AAs of group (iii) in red. Accordingly, consumed amounts of AAs of group (ii) exceed the biomass need approximately by factor three. AAs from group (iii) poorly satisfied the composition-demand between 0 (Asp) and 52% (Glu).

In silico AA-Uptake and -Consumption Studies With *iMG481*

Validation of stoichiometric network model iMG481

Besides studying the *in vivo* AA consumption of *C. glutamicum* WT during bioprocesses, *in silico* AA uptake and its influence on growth was further analyzed with the expanded stoichiometric network model *iMG481*. To check the suitability of the model, FBA was performed for reference conditions using q_{Glc} = 3.55 mmol g^{-1} h^{-1} as input, leaving q_{O2} and q_{CO2} non-constrained. μ_{Sim} = 0.337 h^{-1} was the output which agrees well with the experimental value (**Table 2**) and with μ_{Sim} obtained from the predecessor model *iEZ475* (Zelle et al., 2015). Because *iMG481* was derived from *iEZ475* by the implementation of additional AA importers, measured AA consumption rates, in particular q_{Arg}, q_{Ser}, and q_{Thr}, could be used as additional inputs yielding μ_{Sim} = 0.481 h^{-1}, which was slightly higher than the experimental μ (0.468 ± 0.003 h^{-1}). Constraining respiration of the *in silico* cell to the experimental values reduced the predicted growth rate by ca. 20% in all tested cases. Therefore, following investigations were performed with unconstrained oxygen consumption or carbon dioxide emission.

Comparing predicted intracellular fluxes of *iEZ475* with *iMG481* under reference conditions revealed that the new reaction "alaT" (using Glu as amino donor for Ala-synthesis) was used by *iMG481* instead of the alternative route "NCgl0388" using Val as amino donor. This result was in accordance with Marienhagen and Eggeling (2008) describing the former reaction as the main synthesis route for Ala in *C. glutamicum*. Furthermore, under AA supplementation conditions, the new Gln hydrolysis reaction "glsK" was used by the *in silico* cell instead of reactions "glmS" and "pyrG_2gln" which, likewise to "glsK," produce Glu from exceeding amounts of Gln.

Apart from the two new synthesis pathways, *iMG481* has a broader transport variability than *iEZ475* by incorporation of additional transporters for Ala, Asp, and Met. Accordingly, different uptake options for Ala, Asn, Asp, Glu, Ile, Leu, Met, Phe, and Val were available which were tested with regard to the preferred uptake system of the *in silico* cell. When AA uptake was unconstrained and at least one of the said AA was assumed to be active, the highest μ_{Sim} was always achieved by the least-energy demanding uptake system. The ranking found that diffusion was preferred to ion exchange assigning ATP-requiring uptake the least attraction. For further investigations, all transporters which were supposed to be active under non-limited substrate conditions were considered (**Supplementary Table S1**).

Sensitivity analysis: impact of AA uptake on μ

The impact of AA supplementation on the simulated growth rate μ_{Sim} was studied by means of sensitivity analysis. Substrate

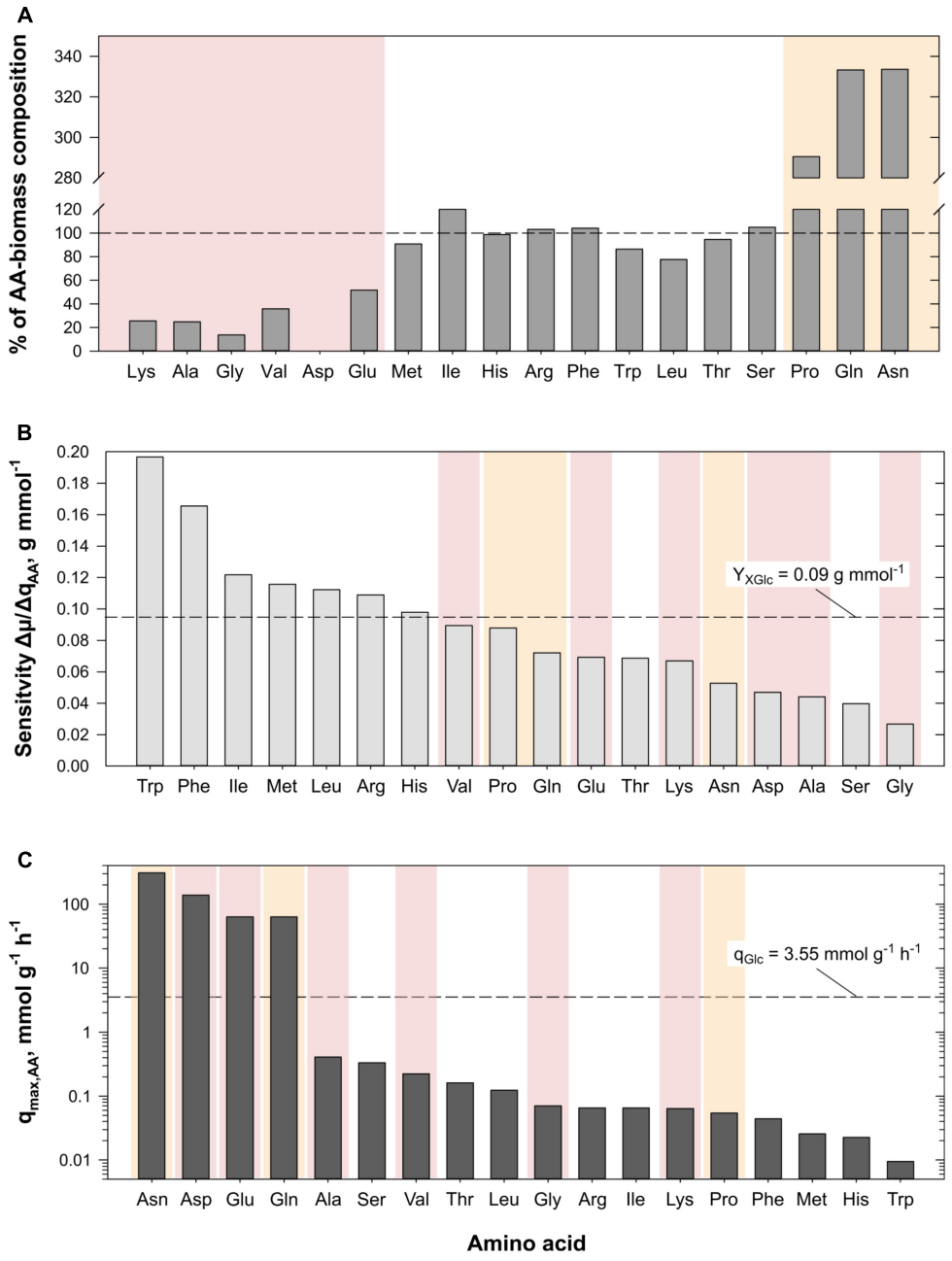

FIGURE 4 | (A) Illustration of percentage amino acid (AA)-biomass yields (mmol g^{-1}) calculated from AA supplementation experiments in relation to the mean AA-composition of biomass from different *C. glutamicum* strains (cf. **Table 4**). AA-amounts consumed during the experiments which were higher (above 100%) or lower (below 100%) than the published values are highlighted in yellow and red, respectively. **(B)** Results of the sensitivity analyses indicating the impact of AA-uptake on the growth rate of the *in silico* cell (cf. Eq. 8). The experimental biomass-glucose yield (Y_{XGlc}) observed for the strain grown in CGXII [4% (w/v) glucose, **Table 2**] is given as reference. Color-coding is adapted from panel (A). **(C)** Results of unbound AA-uptake ($q_{max,AA}$) by the *in silico* cell. The experimental glucose consumption rate (q_{Glc}) observed for growth in CGXII [4% (w/v) glucose, **Table 2**] is given as reference. Color-coding is adapted from panel (A).

consumption rates under exponential growth conditions were taken as the reference. The impact on growth increase was investigated by adding infinitesimal amounts of singular AAs with 3.5 nmol g^{-1} h^{-1} which represented 1/1000 of the glucose uptake rate constraint. Thereby, the AA-related sensitivity on growth induced by each of the 18 AAs was obtained employing Eq. (8). **Figure 4B** ranks the growth sensitivities of these AAs giving the experimental biomass-glucose yield (Y_{XGlc}, **Table 2**) as reference (dashed line). As a result, Trp, Phe, Ile, Met, Leu, Arg, and His showed sensitivities above the reference and therefore had the highest impact on μ_{Sim}. Interestingly, this group of AAs was already identified in the

experimental approach as AAs being consumed according to the AA-biomass composition (cf. **Table 4**), as highlighted by the color scheme adopted from **Figure 4A**. *Vice versa*, AAs exerting non-growth coupled impact on μ_{Sim} (e.g., Pro, Glu, Gln, etc.) were either consumed in lower or higher than expected amounts taking cellular AA-biomass composition as threshold.

Unbound AA-uptake

Complementary to the sensitivity analysis, the consequence of extreme AA uptake has also been studied. The simulations considered constant glucose uptake (3.5 mmol g^{-1} h^{-1}) and eliminated any upper limit of AA uptake. The results pictured in **Figure 4C** show that Asn, Asp, Glu, and Gln surpassed the molar uptake of glucose (dashed line) by up to 85 times. Calculating the AA-biomass yield with the help of the simulated AA uptake and corresponding growth rate according to Eq. (1) (data not shown) further revealed that apart from the four mentioned AAs, Ala, Leu, Ser, Thr, and Val were taken up in higher amounts than expected from the model's AA-biomass composition (cf. reaction "PROTEIN_a"). Gly, however, was the only AA with a taken-up amount below the composition value. Comparison of these AAs to the experimental AA-grouping and color scheme of **Figure 4A** identifies these AA (apart from Ser) as AAs exhibiting non-proportional uptake in the experiments.

DISCUSSION

The study was motivated by the fundamental question to elucidate the physiological response of *C. glutamicum* ATCC 13032 on increasingly nutrient-rich growth conditions. Therefore, a two-staged supplementation analysis was performed. In the first part, standard minimal medium CGXII with glucose as sugar source was supplemented with varying amounts of BHI to identify the cellular maximum of metabolic capacity. Since AAs are crucial components of BHI (in free or peptide-bound form), their influence on growth was analyzed in the second part of the study by adding an AA-cocktail comprising 18 AAs with individual concentrations of 5 mM. Using AA supplementation in synthetic medium enabled further *in silico* FBA studies. Both BHI and AA supplementation are discussed in the following.

Impact of BHI and AAs on Growth and Carbon Consumption of *C. glutamicum*

Previous growth studies by Grünberger et al. (2013) showed that the strain achieved maximum growth rates of 0.42 ± 0.03 h^{-1} when cultivated in lab-scale bioreactors using CGXII. Thereof, Unthan et al. (2014) identified the supplement protocatechuic acid (PCA) in CGXII as growth-accelerating compound. Strictly speaking, it is not yet fully unraveled whether PCA serves as additional carbon source, affects iron transport, enhances growth by a combinatorial effect, or may even support metabolism by other means. Accordingly, CGXII minimal medium without PCA was used in our investigations. As expected, growth rates of 0.32 ± 0.02 h^{-1} were observed in non-supplemented conditions which could be increased to 0.45 ± 0.01 h^{-1} when PCA was used (data not shown). In the following, CGXII always implies PCA-free minimal medium with glucose as standard carbon source.

Adding varying amounts of BHI (1–37 g BHI L^{-1}) to CGXII [2% (w/v) glucose] significantly increased μ from 0.32 ± 0.02 h^{-1} to a maximum of 0.67 ± 0.03 h^{-1} revealing Monod-type dependence of the growth rate increase ($\Delta\mu_{max}$) on BHI-concentration. Interesting enough, K_{BHI} of 2.73 g L^{-1} indicates the existence of a growth boosting component in BHI that is crucial for growth acceleration in low amounts but achieves saturating levels in BHI > 5 g L^{-1}.

To elucidate whether the growth enhancement was due to AAs present in BHI, 18 AAs were added to CGXII [4% (w/v) glucose]. To ensure maximum AA uptake rates, abundant AA concentrations of 5 mM were installed which were sufficiently higher than published K_M-values of the strain's AA transporters (cf. **Supplementary Table S1**). Hence, an equally high growth rate of about 0.6 h^{-1} as induced by 37 g BHI L^{-1} was expected, if AAs were the only growth enhancing factors in BHI. Surprisingly, a remarkably smaller exponential μ_{max} of 0.468 ± 0.003 h^{-1} was observed which equaled the addition of 2 g BHI L^{-1} (**Figure 2**). However, quantification of free and peptide-bound AAs in BHI (data not shown) revealed that only about 8 mM AAs were available in 2 g BHI L^{-1} which was significantly lower than the total amount used in the AA experiments (90 mM). Since these findings indicated that AAs were not the only growth enhancing factors in BHI, we evaluated the findings by further energetic analysis.

Therefore, we qualified the substrates by estimating the ATP-biomass yields of the different nutrient scenarios. Assuming that total consumed carbon (supplied by glucose and BHI) was used to produce biomass, CO_2, and no by-products, CO_2 emission rates and O_2 consumption rates were calculated (**Table 1**) and compared to experimentally determined rates (**Table 2**) of the glucose reference conditions. ATP formation was calculated assuming a growth medium-independent P/O-ratio of 1.2 which represents a realistic estimation based on own observations. Moreover, we presumed that ATP formation equaled consumption. Accordingly, the ATP-yield of about 26 mmol g^{-1} for reference conditions was observed (**Table 1**). The estimation fits well with findings of Cocaign-Bousquet et al. (1996) (29.1 mmol g^{-1}), but differs from the 60 mmol g^{-1} determined by Pfelzer (2016). For comparison, *E. coli* shows demands of 71 mmol g^{-1} (Varma et al., 1993). However, estimations strictly depend on the choice of P/O-ratio. For example, choosing the P/O ratio of two yields 43 mmol g^{-1}. Accordingly, estimated Y_{ATPX} values only show tendencies allowing comparison of the different media.

Almost identical Y_{ATPX} of 23.9 ± 3.04 and 24.3 ± 2.2 mmol g^{-1} were observed for the addition of 1 g BHI L^{-1} and AA supplementation, respectively. The observation somewhat mirrors the Monod-type growth increase after BHI addition (**Figure 2**) compared to the growth rise after AA supplementation. Both revealed similar growth benefits,

apparently resembling similar energetic status of the cells. However, adding BHI $\geq$ 5 g L^{-1}, steadily decreased Y_{ATPX} to about 14 mmol g^{-1} which corresponds to a 46% drop with respect to the reference. Several hypothesis can be formulated: (i) under reference, 1 g BHI L^{-1}-, and AA-supplemented conditions, ATP demanding futile cycles existed which disappeared under BHI-rich conditions; (ii) P/O ratios are not constant but increase under BHI-rich conditions which would compensate the Y_{ATPX} drop; and (iii) BHI-rich media provide crucial precursors, thereby preventing own ATP-demanding cellular synthesis. Hypothesis (i) appears unlikely qualifying a 46% share of ATP production for futile cycling production as too high. Hypothesis (ii) requires for detailed (^{13}C based) metabolic flux analysis which is beyond the scope of this study. Ruling out options (i) and (ii), hypothesis (iii) was taken as the guiding idea for subsequent analysis.

Accordingly, net ATP costs for AA biosynthesis starting from central metabolism precursors were estimated modifying the approach of Kaleta et al. (2013) who calculated the net ATP costs for AA synthesis routes in *E. coli* by considering ATP costs in the synthesis pathways but also accounted for the amount of produced ATP by precursor synthesis (cf. **Table 4** and **Supplementary Tables S2**, **S3**). In contrast to Kaleta et al. (2013), NADPH was not considered as energy (ATP) yielding precursor in respiration of *C. glutamicum* because the strain does not possess nicotinamide nucleotide-dependent transhydrogenases like *E. coli* (Kabus et al., 2007). As a result, ATP costs of about 4 mmol for 1 g biomass were calculated that represents less than 15% of the net ATP formation from glucose (about 26 mmol g^{-1}, **Table 1**) considering the P/O ratio of 1.2. Accordingly, enriching the medium by AAs did create only minor energetic benefit as shown for the AA supplemented medium compared to the reference (difference of approximately 2 mmol g^{-1}). Studies of Ingraham et al. (1983) analyzing ATP demands of *E. coli* grown in minimal and rich medium further support the observation: ATP demands of protein formation outnumber those of AA formation by far. Similar to our findings for *C. glutamicum, E. coli* revealed 40% reduced Y_{ATPX} values when cultivated in rich medium compared to minimal medium (Ingraham et al., 1983). Apparently, the reduction of 46% observed for *C. glutamicum* agrees well. Most likely, other ATP-demanding building blocks, such as fatty acids or nucleotides, are consumed in highly concentrated BHI environments which relieves the cellular need to create ATP thereby reducing the glucose uptake accordingly. Therefore, the growth phenotype resulting from different nutrient supplies can be explained as follows: *C. glutamicum* benefits from the abundant addition of AAs by omitting the related AA biosynthesis which yields a moderate μ increase. Growth advantages of AA supplementation may be rooted in the elimination of kinetics limits. For instance, external supply of AAs may fuel intracellular transaminases thereby preventing own "slow" biosynthesis. Alternatively, external supply may meet short-term needs for charging tRNAs as a prerequisite of fast translation for protein formation (Nieß et al., 2017). Adding high amounts of BHI further released the cell of ATP-costly fatty acid and nucleotide synthesis enhancing μ to its apparent limit of 0.67 h^{-1}. Necessary ATP production was reduced to about 14 mmol ATP per g biomass resembling the remaining cellular needs for maintenance and biosynthesis. The strong growth boosting effect of 1 g BHI L^{-1} (**Figure 2**) anticipates that other growth stimulating components beside AAs (about 4 mM, cf. above) play a role, too. Likely candidates are trace elements or vitamins. The latter have been tested (supplementation of 0.2 mg thiamine-HCl L^{-1} in CGXII) and an elevated growth rate of approximately 0.4 h^{-1} was determined (data not shown).

Biomass specific glucose uptake rates q_{Glc} also showed particularities for different nutrient-rich media. Whereas 1 g BHI L^{-1} caused q_{Glc} increase, further BHI supplementation yielded decreasing rates (**Table 1**) reaching reference-like levels in 37 g BHI L^{-1} and in the AA supplementation experiments. Notably, TC consumption increased proportionally with μ showing a biomass-carbon yield Y_{XC} of 18.47 g C-mol^{-1}. The observations agree with findings of Dominguez et al. (1997) who found Y_{XC} of 17.6 g C-mol^{-1} for the consumption of different glucose-fructose mixtures. Wendisch et al. (2000) observed 12 g C-mol^{-1} for the consumption of glucose-acetate mixtures and Frunzke et al. (2008) measured 13 g C-mol^{-1} for glucose, gluconate, and glucose–gluconate mixtures in shaking flask cultivations. Our study somewhat differs from the others by considering not only carbon uptake alone but also the parallel consumption of nitrogen containing AAs. Consequently, the maximum value of 18.47 g C-mol^{-1} may reflect the total cellular capacity limit of processing carbon and nitrogen (via AAs) through metabolism and translation, whereas Y_{XC} of 17.6 g C-mol^{-1} mirrors limits of sugar uptake and metabolism. Interestingly, both values are similar which hints to optimized carbon-to-biomass conversion irrespective of the medium composition and to equally adjusted capacities for AA processing, i.e., protein formation.

Amino Acid Consumption of the *in vivo* and *in silico* Cell

The addition of an abundant supply of 18 AAs in minimal medium revealed three groups of AAs with distinctive consumption characteristics. AAs of the first group, consisting of Arg, His, Ile, Leu, Met, Phe, Ser, Thr, and Trp, were consumed according to AA-biomass composition. Biosynthesis pathways of most of these AAs, e.g., Met, Trp, or Phe, are energy-intensive, i.e., they have a positive net ATP-cost (**Supplementary Table S3**). Consequently, the cell safes energy when the AAs are consumed instead of being synthesized. The experimental observation agrees well with *in silico* analyses: growth rate-sensitivity studies revealed that the same AAs (apart from Thr and Ser) had the strongest influence on μ. Except for serving as AA building block like the other AAs, Ser may serve as carbon source in the absence of other available C-sources (Netzer et al., 2004). It is a precursor for synthesis of activated C_1-compounds and for L-cysteine synthesis (Wada and Takagi, 2006). The latter was not supplemented in the experiments.

The second group consisted of Asn, Gln, and Pro showing consumption rates more than threefold higher than expected

from the AA-biomass composition. In contrast, the third group of AAs (Ala, Asp, Glu, Gly, Lys, Val) was consumed remarkably below the expected threshold. The consumption rate of Gln was the highest of all AAs (0.694 mmol g^{-1} h^{-1}) and approximated the maximum uptake rate of the Gln transporter (Siewe et al., 1995; **Supplementary Table S1**). Notably, Gln may serve carbon and nitrogen demands at the same time being decomposed by hydrolysis or deamination via glutaminase Glsk or comparable enzymes (Buerger et al., 2016). Glu and ammonia are the products which correlates increased Gln uptake with the reduced need of Glu and ammonia consumption. In case of Glu, the inadequate consumption of the AA might have been caused by the presence of glucose in the medium causing catabolite repression (Krämer et al., 1990; Kronemeyer et al., 1995). Likewise, the aforementioned compensation via Gln uptake may explain the observed low Glu consumption rates. Taking Gln instead of Glu also saves ATP which would have been needed when Gln had to be synthesized from Glu via Gln synthase. Irrespective whether Glu is produced from Gln, taken up, or synthesized from alpha ketoglutarate via glutamate dehydrogenase, Glu may serve as amino donor in transaminase reactions such as aspartate transaminase (AspB) or alanine transferase (AlaT, Marienhagen and Eggeling, 2008) thereby forming Asp or Ala, respectively. Accordingly, Asp and Ala uptake rates are likely to be reduced as observed in the experiments. Ala itself may serve as amino donor for Val production via AvtA-reaction (Marienhagen and Eggeling, 2008) which finally links low Val, Ala, Asp, and Glu uptakes with tremendously high Gln consumption. For completion, Ala uptake via MetP (Trötschel et al., 2008; **Supplementary Table S1**) may have been hampered further by competition with Met, while Lange et al. (2003) showed that *C. glutamicum* WT cannot use Val as sole carbon or nitrogen source if supplemented in CGXII shaking flask experiments. Similar to Gln, the immense Asn uptake likewise reduced the uptake of other AAs of the Asp-family. Aparaginase AnsA which is suspected to act as an overflow enzyme (Mesas et al., 1990) might have been active to hydrolyze Asn to Asp and ammonia thereby minimizing the need for Asp uptake. Besides, Ziert (2014) showed that Asp is a poor nitrogen source, is even less attractive as carbon source, and was therefore not consumed in batch Asp supplementation experiments conducted in microflower plates. Interesting enough, Asp is a precursor for Lys biosynthesis which may explain why immense Asn uptake and its conversion to Asp may finally reduce Lys uptake to 26% of the biomass needs. The corresponding consumption rate (0.025 mmol g^{-1} h^{-1}) was in the same range as the Lys uptake determined in isotopic studies by Seep-Feldhaus et al. (1991) (0.015 mmol g^{-1} h^{-1}). Both rates are significantly lower than the rate needed to satisfy the composition demand at the measured growth rate of 0.468 h^{-1} (0.099 mmol g^{-1} h^{-1}). Summarizing, the immense uptake of Gln and Asn was likely to minimize the uptakes of Ala, Asp, Glu, Lys, and Val, which is also reflected by FBA assuming unlimited uptake of one single AA. In particular, Asn, Asp, Gln, and Glu, the protagonists of the transaminase network, revealed maximum (theoretical) uptake rates in addition to glucose (**Figure 4C**).

So far, no clear experimental observations give evidence on crucial Pro consumption (Bott and Niebisch, 2003; Jensen and Wendisch, 2013) although *putA* (*cg0129*) has been annotated in the genome of *C. glutamicum* encoding proline dehydrogenase which would ultimately provide Glu and NADH (Ling et al., 1994). Besides, the low consumption of Gly (14% with respect to the biomass composition) might be explained by its intracellular production via serine hydroxymethyltransferase being a by-product of 5,10-methylenetetrahydrofolate (MTHF) synthesis (Simic et al., 2002). FBA simulations supported the hypothesis: unlimited Gly uptake as a co-substrate of limited glucose uptake revealed that only 60% of the consumed Gly replenished the *in silico* cell's demand for Gly, while the remaining amount was available as by-product of the MTHF pathway.

CONCLUSION

In this two-staged study, physiological investigations were conducted to improve growth and nutrient consumption of the industrial production host *C. glutamicum*. Supplementation of minimal medium with complex compounds (BHI) relieved the strain of energy intensive biosynthesis, most likely of proteins and fatty acids, subsequently reducing the ATP demand of the cell. In turn, growth was accelerated to the WT strain's apparent maximum of 0.67 h^{-1} in 37 g BHI L^{-1}, while the TC consumption was proportionally increased. However, glucose consumption was only stimulated slightly under certain circumstances (1–10 g BHI L^{-1}) and revealed falling tendencies in rich environments. Besides, biomass carbon yields deduced from BHI and AA supplementation experiments revealed nutrient-irrespective limits of about 18 g C-mol^{-1} that may be a target of further strain engineering studies. Experimental consumption rates of 18 AAs under process-relevant conditions were reported, and Asn and Gln were identified as main protagonists due to their role in the transaminase network of *C. glutamicum*. FBA simulations with *iMG481* confirmed the experimental findings. Summarizing, the revealed AA uptake kinetics, the ranking of individual AA needs, observed AA exchange abilities, the properties of BHI supplementation, and the unraveled apparent limit of carbon-to-biomass conversion offer a highly fruitful basis for improving process productivities and for metabolic engineering. Such studies may expand the application of *C. glutamicum* not only as an AAs producer but also for the production of rather growth coupled products such as technical proteins.

AUTHOR CONTRIBUTIONS

MG designed the study, carried out the bioreactor experiments, analyzed the datasets, and drafted the manuscript. MG and JZ expanded the stoichiometric network model and performed the flux balance analyses. TH and AN analyzed the datasets and corrected the manuscript. BB and RT conceived the whole study and corrected the manuscript. All authors read and approved the final manuscript.

FUNDING

The authors gratefully acknowledge the funding of this work by the German Federal Ministry of Education and Research (BMBF; Grant 031A302A).

ACKNOWLEDGMENTS

We thank Anna-Lena Mayer, Salaheddine Laghrami, and Andreas Freund for excellent support with bioreactor fermentations, as well as Mira Lenfers-Lücker for assistance with the HPLC analyses. Moreover, we thank all members of the 0.6 plus project group for valuable comments on the topic and for their great cooperation.

SUPPLEMENTARY MATERIAL

The Supplementary Material for this article can be found online at: https://www.frontiersin.org/articles/10.3389/fmicb.2018.02058/full#supplementary-material

REFERENCES

Baev, M. V., Baev, D., Radek, A. J., and Campbell, J. W. (2006a). Growth of *Escherichia coli* MG1655 on LB medium: monitoring utilization of sugars, alcohols, and organic acids with transcriptional microarrays. *Appl. Microbiol. Biotechnol.* 71, 310–316. doi: 10.1007/s00253-006-0317-6

Baev, M. V., Baev, D., Radek, A. J., and Campbell, J. W. (2006b). Growth of *Escherichia coli* MG1655 on LB medium: monitoring utilization of amino acids, peptides, and nucleotides with transcriptional microarrays. *Appl. Microbiol. Biotechnol.* 71, 317–322. doi: 10.1007/s00253-005-0310-5

Baev, M. V., Baev, D., Radek, A. J., and Campbell, J. W. (2006c). Growth of *Escherichia coli* MG1655 on LB medium: determining metabolic strategy with transcriptional microarrays. *Appl. Microbiol. Biotechnol.* 71, 323–328. doi: 10.1007/s00253-006-0392-8

Bäumchen, C., Knoll, A., Husemann, B., Seletzky, J., Maier, B., Dietrich, C., et al. (2007). Effect of elevated dissolved carbon dioxide concentrations on growth of *Corynebacterium glutamicum* on D-glucose and L-lactate. *J. Biotechnol.* 128, 868–874. doi: 10.1016/j.jbiotec.2007.01.001

Becker, J., and Wittmann, C. (2012). Bio-based production of chemicals, materials and fuels–*Corynebacterium glutamicum* as versatile cell factory. *Curr. Opin. Biotechnol.* 23, 631–640. doi: 10.1016/j.copbio.2011.11.012

Blombach, B., Buchholz, J., Busche, T., Kalinowski, J., and Takors, R. (2013). Impact of different CO2/HCO3- levels on metabolism and regulation in *Corynebacterium glutamicum*. *J. Biotechnol.* 168, 331–340. doi: 10.1016/j.jbiotec.2013.10.005

Bott, M., and Niebisch, A. (2003). The respiratory chain of *Corynebacterium glutamicum*. *J. Biotechnol.* 104, 129–153. doi: 10.1016/S0168-1656(03)00144-5

Bröer, S., and Krämer, R. (1990). Lysine uptake and exchange in *Corynebacterium glutamicum*. *J. Bacteriol.* 172, 7241–7248. doi: 10.1128/jb.172.12.7241-7248.1990

Buchholz, J., Graf, M., Blombach, B., and Takors, R. (2014a). Improving the carbon balance of fermentations by total carbon analyses. *Biochem. Eng. J.* 90, 162–169. doi: 10.1016/j.bej.2014.06.007

Buchholz, J., Graf, M., Freund, A., Busche, T., Kalinowski, J., Blombach, B., et al. (2014b). CO 2/HCO 3- perturbations of simulated large scale gradients in a scale-down device cause fast transcriptional responses in *Corynebacterium glutamicum*. *Appl. Microbiol. Biotechnol.* 98, 8563–8572. doi: 10.1007/s00253-014-6014-y

Buerger, J., Rehm, N., Grebenstein, L., and Burkovski, A. (2016). Glutamine metabolism of *Corynebacterium glutamicum*: role of the glutaminase GlsK. *FEMS Microbiol. Lett.* 363:fnw230. doi: 10.1093/femsle/fnw230

Burkovski, A., Weil, B., and Krämer, R. (1996). Characterization of a secondary uptake system for L-glutamate in *Corynebacterium glutamicum*. *FEMS Microbiol. Lett.* 136, 169–173. doi: 10.1111/j.1574-6968.1996.tb08044.x

Cocaign-Bousquet, M., Guyonvarch, A., and Lindley, N. D. (1996). Growth rate-dependent modulation of carbon Flux through central metabolism and the kinetic consequences for glucose-limited chemostat cultures of *Corynebacterium glutamicum*. *Appl. Environ. Microbiol.* 62, 429–436.

Coello, N., Montiel, E., Concepcion, M., and Christen, P. (2002). Optimisation of a culture medium containing fish silage for L-lysine production by *Corynebacterium glutamicum*. *Bioresour. Technol.* 85, 207–211. doi: 10.1016/S0960-8524(02)00084-6

Cox, R. A. (2004). Quantitative relationships for specific growth rates and macromolecular compositions of *Mycobacterium tuberculosis*, *Streptomyces coelicolor* A3(2) and *Escherichia coli* B/r: an integrative theoretical approach. *Microbiology* 150, 1413–1426. doi: 10.1099/mic.0.26560-0

Dominguez, H., Cocaign-Bousquet, M., and Lindley, N. D. (1997). Simultaneous consumption of glucose and fructose from sugar mixtures during batch growth of *Corynebacterium glutamicum*. *Appl. Microbiol. Biotechnol.* 47, 600–603. doi: 10.1007/s002530050980

Dominguez, H., Nezondet, C., Lindley, N. D., and Cocaign, M. (1993). Modified carbon flux during oxygen limited growth of *Corynebacterium glutamicum* and the consequences for amino acid overproduction. *Biotechnol. Lett.* 15, 449–454. doi: 10.1007/BF00129316

Frunzke, J., Engels, V., Hasenbein, S., Gätgens, C., and Bott, M. (2008). Co-ordinated regulation of gluconate catabolism and glucose uptake in *Corynebacterium glutamicum* by two functionally equivalent transcriptional regulators, GntR1 and GntR2. *Mol. Microbiol.* 67, 305–322. doi: 10.1111/j.1365-2958.2007.06020.x

Gong, S., Richard, H., and Foster, J. W. (2003). YjdE (AdiC) is the arginine: agmatine antiporter essential for arginine-dependent acid resistance in *Escherichia coli*. *J. Bacteriol.* 185, 4402–4409. doi: 10.1128/JB.185.15.4402-4409.2003

Gourdon, P., Raherimandimby, M., Dominguez, H., Cocaign-Bousquet, M., and Lindley, N. D. (2003). Osmotic stress, glucose transport capacity and consequences for glutamate overproduction in *Corynebacterium glutamicum*. *J. Biotechnol.* 104, 77–85. doi: 10.1016/S0168-1656(03)00165-2

Grünberger, A., van Ooyen, J., Paczia, N., Rohe, P., Schiendzielorz, G., Eggeling, L., et al. (2013). Beyond growth rate 0.6: *Corynebacterium glutamicum* cultivated in highly diluted environments. *Biotechnol. Bioeng.* 110, 220–228. doi: 10.1002/bit.24616

Heirendt, L., Arreckx, S., Pfau, T., Mendoza, S. N., Richelle, A., Heinken, A., et al. (2017). Creation and analysis of biochemical constraint-based models: the COBRA Toolbox v3.0. [Preprint]. Available at: https://arxiv.org/abs/1710.04038

Hermann, T. (2003). Industrial production of amino acids by coryneform bacteria. *J. Biotechnol.* 104, 155–172. doi: 10.1016/S0168-1656(03)00149-4

Ikeda, M., and Nakagawa, S. (2003). The *Corynebacterium glutamicum* genome: features and impacts on biotechnological processes. *Appl. Microbiol. Biotechnol.* 62, 99–109. doi: 10.1007/s00253-003-1328-1

Ingraham, J. L., Maaløe, O., and Neidhardt, F. C. (1983). *Growth of the Bacterial Cell*. Sunderland, MA: Sinauer Associates.

Jensen, J. V. K., and Wendisch, V. F. (2013). Ornithine cyclodeaminase-based proline production by *Corynebacterium glutamicum*. *Microb. Cell Fact.* 12:63. doi: 10.1186/1475-2859-12-63

Jeon, J. M., Song, E. J., and Lee, H. W. (2013). Media optimization of *Corynebacterium glutamicum* for succinate production under oxygen-deprived condition. *J. Microbiol. Biotechnol.* 23, 211–217. doi: 10.4014/jmb.1206.06057

Kabus, A., Georgi, T., Wendisch, V. F., and Bott, M. (2007). Expression of the *Escherichia coli pntAB* genes encoding a membrane-bound transhydrogenase in *Corynebacterium glutamicum* improves L-lysine formation. *Appl. Microbiol. Biotechnol.* 75, 47–53. doi: 10.1007/s00253-006-0804-9

Kaleta, C., Schäuble, S., Rinas, U., and Schuster, S. (2013). Metabolic costs of amino acid and protein production in *Escherichia coli*. *Biotechnol. J.* 8, 1105–1114. doi: 10.1002/biot.201200267

Kalinowski, J., Bathe, B., Bartels, D., Bischoff, N., Bott, M., Burkovski, A., et al. (2003). The complete *Corynebacterium glutamicum* ATCC 13032 genome sequence and its impact on the production of L-aspartate-derived amino acids and vitamins. *J. Biotechnol.* 104, 5–25. doi: 10.1016/S0168-1656(03)00154-8

Käß, F., Hariskos, I., Michel, A., Brandt, H. J., Spann, R., Junne, S., et al. (2014a). Assessment of robustness against dissolved oxygen/substrate oscillations for *C. glutamicum DM*1933 in two-compartment bioreactor. *Bioprocess Biosyst. Eng.* 37, 1151–1162. doi: 10.1007/s00449-013-1086-0

Käß, F., Junne, S., Neubauer, P., Wiechert, W., and Oldiges, M. (2014b). Process inhomogeneity leads to rapid side product turnover in cultivation of *Corynebacterium glutamicum*. *Microb. Cell Fact.* 13:6. doi: 10.1186/1475-2859-13-6

Kimura, K. (1963). The effect of biotin on the amino acid biosynthesis by *Micrococcus glutamicus*. *J. Gen. Appl. Microbiol.* 9, 205–212. doi: 10.2323/jgam.9.205

Kind, S., Jeong, W. K., Schröder, H., Zelder, O., and Wittmann, C. (2010). Identification and elimination of the competing N-acetyldiaminopentane pathway for improved production of diaminopentane by *Corynebacterium glutamicum*. *Appl. Environ. Microbiol.* 76, 5175–5180. doi: 10.1128/AEM.00834-10

Kinoshita, S., Udaka, S., and Shimono, M. (1957). Studies on the amino acid fermentation. *J. Gen. Appl. Microbiol.* 3, 193–205. doi: 10.2323/jgam.3.193

Kjeldsen, K. R., and Nielsen, J. (2009). In silico genome-scale reconstruction and validation of the *Corynebacterium glutamicum* metabolic network. *Biotechnol. Bioeng.* 102, 583–597. doi: 10.1002/bit.22067

Krämer, R., Lambert, C., Hoischen, C., and Ebbighausen, H. (1990). Uptake of glutamate in *Corynebacterium glutamicum*. *Eur. J. Biochem.* 194, 929–935. doi: 10.1111/j.1432-1033.1990.tb19488.x

Kronemeyer, W., Peekhaus, N., Krämer, R., Sahm, H., and Eggeling, L. (1995). Structure of the *gluABCD* cluster encoding the glutamate uptake system of *Corynebacterium glutamicum*. *J. Bacteriol.* 177, 1152–1158. doi: 10.1128/jb.177.5.1152-1158.1995

Lange, C., Rittmann, D., Wendisch, V. F., Bott, M., and Sahm, H. (2003). Global expression profiling and physiological characterization of *Corynebacterium glutamicum* grown in the presence of L-valine. *Appl. Environ. Microbiol.* 69, 2521–2532. doi: 10.1128/AEM.69.5.2521-2532.2003

Lange, J., Müller, F., Bernecker, K., Dahmen, N., Takors, R., and Blombach, B. (2017). Valorization of pyrolysis water: a biorefinery side stream, for 1, 2-propanediol production with engineered *Corynebacterium glutamicum*. *Biotechnol. Biofuels* 10:277. doi: 10.1186/s13068-017-0969-8

Lee, J., Sim, S. J., Bott, M., Um, Y., Oh, M. K., and Woo, H. M. (2014). Succinate production from CO2-grown microalgal biomass as carbon source using engineered *Corynebacterium glutamicum* through consolidated bioprocessing. *Sci. Rep.* 4:5819. doi: 10.1038/srep05819

Liebl, W. (2006). "Corynebacterium–nonmedical," in *The Prokaryotes*, eds M. Dworkin and S. Falkow (New York, NY: Springer), 796–818. doi: 10.1007/0-387-30743-5_30

Ling, M., Allen, S. W., and Wood, J. M. (1994). Sequence analysis identifies the proline dehydrogenase and Δ1-pyrroline-5-carboxylate dehydrogenase domains of the multifunctional *Escherichia coli* PutA protein. *J. Mol. Biol.* 243, 950–956. doi: 10.1006/jmbi.1994.1696

Marienhagen, J., and Eggeling, L. (2008). Metabolic function of *Corynebacterium glutamicum* aminotransferases AlaT and AvtA and impact on L-valine production. *Appl. Environ. Microbiol.* 74, 7457–7462. doi: 10.1128/AEM.01025-08

Marin, K., and Krämer, R. (2007). "Amino acid transport systems in biotechnologically relevant bacteria," in *Amino Acid Biosynthesis - Pathways, Regulation and Metabolic Engineering*, ed. V. F. Wendisch (Berlin: Springer), 289–325.

Marx, A., de Graaf, A. A., Wiechert, W., Eggeling, L., and Sahm, H. (1996). Determination of the fluxes in the central metabolism of *Corynebacterium glutamicum* by nuclear magnetic resonance spectroscopy combined with metabolite balancing. *Biotechnol. Bioeng.* 49, 111–129. doi: 10.1002/(SICI)1097-0290(19960120)49:2<111::AID-BIT1>3.0.CO;2-T

Marx, A., Striegel, K., de Graaf, A. A., and Eggeling, L. (1997). Response of central metabolism of *Corynebacterium glutamicum* to different flux burdens. *Biotechnol. Bioeng.* 56, 168–180. doi: 10.1002/(SICI)1097-0290(19971020)56:2

Mesas, J. M., Gil, J. A., and Martín, J. F. (1990). Characterization and partial purification of L-asparaginase from *Corynebacterium glutamicum*. *Microbiology* 136, 515–519. doi: 10.1099/00221287-136-3-515

Michel, A., Koch-Koerfges, A., Krumbach, K., Brocker, M., and Bott, M. (2015). Anaerobic growth of *Corynebacterium glutamicum* via mixed-acid fermentation. *Appl. Environ. Microbiol.* 81, 7496–7508. doi: 10.1128/AEM.02413-15

Monod, J. (1949). The growth of bacterial cultures. *Annu. Rev. Microbiol.* 3, 371–394. doi: 10.1146/annurev.mi.03.100149.002103

Netzer, R., Peters-Wendisch, P., Eggeling, L., and Sahm, H. (2004). Cometabolism of a nongrowth substrate: L-serine utilization by *Corynebacterium glutamicum*. *Appl. Environ. Microbiol.* 70, 7148–7155. doi: 10.1128/AEM.70.12.7148-7155.2004

Nieß, A., Failmezger, J., Kuschel, M., Siemann-Herzberg, M., and Takors, R. (2017). Experimentally validated model enables debottlenecking of in vitro protein synthesis and identifies a control shift under *in vivo* conditions. *ACS Synth. Biol.* 6, 1913–1921. doi: 10.1021/acssynbio.7b00117

Nishimura, T., Vertès, A. A., Shinoda, Y., Inui, M., and Yukawa, H. (2007). Anaerobic growth of *Corynebacterium glutamicum* using nitrate as a terminal electron acceptor. *Appl. Microbiol. Biotechnol.* 75, 889–897. doi: 10.1007/s00253-007-0879-y

Okino, S., Inui, M., and Yukawa, H. (2005). Production of organic acids by *Corynebacterium glutamicum* under oxygen deprivation. *Appl. Microbiol. Biotechnol.* 68, 475–480. doi: 10.1007/s00253-005-1900-y

Palmieri, L., Berns, D., Krämer, R., and Eikmanns, M. (1996). Threonine diffusion and threonine transport in *Corynebacterium glutamicum* and their role in threonine production. *Arch. Microbiol.* 165, 48–54. doi: 10.1007/s002030050295

Pfelzer, N. (2016). *Experimentelle Bestimmung zellulärer Energiezustände und Analyse des Glykogenstoffwechsels in Corynebacterium glutamicum*. Doctoral dissertation, Aachen, RWTH Aachen University.

Sambrook, J. (2001). *Molecular Cloning: A Laboratory Manual*. Cold Spring Harbor, NY: Cold Spring Harbor Laboratory Press.

Sauer, U., Canonaco, F., Heri, S., Perrenoud, A., and Fischer, E. (2004). The soluble and membrane-bound transhydrogenases UdhA and PntAB have divergent functions in NADPH metabolism of *Escherichia coli*. *J. Biol. Chem.* 279, 6613–6619. doi: 10.1074/jbc.M311657200

Scheele, S., Oertel, D., Bongaerts, J., Evers, S., Hellmuth, H., Maurer, K. H., et al. (2013). Secretory production of an FAD cofactor-containing cytosolic enzyme (sorbitol–xylitol oxidase from *Streptomyces coelicolor*) using the twin-arginine translocation (Tat) pathway of *Corynebacterium glutamicum*. *Microb. Biotechnol.* 6, 202–206. doi: 10.1111/1751-7915.12005

Seep-Feldhaus, A. H., Kalinowski, J., and Pühler, A. (1991). Molecular analysis of the *Corynebacterium glutamicum* gene involved in lysine uptake. *Mol. Microbiol.* 5, 2995–3005. doi: 10.1111/j.1365-2958.1991.tb01859.x

Sezonov, G., Joseleau-Petit, D., and D'Ari, R. (2007). *Escherichia coli* physiology in Luria-Bertani broth. *J. Bacteriol.* 189, 8746–8749. doi: 10.1128/JB.01368-07

Shang, X., Zhang, Y., Zhang, G., Chai, X., Deng, A., Liang, Y., et al. (2013). Characterization and molecular mechanism of AroP as an aromatic amino acid and histidine transporter in *Corynebacterium glutamicum*. *J. Bacteriol.* 195, 5334–5342. doi: 10.1128/JB.00971-13

Shinfuku, Y., Sorpitiporn, N., Sono, M., Furusawa, C., Hirasawa, T., and Shimizu, H. (2009). Development and experimental verification of a genome-scale metabolic model for *Corynebacterium glutamicum*. *Microb. Cell Fact.* 8:43. doi: 10.1186/1475-2859-8-43

Siewe, R. M., Weil, B., and Krämer, R. (1995). Glutamine uptake by a sodium-dependent secondary transport system in *Corynebacterium glutamicum*. *Arch. Microbiol.* 164, 98–103. doi: 10.1007/BF02525314

Simic, P., Willuhn, J., Sahm, H., and Eggeling, L. (2002). Identification of *glyA* (encoding serine hydroxymethyltransferase) and its use together with the exporter ThrE to increase L-threonine accumulation by *Corynebacterium glutamicum*. *Appl. Environ. Microbiol.* 68, 3321–3327. doi: 10.1128/AEM.68.7.3321-3327.2002

Takors, R., Bathe, B., Rieping, M., Hans, S., Kelle, R., and Huthmacher, K. (2007). Systems biology for industrial strains and fermentation processes—example: amino acids. *J. Biotechnol.* 129, 181–190. doi: 10.1016/j.jbiotec.2007.01.031

Tao, H., Bausch, C., Richmond, C., Blattner, F. R., and Conway, T. (1999). Functional genomics: expression analysis of *Escherichia coli* growing on minimal and rich media. *J. Bacteriol.* 181, 6425–6440.

Trötschel, C., Follmann, M., Nettekoven, J. A., Mohrbach, T., Forrest, L. R., Burkovski, A., et al. (2008). Methionine uptake in *Corynebacterium glutamicum* by MetQNI and by MetPS, a novel methionine and alanine importer of the NSS neurotransmitter transporter family. *Biochemistry* 47, 12698–12709. doi: 10.1021/bi801206t

Unthan, S., Grünberger, A., van Ooyen, J., Gätgens, J., Heinrich, J., Paczia, N., et al. (2014). Beyond growth rate 0.6: what drives *Corynebacterium glutamicum* to higher growth rates in defined medium. *Biotechnol. Bioeng.* 111, 359–371. doi: 10.1002/bit.25103

Varma, A., Boesch, B., and Palsson, B. (1993). Stoichiometric interpretation of *Escherichia coli* glucose catabolism under various oxygenation rates. *Appl. Environ. Microbiol.* 59, 2465–2473.

Vertès, A. A., Inui, M., and Yukawa, H. (2012). Postgenomic approaches to using corynebacteria as biocatalysts. *Annu. Rev. Microbiol.* 66, 521–550. doi: 10.1146/annurev-micro-010312-105506

Wada, M., and Takagi, H. (2006). Metabolic pathways and biotechnological production of L-cysteine. *Appl. Microbiol. Biotechnol.* 73, 48–54. doi: 10.1007/s00253-006-0587-z

Wendisch, V. F., Bott, M., and Eikmanns, B. J. (2006). Metabolic engineering of *Escherichia coli* and *Corynebacterium glutamicum* for biotechnological production of organic acids and amino acids. *Curr. Opin. Microbiol.* 9, 268–274. doi: 10.1016/j.mib.2006.03.001

Wendisch, V. F., Brito, L. F., Lopez, M. G., Hennig, G., Pfeifenschneider, J., Sgobba, E., et al. (2016). The flexible feedstock concept in industrial biotechnology: metabolic engineering of *Escherichia coli*, *Corynebacterium glutamicum*, *Pseudomonas*, *Bacillus* and yeast strains for access to alternative carbon sources. *J. Biotechnol.* 234, 139–157. doi: 10.1016/j.jbiotec.2016.07.022

Wendisch, V. F., de Graaf, A. A., Sahm, H., and Eikmanns, B. J. (2000). Quantitative determination of metabolic fluxes during coutilization of two carbon sources: comparative analyses with *Corynebacterium glutamicum* during growth on acetate and/or glucose. *J. Bacteriol.* 182, 3088–3096. doi: 10.1128/JB.182.11.3088-3096.2000

Wieschalka, S., Blombach, B., and Eikmanns, B. J. (2012). Engineering *Corynebacterium glutamicum* for the production of pyruvate. *Appl. Microbiol. Biotechnol.* 94, 449–459. doi: 10.1007/s00253-011-3843-9

Zelle, E., Nöh, K., and Wiechert, W. (2015). "Growth and production capabilities of *Corynebacterium glutamicum*: interrogating a genome-scale metabolic network model", in *Corynebacterium glutamicum: from Systems Biology to Biotechnological Applications*, ed. A. Burkovski (Norfolk, VA: Caister Academic Press), 39–54. doi: 10.21775/9781910190050.04

Zhang, Y., Cai, J., Shang, X., Wang, B., Liu, S., Chai, X., et al. (2017). A new genome-scale metabolic model of *Corynebacterium glutamicum* and its application. *Biotechnol. Biofuels* 10:169. doi: 10.1186/s13068-017-0856-3

Ziert, C. (2014). *Metabolic Engineering of Corynebacterium glutamicum for the Production of L-aspartate and its Derivatives* β*-Alanine and Ectoine*. Doctoral dissertation, Bielefeld, Universität Bielefeld

Conflict of Interest Statement: The authors declare that the research was conducted in the absence of any commercial or financial relationships that could be construed as a potential conflict of interest.

B. Manuscript 2

'Continuous Adaptive Evolution of a Fast-Growing *Corynebacterium glutamicum* Strain Independent of Protocatechuate'

frontiers in Microbiology

ORIGINAL RESEARCH
published: 06 August 2019
doi: 10.3389/fmicb.2019.01648

Continuous Adaptive Evolution of a Fast-Growing *Corynebacterium glutamicum* Strain Independent of Protocatechuate

*Michaela Graf[1†], Thorsten Haas[1†], Felix Müller[1], Anina Buchmann[1], Julia Harm-Bekbenbetova[1], Andreas Freund[1], Alexander Nieß[1], Marcus Persicke[2], Jörn Kalinowski[2], Bastian Blombach[1,3] and Ralf Takors[1]**

[1]Institute of Biochemical Engineering, University of Stuttgart, Stuttgart, Germany, [2]Center for Biotechnology (CeBiTec), Bielefeld University, Bielefeld, Germany, [3]Microbial Biotechnology, Campus Straubing for Biotechnology and Sustainability, Technical University of Munich, Straubing, Germany

OPEN ACCESS

Edited by:
George Tsiamis,
University of Patras, Greece

Reviewed by:
Nicolai Kallscheuer,
Radboud University Nijmegen, Netherlands
João Manuel Pereira Jorge,
University of Porto, Portugal

***Correspondence:**
Ralf Takors
takors@ibvt.uni-stuttgart.de

Specialty section:
This article was submitted to Systems Microbiology, a section of the journal Frontiers in Microbiology

[†]These authors have contributed equally to this work

Received: 16 March 2019
Accepted: 03 July 2019
Published: 06 August 2019

Citation:
Graf M, Haas T, Müller F, Buchmann A, Harm-Bekbenbetova J, Freund A, Nieß A, Persicke M, Kalinowski J, Blombach B and Takors R (2019) Continuous Adaptive Evolution of a Fast-Growing Corynebacterium glutamicum Strain Independent of Protocatechuate. Front. Microbiol. 10:1648. doi: 10.3389/fmicb.2019.01648

Corynebacterium glutamicum is a commonly applied host for the industrial production of amino acids. While valued for its robustness, it is somewhat inferior to competing strains such as *Escherichia coli* because of the relatively low growth rate of 0.40 h^{-1} in synthetic, industrial media. Accordingly, adaptive laboratory evolution (ALE) experiments were performed in continuous cultivation mode to select for a growth-improved host. To ensure industrial attractiveness, this ALE study aimed at a reduction of dependency on costly growth-boosting additives such as protocatechuate (PCA) or complex media supplements. Consequently, double selection pressures were installed consisting of a steady increase in growth rate demands and a parallel reduction of complex medium fractions. Selection yielded *C. glutamicum* EVO5 achieving 0.54 h^{-1} and 1.03 $g_{Glc}\ g_{CDW}^{-1}\ h^{-1}$ in minimal medium without abovementioned supplements. Sequencing revealed 10 prominent mutations, three of them in key regulator genes.

Keywords: *Corynebacterium glutamicum*, adaptive laboratory evolution, continuous adaptive evolution, increased growth, protocatechuate, RamA, DtxR, RpoA

INTRODUCTION AND MOTIVATION

Microbial bioprocesses play a major role in the production of biofuels, foods, food ingredients, feeds, cosmetics, and pharmaceuticals (Straathof, 2013). To ensure their economic competitiveness, processes are developed such that their performance is ideal under large-scale production conditions by either optimizing the producing biocatalysts, i.e., pro-/eukaryotic organisms or cellular parts (for example enzymes), or the surrounding process conditions. The latter comprises elements such as technical process setup, production strategy and corresponding process parameters, and the cultivation medium. Most often, the technical equipment is established in a production plant limiting optimization procedures to the process format and to the process parameters. Production media can be optimized regarding complexity and cost by utilization of simple salts as nitrogen-, phosphorus-, and sulfur sources and a cheap carbon source, e.g., molasses or corn steep liquor. Apart from extracellular process parameters, the

production host can be improved as well. For this, metabolic engineering strategies, optionally combined with omics techniques (Becker and Wittmann, 2018), are applied to influence cell-specific attributes, e.g., growth rate, substrate spectrum, and uptake rate, or production rate, ultimately boosting productivity (Löffler et al., 2016; Nielsen and Keasling, 2016; Michalowski et al., 2017) or reducing cultivation media costs.

In contrast to targeted genome alterations applied in metabolic engineering, adaptive laboratory evolution (ALE) is used as a more traditional way to optimize the same attributes of a production organism (Dragosits and Mattanovich, 2013; LaCroix et al., 2015; Sandberg et al., 2016; Rugbjerg et al., 2018; Stella et al., 2019). In an ALE experiment, cells are exposed to specific selection pressures by creating clearly defined environmental conditions for a prolonged time period. Thereby, formation of evolved subpopulations is promoted and populations best adapted to the installed growth environment outperform the residual ones. This increase in fitness is caused by mutations in the genome of the evolved strain and is extrinsically observable by changed phenotypic characteristics, e.g., higher biomass-substrate yields, higher substrate consumption rates, or higher growth rates (Dettman et al., 2012; Ryall et al., 2012). Thus, ALE can be used in an industrial context to select for favorable mutations in a production host, e.g., robustness to (toxic) by-products (Tremblay et al., 2015; Mohamed et al., 2017; McCloskey et al., 2018), or adaption to non-native carbon sources (Lee and Palsson, 2010). In general, an ALE is performed in either batch or continuous process mode. While repetitive batch experiments are easy to conduct, environmental process conditions vary strongly. Besides decreasing nutrient supply and increasing population densities, pH and dissolved oxygen additionally fluctuate in non-controlled batch reactors such as shake flasks, potentially biasing the pursued outcome of the ALE. To prevent this, continuous bioreactors (e.g., chemostats) are employed to provide controlled process conditions, constant nutrient supply, and consequently constant population densities. Compared to repetitive batches, experimental efforts and costs of chemostats are potentially higher but justified considering that desired mutations are more likely to occur than in a batch ALE experiment (Dragosits and Mattanovich, 2013).

In this study, the Gram-positive microorganism *Corynebacterium glutamicum* was cultivated in a chemostat ALE experiment. This bacterium is considered an industrial workhorse of industrial biotechnology and has been engineered for production of numerous compounds, e.g., organic acids (Wieschalka et al., 2013), amino acids (Wendisch et al., 2016), bio-based fuels (Becker and Wittmann, 2012), diamines (Wendisch et al., 2018), heterologous proteins (Freudl, 2017), and grows on a wide range of substrates (summarized in Becker et al., 2016). Moreover, *C. glutamicum* shows physiological attributes that agree with large-scale production conditions: it is facultative anaerobic (Nishimura et al., 2007) and can endure fluctuating substrate concentrations, dissolved CO_2 (Bäumchen et al., 2007; Blombach et al., 2013) and pH gradients (Follmann et al., 2009), and cannot be lysed by bacteriophages. Nevertheless, the most obvious drawback of this workhorse is the relatively small maximum growth rate (μ) of about 0.4 h^{-1} under conventional growth conditions using synthetic media, and of 0.6 h^{-1} installing specific process formats (Bäumchen et al., 2007; Grünberger et al., 2013) or growth media (Unthan et al., 2014; Graf et al., 2018). Considering that the overall process productivity is positively influenced by high growth rates for growth-coupled (Feist et al., 2009) and growth-decoupled cultivations, increasing μ would further boost the attractiveness of *C. glutamicum* in industrial applications. For this reason, two independent ALE experiments were recently performed with *C. glutamicum*, and indeed, the growth rate could be increased by employing repetitive batch ALEs (Pfeifer et al., 2017; Wang et al., 2018). But as pointed out above, the growth environment of the producing cell is another parameter that can be simultaneously targeted in an ALE to increase the overall process performance. In most (research-related) applications, *C. glutamicum* is cultivated in the standard mineral medium CGXII (Keilhauer et al., 1993; Kind et al., 2010) or MM (Liebl et al., 1989) with a carbon source of choice. Both media contain iron-chelators, i.e., protocatechuate (PCA, in CGXII) or catechol (in MM) that are believed to facilitate iron acquisition (Liebl et al., 1989) or may serve as additional carbon source fueling the citric acid cycle (Shen et al., 2012; Unthan et al., 2014). Aside from their unclear cellular function, especially PCA is a relatively costly medium component that is estimated to be 50–100 fold more expensive than the carbon source and should be prevented as additive to minimize media costs.

Consequently, this investigation had two aims: improving the growth performance of *C. glutamicum* and adapting the strain to an iron-chelator-free minimal medium. Thereby, both parameters should be optimized simultaneously to elevate cellular productivity that makes the organism an ideal choice for large-scale applications. To reach these goals, we employed a time-efficient serial continuous ALE concept and imposed increasingly challenging selection pressures on the strain. In that way, we especially aimed for the selection of mutations in regulatory genes that enhance the cell's performance in the desired ways. Following this approach, we subsequently sequenced evolved strains to gain insights into genome mutations.

MATERIALS AND METHODS

Genome Sequencing of *C. glutamicum* Strains ATCC 13032 and EVO5

For genome (re-)sequencing, DNA of *C. glutamicum* ATCC 13032 and the EVO5 strain was isolated by the NucleoSpin Microbial DNA Kit (Macherey-Nagel, Düren, Germany) according to the manufacturer's instructions. The Illumina TruSeq PCR-free sample preparation Kit was used for library preparation, which was sequenced on a MiSeq system (Illumina, San Diego, CA, USA) by paired-end sequencing with a read-length of 2 × 300 bases. The sequencing reads were assembled by Newbler v2.8 (Roche, Branford, CT, USA) and genome finishing was done using the Consed software (Gordon, 2003). For detection of SNPs, the genome sequence of EVO5 was aligned to the reference genome ATCC 13032 by the software Snapgene v4.3

(GSL Biotech, available at snapgene.com), whereby SNPs were automatically detected.

Bacterial Strains, Preculture, and Media

The wild-type strain *C. glutamicum* ATCC 13032 (WT) obtained from the American Type Culture Collection (ATCC, Manassas, VA, USA) was used in this study. *C. glutamicum* cells from a glycerol cell culture stock where spread on a 2× tryptone-yeast extract (YE) (2× TY, Sambrook, 2001) agar plate which was incubated at 30°C for 48 h. Subsequently, colonies extracted from the agar plate were used to inoculate 5 ml 2× TY medium in glass reaction tubes and incubated for 8 h at 30°C under constant agitation (120 rpm) on a bench-top rotary shaker (Infors HT, Bottmingen, Switzerland). Sterile 500 ml baffled shaking flasks were filled with 50 ml of modified minimal medium CGXII (Buchholz et al., 2014) supplemented with 4% (w/v) glucose. Individual pre-culture minimal medium flasks were inoculated with 5 ml from the pre-culture in glass reactions tubes and incubated overnight at 30°C and constant agitation (120 rpm).

Bioreactor Batch Cultivations

Characterization experiments of strains *C. glutamicum* WT and EVO 5 were performed in a bioreactor (Bioengineering, Wald, Switzerland) with a volume of 3 L, equipped with a six-blade Rushton impeller, a dissolved oxygen (pO_2)-, and pH-probe (Mettler Toledo GmbH, Albstadt, Germany). Off-gas analysis was enabled by non-dispersive (photometric) infrared gas analyzers ($BCPO_2$ and $BCPCO_2$, BlueSens, Herten, Germany) to determine molar O_2 and CO_2 fractions. Cultivations were conducted at 30°C and at a total pressure of 1.5 bar. pH was kept constant at 7.4 by titration with 25% (v/v) NH_4OH. Abundance of oxygen was ensured by keeping the oxygen saturation above 30% through increase of the impeller speed in steps of 50 rpm and by stepwise increase of the aeration rate by 0.15 L min^{-1}. The initial impeller speed was 250 rpm and the aeration rate 0.15 L min^{-1} (0.1 vvm). The amount of biomass needed to inoculate 1.5 L of media with an initial optical density (OD_{600}) of 1 was harvested from the pre-culture shaking flasks, centrifuged at 4,000 × *g* (5430 R, Eppendorf, Hamburg, Germany) for 10 min and 4°C and resuspended in 100 ml sterile 0.9% (w/v) NaCl solution. The resulting biosuspension was used to inoculate 1.4 L CGXII minimal medium (Buchholz et al., 2014) supplemented with 2% (w/v) glucose. Antifoam agent (Struktol® J 647, Schill + Seilacher, Hamburg, Germany) was added manually when necessary. Batch cultivations were performed in independent biological triplicates.

Continuous Evolution Experiments

Control Scheme of the Continuous Bioreactor

Continuous evolution experiments were performed with the same bioreactor setup as described in Section "Bioreactor Batch Cultivations." During the continuous process mode, feed medium was constantly added from a reservoir with a peristaltic pump (Watson Marlow 120 U/DV 200 RPM, Falmouth, UK) and simultaneously, the same volume of the fermentation broth was harvested with a second pump. An accurate feed rate was automatically ensured by a controller (**Figure 1**) that continuously monitored the weight of the harvested material (laboratory scale Combics 3, Sartorius, Göttingen, Germany). It converted the measured mass flow into volume flow (density of the biosuspension: 1.01 kg L^{-1}) and adjusted the influx by regulating the pumping speed when the deviation from the desired flux got larger than 2%. The reaction volume of 1.2 L was kept constant by monitoring the weight of the total reactor using a laboratory scale (Combics 3, Sartorius, Göttingen, Germany) and by automatically adjusting the speed of the harvest pump with a second controller which allowed deviation from the setpoint weight of 0.2%. This setup enabled setting dilution rates with a precision of 0.01 h^{-1}. The regulation scheme was implemented in a custom process control system using the software LabVIEW (LabVIEW® 2010, National Instruments, Austin, TX, USA).

Execution of the Evolution Experiments

To start a continuous evolution bioprocess, sterile medium from the feed reservoir containing CGXII minimal medium (Buchholz et al., 2014) supplemented with 1% (w/v) glucose and varying amounts of YE was pumped into the sterile bioreactor until a volume of 1.1 L was reached. A batch cultivation was initiated using the same protocol as described in Section "Bioreactor Batch Cultivations" with a total reaction volume of 1.2 L and initial aeration rate of 0.12 L min^{-1}. At the end of the batch phase, indicated by a sharp rise of the pO_2 signal, the stirrer speed was set to 650 rpm and the aeration rate to 1.2 L^{-1} (1 vvm). Next, feed and harvest pumps were started and the pumping speed adjusted so that the primary dilution rate was equal to the exponential growth rate determined during the batch phase. About 60 µl h^{-1} of antifoam agent was added constantly with a syringe pump (LA-30, Landgraf HLL, Langenhagen, Germany). Whenever a steady state was reached, indicated by constant process parameters (pO_2 and off-gas signals), the dilution rate was increased to approximate the maximum growth rate of *C. glutamicum* under current growth conditions. Additionally, the YE content of the feed medium was reduced stepwise as indicated in **Figure 2**. Each evolution experiment was performed for an average of 3 weeks. At the end of each experiment, samples of the presumably evolved strain were preserved in glycerol stocks and the most recent one was used to inoculate the following process.

Re-engineering of a Mutation From Evolved Strain EVO5 Into *C. glutamicum* Wild Type

To re-engineer the genomic *ramA* mutation (C → G at nucleotide position 302 in the gene) in *C. glutamicum* ATCC 13032 wild type (WT) that was identified in evolved strain EVO5 (c.f., Section "Mutations in Evolved Strain EVO5 and Growth Characterization") encoding RamA(S101C), the pK19*mobsacB* vector (Schäfer et al., 1994) was used.

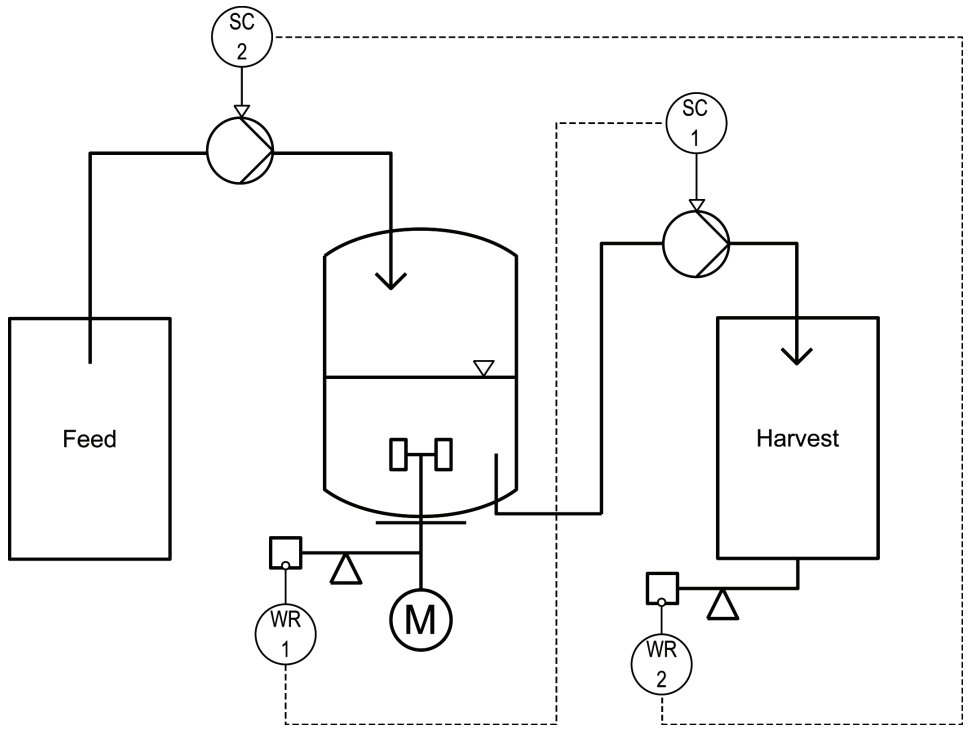

FIGURE 1 | Control scheme of the continuous bioreactor for installment of near wash-out dilution rates. The first controller ensured an accurate reaction volume of 1.2 L by using the bioreactor weight (WR 1) as setpoint and adjusting the pumping rate of the harvest pump (SC 1) if the deviation was >0.2%. An accurate feed rate was automatically installed with the second controller that used the weight of the harvest (WR 2) and deduced mass flow as setpoint to adjust the speed of the feeding pump (SC 2) if the deviation larger than 2%.

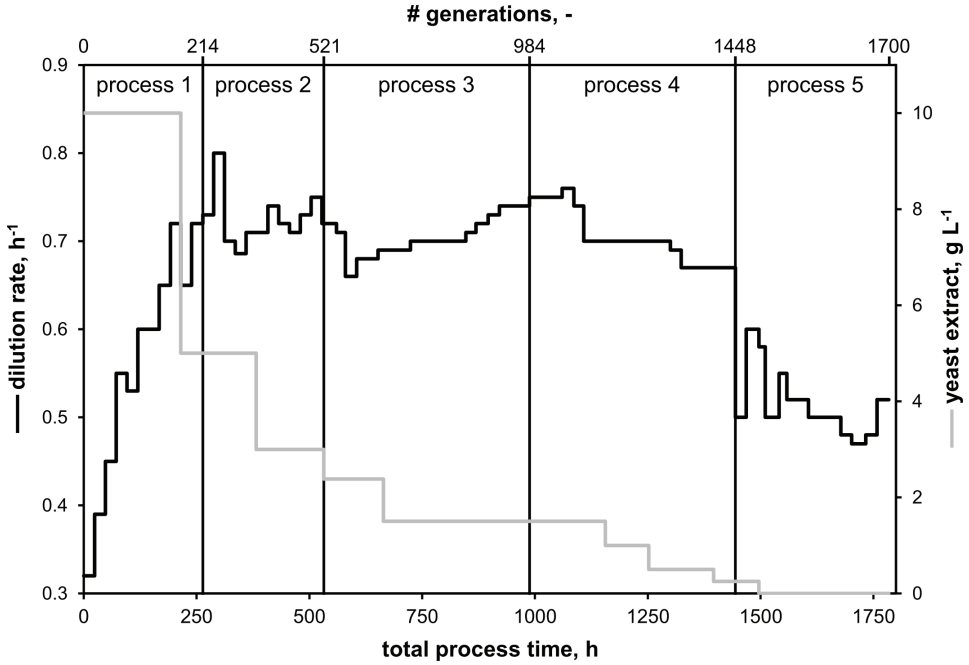

FIGURE 2 | Overview of continuous evolution processes starting with *C. glutamicum* WT. Five processes were conducted using CGXII minimal medium supplemented with 1% (w/v) glucose and varying amounts of yeast extract (YE). The set dilution rate equaled the growth rate of the culture. After the first process, following processes were inoculated with potentially mutated strains from the respective previous process.

The 500-bp sequences flanking the point mutation were amplified with the primer pairs fw_ramA-flank1 + rev_ramA-flank1 (upstream region) and fw_ramA-flank2 + rev_ramA-flank2 (downstream region), respectively. The C → G mutation itself was encoded in the primer rev_ramA-flank1 and fw_ramA-flank2, respectively (**Supplementary Table S1**, marked in bold letters). Amplification products were inserted simultaneously in *Hin*dIII and *Bam*HI linearized pK19*mobsacB* by isothermal assembling in accordance with the protocol provided by Gibson (2011) yielding pK19*mobsacB-ramA*(S101C). Plasmids were amplified in *Escherichia coli* DH5α and purified using a commercially available kit (*E.Z.N.A. Plasmid Mini kit I*, Omega Bio-Tek Inc., Norcross, Georgia, USA). The insert was free of undesired mutations as verified by sequencing with primers fw_pK19-seq and rev_pK19-seq (GATC light run service). The point mutation was eventually introduced in the genomic background of *C. glutamicum* WT by a cassette exchange using pK19*mobsacB-ramA*(S101C) with the work-flow outlined by Schäfer et al. (1994). Electrocompetent cells of *C. glutamicum* ATCC 13032 were prepared according to the protocol provided by Tauch et al. (2002) with slight modifications: cultures were harvested at an OD_{600} of 1.75 and washed three times with 10% (v/v) glycerol. Transformation of competent *C. glutamicum* cells with 300–800 ng of purified plasmid by electroporation (Eppendorf Eporator, 2,500 V, 2 mm gap width, achieving time constants of 4.3–4.7 ms) was carried out following the optimized protocol by van der Rest et al. (1999). Strains carrying the correct *ramA* mutation were identified by sequencing. The mutated region was amplified with primers fw_ramA-flank1 and rev_ramA-flank2 and sequenced with primer fw_ramA-seq and rev_ramA-seq. Oligonucleotide sequences are provided in **Supplementary Table S1**.

Analytical Methods

During batch cultivations in bioreactors, biosuspension was sampled hourly to determine the biomass concentration and the total inorganic carbon (TIC) species and to analyze substrate- and by-product concentrations in cell-free filtrates. Biomass formation was determined by measuring the OD_{600} (DR 3900, Dr. Lange, Berlin, Germany) and by preparation of cell-dry-weight (CDW) samples. For the latter, 1 ml biosuspension was washed twice in deionized water and centrifuged between each washing steps for 2 min at 20,173 × *g* and 4°C (5430 R, Eppendorf, Hamburg, Germany). The washed biomass was transferred to glass vials and dried for at least 24 h in a convection oven (Heraeus, Hanau, Germany) at 105°C. After cooling in a desiccator, vials were weighed on a micro-scale (AE 200, Mettler Toledo, Gießen, Germany). A correlation factor of 0.27 g L^{-1} for OD_{600}-measurements to CDW was obtained. Cell-free samples were produced by filtering the biosuspension through 0.2 µm pore size syringe filters (Rotilabo®, Carl Roth, Karlsruhe, Germany). The filtrates were stored at −20°C until measurement. Glucose and pyruvate concentrations were determined with enzymatic assays following the manufacturer's instructions (R-biopharma, Darmstadt, Germany). TIC amounts in biosuspension samples were determined as described by Buchholz et al. (2014) to correct for underestimated CO_2 values gained by off-gas analysis during the batch cultivations. Biomass formation during shaking flask main cultivations was determined using hourly OD_{600} measurements. During evolution experiments, OD_{600} and cell-free samples were taken at least once per day.

Determination of Kinetic Parameters

Growth Rate

The exponential growth rate (μ) in batch cultivations (shaking flask and bioreactor) was determined by linear regression of the logarithmic biomass concentration over the respective process time. During continuous bioprocesses, the set dilution rate (D) equals the growth rate since the feed rate and the bioreaction volume remained constant. This was ensured by the described controller scheme in Section "Control Scheme of the Continuous Bioreactor."

Consumption Rates and Yields

The biomass-substrate yield (Y_{XS}) was determined by linear regression of substrate and biomass concentration curves. The biomass-specific glucose consumption (q_{Glc}) of *C. glutamicum* strains was calculated by dividing the determined exponential growth rate or the installed dilution rate (D) by Y_{XS}.

Respiratory Rates

The biomass-specific respiratory rates $\left(q_{O_2}, q_{CO_2}\right)$ were obtained by dividing the volumetric oxygen consumption or carbon dioxide emission rates by the biomass concentration. As previously described (see above), the carbon dioxide emission rate was then corrected by TIC-measurements using a total carbon (TC) analyzer (Multi N/C 2100s, Analytik Jena, Jena, Germany).

RESULTS

Evolution Experiments

A total of five consecutive continuous bioreactor processes were conducted with the goal of increasing the growth rate of *C. glutamicum* with an evolutionary approach thereby selecting for the fastest-growing subpopulation. Minimal medium CGXII supplemented with 1% (w/v) glucose, omitting the standard CGXII component PCA (Keilhauer et al., 1993; Kind et al., 2010), and varying amounts of YE was used as growth medium. All processes are illustrated in **Figure 2** with the total process time as sum of all cultivations. By analogy, total numbers of generations are calculated from the respective dilution rates and corresponding time periods. The first cultivation started with *C. glutamicum* WT and supplementation of 10 g YE L^{-1} in the feed medium. The initial dilution rate (D), mirroring the growth rate, was increased stepwise from 0.32 to 0.72 h^{-1} within 8 days (d, corresponds to 142 generations, black curve in **Figure 2**) without any indication of culture wash out. Then, the amount of YE in the feed was reduced to 5 g L^{-1} (gray curve in **Figure 2**), and D was set to 0.65 h^{-1} to prevent a potential wash out. At process time 10 day, D was increased

to 0.72 h^{-1} without detectable loss of biomass. After 11 day, a sample of the biomass was harvested and preserved in glycerol stocks, and the process was stopped. The subsequent two continuous processes (c.f., **Figure 2**) were conducted in the same way: whenever stable process conditions were reached (indicated by off-gas analysis), *D* was increased and the amount of YE was decreased afterward (16 day: 3 g L^{-1}, 28 day: 1.5 g L^{-1}). Notably, the final subpopulation of the preceding process always served as the inoculum for the subsequent experiment. In the fourth process starting at process time 41 day and with 1.5 g YE L^{-1}, a maximum growth rate of 0.76 h^{-1} was set at approx. 42 day which had to be reduced to 0.7 h^{-1} due to the wash out of the culture. Thereupon, YE was reduced several times to 1 g L^{-1} (48 day), 0.5 g L^{-1} (52 day), and 0.25 g L^{-1} (58 day). During this process the dilution rate had to be lowered repeatedly to D = 0.67 h^{-1} to avoid a wash-out. After 62 day (1,490 generations), YE could be omitted completely from the feed medium. Hence, for the following 12 day of the last process, the strain was cultured in minimal medium with glucose as sole carbon source. The final evolved strain was able to sustain a stable growth rate of around 0.52 h^{-1}. Consequently, five potentially evolved strains were harvested over the course of the combined processes: EVO1 (214 generations), EVO2 (520 generations), EVO3 (984 generations), EVO4 (1,448 generations), and EVO5 (1,700 generations).

TABLE 1 | Mutations of *C. glutamicum* strain EVO5 deduced from the final continuous evolution processes (c.f., **Figure 2**).

Locus	Gene	Variant	Mutation/Deletion	Annotation
Pos. 3,168,391		Deletion	G	Intergenic region upstream of *copR*
cg2831	*ramA*	Mutation	S101C (G**G**A → G**C**A)	Bacterial regulatory protein, LuxR family
cg0655	*rpoA*	Mutation	S280F (G**G**A → G**A**A)	DNA-directed RNA polymerase alpha subunit
cg2067		Mutation	L91 V (**T**TG → **G**TG)	Hypothetical protein
cg2069	*psp1*	Mutation	P511 (CC**T** → CC**G**)	Putative secreted protein
cg2103	*dtxR*	Mutation	R103H (C**G**C → C**A**C)	Iron-dependent regulatory protein
cg2293		Deletion, Frameshift	T (nt 139), AA55 stop	Putative indole-3-glycerol phosphate synthase
cg2468		Mutation	N97D (**A**AC → **G**AC)	Branched-chain amino acid ABC-type transport system, permease component
cg2504		Mutation	R265 (CG**T** → CG**C**)	Hypothetical protein
cg2935	*nanP*	Mutation	A265 (GC**C** → GC**T**)	Neuraminidase

The positions of mutations are given in relation to the start codon of respective open reading frames from each gene. EVO5 was harvested after 1,700 generations in solely glucose-supplemented CGXII minimal medium [1% (w/v) glucose].

Mutations in Evolved Strain EVO5 and Growth Characterization

For the final evolved strain EVO5, whole-genome sequencing was applied to identify mutations in its entire genome (**Table 1**) revealing a total of 10 mutations. Among them were mutations in cg0655 (*rpoA*) encoding the DNA-directed RNA polymerase alpha subunit, cg2103 (*dtxR*) encoding the iron-dependent regulator DtxR, cg2831 (*ramA*) that encodes the global carbon regulator RamA, and cg2935 (*nanP*) coding for a neuraminidase. Additionally, mutations appeared in the intergenic region upstream of cg3285 (*copR*, encoding a putative response regulator), in cg2069 (*psp1*, coding for a putative secreted protein) in genes cg2293 and cg2468 that encode a putative indole-3-glycerol phosphate synthase and the permease component of a branched-chain amino acid ABC-type transport system, respectively, as well as in genes cg2067 and cg2504 that both code for hypothetical proteins.

Characterizations of *C. glutamicum* WT, EVO5, and re-engineered mutant strain *C. glutamicum* reRamA (Cg reRamA) were conducted in independent triplicates applying bioreactor batch cultivations. All strains were cultivated under the same conditions in minimal medium CGXII with 2% (w/v) glucose and without PCA. The kinetic parameters determined for each of these strains are listed in **Table 2**. The WT exhibited a growth rate of 0.34 ± 0.03 h^{-1}. EVO5 was characterized by a significantly enhanced growth rate of 0.54 ± 0.01 h^{-1}. This is an improvement of 58% toward the WT performance. Cg reRamA also revealed an elevated growth rate of 0.38 ± 0.03 h^{-1} compared to the WT. Glucose consumption (q_{Glc}) of EVO5 increased by 62% and that of Cg reRamA by 20% compared to the WT (0.64 ± 0.06 g g^{-1} h^{-1}). EVO5 showed likewise proportionally increased respiratory rates of $q_{O_2} = 9.14 \pm 0.31$ mmol g^{-1} h^{-1} and $q_{CO_2} = 9.70 \pm 0.18$ mmol g^{-1} h^{-1} while exhibiting a WT-like biomass-substrate yield of 0.52 ± 0.01 g g^{-1}. While respiratory rates of Cg reRamA were also proportionally increased with the growth rate ($q_{O_2} = 7.04 \pm 0.56$ mmol g^{-1} h^{-1}; $q_{CO_2} = 6.93 \pm 0.55$ mmol g^{-1} h^{-1}), its biomass-substrate yield was below that of the WT (0.49 ± 0.01 g g^{-1}).

Only pyruvate could be detected as by-product of the batch cultivations. Pyruvate concentration in the WT samples (black filled circles, **Figure 3**) started to rise between 3 and 4 h and peaked at about 7 h with a concentration of 60 mg L^{-1}. Afterward, this amount was completely consumed until the end of the processes (9–10 h). EVO5 (black open circles) built up concentrations of approx. 15 mg L^{-1} pyruvate in the medium during the first 3 h of the cultivation. In contrast to the WT, concentrations of pyruvate did not increase markedly and peaked at 5 h (23 mg L^{-1}). The by-product was completely consumed by EVO5 at the end of the cultivation. Cg reRamA accumulated about twice as much pyruvate than the WT (120 mg L^{-1} at process time 6 h) and a residual amount of 30 mg L^{-1} was still detectable after the end of the exponential growth phase (process time 9 h).

DISCUSSION

Adaptive Laboratory Evolution Concept

The aim of the ALE experiments was to increase the growth rate of the industrial workhorse *C. glutamicum* by applying a series of increasingly challenging dilution conditions in

TABLE 2 | Summary of kinetic parameters determined for *C. glutamicum* WT, *C. glutamicum* reRamA (Cg reRamA), and EVO5 grown in CGXII minimal medium supplemented with 2% (w/v) glucose.

Strain	μ h^{-1}	q_{Glc} g g^{-1} h^{-1}	Y_{XS} g g^{-1}	qO_2 mmol g^{-1} h^{-1}	qCO_2 mmol g^{-1} h^{-1}
WT	0.34 ± 0.03	0.64 ± 0.06	0.53 ± 0.01	6.06 ± 0.48	6.17 ± 0.65
Cg reRamA	0.38 ± 0.03	0.77 ± 0.04	0.49 ± 0.01	7.04 ± 0.56	6.93 ± 0.55
EVO5	0.54 ± 0.01	1.03 ± 0.01	0.52 ± 0.01	9.14 ± 0.31	9.70 ± 0.18

Bioreactor batch cultivations were performed at 30°C, 1.5 bar, and pH 7.4 in biological triplicates. Values represent the statistical mean ± standard deviation. μ, exponential growth rate; q_{Glc}, glucose consumption rate; Y_{XS}, biomass-substrate yield; qO_2, oxygen consumption rate; qCO_2, carbon dioxide emission rate.

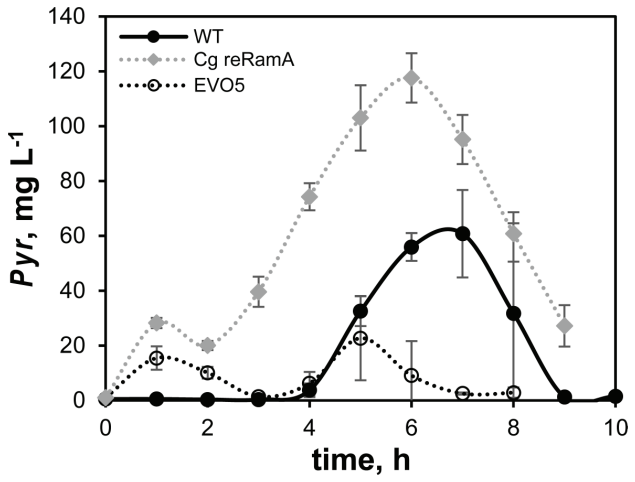

FIGURE 3 | Pyruvate (Pyr) accumulation during exponential growth phases of strains *C. glutamicum* (WT), Cg reRamA, and EVO5 cultivated in CGXII minimal medium supplemented with 2% (w/v) glucose in a bioreactor. Bioreactor batch cultivations were performed at 30°C, 1.5 bar, and pH 7.4 in biological triplicates. Error bars represent ± standard deviation from the mean.

continuously operated bioreactors. Concomitantly, the fraction of YE feeding was reduced finally adding an additional selection pressure. After about 2.5 months of total process time reflecting 1,700 generations, the evolution mutant EVO5 was obtained. This strain exhibited a growth rate of 0.54 h^{-1} which represents an improvement of 58% compared to the WT strain.

Recently, two independent ALE studies also evolved *C. glutamicum* WT with the purpose to improve the growth rate (Pfeifer et al., 2017; Wang et al., 2018). Both approaches followed a different ALE concept by employing repeated batches passaging stationary cells from glucose-depleted minimal medium to glucose-rich medium. Accordingly, cells repetitively encountered highly varying growth environments that were characterized by increasing biomass concentrations, decreasing glucose and oxygen availability, and changing pH over the respective process times (Seletzky et al., 2007) Intrinsically, such conditions are vulnerable to induce by-product formation either due to overflow metabolism (Paczia et al., 2012) or due to oxygen limitation (Lange et al., 2018). As a consequence, such effects may impose additional selection constraints, e.g., selecting for those cells that may withstand said conditions at best, e.g., by co-consuming by-products the fastest. To avoid such additional selection pressures, this study used strictly controlled bioreactor cultivations (pH 7.4; pO_2 > 30%) operating in continuous chemostat mode. Notably, the fine-tuned controller enabled dilution rate (D) settings with a precision of 0.01 h^{-1} close to the growth maximum of the culture. In contrast to batch ALE selections, the continuous mode regime counteracts by-product accumulation by diluting such substances. Besides, operating at a high dilution rate obviously discriminates for the fastest-growing sub-populations while slow growers are washed out (Gostomski et al., 1994). As a side effect, fast-growing subpopulations do not have to compete for nutrients with slow-growers as it is the case in, e.g., (fed-) batch cultivations. Consequently, the described ALE concept exclusively selects for fast-growing subpopulations. Continuous growth selection experiments somewhat differ from batch-wise approaches. Apparently, cells undergo changing nutrient supply in batch cultures, which is only happening in continuous selections when growth kinetics of the selected population changes. Intrinsically, continuous cultures prevent the occurrence of stationary growth that may occur intermediately in sequential batch-wise growth selections. In the continuous experiments of this study, a high number of generations of *C. glutamicum* was produced over the course of the experiments (680 generations per month) which increases the selection speed of an ALE process.

Adaptive Laboratory Evolution Medium and Protocatechuate Deficiency

Unlike other approaches, CGXII medium supplemented with YE was initially used as growth medium. Importantly, the amount of YE was gradually reduced while dilution rates increased. As a consequence, a double selection pressure was imposed on *C. glutamicum*: first to compete with the steadily rising dilution rates by increasing growth and second to increase the own biosynthesis of amino acids because the external supply diminished. Using large amounts of YE liberates the cells from their necessity to produce amino acids from glucose. Accordingly, related demands of precursors, NADPH and ATP, are reduced under amino acid supplementation. Graf et al. (2018) have outlined that *C. glutamicum* WT possesses a maximum glucose uptake rate ($q_{Glc,max}$) of approx. 0.0275 C-mol g_{CDW}^{-1} h^{-1} which equals 0.825 g_{Glc} g_{CDW}^{-1} h^{-1} if synthetic CGXII medium is supplemented with up to 10 g brain-heart-infusion per liter. Further supplementation of the complex media decreased q_{Glc}, while the total carbon

consumption q_C enhanced proportionally with μ yielding a constant biomass-carbon yield of 18.47 g C-mol^{-1}. This phenotype hinted at a maximum catabolic capacity to metabolize glucose for providing precursors of amino acid formation. The selection strategy of our study tackles this fundamental problem. Starting with high YE fractions while concomitantly challenging growth was purposely installed to direct evolution to targets controlling amino acid use and not the precursor supply for amino acid formation. Accordingly, it was expected that genes coding for basic regulatory functions may be evolved rather than genes encoding reactions of the central metabolism. Further reducing the YE fraction while keeping growth selection pressure high was expected to shift selection pressure to genes of central metabolism and related regulons. As such, the selection scenario fundamentally differs from those of previous studies and gives rise to the identification of different mutation sets, as shown in the next paragraph.

Besides, another fact is worth noticing: the growth medium did not contain any PCA. Liebl et al. (1989) had shown that aromatic compounds such as PCA or catechol boost growth of *C. glutamicum* anticipating the facilitated iron acquisition as the key driver. Own studies confirmed that *C. glutamicum* WT only achieved $\mu = 0.33 \pm 0.02$ h^{-1} in PCA-deficient media, whereas 0.45 ± 0.01 and 0.47 ± 0.01 h^{-1} were observed using PCA or catechol, respectively (c.f., **Supplementary Figure S2**). Following the idea to evolve novel *C. glutamicum* strains for industrial application, the study purposely resisted to add PCA to reduce media costs. Accordingly, this constraint may be qualified as an additional threshold compared to the published strains of Pfeifer et al. (2017) and Wang et al. (2018) which used additional iron chelators, i.e., PCA and catechol, respectively. As indicated in **Table 2**, the growth selection using CGXII minimal medium [1% (w/v) glucose] without PCA (Buchholz et al., 2014) improved the growth rate by 58%. Previous studies of Pfeifer et al. (2017) and Wang et al. (2018) only achieved improvements of 26 and 42%, notably still requiring iron chelators. With $\mu_{EVO5} = 0.54$ h^{-1} EVO5 even outperformed the *C. glutamicum* WT growing on PCA containing medium ($\mu_{WT} = 0.45$ h^{-1}). Furthermore, supplementation of PCA under did not boost the growth of EVO5 further (c.f., **Supplementary Figure S3**) which is an interesting target for further research. Summarizing, these findings question the anticipated function on PCA only serving as iron chelator. Another explanation was offered by Shen et al. (2012) who reported that both aromatic compounds can be degraded by *C. glutamicum via* the β-ketoadipate pathway to succinyl-CoA finally fueling the citric acid (TCA) cycle. Unthan et al. (2014) proposed that this effect can explain the improved growth performance in highly diluted environments in presence of PCA. However, such a hypothesis would assume boosting growth of EVO5 after PCA supplementation, which was not observed under the tested conditions. Accordingly, an alternate hypothesis may be valid assigning PCA a regulatory function. Similar observations have been made for numerous siderophores in addition to the iron-chelating properties, but are not yet described for PCA (Johnstone and Nolan, 2015).

Mutations in EVO5

In comparison to the parental WT strain, the genome of EVO5 revealed a total of 10 mutations (c.f., **Table 1**) of which seven mutations were supposedly not responsible for the increased growth performance of EVO5 observed under the tested conditions. The deletion of guanin at Pos. 3168391 was in the intergenic region between cg3285 (*copR*) and cg3286 which is 28 bp ahead of the start codon of *copR* and does not interfere with the binding site of CopR between bp −59 and −78 (Schelder et al., 2011). CopR is a (putative) response regulator and part of the copper-responsive two-component system CopRS serving as key regulatory system in *C. glutamicum* for copper ion resistance (Schelder et al., 2011). However, the transcriptional start site of *copR* was not identified yet (Schelder et al., 2011, Pfeifer-Sancar et al., 2013).

Another mutation was a base exchange in the *psp1* gene that did not lead to an amino acid exchange and therefore should not change the protein's activity. Interestingly, this gene is located in the cryptic prophage element CGP3 (Kalinowski et al., 2003) and was also mutated in the studies of Pfeifer et al. (2017) and Wang et al. (2018). The latter also detected that a 180 kbp fragment of the CGP3 region (cg1890–cg2071) was additionally missing and several mutations were observed in the final part of CGP3 (cg2066–cg2069). Notably, we detected a mutation in cg2067 that is leading to an amino acid exchange in the same region. It seems that mutations in this region are a common occurrence after ALE experiments. Additionally, Baumgart et al. (2013) showed that the removal of this region does not have an adverse effect on growth. Taken together, this makes it likely that mutations in this region do not affect growth and that this mutation is not causative for the improved growth performance.

Nucleotide changes of EVO5 in genes cg2504 and *nanP* did not influence the encoded amino acid either. The gene cg2468, encoding the permease component of a branched-chain amino acid ABC-type transporter, was affected by an amino acid exchange. Possibly, using decreasing amounts of YE as growth supplement in the first ALEs might have provoked this mutation, but it was not lost in the following YE-free phase where minimal medium with glucose as sole carbon source was applied. A deletion of base 139 was observed in cg2293 leading to a frameshift and consequent stop codon at amino acid 55. Since the stop codon occurred at the very beginning of the normally 261 amino acid-long protein, the resulting enzyme (putative indole-3-glycerol phosphate synthase[1]) is most likely not functional.

Three other mutations occurred in genes involved in regulatory processes within EVO5, which is in accordance with the experimental design. They are anticipated to determine the growth phenotype extraordinarily. The RamA protein of *C. glutamicum* was first identified by Cramer and Eikmanns (2007) as a master regulator of acetate metabolism. In the presence of acetate, RamA activates the *pta-ack* genes encoding phosphotransacetylase and acetate kinase as well as *aceA*, and

[1]Information retrieved on 2 December 2018 from CoryneRegNet: www.coryneregnet.de

aceB encoding the enzymes of the glyoxylate shunt isocitrate lyase and malate synthase, respectively. Further studies showed that RamA is a global regulator in the carbon metabolism of *C. glutamicum* and influences genes of carbon uptake, glucose-, ethanol-, and propionate-metabolism, as well as cell wall synthesis (functions of RamA were recently reviewed by Shah et al., 2018). Comparable to our study, the repetitive batch ALE of Wang et al. (2018) triggered a point mutation in the *ramA* gene (yielding $RamA^{A52V}$). The mutation was re-engineered into the WT and into a prophage-free strain (this resulting strain was called LUXR) which led to increased growth rates by 20 and 22%, respectively, compared to the respective parental strains. To test if the mutated $RamA^{S101C}$ obtained in our ALE led to a similar phenotype, we re-engineered the mutation in the WT (called Cg reRamA) and cultivated it under standard batch conditions (CGXII without PCA, 2% (w/v) glucose) in a bioreactor. In contrast to Wang et al. (2018), Cg reRamA exhibited only a slight growth enhancement of 8% compared to the WT-control ($\mu = 0.34 \pm 0.03\ h^{-1}$). However, we observed a non-proportional increase of the glucose consumption rate by 20% (WT: $q_{Glc} = 0.64 \pm 0.06\ g\ g^{-1}\ h^{-1}$) that was comparable to rates determined by Wang et al. (2018). Correspondingly, a two-tailed *t*-test showed that the biomass-substrate yield of Cg reRamA was significantly smaller compared to the WT (Cg reRamA: $0.49 \pm 0.01\ g_{CDW}\ g_{Glc}^{-1}$; WT: $0.53 \pm 0.01\ g_{CDW}\ g_{Glc}^{-1}$, c.f., **Table 2**). The main reason was found by studying the by-product formation of pyruvate. Indeed, Cg reRamA and the WT secreted rising amounts of pyruvate until the mid-exponential growth phase (c.f., **Figure 3**, WT-maximum: 60 mg L^{-1}, Cg reRamA-maximum: 120 mg L^{-1}).

However, Cg reRamA secreted twice as much of the organic acid and was not able to re-consume pyruvate completely. Since pyruvate marks the intersection between glycolysis and TCA, this metabolic overflow phenotype indicated unbalanced fluxes between both central catabolic routes. Apparently, the enhanced glucose consumption rates of Cg reRamA mirrored alleviated glycolytic fluxes, which could not be fueled into the TCA but yielded increased pyruvate secretion instead. This finding is in accordance with results of Wang et al. (2018) who outlined that the *ramA* mutation in LUXR led to an up-regulation of glycolytic genes concomitantly with a slight decrease of TCA activity. The *ramA* point mutations identified by Wang et al. (2018) and in our study are both not located in the DNA-binding site of the protein (HTH motif between positions 214–274 at the C terminus), but in the GAF-2 domain (amino acid positions 8 and 146) at the N terminus (Cramer and Eikmanns, 2007). As summarized in Shah et al. (2018), this domain is (among other functions) associated with gene regulation in bacteria. Cramer and Eikmanns (2007) showed that *C. glutamicum* without HTH-motif in RamA was not able to grow on acetate as sole carbon source. However, the observed GAF-2-mutation in Cg reRamA also impaired growth in CGXII minimal medium with acetate as sole carbon source (c.f., **Supplementary Figure S1**), but did not impair this growth entirely. Besides, the specific mutation S101C in RamA in EVO5 provoked a non-proportional q_{Glc} increase, which was not observed in the RamA-mutants of Wang et al. (2018). A mutation occurred in the gene encoding DtxR, the central regulator of the iron metabolism in *C. glutamicum* (Wennerhold and Bott, 2006). Interestingly, both, DtxR and the previously discussed RamA, have an influence on the regulation of the succinate dehydrogenase operon *sdhCAB* under standard growth conditions (Brune et al., 2006; Bussmann et al., 2009; Auchter et al., 2011) Besides, the *dtxR* mutation may also mirror the cellular need to improve iron availability during growth as outlined by Rolfe et al. (2012).

Another interesting mutation occurred in the gene *rpoA* encoding the alpha-subunit of the RNA polymerase (RNAP). The alpha subunit is part of the RNAP core enzyme and has been described to interact with regulators and to be able to alter transcription initiation (Ross et al., 1993; Dangi et al., 2004; Kim et al., 2012). The alpha-subunit has two domains, the alpha N-terminal domain, essential for RNAP assembly and basal transcription (αNTD), and the alpha C-terminal domain (αCTD), which is interacting with transcriptional regulators and promoter DNA to regulate transcription (Busby and Ebright, 1999; Browning and Busby, 2004). It has been reported that mutations in the αNTD region caused temperature sensitivity (Ishihama et al., 1980), while several mutations in the αCTD induced metabolic changes (Jafri et al., 1995; Klein-Marcuschamer et al., 2009). The present mutation altered the encoded amino acid at position 280, which places it near the center of the αCTD. Because of the range of phenotype changes elicited by mutations in this region, the alpha-subunit of the RNAP was previously proposed as an interesting target for metabolic engineering when global transcriptional changes are required (Klein-Marcuschamer et al., 2009). It is therefore likely that the present mutation in RpoA caused a wide-reaching change in gene expression and might be responsible for the further growth rate improvements. A comparable observation was made by LaCroix et al. (2015) in an *E. coli* ALE study. Among other mutations, reproducible mutations in the gene *rpoB* were observed that together with *rpoC* encodes the beta chain of the RNA polymerase. Even though the mutations manifested at different positions in *rpoB*, each apparently improved *E.coli*'s growth rate.

Summarizing, a set of 10 distinct mutations has been identified in EVO5 of which six supposedly had no influence on the growth performance. Strikingly, three of the residual four mutated genes that most likely were responsible for the growth improvement are global regulators. This accredits the motivation of performing the selection study with the dual pressure to reduce complex media and iron chelator components while challenging growth rates. As such, findings differ from the mutations identified by Pfeifer et al. (2017) in central metabolism genes such as *pyk* (encoding pyruvate kinase; Ozaki and Shiio, 1969; Jetten et al., 1994) and *fruK* (or *pfkB*; cg2119), coding for 1-phosphofructokinase; Sugimoto and Shiio, 1989). Apparently, *C. glutamicum* found ways to adapt to the challenging growth conditions by changing the global regulatory responses, which even allowed the strain to grow without extra iron chelator addition.

Preliminary Characterization of EVO5

Preliminary evaluations of the EVO5 mutant strain with respect to PCA sensitivity as well as acetate, lactate, and gluconate consumption are indicated in the appendix (c.f., **Supplementary Table S2**). Shaking flask experiments were performed and in accordance with the bioreactor cultivations (c.f., Section "Adaptive Laboratory Evolution Medium and PCA Deficiency"; inoculation density: OD_{600} 1), EVO5 shows a maximum growth rate of 0.63 h^{-1} without PCA, superior to the WT growth of 0.36 h^{-1}. Under the same conditions, addition of PCA to the medium does not further accelerate growth of EVO5 while it boosts the growth of *C. glutamicum* WT to 0.55 h^{-1}, which is still lower than the one exhibited by EVO5. Employing an inoculation density of OD 0.5 and supplementing PCA slightly enhanced μ of EVO5 from 0.62 h^{-1} (without PCA) to 0.66 h^{-1}. This growth stimulating effect of PCA in combination with low inoculation densities was previously described for the WT (Unthan et al., 2014) and will be the topic of future research for EVO5. With regard to alternative carbon sources as growth substrate, *C. glutamicum* WT and EVO5 exhibit significantly reduced growth rates on acetate as sole carbon source. In particular, growth of EVO5 is lowered to 0.23 h^{-1}, which is less than WT performance. Apparently, the mutations of EVO5 interact with the strains capacity to metabolize acetate. *C. glutamicum* displays severely reduced growth on lactate as sole carbon source similar to the case of acetate as sole carbon source. While growth rate of the WT is faster than that of EVO5 under these conditions, both rates are the lowest in the experimental study. Although gluconate metabolism differs from glucose uptake and metabolism, its substrate conversion is more comparable to that of glucose than to that of acetate and lactate as alternate carbon sources. Consequently, it may not surprise that gluconate-based growth of EVO5 is faster than of the WT, by trend. Biomass yields of both strains are fairly similar.

CONCLUSION

The installation of a double selection pressure comprising reduction of complex medium supplements and steady increase of growth yielded the successful selection of *C. glutamicum* EVO 5. With μ = 0.54 h^{-1}, the strain outnumbered the WT performance by 58%, noteworthy without using well-known boosters such as PCA. Consequently, the strain is easy-to-transfer in industrial conditions, which allows its use as a novel production platform for growth-coupled products. So far, the relatively low growth rate of *C. glutamicum* restricted its application for partially growth-coupled products only requiring moderate growth associated production kinetics. Now, other applications are in reach further exploiting the native traits of the *C. glutamicum* chassis. Additionally, 10 mutations of which three are regulator genes identified in the growth selections provide a fruitful basis for systems metabolic engineering boosting strain kinetics even further.

DATA AVAILABILITY

All datasets generated for this study are included in the manuscript and/or the **Supplementary Files**.

AUTHOR CONTRIBUTIONS

MG and TH designed the study, analyzed the datasets, and drafted the manuscript. MG, TH, and JH-B carried out the bioreactor experiments, and AF designed the control scheme for the continuous process mode. FM constructed strain *C. glutamicum* reRamA. AB performed characterization studies of *C. glutamicum* WT and EVO5 in shaking flasks. MP performed sequencing of the *C. glutamicum* WT and evolution strain EVO5. JH-B, AF, FM, AB, AN, MP, JK, and BB analyzed the datasets and corrected the manuscript. RT conceived the study and corrected the manuscript. All authors read and approved the final manuscript.

FUNDING

The authors gratefully acknowledge the funding of this work by the German Federal Ministry of Education and Research (BMBF; Grant 031A302A).

ACKNOWLEDGMENTS

The authors thank Anna-Lena Mayer and Salaheddine Laghrami for excellent support with bioreactor fermentations. Moreover, they also thank all members of the "0.6 plus" project group for valuable comments on the topic and for their great cooperation.

SUPPLEMENTARY MATERIAL

The Supplementary Material for this article can be found online at: https://www.frontiersin.org/articles/10.3389/fmicb.2019.01648/full#supplementary-material

REFERENCES

Auchter, M., Cramer, A., Hüser, A., Rückert, C., Emer, D., Schwarz, P., et al. (2011). RamA and RamB are global transcriptional regulators in *Corynebacterium glutamicum* and control genes for enzymes of the central metabolism. *J. Biotechnol.* 154, 126–139. doi: 10.1016/j.jbiotec.2010.07.001

Bäumchen, C., Knoll, A., Husemann, B., Seletzky, J., Maier, B., Dietrich, C., et al. (2007). Effect of elevated dissolved carbon dioxide concentrations on growth of *Corynebacterium glutamicum* on d-glucose and l-lactate. *J. Biotechnol.* 128, 868–874. doi: 10.1016/j.jbiotec.2007.01.001

Baumgart, M., Unthan, S., Rückert, C., Sivalingam, J., Grünberger, A., Kalinowski, J., et al. (2013). Construction of a prophage-free variant of *Corynebacterium*

glutamicum ATCC 13032 for use as a platform strain for basic research and industrial biotechnology. *Appl. Environ. Microbiol.* 79, 6006–6015. doi: 10.1128/AEM.01634-13

Becker, J., Gießelmann, G., Hoffmann, S. L., and Wittmann, C. (2016). "*Corynebacterium glutamicum* for sustainable bioproduction: from metabolic physiology to systems metabolic engineering" in *Synthetic biology – Metabolic engineering. Advances in biochemical engineering/biotechnology*. Vol. 162, eds. H. Zhao and A. P. Zeng (Cham: Springer), 217–263.

Becker, J., and Wittmann, C. (2012). Bio-based production of chemicals, materials and fuels – *Corynebacterium glutamicum* as versatile cell factory. *Curr. Opin. Biotechnol.* 23, 631–640. doi: 10.1016/j.copbio.2011.11.012

Becker, J., and Wittmann, C. (2018). From systems biology to metabolically engineered cells – an omics perspective on the development of industrial microbes. *Curr. Opin. Microbiol.* 45, 180–188. doi: 10.1016/j.mib.2018.06.001

Blombach, B., Buchholz, J., Busche, T., Kalinowski, J., and Takors, R. (2013). Impact of different CO_2/HCO^{3-} levels on metabolism and regulation in *Corynebacterium glutamicum*. *J. Biotechnol.* 168, 331–340. doi: 10.1016/j.jbiotec.2013.10.005

Browning, D. F., and Busby, S. J. W. (2004). The regulation of bacterial transcription initiation. *Nat. Rev. Microbiol.* 2, 57–65. doi: 10.1038/nrmicro787

Brune, I., Werner, H., Hüser, A. T., Kalinowski, J., Pühler, A., and Tauch, A. (2006). The DtxR protein acting as dual transcriptional regulator directs a global regulatory network involved in iron metabolism of *Corynebacterium glutamicum*. *BMC Genomics* 7, 1–19. doi: 10.1186/1471-2164-7-21

Buchholz, J., Graf, M., Blombach, B., and Takors, R. (2014). Improving the carbon balance of fermentations by total carbon analyses. *Biochem. Eng. J.* 90, 162–169. doi: 10.1016/j.bej.2014.06.007

Busby, S., and Ebright, R. H. (1999). Transcription activation by catabolite activator protein (CAP). *Behav. Brain Res.* 99, 153–167. doi: 10.1016/S0166-4328(98)00101-6

Bussmann, M., Emer, D., Hasenbein, S., Degraf, S., Eikmanns, B. J., and Bott, M. (2009). Transcriptional control of the succinate dehydrogenase operon *sdhCAB* of *Corynebacterium glutamicum* by the cAMP-dependent regulator GlxR and the LuxR-type regulator RamA. *J. Biotechnol.* 143, 173–182. doi: 10.1016/j.jbiotec.2009.06.025

Cramer, A., and Eikmanns, B. J. (2007). RamA, the transcriptional regulator of acetate metabolism in *Corynebacterium glutamicum*, is subject to negative autoregulation. *J. Mol. Microbiol. Biotechnol.* 12, 51–59. doi: 10.1128/JB.01061-06

Dangi, B., Gronenborn, A. M., Rosner, J. L., and Martin, R. G. (2004). Versatility of the carboxy-terminal domain of the α subunit of RNA polymerase in transcriptional activation: use of the DNA contact site as a protein contact site for MarA. *Mol. Microbiol.* 54, 45–59. doi: 10.1111/j.1365-2958.2004.04250.x

Dettman, J. R., Rodrigue, N., Melnyk, A. H., Wong, A., Bailey, S. F., and Kassen, R. (2012). Evolutionary insight from whole-genome sequencing of experimentally evolved microbes. *Mol. Ecol.* 21, 2058–2077. doi: 10.1111/j.1365-294X.2012.05484.x

Dragosits, M., and Mattanovich, D. (2013). Adaptive laboratory evolution – principles and applications for biotechnology. *Microb. Cell Factories* 12:64. doi: 10.1186/1475-2859-12-64

Feist, A. M., Zielinski, D. C., Orth, J. D., Schellenberger, J., Herrgard, M. J., and Palsson, B. O. (2009). Model-driven evaluation of the production potential for growth-coupled products of *Escherichia coli*. *Metab. Eng.* 12, 173–186. doi: 10.1016/j.ymben.2009.10.003

Follmann, M., Ochrombel, I., Krämer, R., Trötschel, C., Poetsch, A., Rückert, C., et al. (2009). Functional genomics of pH homeostasis in *Corynebacterium glutamicum* revealed novel links between pH response, oxidative stress, iron homeostasis and methionine synthesis. *BMC Genomics* 10:621. doi: 10.1186/1471-2164-10-621

Freudl, R. (2017). Beyond amino acids: use of the *Corynebacterium glutamicum* cell factory for the secretion of heterologous proteins. *J. Biotechnol.* 258, 101–109. doi: 10.1016/j.jbiotec.2017.02.023

Gibson, D. G. (2011). Enzymatic assembly of overlapping DNA fragments. *Methods Enzymol.* 498, 349–361. doi: 10.1016/B978-0-12-385120-8.00015-2,

Gordon, D. (2003). Viewing and editing assembled sequences using Consed. *Curr. Protoc. Bioinformatics* 2, 11.2.1–11.2.43. doi: 10.1002/0471250953.bi1102s02

Gostomski, P., Mühlemann, M., Lin, Y. H., Mormino, R., and Bungay, H. (1994). Auxostats for continuous culture research. *J. Biotechnol.* 37, 167–177. doi: 10.1016/0168-1656(94)90008-6

Graf, M., Zieringer, J., Haas, T., Nieß, A., Blombach, B., and Takors, R. (2018). Physiological response of *Corynebacterium glutamicum* to increasingly nutrient-rich growth conditions. *Front. Microbiol.* 9, 1–15. doi: 10.3389/fmicb.2018.02058,

Grünberger, A., van Ooyen, J., Paczia, N., Rohe, P., Schiendzielorz, G., Eggeling, L., et al. (2013). Beyond growth rate 0.6: *Corynebacterium glutamicum* cultivated in highly diluted environments. *Biotechnol. Bioeng.* 110, 220–228. doi: 10.1002/bit.24616

Ishihama, A., Shimamoto, N., Aiba, H., Kawakami, K., Nashimoto, H., Tsugawa, A., et al. (1980). Temperature-sensitive mutations in the α subunit gene of *Escherichia coli* RNA polymerase. *J. Mol. Biol.* 137, 137–150. doi: 10.1016/0022-2836(80)90321-6

Jafri, S., Urbanowski, M. L., and Stauffer, G. V. (1995). A mutation in the *rpoA* gene encoding the α subunit of RNA polymerase that affects *metE-metR* transcription in *Escherichia coli*. *J. Bacteriol.* 177, 524–529. doi: 10.1128/jb.177.3.524-529.1995

Jetten, M. S., Gubler, M. E., Lee, S. H., and Sinskey, A. J. (1994). Structural and functional analysis of pyruvate kinase from *Corynebacterium glutamicum*. *Appl. Environ. Microbiol.* 60, 2501–2507.

Johnstone, T. C., and Nolan, E. M. (2015). Beyond iron: non-classical biological functions of bacterial siderophores. *Dalton Trans.* 44, 6320–6339. doi: 10.1039/C4DT03559C

Kalinowski, J., Bathe, B., Bartels, D., Bischoff, N., Bott, M., Burkovski, A., et al. (2003). The complete *Corynebacterium glutamicum* ATCC 13032 genome sequence and its impact on the production of L-aspartate-derived amino acids and vitamins. *J. Biotechnol.* 104, 5–25. doi: 10.1016/S0168-1656(03)00154-8

Keilhauer, C., Eggeling, L., and Sahm, H. (1993). Isoleucine synthesis in *Corynebacterium glutamicum*: molecular analysis of the ilvB-ilvN-ilvC operon. *J. Bacteriol.* 175, 5595–5603. doi: 10.1128/jb.175.17.5595-5603.1993

Kim, J. H., Ham, S. H., and Lee, B. R. (2012). Characterization of the RNA polymerase α subunit operon from *Corynebacterium ammoniagenes*. *World J. Microbiol. Biotechnol.* 28, 669–676. doi: 10.1007/s11274-011-0861-9

Kind, S., Jeong, W. K., Schröder, H., Zelder, O., and Wittmann, C. (2010). Identification and elimination of the competing N-acetyldiaminopentane pathway for improved production of diaminopentane by *Corynebacterium glutamicum*. *Appl. Environ. Microbiol.* 76, 5175–5180. doi: 10.1128/AEM.00834-10

Klein-Marcuschamer, D., Santos, C. N. S., Yu, H., and Stephanopoulos, G. (2009). Mutagenesis of the bacterial RNA polymerase alpha subunit for improvement of complex phenotypes. *Appl. Environ. Microbiol.* 75, 2705–2711. doi: 10.1128/AEM.01888-08

LaCroix, R. A., Sandberg, T. E., O'Brien, E. J., Utrilla, J., Ebrahim, A., Guzman, G. I., et al. (2015). Use of adaptive laboratory evolution to discover key mutations enabling rapid growth of *Escherichia coli* K-12 MG1655 on glucose minimal medium. *Appl. Environ. Microbiol.* 81, 17–30. doi: 10.1128/AEM.02246-14

Lange, J., Münch, E., Müller, J., Busche, T., Kalinowski, J., Takors, R., et al. (2018). Deciphering the adaptation of *Corynebacterium glutamicum* in transition from aerobiosis *via* microaerobiosis to anaerobiosis. *Genes* 9:297. doi: 10.3390/genes9060297

Lee, D. H., and Palsson, B. O. (2010). Adaptive evolution of *Escherichia coli* K-12 MG1655 during growth on a nonnative carbon source, L-1, 2-propanediol. *Appl. Environ. Microbiol.* 76, 4158–4168. doi: 10.1128/AEM.00373-10

Liebl, W., Klamer, R., and Schleifer, K. H. (1989). Requirement of chelating compounds for the growth of *Corynebacterium glutamicum* in synthetic media. *Appl. Microbiol. Biotechnol.* 32, 205–210. doi: 10.1007/BF00165889

Löffler, M., Simen, J. D., Jäger, G., Schäferhoff, K., Freund, A., and Takors, R. (2016). Engineering *E. coli* for large-scale production – strategies considering ATP expenses and transcriptional responses. *Metab. Eng.* 38, 73–85. doi: 10.1016/j.ymben.2016.06.008

McCloskey, D., Xu, S., Sandberg, T. E., Brunk, E., Hefner, Y., Szubin, R., et al. (2018). Adaptation to the coupling of glycolysis to toxic methylglyoxal production in tpiA deletion strains of *Escherichia coli* requires synchronized and counterintuitive genetic changes. *Metab. Eng.* 48, 82–93. doi: 10.1016/j.ymben.2018.05.012

Michalowski, A., Siemann-Herzberg, M., and Takors, R. (2017). *Escherichia coli* HGT: engineered for high glucose throughput even under slowly growing or resting conditions. *Metab. Eng.* 40, 93–103. doi: 10.1016/j.ymben.2017.01.005

Mohamed, E. T., Wang, S., Lennen, R. M., Herrgård, M. J., Simmons, B. A., Singer, S. W., et al. (2017). Generation of a platform strain for ionic liquid tolerance using adaptive laboratory evolution. *Microb. Cell Factories* 16:204. doi: 10.1186/s12934-017-0819-1

Nielsen, J., and Keasling, J. D. (2016). Engineering cellular metabolism. *Cell* 164, 1185–1197. doi: 10.1016/j.cell.2016.02.004

Nishimura, T., Vertès, A. A., Shinoda, Y., Inui, M., and Yukawa, H. (2007). Anaerobic growth of *Corynebacterium glutamicum* using nitrate as a terminal electron acceptor. *Appl. Microbiol. Biotechnol.* 75, 889–897. doi: 10.1007/s00253-007-0879-y

Ozaki, H., and Shiio, I. (1969). Regulation of the TCA and glyoxylate cycles in *Brevibacterium flavum*: II. Regulation of phosphoenolpyruvate carboxylase and pyruvate kinase. *J. Biochem.* 66, 297–311. doi: 10.1093/oxfordjournals.jbchem.a129148

Paczia, N., Nilgen, A., Lehmann, T., Gätgens, J., Wiechert, W., and Noack, S. (2012). Extensive exometabolome analysis reveals extended overflow metabolism in various microorganisms. *Microb. Cell Factories* 11:122. doi: 10.1186/1475-2859-11-122

Pfeifer, E., Gätgens, C., Polen, T., and Frunzke, J. (2017). Adaptive laboratory evolution of *Corynebacterium glutamicum* towards higher growth rates on glucose minimal medium. *Sci. Rep.* 7, 1–14. doi: 10.1038/s41598-017-17014-9

Pfeifer-Sancar, K., Mentz, A., Rückert, C., and Kalinowski, J. (2013). Comprehensive analysis of the *Corynebacterium glutamicum* transcriptome using an improved RNAseq technique. *BMC Genomics* 14:888. doi: 10.1186/1471-2164-14-888

Rolfe, M. D., Rice, C. J., Lucchini, S., Pin, C., Thompson, A., Cameron, A. D. S., et al. (2012). Lag phase is a distinct growth phase that prepares bacteria for exponential growth and involves transient metal accumulation. *J. Bacteriol.* 194, 686–701. doi: 10.1128/JB.06112-11

Ross, W., Gosink, K. K., Salomon, J., Igarashi, K., Zou, C., Ishihama, A., et al. (1993). A third recognition element in bacterial promoters: DNA binding by the alpha subunit of RNA polymerase. *Science* 262, 1407–1413. doi: 10.1126/science.8248780

Rugbjerg, P., Feist, A. M., and Sommer, M. O. A. (2018). Enhanced metabolite productivity of *Escherichia coli* adapted to glucose M9 minimal medium. *Front. Bioeng. Biotechnol.* 6:166. doi: 10.3389/fbioe.2018.00166

Ryall, B., Eydallin, G., and Ferenci, T. (2012). Culture history and population heterogeneity as determinants of bacterial adaptation: the adaptomics of a single environmental transition. *Microbiol. Mol. Biol. Rev.* 76, 597–625. doi: 10.1128/MMBR.05028-11

Sambrook, J. (2001). *Molecular cloning: A laboratory manual*. Cold Spring Harbor, NY: Cold Spring Harbor Laboratory Press.

Sandberg, T. E., Long, C. P., Gonzalez, J. E., Feist, A. M., Antoniewicz, M. R., and Palsson, B. O. (2016). Evolution of *E. coli* on [U-13C] glucose reveals a negligible isotopic influence on metabolism and physiology. *PLoS One* 11:e0151130. doi: 10.1371/journal.pone.0151130

Schäfer, A., Tauch, A., Jäger, W., Kalinowski, J., Thierbach, G., and Pühler, A. (1994). Small mobilizable multi-purpose cloning vectors derived from the *Escherichia coli* plasmids pK18 and pK19: selection of defined deletions in the chromosome of *Corynebacterium glutamicum*. *Gene* 145, 69–73. doi: 10.1016/0378-1119(94)90324-7

Schelder, S., Zaade, D., Litsanov, B., Bott, M., and Brocker, M. (2011). The two-component signal transduction system CopRS of *Corynebacterium glutamicum* is required for adaptation to copper-excess stress. *PLoS One* 6:e22143. doi: 10.1371/journal.pone.0022143

Seletzky, J. M., Noak, U., Fricke, J., Welk, E., Eberhard, W., Knocke, C., et al. (2007). Scale-up from shake flasks to fermenters in batch and continuous mode with *Corynebacterium glutamicum* on lactic acid based on oxygen transfer and pH. *Biotechnol. Bioeng.* 98, 800–811. doi: 10.1002/bit.21359

Shah, A., Blombach, B., Gauttam, R., and Eikmanns, B. J. (2018). The RamA regulon: complex regulatory interactions in relation to central metabolism in *Corynebacterium glutamicum*. *Appl. Microbiol. Biotechnol.*, 102:5901. doi: 10.1007/s00253-018-9085-3

Shen, X. H., Zhou, N. Y., and Liu, S. J. (2012). Degradation and assimilation of aromatic compounds by *Corynebacterium glutamicum*: another potential for applications for this bacterium? *Appl. Microbiol. Biotechnol.* 95, 77–89. doi: 10.1007/s00253-012-4139-4

Stella, R. G., Wiechert, J., Noack, S., and Frunzke, J. (2019). Evolutionary engineering of *Corynebacterium glutamicum*. *Biotechnol. J.* 1800444. doi: 10.1002/biot.201800444

Straathof, A. J. (2013). Transformation of biomass into commodity chemicals using enzymes or cells. *Chem. Rev.* 114, 1871–1908. doi: 10.1021/cr400309c:

Sugimoto, S. I., and Shiio, I. (1989). Fructose metabolism and regulation of 1-phosphofructokinase and 6-phosphofructokinase in *Brevibacterium flavum*. *Agric. Biol. Chem.* 53, 1261–1268. doi: 10.1080/00021369.1989.10869488

Tauch, A., Kirchner, O., Löffler, B., Götker, S., Pühler, A., and Kalinowski, J. (2002). Efficient Electrotransformation of Corynebacterium diphtheriae with a Mini-Replicon Derived from the Corynebacterium glutamicum Plasmid pGA1. *Curr. Microbiol.* 45, 362–367. doi: 10.1007/s00284-002-3728-3

Tremblay, P. L., Höglund, D., Koza, A., Bonde, I., and Zhang, T. (2015). Adaptation of the autotrophic acetogen *Sporomusa ovata* to methanol accelerates the conversion of CO_2 to organic products. *Sci. Rep.* 5:16168. doi: 10.1038/srep16168

Unthan, S., Grünberger, A., van Ooyen, J., Gätgens, J., Heinrich, J., Paczia, N., et al. (2014). Beyond growth rate 0.6: what drives *Corynebacterium glutamicum* to higher growth rates in defined medium. *Biotechnol. Bioeng.* 111, 359–371. doi: 10.1002/bit.25103

van der Rest, M., Lange, C., and Molenaar, D. (1999). A heat shock following electroporation induces highly effcient transformation of *Corynebacterium glutamicum* with xenogeneic plasmid DNA. *Appl. Microbiol. Biotechnol.* 52, 541–545. doi: 10.1007/s002530051557

Wang, Z., Liu, J., Chen, L., Solem, C., and Jensen, P. R. (2018). Alterations in the transcription factors GntR1 and RamA enhance the growth and central metabolism of *Corynebacterium glutamicum*. *Metab. Eng.* 48, 1–12. doi: 10.1016/j.ymben.2018.05.004

Wendisch, V. F., Jorge, J. M., Pérez-García, F., and Sgobba, E. (2016). Updates on industrial production of amino acids using *Corynebacterium glutamicum*. *World J. Microbiol. Biotechnol.* 32:105. doi: 10.1007/s11274-016-2060-1

Wendisch, V. F., Mindt, M., and Pérez-García, F. (2018). Biotechnological production of mono-and diamines using bacteria: recent progress, applications, and perspectives. *Appl. Microbiol. Biotechnol.* 102, 3583–3594. doi: 10.1007/s00253-018-8890-z

Wennerhold, J., and Bott, M. (2006). The DtxR regulon of *Corynebacterium glutamicum*. *J. Bacteriol.* 188, 2907–2918. doi: 10.1128/JB.188.8.2907-2918.2006

Wieschalka, S., Blombach, B., Bott, M., and Eikmanns, B. J. (2013). Bio-based production of organic acids with *Corynebacterium glutamicum*. *Microb. Biotechnol.* 6, 87–102. doi: 10.1111/1751-7915.12013

Conflict of Interest Statement: The authors declare that the research was conducted in the absence of any commercial or financial relationships that could be construed as a potential conflict of interest.

C. Supplementary material to Part I

C.1. DEGs of the PCA supplementation experiment

Table C.1.: Differentially expressed genes obtained from transcriptome analysis of *C. glutamicum* cells grown in $1\,\mathrm{mg\,L^{-1}}$ protocatechuate (PCA) supplemented CGXII ($20\,\mathrm{g\,L^{-1}}$ glucose) batch conditions inducing $\mu = 0.45\,\mathrm{h^{-1}}$. Log fold changes (FC) are based on the unsupplemented reference (Ref) condition. Gene names and functions were retrieved from the CoryneRegNet database (Pauling et al., 2012).

Locus	Name	Function	PCA/Ref
cg0088	*citH*	Putative secondary Mg2+/H+:citrate transporter; CitMHS-family	2.342
cg0111	*cg0111*	Hypothetical protein	-3.219
cg0120	*cg0120*	Putative hydrolase	-1.986
cg0159	*cg0159*	Hypothetical protein	-3.612
cg0160	*cg0160*	Hypothetical protein	-3.479
cg0172	*panD*	Aspartate 1-decarboxylase	2.160
cg0175	*cg0175*	Putative secreted protein	-2.231
cg0179	*cg0179*	Putative membrane protein	1.987
cg0210	*cg0210*	Putative transcriptional regulator; LacI-family	2.032
cg0211	*cg0211*	Putative oxidoreductase	2.183
cg0212	*cg0212*	Phosphate isomerases/epimerase; conserved hypothetical protein	2.325
cg0223	*iolT1*	Putative sugar/metabolite permease; MFS-type	2.326
cg0228	*hkm*	Two-component system; sensory histidine kinase; putative pseudogene	3.707
cg0229	*gltB*	Glutamate synthase (NADPH); large chain	-2.380
cg0310	*katA*	Catalase	2.723
cg0314	*brnF*	Secondary branched-chain amino acid efflux transporter; LIV-E family; large subunit	-2.720
cg0340	*cg0340*	Putative sugar/metabolite permease; MFS-type	2.533
cg0405	*cg0405*	ABC-type putative iron(III) dicitrate transporter; substrate-binding lipoprotein	-4.277
cg0445	*sdhCD*	Succinate dehydrogenase; subunit CD	2.246
cg0446	*sdhA*	Succinate dehydrogenase; subunit A	2.520
cg0447	*sdhB*	Succinate dehydrogenase; subunit B	2.356
cg0465	*cg0465*	Conserved putative membrane protein	-3.642
cg0466	*cg0466*	Conserved putative secreted protein	-3.715
cg0467	*cg0467*	ABC-type putative hemin transporter; substrate-binding lipoprotein	-3.319
cg0468	*cg0468*	ABC-type putative hemin transporter; permease subunit	-2.789
cg0469	*cg0469*	ABC-type putative hemin transporter; ATPase subunit	-3.482
cg0470	*cg0470*	Conserved secreted protein	-7.800
cg0471	*cg0471*	Conserved secreted protein	-7.810
cg0527	*glyR*	Transcriptional activator of glyA; ArsR-family	-2.303
cg0544	*cg0544*	Putative membrane protein	2.019
cg0589	*cg0589*	ABC-type putative iron-siderophore transporter; ATPase subunit	-3.121
cg0590	*cg0590*	ABC-type putative iron-siderophore transporter; permease subunit	-3.389
cg0591	*cg0591*	ABC-type putative iron-siderophore transporter; permease subunit	-3.384
cg0639	*cg0639*	Putative ferredoxin reductase	2.127
cg0641	*fabG2*	Putative secreted short-chain dehydrogenase	2.140
cg0644	*ppsA*	Pyruvate phosphate dikinase; PEP/pyruvate-binding	2.497
cg0645	*cytP*	Putative cytochrome P450	2.433
cg0701	*cg0701*	Putative secondary drug/metabolite transporter	-6.776

Locus	Name	Function	PCA/Ref
cg0712	*cg0712*	Putative secreted protein	1.963
cg0748	*cg0748*	ABC-type putative iron-siderophore transporter; substrate-binding lipoprotein	-2.232
cg0758	*cg0758*	Hypothetical protein	2.041
cg0759	*prpD2*	2-Methylcitrate dehydratase; involved in propionate catabolism	5.441
cg0760	*prpB2*	Methylisocitrate lyase; involved in propionate catabolism	6.734
cg0762	*prpC2*	2-Methylcitrate synthase; involved in propionate catabolism	5.269
cg0767	*cg0767*	Siderophore-interacting protein	-2.853
cg0768	*cg0768*	ABC-type putative iron-siderophore transporter; ATPase subunit	-2.802
cg0769	*cg0769*	ABC-type putative iron-siderophore transporter; permease subunit	-2.865
cg0770	*cg0770*	ABC-type putative iron-siderophore transporter; permease subunit	-2.985
cg0771	*irp1*	ABC-type putative iron-siderophore transporter; substrate-binding lipoprotein	-3.240
cg0921	*cg0921*	Siderophore-interacting protein	-3.472
cg0922	*cg0922*	ABC-type putative iron-siderophore transporter; substrate-binding lipoprotein	-3.614
cg0924	*cg0924*	ABC-type putative iron-siderophore transporter; substrate-binding lipoprotein	-3.435
cg0926	*cg0926*	ABC-type putative iron-siderophore transporter; permease subunit	-2.821
cg0927	*cg0927*	ABC-type putative iron-siderophore transporter; permease subunit	-2.652
cg0928	*cg0928*	ABC-type putative iron-siderophore transporter; ATPase subunit	-2.792
cg0936	*rpf1*	RPF-protein precursor	2.317
cg0961	*cg0961*	Putative hydrolase; alpha/beta-fold	2.867
cg1065	*urtD*	ABC-type putative branched-chain amino acid transporter; ATPase subunit	-2.021
cg1109	*cg1109*	Hypothetical protein	1.980
cg1120	*ripA*	Putative transcriptional regulator; AraC-family	-4.144
cg1129	*aroF*	Putative phospho-2-dehydro-3-deoxyheptonate aldolase	-3.100
cg1156	*ssuD2*	FMNH2-dependent aliphatic sulfonate monooxygenase	-1.976
cg1291	*cg1291*	Putative membrane protein	-2.820
cg1296	*cg1296*	Conserved hypothetical protein; putative non-ribosomal peptide synthetase module	-2.032
cg1298	*cydC*	ABC-type putative multidrug/protein/lipid transporter; ATPase and permease subunit	2.205
cg1299	*cydD*	ABC-type putative multidrug/protein/lipid transporter; ATPase and permease subunit	2.209
cg1300	*cydB*	Cytochrome d ubiquinol oxidase subunit II	2.270
cg1301	*cydA*	Cytochrome d ubiquinol oxidase subunit I	2.506
cg1341	*narI*	Respiratory nitrate reductase 2; gamma chain	2.574
cg1342	*narJ*	Respiratory nitrate reductase 2; delta chain	2.796
cg1343	*narH*	Respiratory nitrate reductase 2; beta chain	2.533
cg1344	*narG*	Respiratory nitrate reductase 2; alpha chain	2.228
cg1345	*narK*	Putative nitrate/nitrite permease; MFS-type	2.109
cg1376	*ssuD1*	FMNH2-dependent aliphatic sulfonate monooxygenase	-2.256
cg1380	*ssuA*	ABC-type aliphatic sulfonate transporter; substrate-binding lipoprotein	-2.348
cg1405	*cg1405*	Siderophore-interacting protein	-2.348
cg1418	*cg1418*	ABC-type putative iron-siderophore transporter; substrate-binding lipoprotein	-2.568
cg1476	*thiC*	Thiamine biosynthesis protein ThiC	-2.555
cg1478	*cg1478*	Hypothetical protein	-5.543
cg1514	*cg1514*	Secreted protein	-2.023
cg1537	*ptsG*	Phosphotransferase system (PTS); glucose-specific enzyme IIBCA component	2.016
cg1580	*argC*	N-acetyl-gamma-glutamyl-phosphate reductase	-2.377
cg1581	*argJ*	Glutamate N-acetyltransferase	-2.545
cg1582	*argB*	Acetylglutamate kinase	-2.437
cg1583	*argD*	Acetylornithine aminotransferase; AT class II	-2.481

Locus	Name	Function	PCA/Ref
cg1584	*argF*	Ornithine carbamoyltransferase	-2.251
cg1585	*argR*	Transcriptional repressor of arginine biosynthesis; ArgR-family	-2.098
cg1595	*uspA2*	Universal stress protein UspA	1.914
cg1612	*cg1612*	Putative acetyltransferase	3.718
cg1626	*cg1626*	Conserved hypothetical protein	-3.051
cg1628	*cg1628*	Putative hydrolase; alpha/beta superfamily	-3.212
cg1695	*cg1695*	Putative antidote protein; HTH-motif XRE family	1.977
cg1696	*cg1696*	Putative antibiotic efflux permease; MFS-type	-2.685
cg1737	*acn*	Aconitate hydratase	2.135
cg1783	*soxA*	Putative oxidase; pseudogene (N-terminal fragment)	-3.088
cg1784	*ocd*	Putative ornithine cyclodeaminase	-3.584
cg1785	*amtA*	Putative secondary ammonium transporter; Amt-family	-3.061
cg1832	*cg1832*	ABC-type putative iron-siderophore transporter; substrate-binding lipoprotein	-3.226
cg1833	*cg1833*	ABC-type putative iron-siderophore transporter; ATPase subunit	-2.822
cg1834	*cg1834*	ABC-type putative iron-siderophore transporter; permease subunit	-2.649
cg1852	*sdaA*	L-Serine dehydratase	-2.393
cg1924	*cg1924*	Hypothetical protein	2.403
cg1930	*cg1930*	Putative secreted hydrolase	-4.143
cg1931	*cg1931*	Putative secreted protein	-3.367
cg2047	*cg2047*	Putative secreted protein	-2.042
cg2117	*ptsI*	Phosphotransferase system (PTS); Enzyme I	2.228
cg2118	*fruR*	transcriptional regulator of sugar metabolism; DeoR family	2.075
cg2119	*pfkB1*	1-Phosphofructokinase	2.213
cg2120	*ptsF*	Phosphotransferase system (PTS); fructose-specific enzyme IIABC component	2.160
cg2135	*miaB*	tRNA methylthiotransferase	1.944
cg2181	*cg2181*	ABC-type putative dipeptide/oligopeptide transporter; substrate-binding lipoprotein	3.909
cg2182	*cg2182*	ABC-type putative dipeptide/oligopeptide transporter; permease subunit	3.962
cg2183	*cg2183*	ABC-type putative dipeptide/oligopeptide transporter; permease subunit	3.672
cg2184	*cg2184*	ABC-type putative dipeptide/oligopeptide transporter; ATPase subunit	3.874
cg2224	*xerC*	Putative site-specific recombinase	-3.129
cg2234	*cg2234*	ABC-type putative iron(III) dicitrate transporter; substrate-binding lipoprotein	-3.176
cg2261	*amtB*	Putative secondary ammonium transporter; Amt-family	-2.420
cg2283	*cg2283*	Conserved hypothetical protein	-2.349
cg2313	*idhA3*	Myo-inositol 2-dehydrogenase	2.099
cg2430	*cg2430*	Hypothetical protein	5.838
cg2444	*cg2444*	Hypothetical protein	-2.299
cg2445	*hmuO*	Heme oxygenase (decyclizing)	-4.271
cg2467	*cg2467*	ABC-type transporter; ATPase subunit	2.150
cg2468	*cg2468*	ABC-type transporter; permease subunit	1.905
cg2545	*cg2545*	Putative secreted or membrane protein	2.366
cg2546	*cg2546*	Putative secondary C4-dicarboxylate transporter	2.400
cg2557	*cg2557*	Putative secondary Na^+/bile acid symporter	3.697
cg2610	*cg2610*	ABC-type putative dipeptide/oligopeptide transporter	3.686
cg2616	*vanA*	Vanillate monooxygenase	2.474
cg2631	*pcaH*	Protocatechuate 3;4-dioxygenase; beta subunit	2.692
cg2636	*catA*	Catechol 1;2-dioxygenase	5.303
cg2665	*cg2665*	Hypothetical protein	-1.961
cg2707	*cg2707*	Conserved hypothetical protein	2.197
cg2708	*msiK1*	ABC-type putative sugar transporter; ATPase subunit	1.990

Locus	Name	Function	PCA/Ref
cg2739	*cg2739*	Putative multidrug efflux permease; MFS-type	-2.206
cg2778	*cg2778*	Conserved hypothetical protein	1.973
cg2796	*cg2796*	Conserved hypothetical protein; MMGE/PRPD-family	-3.861
cg2797	*cg2797*	Conserved hypothetical protein	-2.939
cg2836	*sucD*	Succinate–CoA ligase (ADP-forming); alpha subunit	3.983
cg2837	*sucC*	Succinate–CoA ligase (ADP-forming); beta subunit	3.926
cg2937	*cg2937*	ABC-type putative dipeptide/oligopeptide transporter; substrate-binding lipoprotein	2.379
cg2939	*cg2939*	ABC-type putative dipeptide/oligopeptide transporter; ATPase subunit	1.982
cg2940	*cg2940*	ABC-type putative dipeptide/oligopeptide transporter; ATPase subunit	2.144
cg2962	*cg2962*	Hypothetical protein; uncharacterized enzyme involved in biosynthesis of extracellular polysaccharides	-3.872
cg2966	*cg2966*	Putative phenol 2-monooxygenase	2.058
cg3047	*ackA*	Acetate kinase	3.172
cg3048	*pta*	Phosphate acetyltransferase	3.094
cg3082	*cg3082*	Putative transcriptional regulator; ArsR-family	2.456
cg3107	*adhA*	Alcohol dehydrogenase	3.417
cg3124	*cg3124*	Conserved hypothetical protein	2.371
cg3126	*tctB*	Citrate uptake transporter; membrane subunit	2.121
cg3141	*hmp*	Globin-like flavohaemoprotein; putative nitric oxide dioxygenase	-2.115
cg3156	*cg3156*	Putative secreted protein	-7.289
cg3195	*cg3195*	Putative flavin-containing monooxygenase	5.156
cg3216	*gntP*	Putative secondary gluconate symporter; gluconate:H^+ symporter (GntP) family	3.120
cg3226	*cg3226*	Putative MFS-type L-lactate permease	2.473
cg3329	*cg3329*	Conserved hypothetical protein	-2.060
cg3344	*cg3344*	Putative nitroreductase	-2.678
cg3372	*cg3372*	Conserved hypothetical protein	-3.054
cg3374	*cye1*	Putative NADH-dependent flavin oxidoreductase	-2.176
cg3395	*proP*	Putative proline/betaine permease; MFS-type	2.198
cg3401	*cg3401*	Hypothetical protein	-2.088
cg3404	*cg3404*	ABC-type putative iron(III) dicitrate transporter; substrate-binding lipoprotein	-2.337
cg4005	*cg4005*	Putative secreted protein	-2.048

C.2. DEGs of the BHI supplementation experiment

Table C.2.: Differentially expressed genes obtained from transcriptome analysis of *C. glutamicum* cells grown in $37\,g\,L^{-1}$ brain-heart-infusion (37 BHI) supplemented CGXII ($20\,g\,L^{-1}$ glucose) batch conditions inducing $\mu = 0.67\,h^{-1}$. Log fold changes (FC) are based on the unsupplemented reference (Ref) condition. Gene names and functions were retrieved from the CoryneRegNet database (Pauling et al., 2012).

Locus	Name	Function	37 BHI/Ref
cg0012	*ssuR*	Transcriptional activator of sulfonate(ester) utilization; ROK-family	-2.495
cg0044	*cg0044*	ABC-type putative sugar transporter; substrate-binding lipoprotein	-3.467
cg0045	*cg0045*	ABC-type putative sugar transporter; permease subunit	-3.242
cg0046	*cg0046*	ABC-type putative sugar transporter; ATPase subunit	-3.464
cg0083	*cg0083*	Putative nicotinamide mononucleotide uptake permease; PnuC family	-2.680

Locus	Name	Function	37 BHI/Ref
cg0111	*cg0111*	Hypothetical protein	-2.548
cg0120	*cg0120*	Putative hydrolase	-2.954
cg0159	*cg0159*	Hypothetical protein	-5.238
cg0160	*cg0160*	Hypothetical protein	-3.860
cg0175	*cg0175*	Putative secreted protein	-2.72
cg0177	*cg0177*	Hypothetical protein	-3.351
cg0197	*iolC*	Putative 5-dehydro-2-deoxygluconokinase	4.695
cg0198	*cg0198*	Conserved hypothetical protein; probably involved in myo-inositol metabolism	4.731
cg0199	*iolA*	Methylmalonate-semialdehyde dehydrogenase	4.899
cg0201	*iolB*	Uncharacterized enzyme involved in inositol metabolism	3.447
cg0202	*iolD*	Putative acetolactate synthase; large subunit	3.813
cg0203	*iolE*	Putative myo-inosose-2 dehydratase	3.887
cg0204	*iolG*	Myo-inositol 2-dehydrogenase	3.972
cg0205	*iolH*	Myo-inositol catabolism protein	3.636
cg0210	*cg0210*	Putative transcriptional regulator; LacI-family	3.319
cg0223	*iolT1*	Putative sugar/metabolite permease; MFS-type	6.465
cg0228	*hkm*	Two-component system; sensory histidine kinase; putative pseudogene	2.542
cg0229	*gltB*	Glutamate synthase (NADPH); large chain	-4.133
cg0230	*gltD*	Glutamate synthase (NADPH); small chain	-2.919
cg0293	*cg0293*	Hypothetical protein	-2.508
cg0310	*katA*	Catalase	3.391
cg0404	*cg0404*	Conserved hypothetical protein; nitroreductase-family	-2.532
cg0405	*cg0405*	ABC-type putative iron(III) dicitrate transporter; substrate-binding lipoprotein	-5.262
cg0446	*sdhA*	Succinate dehydrogenase; subunit A	2.628
cg0447	*sdhB*	Succinate dehydrogenase; subunit B	2.506
cg0465	*cg0465*	Conserved putative membrane protein	-4.406
cg0466	*cg0466*	Conserved putative secreted protein	-4.871
cg0467	*cg0467*	ABC-type putative hemin transporter; substrate-binding lipoprotein	-3.719
cg0468	*cg0468*	ABC-type putative hemin transporter; permease subunit	-3.231
cg0469	*cg0469*	ABC-type putative hemin transporter; ATPase subunit	-3.624
cg0470	*cg0470*	Conserved secreted protein	-8.389
cg0471	*cg0471*	Conserved secreted protein	-8.235
cg0534	*cg0534*	Putative integral membrane protein	-2.568
cg0566	*gabT*	Putative 4-aminobutyrate aminotransferase; AT class II	2.667
cg0589	*cg0589*	ABC-type putative iron-siderophore transporter; ATPase subunit	-3.620
cg0590	*cg0590*	ABC-type putative iron-siderophore transporter; permease subunit	-3.724
cg0591	*cg0591*	ABC-type putative iron-siderophore transporter; permease subunit	-3.895
cg0635	*cg0635*	Putative NAD-dependent aldehyde dehydrogenase	-3.022
cg0701	*cg0701*	Putative secondary drug/metabolite transporter	-6.752
cg0737	*cg0737*	ABC-type methionine transporter; substrate-binding lipoprotein (TC 3.A.1.24.1)	-2.587
cg0754	*metX*	Homoserine O-acetyltransferase	-2.915
cg0755	*metY*	O-Acetylhomoserine sulfhydrylase	-2.861
cg0760	*prpB2*	Methylisocitrate lyase; involved in propionate catabolism	3.228
cg0767	*cg0767*	Siderophore-interacting protein	-3.446
cg0768	*cg0768*	ABC-type putative iron-siderophore transporter; ATPase subunit	-3.685
cg0769	*cg0769*	ABC-type putative iron-siderophore transporter; permease subunit	-3.008
cg0770	*cg0770*	ABC-type putative iron-siderophore transporter; permease subunit	-3.132
cg0771	*cg0771*	ABC-type putative iron-siderophore transporter; substrate-binding lipoprotein	-3.323
cg0825	*cg0825*	Putative short chain dehydrogenase related to 3-oxoacyl-(acyl-carrier protein) reductase	-6.265

Locus	Name	Function	37 BHI/Ref
cg0921	*cg0921*	Siderophore-interacting protein	-5.342
cg0922	*cg0922*	ABC-type putative iron-siderophore transporter; substrate-binding lipoprotein	-5.404
cg0924	*cg0924*	ABC-type putative iron-siderophore transporter; substrate-binding lipoprotein	-3.796
cg0926	*cg0926*	ABC-type putative iron-siderophore transporter; permease subunit	-2.962
cg0927	*cg0927*	ABC-type putative iron-siderophore transporter; permease subunit	-2.913
cg0928	*cg0928*	ABC-type putative iron-siderophore transporter; ATPase subunit	-3.061
cg0936	*rpf1*	RPF-protein precursor	2.501
cg1064	*urtC*	ABC-type putative branched-chain amino acid transporter; permease subunit	-2.989
cg1120	*ripA*	Putative transcriptional regulator; AraC-family	-5.069
cg1129	*aroF*	Putative phospho-2-dehydro-3-deoxyheptonate aldolase	-3.544
cg1139	*cg1139*	Allophanate hydrolase subunit 2	3.576
cg1140	*cg1140*	Allophanate hydrolase subunit 1	3.599
cg1141	*cg1141*	Conserved hypothetical protein; UPF0271-family	3.603
cg1142	*cg1142*	Putative Mn2+ transporter; metal ion (Mn2+-iron) transporter (Nramp) family	3.629
cg1147	*ssuI*	NAD(P)H-dependent FMN reductase	-2.894
cg1151	*seuA*	FMNH2-dependent monooxygenase; involved in sulfonate ester degradation	-2.540
cg1152	*seuB*	FMNH2-dependent monooxygenase; involved in sulfonate ester degradation	-3.465
cg1156	*ssuD2*	FMNH2-dependent aliphatic sulfonate monooxygenase	-3.402
cg1214	*nadS*	Putative cysteine desulfurase; AT class IV	-4.261
cg1215	*nadC*	Putative nicotinate-nucleotide pyrophosphorylase	-4.448
cg1216	*nadA*	Quinolinate synthetase; subunit A	-4.187
cg1218	*ndnR*	ADP-ribose pyrophosphatase	-4.181
cg1227	*cg1227*	Putative membrane protein	-9.653
cg1228	*cg1228*	ABC-type putative cobalt transporter; ATPase subunit	-10.099
cg1229	*cg1229*	ABC-type putative cobalt transporter; permease subunit	-10.192
cg1230	*cg1230*	Conserved hypothetical protein	-8.371
cg1231	*chaA*	Putative secondary Na+/Ca2+ antiporter; Ca2+:cation antiporter (CaCA) Family	-5.022
cg1290	*metE*	5-Methyltetrahydropteroyltriglutamate– homocysteine methyltransferase	-7.108
cg1296	*cg1296*	Conserved hypothetical protein; putative non-ribosomal peptide synthetase module	-3.332
cg1341	*narI*	Respiratory nitrate reductase 2; gamma chain	2.974
cg1342	*narJ*	Respiratory nitrate reductase 2; delta chain	3.183
cg1343	*narH*	Respiratory nitrate reductase 2; beta chain	2.922
cg1344	*narG*	Respiratory nitrate reductase 2; alpha chain	2.718
cg1345	*narK*	Putative nitrate/nitrite permease; MFS-type	2.658
cg1376	*ssuD1*	FMNH2-dependent aliphatic sulfonate monooxygenase	-3.601
cg1377	*ssuC*	ABC-type aliphatic sulfonate transporter; permease subunit	-5.171
cg1379	*ssuB*	ABC-type aliphatic sulfonate transporter; ATPase subunit	-4.320
cg1380	*ssuA*	ABC-type aliphatic sulfonate transporter; substrate-binding lipoprotein	-3.928
cg1418	*cg1418*	ABC-type putative iron-siderophore transporter; substrate-binding lipoprotein	-3.090
cg1419	*cg1419*	Putative secondary Na+/bile acid symporter; bile acid:Na+ symporter (BASS) family	-2.585
cg1473	*cg1473*	Conserved hypothetical protein	-2.977
cg1476	*thiC*	Thiamine biosynthesis protein ThiC	-10.090
cg1478	*cg1478*	Hypothetical protein	-8.165
cg1514	*cg1514*	Secreted protein	-5.993
cg1518	*cg1518*	Hypothetical protein	-2.662
cg1562	*cg1562*	Putative membrane protein	-2.691
cg1580	*argC*	N-acetyl-gamma-glutamyl-phosphate reductase	-3.362

Locus	Name	Function	37 BHI/Ref
cg1581	*argJ*	Glutamate N-acetyltransferase	-3.279
cg1582	*argB*	Acetylglutamate kinase	-3.375
cg1583	*argD*	Acetylornithine aminotransferase; AT class II	-3.395
cg1584	*argF*	Ornithine carbamoyltransferase	-3.262
cg1585	*argR*	Transcriptional repressor of arginine biosynthesis; ArgR-family	-3.190
cg1653	*pgp1*	Putative phosphoglycolate phosphatase	2.535
cg1654	*thiD1*	Phosphomethylpyrimidine kinase/thiamine-phosphate diphosphorylase	-4.603
cg1655	*thiM*	Hydroxyethylthiazole kinase	-3.884
cg1665	*cg1665*	Putative secreted protein	-3.134
cg1701	*metH*	Methionine synthase	-3.717
cg1739	*cg1739*	Glutamine amidotransferase domain	-2.574
cg1783	*soxA*	Putative oxidase; pseudogene (N-terminal fragment)	-3.348
cg1784	*ocd*	Putative ornithine cyclodeaminase	-4.602
cg1785	*amtA*	Putative secondary ammonium transporter; Amt-family	-4.044
cg1806	*metK*	Methionine adenosyltransferase	-2.545
cg1930	*cg1930*	Putative secreted hydrolase	-5.121
cg1931	*cg1931*	Putative secreted protein	-4.041
cg1932	*ppp2*	Putative protein phosphatase	-4.714
cg1940	*cg1940*	Putative secreted protein	-3.773
cg2181	*cg2181*	ABC-type putative dipeptide/oligopeptide transporter; substrate-binding lipoprotein	3.636
cg2182	*cg2182*	ABC-type putative dipeptide/oligopeptide transporter; permease subunit	3.889
cg2183	*cg2183*	ABC-type putative dipeptide/oligopeptide transporter; permease subunit	3.642
cg2184	*cg2184*	ABC-type putative dipeptide/oligopeptide transporter; ATPase subunit	3.887
cg2224	*xerC*	Putative site-specific recombinase	-3.536
cg2234	*cg2234*	ABC-type putative iron(III) dicitrate transporter; substrate-binding lipoprotein	-3.461
cg2236	*thiE*	Thiamine-phosphate diphosphorylase	-5.670
cg2237	*thiO*	Putative D-amino acid dehydrogenase; small subunit	-5.676
cg2238	*thiS*	Sulfur transfer protein involved in thiamine biosynthesis; ThiS-like	-4.820
cg2239	*thiG*	Thiamine biosynthesis protein; ThiG-like	-5.085
cg2240	*thiF*	Putative Dinucleotide-utilizing enzyme involved in thiamine biosynthesis	-5.325
cg2261	*amtB*	Putative secondary ammonium transporter; Amt-family	-2.901
cg2430	*cg2430*	Hypothetical protein	3.504
cg2445	*hmuO*	Heme oxygenase (decyclizing)	-4.991
cg2545	*cg2545*	Putative secreted or membrane protein	2.907
cg2546	*cg2546*	Putative secondary C4-dicarboxylate transporter; tripartite ATP-independent transporter (TRAP-T) family	3.138
cg2559	*aceB*	Malate synthase	-3.013
cg2560	*aceA*	Isocitrate lyase	-2.953
cg2610	*cg2610*	ABC-type putative dipeptide/oligopeptide transporter; substrate-binding lipoprotein	3.225
cg2636	*catA*	Catechol 1;2-dioxygenase	4.651
cg2687	*metB*	Cystathionine gamma-synthase	-2.492
cg2796	*cg2796*	Conserved hypothetical protein; MMGE/PRPD-family; putative involved in propoinate catabolism	-4.122
cg2797	*cg2797*	Conserved hypothetical protein	-3.317
cg2836	*sucD*	Succinate–CoA ligase (ADP-forming); alpha subunit	3.322
cg2837	*sucC*	Succinate–CoA ligase (ADP-forming); beta subunit	3.323
cg2870	*dctA*	Putative secondary H+/Na+:C4-dicarboxylate symporter; dicarboxylate/amino acid:cation symporter (DAACS) family	3.001

Locus	Name	Function	37 BHI/Ref
cg2875	*cg2875*	Hypothetical protein	2.583
cg2962	*cg2962*	Hypothetical protein; uncharacterized enzyme involved in biosynthesis of extracellular polysaccharides	-4.028
cg3111	*cg3111*	Putative secreted protein	-2.562
cg3119	*fpr2*	Ferredoxin–NADP(+) reductase	-2.826
cg3156	*cg3156*	Putative secreted protein	-6.872
cg3195	*cg3195*	Putative flavin-containing monooxygenase	2.746
cg3323	*cg3323*	Inositol-3-phosphate synthase	-8.210
cg3329	*cg3329*	Conserved hypothetical protein	-3.626
cg3344	*cg3344*	Putative nitroreductase	-2.821
cg3372	*cg3372*	Conserved hypothetical protein	-8.019
cg3374	*cg3374*	Putative NADH-dependent flavin oxidoreductase	-5.467
cg3375	*cg3375*	Predicted nucleoside-diphosphate-sugar epimerase	-2.489
cg3389	*cg3389*	Predicted oxidoreductase	3.785
cg3390	*cg3390*	Putative sugar phosphate isomerase/epimerase	5.537
cg3391	*idhA1*	Inositol 2-dehydrogenase	5.283
cg3392	*idhA2*	Inositol 2-dehydrogenase	4.786
cg3401	*cg3401*	Hypothetical protein	-3.884
cg4005	*cg4005*	Putative secreted protein	-5.967

C.3. Growth rate-dependent DEGs of supplementation experiments

Table C.3.: Differentially expressed genes obtained from transcriptome analysis of *C. glutamicum* cells grown in supplemented CGXII ($20\,g\,L^{-1}$ glucose) batch conditions featuring $10\,mg\,L^{-1}$ protocatechuate (PCA), or $1\,g\,L^{-1}$, $5\,g\,L^{-1}$, $10\,g\,L^{-1}$ and $37\,g\,L^{-1}$ BHI (1, 5, 10, 37 BHI) inducing $\mu = 0.45\,h^{-1}$, $0.44\,h^{-1}$, $0.54\,h^{-1}$, $0.59\,h^{-1}$ and $0.67\,h^{-1}$, respectively. Log fold changes (FC) are based on the lowest growth rate of $0.32\,h^{-1}$ (unsupplemented reference condition, Ref) as indicated. Gene names and functions were retrieved from the CoryneRegNet database (Pauling et al., 2012).

Locus	Name	Function	FC 1 BHI/Ref	FC PCA/Ref	FC 5 BHI/Ref	FC 10 BHI/Ref	FC 37 BHI/Ref
cg0120	*cg0120*	Putative hydrolase	-2.275	-1.986	-2.941	-2.380	-2.954
cg0228	*cg0228*	Two-component system; sensory histidine kinase; putative pseudogene	1.799	3.707	3.429	3.812	2.542
cg0229	*gltB*	Glutamate synthase (NADPH); large chain	-3.356	-2.380	-2.19	-3.121	-4.133
cg0701	*cg0701*	Putative secondary drug/metabolite transporter	-5.517	-6.776	-6.882	-7.273	-6.752
cg0760	*prpB2*	Methylisocitrate lyase; involved in propionate catabolism	5.069	6.734	8.648	4.913	3.228
cg0936	*rpf1*	RPF-protein precursor	2.129	2.317	2.483	2.551	2.501
cg1129	*aroF*	Putative phospho-2-dehydro-3-deoxyheptonate aldolase	-2.008	-3.100	-4.652	-5.288	-3.544
cg1296	*cg1296*	Conserved hypothetical protein; putative non-ribosomal peptide synthetase module	-1.546	-2.032	-2.300	-2.451	-3.332
cg1376	*ssuD1*	FMNH2-dependent aliphatic sulfonate monooxygenase	-1.846	-2.256	-2.555	-4.284	-3.601
cg1380	*ssuA*	ABC-type aliphatic sulfonate transporter; substrate-binding lipoprotein	-1.723	-2.348	-2.532	-4.324	-3.928
cg1476	*thiC*	Thiamine biosynthesis protein ThiC	-1.41	-2.555	-5.054	-7.884	-10.090
cg1478	*cg1478*	Hypothetical protein	-5.280	-5.543	-2.170	-7.114	-8.165
cg1580	*argC*	N-acetyl-gamma-glutamyl-phosphate reductase	-2.238	-2.377	-1.922	-3.050	-3.362
cg1581	*argJ*	Glutamate N-acetyltransferase	-2.339	-2.545	-2.177	-3.409	-3.279
cg1582	*argB*	Acetylglutamate kinase	-2.354	-2.437	-2.252	-3.408	-3.375
cg1583	*argD*	Acetylornithine aminotransferase; AT class II	-2.189	-2.481	-2.356	-3.588	-3.395
cg1584	*argF*	Ornithine carbamoyltransferase	-2.107	-2.251	-2.399	-3.782	-3.262
cg1585	*argR*	Transcriptional repressor of arginine biosynthesis; ArgR-family	-2.194	-2.098	-2.814	-4.021	-3.19
cg1783	*soxA'*	Putative oxidase; pseudogene (N-terminal fragment)	-2.103	-3.088	-3.152	-3.351	-3.348
cg1784	*ocd*	Putative ornithine cyclodeaminase	-3.115	-3.584	-3.596	-6.501	-4.602
cg1785	*amtA*	Putative secondary ammonium transporter; Amt-family	-2.822	-3.061	-4.084	-4.546	-4.044
cg2181	*cg2181*	ABC-type putative dipeptide/oligopeptide transporter; substrate-binding lipoprotein	3.526	3.909	2.839	2.567	3.636
cg2182	*cg2182*	ABC-type putative dipeptide/oligopeptide transporter; permease subunit	3.588	3.962	3.369	3.395	3.889
cg2183	*cg2183*	ABC-type putative dipeptide/oligopeptide transporter; permease subunit	3.375	3.672	2.864	2.708	3.642
cg2184	*cg2184*	ABC-type putative dipeptide/oligopeptide transporter; ATPase subunit	3.474	3.874	3.534	3.553	3.887
cg2261	*amtB*	Putative secondary ammonium transporter; Amt-family	-2.218	-2.42	-2.325	-2.577	-2.901
cg2430	*cg2430*	Hypothetical protein	5.034	5.838	6.170	6.872	3.504
cg2546	*cg2546*	Putative secondary C4-dicarboxylate transporter	1.475	2.400	2.621	2.415	3.138
cg2610	*cg2610*	ABC-type putative dipeptide/oligopeptide transporter; substrate-binding lipoprotein	2.630	3.686	4.312	4.673	3.225
cg2636	*catA*	Catechol 1;2-dioxygenase	2.657	5.303	5.488	6.554	4.651
cg2836	*sucD*	Succinate–CoA ligase (ADP-forming); alpha subunit	3.292	3.983	3.531	4.454	3.322
cg2837	*sucC*	Succinate–CoA ligase (ADP-forming); beta subunit	3.361	3.926	3.302	4.209	3.323
cg2962	*cg2962*	Hypothetical protein; uncharacterized enzyme involved in biosynthesis of extracellular polysaccharides	-1.906	-3.872	-3.319	-3.698	-4.028
cg3195	*cg3195*	Putative flavin-containing monooxygenase	3.525	5.156	4.571	5.628	2.746
cg3329	*cg3329*	Conserved hypothetical protein	-1.459	-2.06	-2.564	-2.837	-3.626
cg3344	*cg3344*	Putative nitroreductase	-2.272	-2.678	-2.356	-2.516	-2.821
cg3372	*cg3372*	Conserved hypothetical protein	-2.216	-3.054	-2.184	-6.226	-8.019
cg3374	*cg3374*	Putative NADH-dependent flavin oxidoreductase	-1.653	-2.176	-2.537	-5.454	-5.467

D. Supplementary material to Part II

D.1. Determination of μ_{max}

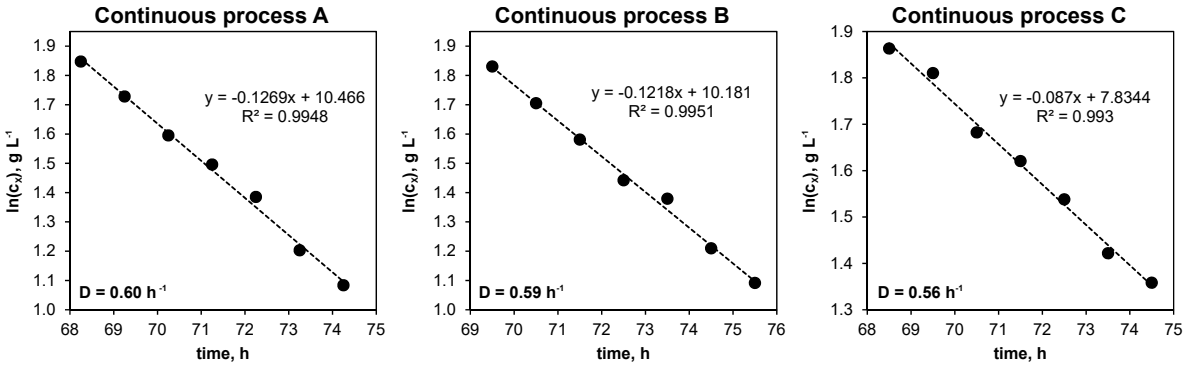

Figure D.1.: Illustration of half- logarithmic linear regression of biomass-time courses to determined the maximum growth rate of *C. glutamicum* cultivated in CGXII minimal medium ($12\,\mathrm{g\,L^{-1}}$ glucose. $30\,\mathrm{mg\,L^{-1}}$ protocatechuate) by wash out experiments in continuous processes A, B, C.

D.2. Simulation of steady state concentrations

Table D.4.: Simulation of metabolic steady state concentrations derived from experimental data of continuous chemostat process A ($c_{s,in} = 12.86\,\mathrm{g\,L^{-1}}$), mass balances of the continuous bioreactor, Monod-kinetics [$\mu_{max} = 0.62\,\mathrm{h^{-1}}$, Grünberger et al. (2013); $K_S = 14\,\mu\mathrm{mol\,L^{-1}}$; Lindner et al. (2011)], and maintenance after Pirt [m_s: $(0.08 \pm 0.02)\,\mathrm{mmol\,g^{-1}\,h^{-1}}$; $1/Y_{XS}^{real}$: $(7.74 \pm 0.16)\,\mathrm{mmol\,g^{-1}}$], Koch-Koerfges et al. (2013)]. $\tilde{c_s}$: simulated substrate concentration in metabolic steady state; $\tilde{c_x}$: simulated biomass concentration in metabolic steady state.

μ, $\mathrm{h^{-1}}$	0.2	0.3	0.4
$\tilde{c_s}$, $\mathrm{g\,L^{-1}}$	0.0012	0.0024	0.0046
$\tilde{c_x}$, $\mathrm{g\,L^{-1}}$	8.77	8.91	8.77

D.3. Intracellular metabolite pool sizes

Table D.5.: Biomass specific metabolite pool concentrations calculated from three biological replicates of *C. glutamicum* cultures cultivated in chemostat mode (processes A, B, C) at growth rates of $0.2\,h^{-1}$, $0.3\,h^{-1}$ and $0.4\,h^{-1}$. Values represent means ± standard deviations of four individual biomass samples.

	Biomass-specific intracellular metabolite pools. $\mu mol\,g^{-1}_{CDW}$								
	$\mu = 0.2\,h^{-1}$			$\mu = 0.3\,h^{-1}$			$\mu = 0.4\,h^{-1}$		
Process/ Metabolite	A	B	C	A	B	C	A	B	C
G6P	1.52 ± 0.10	1.23 ± 0.01	1.22 ± 0.05	4.87 ± 0.40	4.46 ± 0.15	3.64 ± 0.19	7.07 ± 0.09	6.63 ± 0.74	6.24 ± 0.43
F6P	0.76 ± 0.08	0.61 ± 0.04	0.56 ± 0.01	2.43 ± 0.15	2.21 ± 0.03	1.84 ± 0.07	3.56 ± 0.04	3.19 ± 0.19	2.99 ± 0.15
FbP	1.05 ± 0.18	0.78 ± 0.09	0.72 ± 0.00	6.24 ± 0.05	4.12 ± 0.12	3.26 ± 0.24	11.42 ± 0.81	8.68 ± 1.21	7.89 ± 1.22
DHAP	0.2 ± 0.4	0.16 ± 0.03	0.12 ± 0.01	0.63 ± 0.06	0.45 ± 0.05	0.47 ± 0.02	0.86 ± 0.13	0.49 ± 0.00	0.55 ± 0.01
2/3PG	1.24 ± 0.09	0.88 ± 0.08	1.03 ± 0.04	1.2 ± 1.0	0.81 ± 0.10	0.87 ± 0.15	0.56 ± 0.06	0.68 ± 0.01	0.73 ± 0.04
PEP	1.71 ± 0.10	1.35 ± 0.06	1.37 ± 0.01	1.41 ± 0.06	1.22 ± 0.06	1.17 ± 0.07	0.89 ± 0.05	0.86 ± 0.07	0.94 ± 0.03
Cit/IsoCit	0.00 ± 0.00	0.00 ± 0.00	0.00 ± 0.00	0.01 ± 0.00	0.01 ± 0.00	0.01 ± 0.00	0.01 ± 0.00	0.02 ± 0.00	0.01 ± 0.00
AKG	0.62 ± 0.10	0.88 ± 0.11	0.74 ± 0.04	0.63 ± 0.02	0.56 ± 0.01	0.56 ± 0.03	0.67 ± 0.05	0.52 ± 0.02	0.56 ± 0.03
Suc	7.87 ± 1.59	6.96 ± 0.17	6.53 ± 0.07	10.9 ± 1.5	8.56 ± 0.03	8.33 ± 0.41	9.08 ± 0.88	8.43 ± 0.77	8.61 ± 1.03
Fum	0.06 ± 0.01	0.05 ± 0.00	0.06 ± 0.00	0.11 ± 0.01	0.08 ± 0.00	0.09 ± 0.01	0.10 ± 0.01	0.11 ± 0.01	0.10 ± 0.01
Mal	0.35 ± 0.03	0.32 ± 0.01	0.36 ± 0.01	0.67 ± 0.02	0.55 ± 0.01	0.59 ± 0.04	0.7 ± 0.5	0.80 ± 0.06	0.74 ± 0.05
P5P	0.98 ± 0.05	0.82 ± 0.04	0.87 ± 0.02	0.91 ± 0.04	0.81 ± 0.04	0.76 ± 0.06	1.12 ± 0.07	0.94 ± 0.00	0.95 ± 0.10
S7P	0.50 ± 0.08	0.42 ± 0.03	0.40 ± 0.00	0.84 ± 0.03	0.74 ± 0.03	0.69 ± 0.02	0.81 ± 0.01	0.84 ± 0.04	0.84 ± 0.05
Ala	5.12 ± 0.57	4.99 ± 0.07	5.45 ± 1.08	6.17 ± 0.17	5.27 ± 0.12	5.32 ± 0.66	6.92 ± 0.18	6.14 ± 0.02	6.05 ± 0.16
Val	2.37 ± 0.26	2.26 ± 0.15	2.11 ± 0.02	3.30 ± 0.05	2.82 ± 0.06	3.00 ± 0.18	2.49 ± 0.03	2.46 ± 0.04	2.96 ± 0.13
Phe	0.05 ± 0.01	0.05 ± 0.00	0.05 ± 0.00	0.08 ± 0.00	0.08 ± 0.00	0.07 ± 0.01	0.14 ± 0.00	0.14 ± 0.01	0.12 ± 0.01
Trp	0.02 ± 0.00	0.02 ± 0.00	0.02 ± 0.00	0.03 ± 0.00	0.03 ± 0.00	0.03 ± 0.01	0.03 ± 0.00	0.03 ± 0.00	0.03 ± 0.00
Tyr	0.04 ± 0.00	0.04 ± 0.00	0.03 ± 0.00	0.07 ± 0.00	0.06 ± 0.00	0.05 ± 0.01	0.10 ± 0.01	0.09 ± 0.00	0.09 ± 0.00
Leu	0.69 ± 0.10	0.64 ± 0.03	0.64 ± 0.02	0.70 ± 0.01	0.58 ± 0.01	0.63 ± 0.04	0.40 ± 0.01	0.37 ± 0.01	0.47 ± 0.03
Ser	0.94 ± 0.04	1.03 ± 0.08	1.01 ± 0.03	1.42 ± 0.07	1.44 ± 0.04	1.53 ± 0.08	1.56 ± 0.09	1.56 ± 0.02	1.72 ± 0.09
Gly	1.42 ± 0.09	1.39 ± 0.06	1.49 ± 0.04	2.07 ± 0.09	1.98 ± 0.07	1.88 ± 0.11	3.38 ± 0.12	3.11 ± 0.15	2.92 ± 0.02
Glu	259.73 ± 11.67	256.64 ± 2.08	249.67 ± 2.82	272.23 ± 4.25	249.72 ± 6.65	237.74 ± 12.85	249.71 ± 5.14	250.48 ± 3.02	245.55 ± 10.34
Gln	6.03 ± 0.41	6.27 ± 0.27	6.38 ± 0.07	7.21 ± 0.13	6.62 ± 0.24	6.55 ± 0.32	10.96 ± 0.33	9.86 ± 0.28	9.57 ± 0.13
Arg	0.25 ± 0.02	0.23 ± 0.01	0.24 ± 0.01	0.28 ± 0.01	0.24 ± 0.00	0.24 ± 0.01	0.30 ± 0.01	0.28 ± 0.01	0.27 ± 0.01
Pro	0.64 ± 0.02	0.64 ± 0.01	0.90 ± 0.56	1.31 ± 0.25	1.03 ± 0.02	0.94 ± 0.14	5.11 ± 0.21	3.63 ± 0.09	2.93 ± 0.05
Asp	5.51 ± 0.37	5.24 ± 0.07	5.59 ± 0.64	5.25 ± 0.28	4.66 ± 0.27	4.70 ± 0.46	6.52 ± 0.22	5.6 ± 1.3	5.47 ± 0.26
Lys	0.72 ± 0.02	0.80 ± 0.13	0.82 ± 0.11	1.34 ± 0.03	1.15 ± 0.10	1.12 ± 0.14	1.67 ± 0.30	1.36 ± 0.16	1.31 ± 0.10
Thr	0.90 ± 0.06	0.82 ± 0.03	0.85 ± 0.01	1.21 ± 0.00	1.06 ± 0.05	1.06 ± 0.03	1.42 ± 0.03	1.32 ± 0.05	1.31 ± 0.04
Asn	0.01 ± 0.00	0.01 ± 0.00	0.01 ± 0.00	0.01 ± 0.00	0.01 ± 0.00	0.01 ± 0.00	0.01 ± 0.00	0.01 ± 0.00	0.01 ± 0.00
Ile	0.53 ± 0.07	0.50 ± 0.03	0.47 ± 0.01	0.81 ± 0.01	0.70 ± 0.00	0.69 ± 0.05	0.61 ± 0.00	0.59 ± 0.01	0.71 ± 0.02
Met	0.65 ± 0.08	0.61 ± 0.05	0.59 ± 0.02	0.51 ± 0.02	0.47 ± 0.01	0.46 ± 0.02	0.29 ± 0.00	0.29 ± 0.00	0.33 ± 0.01

D.4. Growth rate-dependent DEGs from chemostat experiments

Table D.6.: Differentially expressed genes obtained from transcriptome analysis of *C. glutamicum* cells grown in chemostat cultures ($\mu = 0.2\,h^{-1}$, $0.3\,h^{-1}$ and $0.4\,h^{-1}$) were clustered in two groups (cluster 1 and 2) based on their growth rate-dependent gene expression. Listed genes below belong to cluster 1 and revealed increasing expression over rising μ. Log fold changes (FC) are based on the lowest growth rate of $0.2\,h^{-1}$ as indicated. Gene names and functions were retrieved from the CoryneRegNet database (Pauling et al., 2012).

Locus	Name	Function	FC 0.3/0.2	FC 0.4/0.2
cg0010	*cg0010*	Conserved hypothetical protein	0.397	0.549
cg0039	*cg0039*	Putative transcriptional regulator	0.284	0.504
cg0082	*cg0082*	Chloride ion channel; ClC-family	0.726	1.295
cg0095	*bioB*	Biotin synthase	0.406	0.591
cg0121	*cg0121*	Putative multidrug efflux permease; MFS-type	0.278	0.484
cg0122	*cg0122*	Hypothetical protein	0.042	0.118
cg0148	*panC*	Pantoate–beta-alanine ligase	0.268	0.494
cg0156	*cysR*	Transcriptional activator of assimilatory sulfate reduction; ROK-family	0.106	0.415
cg0158	*cg0158*	Putative drug efflux permease; MFS-type	0.571	0.793
cg0183	*cg0183*	Putative threonine efflux transporter; resistance to homoserine/threonine (RhtB) family	0.125	0.408
cg0197	*iolC*	Putative 5-dehydro-2-deoxygluconokinase	0.270	0.567
cg0198	*cg0198*	Conserved hypothetical protein; probably involved in myo-inositol metabolism	0.169	0.491
cg0199	*iolA*	Methylmalonate-semialdehyde dehydrogenase	0.170	0.325
cg0223	*iolT1*	Putative sugar/metabolite permease; MFS-type	0.279	0.465
cg0235	*embC*	arabinofuranosyltransferase	0.253	0.602
cg0243	*cg0243*	Putative membrane protein	0.358	0.949
cg0244	*cg0244*	Putative membrane protein	0.263	0.762
cg0245	*cg0245*	Conserved hypothetical protein	0.214	0.793
cg0286	*cg0286*	Conserved putative membrane protein	0.883	1.556
cg0298	*recR*	DNA repair protein (RecF pathway)	0.333	0.882
cg0303	*leuA*	2-Isopropylmalate synthase	0.204	0.392
cg0307	*asd*	Aspartate-semialdehyde dehydrogenase	0.155	0.355
cg0308	*cg0308*	Putative membrane protein	0.204	0.347
cg0356	*cg0356*	Putative membrane-associated serine protease; membrane protein	0.111	0.398
cg0373	*topA*	DNA topoisomerase I	0.064	0.198
cg0391	*rmlB2*	Putative dTDP-glucose 4.6-dehydratase	0.247	0.412
cg0403	*rmlB1*	dTDP-glucose 4.6-dehydratase	0.333	0.643
cg0404	*cg0404*	Conserved hypothetical protein; nitroreductase-family	0.680	1.166
cg0411	*cg0411*	Putative membrane protein	0.578	1.274
cg0413	*cmt1*	Trehalose corynomycolyl transferase	0.100	0.366
cg0414	*wzz*	Cell surface polysaccharide biosynthesis/chain length determinant	0.395	0.755
cg0416	*cg0416*	Putative secreted protein; carrying a eukaryotic domain	0.263	0.413
cg0418	*cg0418*	Putative aminotransferase; involved in cell wall biosynthesis	0.196	0.401
cg0472	*cg0472*	Conserved hypothetical protein	0.246	0.809
cg0502	*qsuB*	putative dehydroshikimate dehydratase; 2 domain protein	0.308	0.405
cg0503	*aroD*	Probable 3-dehydroquinate dehydratase	0.347	0.504

Locus	Name	Function	FC 0.3/0.2	FC 0.4/0.2
cg0507	*cg0507*	ABC-type putative spermidine/putrescine/iron(III) transporter; permease subunit	0.424	0.628
cg0544	*cg0544*	Putative membrane protein	0.611	1.055
cg0563	*rplK*	50S ribosomal protein L11	0.356	0.716
cg0564	*rplA*	50S ribosomal protein L1	0.340	0.729
cg0572	*rplJ*	50S ribosomal protein L10	0.281	0.659
cg0573	*rplL*	Putative 50S ribosomal protein L7/L12	0.27	0.635
cg0581	*rpsL*	30S ribosomal protein S12	0.255	0.543
cg0582	*rpsG*	30S ribosomal protein S7	0.231	0.66
cg0593	*rpsJ*	30S ribosomal protein S10	0.218	0.606
cg0594	*rplC*	50S ribosomal protein L3	0.187	0.595
cg0596	*rplD*	50S ribosomal protein L4	0.171	0.513
cg0600	*rplV*	50S ribosomal protein L22	0.118	0.423
cg0604	*rpsQ*	30S ribosomal protein S17	0.220	0.576
cg0607	*cg0607*	Putative secreted protein	0.209	0.658
cg0608	*rplN*	50S ribosomal protein L14	0.190	0.562
cg0609	*rplX*	50S ribosomal protein L24	0.208	0.503
cg0628	*rpsH*	30S ribosomal protein S8	0.276	0.595
cg0629	*rplF*	50S ribosomal protein L6	0.218	0.636
cg0630	*rplR*	50S ribosomal protein L18	0.217	0.643
cg0631	*rpsE*	30S ribosomal protein S5	0.234	0.598
cg0634	*rplO*	50S ribosomal protein L15	0.241	0.487
cg0651	*infA*	Translation initiation factor IF-1	0.260	0.508
cg0652	*rpsM*	30S ribosomal protein S13	0.251	0.614
cg0653	*rpsK*	30S ribosomal protein S11	0.178	0.464
cg0654	*rpsD*	30S ribosomal protein S4	0.198	0.572
cg0673	*rplM*	50S ribosomal protein L13	0.337	0.783
cg0674	*rpsI*	30S ribosomal protein S9	0.332	0.72
cg0676	*cg0676*	Conserved hypothetical protein	0.542	0.993
cg0697	*cg0697*	Conserved hypothetical protein	0.095	0.559
cg0714	*cg0714*	Hypothetical protein	0.391	0.871
cg0732	*cg0732*	ABC-type transporter; permease subunit	0.363	0.789
cg0752	*cg0752*	Putative secreted or membrane protein	0.549	0.95
cg0756	*cstA*	Putative carbon starvation protein A	0.233	0.47
cg0757	*cg0757*	Conserved hypothetical protein	0.175	0.581
cg0779	*trpS*	Tryptophanyl-tRNA synthetase	0.250	0.451
cg0782	*dac*	D-alanyl-D-alanine carboxypeptidase	0.355	1.047
cg0790	*lpdA*	flavoprotein disulfid reductase family protein	0.132	0.438
cg0792	*cg0792*	Hypothetical protein	1.530	2.082
cg0793	*cg0793*	Putative secreted protein	1.194	1.594
cg0809	*maf*	Septum formation protein Maf	0.401	0.551
cg0816	*purK*	Phosphoribosylaminoimidazole carboxylase; ATPase subunit	0.208	0.399
cg0825	*cg0825*	Putative short chain dehydrogenase related to 3-oxoacyl-(acyl-carrier protein) reductase	0.285	0.533
cg0844	*cg0844*	Type II restriction enzyme; methylase subunit	0.067	0.206
cg0845	*cg0845*	DNA/RNA helicase; superfamily II	0.058	0.247
cg0848	*wbbL*	Putative glycosyltransferase	0.299	0.531
cg0861	*tmk*	Putative thymidylate kinase	0.272	0.579
cg0893	*cg0893*	Putative secreted protein; containing a PDZ-domain	0.303	0.606
cg0898	*pdxS*	pyridoxal 5'-phosphate (PLP) synthase subunit	0.365	0.66

Locus	Name	Function	FC 0.3/0.2	FC 0.4/0.2
cg0899	*pdxT*	pyridoxal 5'-phosphate (PLP) synthase subunit; glutamine amidotransferase	0.373	0.7
cg0936	*rpf1*	RPF-protein precursor	0.212	0.788
cg0938	*cspB*	Cold shock protein	0.239	0.686
cg0940	*cg0940*	Glutamine cyclotransferase	0.311	0.492
cg0948	*serC*	Phosphoserine transaminase; AT class IV	0.184	0.276
cg0949	*gltA*	Citrate synthase	0.290	0.558
cg0982	*cg0982*	Putative membrane protein	0.073	0.343
cg0983	*purN*	Phosphoribosylglycinamide formyltransferase	0.171	0.284
cg0989	*rpsN*	30S ribosomal protein S14	0.312	0.698
cg0990	*rpmG*	50S ribosomal protein L33	0.297	0.734
cg0991	*rpmB*	50S ribosomal protein L28	0.263	0.797
cg0993	*cg0993*	Putative transcriptional regulator; ArsR-family	0.402	0.612
cg0994	*rpmE*	Putative 50S ribosomal protein L31	0.098	0.406
cg1007	*cg1007*	Putative membrane protein	0.054	0.169
cg1014	*pmt*	Protein O-mannosyltransferase	0.118	0.374
cg1048	*cg1048*	Putative hydrolase; HAD superfamily	0.350	0.807
cg1052	*cmt3*	Corynomycolyl transferase	0.370	0.657
cg1067	*pth2*	Peptidyl-tRNA hydrolase	0.374	0.834
cg1076	*glmU*	Putative UDP-N-acetylglucosamine diphosphorylase	0.154	0.323
cg1171	*cg1171*	Putative GTPase	0.296	0.571
cg1219	*cg1219*	Putative membrane protein	0.364	0.798
cg1248	*cg1248*	Putative GTPase; probably involved in stress response	0.343	0.597
cg1252	*fdxC*	Ferredoxin	0.250	0.594
cg1290	*metE*	5-Methyltetrahydropteroyltriglutamate–homocysteine methyltransferase	0.355	0.784
cg1305	*cg1305*	Putative secondary proline transporter; amino acid-polyamine-organocation (APC) family	0.812	1.58 0
cg1332	*cg1332*	Putative secreted hydrolase	0.295	0.604
cg1364	*atpF*	ATP synthase F0; B chain	0.142	0.32
cg1398	*cg1398*	Conserved hypothetical protein	0.228	0.412
cg1417	*cg1417*	Putative acetyltransferase	0.339	0.568
cg1437	*ilvC*	Ketopantoate reductase	0.403	0.755
cg1458	*odx*	Putative hydrolase. FAA-family	0.157	0.379
cg1479	*glgP1*	Putative glycogen phosphorylase	0.180	0.420
cg1482	*cg1482*	Putative Zn-dependent hydrolase	0.230	0.454
cg1486	*ltbR*	Transcriptional regulator; IclR-family	0.316	0.872
cg1487	*leuC*	3-Isopropylmalate dehydratase; large subunit	0.552	1.352
cg1488	*leuD*	3-Isopropylmalate dehydratase; small subunit	0.569	1.411
cg1492	*gpsA*	Glycerol-3-phosphate dehydrogenase (NAD(P)(+))	0.421	0.757
cg1522	*cg1522*	Putative membrane protein	0.642	1.479
cg1531	*rpsA*	30S ribosomal protein S1	0.170	0.404
cg1553	*qor2*	quinone oxidoreductase involve in disulfide stress response	0.272	0.712
cg1563	*infC*	Translation initiation factor IF-3	0.162	0.412
cg1564	*rpmI*	50S ribosomal protein L35	0.149	0.428
cg1572	*glpQ2*	Putative glycerophosphodiester phosphodiesterase	0.397	0.804
cg1574	*pheS*	Phenylalanyl-tRNA synthetase; alpha chain	0.177	0.292
cg1595	*uspA2*	Universal stress protein UspA	0.331	0.793
cg1602	*recN*	DNA repair protein RecN	0.259	0.544
cg1611	*scpA*	Putative segregation and condensation protein A	0.105	0.376

Locus	Name	Function	FC 0.3/0.2	FC 0.4/0.2
cg1613	*sseA2*	Rhodanese-related sulfurtransferase	0.219	0.503
cg1614	*scpB*	Putative segregation and condensation protein B	0.345	0.569
cg1622	*cg1622*	ABC-type putative multidrug transporter; ATPase and permease subunit	0.622	1.082
cg1638	*cg1638*	Conserved hypothetical protein	0.228	0.451
cg1661	*cg1661*	Putative secondary arsenite transporter; arsenical resistance-3 (ACR3) family	0.326	0.552
cg1698	*hisG*	ATP phosphoribosyltransferase	0.273	0.48
cg1710	*bacA*	Putative undecaprenol kinase	0.461	0.685
cg1782	*tnp13b*	Transposase	0.315	0.557
cg1845	*cg1845*	Conserved hypothetical protein	0.088	0.353
cg1857	*ppiB*	Peptidyl-prolyl cis-trans isomerase	0.350	0.591
cg1867	*secD*	Preprotein translocase; SecD subunit	0.174	0.388
cg1881	*cg1881*	Conserved putative secreted protein; iron-dependent peroxidase	0.358	0.596
cg1883	*cg1883*	Putative secreted protein	0.312	0.566
cg1916	*cg1916*	Hypothetical protein	0.371	0.700
cg1918	*cg1918*	Putative secreted protein	0.414	0.845
cg1920	*cg1920*	Hypothetical protein	0.644	1.734
cg1926	*cg1926*	Hypothetical protein	0.276	0.557
cg1929	*res*	Putative resolvase; family recombinase	0.490	0.900
cg1957	*cg1957*	Hypothetical protein	0.343	0.559
cg1963	*cg1963*	Putative DNA/RNA helicase; superfamily II	0.164	0.623
cg1997	*cglIR*	Putative type II restriction endonuclease	0.266	0.454
cg1998	*cglIIR*	ATP-dependent helicase probaly involved in restriction and/or modification	0.238	0.378
cg2047	*cg2047*	Putative secreted protein	0.498	1.001
cg2117	*ptsI*	Phosphotransferase system; Enzyme I	0.206	0.518
cg2124	*cg2124*	Putative transcriptional regulator; AraC family	0.114	0.388
cg2125	*uraA*	Putative xanthine/uracil symporter; nucleobase:cation symporter-2 (NCS2) family	0.246	0.542
cg2130	*miaA*	tRNA isopentenyltransferase	0.129	0.291
cg2135	*miaB*	tRNA methylthiotransferase	0.213	0.355
cg2163	*dapB*	Dihydrodipicolinate reductase	0.329	0.510
cg2167	*rpsO*	30S ribosomal protein S15	0.277	0.776
cg2168	*iunH2*	Nucleoside hydrolase; inosine-uridine preferring	0.304	0.471
cg2178	*nusA*	Putative transcriptional termination/antitermination factor	0.320	0.598
cg2184	*cg2184*	ABC-type putative dipeptide/oligopeptide transporter; ATPase subunit	0.317	0.453
cg2194	*mtr*	Putative NADPH-dependent mycothiol reductase	0.181	0.260
cg2200	*chrA*	Two-component system; transcriptional response regulator	0.293	0.220
cg2216	*cdsA*	Phosphatidate cytidylyltransferase	0.159	0.357
cg2222	*rpsB*	30S ribosomal protein S2	0.297	0.613
cg2230	*rnhB*	Ribonuclease HII	0.429	0.791
cg2239	*thiG*	Thiamine biosynthesis protein; ThiG-like	0.159	0.502
cg2302	*cg2302*	Putative membrane protein	0.249	0.431
cg2307	*cg2307*	Putative membrane protein	0.260	0.412
cg2308	*cg2308*	Putative secreted protein	0.114	0.327
cg2320	*cg2320*	Putative transcriptional regulator; ArsR-family	0.077	0.393
cg2324	*cg2324*	Conserved hypothetical protein	0.183	0.438
cg2336	*cg2336*	Putative secreted protein	0.354	0.673

Locus	Name	Function	FC 0.3/0.2	FC 0.4/0.2
cg2337	*cg2337*	Hypothetical protein	0.242	0.515
cg2359	*ileS*	Isoleucine–tRNA ligase	0.175	0.327
cg2367	*ftsQ*	Cell division septal protein	0.109	0.238
cg2373	*murF*	UDP-N-acetylmuramoyl-tripeptide–D-alanyl-D-alanine ligase	0.077	0.358
cg2374	*murE*	UDP-N-acetylmuramoylalanyl-D-glutamate–2.6-diaminopimelate ligase	0.047	0.364
cg2394	*cmt4*	Corynomycolyl transferase	0.160	0.446
cg2395	*cg2395*	Putative secreted or membrane protein	0.298	0.763
cg2409	*ctaC*	Cytochrome c oxidase subunit II	0.239	0.344
cg2410	*ltsA*	Asparagine synthase (glutamine-hydrolyzing)	0.179	0.400
cg2437	*thrC*	Threonine synthase	0.378	0.587
cg2449	*cg2449*	Conserved hypothetical protein	0.401	1.042
cg2452	*galK*	Galactokinase	0.299	0.631
cg2514	*cg2514*	Conserved hypothetical protein	0.210	0.307
cg2543	*glcD*	Putative (S)-2-hydroxy-acid oxidase	0.385	0.667
cg2546	*cg2546*	Putative secondary C4-dicarboxylate transporter; tripartite ATP-independent transporter (TRAP-T) family	0.294	0.871
cg2556	*cg2556*	Putative integral membrane protein	0.221	0.526
cg2557	*cg2557*	Putative secondary Na+/bile acid symporter; bile acid:Na+ symporter (BASS) family	0.527	1.161
cg2579	*cg2579*	Conserved hypothetical protein; DegV-family	0.230	0.365
cg2581	*cg2581*	Putative fructose-2.6-bisphosphatase	0.217	0.408
cg2592	*cg2592*	Hypothetical protein	0.155	0.284
cg2595	*rplU*	50S ribosomal protein L21	0.116	0.389
cg2601	*cg2601*	Pirin-related protein; putative pseudogen (C-terminal fragment)	0.259	0.436
cg2647	*tig*	Putative Trigger factor; invoved in cell division	0.160	0.472
cg2687	*metB*	Cystathionine gamma-synthase	0.256	0.716
cg2691	*cg2691*	Conserved hypothetical protein	0.389	0.622
cg2719	*cg2719*	Putative enterochelin esterase	0.796	1.667
cg2809	*cg2809*	Putative membrane protein	0.183	0.431
cg2811	*cg2811*	ABC-type lipoprotein release transporter; permease subunit	0.426	0.614
cg2829	*murA2*	UDP-N-acetylglucosamine 1-carboxyvinyltransferase	0.25	0.427
cg2834	*cysE*	Serine O-acetyltransferase	0.223	0.45
cg2870	*dctA*	Putative secondary H+/Na+:C4-dicarboxylate symporter; dicarboxylate/amino acid:cation symporter (DAACS) family	0.196	0.617
cg2873	*ptrB*	Oligopeptidase B	0.247	0.396
cg2922	*cg2922*	Putative transcriptional regulator; IclR-family	0.296	0.831
cg2925	*ptsS*	Phosphotransferase system; sucrose-specific enzyme IIBCA component	0.465	1.109
cg2942	*cg2942*	Putative transcriptional regulator; AsnC-family	0.166	0.352
cg2945	*ispD*	Putative 2-C-methyl-D-erythritol 4-phosphate cytidylyltransferase	0.178	0.366
cg2952	*cg2952*	Putative secreted protein	0.262	0.526
cg2964	*guaB1*	IMP dehydrogenase	0.286	0.608
cg3011	*groEL2*	Chaperonin Cpn60 (60Kd subunit)	0.346	0.541
cg3031	*cg3031*	Conserved hypothetical protein; glutamate-cysteine ligase family	0.195	0.265
cg3032	*cg3032*	Putative secreted protein	0.154	0.482
cg3047	*ackA*	Acetate kinase	0.447	0.874
cg3048	*pta*	Phosphate acetyltransferase	0.434	0.913
cg3066	*cg3066*	Putative membrane protein	0.149	0.317
cg3074	*cg3074*	Conserved hypothetical protein	0.361	1.134

Locus	Name	Function	FC 0.3/0.2	FC 0.4/0.2
cg3098	*dnaJ*	Chaperone DnaJ; heat shock protein	0.244	0.441
cg3133	*cg3133*	ABC-type putative cobalt/sugar transporter; ATPase subunit	0.466	0.897
cg3134	*cg3134*	ABC-type putative cobalt/sugar transporter; permease subunit	0.519	1.017
cg3135	*cg3135*	Putative membrane protein	0.429	0.939
cg3138	*ppmA*	Band 7 domain-containing protein; stomatin/prohibitin homolog	0.346	1.395
cg3139	*cg3139*	Conserved hypothetical protein	0.414	1.479
cg3140	*tagA1*	DNA-3-methyladenine glycosylase I	0.358	1.456
cg3178	*pks*	Putative polyketide synthase; PksM-like	0.087	0.322
cg3180	*cg3180*	Putative secreted protein	0.232	0.512
cg3181	*cg3181*	Putative secreted protein	0.232	0.520
cg3182	*cop1*	Trehalose corynomycolyl transferase	0.215	0.403
cg3189	*ubiA*	Polyprenyltransferase. involved in decaprenol phosphoarabinose synthesis	0.253	0.582
cg3190	*cg3190*	Membrane-associated decaprenylphosphoryl-5-phosphoribose phosphatase	0.205	0.508
cg3191	*glfT*	Putative glycosyltransferase	0.207	0.449
cg3197	*psp5*	Putative secreted protein	0.438	0.795
cg3206	*cg3206*	Putative phosphoglycerate mutase	0.286	0.650
cg3214	*cg3214*	Conserved hypothetical protein	0.337	0.709
cg3243	*cg3243*	Conserved hypothetical protein; RecB-family nuclease	0.255	0.534
cg3323	*ino1*	Inositol-3-phosphate synthase	0.415	0.584
cg3344	*cg3344*	Putative nitroreductase	0.265	0.724
cg3374	*cye1*	Putative NADH-dependent flavin oxidoreductase	0.543	1.141
cg3375	*cg3375*	Predicted nucleoside-diphosphate-sugar epimerase	0.263	0.613
cg3395	*proP*	Putative proline/betaine permease; MFS-type	0.306	1.048
cg3409	*thiD2*	Phosphomethylpyrimidine kinase	0.448	0.835
cg3423	*trxC*	Thioredoxin	0.072	0.271
cg3424	*cwlM*	N-Acetylmuramoyl-L-alanine amidase	0.111	0.352

Table D.7.: Differentially expressed genes obtained from transcriptome analysis of *C. glutamicum* cells grown in chemostat cultures ($\mu = 0.2\,h^{-1}$, $0.3\,h^{-1}$ and $0.4\,h^{-1}$) were clustered in two groups (cluster 1 and 2) based on their growth rate-dependent gene expression. Listed genes below belong to cluster 2 and revealed decreasing expression over rising μ. Gene names and functions were retrieved from the CoryneRegNet database (Pauling et al., 2012).

Locus	Name	Function	FC 0.3/0.2	FC 0.4/0.2
cg0064	*cg0064*	Conserved hypothetical protein; FHA dpmain	-0.122	-0.194
cg0109	*lip1*	Triacylglycerol lipase	-0.313	-0.605
cg0120	*cg0120*	Putative hydrolase	-0.585	-1.294
cg0138	*cg0138*	ATP/GTP-binding protein	-0.261	-0.496
cg0139	*cg0139*	Putative transcriptional regulator; DeoR-family	-0.368	-0.807
cg0170	*cg0170*	Putative membrane protein	-0.197	-0.425
cg0171	*cg0171*	Putative secreted protein	-0.296	-0.681
cg0175	*cg0175*	Putative secreted protein	-0.874	-1.579
cg0192	*cg0192*	Conserved hypothetical protein	-0.685	-1.249
cg0222	*cg0222*	Putative membrane protein	-0.291	-0.711
cg0291	*cg0291*	Putative dioxygenase	-0.706	-1.404
cg0337	*whcA*	Putative transcriptional regulator; WhiB-family	-0.218	-0.479

Locus	Name	Function	FC 0.3/0.2	FC 0.4/0.2
cg0380	*cg0380*	Hypothetical protein	-0.261	-0.815
cg0432	*cg0432*	Putative lipopolysaccharide modification acyltransferase	-0.111	-0.354
cg0439	*cg0439*	Putative acetyl transferase	-0.203	-0.287
cg0452	*cg0452*	Hypothetical protein	-0.177	-0.410
cg0481	*mshA*	Putative glycosyltransferase; involved in mycothiol biosynthesis	-0.179	-0.347
cg0515	*cg0515*	Putative cation transporting P-type ATPase	-0.168	-0.311
cg0516	*hemE*	Uroporphyrinogen decarboxylase	-0.397	-0.731
cg0519	*cg0519*	Putative phosphoglycerate mutase	-0.277	-0.563
cg0522	*ccsA*	Cytochrome c biogenesis membrane protein; DsbD-family	-0.234	-0.543
cg0524	*ccsB*	Cytochrome c biogenesis membrane protein; CcsA-family	-0.262	-0.365
cg0535	*cg0535*	Putative ketoglutarate semialdehyde dehydrogenase	-0.844	-1.590
cg0536	*cg0536*	Putative 5-dehydro-4-deoxyglucarate dehydratase	-0.647	-1.229
cg0579	*cg0579*	Transcriptional regulatory protein; HTH3-family	-0.194	-0.574
cg0618	*fdhF*	Putative formate dehydrogenase; FdhA-family alpha chain	-0.152	-0.364
cg0638	*cg0638*	Hypothetical protein	-0.186	-0.769
cg0650	*cg0650*	Putative secreted protein	-0.298	-0.651
cg0662	*cg0662*	Conserved hypothetical protein; putative FAD/FMN-containing dehydrogenase	-0.272	-0.514
cg0683	*cg0683*	Putative permease	-0.263	-0.466
cg0745	*cg0745*	Putative NAD-dependent protein deacetylase; SIR2-family	-0.172	-0.418
cg0788	*pmmB*	Phosphoglucomutase/phosphomannomutase	-0.263	-0.771
cg0796	*prpD1*	Putative (2-methyl) citrate dehydratase	-0.777	-1.614
cg0797	*prpB1*	Putative (methyl)isocitrate lyase	-0.853	-1.896
cg0798	*prpC1*	Putative (methyl)citrate synthase	-0.927	-1.805
cg0806	*cg0806*	Conserved hypothetical protein	-0.326	-0.707
cg0807	*cg0807*	Conserved hypothetical protein	-0.172	-0.462
cg0812	*dtsR1*	Acetyl/propionyl-CoA carboxylase; beta chain	-0.227	-0.404
cg0874	*cg0874*	Conserved hypothetical protein	-0.275	-0.445
cg0882	*cg0882*	Conserved hypothetical protein	-0.243	-0.697
cg0896	*cg0896*	Putative membrane protein	-0.068	-0.236
cg0906	*cg0906*	Hypothetical protein	-0.271	-0.528
cg0961	*cg0961*	Putative hydrolase; alpha/beta-fold	-0.225	-0.921
cg0973	*pgi*	Glucose-6-phosphate isomerase	-0.186	-0.319
cg0997	*cgtS2*	Two-component system; sensory histidine kinase	-0.217	-0.445
cg0998	*cg0998*	Trypsin-like serine protease	-0.383	-0.53
cg1018	*cg1018*	Putative ATP-dependent DNA helicase	-0.224	-0.336
cg1028	*cg1028*	Putative restriction-modification system methylase	-0.195	-0.541
cg1043	*cg1043*	Conserved hypothetical protein	-0.309	-0.666
cg1045	*cg1045*	Conserved hypothetical protein	-0.234	-0.561
cg1068	*cg1068*	Putative oxidoreductase	-0.238	-0.776
cg1073	*cg1073*	Putative lactoylglutathione lyase	-0.167	-0.704
cg1080	*cg1080*	Putative multicopper oxidase	-0.487	-0.861
cg1085	*cg1085*	Hypothetical protein	-0.45	-1.18
cg1087	*cg1087*	Putative membrane protein	-0.465	-1.256
cg1088	*cg1088*	ABC-type putative multidrug transporter; ATPase and permease subunit	-0.468	-1.195
cg1090	*ggtB*	Putative gamma-glutamyltranspeptidase	-0.104	-0.723
cg1091	*cg1091*	Hypothetical protein	-0.364	-0.902
cg1099	*mfd*	Transcription-repair coupling factor (TRCF)	-0.063	-0.131
cg1106	*cg1106*	conserved hypothetical protein	-0.358	-0.603

Locus	Name	Function	FC 0.3/0.2	FC 0.4/0.2
cg1137	*cg1137*	Putative transcriptional regulator; LysR-family	-0.153	-0.444
cg1144	*cg1144*	Hypothetical protein	-0.274	-0.449
cg1166	*cg1166*	Putative membrane protein	-0.201	-0.568
cg1174	*arcB*	Putative ornithine carbamoyltransferase	-0.336	-0.561
cg1179	*cg1179*	Putative membrane protein	-0.249	-0.717
cg1182	*cg1182*	Putative membrane protein	-0.360	-0.698
cg1190	*cg1190*	Hypothetical protein	-0.524	-1.001
cg1195	*cg1195*	Putative permease; sulfate permease (SulP) family	-0.254	-0.726
cg1204	*cg1204*	Conserved hypothetical protein; similar to 2.3-PDG dependent phosphoglycerate mutase	-0.324	-0.749
cg1205	*cg1205*	Conserved hypothetical protein	-0.254	-0.835
cg1206	*cg1206*	Conserved hypothetical protein	-0.196	-0.674
cg1220	*cg1220*	Putative Zn-dependent hydrolase; beta-lactamase fold	-0.409	-0.640
cg1224	*cg1224*	Conserved hypothetical protein	-0.386	-1.094
cg1237	*cg1237*	Putative membrane protein	-0.121	-0.221
cg1238	*cg1238*	Putative membrane protein	-0.307	-0.561
cg1244	*cg1244*	Arsenate reductase or related protein; glutaredoxin-family	-0.159	-0.353
cg1265	*cg1265*	Conserved hypothetical protein	-0.128	-0.294
cg1267	*cg1267*	Beta-fructosidase (levanase/invertase)	-0.251	-0.510
cg1271	*sigE*	RNA polymerase sigma factor; ECF-family	-0.413	-0.687
cg1276	*mgtE1*	Putative Mg2+ transporter; Mg2+ transporter-E (MgtE) family	-0.206	-0.440
cg1283	*aroE2*	Putative shikimate/quinate 5-dehydrogenase	-0.050	-0.240
cg1284	*lipT*	Putative carboxylesterase; type B	-0.247	-0.546
cg1285	*cg1285*	Conserved hypothetical protein	-0.204	-0.415
cg1286	*cg1286*	Conserved hypothetical protein	-0.046	-0.272
cg1298	*cydC*	ABC-type putative multidrug/protein/lipid transporter; ATPase and permease subunit	-0.096	-0.335
cg1299	*cydD*	ABC-type putative multidrug/protein/lipid transporter; ATPase and permease subunit	-0.15	-0.365
cg1301	*cydA*	Cytochrome d ubiquinol oxidase subunit I	-0.181	-0.542
cg1313	*cg1313*	Putative secreted lipoprotein	-0.422	-0.825
cg1314	*putP*	Putative Na+/proline symporter; solute:sodium symporter (SSS) family	-0.222	-0.502
cg1317	*cg1317*	Conserved hypothetical protein	-0.159	-0.25
cg1352	*moaA*	Molybdopterin biosynthesis protein A	-0.258	-0.563
cg1381	*glgB*	1.4-alpha-glucan branching enzyme	-0.141	-0.350
cg1382	*glgE*	Putative alpha-amylase	-0.100	-0.311
cg1396	*cg1396*	Hypothetical protein	-0.101	-0.545
cg1423	*cg1423*	Putative oxidoreductase; aldo/keto reductase family	-0.289	-0.691
cg1426	*gst*	Putative glutathione S-transferase	-0.197	-0.335
cg1454	*cg1454*	ABC-type putative aliphatic sulfonates transporter; substrate-binding lipoprotein	-0.494	-1.223
cg1474	*cg1474*	Hypothetical protein	-0.253	-0.428
cg1483	*cg1483*	Putative membrane protein	-0.110	-0.542
cg1485	*cg1485*	Putative metal dependent phosphohydrolase; RelA/SpoT-like	-0.272	-0.831
cg1498	*cg1498*	ATP-dependent DNA helicase; RecG-like	-0.164	-0.393
cg1545	*uriT*	Putative multidrug efflux permease; MFS-type	-0.357	-0.451
cg1550	*uvrB*	Excinuclease ABC; subunit B	-0.199	-0.460
cg1551	*uspA1*	Universal stress protein UspA	-0.187	-0.682
cg1562	*cg1562*	Putative membrane protein	-0.374	-0.754

Locus	Name	Function	FC 0.3/0.2	FC 0.4/0.2
cg1589	*cg1589*	Putative secreted protein	-0.515	-1.176
cg1590	*cg1590*	Conserved putative secreted protein	-0.598	-1.204
cg1591	*cg1591*	Putative secreted protein	-0.327	-0.696
cg1612	*cg1612*	Putative acetyltransferase	-0.224	-0.844
cg1619	*cg1619*	Putative transcriptional regulator; AraC family	-0.237	-0.667
cg1630	*cg1630*	Putative signal transduction protein; FHA-domain	-0.152	-0.394
cg1635	*cg1635*	Putative membrane protein	-0.351	-0.631
cg1646	*cg1646*	ABC-type multidrug transport system; ATPase subunit	-0.285	-0.660
cg1647	*cg1647*	ABC-type multidrug transport system; permease subunit	-0.274	-0.882
cg1665	*cg1665*	Putative secreted protein	-0.828	-1.787
cg1671	*cg1671*	Putative membrane-associated GTPase	-0.206	-0.410
cg1673	*ppmN*	Polyprenol-phosphate-mannose synthase domain 2	-0.077	-0.180
cg1676	*lip*	Putative lipase	-0.140	-0.450
cg1683	*cg1683*	DNA/RNA helicase; superfamily II	-0.350	-0.724
cg1693	*pepC*	putative aspartyl aminopeptidase	-0.140	-0.423
cg1697	*aspA*	Aspartate ammonia-lyase	-0.281	-0.588
cg1703	*cg1703*	Putative FAD-dependent pyridine nucleotide-disulphide oxidoreductase	-0.314	-0.541
cg1705	*arsB1*	Putative secondary arsenite transporter; arsenical resistance-3 (ACR3) family	-0.234	-0.317
cg1706	*arsC1*	Putative arsenate reductase (arsenical pump modifier)	-0.145	-0.543
cg1730	*cg1730*	Putative secreted protease subunit; stomatin/prohibitin-like	-0.147	-0.258
cg1734	*hemH*	Ferrochelatase	-0.494	-0.926
cg1740	*cg1740*	Putative nucleoside-diphosphate-sugar epimerase	-0.260	-0.560
cg1741	*cg1741*	Putative membrane protein	-0.272	-0.750
cg1742	*cg1742*	Conserved hypothetical protein; containing an ACT-domain	-0.143	-0.286
cg1744	*pacL*	Putative cation transporting P-type ATPase	-0.081	-0.397
cg1759	*cg1759*	Putative metal-sulfur cluster biosynthetic enzyme	-0.359	-0.569
cg1760	*sufU*	Protein involved in Fe-S cluster formation; NifU-family	-0.316	-0.554
cg1761	*sufS*	cysteine desulfurase	-0.356	-0.588
cg1762	*sufC*	FeS cluster assembly ATPase; SufC-family	-0.373	-0.617
cg1763	*sufD*	FeS cluster assembly protein; SufD-family	-0.343	-0.572
cg1764	*sufB*	FeS cluster assembly protein; SufB-family	-0.37	-0.584
cg1766	*mptB*	Putative membrane protein	-0.237	-0.485
cg1771	*qor*	Putative NADPH:quinone reductase; zeta-crystallin	-0.044	-0.263
cg1792	*cg1792*	Putative transcriptional regulator; WhiB-family	-0.271	-0.551
cg1793	*cg1793*	Conserved hypothetical protein	-0.337	-0.596
cg1794	*cg1794*	Conserved hypothetical protein; P-loop ATPase protein family	-0.186	-0.427
cg1800	*ribG*	Riboflavin-specific deaminase/reductase	-0.108	-0.302
cg1807	*dfp*	Putative flavoprotein. involved CoA metabolism	-0.151	-0.394
cg1812	*pyrF*	Orotidine-5'-phosphate decarboxylase	-0.328	-0.724
cg1813	*carB*	Carbamoyl-phosphate synthase. large chain	-0.423	-0.712
cg1815	*pyrC*	Dihydroorotase	-0.414	-0.679
cg1817	*pyrR*	Putative RNA-binding regulatory protein; phosphoribosyltransferase domain	-0.321	-0.522
cg1840	*cg1840*	Conserved hypothetical protein	-0.217	-0.468
cg1852	*sdaA*	L-Serine dehydratase	-0.357	-0.675
cg1859	*cg1859*	Putative secreted protein	-0.206	-0.396
cg1861	*rel*	GTP diphosphokinase	-0.239	-0.500
cg1872	*cg1872*	Conserved hypothetical protein	-0.141	-0.210

Locus	Name	Function	FC 0.3/0.2	FC 0.4/0.2
cg1895	*cg1895*	Putative secreted protein	-0.128	-0.318
cg1904	*cg1904*	ABC-type transporter; permease subunit	-0.219	-0.412
cg1905	*cg1905*	Hypothetical protein	-0.174	-0.582
cg1907	*cg1907*	Putative phosphopantothenoylcysteine synthetase/decarboxylase	-0.334	-0.87
cg1908	*cg1908*	Hypothetical protein	-0.299	-0.822
cg1917	*cg1917*	Hypothetical protein	-0.500	-0.618
cg1942	*cg1942*	Putative secreted protein	-0.160	-0.796
cg1943	*cg1943*	Hypothetical protein	-0.240	-0.832
cg2026	*cg2026*	Hypothetical protein	-0.389	-0.823
cg2029	*cg2029*	Hypothetical protein	-0.404	-0.843
cg2034	*cg2034*	Hypothetical protein	-0.176	-0.453
cg2038	*cg2038*	Hypothetical protein	-0.165	-0.370
cg2046	*cg2046*	Hypothetical protein	-0.313	-0.724
cg2056	*cg2056*	Putative membrane protein	-0.180	-0.427
cg2060	*cg2060*	Hypothetical protein	-0.223	-0.566
cg2076	*ribD*	Putative riboflavin specific deaminase	-0.281	-0.702
cg2090	*suhB*	Myo-inositol-1(or 4)-monophosphatase	-0.273	-0.508
cg2094	*cg2094*	Hypothetical protein	-1.105	-1.685
cg2102	*sigB*	RNA polymerase sigma factor rpoD (Sigma-A)	-0.427	-0.807
cg2106	*cg2106*	Conserved hypothetical protein	-0.284	-0.445
cg2111	*hrpA*	Putative ATP-dependent helicase	-0.204	-0.251
cg2115	*sugR*	Transcriptional regulator; DeoR-family	-0.233	-0.372
cg2116	*cg2116*	Putative phosphofructokinase	-0.145	-0.436
cg2136	*gluA*	ABC-type glutamate transporter; ATPase subunit (TC 3.A.1.3.9)	-0.090	-0.358
cg2152	*clgR*	Transcriptional activator of Clp protease genes	-0.250	-0.514
cg2173	*dinF*	Putative MATE multidrug efflux protein; multidrug/oligosaccharidyl-lipid/polysaccharide (MOP) flippase	-0.053	-0.586
cg2175	*rbfA*	Ribosome-binding factor A	-0.181	-0.313
cg2191	*cg2191*	Conserved hypothetical protein	-0.144	-0.406
cg2196	*cg2196*	Putative secreted or membrane protein	-0.177	-0.487
cg2215	*cg2215*	Putative membrane protein	-0.243	-0.580
cg2250	*cg2250*	Putative secreted protein	-0.307	-0.714
cg2255	*cg2255*	ABC-type putative daunorubicin transporter; permease subunit	-0.261	-0.993
cg2256	*cg2256*	ABC-type putative daunorubicin transporter; ATPase subunit	-0.232	-0.542
cg2266	*cg2266*	Putative acylphosphatase	-0.641	-1.198
cg2328	*cg2328*	Hypothetical protein	-0.134	-0.333
cg2338	*dnaE1*	DNA-directed DNA polymerase. polymerase III; alpha chain	-0.187	-0.502
cg2340	*cg2340*	ABC-type putative amino acid transporter; substrate-binding lipoprotein	-0.247	-0.558
cg2341	*cg2341*	Putative Co/Zn/Cd cation transporter	-0.232	-0.522
cg2342	*cg2342*	Putative oxidoreductase	-0.242	-0.639
cg2343	*cg2343*	Putative decarboxylase	-0.195	-0.525
cg2380	*cg2380*	Putative membrane protein	-0.193	-0.507
cg2388	*pknL*	Putative serine/threonine protein kinase	-0.307	-0.583
cg2417	*cg2417*	Putative short-chain type oxidoreductase	-0.147	-0.355
cg2430	*cg2430*	Hypothetical protein	-0.149	-0.531
cg2438	*cg2438*	Hypothetical protein	-0.478	-1.178
cg2446	*glnE*	Glutamate–ammonia-ligase adenylyltransferase	-0.386	-0.816
cg2447	*glnA2*	Glutamate–ammonia ligase	-0.191	-0.453
cg2453	*cg2453*	Putative exoribonuclease	-0.141	-0.306

Locus	Name	Function	FC 0.3/0.2	FC 0.4/0.2
cg2457	*cg2457*	Conserved hypothetical protein	-0.203	-0.668
cg2462	*cg2462*	Putative transcriptional regulator; TetR-family	-0.140	-0.279
cg2477	*cg2477*	Conserved hypothetical protein	-0.262	-0.587
cg2500	*znr*	Putative transcriptional regulator; ArsR-family	-0.384	-0.693
cg2502	*zur*	Putative transcriptional regulator; FUR-family	-0.686	-1.342
cg2516	*hrcA*	Putative transcriptional regulator; HrcA-family	-0.379	-0.746
cg2518	*cg2518*	Putative secreted protein	-0.233	-0.547
cg2521	*fadD15*	Long-chain-fatty-acid–CoA ligase	-0.172	-0.61
cg2558	*cg2558*	Putative aldose 1-epimerase	-0.168	-0.327
cg2559	*aceB*	Malate synthase	-0.243	-0.667
cg2564	*cg2564*	conserved hypothetical protein	-0.172	-0.549
cg2565	*cg2565*	Hypothetical protein	-0.180	-0.526
cg2566	*cg2566*	Putative secreted protein	-0.275	-0.924
cg2572	*cg2572*	Conserved hypothetical protein	-0.219	-0.741
cg2589	*cg2589*	Predicted GTPase	-0.228	-0.707
cg2613	*mdh*	Malate dehydrogenase	-0.166	-0.339
cg2620	*clpX*	ATP-dependent clp protease ATPase subunit	-0.286	-0.683
cg2628	*pcaC*	Putative 4-carboxymuconolactone decarboxylase	-0.084	-0.325
cg2629	*pcaB*	Putative 3-carboxy-cis.cis-muconate cycloisomerase	-0.392	-0.984
cg2630	*pcaG*	Protocatechuate 3.4-dioxygenase; alpha subunit	-0.315	-0.855
cg2631	*pcaH*	Protocatechuate 3.4-dioxygenase; beta subunit	-0.407	-0.833
cg2635	*catB*	Putative muconate cycloisomerase	-0.488	-1.115
cg2662	*pepN*	Membrane alanyl aminopeptidase	-0.327	-0.801
cg2665	*cg2665*	Hypothetical protein	-0.130	-0.383
cg2686	*cg2686*	Putative transcriptional regulator; TetR-family	-0.081	-0.332
cg2704	*cg2704*	ABC-type putative sugar transporter; permease subunit	-0.278	-0.588
cg2748	*cg2748*	Conserved putative membrane protein	-0.111	-0.249
cg2767	*cg2767*	Putative membrane protein	-0.468	-0.637
cg2795	*cg2795*	NADPH:quinone reductase or related Zn-dependent oxidoreductase	-0.216	-0.648
cg2822	*cg2822*	Sugar phosphate isomerase/epimerase	-0.227	-0.630
cg2830	*pduO*	Putative adenosylcobalamin-dependent diol dehydratase	-0.167	-0.531
cg2836	*sucD*	Succinate–CoA ligase (ADP-forming); alpha subunit	-0.17	-0.391
cg2837	*sucC*	Succinate–CoA ligase (ADP-forming); beta subunit	-0.628	-1.609
cg2889	*cg2889*	Putative transcriptional regulator; MerR family	-0.726	-1.660
cg2890	*cg2890*	Hypothetical protein; putative amino acid processing enzyme	-0.285	-0.748
cg2891	*pqo*	Pyruvate:quinone oxidoreductase	-0.255	-0.860
cg2958	*butA*	L-2.3-Butanediol dehydrogenase/acetoin reductase	-0.351	-0.864
cg2959	*cg2959*	Putative secreted protein	-0.183	-0.296
cg2965	*cg2965*	Putative transcriptional regulator; AraC-family	-0.212	-0.595
cg2966	*cg2966*	Putative phenol 2-monooxygenase	-0.108	-0.283
cg2968	*cg2968*	Conserved hypothetical protein	-0.280	-1.171
cg2981	*folX*	Dihydroneopterin aldolase	-0.163	-0.553
cg2985	*hpt*	Hypoxanthine phosphoribosyltransferase	-0.122	-0.234
cg2999	*cg2999*	Putative ferredoxin reductase	-0.218	-0.334
cg3001	*cg3001*	Putative transcriptional regulator; MarR-family	-0.298	-0.882
cg3024	*mrpA*	Putative secondary Na+/H+ antiporter; monovalent cation:proton antiporter-3 (CPA3) family	-0.195	-0.318
cg3043	*cg3043*	Putative NTP pyrophosphohydrolase/oxidative damage repair enzyme	-0.219	-0.381
cg3044	*cg3044*	Putative membrane protein	-0.243	-0.451

Locus	Name	Function	FC 0.3/0.2	FC 0.4/0.2
cg3045	*cg3045*	ABC-type putative glutamine transporter; substrate-binding lipoprotein	-0.357	-0.888
cg3051	*cg3051*	Putative secreted protein	-0.447	-0.869
cg3052	*cg3052*	Putative secreted protein	-0.434	-0.837
cg3075	*cmr*	Putative multidrug efflux permease; MFS-type	-0.177	-0.291
cg3092	*cg3092*	Putative 2-polyprenylphenol hydroxylase or related flavodoxin oxidoreductase	-0.386	-0.998
cg3118	*cysI*	Ferredoxin-sulfite reductase	-0.124	-0.306
cg3120	*cg3120*	Conserved hypothetical protein	-0.159	-0.276
cg3122	*phnB1*	Hypothetical protein; PhnB-like	-0.219	-0.333
cg3169	*pck*	Phosphoenolpyruvate carboxykinase (GTP)	-0.337	-0.927
cg3192	*cg3192*	Putative secreted or membrane protein	-0.347	-0.963
cg3195	*cg3195*	Putative flavin-containing monooxygenase	-0.181	-0.424
cg3219	*ldh*	L-Lactate dehydrogenase	-0.189	-0.808
cg3236	*msrA*	Protein-methionine-S-oxide reductase	-0.147	-0.319
cg3270	*cg3270*	Putative membrane protein; putative pseudogene (N-terminal fragment)	-0.183	-0.425
cg3304	*dnaB*	Putative replicative DNA helicase	-0.403	-0.980
cg3309	*cg3309*	Putative secreted protein	-0.158	-0.418
cg3331	*ogt*	Methylated-DNA-[protein]-cysteine S-methyltransferase	-0.465	-0.885
cg3332	*cg3332*	NADPH:quinone reductase	-0.256	-0.587
cg3367	*cg3367*	ABC-type putative multidrug transporter; ATPase subunit	-0.239	-0.569
cg3368	*cg3368*	ABC-type putative multidrug transporter; permease subunit	-0.365	-0.980
cg3378	*cg3378*	Conserved hypothetical protein	-0.626	-1.134
cg3385	*rhcD2*	Hydroxyquinol 1.2-dioxygenase	-0.492	-0.206
cg3388	*cg3388*	Putative transcriptional regulator; IclR-family	-0.191	-0.510
cg3389	*cg3389*	Predicted oxidoreductase	-0.088	-0.251
cg3390	*cg3390*	Putative sugar phosphate isomerase/epimerase	-0.267	-0.558
cg3391	*idhA1*	Inositol 2-dehydrogenase	-0.401	-0.669
cg3396	*cg3396*	Putative membrane protein; stomatin/prohibitin homolog-like	-0.584	-0.909
cg3418	*cg3418*	Putative secreted protein	-0.477	-0.729

D.5. Sampling plan of continuous ^{13}C-labeling process

Table D.8.: Sampling plan of the stationary ^{13}C-tracer experiment performed in chemostat mode at μ = 0.4 h^{-1} featuring fast-sampling after switching from ^{12}C- to ^{13}C-labeled glucose. RT: residence time

Sample no.	Time	Time unit	RT. h (2.5 h)$^{-1}$
1	0	s	0.0000
2	4	s	0.0004
3	8	s	0.0009
4	12	s	0.0013
5	16	s	0.0018
6	20	s	0.0022
7	25	s	0.0028
8	41	s	0.0046
9	61	s	0.0068
10	80	s	0.0089
11	120	s	0.0133
12	180	s	0.0200
13	6	min	0.0400
14	12	min	0.0800
15	24.15	min	0.1610
16	48	min	0.3200
17	96	min	0.6400
18	2.50	h	1.0000
19	5.00	h	2.0000
20	7.50	h	3.0000
21	9.50	h	3.8000
22	9.67	h	3.8667
23	9.83	h	3.9333
24	10.00	h	4.0000
25	10.17	h	4.0667

D.6. Isotopologue distributions in the first 180 s of ^{13}C-labeling

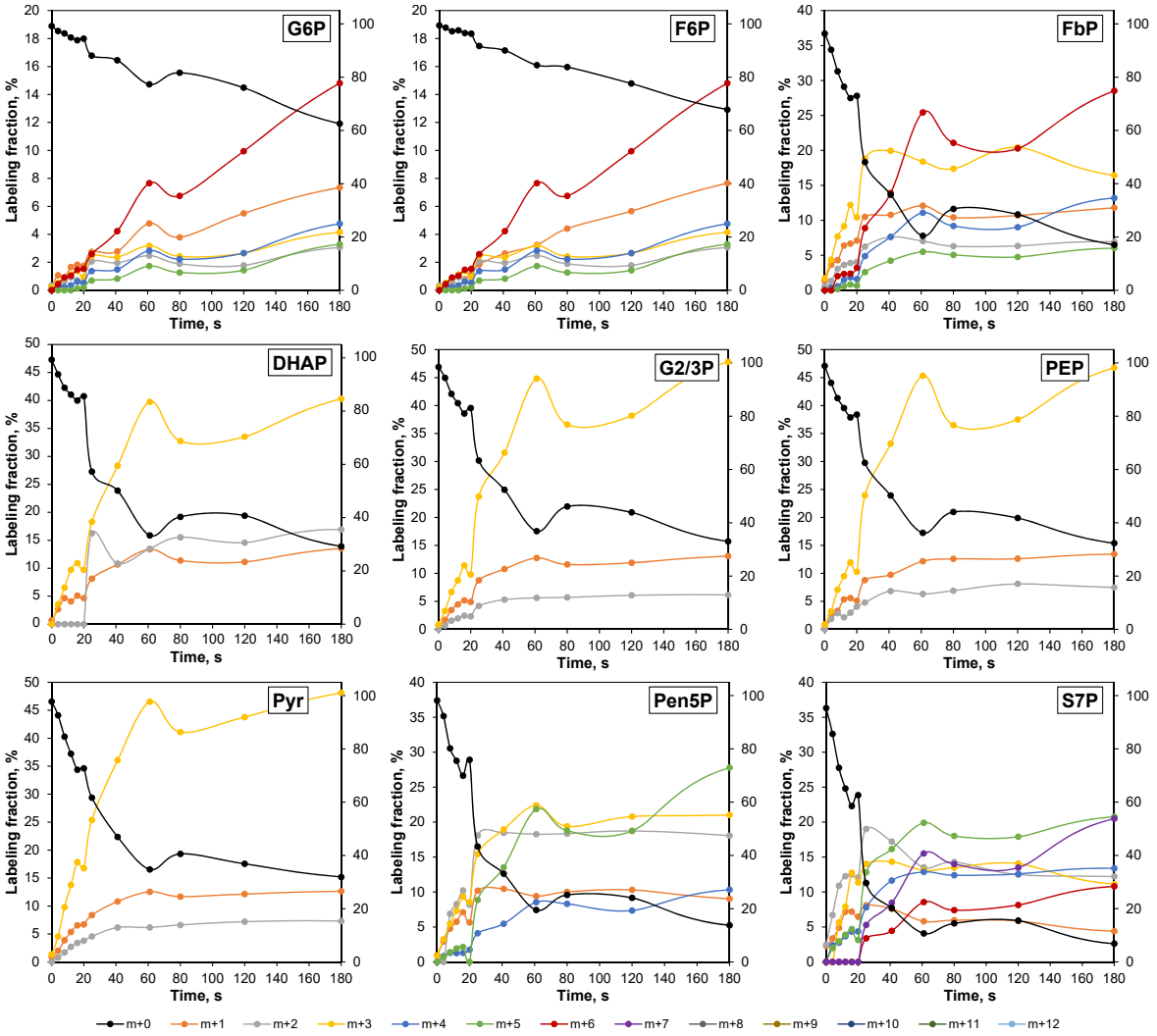

Figure D.2.: Isotopologue distributions of metabolites from glycolysis and PPP in the first 180 s of introducing ^{13}C-labeled glucose into the chemostat process. The y-axis on the right-hand side is the scale for the unlabeled $m+0$-trace.

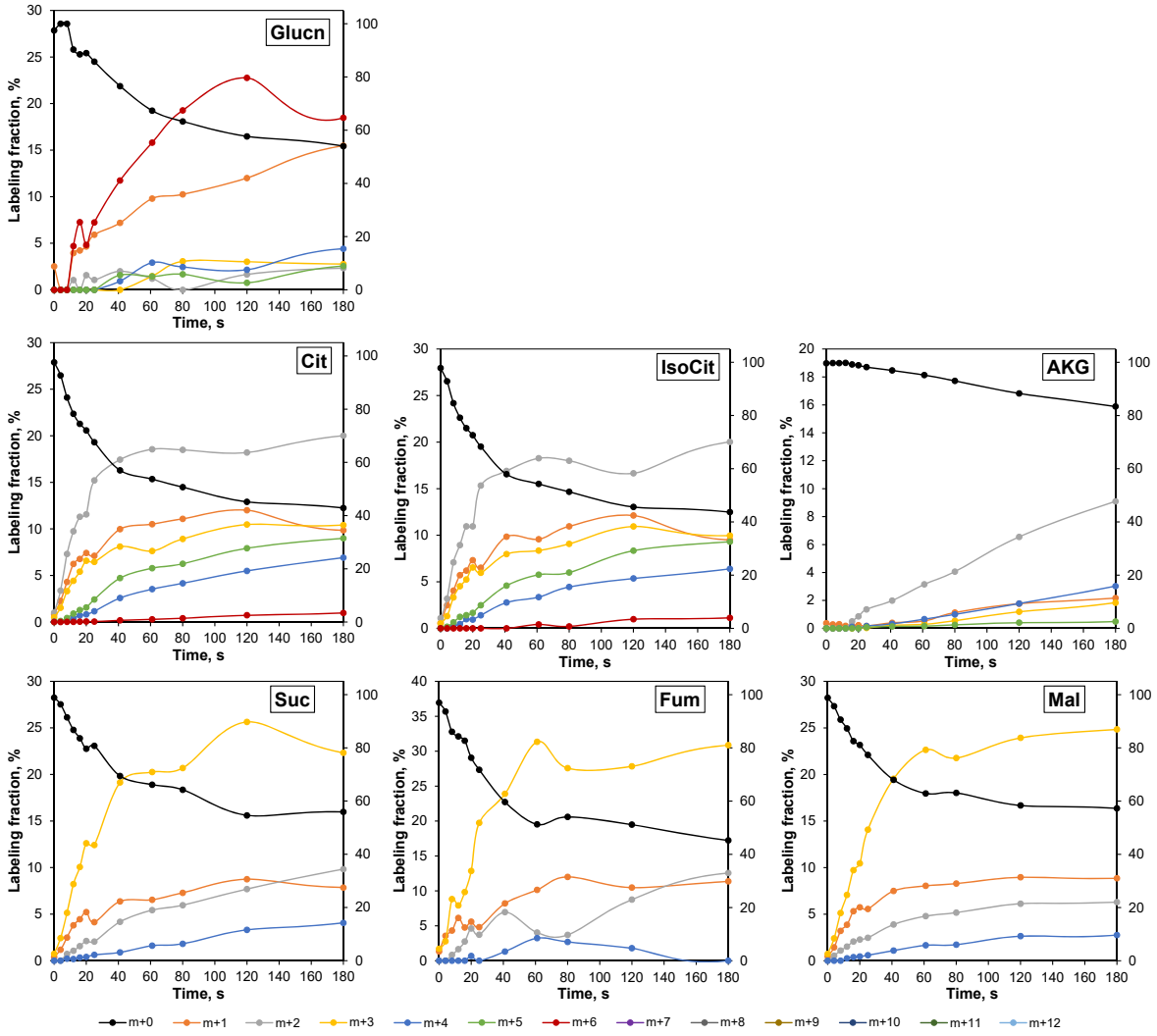

Figure D.3.: Isotopologue distributions of gluconate and metabolites from TCA in the first 180 s of introducing ^{13}C-labeled glucose into the chemostat process. The y-axis on the right-hand side is the scale for the unlabeled $m+0$-trace.

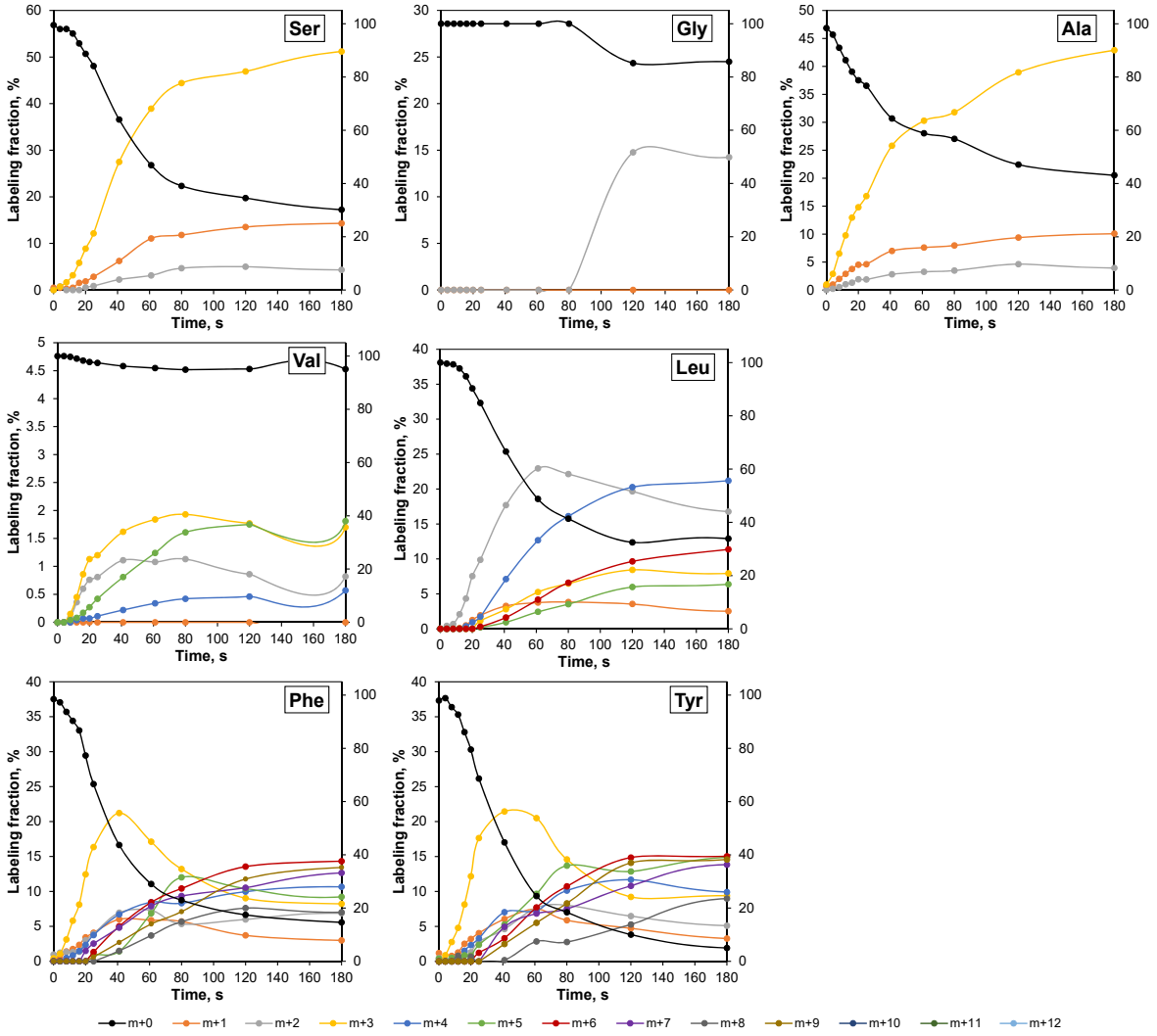

Figure D.4.: Isotopologue distributions of Ser, Gly, Ala, Val, Leu, Phe, and Tyr in the first 180 s of introducing ^{13}C-labeled glucose into the chemostat process. The y-axis on the right-hand side is the scale for the unlabeled $m+0$-trace.

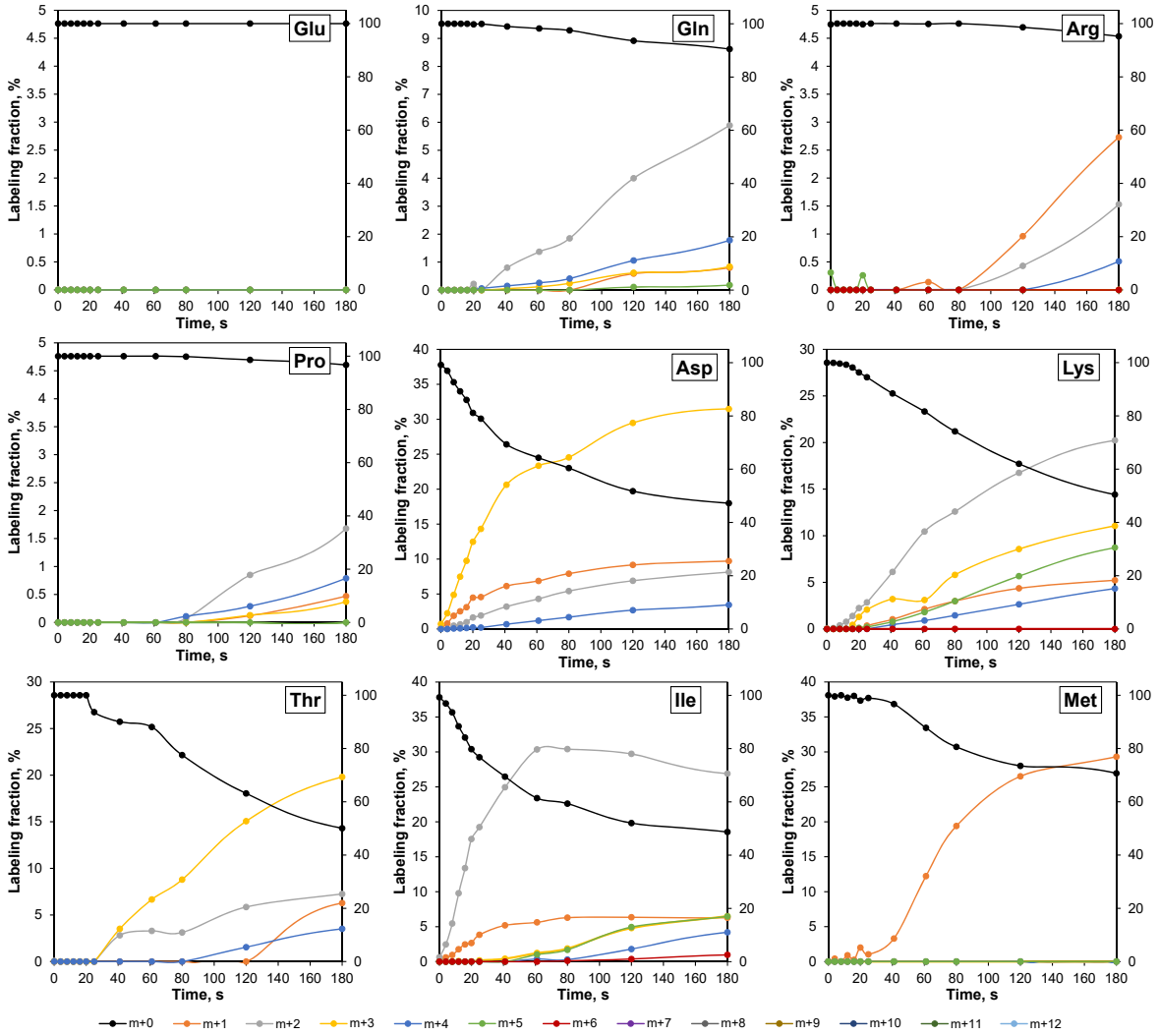

Figure D.5.: Isotopologue distributions of Glu, Gln, Arg, pro, Asp, Lys, Thr, Ile, and Met in the first 180 s of introducing ^{13}C-labeled glucose into the chemostat process. The y-axis on the right-hand side is the scale for the unlabeled $m+0$-trace.

D.7. Isotopologue distributions of intracellular metabolites

Table D.9.: Isotopologue distributions in % of 33 analyzed intracellular metabolites of each sample (0 s to 10.67 h) withdrawn after switching from ^{12}C- to ^{13}C-glucose feed (t = 0 h) at $\mu = 0.4\,h^{-1}$. $\sum$ represents the sum of all isotopologues ($\sum_{i=1}^{n} m+n$) detected for respective metabolites.

	Sample time, s											Sample time, min					Sample time, h								
	0	4	8	12	16	20	25	41	61	80	120	180	6	12	24.15	48	96	2.5	5	7.5	9.5	9.67	9.83	10	10.17
G6P																									
m+0	99.2	97.3	96.4	94.9	93.9	94.5	88.1	86.3	77.3	81.7	76.1	62.6	43.7	39.8	30.3	20.3	6.7	2.9	1.0	0.7	1.5	0.8	1.1	0.9	0.6
m+1	0.3	1.1	0.9	1.7	1.8	1.8	2.7	2.8	4.8	3.8	5.5	7.4	10.5	11.2	13.1	17.8	20.8	21.3	23.0	24.6	23.0	23.7	23.8	22.9	23.3
m+2	0.3	0.3	0.7	0.9	0.7	0.6	2.1	2.0	2.5	1.9	1.8	3.1	3.8	3.8	3.6	3.0	3.7	3.8	3.8	2.9	3.2	2.9	3.3	3.7	3.4
m+3	0.2	0.5	0.9	1.1	1.4	1.0	2.5	2.4	3.2	2.4	2.7	4.2	5.0	5.4	5.8	4.9	5.0	5.3	4.6	3.9	4.8	4.5	4.5	4.6	4.4
m+4	0.0	0.3	0.2	0.4	0.6	0.5	1.4	1.5	2.8	2.2	2.7	4.8	7.0	6.5	7.4	7.1	7.0	7.9	7.1	6.6	6.6	6.1	6.3	7.4	6.6
m+5	0.0	0.0	0.0	0.0	0.1	0.2	0.7	0.8	1.7	1.3	1.4	3.3	4.3	4.6	5.3	4.5	4.8	5.6	4.8	3.9	4.8	4.5	4.2	5.0	4.8
m+6	0.0	0.4	0.9	1.0	1.5	1.5	2.6	4.2	7.7	6.8	9.9	14.8	25.7	28.7	34.4	42.5	52.1	53.2	55.6	57.3	56.1	57.5	56.7	55.6	56.8
$\sum$	0.8	2.7	3.6	5.1	6.1	5.5	11.9	13.7	22.7	18.3	23.9	37.4	56.3	60.2	69.7	79.7	93.3	97.1	99.1	99.3	98.5	99.2	98.9	99.1	99.4
F6P																									
m+0	99.4	98.6	97.2	97.6	96.6	96.3	91.7	90.0	84.5	83.8	77.6	67.8	50.0	36.8	23.3	11.6	4.2	2.3	1.0	0.7	1.0	0.4	0.8	0.7	0.7
m+1	0.3	0.4	0.7	0.3	0.8	1.1	1.9	2.6	3.2	4.4	5.7	7.7	12.1	15.0	18.9	21.8	23.0	22.8	24.5	24.3	25.1	25.5	24.3	24.3	25.2
m+2	0.0	0.4	0.6	0.4	0.4	0.2	1.2	0.9	0.7	1.2	1.0	1.5	2.1	2.0	2.5	2.8	3.5	3.0	3.0	2.7	2.7	2.7	2.9	2.8	2.4
m+3	0.1	0.2	0.6	0.4	0.6	0.7	1.7	1.6	1.8	1.4	1.9	2.6	3.1	4.0	4.2	4.5	3.8	4.6	4.4	4.2	4.1	4.1	4.0	3.9	4.1
m+4	0.0	0.0	0.2	0.3	0.4	0.2	0.8	0.7	1.3	0.0	1.5	2.5	4.0	4.9	5.3	5.6	6.2	6.8	6.6	6.2	6.3	6.8	6.3	6.9	6.3
m+5	0.0	0.0	0.0	0.0	0.1	0.0	0.2	0.5	1.0	0.7	0.9	1.6	2.2	3.0	3.6	3.1	3.9	4.2	4.0	3.5	3.5	3.5	3.5	3.8	3.5
m+6	0.2	0.5	0.7	1.0	1.2	1.5	2.6	3.7	7.5	8.5	11.4	16.3	26.5	34.4	42.2	50.6	55.5	56.4	56.6	58.5	57.3	56.8	58.2	57.6	57.8
$\sum$	0.6	1.4	2.8	2.4	3.5	3.7	8.3	10.0	15.5	16.2	22.4	32.2	50.0	63.2	76.7	88.4	95.8	97.7	99.0	99.3	99.0	99.6	99.2	99.4	99.3
FbP																									
m+0	96.4	90.3	82.2	76.4	72.1	73.0	48.1	35.9	20.5	30.5	28.5	17.1	7.9	5.8	5.5	5.6	3.1	2.2	2.0	2.1	1.9	1.8	2.1	2.0	2.3
m+1	1.4	3.6	4.3	6.4	6.7	7.1	10.5	10.8	12.1	10.4	10.7	11.8	14.4	14.2	13.0	11.3	12.0	12.9	12.7	11.8	13.0	12.6	12.3	11.6	13.5
m+2	0.6	1.3	3.1	3.6	3.9	4.0	6.2	7.6	7.0	6.3	6.3	6.9	5.2	4.6	4.9	5.0	5.3	5.4	5.1	5.4	5.4	5.5	5.4	5.4	5.4
m+3	1.7	4.4	7.7	9.2	12.2	10.4	18.8	19.9	18.4	17.4	20.4	16.4	13.0	12.4	14.0	15.1	13.9	12.4	13.2	13.2	12.7	13.2	13.1	13.6	13.6
m+4	0.0	0.4	0.6	1.5	1.9	1.6	4.9	7.6	11.1	9.2	9.0	13.2	12.5	13.8	14.3	15.4	15.1	15.2	15.5	16.1	15.3	15.4	15.0	16.1	14.5
m+5	0.0	0.0	0.2	0.6	0.8	0.6	2.6	4.2	5.5	5.1	4.8	6.0	5.8	6.9	7.1	8.4	8.4	8.0	7.3	7.5	7.8	7.7	7.9	7.7	8.7
m+6	0.0	0.0	2.0	2.3	2.4	3.2	8.9	13.9	25.4	21.1	20.3	28.5	41.1	42.2	41.2	39.2	42.2	44.0	44.2	44.0	43.9	43.8	44.2	43.7	42.0
$\sum$	3.7	9.7	17.8	23.6	27.9	27.0	51.9	64.1	79.5	69.5	71.5	82.9	92.1	94.2	94.5	94.4	96.9	97.9	98.0	97.9	98.1	98.2	97.9	98.1	97.7
DHAP																									
m+0	99.3	93.8	88.8	86.2	84.0	85.6	57.3	50.1	33.3	40.3	40.8	29.2	19.7	17.8	16.6	19.0	13.6	13.6	13.3	12.7	12.3	12.8	12.4	12.8	12.4
m+1	0.7	2.7	4.7	4.1	5.1	4.7	8.2	10.7	13.4	11.4	11.1	13.5	15.9	16.3	16.1	17.5	16.4	15.9	16.0	16.5	16.3	17.0	16.7	15.7	15.5
m+2	0.0	0.0	0.0	0.0	0.0	0.0	16.3	10.8	13.5	15.5	14.6	16.9	13.2	13.3	14.0	0.0	16.5	14.5	14.8	15.0	16.9	13.2	14.1	14.5	17.2
m+3	0.0	3.5	6.6	9.7	10.9	9.7	18.3	28.3	39.8	32.8	33.5	40.3	51.3	52.7	53.3	63.5	53.5	56.0	55.9	55.9	54.5	57.0	56.8	56.9	55.0
$\sum$	0.7	6.2	11.2	13.8	16.0	14.4	42.7	49.9	66.7	59.7	59.2	70.8	80.3	82.2	83.4	81.0	86.5	86.4	86.7	87.3	87.7	87.2	87.6	87.2	87.6
2/3PG																									
m+0	98.5	94.4	88.4	84.9	81.0	83.0	63.3	52.4	36.8	46.1	43.9	33.0	23.9	21.9	20.2	19.3	16.7	17.2	16.9	16.4	16.5	16.3	16.8	16.7	17.1
m+1	0.7	1.7	3.4	4.4	5.2	4.9	8.8	10.8	12.8	11.6	11.9	13.1	14.3	14.5	14.7	15.4	15.5	15.0	14.8	15.3	15.5	15.5	14.9	15.0	15.1
m+2	0.0	0.7	1.6	2.0	2.4	2.3	4.2	5.3	5.6	5.7	6.1	6.1	4.9	5.1	5.3	6.9	7.1	5.5	5.7	5.9	6.1	6.1	6.0	5.7	6.5
m+3	0.9	3.3	6.7	8.7	11.4	9.8	23.7	31.6	44.8	36.6	38.2	47.8	56.9	58.5	59.8	58.5	60.7	62.4	62.7	62.4	61.9	62.2	62.3	62.6	61.4
$\sum$	1.5	5.6	11.7	15.1	19.0	17.0	36.7	47.6	63.2	53.9	56.1	67.0	76.1	78.1	79.8	80.7	83.3	82.8	83.1	83.6	83.5	83.7	83.2	83.3	82.9

	Sample time, s											Sample time, min					Sample time, h								
	0	4	8	12	16	20	25	41	61	80	120	180	6	12	24.15	48	96	2.5	5	7.5	9.5	9.67	9.83	10	10.17
PEP																									
m+0	98.9	92.5	86.8	83.1	79.5	80.6	62.5	50.2	36.2	44.0	41.8	32.3	23.5	22.6	19.5	17.5	15.7	17.1	16.1	16.0	15.2	14.9	15.3	17.5	23.3
m+1	0.3	2.4	3.3	5.3	5.6	5.1	8.8	9.7	12.2	12.6	12.6	13.5	13.5	14.7	14.5	15.5	15.6	15.5	14.8	14.8	14.6	14.9	16.4	14.4	16.5
m+2	0.0	1.8	2.9	2.1	3.0	4.1	4.8	6.8	6.3	6.9	8.1	7.5	6.3	6.5	7.5	8.3	9.6	6.7	7.7	8.1	9.3	7.5	9.9	9.3	6.8
m+3	0.9	3.2	7.1	9.5	11.9	10.3	23.9	33.2	45.3	36.5	37.5	46.8	56.8	56.3	58.5	58.8	59.2	60.7	61.4	61.1	61.0	62.8	58.4	58.8	53.5
Σ	1.1	7.5	13.2	17.0	20.5	19.4	37.5	49.8	63.8	56.0	58.2	67.7	76.5	77.4	80.5	82.5	84.4	82.9	83.9	84.1	84.8	85.1	84.7	82.6	76.7
Pyr																									
m+0	97.8	92.6	84.6	78.2	72.2	72.7	61.7	46.9	34.8	40.6	36.9	31.9	24.4	21.6	19.3	17.1	15.5	15.4	15.3	15.0	15.3	15.3	15.1	15.7	15.5
m+1	0.9	2.0	3.9	5.4	6.6	6.7	8.4	10.8	12.6	11.7	12.2	12.7	13.3	13.5	14.1	14.7	14.9	14.1	14.5	14.6	14.4	14.4	14.3	14.1	14.2
m+2	0.0	0.8	1.7	2.7	3.4	3.8	4.6	6.2	6.2	6.6	7.2	7.3	6.0	6.1	7.0	8.4	8.4	6.9	6.9	7.2	8.1	7.1	7.8	6.7	8.1
m+3	1.4	4.6	9.8	13.8	17.9	16.8	25.4	36.1	46.5	41.1	43.8	48.1	56.3	58.9	59.7	59.8	61.3	63.5	63.3	63.2	62.2	63.2	62.8	63.6	62.3
Σ	2.2	7.4	15.4	21.8	27.8	27.3	38.3	53.1	65.3	59.4	63.1	68.1	75.6	78.4	80.7	82.9	84.6	84.6	84.7	85.0	84.7	84.7	84.9	84.3	84.5
AceCoA																									
m+0	82.9	69.4	84.9	76.4	70.1	69.5	72.4	55.4	43.5	50.5	46.9	38.0	37.6	28.8	25.2	15.6	7.5	3.6	0.0	0.0	0.0	0.0	0.0	0.0	0.0
m+1	15.1	15.2	5.5	6.9	11.7	12.3	5.1	9.5	9.9	10.0	10.6	12.7	10.6	11.3	11.4	8.2	4.5	1.9	0.0	0.0	0.0	0.0	0.0	0.0	0.0
m+2	2.0	11.4	9.6	15.6	16.7	18.2	21.5	34.3	43.9	36.9	38.8	48.1	47.9	49.9	43.4	26.6	15.6	7.1	1.1	0.0	0.0	0.0	0.0	0.0	0.0
m+3	0.0	1.7	0.0	1.1	1.5	0.0	0.7	0.8	2.8	2.7	3.7	0.0	2.4	2.6	3.8	2.8	2.1	1.6	0.0	0.0	0.0	0.0	0.0	0.0	0.0
m+4	0.0	0.0	0.0	0.0	0.0	0.0	0.4	0.0	0.0	0.0	0.0	1.3	1.1	0.9	2.5	2.7	1.4	1.5	0.0	0.0	0.0	0.0	0.0	0.0	0.0
m+5	0.0	0.0	0.0	0.0	0.0	0.0	0.0	0.0	0.0	0.0	0.0	0.0	0.0	1.3	1.2	2.4	2.0	1.9	1.4	0.0	0.0	0.0	0.0	0.0	0.0
m+6	0.0	0.0	0.0	0.0	0.0	0.0	0.0	0.0	0.0	0.0	0.0	0.0	0.0	0.7	1.4	4.3	3.5	2.4	1.0	0.0	0.0	0.0	0.0	0.0	0.0
m+7	0.0	0.0	0.0	0.0	0.0	0.0	0.0	0.0	0.0	0.0	0.0	0.0	0.4	1.8	2.8	3.3	4.4	3.4	2.0	0.0	0.0	0.0	0.0	0.6	0.3
m+8	0.0	0.0	0.0	0.0	0.0	0.0	0.0	0.0	0.0	0.0	0.0	0.0	0.0	0.5	3.2	6.0	4.9	4.3	2.2	1.3	0.0	0.0	0.0	1.0	1.2
m+9	0.0	0.0	0.0	0.0	0.0	0.0	0.0	0.0	0.0	0.0	0.0	0.0	0.0	2.2	1.7	4.8	5.9	5.5	3.7	2.4	1.6	1.3	1.1	1.5	1.3
m+10	0.0	0.0	0.0	0.0	0.0	0.0	0.0	0.0	0.0	0.0	0.0	0.0	0.0	0.0	1.3	4.8	5.7	5.2	4.4	2.5	3.0	2.2	2.5	2.2	2.0
m+11	0.0	0.0	0.0	0.0	0.0	0.0	0.0	0.0	0.0	0.0	0.0	0.0	0.0	0.0	1.1	2.8	5.5	5.6	5.4	4.4	3.3	3.8	4.2	3.8	4.0
m+12	0.0	0.0	0.0	0.0	0.0	0.0	0.0	0.0	0.0	0.0	0.0	0.0	0.0	0.0	0.0	2.8	4.6	5.2	5.4	5.6	4.9	5.1	3.9	4.9	4.4
m+13	0.0	0.0	0.0	0.0	0.0	0.0	0.0	0.0	0.0	0.0	0.0	0.0	0.0	0.0	0.0	1.7	4.3	5.9	7.8	7.0	6.7	6.5	7.7	6.7	6.4
m+14	0.0	0.0	0.0	0.0	0.0	0.0	0.0	0.0	0.0	0.0	0.0	0.0	0.0	0.0	1.1	3.0	4.0	5.5	7.1	9.9	10.6	9.4	10.7	8.2	7.9
m+15	0.0	0.0	0.0	0.0	0.0	0.0	0.0	0.0	0.0	0.0	0.0	0.0	0.0	0.0	0.0	2.2	5.5	7.0	9.0	8.9	9.5	10.9	8.5	10.1	10.2
m+16	0.0	0.0	0.0	0.0	0.0	0.0	0.0	0.0	0.0	0.0	0.0	0.0	0.0	0.0	0.0	2.3	5.8	6.3	9.8	11.9	10.4	11.5	11.9	11.4	10.8
m+17	0.0	0.0	0.0	0.0	0.0	0.0	0.0	0.0	0.0	0.0	0.0	0.0	0.0	0.0	0.0	1.8	3.7	6.6	10.0	10.9	12.6	11.7	11.1	11.1	12.2
m+18	0.0	0.0	0.0	0.0	0.0	0.0	0.0	0.0	0.0	0.0	0.0	0.0	0.0	0.0	0.0	1.6	3.8	7.3	10.0	10.5	10.4	11.3	13.1	11.1	11.4
m+19	0.0	0.0	0.0	0.0	0.0	0.0	0.0	0.0	0.0	0.0	0.0	0.0	0.0	0.0	0.0	0.4	3.0	5.3	6.9	8.6	10.1	9.7	9.9	10.1	9.8
m+20	0.0	2.2	0.0	0.0	0.0	0.0	0.0	0.0	0.0	0.0	0.0	0.0	0.0	0.0	0.0	0.0	2.3	3.8	5.9	8.5	8.9	7.8	8.8	7.9	8.7
m+21	0.0	0.0	0.0	0.0	0.0	0.0	0.0	0.0	0.0	0.0	0.0	0.0	0.0	0.0	0.0	0.0	0.0	2.0	4.2	4.9	5.9	5.6	5.0	5.4	5.5
m+22	0.0	0.0	0.0	0.0	0.0	0.0	0.0	0.0	0.0	0.0	0.0	0.0	0.0	0.0	0.0	0.0	0.0	1.3	2.5	2.3	2.3	2.4	1.7	3.5	3.0
m+23	0.0	0.0	0.0	0.0	0.0	0.0	0.0	0.0	0.0	0.0	0.0	0.0	0.0	0.0	0.0	0.0	0.0	0.0	0.5	0.5	0.0	0.9	0.0	0.6	1.1
Σ	17.1	30.6	15.1	23.6	29.9	30.5	27.6	44.6	56.5	49.5	53.1	62.1	62.4	71.2	74.8	84.5	92.5	96.4	100.0	100.0	100.0	100.0	100.0	100.0	100.0
Cit																									
m+0	97.6	92.7	84.4	78.3	74.5	72.0	67.6	57.0	53.7	50.7	45.2	42.9	29.9	16.1	5.6	2.5	1.2	0.9	0.8	0.9	0.9	0.8	0.8	0.8	0.9
m+1	0.8	2.3	4.3	6.2	6.8	7.4	7.1	10.0	10.5	11.1	12.0	9.9	11.4	11.4	7.2	4.8	3.4	3.0	3.0	3.0	3.0	3.0	3.0	2.9	2.9
m+2	1.0	3.4	7.3	9.7	11.3	11.6	15.2	17.4	18.6	18.5	18.2	20.0	22.1	20.7	16.1	11.1	8.5	7.9	7.9	7.8	7.8	7.8	7.8	7.8	7.7
m+3	0.5	1.5	3.3	4.4	5.4	6.6	6.5	8.1	7.6	8.9	10.5	10.4	12.7	16.7	19.0	18.5	16.8	15.9	15.7	15.6	15.9	15.8	15.8	15.9	16.1
m+4	0.0	0.1	0.2	0.4	0.7	0.8	1.2	2.6	3.5	4.2	5.5	6.9	10.6	15.4	20.2	22.7	23.4	24.0	24.0	23.9	23.7	23.8	24.0	23.8	24.0
m+5	0.0	0.1	0.4	0.9	1.3	1.6	2.4	4.7	5.8	6.3	7.9	9.0	10.9	14.7	20.5	22.9	23.3	23.7	23.2	23.0	22.8	23.0	23.4	23.4	23.5

	Sample time, s											Sample time, min					Sample time, h								
	0	4	8	12	16	20	25	41	61	80	120	180	6	12	24.15	48	96	2.5	5	7.5	9.5	9.67	9.83	10	10.17
m+6	0.0	0.0	0.0	0.0	0.0	0.1	0.1	0.2	0.3	0.4	0.7	1.0	2.3	5.0	11.4	17.6	23.6	24.7	25.5	25.8	25.8	25.7	25.3	25.5	25.0
Σ	2.4	7.3	15.6	21.8	25.5	28.0	32.4	43.0	46.3	49.3	54.8	57.1	70.1	83.9	94.5	97.6	98.9	99.1	99.2	99.1	99.1	99.2	99.2	99.2	99.1
IsoCit																									
m+0	97.8	92.9	84.6	79.2	75.2	72.6	68.3	57.9	54.3	51.3	45.6	43.7	30.9	16.6	6.2	3.3	1.9	1.2	1.3	1.4	1.3	1.0	1.1	1.2	1.2
m+1	0.6	2.5	4.1	5.7	6.2	7.3	6.5	9.8	9.6	11.0	12.1	9.5	10.9	11.0	7.1	4.6	3.4	3.1	3.0	3.0	2.9	3.2	3.1	3.0	3.0
m+2	1.1	3.2	7.1	8.9	11.0	11.0	15.3	16.9	18.3	18.0	16.7	20.0	22.0	20.9	16.0	11.3	8.4	8.2	8.1	7.9	7.8	7.9	7.4	7.5	7.8
m+3	0.5	1.3	3.3	4.5	5.2	6.5	6.0	8.0	8.4	9.1	10.9	10.0	12.4	17.0	19.5	18.5	16.8	15.4	15.5	15.4	15.7	15.8	16.2	16.0	15.8
m+4	0.0	0.0	0.3	0.5	1.0	0.9	1.4	2.8	3.4	4.4	5.4	6.4	10.5	15.3	20.5	22.6	23.3	24.0	24.0	24.1	23.7	23.8	24.0	24.1	24.1
m+5	0.0	0.2	0.6	1.2	1.4	1.7	2.5	4.6	5.8	6.0	8.3	9.3	11.0	14.4	20.1	22.4	23.3	23.7	23.0	23.0	23.2	22.8	23.3	23.2	23.6
m+6	0.0	0.0	0.0	0.0	0.0	0.0	0.0	0.0	0.4	0.2	1.0	1.1	2.3	4.8	10.7	17.3	22.9	24.4	25.2	25.3	25.4	25.6	24.9	25.1	24.5
Σ	2.2	7.1	15.4	20.9	24.8	27.4	31.7	42.1	45.7	48.7	54.4	56.3	69.1	83.4	93.9	96.7	98.1	98.8	98.7	98.6	98.7	99.0	98.9	98.8	98.8
AKG																									
m+0	99.6	99.7	99.7	99.8	99.2	98.9	98.2	96.9	95.2	93.0	88.3	83.4	68.0	44.5	21.3	7.0	2.7	2.9	1.7	1.6	1.2	1.4	1.4	1.3	1.3
m+1	0.4	0.3	0.3	0.2	0.2	0.2	0.2	0.4	0.5	1.1	1.8	2.2	3.6	5.9	6.8	5.8	4.7	4.4	4.3	4.0	4.5	4.6	4.4	4.5	4.4
m+2	0.0	0.0	0.0	0.0	0.5	0.9	1.4	2.0	3.2	4.1	6.6	9.1	15.3	22.9	23.8	18.2	13.9	12.7	12.2	12.8	12.3	12.5	12.6	12.5	12.2
m+3	0.0	0.0	0.0	0.0	0.0	0.0	0.0	0.2	0.3	0.6	1.2	1.8	4.7	9.5	17.6	23.9	25.1	24.7	24.8	25.5	25.4	25.1	25.2	25.1	25.9
m+4	0.0	0.0	0.0	0.0	0.1	0.0	0.2	0.3	0.7	1.0	1.8	3.0	7.0	13.1	20.3	25.2	25.9	25.5	25.8	26.0	26.1	25.8	25.7	25.7	25.4
m+5	0.0	0.0	0.0	0.0	0.0	0.0	0.1	0.1	0.2	0.3	0.4	0.5	1.4	4.1	10.2	19.9	27.7	29.9	31.1	30.2	30.5	30.6	30.8	31.0	30.8
Σ	0.4	0.3	0.3	0.2	0.8	1.1	1.8	3.1	4.8	7.0	11.7	16.6	32.0	55.5	78.7	93.0	97.3	97.2	98.3	98.4	98.8	98.6	98.6	98.8	98.7
Suc																									
m+0	98.9	96.4	91.5	86.8	83.6	79.7	80.8	69.4	66.2	64.2	54.6	55.9	51.2	33.7	17.8	8.8	5.6	5.0	4.4	4.7	4.6	4.5	4.8	4.6	4.6
m+1	0.4	1.2	2.5	3.8	4.5	5.2	4.1	6.4	6.5	7.3	8.8	7.9	7.7	10.5	11.8	12.8	12.4	10.3	11.2	11.5	11.2	11.7	10.9	11.4	11.0
m+2	0.0	0.0	0.7	1.1	1.6	2.1	2.1	4.2	5.4	6.0	7.7	9.8	15.2	19.5	21.1	18.4	17.7	19.7	19.4	18.3	19.2	18.5	19.2	18.6	19.4
m+3	0.7	2.4	5.1	8.2	10.1	12.6	12.4	19.1	20.3	20.7	25.6	22.3	18.0	22.8	26.4	27.8	25.0	24.7	23.9	24.1	23.9	24.0	24.2	23.9	24.3
m+4	0.0	0.0	0.2	0.2	0.3	0.4	0.6	0.9	1.6	1.8	3.3	4.1	7.9	13.6	22.8	32.3	39.3	40.3	41.2	41.4	41.2	41.4	41.0	41.5	40.8
Σ	1.1	3.6	8.6	13.3	16.4	20.4	19.2	30.6	33.9	35.8	45.4	44.1	48.8	66.3	82.2	91.2	94.4	95.1	95.6	95.3	95.4	95.6	95.2	95.4	95.4
Fum																									
m+0	97.0	93.7	86.1	84.3	82.7	76.3	71.8	59.6	51.3	54.1	51.2	45.2	32.4	31.1	16.9	11.0	7.1	4.5	4.3	4.2	5.0	3.4	6.8	6.2	5.6
m+1	1.3	3.6	4.3	6.1	4.8	5.6	4.8	8.2	10.1	12.0	10.5	11.4	13.9	13.9	13.9	14.3	14.0	12.4	13.3	14.1	13.5	14.4	12.0	12.7	13.5
m+2	0.0	0.0	0.8	1.7	2.7	4.6	3.7	7.0	4.0	3.7	8.8	12.6	13.3	16.9	19.4	16.4	16.7	17.2	16.4	15.9	17.1	16.7	17.6	17.0	17.1
m+3	1.7	2.8	8.8	7.9	9.8	12.9	19.7	23.9	31.3	27.6	27.8	30.9	31.8	27.3	28.1	30.1	25.3	24.2	23.4	21.9	23.9	23.9	23.6	22.0	25.9
m+4	0.0	0.0	0.0	0.0	0.0	0.7	0.0	1.3	3.2	2.7	1.8	0.0	8.6	10.9	21.7	28.2	36.9	41.6	42.6	43.9	40.5	41.7	40.0	42.0	37.9
Σ	3.0	6.3	14.0	15.7	17.3	23.7	28.2	40.4	48.8	46.0	48.8	54.8	67.6	68.9	83.1	89.0	92.9	95.5	95.7	95.9	95.1	96.7	93.2	93.8	94.4
Mal																									
m+0	98.8	95.7	90.6	87.3	82.5	81.1	77.3	68.0	62.9	63.1	58.4	57.3	50.0	36.7	27.9	17.0	9.5	5.7	4.6	4.5	4.8	4.6	4.8	4.5	4.5
m+1	0.5	1.4	3.2	3.9	5.3	5.7	5.6	7.5	8.0	8.3	9.0	8.9	9.8	11.7	12.5	13.2	13.1	13.0	13.5	13.0	13.1	13.3	13.0	12.9	12.9
m+2	0.0	0.5	1.1	1.5	2.1	2.3	2.5	3.9	4.8	5.2	6.1	6.3	7.9	11.2	13.1	15.2	15.6	16.4	16.4	16.4	16.7	16.4	17.1	16.4	16.8
m+3	0.7	2.4	5.1	7.1	9.7	10.5	14.1	19.5	22.6	21.8	23.9	24.8	26.5	29.3	28.2	26.5	25.4	24.4	23.9	24.6	24.6	24.0	25.0	24.0	24.5
m+4	0.0	0.0	0.0	0.3	0.4	0.5	0.6	1.1	1.7	1.7	2.6	2.8	5.7	11.2	18.3	28.2	36.4	40.5	41.7	41.6	40.9	41.6	40.1	42.3	41.3
Σ	1.2	4.4	9.4	12.7	17.5	18.9	22.7	32.0	37.1	36.9	41.7	42.7	50.0	63.3	72.1	83.0	90.5	94.3	95.4	95.6	95.2	95.4	95.2	95.5	95.6
Pen5P																									
m+0	98.2	92.3	80.2	75.5	69.9	75.9	43.3	33.1	19.5	25.2	24.1	13.8	10.3	9.1	8.0	6.8	5.5	5.6	5.5	5.9	5.5	5.6	6.1	5.2	5.9
m+1	0.9	2.9	4.8	5.8	7.1	5.7	10.2	10.5	9.4	10.0	10.3	9.0	7.2	6.7	6.7	6.6	5.9	6.0	6.3	6.0	5.8	6.0	5.5	5.9	6.0

	Sample time, s											Sample time, min					Sample time, h								
	0	4	8	12	16	20	25	41	61	80	120	180	6	12	24.15	48	96	2.5	5	7.5	9.5	9.67	9.83	10	10.17
m+2	0.0	0.0	6.9	8.3	10.2	8.2	18.1	18.5	18.3	18.4	18.7	18.1	14.7	14.6	14.6	14.3	13.9	12.9	12.7	13.6	13.7	13.8	13.1	13.6	13.0
m+3	0.9	3.2	5.5	7.3	9.3	8.5	15.4	19.0	22.4	19.4	20.8	21.0	22.2	22.0	21.7	22.2	21.1	21.2	21.3	21.1	20.9	22.1	21.5	21.5	20.8
m+4	0.0	0.8	1.3	1.3	1.3	1.8	4.1	5.5	8.6	8.3	7.4	10.3	10.6	10.8	11.5	13.7	15.1	13.4	13.4	12.9	13.1	12.9	12.3	13.2	14.5
m+5	0.0	0.7	1.4	1.9	2.1	0.0	8.9	13.5	21.9	18.8	18.7	27.8	35.1	36.9	37.7	36.5	38.5	41.0	40.7	40.6	41.0	39.7	41.6	40.6	39.8
Σ	1.8	7.7	19.8	24.5	30.1	24.1	56.7	66.9	80.5	74.8	75.9	86.2	89.7	90.9	92.1	93.2	94.5	94.4	94.5	94.1	94.5	94.4	93.9	94.8	94.1
S7P																									
m+0	95.3	85.6	72.9	65.1	58.5	62.6	29.6	20.2	10.7	14.5	15.5	6.8	4.9	3.9	3.2	2.7	2.2	2.3	2.5	2.3	2.5	2.2	2.2	2.3	2.1
m+1	2.3	3.4	4.9	7.2	7.2	6.5	8.1	7.6	5.8	6.0	5.9	4.4	3.9	3.6	3.5	3.1	2.7	3.0	2.7	2.7	3.0	2.9	2.8	3.0	3.0
m+2	2.4	6.7	10.9	12.3	12.5	12.1	19.0	17.2	13.5	14.3	12.5	12.2	11.8	10.9	10.2	8.1	8.4	9.7	9.1	8.9	9.0	8.9	9.3	9.1	8.6
m+3	0.0	0.0	5.6	7.9	12.8	11.4	14.0	14.3	13.1	13.5	14.1	11.1	9.7	10.3	9.9	11.2	10.3	9.3	9.4	9.7	9.9	9.5	9.6	9.3	9.3
m+4	0.0	2.4	2.8	3.7	4.3	4.4	7.8	11.6	12.9	12.4	12.6	13.4	11.6	12.0	11.8	13.3	13.0	11.5	11.9	12.0	11.9	11.6	11.3	11.6	12.6
m+5	0.0	2.0	2.9	3.9	4.7	3.1	12.8	16.2	19.9	18.0	17.9	20.8	21.5	21.8	22.4	22.1	21.9	22.2	22.2	23.0	22.8	22.2	22.6	22.7	21.9
m+6	0.0	0.0	0.0	0.0	0.0	0.0	3.4	4.4	8.6	7.4	8.1	10.8	11.0	11.3	12.0	13.8	14.9	12.8	13.4	13.0	12.8	13.4	13.2	13.1	14.5
m+7	0.0	0.0	0.0	0.0	0.0	0.0	5.3	8.5	15.5	14.0	13.5	20.5	25.6	26.1	27.1	25.8	26.7	29.2	28.8	28.4	28.3	29.3	29.0	29.1	27.9
Σ	4.7	14.4	27.1	34.9	41.5	37.4	70.4	79.8	89.3	85.5	84.5	93.2	95.1	96.1	96.9	97.3	97.8	97.7	97.5	97.7	97.6	97.8	97.8	97.7	97.9
Ser																									
m+0	99.5	98.0	98.1	96.3	92.6	88.7	84.1	64.0	46.9	39.1	34.5	30.2	26.1	23.8	20.7	21.2	19.9	18.6	17.7	18.4	18.8	17.7	18.2	18.3	17.8
m+1	0.5	0.5	0.3	0.5	1.5	1.9	2.8	6.2	11.1	11.8	13.5	14.3	14.5	14.7	14.8	13.6	14.6	14.1	14.5	14.0	14.2	14.3	14.5	14.1	14.5
m+2	0.0	0.8	0.0	0.0	0.0	0.6	0.9	2.2	3.1	4.7	5.0	4.3	4.8	5.1	5.5	5.9	5.6	6.0	5.7	5.7	5.5	6.3	5.7	5.7	6.5
m+3	0.0	0.7	1.7	3.2	5.8	8.9	12.2	27.5	38.9	44.4	46.9	51.2	54.7	56.4	59.1	59.2	59.9	61.3	62.0	61.9	61.6	61.8	61.6	61.8	61.3
Σ	0.5	2.0	1.9	3.7	7.4	11.3	15.9	36.0	53.1	60.9	65.5	69.8	73.9	76.2	79.3	78.8	80.1	81.5	82.3	81.6	81.3	82.4	81.8	81.7	82.2
Gly																									
m+0	100.0	100.0	100.0	100.0	100.0	100.0	100.0	100.0	100.0	100.0	85.2	85.8	82.0	62.5	45.9	32.8	38.7	26.7	26.6	31.8	35.7	23.9	30.3	25.7	19.5
m+1	0.0	0.0	0.0	0.0	0.0	0.0	0.0	0.0	0.0	0.0	0.0	0.0	0.0	0.0	0.0	0.0	0.0	0.0	0.0	0.0	0.0	0.0	0.0	0.0	0.0
m+2	0.0	0.0	0.0	0.0	0.0	0.0	0.0	0.0	0.0	0.0	14.8	14.2	18.0	37.5	54.1	67.2	61.3	73.3	73.4	68.2	64.4	76.1	69.7	74.3	80.5
Σ	0.0	0.0	0.0	0.0	0.0	0.0	0.0	0.0	0.0	0.0	14.8	14.2	18.0	37.5	54.1	67.2	61.3	73.3	73.4	68.2	64.4	76.1	69.7	74.3	80.5
Ala																									
m+0	98.4	95.9	91.0	86.3	82.0	78.8	76.7	64.4	58.9	56.8	47.1	43.1	35.8	27.7	22.6	19.5	18.0	17.9	17.3	17.3	17.4	17.2	17.0	17.6	17.3
m+1	0.7	1.0	2.0	2.9	3.8	4.5	4.6	7.0	7.6	8.0	9.4	10.1	10.6	12.4	13.2	13.4	13.3	13.0	13.4	13.4	13.4	13.6	13.1	13.4	13.2
m+2	0.0	0.2	0.5	1.0	1.3	1.9	1.9	2.8	3.3	3.5	4.6	3.9	4.1	5.5	5.6	6.6	6.7	6.2	6.0	6.1	6.1	6.3	6.2	6.1	6.6
m+3	1.0	2.9	6.5	9.8	12.9	14.8	16.8	25.8	30.3	31.8	38.9	42.9	49.5	54.5	58.6	60.4	62.0	63.0	63.3	63.2	63.1	62.9	63.7	62.9	62.9
Σ	1.6	4.1	9.0	13.7	18.0	21.2	23.3	35.6	41.1	43.2	52.9	56.9	64.2	72.3	77.4	80.5	82.0	82.2	82.7	82.7	82.6	82.8	83.0	82.4	82.7
Val																									
m+0	100.0	100.0	99.7	99.1	98.3	97.8	97.5	96.2	95.5	94.9	95.2	95.1	29.4	24.0	18.3	12.5	8.8	7.3	6.6	6.6	6.5	6.3	6.2	6.3	6.7
m+1	0.0	0.0	0.0	0.0	0.0	0.0	0.0	0.0	0.0	0.0	0.0	0.0	5.0	5.0	4.3	5.8	5.7	5.9	5.8	5.5	5.3	5.5	5.7	6.0	5.9
m+2	0.0	0.0	0.1	0.4	0.6	0.8	0.8	1.1	1.1	1.1	0.9	0.8	14.7	14.1	15.1	15.1	15.3	15.1	15.0	15.3	15.1	14.9	14.9	15.1	14.6
m+3	0.0	0.0	0.2	0.5	0.9	1.1	1.2	1.6	1.8	1.9	1.8	1.7	19.3	20.3	20.6	21.5	21.8	22.5	22.9	22.4	22.5	22.3	22.7	22.9	22.9
m+4	0.0	0.0	0.0	0.0	0.1	0.1	0.1	0.2	0.3	0.4	0.5	0.6	7.3	8.5	10.3	10.8	11.6	11.7	12.0	12.0	11.9	12.3	11.9	11.9	12.1
m+5	0.0	0.0	0.0	0.1	0.2	0.3	0.4	0.8	1.2	1.6	1.8	1.8	24.2	28.0	31.5	34.3	36.9	37.4	37.7	38.3	38.7	38.8	38.6	37.9	37.8
Σ	0.0	0.0	0.3	0.9	1.7	2.2	2.6	3.8	4.5	5.1	4.8	4.9	70.6	76.0	81.7	87.5	91.3	92.7	93.4	93.4	93.5	93.7	93.8	93.7	93.3
Leu																									
m+0	100.0	99.6	99.3	97.8	94.8	90.3	84.8	66.6	48.8	41.4	32.5	33.9	20.4	16.6	10.4	6.0	4.9	3.0	1.8	2.3	2.4	1.4	1.8	2.0	2.5
m+1	0.0	0.0	0.0	0.1	0.5	1.3	1.9	3.3	3.8	3.8	3.6	2.5	3.4	3.2	2.5	2.3	2.0	2.0	1.9	1.7	2.0	1.9	2.0	1.9	1.8

	Sample time, s											Sample time, min					Sample time, h								
	0	4	8	12	16	20	25	41	61	80	120	180	6	12	24.15	48	96	2.5	5	7.5	9.5	9.67	9.83	10	10.17
m+2	0.0	0.4	0.7	2.1	4.3	7.5	9.9	17.7	23.0	22.1	19.7	16.8	15.7	14.0	13.4	11.2	9.9	9.3	9.6	9.3	8.9	9.8	9.9	8.9	9.7
m+3	0.0	0.0	0.0	0.0	0.0	0.0	1.1	2.8	5.3	6.5	8.4	7.9	10.7	11.6	11.1	11.6	11.1	11.7	12.3	12.0	11.5	11.6	11.8	11.7	11.3
m+4	0.0	0.0	0.0	0.0	0.4	0.9	1.7	7.1	12.7	16.1	20.3	21.2	25.0	26.3	27.7	29.1	28.9	29.9	29.6	29.6	29.9	30.3	29.4	30.5	29.7
m+5	0.0	0.0	0.0	0.0	0.0	0.0	0.2	0.9	2.4	3.5	6.0	6.4	9.3	11.4	13.9	15.4	17.0	17.3	17.5	17.8	17.5	17.7	17.6	18.3	17.7
m+6	0.0	0.0	0.0	0.0	0.0	0.0	0.3	1.6	4.2	6.6	9.6	11.4	15.4	17.0	21.1	24.4	26.3	26.7	27.4	27.4	27.9	27.4	27.6	26.9	27.3
Σ	0.0	0.4	0.7	2.2	5.2	9.7	15.2	33.4	51.2	58.7	67.5	66.1	79.6	83.4	89.6	94.0	95.1	97.1	98.2	97.7	97.6	98.6	98.2	98.1	97.5
Phe																									
m+0	98.5	97.3	93.7	90.3	86.7	77.3	66.5	43.7	29.0	22.9	17.5	14.6	10.8	9.9	6.5	6.3	4.9	0.0	0.0	0.0	2.5	0.0	0.0	0.0	3.4
m+1	0.1	0.4	1.4	1.8	2.4	3.4	4.1	6.0	5.9	5.7	3.7	3.0	2.4	2.2	2.3	1.8	1.3	2.2	2.0	1.5	2.0	1.7	1.6	1.3	1.7
m+2	1.0	1.2	1.3	1.3	1.4	3.0	3.9	7.0	7.3	5.3	6.0	6.9	5.1	5.9	5.3	4.3	4.5	3.7	4.1	4.4	4.5	3.9	3.6	4.0	3.7
m+3	0.4	1.1	3.1	5.8	8.1	12.4	16.3	21.2	17.1	13.2	9.0	8.2	8.0	7.8	6.8	6.2	5.9	6.5	6.4	6.3	6.0	6.9	6.2	6.6	6.8
m+4	0.0	0.0	0.5	0.8	1.5	2.4	3.8	6.7	8.5	8.3	10.0	10.7	9.3	8.7	8.4	8.3	8.3	8.1	8.4	8.2	8.0	8.2	7.0	7.9	8.2
m+5	0.0	0.0	0.0	0.0	0.0	0.0	0.9	1.4	6.9	12.0	10.4	9.2	13.8	11.1	14.0	14.0	13.9	13.2	15.1	16.2	16.1	16.1	18.7	15.2	15.6
m+6	0.0	0.0	0.0	0.0	0.0	0.0	1.3	5.0	8.4	10.4	13.5	14.3	14.8	14.6	14.6	14.5	15.3	16.7	14.2	14.8	14.5	14.2	14.4	14.9	14.6
m+7	0.0	0.0	0.0	0.0	0.0	1.5	2.5	4.8	7.9	9.3	10.5	12.7	13.1	13.5	13.8	14.7	15.0	14.8	14.8	14.9	14.4	15.7	12.6	15.3	14.6
m+8	0.0	0.0	0.0	0.0	0.0	0.0	0.0	1.5	3.7	5.7	7.6	7.0	8.3	9.0	9.8	9.9	10.4	12.2	12.1	10.4	10.6	12.3	12.8	11.9	10.5
m+9	0.0	0.0	0.0	0.0	0.0	0.0	0.6	2.7	5.3	7.1	11.8	13.4	14.6	17.4	18.5	20.1	20.5	22.7	23.0	23.4	21.4	21.2	23.2	22.7	21.0
Σ	1.5	2.7	6.3	9.7	13.3	22.7	33.5	56.3	71.0	77.1	82.6	85.4	89.2	90.1	93.5	93.8	95.1	100.0	100.0	100.0	97.5	100.0	100.0	100.0	96.6
Tyr																									
m+0	98.0	98.9	95.5	92.7	86.1	79.5	68.7	44.7	24.5	18.4	10.0	5.0	4.6	0.0	2.8	0.0	0.0	0.0	0.0	0.0	1.2	0.0	0.0	0.0	0.0
m+1	1.2	0.0	0.8	1.3	2.5	3.2	4.0	6.1	7.5	5.9	4.7	3.3	2.0	2.8	1.1	1.7	0.0	0.0	1.4	0.0	0.0	0.0	0.0	1.2	0.9
m+2	0.5	0.3	0.5	0.4	0.9	1.3	2.8	4.6	7.7	8.0	6.5	5.1	4.7	2.9	2.8	2.7	1.7	0.0	1.6	0.0	0.0	2.8	0.0	0.0	0.0
m+3	0.0	0.9	2.8	4.8	8.1	12.2	17.6	21.5	20.5	14.6	9.2	9.4	9.3	10.5	8.7	7.2	7.7	8.0	7.6	7.6	7.4	7.4	7.0	7.7	7.7
m+4	0.0	0.0	0.0	0.0	1.5	2.3	3.3	7.0	7.3	10.1	11.7	9.9	9.4	9.9	7.7	8.1	9.3	8.4	7.7	8.3	9.3	7.8	8.4	8.6	7.7
m+5	0.4	0.0	0.5	0.0	0.9	0.8	2.4	5.3	9.7	13.7	12.9	14.9	16.4	16.0	15.7	16.7	14.1	15.2	15.8	17.7	16.5	15.4	17.0	17.3	15.6
m+6	0.0	0.0	0.0	0.0	0.0	0.0	1.2	3.3	7.7	10.7	14.9	15.0	16.4	16.6	17.7	17.7	16.3	17.4	15.3	16.8	15.5	17.1	16.6	15.0	16.2
m+7	0.0	0.0	0.0	0.0	0.0	0.0	0.0	4.9	6.8	7.5	10.8	13.8	11.5	12.6	14.1	13.7	14.0	16.8	16.5	15.5	15.2	15.4	16.1	17.4	16.3
m+8	0.0	0.0	0.0	0.8	0.0	0.7	0.0	0.2	2.9	2.8	5.3	9.0	7.7	10.7	10.0	11.9	11.0	11.3	10.4	12.2	12.5	12.2	11.6	11.5	12.0
m+9	0.0	0.0	0.0	0.0	0.0	0.0	0.0	2.5	5.5	8.3	14.1	14.6	18.2	18.0	19.4	20.4	26.0	23.0	23.7	21.9	22.5	21.9	23.4	21.3	23.6
Σ	2.0	1.1	4.5	7.3	13.9	20.5	31.3	55.3	75.5	81.6	90.0	95.0	95.4	100.0	97.2	100.0	100.0	100.0	100.0	100.0	98.8	100.0	100.0	100.0	100.0
Glu																									
m+0	100.0	100.0	100.0	100.0	100.0	100.0	100.0	100.0	100.0	100.0	100.0	100.0	100.0	44.1	20.5	6.1	2.0	1.5	1.3	1.2	1.2	1.3	1.2	1.3	1.3
m+1	0.0	0.0	0.0	0.0	0.0	0.0	0.0	0.0	0.0	0.0	0.0	0.0	0.0	6.2	7.1	6.4	5.0	4.7	4.6	4.6	4.5	4.6	4.6	4.7	4.8
m+2	0.0	0.0	0.0	0.0	0.0	0.0	0.0	0.0	0.0	0.0	0.0	0.0	0.0	23.2	24.0	18.6	13.8	13.0	12.5	12.1	12.4	12.6	12.6	12.1	12.5
m+3	0.0	0.0	0.0	0.0	0.0	0.0	0.0	0.0	0.0	0.0	0.0	0.0	0.0	9.9	17.7	23.5	25.3	25.4	25.8	25.9	25.9	26.3	25.6	26.0	25.8
m+4	0.0	0.0	0.0	0.0	0.0	0.0	0.0	0.0	0.0	0.0	0.0	0.0	0.0	12.6	20.6	25.6	26.0	25.4	25.7	25.9	25.7	25.2	25.7	25.6	25.9
m+5	0.0	0.0	0.0	0.0	0.0	0.0	0.0	0.0	0.0	0.0	0.0	0.0	0.0	4.0	10.1	19.9	27.9	30.1	30.2	30.3	30.4	30.1	30.3	30.3	29.8
Σ	0.0	0.0	0.0	0.0	0.0	0.0	0.0	0.0	0.0	0.0	0.0	0.0	0.0	55.9	79.5	93.9	98.0	98.5	98.7	98.8	98.8	98.8	98.8	98.7	98.7
Gln																									
m+0	100.0	100.0	100.0	100.0	100.0	99.8	99.9	99.0	98.3	97.5	93.6	90.5	75.4	50.3	23.2	6.9	2.6	1.9	1.4	1.4	1.3	1.2	1.3	1.3	1.3
m+1	0.0	0.0	0.0	0.0	0.0	0.0	0.0	0.0	0.0	0.0	0.6	0.8	2.6	5.1	6.9	6.2	4.8	4.4	4.4	4.4	4.5	4.5	4.5	4.6	4.5
m+2	0.0	0.0	0.0	0.0	0.0	0.2	0.0	0.8	1.4	1.9	4.0	5.9	12.4	21.4	23.8	18.5	13.8	12.9	12.3	12.6	12.6	12.3	12.2	12.3	12.3
m+3	0.0	0.0	0.0	0.0	0.0	0.0	0.0	0.1	0.1	0.2	0.6	0.8	3.4	8.5	16.9	23.6	25.0	25.2	25.7	25.1	25.4	25.5	25.9	25.6	25.5
m+4	0.0	0.0	0.0	0.0	0.0	0.0	0.1	0.2	0.3	0.4	1.1	1.8	5.2	11.6	20.1	25.7	25.9	25.6	25.9	25.7	25.5	25.9	25.4	25.6	25.9
m+5	0.0	0.0	0.0	0.0	0.0	0.0	0.0	0.0	0.0	0.0	0.1	0.2	1.0	3.2	9.2	19.3	27.9	30.1	30.4	30.9	30.7	30.5	30.8	30.7	30.5

	Sample time, s											Sample time, min					Sample time, h								
	0	4	8	12	16	20	25	41	61	80	120	180	6	12	24.15	48	96	2.5	5	7.5	9.5	9.67	9.83	10	10.17
Σ	0.0	0.0	0.0	0.0	0.0	0.2	0.1	1.0	1.8	2.5	6.4	9.5	24.6	49.7	76.8	93.1	97.4	98.2	98.6	98.7	98.7	98.8	98.7	98.8	98.7
Arg																									
m+0	99.7	100.0	100.0	100.0	100.0	99.7	100.0	100.0	99.9	100.0	98.6	95.2	82.2	57.1	21.9	8.7	3.8	2.6	1.6	1.8	1.1	1.0	1.0	1.2	1.1
m+1	0.0	0.0	0.0	0.0	0.0	0.0	0.0	0.0	0.1	0.0	1.0	2.7	7.0	12.5	13.3	6.6	3.4	2.4	2.3	2.2	2.6	2.9	2.2	2.3	2.2
m+2	0.0	0.0	0.0	0.0	0.0	0.0	0.0	0.0	0.0	0.0	0.4	1.5	6.5	16.0	17.1	12.0	7.7	7.3	7.2	6.5	6.5	7.0	6.5	7.4	6.8
m+3	0.0	0.0	0.0	0.0	0.0	0.0	0.0	0.0	0.0	0.0	0.0	0.0	0.0	0.0	18.1	21.1	17.3	16.7	17.0	17.0	17.8	16.8	15.8	16.2	17.1
m+4	0.0	0.0	0.0	0.0	0.0	0.0	0.0	0.0	0.0	0.0	0.0	0.5	2.9	9.1	16.1	22.2	25.5	25.2	24.4	25.8	25.8	25.1	26.1	25.6	25.3
m+5	0.3	0.0	0.0	0.0	0.0	0.3	0.0	0.0	0.0	0.0	0.0	0.0	1.4	4.8	10.5	20.4	25.1	25.7	26.1	25.7	25.2	26.6	26.3	26.2	26.3
m+6	0.0	0.0	0.0	0.0	0.0	0.0	0.0	0.0	0.0	0.0	0.0	0.0	0.0	0.5	2.8	8.9	17.1	20.1	21.5	20.9	21.0	20.7	22.1	21.0	21.2
Σ	0.3	0.0	0.0	0.0	0.0	0.3	0.0	0.0	0.1	0.0	1.4	4.8	17.8	42.9	78.1	91.3	96.2	97.4	98.5	98.2	98.9	99.0	99.0	98.8	98.9
Pro																									
m+0	100.0	100.0	100.0	100.0	100.0	100.0	100.0	100.0	100.0	99.8	98.6	96.7	85.7	61.7	30.5	9.6	3.1	2.0	1.5	1.3	1.3	1.3	1.3	1.2	1.2
m+1	0.0	0.0	0.0	0.0	0.0	0.0	0.0	0.0	0.0	0.0	0.1	0.5	1.8	4.1	6.6	6.2	4.7	4.6	4.6	4.7	4.6	4.6	4.5	4.6	4.5
m+2	0.0	0.0	0.0	0.0	0.0	0.0	0.0	0.0	0.0	0.1	0.9	1.7	7.0	17.0	23.0	19.1	14.0	12.7	12.3	12.3	12.2	12.4	12.5	12.3	12.4
m+3	0.0	0.0	0.0	0.0	0.0	0.0	0.0	0.0	0.0	0.0	0.1	0.4	2.0	6.3	14.3	22.3	24.9	25.4	25.3	25.6	25.7	25.3	25.6	25.5	25.5
m+4	0.0	0.0	0.0	0.0	0.0	0.0	0.0	0.0	0.0	0.1	0.3	0.8	3.0	8.8	17.8	24.8	25.7	25.6	25.6	25.8	25.6	25.9	25.5	25.7	25.8
m+5	0.0	0.0	0.0	0.0	0.0	0.0	0.0	0.0	0.0	0.0	0.0	0.0	0.6	2.2	7.8	18.1	27.5	29.6	30.7	30.3	30.6	30.5	30.7	30.8	30.7
Σ	0.0	0.0	0.0	0.0	0.0	0.0	0.0	0.0	0.0	0.2	1.4	3.3	14.3	38.3	69.5	90.4	96.9	98.0	98.5	98.7	98.7	98.7	98.7	98.8	98.8
Asp																									
m+0	99.2	97.0	92.7	89.3	86.0	81.2	79.0	69.3	64.3	60.4	51.8	47.2	41.2	29.1	16.2	8.5	5.5	4.5	4.4	4.4	4.4	4.4	4.0	4.4	4.3
m+1	0.1	0.8	1.9	2.5	3.1	4.5	4.6	6.1	6.9	7.9	9.2	9.7	10.6	12.4	13.6	13.9	13.2	13.1	13.0	12.9	13.0	12.9	12.8	12.6	12.6
m+2	0.0	0.0	0.5	0.7	1.0	1.6	1.9	3.2	4.3	5.4	6.9	8.1	11.1	15.0	17.3	17.2	16.7	17.0	16.8	16.7	17.1	17.0	17.1	17.4	17.2
m+3	0.7	2.3	4.9	7.5	9.8	12.5	14.3	20.6	23.4	24.6	29.5	31.5	30.2	30.7	31.0	28.2	25.1	24.0	23.9	23.6	23.8	23.6	24.0	23.8	24.2
m+4	0.0	0.0	0.1	0.1	0.1	0.2	0.2	0.7	1.2	1.7	2.7	3.5	7.0	12.8	21.9	32.3	39.6	41.5	41.9	42.4	41.7	42.1	42.1	42.0	41.7
Σ	0.8	3.0	7.3	10.8	14.0	18.8	21.0	30.7	35.7	39.6	48.2	52.8	58.8	70.9	83.8	91.5	94.6	95.5	95.6	95.6	95.6	95.6	96.0	95.7	95.7
Lys																									
m+0	100.0	99.9	99.6	99.2	98.2	96.3	94.5	88.4	81.6	74.2	62.0	50.4	32.5	21.3	15.5	10.9	4.7	2.6	1.3	1.0	1.2	1.1	1.0	1.0	1.0
m+1	0.0	0.0	0.0	0.0	0.0	0.0	0.4	1.0	2.1	3.0	4.4	5.2	6.9	6.9	5.2	3.9	3.4	3.4	3.5	3.5	3.1	3.3	3.2	3.2	3.4
m+2	0.0	0.1	0.4	0.8	1.4	2.2	2.9	6.1	10.5	12.6	16.8	20.2	23.0	20.6	15.0	11.0	8.9	8.4	8.2	8.3	8.1	8.4	8.1	8.0	8.4
m+3	0.0	0.0	0.0	0.0	0.4	1.3	2.1	3.2	3.1	5.8	8.6	11.1	15.9	17.2	17.7	16.6	16.1	16.2	16.1	15.4	16.0	15.4	16.2	16.4	16.9
m+4	0.0	0.0	0.0	0.0	0.0	0.0	0.0	0.5	0.9	1.5	2.6	4.3	8.2	13.3	17.6	19.9	22.1	22.6	22.5	23.7	23.4	23.2	23.0	22.9	22.9
m+5	0.0	0.0	0.0	0.0	0.0	0.1	0.2	0.8	1.8	3.0	5.7	8.7	13.5	16.7	19.1	20.7	21.3	21.4	22.1	21.4	21.7	22.1	22.0	21.9	21.8
m+6	0.0	0.0	0.0	0.0	0.0	0.0	0.0	0.0	0.0	0.0	0.0	0.0	0.0	4.0	9.9	17.0	23.6	25.4	26.3	26.7	26.7	26.7	26.5	26.7	25.7
Σ	0.0	0.1	0.4	0.8	1.8	3.7	5.5	11.6	18.4	25.8	38.0	49.6	67.5	78.7	84.5	89.2	95.3	97.4	98.7	99.0	98.8	98.9	99.0	99.0	99.0
Thr																									
m+0	99.9	100.0	100.0	100.0	100.0	100.0	100.0	93.7	90.1	88.1	77.5	63.2	50.1	36.6	18.7	11.3	6.7	5.8	5.3	5.0	5.1	4.5	4.6	5.2	4.7
m+1	0.0	0.0	0.0	0.0	0.0	0.0	0.0	0.0	0.0	0.0	0.0	6.3	7.4	9.5	12.2	12.1	13.0	11.4	11.5	16.6	11.4	14.3	12.3	11.9	15.1
m+2	0.1	0.0	0.0	0.0	0.0	0.0	0.0	2.8	3.3	3.1	5.9	7.3	10.5	15.3	18.9	18.0	17.9	18.2	18.9	16.7	18.0	18.8	19.0	17.3	17.1
m+3	0.0	0.0	0.0	0.0	0.0	0.0	0.0	3.5	6.7	8.8	15.1	19.8	25.9	27.0	29.8	27.0	23.3	24.4	23.2	22.5	24.2	22.4	23.1	24.9	22.1
m+4	0.0	0.0	0.0	0.0	0.0	0.0	0.0	0.0	0.0	0.0	1.5	3.5	6.1	11.7	20.4	31.6	39.1	40.3	41.2	39.2	41.3	40.0	41.1	40.8	41.0
Σ	0.1	0.0	0.0	0.0	0.0	0.0	0.0	6.3	10.0	11.9	22.5	36.9	49.9	63.4	81.3	88.8	93.3	94.2	94.7	95.0	94.9	95.5	95.4	94.8	95.3
Ile																									
m+0	99.3	96.9	93.6	88.4	84.2	79.8	76.7	69.4	61.4	59.3	52.0	48.7	36.0	28.3	16.6	8.9	5.0	3.1	2.0	1.9	1.8	1.5	1.6	1.7	1.5

	Sample time, s											Sample time, min					Sample time, h								
	0	4	8	12	16	20	25	41	61	80	120	180	6	12	24.15	48	96	2.5	5	7.5	9.5	9.67	9.83	10	10.17
m+1	0.1	0.6	1.0	1.8	2.5	2.7	3.8	5.2	5.6	6.3	6.4	6.3	7.0	6.3	5.5	4.4	3.4	3.0	3.3	3.2	3.4	3.3	3.5	3.1	3.0
m+2	0.6	2.5	5.5	9.8	13.4	17.5	19.2	24.9	30.4	30.4	29.7	26.9	25.4	21.7	17.6	12.0	9.5	8.9	7.9	8.2	8.1	8.3	8.2	8.2	7.6
m+3	0.0	0.0	0.0	0.1	0.0	0.0	0.2	0.4	1.2	1.9	4.8	6.5	11.0	13.3	15.2	16.2	15.3	15.1	16.0	15.6	15.6	15.1	15.6	15.1	16.4
m+4	0.0	0.0	0.0	0.0	0.0	0.0	0.0	0.0	0.4	0.3	1.8	4.2	7.6	11.2	16.6	20.4	22.3	23.0	23.5	23.1	22.8	24.1	22.8	23.8	23.5
m+5	0.0	0.0	0.0	0.0	0.0	0.0	0.0	0.0	1.0	1.7	5.0	6.5	11.3	14.0	18.2	20.3	20.1	21.9	20.5	21.2	20.7	20.6	21.1	20.7	21.7
m+6	0.0	0.0	0.0	0.0	0.0	0.0	0.0	0.0	0.0	0.1	0.4	1.0	1.9	5.2	10.4	18.0	24.3	25.0	26.8	26.8	27.7	27.1	27.3	27.3	26.4
Σ	0.7	3.1	6.4	11.6	15.8	20.2	23.3	30.6	38.6	40.7	48.0	51.3	64.1	71.7	83.5	91.1	95.0	96.9	98.0	98.1	98.2	98.5	98.4	98.3	98.5
Met																									
m+0	100.0	99.6	100.0	99.1	99.8	98.0	99.0	96.7	87.8	80.6	73.5	70.7	41.1	21.3	12.4	7.0	4.2	1.9	2.1	1.9	2.1	1.5	1.5	0.0	1.7
m+1	0.0	0.4	0.0	0.9	0.3	2.0	1.0	3.3	12.2	19.4	26.5	29.3	37.3	29.2	19.7	12.9	8.1	6.3	5.9	6.6	4.7	5.9	6.3	6.1	5.3
m+2	0.0	0.0	0.0	0.0	0.0	0.0	0.0	0.0	0.0	0.0	0.0	0.0	4.7	8.3	12.7	11.4	13.9	15.2	12.9	12.4	12.9	14.3	12.8	13.9	11.5
m+3	0.0	0.0	0.0	0.0	0.0	0.0	0.0	0.0	0.0	0.0	0.0	0.0	0.0	12.7	17.9	21.1	18.8	19.5	20.3	19.4	21.1	17.4	19.4	19.5	20.1
m+4	0.0	0.0	0.0	0.0	0.0	0.0	0.0	0.0	0.0	0.0	0.0	0.0	16.9	23.6	24.9	25.8	29.3	27.3	28.3	30.7	29.1	29.9	29.4	30.8	31.4
m+5	0.0	0.0	0.0	0.0	0.0	0.0	0.0	0.0	0.0	0.0	0.0	0.0	0.0	5.0	12.4	21.8	25.7	29.9	30.5	29.2	29.9	31.1	30.6	29.8	30.0
Σ	0.0	0.4	0.0	0.9	0.3	2.0	1.0	3.3	12.2	19.4	26.5	29.3	58.9	78.8	87.7	93.0	95.8	98.1	97.9	98.1	97.9	98.5	98.5	100.0	98.3
Glucn																									
m+0	97.5	100.0	100.0	90.3	88.5	89.0	85.8	76.6	67.4	63.3	57.7	54.0	33.6	23.3	19.5	29.1	17.3	18.4	12.1	9.0	14.8	13.9	11.0	9.0	7.5
m+1	2.5	0.0	0.0	4.0	4.2	4.7	5.9	7.2	9.8	10.3	12.0	15.5	18.5	21.7	22.0	20.6	23.1	25.0	26.9	26.7	24.9	30.3	24.1	25.7	23.8
m+2	0.0	0.0	0.0	1.1	0.0	1.6	1.1	2.0	1.2	0.0	1.7	2.3	2.5	2.6	3.3	3.1	2.8	2.7	2.3	2.9	3.0	0.0	3.2	1.8	2.6
m+3	0.0	0.0	0.0	0.0	0.0	0.0	0.0	0.0	1.5	3.1	3.0	2.8	3.0	3.1	3.7	0.0	3.2	0.0	3.2	0.0	0.0	0.0	0.0	3.6	3.6
m+4	0.0	0.0	0.0	0.0	0.0	0.0	0.0	0.9	2.9	2.5	2.2	4.4	4.4	4.5	0.0	0.0	0.0	2.7	0.0	0.0	0.0	0.0	0.0	0.0	0.0
m+5	0.0	0.0	0.0	0.0	0.0	0.0	0.0	1.6	1.4	1.7	0.8	2.6	3.6	2.7	4.1	3.7	3.3	2.8	3.5	4.3	3.2	8.7	3.7	4.0	4.5
m+6	0.0	0.0	0.0	4.7	7.3	4.8	7.2	11.7	15.8	19.3	22.8	18.5	34.5	42.2	47.5	43.5	50.5	48.4	51.9	57.2	54.1	47.2	58.0	55.9	58.1
Σ	2.5	0.0	0.0	9.7	11.5	11.0	14.2	23.4	32.7	36.7	42.3	46.0	66.4	76.7	80.6	70.9	82.7	81.6	87.9	91.0	85.2	86.1	89.0	91.0	92.6

D.8. Simulated intracellular metabolite fluxes at $\mu = 0.4\,h^{-1}$

Table D.10.: Results of the simulated metabolic flux analysis for *C. glutamicum* cultivated at $\mu = 0.4\,h^{-1}$ for all reactions that were integrated in the metabolic network model. Fluxes are given in relation to the glucose consumption uptake rate ($q_{Glc} = 4.13\,mmol\,h^{-1}$). LB: lower bound; UB: upper bound; best fit obtained with the profile likelihoods method.

Reaction name	LB, %	Best fit, %	UB,%	Reaction name	LB, %	Best fit, %	UB, %
acnA	55.6	66.1	76.7	metXH	1.3	1.3	1.4
acnB	55.6	66.1	76.7	met-bm	1.3	1.3	1.4
acoa-bm	22.5	22.5	23.9	mez	-139	-80.7	71.4
akg-bm	2.5	2.5	2.6	mqo-mdh	-18.4	135.6	199.5
ala-bm	5.4	5.4	5.8	oaa-bm	4.4	4.4	4.6
aro	1.9	1.9	2	odh-1	22.2	27.4	32.7
aspB	11	11	11.7	odh-2	22.2	27.4	32.7
asx-bm	3.6	3.6	3.8	p5p-bm	7.9	7.9	8.4
co2-out	220.8	256.3	287.9	pck-ppc	-92.2	-40.3	34.8
cys-bm	0.8	0.8	0.8	pdh	82.2	92.5	96.8
e4p-bm	0.5	0.5	0.5	pep-bm	1	1	1.0
eno	140.9	146.8	155.5	pfk	67.1	73.7	80.4
f6p-bm	0.6	0.6	0.7	pga-bm	5.6	5.6	5.9
fda	67.1	73.7	80.4	pgi	26.6	44.9	62.9
fumC-1	22.2	27.4	32.7	phe-bm	1.2	1.2	1.3
fumC-2	22.2	27.4	32.7	phoAB	1.2	1.2	1.3
g6p-bm	1.8	1.8	2	proG	1.5	1.5	1.6
gapA	153.8	159.7	170.8	pro-bm	1.5	1.5	1.6
gap-bm	1.2	1.2	1.2	pts	94.1	100	105.2
gdh	8.8	8.8	9.3	pyc-odx	-72.5	-13.8	136.1
glc-upt	94.1	100	105.2	pyk	5.9	82.3	134.9
glnA	1.8	1.8	1.9	pyr-bm	2.1	2.1	2.2
gln-bm	1.8	1.8	1.9	sdh-1	22.2	27.4	32.7
gltA	55.6	66.1	76.7	sdh-2	22.2	27.4	32.7
glu-bm	5.5	5.5	5.8	serC	7.4	7.4	7.8
glyA	3.2	3.2	3.4	ser-bm	2	2	2.1
gly-bm	3.2	3.2	3.4	tal	9.4	15.9	22.7
gnd	33.8	53.3	73.3	thf-out	1.9	1.9	2.1
icd	55.6	66.1	76.7	thrB	4.3	4.3	4.6
ile-bm	1.8	1.8	1.9	thr-bm	2.5	2.5	2.6
ilvAE	1.8	1.8	1.9	tkt1	11.7	15.9	22.8
ilvB	6.5	6.5	6.9	tkt2	7	13.5	20.2
ilvEa	5.4	5.4	5.8	tpi	67.1	73.7	80.4
ilvEv	8	8	8.5	tyrAB	0.7	0.7	0.8
leuAP	4	4	4.2	tyr-bm	0.7	0.7	0.8
leu-bm	4	4	4.2	val-bm	2.6	2.6	2.7
ltsA	3.6	3.6	3.8				
lysCA-1	0.9	0.9	1				
lysCA-2	0.9	0.9	1				
lysC-hom	5.6	5.6	5.9				
lys-bm	1.8	1.8	1.9				

Declaration of authorship

I hereby declare that this dissertation is entirely my own work and that I used no other references or sources than those indicated. Passages or ideas from other references are clearly indicated.

Hiermit versichere ich, dass ich diese Dissertation selbstständig angefertigt und keine anderen Quellen oder Hilfsmittel als angegeben verwendet habe. Passagen und Gedanken aus anderen Quellen sind als solche kenntlich gemacht.

Ulm, 1. November 2019

Michaela Graf

Curriculum Vitae

Personal information

Name:	Michaela Graf
Date of birth:	07.12.1988, Ulm a.d. Donau, Germany

Employment

Since 11/2018	**Transfer Engineer** Upstream Manufacturing, Boehringer Ingelheim Pharma GmbH & Co. KG, Biberach, Germany
04/2014–03/2018	**Research Associate**, Institute of Biochemical Engineering, University of Stuttgart, Germany

Education

2019	Intended final qualification: Dr.-Ing.
Since 04/2014	**Ph.D. Student** Biochemical Engineering, Institute of Biochemical Engineering, University of Stuttgart, Germany
10/2011–03/2014	**M. Sc. Process Engineering** Major studies in chemical and biochemical engineering, Master Thesis: '*Characterization and Application of a Cascade Bioreactor to Analyze the Scale-Up dependent CO_2/HCO_3 Stimulus in* Corynebacterium glutamicum*'* Institute of Biochemical Engineering, University of Stuttgart, Germany
10/2008–09/2011	**B. Sc. Process Engineering** Bachelor Thesis: '*Kinetische Vermessung der katalytischen Aktivität beschichteter Metallschäume*' Institute of Chemical Engineering, University of Stuttgart, Germany
09/1999–07/2008	**Allgemeine Hochschulreife**, Schubart Gymnasium, Ulm, Germany

Work experience

01/2014–03/2014	**Internship**, Up- & Downstream bioprocess development, Boehringer Ingelheim Pharma GmbH & Co. KG, Biberach, Germany
04/2013–12/2013	**Tutor** in Technical Thermodynamics, Institute of Thermodynamics and Thermal Process Engineering, University of Stuttgart, Germany
10/2012–03/2013	**Research Associate**, Institute of Biochemical Engineering, University of Stuttgart, Germany
07/2010–12/2010	**Student Research Associate**, Institute of Chemical Engineering, University of Stuttgart, Germany
04/2009–09/2012	**Working Student**, Siemens AG, Stuttgart, Germany